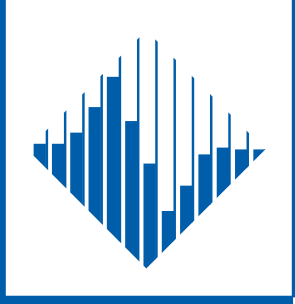

PACIFIC EARTHQUAKE ENGINEERING RESEARCH CENTER

Improving Earthquake Mitigation through Innovations and Applications in Seismic Science, Engineering, Communication, and Response

Proceedings of a U.S.-Iran Seismic Workshop
June 29–July 1, 2009
Irvine, California

PEER 2009/02
OCTOBER 2009

Improving Earthquake Mitigation through Innovations and Applications in Seismic Science, Engineering, Communication, and Response

Proceedings of a U.S.-Iran Seismic Workshop
June 29–July 1, 2009

Arnold and Mabel Beckman Center of the
National Academies of Sciences and Engineering
100 Academy Way
Irvine, California

PEER Report 2009/02
Pacific Earthquake Engineering Research Center
College of Engineering
University of California, Berkeley

October 2009

ABSTRACT

The second U.S.-Iran seismic workshop was held on June 29–July 1, 2009, at the Arnold and Mabel Beckman Center of the National Academies of Sciences and Engineering, Irvine, California. The workshop was supported by the U.S. National Academy of Sciences in collaboration with the Pacific Earthquake Engineering Research Center, and Sharif University of Technology. The theme of this workshop was *Improving Earthquake Mitigation through Innovations and Applications in Seismic Science, Engineering, Communication, and Response*.

This report contains the collection of the papers presented at the 2009 workshop, and participants' recommendations for future collaboration between U.S. and Iranian earthquake scientists and engineers.

Yousef Bozorgnia, Sanaz Rezaeian, and William Anderson

INTRODUCTION

2008 Seismic Workshop

Following an extended period of planning, on June 8–9, 2008, a U.S.-Iran invitational workshop on the "Seismic Performance of Adobe and Masonry Structures" was held at Sharif University of Technology in Tehran. The workshop was organized by Sharif University of Technology (SUT), in collaboration with the U.S. National Academy of Sciences and the Pacific Earthquake Engineering Research Center (PEER), UC Berkeley. The workshop involved specialists from 14 Iranian institutions and an American delegation comprising Daniel Abrams of the University of Illinois at Urbana-Champaign; William Anderson representing the U.S. National Academy of Sciences; Yousef Bozorgnia of PEER, UC Berkeley; Ahmad Hamid of Drexel University; Robert Hamilton representing the U.S. National Academy of Sciences; Richard Klingner of the University of Texas at Austin; and Fred Webster of Fred Webster and Associates in Menlo Park, California.

Sharif University of Technology, Tehran, June 9, 2008

The topic of adobe and masonry vulnerability was selected because of the extensive damage to this form of construction from earthquakes in Iran, including the Bam earthquake of December 26, 2003. Twenty-three technical papers were presented. The workshop concluded with a panel session that identified topics for future research collaboration. The workshop was followed with a one-day public seminar on June 10, 2008, on "Seismic Hazard Reduction," also held at Sharif University.

In the last session of the public seminar, the participants suggested research topics for future seismic cooperation. Those topics are listed in the appendix of this report.

2009 Seismic Workshop

The second U.S.-Iran seismic workshop was held on June 29–July 1, 2009, at the Arnold and Mabel Beckman Center of the National Academies of Sciences and Engineering, Irvine, California. The workshop was supported by the U.S. National Academy of Sciences, in collaboration with the Pacific Earthquake Engineering Research Center (PEER), and Sharif University of Technology (SUT). The theme of this workshop was ***Improving Earthquake Mitigation through Innovations and Applications in Seismic Science, Engineering, Communication, and Response***. Numerous U.S. and Iranian earthquake engineers and scientists participated in the workshop and gave presentations. The agenda of the workshop is attached. The papers presented at the workshop were edited by **Yousef Bozorgnia** (PEER, UC Berkeley), **Sanaz Rezaeian** (PEER, UC Berkeley), and **William Anderson** (U.S. National Academy of Sciences).

On July 1, 2009, the final day of the workshop, the participants had an open discussion about possibilities for future cooperation between seismic experts from both countries. A summary of the open discussion is attached.

We thank all participants of the workshops from both countries for their time and efforts. These workshops in 2008 and 2009 would not have been possible without the continuous support and encouragement of **Glenn Schweitzer** of the U.S. National Academy of Sciences. **Dr. Tabatabaee** (SUT), **Dr. Vafai** (SUT), and **Dr. Pak** (SUT) spent an enormous amount of time coordinating the efforts of the Iranian seismic researchers. We gratefully appreciate their time, efforts, and cooperation. **Sanaz Rezaeian** (PEER, UC Berkeley) diligently assisted in organizing the proceedings of the workshop; her efforts are greatly appreciated. **Merc Fox** (U.S. National Academy of Sciences) carefully worked on all details of the logistics for the 2009 workshop; we appreciate her dedication.

Yousef Bozorgnia and William Anderson

Irvine, California, July 1, 2009

SUMMARY OF THE WORKSHOP CONCLUDING SESSION

On July 1, 2009, the final day of the U.S.-Iran Seismic Workshop, the participants had an open discussion about possibilities for the future cooperation between seismic experts from both countries. The following topics were recommended for future seismic cooperation by the workshop participants:

I. Priority List of Technical Topics for Seismic Cooperation:

1. Seismic performance and retrofit of adobe and masonry buildings, especially residential and school buildings, including a pilot program for implementing candidate retrofit designs.
2. Multidisciplinary seismic risk reduction of lifelines, including lifelines components, structures, systems and networks.
3. Seismic risk reduction of geological and geotechnical hazards such as liquefaction and landslides.
4. Integrated multidisciplinary seismic risk management, including reducing the socio-economic impacts of earthquakes, emergency response management, public risk management and policy.
5. Development of a global risk evaluation system encompassing the derivation of urban and regional vulnerability functions (city inventory and human loss).
6. Earth science, paleoseismological, earthquake source, and seismic hazard studies.
7. Other seismic issues of interest to both the U.S. and Iranian earthquake research communities.

II. Framework of Technical Cooperation. The following was recommended by the participants:

1. Scientific and engineering interactions among researchers, practitioners, academic institutions, and other research and educational organizations in the two countries are encouraged.
2. Creation of a non-governmental joint committee to draft planning details for seismic cooperation. The responsibilities of the joint committee should include:
   - Recommendations on duration, scope, budget, potential funding agencies, etc., for the seismic cooperative program.
   - Creation of sub-committees for each of the technical topics listed above, and coordination of their activities.
3. Sharif University of Technology and the Pacific Earthquake Engineering Research Center, together with other interested scientific organizations in the two countries, will act as points of contact in promoting the process of seismic cooperation as listed above.

AGENDA

MONDAY JUNE 29, 2009

7:45 – 8:30 **Breakfast**

8:30 – 9:00 **Opening—Thomas Jordan, Ali Pak, and Yousef Bozorgnia**

9:00 – 10:00 **Keynote Presentation—Lucile Jones,** United States Geological Survey:
Engaging a Community in Seismic Risk Reduction: Lessons in Science and Communication from the Great Southern California Shakeout

10:00 – 10:15 **Break**

10:15 – 12:15 **Seismic Hazard—Daniel Abrams,** Session Chair

- **Thomas Jordan**, University of Southern California:
  Opportunities for Seismic Risk Reduction Using Earthquake System Science
- **Manuchehr Ghorashi,** Geological Survey of Iran:
  Living with Earthquakes: Know Your Faults
- **Eric Fielding**, Jet Propulsion Laboratory:
  Studies of Earthquake Ruptures and Fault Zone Characteristics with SAR Interferometry (InSAR)
- **Sanaz Rezaeian**, University of California at Berkeley:
  Simulation of Ground Motion Time-Histories

12:15 – 1:15 **Lunch**

1:15 – 2:45 **Multi-Disciplinary Research and Risk Reduction—Richard Klingner,** Session Chair

- **Yousef Bozorgnia**, University of California at Berkeley:
  Crucial Role of Coordinated Multi-Disciplinary Seismic Research
- **Maziar Hosseini**, Tehran Disaster Mitigation and Management Organization: *Seismic Reduction: A Community-Based Approach*
- **Hamzeh Shakib**, Tarbiat Modares University:
  Seismic Vulnerability Assessment of Unreinforced Masonry Buildings: A Guideline

2:45 – 3:00 **Break**

3:00 – 4:15 **Seismic Risk Reduction II and Recovery — Richard Klingner,** Session Chair

- **Laurie Johnson**, Laurie Johnson Consulting:
  Recovery with an Emphasis on Kobe and New Orleans Recoveries
- **Brian Tucker**, GeoHazards International:
  A Proposal for US-Iranian Collaboration: Improving School Earthquake Safety in Central Asia

4:15 – 5:30 **Reception**

5:30 – 7:00 **Banquet**

TUESDAY JUNE 30, 2009

7:45 – 8:30 Breakfast

8:30 – 9:45 Masonry & Adobe Buildings I—Brian Tucker, Session Chair

- **Richard Klingner**, The University of Texas at Austin:
  Earthquake Resistance of Modern Reinforced Masonry Construction
- **Ali Bakhshi**, Sharif University of Technology:
  Seismic Performance of Existing and Retrofitted Masonry and Adobe Houses in Iran Using Shaking Table Tests
- **Ahmad Hamid**, Drexel University:
  Seismic Performance of Partially Grouted Reinforced Concrete Masonry Buildings

9:45 – 11:00 Masonry & Adobe Buildings II—Brian Tucker, Session Chair

- **Daniel Abrams**, University of Illinois at Urbana-Champaign:
  Innovative Seismic Risk Mitigation for Masonry Buildings
- **Abdolreza Sarvghad-Moghadam**, International Institute of Earthquake Engineering and Seismology:
  Role Seismic Retrofitting of Building in Earthquake Risk Mitigation and Disaster Planning for Iran
- **Fred Webster**, Fred Webster Associates:
  California Mission Church Seismic Analysis Project

11:00 – 11:15 Break

11:15 – 12:30 Seismic Response of Buildings I—Fred Webster, Session Chair

- **Mohammad Ghannad**, Sharif University of Technology:
  Effect of Soil on Seismic Performance of Structures
- **Hassan Moghaddam**, Sharif University of Technology:
  On the Optimum Performance-Based Design of Structures
- **Homayoon Estekanchi**, Sharif University of Technology:
  Endurance Time Method: From Ideation to Application

12:30 – 1:30 Lunch

1:30 – 2:30 Seismic Response of Buildings II—Fred Webster, Session Chair

- **Farzin Zareian**, University of California at Irvine:
  Prediction of Collapse of Buildings under Earthquake Ground Motion
- **Mohammad Kazemi**, Sharif University of Technology:
  VM Link Element for Seismic Analysis of Steel Frames

2:30 – 4:30 Geotechnical Earthquake Engineering—Fred Webster, Session Chair

- **Amir Khoei**, Sharif University of Technology:
  SUT−DAM 3D: An Integrated Software Environment for Multi-Disciplinary Geotechnical Engineering
- **Scott Brandenberg**, University of California at Los Angeles:
  Bridge Foundations in Liquefied and Laterally Spreading Ground
- **Mohsen Haeri**, Sharif University of Technology:
  An Overview of the Geotechnical Earthquake Engineering Research of the Civil Engineering Department of Sharif University of Technology
- **Ali Pak**, Sharif University of Technology:
  Evaluating the Effectiveness of Soil Densification for Mitigating Liquefaction-Induced Settlement of Buildings

4:30 – 4:45 Break

4:45 – 5:45 Future of Seismic Cooperation Discussion I—Glenn Schweitzer, Session Chair

WEDNESDAY JULY 1, 2009

7:45 – 8:30 **Breakfast**

8:30 – 9:45 **Seismic Performance of Lifelines—Ahmad Hamid,** Session Chair

- **Masanobu Shinozuka**, University of California at Irvine: *Assessment of Seismic Risk in Lifeline Systems*
- **Mark Mahan**, California Department of Transportation: *Seismic Design and Retrofit of California Bridges*
- **Mohammad Ahmadi**, Tarbiat Modares University: *Seismic Load Definition for Structures in Canyon Site*s

9:45 – 11:00 **Future of Seismic Cooperation Discussion II—Glenn Schweitzer,** Session Chair

11:00 – 11:30 **Closing Session—Ali Pak and Yousef Bozorgnia**

11:30 – 12:30 **Farewell Lunch**

CONTENTS

PREPARING A POPULATION FOR AN EARTHQUAKE LIKE CHI-CHI: THE GREAT SOUTHERN CALIFORNIA SHAKEOUT

Lucile M. Jones[1*] and The ShakeOut Team[2]

[1] Chief Scientist, Multi Hazards Demonstration Project, United States Geological Survey (USA)

[2] Hundreds of experts contributed to the creation of the ShakeOut Scenario and Exercise (USA)

ABSTRACT

The Great Southern California ShakeOut was a week of special events featuring the largest earthquake drill in United States history. On November 13, 2008, over 5 million southern Californians pretended that a magnitude-7.8 earthquake had occurred and practiced actions that could reduce its impact on their lives. The primary message of the ShakeOut is that what we do now, before a big earthquake, will determine what our lives will be like after. The drill was based on a scenario of the impacts and consequences of such an earthquake on the Southern San Andreas Fault, developed by over 300 experts led by the U.S. Geological Survey in partnership with the California Geological Survey, the Southern California Earthquake Center, Earthquake Engineering Research Institute, lifeline operators, emergency services and many other organizations. The ShakeOut campaign was designed and implemented by earthquake scientists, emergency managers, sociologists, art designers and community participants. The means of communication were developed using results from sociological research on what encouraged people to take action. This was structured around four objectives: 1) consistent messages – people are more inclined to believe something when they hear the same thing from multiple sources; 2) visual reinforcement – people are more inclined to do something they see other people doing; 3) encourage "milling" or discussing contemplated action – people need to discuss an action with others they care about before committing to undertaking it; and 4) focus on concrete actions – people are more likely to prepare for a set of concrete consequences of a particular hazard than for an abstract concept of risk. The goals of the ShakeOut were established in Spring 2008 and were: 1) to register 5 million people to participate in the drill; 2) to change the culture of earthquake preparedness in southern California; and 3) to reduce earthquake losses in southern California. All of these goals were met. The final registration at www.shakeout.org for the 2008 ShakeOut was 5.47 million people, or one-quarter of the population of the region. A survey conducted with the registered participants showed that the messages they took from the ShakeOut were the concepts intended, including the importance of "Drop, Cover, Hold On", the interdependency of earthquake risk ("We are all in this together") and the possibility of reducing losses through preparation and mitigation. Sales data from the Home Depot hardware stores in southern California showed a 260% increase in the sale of earthquake safety products during the month of the ShakeOut, November 2008.

Keywords: earthquake preparedness, risk communication, earthquake scenarios

INTRODUCTION

The idea for the Great Southern California ShakeOut arose after Hurricane Katrina hit the U.S. Gulf Coast in 2005 in response to the urgent need to transform the way that southern Californians think - and act – about natural disasters, beginning with earthquakes. Earthquakes

[*] Corresponding author: Lucile M. Jones, USGS, 525 S. Wilson Ave., Pasadena, CA 91106; jones@usgs.gov

are inevitable and we cannot stop them. What we *can* change is how we prepare for them - in our homes, our schools, our businesses, and our communities. If we instead maintain the status quo, then one of these disasters will become a catastrophe, and cripple the long-term economic and social stability of our society.

The ShakeOut was based on a comprehensive scenario of a plausible great earthquake (M7.8) on the southern San Andreas Fault ([1,2] The USGS partnered with the California Geological Survey, Southern California Earthquake Center, earthquake Engineering Research Institute, utility lifeline operators, emergency services, public health, local government and many other organizations to bring 300 scientists and engineers together to build the scenario. This group's mission was to create a plausible earthquake disaster scenario for planning purposes, to examine the impacts of a giant southern California earthquake on the San Andreas fault, from seconds to decades after the event. Ultimately, the goal is to establish a resilient society, and this transformation requires concerted and repeated effort over many years – doing the best science we can and getting our messages to the community in ways that they will be truly heard, used, and applied. We focused on identifying "low hanging fruit" – changes we can make *before* the event that are relatively easy and inexpensive to accomplish, which will have enormous consequences in reducing casualties and losses *after* the event.

The earthquake professionals from federal, State and local agencies as well as private companies formed the Earthquake Country Alliance to communicate earthquake risk to the people of southern California using the results of the scenario. The Alliance used a variety of media, especially the ShakeOut.org website to encourage residents to participate in an earthquake drill at the same time on November 13, 2008. At the same time, the State of California used the scenario as the basis of the emergency responders exercise called Golden Guardian. The City of Los Angeles began planning for an international conference on earthquake safety policy, and a major art college, the Art Center College of Design, began a program to apply design to emergency readiness. As plans for all of these activities matured, the organizers decided to join forces to become The Great Southern California ShakeOut.

THE SHAKEOUT SCENARIO

The ShakeOut Earthquake Scenario is a comprehensive assessment of the physical, social and economic consequences of a great earthquake in southern California, detailing the physical damages (casualties and losses) caused by the earthquake and the impact of those damages on our social and economic systems. To create this assessment, we needed to first construct a plausible earthquake. The earthquake ground motions and fault rupture were based on a wide range of earthquake research information, from trenching and exposed evidence of prehistoric earthquakes, to analysis of instrumental recordings of large earthquakes and the latest theory in earthquake source physics [3]. This information was then fed forward into the rest of the ShakeOut scenario and used by experts to estimate the impact on southern California.

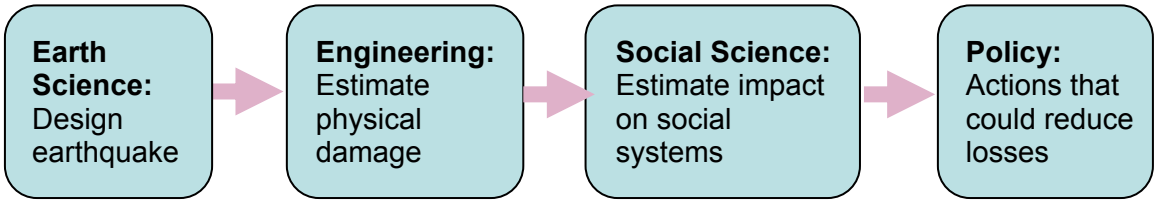

Fig. 1. Flow diagram for the earthquake scenario construction.

The ShakeOut scenario earthquake is a magnitude 7.8 earthquake on the southernmost 300 km (200 mi) of the San Andreas fault (between the Salton Sea and Lake Hughes), a plausible event on the fault most likely to produce a great earthquake [4]. The hypothesized rupture starts at the southern end of the San Andreas and ruptures northwest for 300 km. We estimated the ground motions with physics-based computer simulations of the earthquake with computer systems developed by the Southern California Earthquake Center Information Technology research program.

For the past thirty years, before the recent advances in information technology, ground motion predictions have typically been made using **attenuation relations**, which forecast the expected shaking at a site from the magnitude and distance from the fault. Attenuation relations do not include the additional factors that can affect the shaking such as site effects, directivity and radiation pattern and thus cannot predict pockets of shaking that are lower or higher than the mean. Our physics-based simulations modelled all of the factors, primary and secondary, that affect ground shaking, using two inputs: the ShakeOut kinematic rupture description and a *velocity model* that describes the seismic characteristics of the southern California rocks through which the waves propagate. The results are shown to be consistent with the newest attenuation relations developed by the Next Generation Attenuation (NGA) Models Project [5]

The damage impacts of the scenario earthquake were estimated through a three-step process. First, FEMA's loss estimation program, HAZUS-MH, was run using the physics-based ground motion model [6]. For Los Angeles and Orange Counties, HAZUS used a refined database of structures created from tax assessor's data. For the other counties, this was not available and the default HAZUS database was used. Once HAZUS work had been completed, expert opinion was collected on potential earthquake aftermath through 13 special studies and 6 expert panels. Panels were convened to estimate impacts on dams public utilities, especially where multiple utility companies provide a public service such as water supply or electricity. Engineers and operators were invited to attend the half-day panel discussions, and were presented the results of prior earth sciences studies (shaking, faulting, etc.) as well as damage to other interacting lifelines that had already been assessed. They were then asked to put forward a realistic scenario of damage, service interruption, restoration, and to suggest promising mitigation options. To complement the panels, special studies were used for buildings and for lifelines where the panel process was impractical, such as private utilities or infrastructure (such as highways) where in-depth analysis was desired. In these cases, contributors were selected for their specialized expertise. They too were presented with all previously estimated earth-science and relevant utility impacts, and asked to summarize assets exposed to damage, evidence of past seismic vulnerability, and to posit (repetitive-word choice) a realistic scenario of damage, loss of

function, restoration, and promising mitigation measures. Panels of highly qualified experts reviewed crucial special studies. In the next step of the process, the expert evaluations were merged with the HAZUS results to create the final estimates of probable damages.

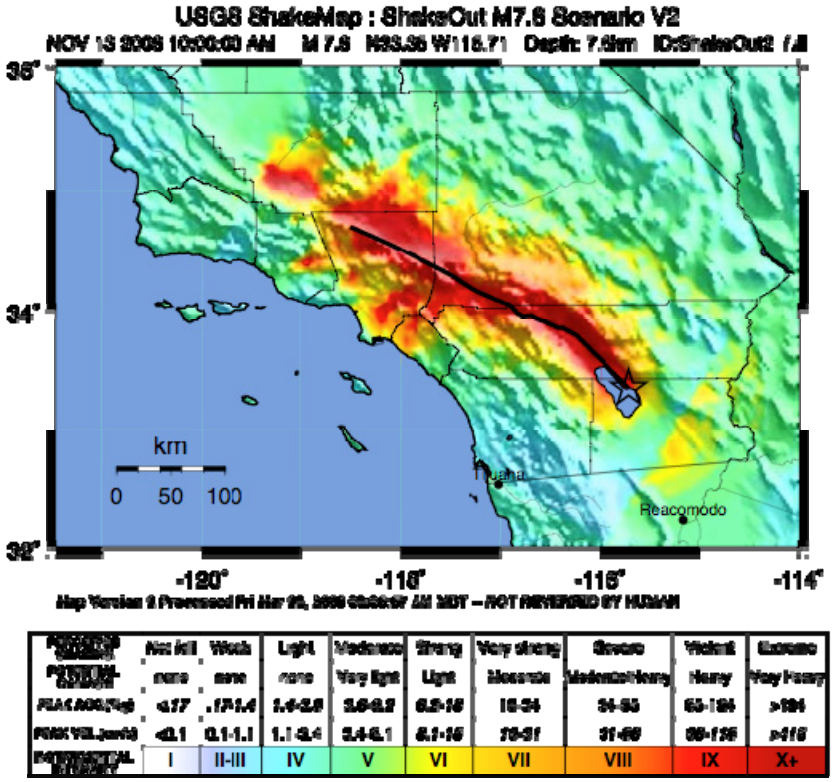

Fig. 2. This "ShakeMap" is a representation of the shaking that will be produced by the ShakeOut earthquake. The colours represent the Modified Mercalli Intensity with the warmer colours representing areas of greater damage. (http://earthquake.usgs.gov/eqcenter/ shakemap/list.php?y=2008&n=sc&s=1

The damage to the built environment propagates through and damages the social systems of the region. This study investigated the impacts of the earthquake on emergency services, human health, the regional economy and trade operations from the Ports of Los Angeles and Long Beach. The major losses for this earthquake fall into four categories: building damages, non-structural damages, damage to lifelines and infrastructure, and fire losses. Within each category, the analysis found types of losses that are well understood – that have been seen in previous earthquakes and the vulnerabilities recognized but not removed – and types of losses that had been less obvious – where the type of failure is only recently understood or the extent of the problem not yet fully recognized. The study also found numerous areas where mitigation conducted over the last few decades by state agencies, utilities and private owners, has greatly reduced the vulnerability. Because of these mitigation measures, the total financial impact of this earthquake is estimated to be "only" about $200 billion with approximately 2,000 fatalities.

Steel moment frame high-rise buildings were found to form cracks in their welds during the 1994 Northridge earthquake [7]. Two special studies were conducted to analyse the behaviour of steel

frame high-rise buildings in the ground motions modelled for this earthquake. This event shows amplified long period motions caused by resonance in the sedimentary basins, particularly the very deep Los Angeles basin. A special panel of structural engineers evaluated these studies and concluded, "Given these ground motions, the collapse of pre-1994 welded steel moment frame buildings is a credible scenario." Since this result comes from the long period ground motions, the area where this type of damage is possible is relatively large and includes much of the urbanized areas of Los Angeles, Orange, Riverside and San Bernardino Counties.

California's investments in mitigation have paid off most obviously in increased robustness and resiliency of the region's lifelines. The retrofitting of highway bridges, conversion of ceramic insulators in the electric grid to polymers, and replacement of cast iron pipes mean that many of the utilities will be able to restore function much more quickly after the earthquake. However, the lifelines that cross the fault will all break when the fault moves. This will disrupt the movement of water, petroleum products, telecommunications, and general transportation. Repair of the lifelines will be slowed because the lifelines all cross the fault at just a few passes in the mountains and therefore interact with each other. For instance, repairing pipelines broken at Cajon Pass will require access that depends upon repair to Interstate 15. That in turn could be delayed if a wildfire starts after damage to the electric lines in the same location.

Southern California is unfortunately well situated to generate major fires following earthquakes. The number of ignitions that will create fires large enough to call the fire department can be extrapolated from previous earthquakes and depends upon the number of households at different levels of seismic shaking. This leads to an estimate of 1,600 ignitions, of which 1,200 will be too large to be controlled by one fire company. In areas of dense wood-frame construction, these fires if not controlled will grow quickly to involve tens or hundreds of city blocks. The fire risk is increased by the damage to the water distribution system and by the traffic gridlock. The fire losses double the total losses from the earthquake.

An emergency response matrix has been developed to help understand what the demands for emergency services will be like. Seventeen functions of emergency services are grouped into seven general classes of activities including: crisis information (public information and responder communications), search and rescue, victim services (shelter, provision of food and water and the management and distribution of donated goods and services), access management and law enforcement (control and security and traffic control), the staffing and functioning of emergency operations centres, fire suppression, medical emergency response, and finally service restoration which includes repair of utilities, route recovery and debris removal.

All of these losses and responses have been considered in assessing the final economic and social costs of this earthquake. The disruption to lifelines and transportation across the San Andreas Fault would lead to long-term business interruption with consequences throughout the American economy. The potential for catastrophic fire propagation has emphasized that fire risk reduction may be the most important arena for community mitigation.

THE SHAKEOUT EXERCISE

The ShakeOut campaign was designed and implemented by earthquake scientists, emergency managers, sociologists, art designers and community participants. The original idea was proposed at a meeting of the senior leaders of the scenario development team. The California Emergency Management Agency representative proposed to use the scenario for a drill of emergency managers (called "Golden Guardian") and others proposed engaging the public as well, inspired by the "Earthquake Day" held every September 1 in Japan. This group evolved into the Earthquake Country Alliance, merging with the group of emergency preparedness communicators that had formed at the tenth anniversary of the 1994 Northridge earthquake.

As the scenario and the possibility of a first ever public drill developed, other organizations in southern California that were working towards various earthquake preparedness efforts joined forces with the US Geological Survey, the Southern California Earthquake Center and the emergency mangers working with them. The two other activities being planned were an International Earthquake Policy Conference proposed by the City of Los Angeles and an Earthquake Rally proposed by the Art Center College of Design. About one year before the event, a decision was made to combine these four efforts (Golden Guardian, public drill, Earthquake Conference and Earthquake Rally) into one effort called the Great Southern California ShakeOut, to be produced by the Earthquake Country Alliance. This was created without dedicated government funding. Organizations contributed time and some resources from existing funding and donations from a few private entities.

The goals of the ShakeOut were established in Spring 2008 and were to:

1. Register 5 million people to participate in the drill;
   We wanted to reach out to all sectors of society and reach as broad of a group of participants as we could. The goal of 5 million participants was set as approximately one-quarter of the total population of 22 million residents of the region.
2. Change the culture of earthquake preparedness in southern California; and
   The purpose for the public communication was to encourage people to think about earthquakes in a different way. Many people living in areas at risk from earthquakes do not think much about earthquake safety. They feel that earthquakes are inevitable but they still want to live in southern California for other reasons and they try to just not think about earthquakes most of the time. Our goal was to get them to say "I want to live here; earthquakes are inevitable, so I will figure out how to reduce the risk."
3. Reduce earthquake losses in southern California.

Both of the first two goals are means to achieve this third one. This goal is more difficult to measure; maybe impossible until the next big earthquake occurs.

The leaders of these four efforts formed the original ShakeOut Steering Committee under the banner of the Earthquake Country Alliance. In the year leading up to the ShakeOut other members joined as they and their organization became committed to the project (Table 1). All members of the Steering Committee were expected to donate significant effort to planning and promotion ShakeOut and to contribute other resources from their agency.

Table 1. ShakeOut Steering Committee Membership.

Member	Organization	Activities and Expertise
Lucy Jones	U.S. Geological Survey	Chief Scientist for the scenario project and Founding member of the Earthquake Country Alliance.
Mark Benthien	Southern California Earthquake Center	Director for Communication, Education and Outreach. Managed fundraising and media purchases. Developed registration system and webpages.
Monica Buchanan	State Farm Insurance	State Farm donated Monica's time to support the ShakeOut. Outreach to the business community and organization for ShakeOut.
John Bwarie	City of Los Angeles; Councilman Greig Smith's Office	Organizer of the International Earthquake Conference.
Dale Cox	U. S. Geological Survey	The earthquake scenario and connections to the local government and military participants.
Kate Long	California Emergency Management Agency	Interface with Golden Guardian exercise. Connections with Hollywood-based partners.
Ines Pearce	Pearce Global Partners	Connections to the business community and contingency planners.
Jack Popejoy	CBS News Radio	Interface with local media.
Sohini Sinha	Art Center College of Design	Organizer of the Get Ready Rally.
Steven Storbakken and Connie Lackey	Providence Health Care Hospitals Emergency Management	Connection to the healthcare community. Organized almost 200 hospitals in southern California to participate in ShakeOut.
Margaret Vinci	California Institute of Technology, Director of Earthquake Research Affiliates	Interface between the business community and the earthquake monitoring network, California Integrated Seismic Network.
Auxiliary members provided expertise and connections to particular subsets of the activities		Included Ken Hudnut and Sue Perry (U. S. Geological Survey), Peggy Brustche (American Red Cross), Joanne McLaughlin (Illusion Factory)

Agreement was reached early in the process to keep the messages simple and consistent between the many agencies and organizations transmitting the messages. When the July 2008 magnitude-5.4 Chino Hills earthquake [8] showed that few Californians followed "Drop, Cover and Hold On" during an earthquake, the decision was made to focus on that message for this first campaign, with a secondary emphasis on "Secure Your Space" to promote earthquake mitigation.

The means of communication with the public were developed using results from sociological research on what encouraged people to take action [9]. This was structured around four objectives: 1) consistent messages – people are more inclined to believe something when they hear the same thing from multiple sources; 2) visual reinforcement – people are more inclined to do something they see other people doing; 3) encourage "milling" or discussion of the proposed

action – people need to discuss an action with others they care about before committing to undertaking the action; and 4) focus on concrete actions – people are more likely to prepare for a set of concrete consequences of a particular hazard than for an abstract concept of risk.

Consistent messaging was particularly difficult because of the large and diverse number of people and organizations that encompassed potential ShakeOut participants. In many regions, the population has limited experience with very damaging earthquakes and the earthquake professionals (e.g., geologists, operators of seismic networks, structural engineers) become the primary conveyors of earthquake safety information. The history of damaging earthquakes in southern California, however, has been extensive enough, that many different organizations including local government emergency managers and fire departments, the Red Cross, Community Emergency Response Teams, universities as well as State and federal researchers have some experience communicating earthquake safety messages. Multiple messengers with variations iterations of that message have sometimes led to confusion. One of the goals in the ShakeOut was to not let the messenger get in the way of the message. Thus ShakeOut members agreed to develop a simple set of messages and to commit their organization to stick with those messages. We also agreed to use ShakeOut visuals – graphic arts elements designed by the Art Center for this particular event and not use any logos or graphic elements from our own organizations.

Fig. 3. Examples of graphic communication for the ShakeOut drill.

To achieve visual reinforcement of the message, we worked with broadcast media in southern California to make the ShakeOut activities appealing for news coverage. We communicated with some of the businesses that planned to participate and encouraged them to create media opportunities to increase coverage. To encourage more visual coverage, we released compelling graphics the day before the ShakeOut portraying the earthquake rupture and wave propagation.

The primary activity to encourage milling was to encourage a multi-faceted community-based drill with different types of organizations participating so that multiple family members and friends would take part in different locations at the same time, thus encouraging them to talk about the event at home. We specifically solicited participation by government agencies, businesses, schools, medical facilities, colleges and universities, senior centers and scout troops.

The fourth goal of focusing on concrete actions arose naturally from the use of a drill as the organizing event. But we also spent considerable effort clarifying a limited set of concrete requested actions. We also prepared materials emphasizing these specific actions, from education materials (e.g. the preparedness booklet *Putting Down Roots in Earthquake Country* published in English and Spanish versions and a new business-oriented supplement [10]), drill broadcasts – audio sequences that could be broadcast at the time of the drill and drill scripts to suggest several levels of possible involvement.

APPROACH TO THE SHAKEOUT

The fundamental goal of the Shakeout was to get a high percentage of southern Californians to undertake activities that would make them safer in the next big earthquake. With such a large potential audience and a multitude of possible messengers, it was important to keep the message simple. We therefore chose to focus on a very limited definition of what earthquake safety entailed. First we focused on "Drop Cover, Hold On", the appropriate actions to take during a big earthquake. During the magnitude-5.4 Chino Hills earthquake that occurred in July 2008, news coverage showed many people, especially adults, who reacted in an unsafe manner. It was clear that the only venue in which "Drop, Cover and Hold On" is taught in California is the elementary and secondary schools. Any adult who did not attend California schools, probably had not heard this message and most had heard it only in school. Special graphics were developed and promoted through websites (www.dropcoverholdon.org) and billboards, and T-shirts. The secondary message was "Secure Your Space" and encouraged people to reduce seismic risk, both structural and non-structural. A large home improvement store chain (Home Depot) helped pay for promotion.

The ShakeOut.org website was the center of the recruitment effort. Groups would register through the website and every group that registered at last 500 people was personally contacted to confirm that this number reflected those participating (for instance, the members of a neighborhood association that participated in the drill rather than the number of people who live in that neighborhood). This registration system allowed us to communicate with participants by email and to receive feedback and reports of activities of the ShakeOut. To help standardize the communication of the preparedness message, many products were developed to support non-scientists communicate the basic messages. Products of the ShakeOut are shown in Table 2.

Table 2. Example communication products created by the ShakeOut Steering Committee for use by ShakeOut associates.

Product	Description and Uses
ShakeOut scenario narratives	A narrative of life in southern California from 10 minutes before the earthquake until 1 year after based on the scientific scenario but told in a personalized form [2]
Posters	Graphics designed by Art Center College of Design to post in workplaces to promote participation in the drill
PowerPoint presentations	Distributed to trained ShakeOut Associates to explain the earthquake scenario and earthquake preparedness
Drill broadcast	Audio and video recordings lasting 90 seconds to broadcast during the drill. Used by some radio and TV stations and PA systems in corporations
Beat the Quake	Online video game (dropcoverholdon.org) to promote non-structural mitigation
Drill manuals	Suggestions for creating an earthquake drill at multiple levels from simple drop, cover, hold to evacuation, triage and reunification plans
Preparedness Now	4 minute video made about the scenario. Distributed through YouTube.
Putting Down Roots in Earthquake Country *Seven Steps to an Earthquake Resilient Business*	Handbooks for the public that explain the earthquake risk and steps for improved earthquake safety. Also distributed through the website earthquakecountry.info

In July 2008, the ShakeOut Steering Committee worked with officials in the counties of southern California to form county-based ShakeOut Associates. These groups (of 500-100 members per county) were trained by the Steering Committee to take the message to local groups in their counties. About two months before the ShakeOut, the Steering Committee made a formal decision to stop trying to maintain a connection with all of the participants of the ShakeOut. We recognized that if we insisted on contact with all groups, we would limit the number of participants, due to a lack of time and manpower. This means that we will never know all that happened during the ShakeOut. We have, however, collected stories from some of the participants, one of which is shown in Table 3.

Table 3. Example report of activities in a community leading up to and during the ShakeOut.

Interview with Blake Goetz, Fire Chief of Palm Springs, CA	**Response**
What did your city do for the ShakeOut?	We held several community outreach meetings to inform the public about the results of the USGS Earthquake analysis and tied it to personal responsibility about being prepared at home and work. Informational ShakeOut flyers were distributed by e-mail and in person. The media was informed about Shakeout and they spread the word and wrote in depth articles about the EQ potential here in the Coachella Valley. A large 30" ShakeOut Banner was strung across Palm Canyon to inform the public and presentations were made at televised City Council meetings. All City 500+ city employees duck, covered and held on at 1000 hr's and they were all register on the ShakeOut Website. The Fire Department exercised their newly developed SOP for actions immediately after an earthquake (three times over three days) and conducted field damages assessments of the pre-identified target hazards. Each Engine company had index cards to open and read at specific times and had to report their findings (simulated damage) to the Incident Commander. The biggest and most valuable part of the ShakeOut was participation in a Regional two-day Tabletop Exercise involving 220 different public, private and non-profit organizations that met at the Riviera Hotel Ballroom. There were two 4-hour sessions scripted to the USGS scenario. Much time was given for discipline specific groups to interact and describe what their plans and actions would be. They all Ducked and covered at 10 AM to the earthquake sound coming from a 3'x3' subwoofer. It was so realistic. The walls were shaking and glasses rattled. Everyone's nerves were on edge and that forced the issue of preparedness home. Many of the groups had never worked with each other and the media participated as participants not reporters although significant reporting was accomplished. In fact the Editor of the Desert Sun wrote an editorial in the paper recommending that a regional Emergency Manager be hired at the Coachella Valley Association of Governments to continue the fine work we did. CERT teams participated in skills exercises the following Saturday and significant after action reports were developed.
What, if any, lessons did your city take from the ShakeOut and enact to become more prepared for a large earthquake?	Overall, public and professional earthquake awareness and preparedness was taken to a new level never before seen. What was once public apathy, is now ingrained as a personal and professional responsibility. The fire department learned that field reports coming in from the engine companies overwhelmed the IC so our SOP has been modified to require field units to wait for a roll call status report so it can organize and prioritize. More EQ supplies were purchased including 700 heater Meals. Two 40' insulated and air-conditioned shipping containers were purchased and stocked with over $100,000 of supplies. An agreement with the Convention Center Caterer was signed that now requires 9,000 meals to be prepared (with food in stock) so we can feed 1,000 emergency workers three meals a day for three days. They will also become the Food Unit Leader on behalf of the City to organize food donations from restaurants when the electricity goes out. I could go on and on.....

Table 3—Continued

Interview with Blake Goetz, Fire Chief of Palm Springs, CA	**Response**
Do you have any statistics on your ShakeOut activities or after-action mitigation?	Over 220 organizations in the Western Coachella Valley met beneath one roof for the first time to focus on EQ preparedness and response for the first time. If it had not been for the scientific research done by the USGS Partners, ShakeOut would not have the credibility it had. **ShakeOut was the most impressive display of community action I have ever scene in 32 years of emergency management!**

OUTCOMES OF THE SHAKEOUT

All three of the goals set for the ShakeOut drill were met. The final registration at www.shakeout.org for the 2008 ShakeOut was 5.47 million people, or one-quarter of the population of the region. A survey conducted with the registered participants showed that the messages they took from the ShakeOut were the concepts intended, including the importance of "Drop, Cover, Hold On", the interdependency of earthquake risk ("We are all in this together") and the possibility of reducing losses through preparation and mitigation. Sales data from the Home Depot hardware stores in southern California showed a 260% in crease in the sale of earthquake safety products during the month of the ShakeOut, November 2008. The breakdown of participants is in Table 4.

Table 4. Participants in the ShakeOut public earthquake drill.

Categories	Participants	Individual Registrations
Schools	3.95 million	1589, including 207 school districts and over 650 private schools
Colleges	564,000	121, including University of Southern California, University of California at three campuses- Los Angeles, Irvine and Riverside, California Institute of Technology, all the local California State Universities and many community colleges.
Businesses	342,000	2531, including State Farm, Home Depot, Wal-Mart, Nestle, Bank of America, Wells Fargo, Southern California Edison, San Diego Zoo, Marriott, Warner Brothers, AT&T
Government	289,600	593, including all employees of San Bernardino, Los Angeles, Orange and Kern Counties.
Faith and Community Organizations	142,000	1161
Medical	107,000	280, including Providence Group, Kaiser Permanente, Cedars-Sinai, UCLA, Loma Linda
Individuals/families	57,600	19,200

The partnerships, energy and ideas from the ShakeOut continue to grow within the southern California community. Earthquake safety advocates in northern California have joined the Earthquake Country Alliance and they are preparing for a second ShakeOut, expanded to the whole state of California in October 2009. Perhaps the most lasting effect will be the deepened partnerships between scientists, engineers and the community. The utility companies have continued to apply the scenarios and are working with the scientists to improve instrumentation and their distribution systems. Some of the most active participants from the private sector and local government are now working with the regional seismic network to prototype application of earthquake early warning systems. What was initially conceived as a one-time ShakeOut turned out to not be the start of something much larger.

CONCLUSIONS

The ShakeOut provides some lessons for other scientists interested in policy communication. First, the evidence of "good science" – the reputable agencies and consensus results – in the scenario were repeatedly cited as reasons to believe the scenario. Our science does matter. Second, the effort to have not just good earth science, but to extend the study into engineering and the social sciences to create a product that could be directly applied to decision-making, increased the use of the resulting product. Users did not have to work hard to see why the results mattered to them. Fourth, the accessibility of the results as communicated through a narrative and professional designed movies increased the impact.

Perhaps the most enduring effect will be the strengthened partnerships between scientists, engineers and the community. The utility companies have continued to apply the scenarios and are working with the scientists to improve instrumentation and their distribution systems. Some of the most active participants from the private sector and local government are now working with the seismic network to prototype application of earthquake early warning systems.

ACKNOWLEDGMENTS

Public sector support for the organization of the ShakeOut came from the U.S. Geological Survey, Southern California Earthquake Center (funded by National Science Foundation and USGS), California Earthquake Authority, California Office of Emergency Services, California Geological Survey, City of Los Angeles, and the Federal Emergency Management Agency. Private sector supporters included Time Warner Cable, The Home Depot, State Farm Insurance, Illusion Factory, Kaiser Permanente, , Tyco Electronics, QuakeHold!, Westfield, ABC7 Los Angeles, IBHS DisasterSafety.org, Pearce Global Partners, ServPro, NPA, and 3n. We gratefully acknowledge all these contributions and the commitment to earthquake safety of 5.5 million of our fellow residents of southern California.

REFERENCES

[1] Jones, Lucile M., Bernknopf, Richard, Cox, Dale, Goltz, James, Hudnut, Kenneth, Mileti, Dennis, Perry, Suzanne, Ponti, Daniel, Porter, Keith, Reichle, Michael, Seligson, Hope, Shoaf, Kimberley, Treiman, Jerry, and Wein, Anne, (2008), "The ShakeOut Scenario," U.S. Geological Survey Open-File Report 2008-1150 and California Geological Survey Preliminary Report 25 [http://pubs.usgs.gov/of/2008/1150/].

[2] Perry, Suzanne, Cox, Dale, Jones, Lucile, Bernknopf, Richard, Goltz, James, Hudnut, Kenneth, Mileti, Dennis, Ponti, Daniel, Porter, Keith, Reichle, Michael, Seligson, Hope, Shoaf, Kimberley, Treiman, Jerry, and Wein, Anne, (2008), "The

ShakeOut Earthquake Scenario; a story that southern Californians are writing," U.S. Geological Survey Circular 1324 and California Geological Survey Special Report 207, 16 p. [http://pubs.usgs.gov/circ/1324/]

[3] Graves R.W., B. T. Aagard, K. W. Hudnut, L.M. Star, J. P. Stewart, and T. H. Jordan, (2008), "Broadband simulations for Mw7.8 earthquakes: Ground motion sensitivity to rupture speed," *Geophys. Res. Lett.* V. 35, p. L32202.

[4] Petersen, Mark D., Frankel, Arthur D., Harmsen, Stephen C., Mueller, Charles S., Haller, Kathleen M., Wheeler, Russell L., Wesson, Robert L., Zeng, Yuehua, Boyd, Oliver S., Perkins, David M., Luco, Nicolas, Field, Edward H., Wills, Chris J., and Rukstales, Kenneth S., (2008), "Documentation for the 2008 Update of the United States National Seismic Hazard Maps," U.S. Geological Survey Open-File Report 2008–1128, 61 p.

[5] Earthquake Spectra 24:1, (2008) "The Next Generation Attenuation Special Issue."

[6] FEMA, 2003, Multi-hazard loss estimation methodology earthquake model, HAZUS-MH MR3 Technical Manual: developed by Department of Homeland Security Emergency Preparedness and Response Directorate, FEMA Mitigation Division, Washington D.C., http://www.fema.gov/plan/prevent/hazus/hz_manuals.shtm, 699 p.

[7] Scientists of the USGS and SCEC (1994), The magnitude 6.7 Northridge, California, earthquake of January 17, 1994, *Science,* **266**, 389-397

[8] Hauksson, E., K. Felzer, D. Given, M. Giveon, S. Hough, K. Hutton, H. Kanamori, V. Sevilgen, S. Wei, and A. Yong, (2008) "Preliminary Report on the 29 July 2008 Mw5.4 Chino Hills, Eastern Los Angeles Basin, California, Earthquake Sequence," *Seismo. Res. Letters*, vol. 79, p. 855- 868.

[9] Mileti, Dennis S., Colleen Fitzpatrick and Barbara C. Farhar, (1992), "Fostering Public Preparations for Natural Hazards: Lessons from the Parkfield Earthquake Prediction," Environment 34(3): 16-20 and 36-39.

[10] Jones, Lucile M., and M. Benthien, (1995, updated 2008)"Putting Down Roots in Earthquake County," Special Publication of the Southern California Earthquake Center. , M/ Benthien and I. Pearce (2008), "Sven Steps to an Earthquake-Resilient Business," Special Publication of the Southern California Earthquake Center

REDUCING SEISMIC RISK THROUGH INTERNATIONAL COOPERATION IN EARTHQUAKE SYSTEM SCIENCE[1]

Thomas H. Jordan
Director, Southern California Earthquake Center, University of Southern California, Los Angeles, CA 90089-0742 USA; tjordan@usc.edu

Earthquakes and their effects pose the greatest natural threat to life and property in many urban regions. Two prominent examples are Los Angeles, California, where I live and work, and Tehran, Iran, the host city for the international workshop on *Science: A Gateway to Understanding*. From my perspective as a geoscientist, these megacities are remarkably similar. Each is bounded by high mountains rising thousands of meters above fertile alluvial slopes and arid sedimentary plains. Their stunning but seismic geographies are being actively shaped by folding and faulting in the boundary zones between gigantic tectonic plates.

Tehran and LA each comprise more than 12 million people; consequently, they account for much of their national earthquake risk. Measured as annualized economic losses, almost half of the total earthquake risk for the United States comes from Southern California, about 25% of it from the Los Angeles metropolitan area alone (FEMA, 2000). I am not aware of a comparable synoptic risk quantification for Iran, but hazard assessments and studies of building fragility suggest that Tehran's fraction of the national earthquake risk may be even higher (Tavakoli & Ashtiany, 1999; CEST-JICA, 2000; EMI, 2006; Ashtari Jafari, 2007). Megacity earthquakes can jeopardize prosperity and social welfare. Clearly, we need to know more about them and learn to work together to reduce the societal risks.

Iran's long history of civilization has provided a remarkable record of earthquake activity pertinent to this goal (Ambraseys & Melville, 1982; Berberian, 1994). During the past thirteen centuries, nine earthquakes with magnitudes greater than 7 have occurred less than 200 km from Tehran. The last, in 1962, killed more than 12,000 people. Even much smaller, more frequent events can cause considerable damage. The magnitude-6.2 Firuzabad-Kojur earthquake, which struck a mountainous region 70 km north of Tehran on May 28, 2004, killed 35 people, and preliminary assessments of its economic damage exceeded 125 billion Rials.

As citizens of "earthquake country," many of us at this workshop share an interest in the earthquake problem. My focus will be on its scientific dimensions. In particular, I will outline some of the key areas where scientific collaboration among Iran, the United States, and other countries might lead to new understanding of earthquake behavior that can help us reduce risk. My discussion is intended to support a broader thesis: the potential for scientific cooperation to address our common environmental problems—water and energy supply, pollution, climate change, ecological degradation, as well as earthquakes—can be a strong force for developing cross-cultural understanding and improving international relations.

[1] Reprint with permission from the U.S. National Academy of Sciences, from "Science as a Gateway to Understanding: International Workshop Proceedings, Tehran, Iran," The National Academies Press.

SEISMIC RISK ANALYSIS

Earthquakes proceed as cascades in which the primary effects of faulting and ground shaking induce secondary effects, such as landslides, liquefaction and tsunami, and set off destructive processes within the built environment, such as fires and dam failures (NRC, 2003). *Seismic hazard* can be defined as a forecast of how intense these effects will be at a specified site on Earth's surface during a future interval of time.

In contrast, *seismic risk* is a forecast of the damage to society that will be caused by earthquakes, usually measured in terms of casualties and economic losses in a specified area. Risk depends on the hazard, but it is compounded by a community's *exposure*—its population and the extent and density of its built environment—as well as its *fragility*, the vulnerability of its built environment to seismic hazards. Risk is lowered by *resiliency*, how quickly a community can recover from earthquake damage. The "risk equation" expresses these relationships in a compact (though simplistic) notation:

$$risk = hazard \times exposure \times fragility \div resiliency$$

Risk analysis seeks to quantify the risk equation in a framework that allows the impact of political policies and economic investments to be evaluated and thereby to inform the decision-making processes relevant to risk reduction.

Risk quantification is a difficult problem, because it requires detailed knowledge of the natural and the built environments, as well as an understanding of both earthquake and human behaviors. Moreover, risk is a rapidly moving target, owing to the exponential rise in the urban exposure to seismic hazards; calculating risk involves predictions of how civilization will continue to develop, which are highly uncertain. Not surprisingly, the best risk models are maintained by the insurance industry, where the losses and payoffs can be huge. However, the information from insurance risk models is usually proprietary and restricted to portfolios that represent (by design) a small fraction of the total exposure.

The synoptic risk studies needed for policy formulation are the responsibility of public agencies, and their accuracy and efficacy depends on technological resources not yet available in many seismically active regions. Risk assessments can be improved worldwide through international collaborations that share the expertise of earthquake scientists and engineers from countries with well-developed risk reduction programs. For example, many countries have benefited from the information about regional hazards produced by the Global Seismic Hazard Assessment Program during the United Nations International Decade for Natural Disaster Reduction (Giardini et al., 1999; Tavakoli & Ashtiany, 1999).

The first synoptic view of earthquake risk in the United States was published by the Federal Emergency Management Agency less than a decade ago (FEMA, 2000). This study obtained an annualized earthquake loss for California of $3.3 billion per year. However, it was based on a rather limited database of building stock and did not consider local site effects (e.g., soft soils) in computing the seismic hazard. A parallel but more detailed study by the California Division of Mines and Geology (now called the California Geological Survey) obtained a statewide expected

value that was twice as large (CDMG, 2000). A revision of FEMA (2000) is currently underway using a more advanced methodology and better inventories of buildings and lifelines.

Risk estimates have been published for California earthquake scenarios adapted from historical events, such as the 1906 San Francisco earthquake (Kircher et al., 2006), or inferred from geologic data on the locations and magnitudes of prehistoric fault ruptures, such as the Puente Hills blind thrust system that runs beneath central Los Angeles (Field et al., 2005). The results are sobering. The ground shaking from a major earthquake on the Puente Hills fault (magnitude 7.1-7.5), if it occurred during working hours, would probably kill 3,000 to 18,000 people and cause direct economic losses of $80 billion to $250 billion (Field et al., 2005). The large range in the loss estimates comes from two types of uncertainty: the natural variability assigned to the earthquake scenario (aleatory uncertainty) as well as our lack of knowledge about the true risks involved (epistemic uncertainty).

According to a similar scenario study, the loss of life caused by earthquakes of magnitude 6.7-7.1 on the North Tehran, Mosha, or Ray faults in greater Tehran ranges from 120,000 to 380,000 (CEST-JICA, 2000). The casualty figures for comparable earthquake scenarios in Los Angeles and Tehran thus show an order-of-magnitude difference, which derives primarily from the greater fragility of the built environment in Tehran. This comparison underlines the fact that the implementation of seismic safety engineering is the key to seismic risk reduction in urban areas.

STRATEGIES FOR SEISMIC RISK REDUCTION

I will illustrate the basic strategies for reducing seismic risk using California examples. The strategies can be categorized according to the four factors in the risk equation. For example, the exposure to hazard can be limited by land-use policies, such as the Natural Hazards Disclosure Act, passed by the California state legislature in 1998. The law requires that sellers of real property and their agents provide prospective buyers with a "natural hazard disclosure statement" when the property being sold lies near an active fault or within other state-mapped seismic hazard zones. This type of *caveat emptor* is typical of the weak compliance provisions in most land-use regulations. The high land values and population pressures in Los Angeles, where "sprawl has hit the wall," make the enactment of more stringent land-use policies quite difficult. We can thus expect seismic exposure to continue rising in proportion to urban expansion and densification.

A more effective strategy is to reduce the structural and non-structural fragility of buildings using building codes and other seismic safety regulations, performance-based design, and seismic retrofitting. The seismic safety provisions in the California building codes have been substantially improved by the tough lessons learned from historical earthquakes; in particular, revisions have corrected the design deficiencies identified in the aftermath of the destructive 1933 Long Beach, 1971 San Fernando, 1989 Loma Prieta, and 1994 Northridge earthquakes.

The efforts to promote seismic retrofitting have achieved mixed results. A 1981 Los Angeles city ordinance led to the demolition or retrofitting of almost its entire stock of unreinforced masonry buildings, the most fragile and dangerous class of inhabited structures. However, a state law regulating the seismic safety of hospitals, passed after the 1994 Northridge earthquake, has

proven to be economically infeasible. Faced with the specter that many hospitals would be shut down rather than be retrofit, the legislature has postponed the compliance date for basic life-safety provisions of the law and is back-peddling on its long-term goal that all hospitals be capable of serving the public after earthquake disasters.

The latter requirement typifies performance-based design. Performance-based design goes beyond the building-code requirements for life-safety by improving the ability of structures to retain a specified degree of functionality after episodes of seismic shaking (SEAOC, 1995). The impetus for performance-based design, largely economic, has raised new challenges for earthquake science and engineering (FEMA, 2006). In particular, engineers must be able to predict more accurately the damage state of structural systems—not just the system components—requiring more detailed descriptions of the ground motion. A full structural analysis uses complete time histories of ground motion to account for the nonlinearities in the structural response and in its coupling with near-surface soil layers. In California, the Pacific Earthquake Engineering Research (PEER) Center at Berkeley has organized a multi-institutional research program for advancing performance-based design (see http://peer.berkeley.edu/).

Community resiliency can be enhanced through better emergency response, insurance investments, catastrophe bonding, and state-funded recovery assistance. All of these tools are applicable to a wide range of natural and human hazards, including wildfires, severe storms, floods, epidemics, and terrorism. However, effective preparation and response to multiple hazards depends on a balanced view of relative risks. In the United States, there is concern that the recent emphasis on terrorist threats has distracted efforts to prepare for natural disasters. The poor performance of the emergency response to Hurricane Katrina and subsequent disaster-recovery programs, especially in the hard-hit city of New Orleans, illustrate the need for better coordination and planning among local, state, and federal agencies (White House, 2006). One mechanism for improving coordination and planning is to conduct emergency response exercises based on realistic disaster scenarios.

Disaster mitigation can be enhanced by education. Public education is especially critical in preparing the response of megacities to catastrophic event cascades, during which government aid to the population might be insufficient and delayed (Perry et al., 2008). In the case of earthquakes, public awareness of the problem is greatly heightened after disruptive events, which motivate people to prepare for future disasters. Even small earthquakes, if widely felt, can provide "teachable moments," as can the anniversaries of famous disasters. Two years ago, the centenary of the 1906 San Francisco earthquake motivated an extensive and successful public education campaign throughout California (USGS, 2006).

The first factor in the risk equation—the seismic hazard—is qualitatively different from the other three. We have no direct means to reduce the primary hazards of faulting and ground shaking; earthquakes involve great forces of nature that will remain beyond human control for the foreseeable future. Nevertheless, the hazard level sets the risk, and the properly characterizing seismic hazard—forecasting earthquakes and their effects; charting earthquake cascades as they are happening—is therefore critical to risk reduction. For instance, current hazard forecasts contain large epistemic errors, which compromises effectiveness of risk analysis in guiding

political policies and economic decisions. One role of earthquake system science is to reduce these uncertainties by improving our statistical and physical models of earthquake processes.

EARTHQUAKE SYSTEM SCIENCE

A geosystem is a representation of nature defined by the terrestrial behavior it seeks to explain (NRC, 2000). In the case of an active fault system, the ground motion due to a fault rupture is one of the most interesting behaviors from a practical perspective, because experience tells us that fault displacement and the attendant ground shaking are the primary seismic hazards for cities such as Tehran and Los Angeles. System-level hazard analysis can be exemplified by the following set of problems:

1. Identify the active fault traces in a region and predict the maximum displacements that might occur across them.
2. From the shaking intensities recorded on a sparse network of seismometers during an earthquake, predict the intensities everywhere in the region occupied by the network.
3. Forecast the distribution the shaking intensities in a region from all future earthquakes.

A basic methodology for solving the seismic forecasting problem (3) is probabilistic seismic hazard analysis (PSHA). Originally developed by earthquake engineers, PSHA estimates the probability that the ground motions generated at a geographic site from all regional earthquakes will exceed some intensity measure during a time interval of interest, usually a few decades. A plot of the exceedance probability as a function of the intensity measure is called the *hazard curve* for the site. In downtown Los Angeles, for instance, typical estimates of the exceedance probabilities for peak ground acceleration (PGA)—a commonly used intensity measure—are 10% in 50 years for PGA $\geq 0.6\,g$ and 2% in 50 years for PGA $\geq 1.0\,g$, where g is the acceleration of gravity at Earth's surface (9.8 m/s^2). Other useful intensity measures are peak ground velocity (PGV) and the maximum spectral acceleration at a particular shaking frequency. From hazard curves, engineers can estimate the likelihood that buildings and other structures will be damaged by earthquakes during their expected lifetimes, and they can apply the performance-based design and seismic retrofitting to reduce structural fragility to levels appropriate for life-safety and operational requirements.

A *seismic hazard map* is a plot of the intensity measure as a function of site position for fixed exceedance probability. The official seismic hazard maps for the United States are produced by the National Seismic Hazard Mapping Project, managed by the U.S. Geological Survey. Seismic hazard maps are critical ingredients to regional risk analysis. For example, the FEMA (2000) and CDMG (2000) risk studies were based on the 1995 edition of the National Seismic Hazard Map (NSHMP, 1996). The underway revisions to the FEMA assessment are incorporating the better knowledge of seismic hazards encoded in NSHMP (2002) edition. The latest edition, NSHMP (2008), has just been released, and it will be used for the 2012 revisions to the Uniform Building Code.

The system-level study of earthquake hazards is "big science", requiring a top-down, interdisciplinary, multi-institutional approach. The Southern California Earthquake Center (SCEC) is funded by the U.S. National Science Foundation and U.S. Geological Survey to coordinate an extensive research program in earthquake system science, and the program now

involves more than 600 experts at more than 62 research institutions (Jordan, 2006a; see http://www.scec.org). Southern California's network of several hundred active faults forms a superb natural laboratory for the study of earthquake physics, and its seismic, geodetic, and geologic data are among the best in the world. SCEC's mission is to use this information to develop a comprehensive, physics-based understanding of the Southern California fault system, and to communicate this understanding to society as useful knowledge for reducing seismic risk.

One of the goals of the SCEC program is to improve the techniques of PSHA through physics-based, system-level modeling. PSHA involves the manipulation of two types of subsystem probabilities: the probability for the occurrence of a distinct earthquake source during the time interval of interest, and the probability that the ground motions at a site will exceed some intensity measure conditional on that event having occurred. The first is obtained from an *earthquake rupture forecast* (*ERF*), whereas the second is computed from an *attenuation relationship* (*AR*), which quantifies the distribution of ground motions as they attenuate with distance from the source.

The *ERF* that underlies the current U.S. national seismic map (NSHMP, 2008) is "time-independent" in that it assumes that earthquakes are random in time (Poisson distributed); in other words, it calculates the probabilities of future earthquakes ignoring any information about the occurrence dates of past earthquakes. However, owing to stress-mediated fault interactions and seismicity triggering, earthquakes are known not to be Poisson distributed. A major SCEC research objective is to develop time-dependent forecast models that include more information about the region's earthquake history. In the early 1990's, a SCEC-sponsored Working Group on California Earthquake Probabilities published a time-dependent *ERF* for Southern California (WGCEP, 1995). SCEC has more recently collaborated with the U.S. Geological Survey, and the California Geological Survey to produce the first comprehensive Uniform California Earthquake Rupture Forecast (WGCEP, 2007). The long-term (time-independent) model that underlies the UCERF was developed in partnership with the National Seismic Hazard Mapping Project, which has incorporated the results into its most recent release (NSHMP, 2008).

In the WGCEP forecasting models, the event probabilities are conditioned on the dates of previous earthquakes using stress-renewal models, in which probabilities drop immediately after a large earthquake releases tectonic stress on a fault and rise as the stress re-accumulates. Such models are motivated by the elastic rebound theory of the earthquake cycle and calibrated for variations in the cycle using historical and paleoseismic observations (WGCEP, 2003; Field, 2007b).

WGCEP (2007) estimates that, in the Los Angeles region, the mean 30-year probability of an earthquake with a magnitude equal to or greater than 6.7—the size of the destructive 1994 Northridge event—is about 67%. Because larger earthquakes occur less frequently, the chances of a magnitude $\geq$ 7.5 earthquake in the LA area during the next 30 years drop to about 18%. For the much larger Southern California region, the equivalent odds of a magnitude $\geq$ 7.5 event increase to 37%. The comparable value for Northern California is significantly less, about 15%, primarily because the last ruptures on the southern San Andreas fault, in 1857 and circa 1680, were less recent than the 1906 rupture of the northern San Andreas fault; i.e., sufficient stress has re-accumulated of the southern sections of the fault to make a large rupture more likely. The

UCERF model will be used by decision-makers concerned with land-use planning, the seismic safety provisions of building codes, disaster preparation and recovery, emergency response, and earthquake insurance; engineers who need estimates of maximum seismic intensities for the design of buildings, critical facilities, and lifelines; and organizations that promote public education for mitigating earthquake risk.

A second type of time-dependent *ERF* conditions the probabilities using seismic-triggering models calibrated to account for observed aftershock activity, such as epidemic-type aftershock sequence (ETAS) models (Ogata, 1988). In California, the Short-Term Earthquake Probability (STEP) model of Gerstenberger et al. (2005) has been turned into an operational forecast that is updated hourly (see http://pasadena.wr.usgs.gov/step). The STEP forecast is a useful, though experimental, tool for aftershock prediction as well as the conditioning the long-term probabilities of large earthquakes on small events that are potential foreshocks. It should be emphasized, however, that the current probability gains in the latter application are relatively small.

The SCEC program seeks to improve time-dependent *ERF*s through better understanding of earthquake predictability. We have seen how long-term (decades to centuries) and short-term (hours to days) predictability are being exploited by operational time-dependent forecasting models. The challenge is unify the forecasting models across the temporal scales, which requires a better understanding of intermediate-term (weeks to years) predictability. The research toward such a unification is now focused on gaining insights into the physical processes of stress evolution and seismic triggering (e.g., Toda et al., 2005). The SCEC-USGS Working Group on Regional Earthquake Likelihood Models (RELM) is testing of a variety of intermediate-term models (Field, 2007a; Schorlemmer et al., 2007). Based on this experience, SCEC has formed an international partnership that is extending scientific earthquake prediction experiments to other fault systems through a global infrastructure for comparative testing, called the Collaboratory for the Study of Earthquake Predictability (Jordan, 2006b; CSEP, 2008). In the next section, I will elaborate on the exceptional opportunities presented by CSEP for international cooperation in earthquake system science.

Large earthquakes are rare events, and the strong-motion data from them are sparse. For this reason, a number of key phenomena are difficult to capture through a strictly empirical approach, including the amplification of ground motions in sedimentary basins, source directivity effects, and the variability caused by rupture-process complexity and 3D geologic structure. Therefore, a major objective of the SCEC program is to develop attenuation relationships that correctly model the physics of seismic wave propagation. Numerical simulations of ground motions play a vital role in this area of research, comparable to the situation in climate studies, where the largest, most complex general circulation models are being used to predict the hazards and risks of anthropogenic global change.

With NSF funding, SCEC has developed a cyberinfrastructure for earthquake simulation, the Community Modeling Environment (CME), which allows scientists to construct system-level models of earthquake processes using high-performance computing facilities and advanced information technologies (Jordan & Maechling, 2003; Field et al., 2003). The CME infrastructure includes several computational platforms, each comprising the hardware, software,

and scientific expertise (wetware) needed to execute and manage the results from different types of PSHA simulations. An example is the *TeraShake* platform for simulations of dynamic fault ruptures and ground motions on dense geographical grids. TeraShake simulations of ruptures on the southernmost San Andreas fault have shown how the chain of sedimentary basins between San Bernardino and downtown Los Angeles form an effective waveguide that channels surface waves along the southern edge of the San Bernardino and San Gabriel Mountains (Olsen et al., 2006, 2008). SCEC is now increasing the performance of these computational platforms to take advantage of the petascale computational facilities that will be developed during the next several years. In the not-to-distant future, we will be able to incorporate much more physics into seismic hazard and risk analysis through system-level simulations.

INTERNATIONAL SCIENTIFIC PARTNERSHIPS

Earthquake system science relies on the premise that detailed studies of fault systems in different regions, such as Southern California, Japan, and Iran, can be synthesized into a generic understanding of earthquake phenomena. Achieving such a synthesis will depend on international partnerships that facilitate the development and comparison of well-calibrated regional models. I will briefly outline some of the salient opportunities opened by recent developments in earthquake system science.

Exploring the Earthquake Record. The science of seismic hazard and risk is severely data-limited. Even in the most seismically active areas, the recurrence rates of large earthquakes are long compared to rates of urbanization and technological change. The last large earthquake on the southern San Andreas was in 1857, before the pueblo of Los Angeles became a city and before the pendulum seismometer was invented. According to WGCEP (2007), the 30-year probability of a large (magnitude ≥ 7.8) earthquake in Southern California is about 20%, too large for comfort, but small enough that it may be some time before we directly observe one or more of the "outer-scale" ruptures which dominate the behavior of the southern San Andreas system.

The power-law statistics of extreme events illustrate why progress in earthquake system science depends so heavily on comparative studies of active faults around the world. International scientific exchange has allowed much to be learned about continental faulting of the San Andreas type; e.g., from large strike-slip earthquakes that have occurred in Turkey, Tibet, and Alaska just during the last decade (Barka, 1999; Heaussler et al., 2004; Klinger et al., 2005). A plausible goal is the creation of an international database—a global reference library—for archiving the field and instrumental information recovered from such rare events.

A second obvious goal is to extend the seismicity catalogs for active fault systems backward in time. Countries like Iran with long historical records have a head start, but our knowledge of past activity can be significantly augmented using the new tools of paleoseismology and neotectonics to decipher the geologic record. Systematic paleoseismic investigations have elucidated a thousand-year history of San Andreas slip (Grant & Lettis, 2002; Weldon et al., 2005), and SCEC's current objective is to define slip rate and earthquake history of southern San Andreas fault system for last 2000 years. Through international scientific exchange, these field-based techniques can be improved and applied to other fault systems.

The tectonics of Tehran and Los Angeles are both characterized by oblique convergence accommodated by complex systems of frontal thrust faults that are raising the Alborz Mountains and Transverse Ranges, respectively. A comparative study of these orogenic systems based on data from seismology, paleoseismology, remote sensing, and space geodesy would be a particularly good target for Iran-U.S. collaboration.

Real-Time Seismic Information Systems. A major advance in seismic monitoring and ground-motion recording is the integration of high-gain regional seismic networks with strong-motion recording networks to form comprehensive seismic information systems. A prime example of international collaboration is in the European-Mediterranean region, where Network of Research Infrastructures for European Seismology (NERIES) is integrating over 100 seismic monitoring systems and observatories in 46 countries into pan-European cyberinfrastructure (Giardini, 2008).

On regional scales, seismic information systems provide essential information for guiding the emergency response to earthquakes, especially in urban settings. Seismic data from a regional network can be processed immediately following an event and the results broadcast to users, such as emergency response agencies and responsible government officials, utility and transportation companies, and other commercial interests. The parameters include traditional estimates of origin time, hypocenter location, and magnitude, as well as "ShakeMaps" of predicted ground motions conditioned on available strong-motion recordings, which can aid in damage assessments (Wald et al., 1999). In California, this type of information is provided by the California Integrated Seismic Network (CISN), which comprises more than a thousand seismic stations telemetered to central processing and data archiving facilities at the University of California, Berkeley, and the California Institute of Technology (http://www.cisn.org/).

Improvements in the real-time capabilities of these systems have opened the door to "earthquake early warning." EEW is the prediction of imminent seismic shaking at a set of target sites, obtained after a fault rupture initiates but in advance of the arrival of potentially damaging seismic waves. There are several EEW strategies (Kanamori, 2005), but the most common relies on a dense network of seismometers to transmit records of the first-arriving (*P*) waves to a central processor that can locate the event, estimate its magnitude, and broadcast predictions to the target sites in near real time. In Southern California, the warning times in Los Angeles for earthquakes on the San Andreas fault could be a minute or more, enough for individuals to prepare for shaking (e.g., by getting under a desk) and for certain types of automated decisions that might reduce damage and increase resiliency: slowing trains, stopping elevators, shutting gas lines, conditioning electrical grids, etc.

Several countries have already invested heavily in EEW systems. Japan's is the most advanced (Horiuchi et al., 2005; see http://www.jma.go.jp/jma/en/Activities/eew.html), but systems are also operational in Mexico, Taiwan, and Turkey. SCEC is participating with Berkeley and Caltech scientists in a USGS-sponsored project to test the performance of three EEW algorithms on the CISN system. However, the United States has been lagging in the development of EEW and could profit from more international involvement in this area.

Dynamical Modeling. Numerical simulations of large earthquakes in well-studied seismically active areas are important tools for basic earthquake science, because they provide a quantitative basis for comparing hypotheses about earthquake behavior with observations. Simulations are playing an increasingly crucial role in our understanding of regional earthquake hazard and risk, because they can extend our knowledge to phenomena not yet observed. Moreover, they can also be used for the interpolation of recorded data in producing ShakeMaps and in the extrapolation of recorded data for earthquake early warning.

SCEC is applying simulation technology to the prediction of salient aspects of earthquake behavior, such as the influence of rupture directivity and basin effects on strong ground motions. Similar capabilities are being developed in Japan and Europe. Making this cyberinfrastructure available for application in other regions is an excellent target for international scientific exchange. Such a program will entail the development of geologic models of regional fault networks and seismic velocity structures. Here, the SCEC experience in synthesizing three-dimensional structural representations may prove useful.

Seismic Risk Analysis. From a practical point of view, the main role of earthquake system science is to promote risk reduction through better characterization of seismic hazards. For megacities like Tehran and Los Angeles, the key problem is holistic: how can we protect the societal infrastructure from extreme events that might "break the system," like Hurricane Katrina broke the city of New Orleans in 2005? Achieving this type of security depends on understanding how the accumulation of damage during event cascades leads to urban-system failure. I will mention two ways earthquake system science is contributing to this goal.

Earthquake simulations can provide cascade scenarios from which we can learn about, and possibly correct, the critical points of failure. In November, 2008, the USGS will coordinate the Great Southern California ShakeOut, a week-long emergency-response exercise based on a SCEC simulation of a magnitude-7.8 rupture of the southern San Andreas fault (Perry et al., 2008). ShakeOut will involve federal, state, and local emergency-response agencies, as well as several million of citizens at schools and places of business. The objective of this disaster exercise is to improve public preparedness at all organizational levels.

SCEC is generating large suites of simulations that sample the likelihoods of future earthquakes. This capability for physics-based prediction of seismic shaking will someday replace empirical attenuation relationships in PSHA. It offers the possibility of an end-to-end ("rupture to rafters") analysis that embeds the built environment in a geologic structure to calculate more realistically earthquake risk for urban systems, not just individual structures.

The interests of basic and applied science converge at the system level. Predictive modeling of earthquake dynamics comprises a very difficult set of computational problems. Taken from end to end, the problem comprises the loading and eventual failure of tectonic faults, the generation and propagation of seismic waves, the response of surface sites, and—in its application to seismic risk—the damage caused by earthquakes to the built environment. This chain of physical processes involves a wide variety of interactions, some highly nonlinear and multiscale. Only through international collaboration can we extend such predictive models to all regions where the seismic risk is high.

Earthquake Prediction. Earthquake prediction *senso stricto*—the advance warning of the locations, times, and magnitudes of potentially destructive fault ruptures—is a great unsolved problem in physical science and, owing to its societal implications, one of the most controversial. Despite more than a century of research, no methodology can reliably predict potentially destructive earthquakes on time scales of a decade or less. Many scientists question whether such predictions will ever contribute significantly to risk reduction, even with substantial improvements in the ability to detect precursory signals; the chaotic nature of brittle deformation may simply preclude useful short-term predictions.

Nevertheless, global research on earthquake predictability is resurgent, motivated by better data from seismology, geodesy, and geology; new knowledge of the physics of earthquake ruptures; and a more comprehensive understanding of how active faults systems actually work. To understand earthquake predictability, scientists must be able to conduct prediction experiments under rigorous, controlled conditions and evaluate them using accepted criteria specified in advance. Retrospective prediction experiments, in which hypotheses are tested against data already available, have their place in calibrating prediction algorithms, but only true (prospective) prediction experiments are really adequate for testing predictability hypotheses.

The scientific controversies surrounding earthquake predictability are often rooted in poor experimental infrastructure, inconsistent data, and the lack of testing standards. Attempts have been made over the years to structure earthquake prediction research on an international scale. For example, the International Association of Seismology and Physics of the Earth's Interior convened a Sub-Commission on Earthquake Prediction for almost two decades, which attempted to define standards for evaluating predictions. However, most observers would agree that our current capabilities for conducting scientific prediction experiments remain inadequate. Individual scientists and groups usually do not have the resources or expertise (or incentives) to conduct and evaluate long-term prediction experiments.

As a remedy, SCEC is working with its international partners to establish a Collaboratory for the Study of Earthquake Predictability. The goals of CSEP project are to support scientific earthquake prediction experiments in a variety of tectonic environments; promote rigorous research on earthquake predictability through comparative testing of prediction hypotheses; and help the responsible government agencies assess the feasibility of earthquake prediction and the performance of proposed prediction algorithms. A shared, open-source cyberinfrastrcuture is being developed to implement and evaluate time-dependent seismic hazard models through comparative testing (CSEP, 2008). Testing centers have been established at SCEC, ETH Zürich, and GNS Science in Wellington, New Zealand, and prediction experiments are now underway in several natural laboratories, including California, Italy, and New Zealand. Scientists from China, Japan, Greece, and Iceland have been participating in the development phase of CSEP, and we are encouraging other countries to initiate CSEP testing programs in the seismically active regions within their borders.

The research objectives of international partnerships in earthquake system science can be organized under four major goals: (1) discover the physics of fault failure and dynamic rupture; (2) improve earthquake forecasts by understanding fault-system evolution and the physical basis for earthquake predictability; (3) predict ground motions and their effects on the built

environment by simulating earthquakes with realistic source characteristics and three-dimensional representations of geologic structures; and (4) improve the technologies that can reduce earthquake risk, provide earthquake early warning, and enhance emergency response. A common theme is the need to deploy cyberinfrastructure that can facilitate the creation and flow of information required to simulate and predict earthquake behaviors.

Toward this end, SCEC proposes the establishment of a Multinational Partnership for Research in Earthquake System Science (MPRESS) to sponsor comparative studies of active fault systems. The partnership would be organized to broaden the training of students and early-career scientists beyond a single discipline by exposing them to research problems that require an interdisciplinary, system-level approach and to enhance their understanding of how scientific research works in different countries, how different societies perceive the scientific enterprise, and how diverse cultures respond to scientific information about natural hazards.

ACKNOWLEDGMENT

This research was supported by the Southern California Earthquake Center. SCEC is funded by NSF Cooperative Agreement EAR-0106924 and USGS Cooperative Agreement 02HQAG0008. The SCEC contribution number for this paper is 1210.

REFERENCES

Ambraseys, N. N., & C. P. Melville (1982). *A History of Persian Earthquakes*, Cambridge, 237 pp., ISBN: 9780521021876.

Ashtari Jafari, (2007). Time-independent seismic hazard analysis in Alborz and surrounding area, *Natural Hazards*, **42**, 237-252.

Barka, A. A. (1999). The 17 August 1999 Izmit earthquake, *Science,* **285**, 1858-1859.

Berberian, M. (1994). Natural hazards and the first earthquake catalogue of Iran, International Institute of Earthquake Engineering and Seismology, **1**, 620.

CEST-JICA (2000). *The Study on Seismic Microzoning of the Greater Tehran Area in the Islamic Republic of Iran*, Center for Earthquake and Environmental Studies of Tehran and Japan International Cooperation Agency, Tehran Municipality, Tehran, Iran.

CDMG (2000). *An Evaluation of Future Earthquake Losses in California*, California Division of Mines and Geology, Sacramento, California, September, 2000, 16 pp.

CSEP (2008). Collaboratory for the Study of Earthquake Predictability, T. H. Jordan, D. Schorlemmer, S. Wiemer, M. Gerstenberger, D. Jackson, P. J. Maechling, M. Liukis & J. D. Zechar, *Collaboratory for the Study of Earthquake Predictability: Progress and Plans*, Southern California Earthquake Center, January, 2008, 12 pp.

EMI (2006). *Tehran Disaster Risk Management Profile*, Earthquakes and Megacities Initiative, Megacities Disaster Risk Management Knowledge Base, Pacific Disaster Center, http://emi.pdc.org/cities/CP-Tehran-July2006.pdf.

FEMA (2000). *HAZUS99 Estimated Annualized Earthquake Losses for the United States*, Federal Emergency Management Agency Report 366, Washington, D.C., September, 2000, 32 pp.; for overview of HAZUS, see http://www.fema.gov/plan/prevent/hazus/ and http://www.nibs.org/hazusweb/overview/overview.php.

FEMA (2006). *Next-Generation Performance-Based Seismic Design Guidelines*, Federal Emergency Management Agency Report 445, Washington, D.C., August, 2006, 128 pp.

Field, E. H. (2007a). Overview of the Working Group for the Development of Regional Earthquake Likelihood Models (RELM), *Seismol. Res. Lett*. **78**, 7-16.

Field, E. H. (2007b). A summary of previous Working Groups on California Earthquake Probabilities, *Bull. Seismol. Soc. Am.*, **97**, p. 1033-1053, doi:10.1785/0120060048.

Field, E. H., T. H. Jordan & C. A. Cornell (2003). OpenSHA: a developing community modeling environment for seismic hazard analysis, *Seismol. Res. Letters*, **74**, 406–419.

Field, , E. H., H. A. Seligson, N. Gupta, V. Gupta, T. H. Jordan & K. Campbell (2005). Probabilistic Loss estimates for a Puente Hills blind-thrust earthquake in Los Angeles, California, *Earthquake Spectra*, **21**, 329-338.

Gerstenberger, M., S. Wiemer, L.M. Jones & P.A. Reasenberg (2005). Real-time forecast of tomorrow's earthquakes in California, *Nature*, **435**, 328-331.

Giardini, D. G. Grünthal, K. Shedlock & P. Zhang (1999). The GSHAP global seismic hazard map, *Ann. Geofisica*, **42**, 1225-1230.

Giardini, D., T. van Eck, R. Bossu & S. Wiemer (2008). Networking Research Infrastructures for Earthquake Seismology in Europe, *Eos*, **89**, 219.

Grant, L. B. & W. R. Lettis, editors (2002). Paleoseismology of the San Andreas Fault System, *Bull. Seismol. Soc. Am*., Special Issue, 92, 2002.

Heaussler, P. J. & 10 others (2004). Surface rupture and slip distribution of the Denali and Totschunda faults in the 3 November 2002 M 7.9 earthquake, Alaska, *Bull. Seismol. Soc. Am.*, **94**, S23-S52.

Horiuchi, S., H. Negishi, K. Abe, A. Kamimura & Y. Fujinawa (2005). An automatic processing system for broadcasting earthquake alarms, *Bull. Seismol. Soc. Am.*, **95**, 708-718.

Jordan, T. H. (2006a). Earthquake system science in Southern California, *Bull. Earthquake Res. Inst. Tokyo*, **81**, 211-219.

Jordan, T. H. (2006b). Earthquake predictability, brick by brick, *Seismol. Res. Lett.*, **77**, 3-6.

Jordan, T. H., & P. Maechling (2003). The SCEC community modeling environment: an information infrastructure for system-level earthquake science, *Seismol. Res. Lett*., 74, 324-328.

Kanamori, H. (2005). Real-time seismology and earthquake damage mitigation, *Ann. Rev. Earth Planet. Sci.*, **33**, 195-214.

Klinger Y., X. Xu, P. Tapponnier, J. Van der Woerd, C. Laserre & G. King (2005). High-resolution satellite imagery mapping of the surface rupture and slip distribution of the Mw ~7.8, November 14, 2001 Kokoxili earthquake (Kunlun fault, Northern Tibet, China), *Bull. Seismol. Soc. Am.*, **95**, 1970-1987.

Kircher, C. A., H. A. Seligson, J. Bouabid & G. C. Morrow (2006). When the Big One strikes again: estimated losses due to a repeat of the 1906 San Francisco earthquake, *Earthquake Spectra*, **22**, S297-S339.

NRC (2000). National Research Council, Committee on Basic Research Opportunities in Earth Science (T. H. Jordan, chair), *Basic Research Opportunities in Earth Science*, National Academy Press, Washington, D.C., 154 pp.

NRC (2003). National Research Council, Committee on the Science of Earthquakes (T. H. Jordan, chair),*Living on an Active Earth: Perspectives on Earthquake Science*, National Academy Press, Washington, D.C., 418 pp.

NSHMP (1996). National Seismic Hazard Mapping Program, A. Frankel, C. Mueller, T. Barnhard, D. Perkins, E. Leyendecker, N. Dickman, S. Hanson & M. Hopper (1996). National seismic-hazard maps: documentation June 1996, U.S. Geol. Surv. Open-file Rept. 1996-532, 110 pp.

NSHMP (2002). National Seismic Hazard Mapping Program, A. D. Frankel, M. D. Petersen, C. S. Muller, K. M. Haller, R. L. Wheeler, E. V. Leyendecker, R. L. Wesson, S. C. Harmsen, C. H. Cramer, D. M. Perkins & K. S. Rukstales, *Documentation for the 2002 Update of the National Seismic Hazard Maps*, U.S. Geol. Surv. Open-file Rept. 2002-420, 33 pp.; see http://earthquake.usgs.gov/hazmaps/.

NSHMP (2008). National Seismic Hazard Mapping Program, M. D. Petersen, A. D. Frankel, S. C. Harmsen, C. S. Mueller[1], Kathleen M. Haller[1], R L. Wheeler, R. L. Wesson, Y Zeng, O. S. Boyd, D. M. Perkins, N. Luco, E. H. Field, C. J. Wills & K. S. Rukstales, Documentation for the 2008 Update of the United States National Seismic Hazard Maps, U. S. Geol. Surv. Open File Rep. 2008-1128.

Ogata, Y. (1988). Statistical models for earthquake occurrence and residual analysis for point processes, *J. Amer. Statist. Assoc*., **83**, 9-27.

Olsen, K. B., S. Day, J. B. Minster, Y. Cui, A. Chourasia, M. Faerman, R. Moore, P. Maechling & T. H. Jordan (2006). Strong Shaking in Los Angeles Expected From Southern San Andreas Earthquake, *Geophys. Res. Lett.*, 33, L07305, doi:10.1029/2005GL025472.

Olsen, K. B., S. M. Day, J. B. Minster, Y. Cui, A Chouasia, R. Moore, P. Maechling & T. Jordan (2008). TeraShake2: spontaneous rupture simulations of Mw 7.7 Earthquakes on the southern San Andreas Fault, *Bull. Seismol. Soc. Am.*, **98**, 1162 -1185, doi: 10.1785/0120070148.

Perry, S., D. Cox, L. Jones, R. Bernknopf, J. Goltz, K. Hudnut, D. Mileti, D. Ponti, M. Reichle, H. Seligson, K. Shoaf, J. Treiman & A. Wein (2008). The ShakeOut Earthquake Scenario—a story that Southern Californians are writing, *USGS Circular 1324*, Washington DC, April, 2008, 16 pp.

SEAOC (1995). *Vision 2000: Performance-Based Seismic Engineering of Buildings*, Structural Engineers Association of California, San Francisco, April, 1995, 115 pp.

Schorlemmer, D., M. C. Gerstenberger, S. Wiemer, D. D. Jackson, and D. A. Rhoades (2007). Earthquake likelihood model testing, *Seismol. Res. Lett.* **78**, 17-29.
Tavakoli, B. & M. Ghafory-Ashtiany (1999). *Seismic Hazard Assessment of Iran*, contributed to the Global Seismic Hazard Assessment Program, http://www.seismo.ethz.ch/gshap/iran/report.html.
Toda, S., R. S. Stein, K. Richards-Dinger & S. Bozkurt (2005). Forecasting the evolution of seismicity in southern California: Animations built on earthquake stress transfer, *J. Geophys. Res.*, **110**, B05S16, doi:10.1029/2004JB003415.
USGS (2006). 100th Anniversary of the 1906 Earthquake, *People, Land & Water*, **12**(13), U. S. Geological Survey, April, 2006, 36 pp. http://www.usgs.gov/homepage/science_features/plw_1906.asp,
Wald, D., V. Quitoriano, T. Heaton, H. Kanamori, C.W. Scrivner & C.B. Worden (1999). TriNet "shakemaps": Rapid generation of instrumental ground motion and intensity maps for earthquakes in Southern California, *Earthquake Spectra,* **15**, 537-55; see http://earthquake.usgs.gov/eqcenter/shakemap/.
WGCEP (1995). Working Group on California Earthquake Probabilities, Seismic hazards in southern California: probable earthquakes, 1994-2024, *Bull. Seismol. Soc. Am.* **85**, 379-439.
WGCEP (2003). Working Group on California Earthquake Probabilities, *Earthquake Probabilities in the San Francisco Bay Region: 2002–2031*, U.S. Geol. Surv. Open-file Rept. *2003-214*.
WGCEP (2007). Working Group on California Earthquake Probabilities, *Uniform California Earthquake Rupture Forecast, Version 2*, U.S. Geol. Surv. Open-file Rept. 2007-1437, Washington DC, December, 2007, 95 pp.
Weldon II, R. J., T. E. Fumal, G. P. Biasi & K. M. Scharer (2005). Past and future earthquakes on the San Andreas fault, *Science*, **308**, 966.
White House (2006). *The Federal Response to Hurricane Katrina: Lessons Learned*, White House Report, Washington DC, 217 pp., http://www.whitehouse.gov/reports/katrina-lessons-learned.pdf.

LIST OF ABBREVIATIONS

AR – Attenuation Relationship
CDMG – California Division of Mines and Geology (now CGS)
CEST – Center for Earthquake and Environmental Studies of Tehran
CGS – California Geological Survey
CISN – California Integrated Seismic Network
CME – Community Modeling Environment
CSEP – Collaboratory for the Study of Earthquake Predictability
EEW – Earthquake Early Warning
ERF – Earthquake Rupture Forecast
ETAS – Epidemic Type Aftershock Sequence
FEMA – Federal Emergency Management Agency
JICA – Japan International Cooperation Agency
MPRESS – Multinational Partnership for Research in Earthquake System Science
NERIES – Network of Research Infrastructures for European Seismology
NSHMP – National Seismic Hazard Mapping Program
PEER – Pacific Earthquake Engineering Research Center
PGA – Peak Ground Acceleration
PGV – Peak Ground Velocity
PSHA – Probabilistic Seismic Hazard Analysis
RELM – Regional Earthquake Likelihood Models
SCEC – Southern California Earthquake Center
SEAOC – Structural Engineers Association of California
STEP – Short Term Earthquake Probability (model)
UCERF – Uniform California Earthquake Rupture Forecast
USGS – United States Geological Survey
WGCEP – Working Group on California Earthquake Probabilities

LIVING WITH EARTHQUAKES: KNOW YOUR FAULTS

Manouchehr Ghorashi
Research Institute for Earth Sciences and Islamic Azad University—North Tehran Branch

ABSTRACT

The great earthquake belt which stretches from the Mediterranean through the Middle East into central Asia results from the ongoing collision between the Eurasian plate and the African, Arabian and Indian plates to the south. Through much of this belt, the topography is created and controlled by fault movement in earthquakes. Many habitations are located at the foot of the fault- controlled mountain range- fronts that bound inhospitable deserts or elevated plateaus, in positions that are favorable for trade-routes, strategic control of access or for water supply. As a result, they are vulnerable to earthquakes, which often seem to have targeted population centers precisely. For many centuries, an uneasy accommodation has been reached between human needs and the earthquake-controlled landscape, sometimes brilliantly exploited by local hydrological engineering, as in Iran. In the old days, occasional earthquakes have occurred in these areas, killing a shocking proportion of the population, but it is important to note that the populations of the settlements themselves have been relatively small. Many once-small rural communities have now grown into towns, cities or megacities, while retaining their vulnerability through poor building standards. Earthquakes that occur in these places today now kill many more than they did in the past, as we have witnessed in the last few years. The only reason that extreme catastrophes have been rare in the last few years is because the exposure of modern megacities to earthquake hazard has been relatively short. An increase in the number of such catastrophes now seems to be inevitable. Over the last two decades understanding of how active faults move in earthquakes, and the ability to recognize them before they move, has increased from a situation in the 1970s when even the most fundamental characteristics of earthquake faults, such as their depth and orientation, were known only crudely. We can now resolve precise details of their shape, position and even slip variation over their surface, without going anywhere near the epicentral region. These advances have come through the combined use of seismology and space-based surveying techniques, particularly GPS (Global Positioning System) and radar interferometry. At the same time we have become much better at identifying active earthquake-generating structures before they move, largely through appreciating the signature they produce in the landscape at the surface. Perhaps we will be less embarrassed in the future than we have been in the recent past by large earthquakes that occurred on faults that were unknown or unappreciated at the time, but most of which could have been identified beforehand, given our better understanding of what to look for. In addition there is a better idea of how to understand the deformation of the continental regions which, after all, are where we live and where earthquakes cause most damage. Some of the processes we can see occurring today require the faulting to evolve with time and it is more or less possible to recognize this in the landscape, identifying faults that grow, interact or even die, becoming inactive.

Keywords: Active faulting, Earthquakes, Seismic Hazard, Iran, Megacities.

1. INTRODUCTION

The active deformation in Iran is caused by Arabian-Eurasia convergence, and nearly all of the shortening is accommodated within the political border of Iran itself.

Recent GPS measurements (McClusky et al. 2003; Vernant et al. 2004) indicate that Arabia moves approximately northwards, with respect to Eurasia, at about 23mm/yr (fig.1). This is lower than previous estimates for plate motion based on pre-GPS plate-circuit models (DeMets et al. 1994). The seismicity within Iran suggests that much of the deformation is concentrated in the Zagros, Alborz and Kopeh Dagh mountains, and in east Iran (fig.2), surrounding Central Iran and the Lut Desert, which is virtually aseismic and behave as relatively rigid blocks (Jackson and MeKenzie, 1984). This view is supported by the available GPS data (Vernant et al. 2004).The Zagros accommodates about half of the northward motion of Arabia (e.g. Tatar et al. 2002), with the Alborz, Central Caspian Sea, and Kopeh Dagh taking up the rest, (Vernant et al. 2004). The northward motion of Arabia is partly accommodated by subduction of the Oman sea oceanic crust beneath the Makran. Shortening north of the Zagros requires N-S right–lateral shear between Central Iran and Afghanistan. This is observed in the N-S right lateral strike-slip fault system either side of the Lut desert, in east Iran (Walker and Jackson, 2004).

The Arabia – Eurasia collision in Iran is relatively young, and as mentioned earlier, the active faults and earthquake distribution are for the most part restricted within the political borders of the country. In addition, the arid desert climate, with an almost complete lack of vegetation and human habitation across much of the country, aids the reservation in the landscape of very subtle indications of surface deformation due to active faulting, making Iran an ideal region for the study of active faulting.

Active faults in Iran have caused many destructive earthquakes in recent years, for example at Dasht-e-Bayaz in 1968; at Tabas in 1978; at Rudbar in 1990; at Golbaf in 1981, 1988; at Zirkuh (Qa'enat) 1997; at Bam in 2003; and at Dahuiyeh (Zarand) in 2005. However relatively little is known at present about the distribution of active faulting in Iran , the rates of deformation and earthquake recurrence in individual regions, and the ways in which the faults in Iran accommodate Arabia-Eurasia convergence. A significant number of earthquakes in Iran have occurred on faults that were not previously well known to exist, as the faults responsible are often "blind" (or partially blind) and expressed at the earths surface as folding in relatively soft and easily eroded Quaternary deposits. By studying recent earthquakes (such as the events at Tabas in 1978;at Sefidabeh in 1994; at Avaj in 2002; and at Bam in 2003), we have found diagnostic geomorphic indications of faulting at depth, which we use to recognize other active fault in areas that have no record of earthquakes(Jackson et al. 1995, Walker and Jackson 2004).

As Jackson (2001) points out, the interests of the earthquake engineer and the tectonic geologist frequently overlap both are interested in active faults: the geologist wants to know how that faults contributes to the regional deformation and the formation of the landscape, while the engineer is concerned with the potential for future earthquakes. That overlap of interest is particularly obvious on the continental regions, which is where most people live and where most engineered structure are erected because the active faults are accessible for study. In particular, space-based geodetic investigations using GPS or INSAR (Synthetic Aperture Radar Interferometry) can be combined with seismological analysis to give a great deal of information about the orientation, size and slip on a fault. This information can in turn, be related to the

surface geomorphological features associated with the fault, observed both from satellite imagery and in the field, to see how repeated slip on that fault has erected the surrounding landscape.

During the twentieth century, the Iranian people have experienced at least one >7.0 magnitude earthquake every seven years, and one 6.0-6.9 magnitude earthquake every two years, culminating in a very large death toll averaging 1.577 person/year (Berberian 2005). Since 1900, more than 164000 people have been killed by earthquake in Iran. During this period, no large-magnitude earthquake has impacted the metropolitan area of Tehran or large provincial capital cities. In the following sections the reason how villages grow and their vulnerability will be discussed.

2. FROM VILLAGES TO MEGACITIES

For centuries, desert rim existence in Iran had established a way of living with earthquakes. Earthquake faults, and the topography they produce, were largely responsible for the water resources and for the locations of habitations and agriculture, as well as some building materials. Occasionally, earthquakes moved those faults, and villages were destroyed. But the return period of earthquakes on individual faults are likely to be in the order of thousands of years and since it is unlikely for these earthquakes to recur on a timescale relevant for human memory, they have kept rebuilding their settlements in those areas. When earthquakes do occur, the destruction, and particularly the mortality; can be shocking, because of the vulnerable local building styles. For example, in the town of Tabas in 1978, more than %80 of the population (11600 of 13000) were killed outright; at Bam in 2003, the figure was near %30. Most places are, nonetheless, rebuilt and resettled because their locations are, at the end, determined by where water is available and agriculture is possible.

The problem is that villages grow, and have grown, rapidly, while building quality remains equally vulnerable, though it may change from weak adobe forms to poorly built multi-storey apartment blocks, and so mortality rates remain appallingly high. Thus the village of Sefeidabeh can become the large rural town of Tabas (11000 killed in the town in 1978; 20000 including other villages of the oasis), or the small city of Bam (40000 killed in 2003) Rudbar (40000 killed in 1990), or the megacity of Tehran, which now has a daytime population of about 12 million. Tehran is situated at the base of the Alborz mountain range front, which is elevated by movement on an active thrust fault. Several other active faults are also situated nearby. In former time, the site was occupied by relatively small towns on a major trade rout. These predecessors of modern Tehran were damaged or destroyed completely in earthquakes of probable Mw ~ 7 in 4th century BC, 855, 958, 1177 and 1830 (Ambraseys and Melville, 1982; Berberian and Yeats, 1999), but the number killed was probably quite small by modern standards. The modern Tehran is a megacity that grew rapidly on the same site in the later twentieth century.

However, there is no sign that the concentration of population into large towns and cities in Iran is accompanied by a decrease in the mortality rate during earthquakes. Many major towns and cities are situated adjacent to range fronts and faults, in places that made sense when they were initiated as agricultural settlement, and they retain that vulnerability to earthquakes. In such places, earthquakes that in the past killed a few hundred of thousand people will now kill tens or hundreds of thousands, or more. The situation is similar throughout much of the Mediterranean-Middle East –Central Asia earthquake belt.

3. CASE STUDIES

For centuries, Iranian civilization and desert existence has lived with, and exploited, this link between, faulting and water supply. Some examples serve to illustrate this relationship.

3.1. The Sefidabeh Earthquake

In February 1994, the small desert village of Sefidabeh in southeast Iran was destroyed by an earthquake (magnitude, Mw 6.1). Most of the approximately 300 buildings in Sefidabeh collapsed, having been built of adobe, or sun dried mud-brick, the traditional indigenous building material from which both walls and heavy roof domes are constructed. The fact that only six people died in this case is attributed to the lucky chance of a foreshock 24 hours beforehand, and to the local time of the mainshock (11:30 am), so that many people were outdoors anyway.

Sefidabeh is a desperately remote and inhospitable location (fig. 2), between two deserts of the Dasht-e-Margo (*lit.* desert of death) In Afghanistan and the Dasht-e-Lut (*lit*. barren desert) of southeast Iran; one of the very few stops on a long , lonely trans-desert trade rout between northeast Iran and the Indian Ocean. It is the only habitation of any size for nearly 100Km in any direction, and yet the earthquake apparently targeted it precisely.

Instead of a fault rupture or scarp at the surface, what formed instead was a fold. A fold of this type, on which slip fail to reach to the surface is called a "blind fault". Slip in a single earthquake is only a meter or two, but repeated earthquakes over hundreds of thousands of years cause the fold to grow into a single ridge. The ridge adjacent to Sefidabeh is about 100m high and obvious (fig. 3). Sefidabeh is built on an old alluvial fan, formed where an ephemeral river that used to flow through the ridge discharged it waters onto the desert plain (Berberian et al. 2000). But repeated earthquakes caused the ridge to grow, not just in height but also by increasing its length towards the northwest, the river had to incise a gorge through it, eventually becoming blocked, as forming a lake. Finally, the river abandoned this course altogether, and now flows round the northwest tip to the ridge instead. The old lake beds remain (fig. 3a), now dry and elevated 70m above the desert plain. From the age of the sediments within them, it can date the switch in the river course to about 100000 years ago (Jackson 2006, Parsons et al. 2006).

Thus, well before the earthquake, all the signals were there in the landscape that Sefidabeh was in a vulnerable location-if people had only seen them and known how to read them (they had not; Sefidabeh was too remote for anyone to have noticed). Blind thrusts are very common in Iran, as the whole country is being squashed in a north-south direction between the converging Arabian and Eurasian plates at about 23mm/yr (Vernant et al. 2004). Earlier devastating Iranian earthquakes of modern times that occurred on blind thrusts include those at Ferdows in 1968 (Mw 6.3, approx. 1000 killed) and Tabas in 1978 (Mw 7.3, approx. 20000 killed). In neither of these cases were the causative faults recognized at the time, though, in retrospect, they are clear in the landscape (Walker et al. 2003). The city of Bam, destroyed in 2003 (Mw 6.8, approx. 40000 killed) was also located on a blind thrust (which was recognized beforehand; Berberian 1976; Walker and Jackson 2002), thought the faulting in that earthquake was more complicated (Talebian et al. 2004; Funning et al. 2005). In each of these cases, at Sefidabeh, Ferdows, Tabas and Bam, although we know about the causative faults, we have not yet explained why the earthquakes apparently scored bull's-eye hits on the only substantial habitations in the desert for tens of kilometers in any direction.

Why Sefidabeh is located there? Sefidabeh means "white water", and the village obtains its water from the white lake beds in the uplifted ridge (fig.3c, d), which leak in a series of springs at its base. In this case, the fault is responsible for the sub-surface aquifer of the lake beds, and ensure that continual uplift and elevation above the plain, causing the formation of springs. Sefidabeh is the only place it is possible to live and attempt a meager agricultural existence, in this extremely inhospitable environment, as it is the only place with water. It is the fault that provides the water, but the fault may kill people when it moves.

This situation is common in Iran. The country is mountainous except for flat regions in the interior, which are barren salt flats. The mountains provide the water, so habitations are common at the foot of range fronts, many of which exist because they are elevated by movement on thrust faults. For centuries, the indigenous people have exploited this situation. Some horticulture is possible on the toes of alluvial fans coming off the ranges, on the finer-grained material away from the coarse debris adjacent to the steep slopes, but only if water is available. The water table is usually elevated at the range front, sometimes exaggeratedly so if there is an active fault, because repeated grinding of rocks on the fault creates a very fine, impermeable clay (called 'fault gouge') that can act as an underground dam to the water table, elevating it still further. Tunnels are dug, by hand, back to the range through the semi- consolidated fan material, to tap the elevated water table at the range front (figures 4 and 5). In Iran, these tunnels are called 'qanat', and are one of the glories of the ancient Persian civilization. They can be several tens of kilometers long, up to 100m deep at the range front, and are marked at the surface by lines of circular craters, where vertical shafts are sunk down to the tunnel to provide access, ventilation and removal of excavated material during construction. Many have been in continuous use for centuries, and the oldest are thought to have been dug more than 2000 years ago.

3.2. The Bam Earthquake

The catastrophic Mw 6.6 earthquake of 2003 at Bam in the Kerman province of south-central Iran attracted much attention, and has been studied with an abundance of observations from synthetic aperture radar, teleseismic seismology, aftershock studies, geomorphology, remote sensing and surface field work (Talebian et al. 2004; Jackson et al. 2006). It effectively destroyed the ancient city of Bam, with a population of around 150000. The number of death will perhaps never be known exactly, but is thought to be between 26000 (the official figure) and 40000. Even in the long and terrible earthquake history of Iran, where event of this nature are not rare (the last comparable one, again killing ~ 40000 people, occurred in 1990; see Berberian et al. 1992), the Bam earthquake was especially destructive.

The most obvious fault in the area is the escarpment running for ~ 12 Km between Bam and Baravat. It is clearly visible in satellite imagery and in the field and is mentioned in several earlier publications on the area (e.g. Berberian 1976; Walker and Jackson 2002). In form, the escarpment is an asymmetric fold with a steep eastern side and an almost-flat top (fig. 6), uplifting and exposing relatively fine-grained alluvium, marls and sands through the encrusted desert pavement. It has all the characteristic of a fold above a blind, west-dipping reverse fault (fig. 6).

After the earthquake, hairline cracks were followed discontinuously along most of the length of the escarpment, close to its base. They were mostly in the form of open fissures less than one cm wide, with no consistent or reliable indication of strike-slip motion. Coseismic cracks and

fissures were observed following the earthquake in several areas north and south of the city of Bam. These ruptures were recognized in the immediate aftermath of the earthquake and none of them indicate surface faulting sufficient to have generated the earthquakes.

The fold ridge is crossed by numerous W-E flowing underground water channels, (qanat), marked at the surface by lines of vertical shafts typically 10-20m apart. These qanats top an uplifted aquifer beneath the fold, in the hanging wall of the blind reverse fault, to bring water to the date-growing region of Baravat in the east. Indeed, the fold, and its uplifted aquifer, provide the main source of water for agricultural purposes, together indicate the reason for the location of the Bam oasis and its agriculture (fig. 5a). It is this fault controlled water supply that determines where Bam is located, and why it was destroyed. Elsewhere in the desert, qanats bring water to fantasy pleasure gardens, with cascading pools of water surrounded by trees and pavilions, such as at Mahan in the Kerman province (fig. 5d). Qanats provide fresh, continuous supplies of water, with little evaporation loss, to thousands of villages in the deserts of Iran and other countries in the Middle East and Central Asia. They are engineering wonders, and the very lifelines by which existence is possible for many. The association between active reverse faulting, uplifted aquifer providing a water supply, and the locations of settlements, is common in the desert regions of Iran (Berberian et al. 2001).

An extraordinary feature of the Envisat ASAR data at Bam was the contrast between the exceptional coherence of successive images in the surrounding desert and the decorrelation of those images along the ruptures south of Bam (fig. 7). This contrast was so extreme and clear that the ruptures themselves were visible (figs. 7 and 8) and this guided us to their previously undiscovered surface location a month after the earthquake (see Talebian et al. 2004; Funning et al. 2005).

4. DISCUSSION AND CONCLUDING REMARKS

Vulnerable urban areas in Iran, in which prominent potential seismic sources have been mapped under heavily populated centers, including megacity of Tehran and several other provincial cities are known with well-documented historical seismic data. All major cities are located on and/or adjacent to numerous major exposed and blind capable faults. The situation leaves the country vulnerable to the catastrophic collapse of large numbers of buildings and infrastructure and large human casualties in the event of a major urban earthquake.

The link between how and where people live and earthquakes is particularly dramatic in Iran, but for many other parts of the great earthquakes and mountain belts that run from Italy to China, the situation is similar. Throughout this region the topography is largely created by fault movement in earthquakes, ultimately the result of the ongoing collision between the Eurasian plate and the African, Arabian and Indian plate to the north. Large tracts of this area are either low, barren, inhospitable deserts, or high, inaccessible and also inhospitable plateaus. Habitations concentrate around the edge of these regions, at the range fronts, because these locations are on trade routs, are of strategic importance controlling access, or are near water supplies. Many have been destroyed in past earthquakes when their populations were relatively small, but have now grown into very large and very vulnerable cities.

The relentless rise in global population and in the growth of megacities in the developing world is discussed by Bilham (1995,1998,2004). Half the world's megacities of more than 10 million

habitants are in locations vulnerable to earthquakes (Fig. 9a). Figure 9b shows the most damaging earthquakes, in terms of lives lost, of the last 1000 years, that updated by Jackson (2006). The map simply distinguishes earthquakes that killed more than 10000 people from those that killed more than 100000. Figure 9b is alarming because it highlight the vulnerability of cities in the Mediterranean-Middle East-Asia earthquake belt, as well as the coastal regions of South and Central America and Indonesia, for which tsunamis pose an additional risk, as demonstrated in Sumatara in 2004. Many of the red dots indicate earthquakes that killed more than 10000 at times when the cities involved had populations far lower than they have today. Of the 113 earthquakes included in figure 9b over the last 1000 years, 34 occurred in the last 100 years alone.

Figure 9c, shows the number of earthquakes killing more than 10000(grey) and 50000 (red) per century for the last 1000 years. The histogram shows the relentless increase in fatalities with the expanding global population after 1600, and it is quite clear where the trend is heading (Jackson, 2006).

ACKNOWLEDGMENT

This paper is a part of more than 25 years of scientific collaboration between the Geological Survey of Iran, the University of Cambridge, and the Centre for Observation and Modeling of Earthquake and Tectonics (COMET). I take this opportunity to express my sincere thanks to Prof. James Jackson of the University of Cambridge for kindly giving me all documents.

REFERENCES

Ambraseys, N. N., and Melville, C.P., 1982, A history of Persian earthquakes, Cambridge University Press, UK, 219 pp.

Berberian, M., 1976, Contribution to the seismotectonics of Iran (Part II), Geol. Surv. Iran, Rep. No. 39.

Berberian, M., 2005, The 2003 Bam Urban earthquake: A predictable seismotectonic pattern along the western margin of the rigid Lut block, southeast Iran. Earthquake Spectra, 21, 535-599.

Berberian , M., and Yeats, R. S. 1999, Patterns of historical earthquakes rupture in the Iranian Plateau. Bull. Seism. Soc. Am., 89, 120-139.

Berberian, M. et al., 1992, The Rudbar-Tarom earthquake of 20 June 1990 in NW Persia: preliminary field and Seismological observations, and its tectonic significance, Bull. Seism. Soc. Am. 82,1726-1755.

Berberian, M. et al., 2000, The Sefidabeh earthquakes in eastern Iran: blind thrusting and bedding-plain slip on a growing anticline, and active tectonics of the Sistan Suture zone, Geophys. J. Int, 142, 283-299.

Berberian, M. et al., 2001, The March 14 1998 Fandoqa earthquake (Mw 6.6) in Kerman Province, SE Iran: Re-rupture of the 1981 Sirch earthquake fault, triggering of slip on adjacent thrusts and the active tectonics of the Gowk fault zone. Geophys. J. Int. 146, 371- 398.

Bilham, R., 1995, Global fatalities from earthquakes in the past 2000 years: prognosis for the next 30. In: Reduction and predictability of natural disasters (eds. J. Rundle, F. Klein and D. Turcott), Santa Fe Institute Studies in the sciences of complexity, vol. xxv, pp. 19-31, Reading, M. A.: Addison Wesley.

Bilham, R., 1998, Earthquakes and urban development, Nature, 336, 625-626.

Bilham, R., 2004, Urban earthquake fatalities: a safer world, or worse to come? Seism. Res. Lett. 75, 706-712.

DeMets, C. et al. 1994, Effects of recent revisions to the geomagnetic timescale on estimates of current plate motions: Geophys. Res. Lett. 21, 2191-2194.

Funning, G. J. et al., 2005, Surface displacements and source, Parameters of the 2003 Bam (Iran) earthquake from Envisat advanced synthetic aperture radar imagery, J. Geophys. Res. 110, Bo 9406 (doi: 10.1029, 2004 JBoo 3338).

Jackson, J. A., 1995, The accommodation of Arabia-Eurasia Plate Convergence in Iran, J. Geophys. Res. 100, 1505-15219.

Jackson, J. A., 2001, Living with earthquakes: Know your faults. J. Earthquake Engineering, 5 (Special Issue I), 5-123.

Jackson, J. A., 2006- Fatal attraction: living with earthquakes, the growth of villages in to megacities, and earthquake vulnerability in the modern world, Phil. Trans. R. Soc. A, 364, 1911-1925.
Jackson, J. A. and McKenzie D.P., 1984, Active tectonics of the Alpine-Himalayan belt between western Turkey and Pakistan, Geophys. J. R. Astorn. Soc. 77,185-264.
Jackson, J. A. et al., 2006, Seismotectonic aspects of the 26 December 2003 Bam, Iran, earthquake, Geophys. J. Int. 166, 1270- 1292.
McClusky, S. et al., 2000, Global Positioning system constraints on plate kinematics and dynamics is the eastern Mediterranean and Caucasus. J. Geophys. Res. 105, 5695-5719.
Parsons, B. et al., 2006, The 1994 Sefidabeh (eastern Iran) earthquakes revisited: new evidence from satellite radar interferometry and carbonate dating about the growth of an active fold above a blind thrust fault, Geophys. J. Int. 164, 202-217.
Talebian, M. et al., 2004, The 2003 Bam (Iran) earthquake: rupture of a blind strike-slip fault, Geophys. Res. Lett. 31, L 11611.
Tatar, M. et al., 2005, The 2003 December 26 Bam earthquake (Iran), Mw 6.6, aftershock sequence, Geophys. J. Int. 162.
Vernant, Ph. et al., 2004, Contemporary crustal deformation and plate kinematics in Middle East constrained by GPS measurements in Iran and northern Oman, J. Geophys. Int. 157, 381-398.
Walker, R. and Jackson, J. A., 2002, Offset and evolution of the Gowk fault, S. E. Iran: a major intra-continental strike-slip system, J. Struct. Geol. 24, 1677-1698.
Walker, R. and Jackson, J. A., 2004, Active tectonics and late Tertiary strain distribution in central and eastern Iran, Tectonophysics, 23, TC5010.
Walker, R. Jackson, J. A. and Baker, J. 2003, Thrust faulting in eastern Iran: Source Parameters and surface deformation of the 1978 Tabas and 1968 Ferdows earthquake sequence, Geophys. J. Int. 152, 749-765.

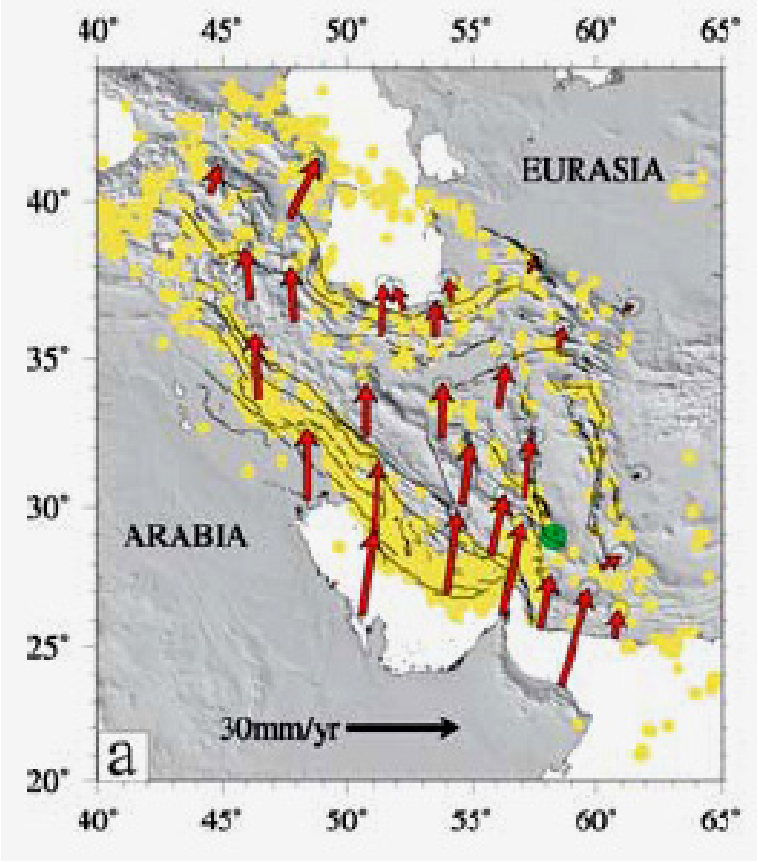

Fig. 1. Yellow circles are earthquakes in the period 1964–2002 from the catalogue of Engdahl et al. (1998) and subsequent updates. Red arrows are velocities (in mm/yr) of points in Iran relative to stable Eurasia, measured by GPS from Vernant et al. 2004). The green circle is the epicentre of the 2003 Bam earthquake.

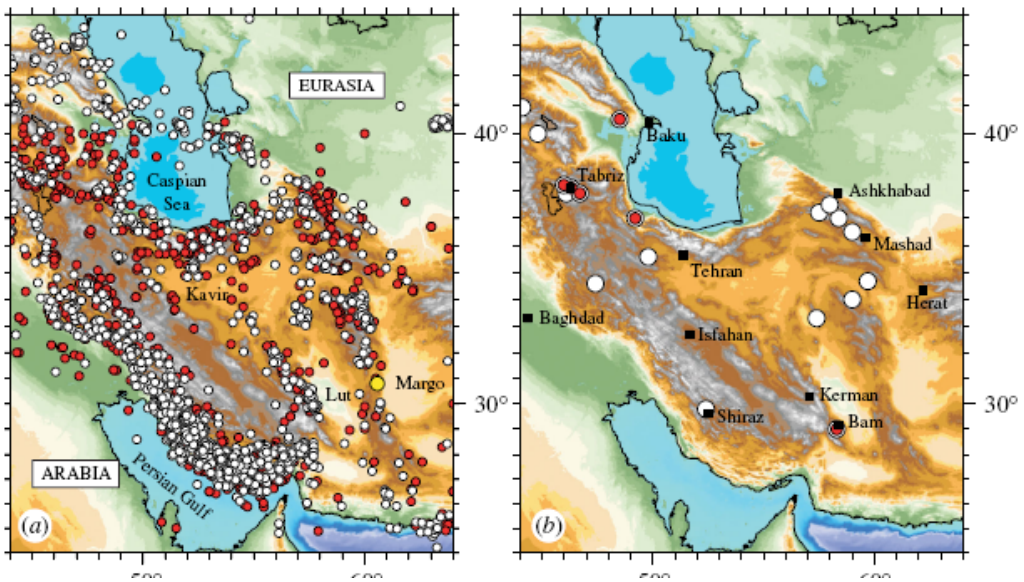

Fig. 2. Earthquakes in Iran and its surroundings. (a) White dots are well-located earthquakes of magnitude greater than 4 during 1963–2002 from the updated catalogue of Engdahl et al. (1998). Red dots are earthquakes of the previous 1000 years, thought to be bigger than magnitude 5, from Ambraseys & Melville (1982), complete only to 418 N. The yellow dot is the location of the village of Sefidabeh, mentioned in the text. The deserts of the Dasht-e-Margo, Dasht-e-Lut and Dashte - Kavir are labelled and relatively free of earthquakes, which concentrate near the edges of the high topography. (b) Earthquakes of the last 1000 years that have killed more than 10,000 (white dots) or 30,000 people (red dots).

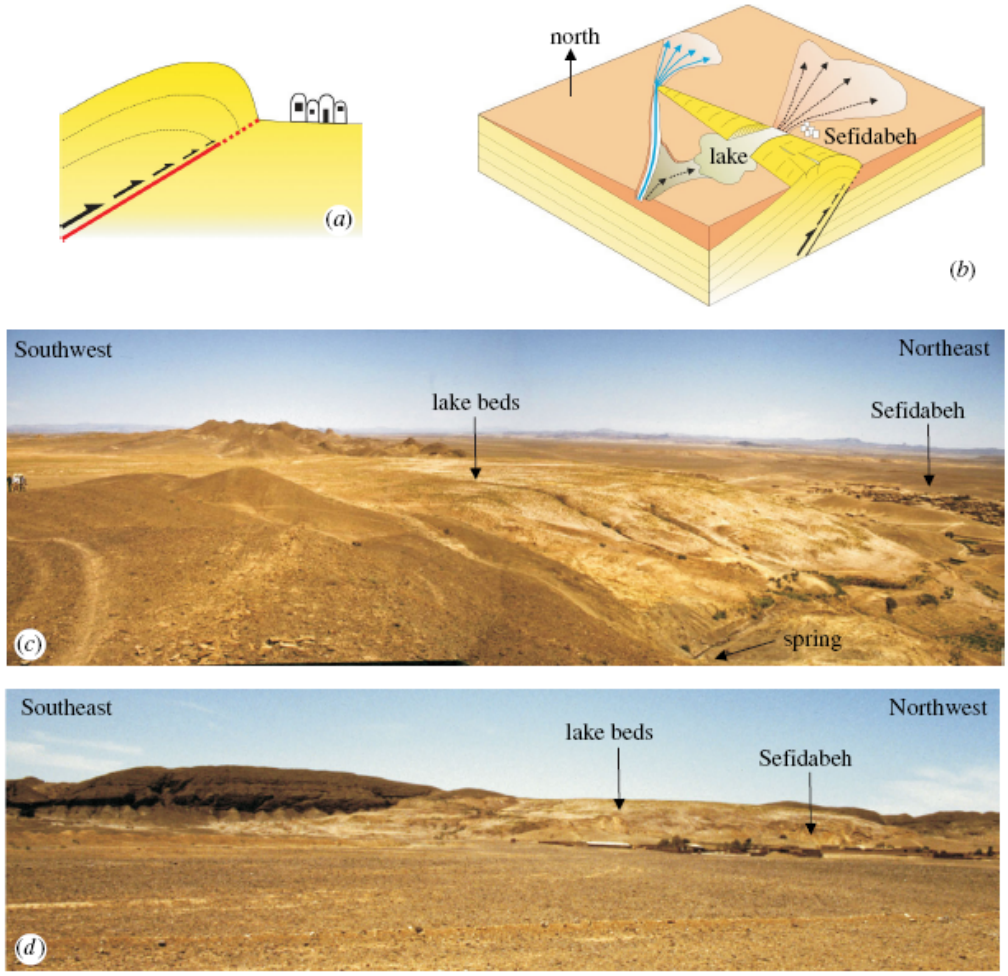

Fig. 3. (a) Schematic cross-section of a 'blind' thrust (or reverse) fault, in red, adjacent to a village (not to scale). Slip on the fault (black arrows) dies out towards the surface, which deforms by creating a fold. (b) Simplified cartoon of a blind thrust and its fold at Sefidabeh. The fold is about 10 km long. As the fold grew in repeated earthquakes, a river that used to flow across it first incised to make a gorge, then flooded to make a lake, and was finally abandoned when the river course switched to flow round the northwest end of the fold (Parsons et al. 2006). (c) View looking northwest across the abandoned lake beds, now uplifted 70 m above the level of Sefidabeh village. Note the spring at the base of the white lake sediments, and the people on the left, for scale. (d) View looking southwest across Sefidabeh to the white lake beds on the ridge behind the village.

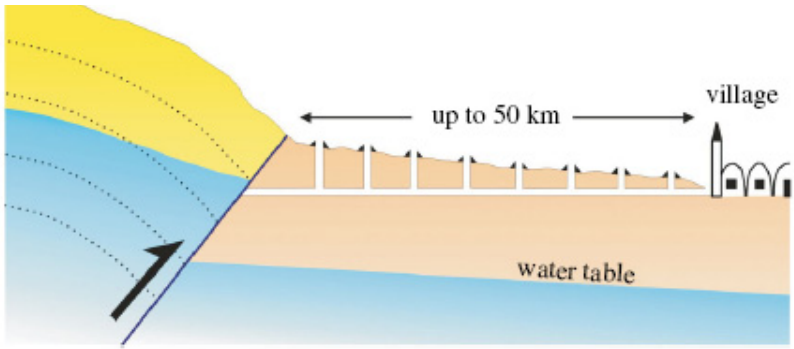

Fig. 4. Cartoon of irrigation tunnel (qanat) dug through alluvium towards a range-front, where water-table is elevated because of impermeable clay ('gouge') on thrust fault. Qanats can be up to 100 m deep at range front.

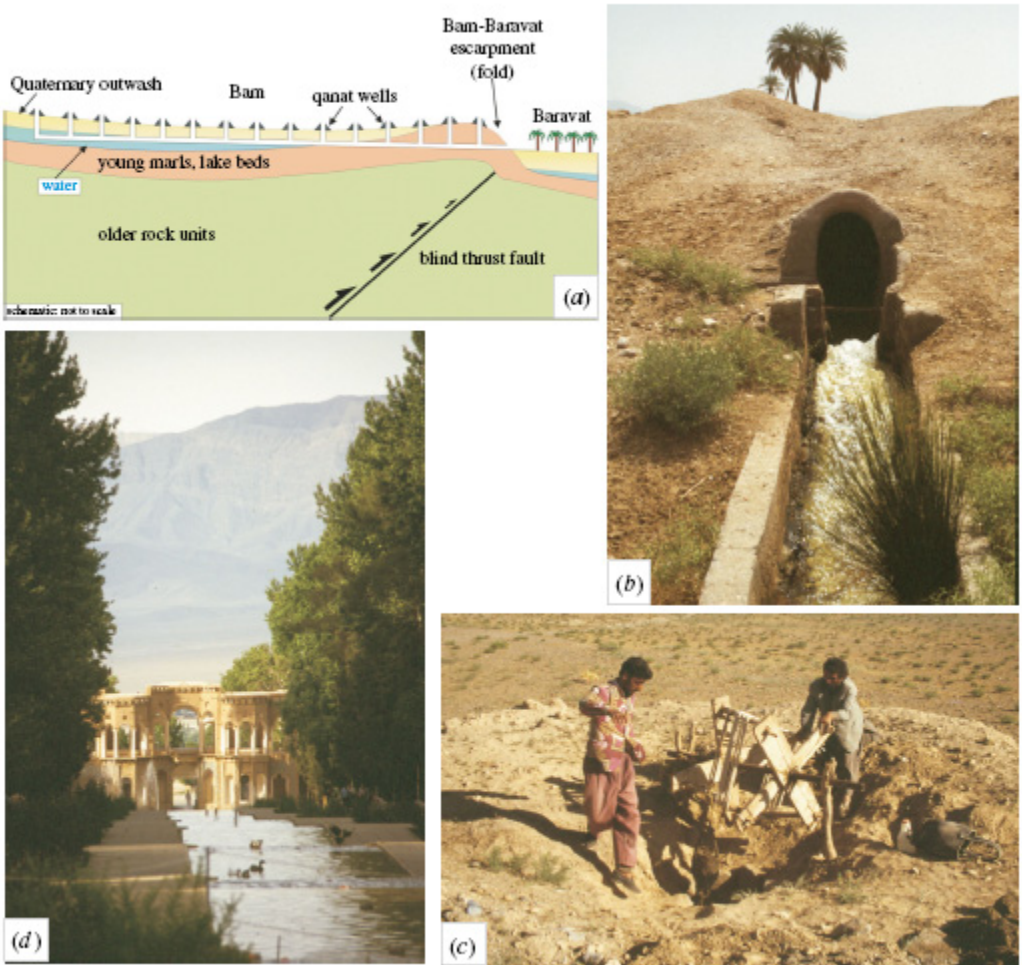

Fig. 5. (a) Schematic section of qanat systems feeding date growing region of Baravat adjacent to Bam. The blind thrust fault has created a fold which ponds sub-surface water flow through Quaternary outwash, as the underlying lake beds (marls) are relatively impermeable. (b) A qanat tunnel emerging near a village. (c) A windlass working at vertical qanat shaft, bringing excavated material to surface from underground worker below. Discarded material forms crater rim at surface, preventing flash-floods from washing material back into hole. (d) Water gardens at Mahan, between Bam and Kerman, fed by qanats from mountains several kilometres away.

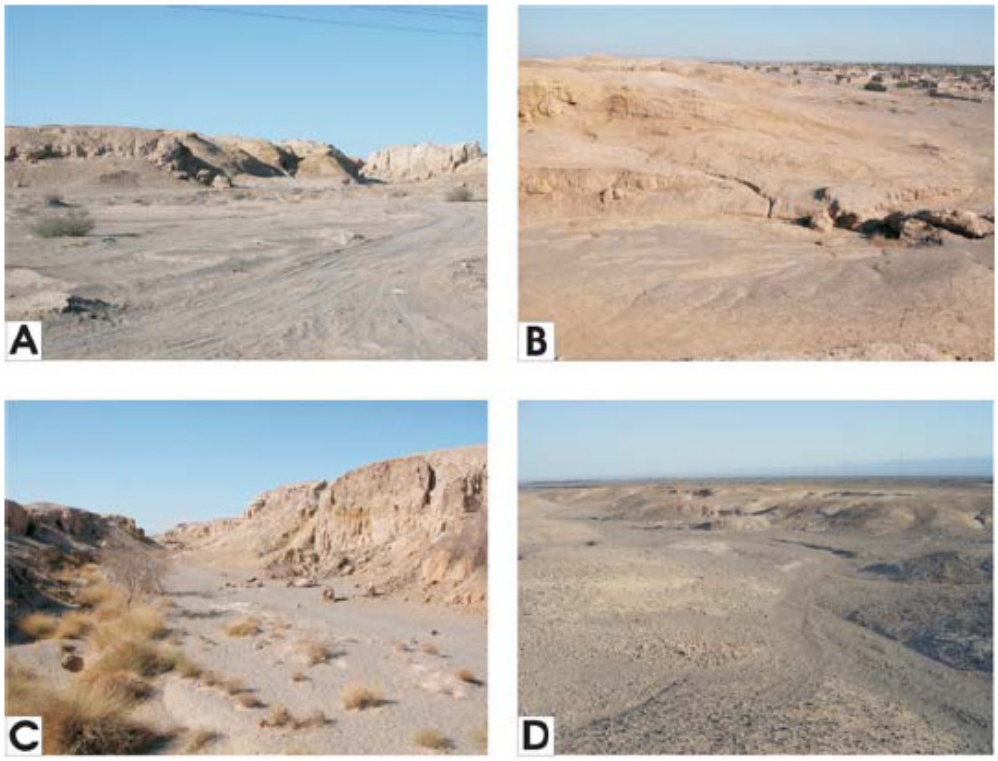

Fig. 6. Field photos of the Bam-Baravat ridge. (a) View west at 29◦ 4.2' N 58◦ 23.9'E, showing the eastern face of the ridge, about 15 m high, and a gully incised through it. (b) View north along the ridge at 29◦ 4.4'N 58◦ 23.9'E. Note the folded easterly dip of the young, fine-grained sediments of the ridge. Baravat is in the distance. (c) A typical gully incised through the uplifted ridge, at 29◦ 5.1'N 58◦ 23.9'E, looking west. (d) An abandoned, uplifted, dry valley on the crest of the ridge near its southern end, looking west.

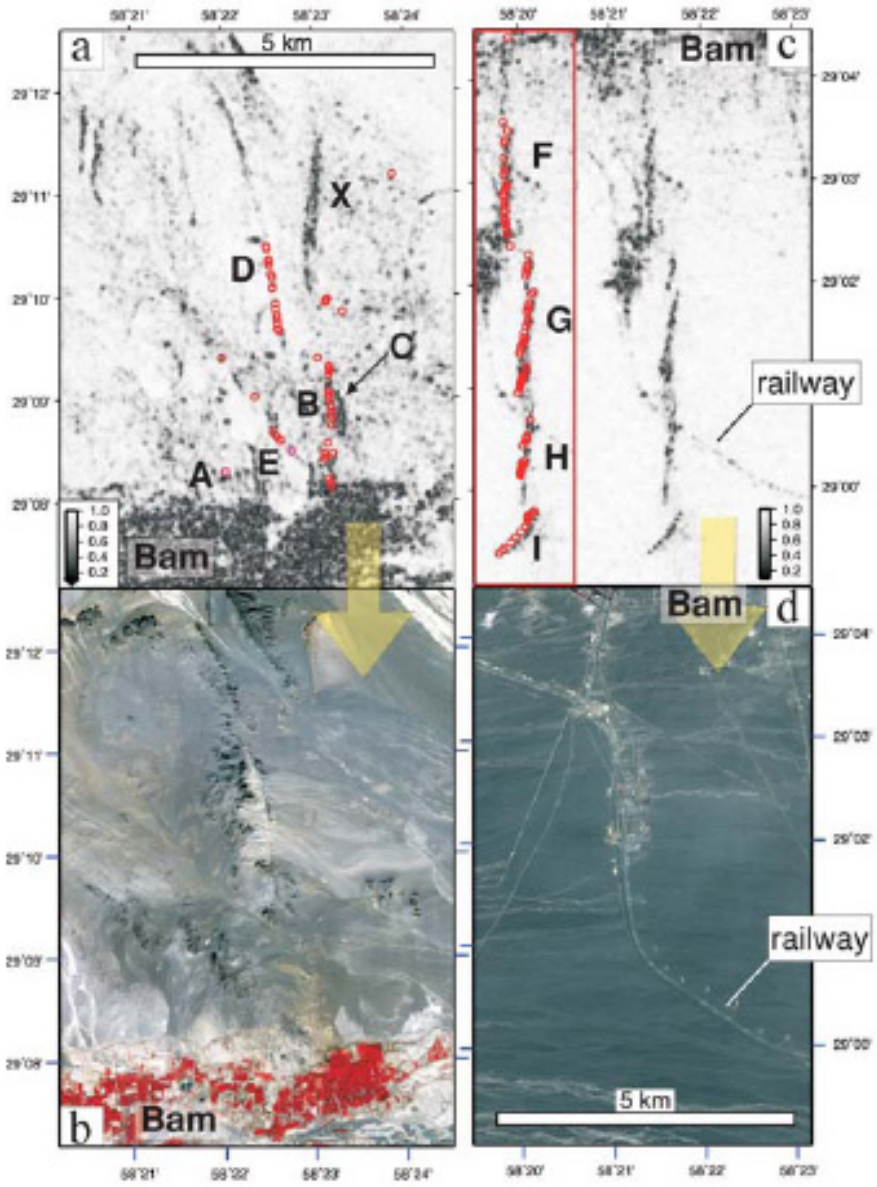

Fig. 7. Satellite images (b, d) and radar decorrelation images (a, c) for regions north (a, b) and south (c, d) of Bam. The big yellow arrows are to indicate that the panels are linked vertically. Boxes outlining the regions are indicated in Fig. 3. (b) and (d) are both ASTER images (bands 321-RGB). The red areas in (b) are cultivated regions north of Bam. (c) and (d) are both made from ENVISAT descending track 120 images acquired on 2003 December 3 and 2004 February 11. (a) Correlation map for the region north of Bam. Black shows a correlation decrease during interval straddling the earthquake. Red circles are GPS locations of surface ruptures observed in the field, with locations A–E discussed in the text. (b) ASTER image of the area in (a). (c) Correlation map, as in (a), for the region south of Bam. The red inset box is a repeat of the central part of the image with the GPS locations of ruptures in the field.

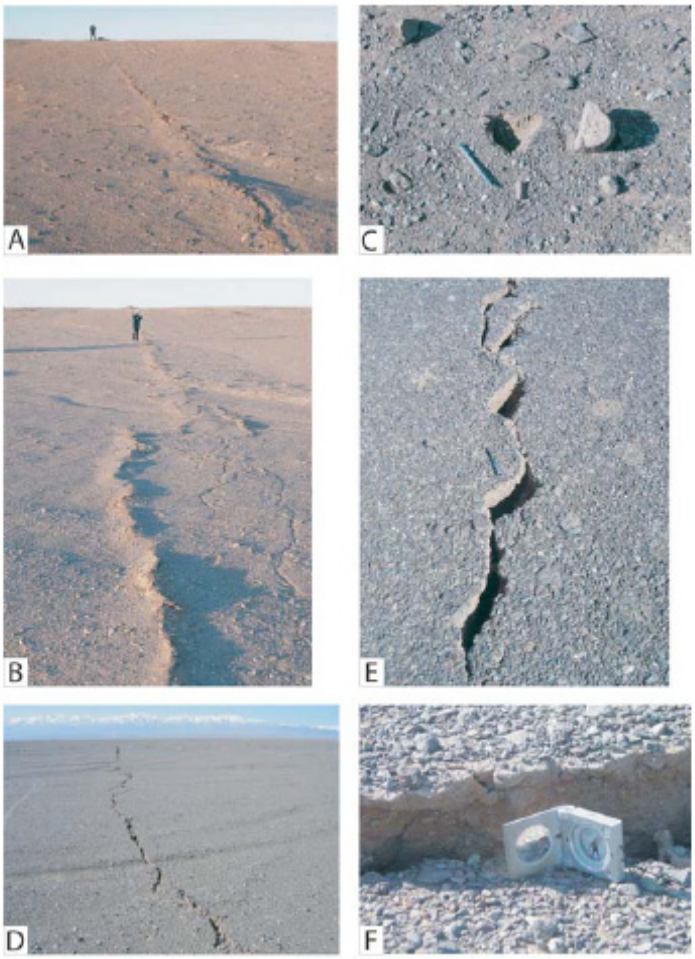

Fig. 8. Field photographs of coseismic surface ruptures. (a) North of Bam at 29° 8.93' N 58° 23.16'E; location B in Fig. 7(a). View is north. The rupture trace cuts the cemented desert pavement. (b) Detail looking south at the same location as (a), showing minor pop-up features in the buckled, cemented desert crust. (c) A stone dislodged from the cemented surface and thrown about 10 cm, at location C in Fig. 7a, north of Bam. (d) View south towards the Jebel Barez mountains along the main rupture trace south of Bam, at 29° 01.390' N 58° 21.565' E, on segment G in Fig. 7(c). (e) Detail of the rupture trace at 29° 01.623' N 58 ° 21.628' E showing the left-stepping tension fractures indicative of right-lateral slip. (f) A vertical offset on segment I of Fig. 7(c), showing the cemented upper few cm of the desert pavement.

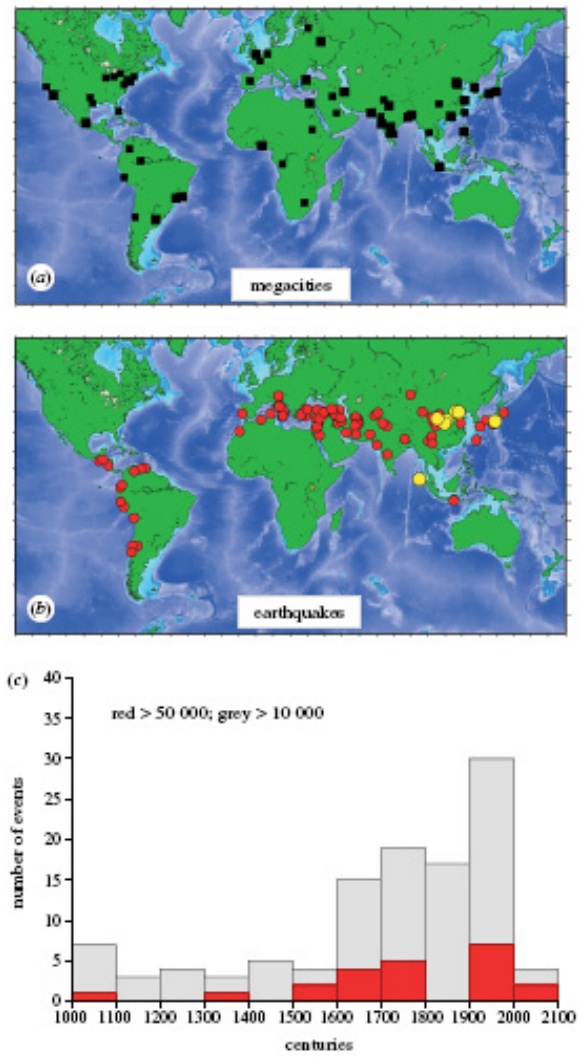

Fig. 9. (a) Cities with more than 5 million (small squares) or 10 million (large squares) population. (b) Earthquakes of the last 1000 years known to have killed more than 10,000 (red dots) or 100,000 (yellow dots) people. There are 113 earthquakes in this figure, many of their symbols overlying each other. A total of 34 of these earthquakes occurred in the last 100 years alone. (c) Histogram of the number of earthquakes killing more than 10,000 (grey) or 50,000 (red) people per century.

COSEISMIC AND ASEISMIC DEFORMATION ON FAULTS IN IRAN FROM INSAR

Eric Fielding, Paul Lundgren
Jet Propulsion Laboratory, California Institute of Technology, Pasadena, California, USA
Morteza Talebian, Hamid Nazari, Manouchehre Ghorashi
Geological Survey of Iran
Tim Wright, Gareth Funning, Richard Walker, Barry Parsons, James Jackson
Centre for Observation and Modelling of Earthquakes and Tectonics (COMET), UK

Interferometric synthetic aperture radar (SAR) or InSAR is becoming a well-accepted technique for measuring ground deformation caused by fault motion or other processes beneath the surface. Soon after the launch of the ERS-1 (Earth Remote Sensing) satellite by the European Space Agency in 1991, the InSAR data from the satellite was analyzed to measure deformation caused by the large 1992 M7.3 Landers, California earthquake (Massonnet et al., 1993). The ERS-1 satellite was joined in 1995 by the identical ERS-2 satellite, and the two ERS satellites were operated in a Tandem mission to acquire InSAR data with a separation of only one day. The ERS-1 satellite failed completely in 2000 and the ERS-2 satellite had a partial failure in January 2001 that caused it to be mostly not usable for InSAR after that time. The ERS satellites have C-band (5.6 cm wavelength) SAR instruments that work best for InSAR in areas with little vegetation.

For the ERS Tandem mission, there was a temporary ground receiving station operated in Central Asia that allowed the acquisition of nearly complete SAR coverage of Iran on many dates between 1996 and 1999, greatly improving on the scattered ERS SAR coverage acquired before that time. The first publication on an earthquake in Iran that exploited InSAR data studied the M6.6 1998 Fandoqa earthquake that ruptured part of the Gowk fault (Berberian et al., 2001). A more in-depth study and modeling of the InSAR data covering the Fandoqa earthquake showed that a large area of the shallow and shallowly dipping Shahdad thrust to the east and south moved during the six months after the earthquake (Fielding et al., 2004). The slip on the Shahdad thrust was apparently aseismic, releasing about the same amount of fault motion as a M6 earthquake without radiating detectable seismic waves. Another study using the early ERS data for InSAR analysis also found that slip on a shallow thrust fault or faults caused the 1994 Sefidabeh earthquake sequence (Parsons et al., 2006).

The European Space Agency (ESA) launched a new satellite called Envisat in 2002 that carries a more advanced SAR. It started acquiring SAR over Iran (and much of the rest of the Earth) regularly in 2003. This data provided the background coverage necessary for coseismic InSAR studies of the devastating 26 December 2003 Bam earthquake (M6.6), the first major earthquake imaged by Envisat SAR. ESA considered the Bam earthquake an event of special interest and makes the Envisat SAR data available to many researchers at no charge, so it has became the most studied InSAR event up to 2009. Two preliminary papers were published soon after the earthquake that utilized InSAR data to estimate the fault parameters of the earthquake (Talebian et al., 2004; Wang et al., 2004). The previously mapped Bam Fault, which is primarily a blind thrust fault that is pushing a fold up between the city of Bam and the town of Baravat, was shown by the InSAR data to not be the main causative fault for the Bam earthquake. The main fault was a strike-slip fault about 5 km to the west of where the Bam Fault reaches the surface. Using the InSAR data, Talebian et al. (2004) located in the field the surface ruptures above this

main fault that ruptured in 2003. Some authors have called this fault the Arg-e-Bam Fault because it projects beneath the city of Bam near the Arg-e-Bam fort that was destroyed in the earthquake.

An additional measurement can be calculated from InSAR data, the correlation or coherence of the InSAR phase. This provides additional information on the amount of change or disruption within the pixels of the SAR interferograms. An extensive study of the InSAR coherence of the Bam coseismic interferograms mapped the details of the surface ruptures, and confirmed the surface ruptures with additional field mapping (Fielding et al., 2005). The field mapping showed that the surface ruptures had a maximum offset of about 25 cm. The coherence changes also show the degree of damage to buildings in the city of Bam, once other causes of coherence changes are removed by taking the ratio of pre-earthquake and coseismic coherence images (Fielding et al., 2005).

Funning et al. (2005) performed an in-depth analysis and modeling of the coseismic deformation of the Bam earthquake. They expanded on the preliminary results of Talebian et al. (2004), showing that the InSAR data require a second fault rupture in addition to the main fault rupture on the Arg-e-Bam Fault. This secondary rupture, which had a significant thrust component, only occurred at depths of about 4-6 km beneath the surface on a fault that might be the down-dip extension of the Bam Fault. Modeling of the slip distribution showed that the main fault slip occurred on a near-vertical (roughly 85 degrees east dip) fault that projects to the surface at the location of the surface ruptures mapped from the InSAR coherence and field mapping. The rupture extends beneath the city of Bam, even though the surface ruptures stop south of the city, and passes about 400 m away from the strong motion station installed at Bam. The peak slip of more than 300 cm was at a depth of about 5 km and decreased upward, which is consistent with the small amount of slip observed in the field (Funning et al., 2005). The slip also decreases downward to terminate at a depth of around 10-12 km.

First-order modeling of the strong motion recording from the Bam station shows that the fault ruptured from south to north and likely started at a depth of around 8 km at the southern edge of the main rupture (Bouchon et al., 2006; Jackson et al., 2006). This means that the rupture propagated upward and northward directly towards the city of Bam, crossing the main patch of very high slip derived from the InSAR analysis. This explains the very large acceleration and velocities observed in the strong motion record and the extreme level of damage to the city. Analysis of teleseismic data for the Bam earthquake also confirms the presence of a secondary thrust slip subevent that occurred after the main strike-slip rupture (Jackson et al., 2006).

Envisat data was acquired over the Bam area regularly for three and a half years after the 2003 earthquake. Time-series analysis of this postseismic record of surface deformation showed that several processes were active (Fielding et al., 2009). There was afterslip on the main fault that ruptured in 2003 (or very close faults), primarily in the areas to the south and north and shallower than the main coseismic slip. This is consistent with a velocity strengthening fault rheology in those areas. There is also an area of postseismic poroelastic rebound in the place where the main coseismic rupture had a constraining bend. The surface directly above the main coseismic slip patch subsided after the earthquake beyond the constraining bend, with a small amount of motion towards the fault. This is consistent with a volume change at shallow depths (<1 km), and was interpreted by Fielding et al. (2009) as recovery of coseismic dilatancy in the material at those depths. The apparent deficit of coseismic slip at the surface compared with the

larger amount of slip at depths below 2 km can be explained by distributed shear in the upper layers, which is likely to cause dilatancy or expansion of the material. This dilatancy then reversed in the years after the earthquake. This observation and the afterslip indicate that the shallow layers above the main coseismic slip do not have a large elastic stress that will need to be released in a future large earthquake, which is some good news for the rebuilding of Bam. Unfortunately, we cannot detect postseismic release of stress on the deeper fault or faults that must extend to the bottom of the crust beneath the main coseismic rupture, deeper than 10-12 km depth. This deeper fault could still rupture in the near future and bring new devastation to the city of Bam, but we don't know what is the geometry or location of the deeper faults.

ACKNOWLEDGMENTS

Part of this work was performed at the Jet Propulsion Laboratory, California Institute of Technology under contract with the National Aeronautics and Space Administration. ERS SAR data are copyrighted and courtesy of the European Space Agency under projects AO3-213 and AO3-371. Envisat SAR data are copyrighted and courtesy of ESA under project AOE-668.

REFERENCES

Berberian, M., Jackson, J.A., Fielding, E.J., Parsons, B.E., Priestley, K., Qorashi, M., Talebian, M., Walker, R., Wright, T.J., and Baker, C., 2001, The 1998 March 14 Fandoqa earthquake (M_w 6.6) in Kerman province, southeast Iran: Re-rupture of the 1981 Sirch earthquake fault, triggering of slip on adjacent thrusts and the active tectonics of the Gowk fault zone: Geophysical Journal International, v. 146, p. 371-398.

Bouchon, M., Hatzfeld, D., Jackson, J.A., and Haghshenas, E., 2006, Some insight on why Bam (Iran) was destroyed by an earthquake of relatively moderate size: Geophys. Res. Lett., v. 33, p. 1-4.

Fielding, E.J., Lundgren, P.R., Bürgmann, R., and Funning, G.J., 2009, Shallow fault-zone dilatancy recovery after the 2003 Bam earthquake in Iran: Nature, v. 458, p. 64-68.

Fielding, E.J., Talebian, M., Rosen, P.A., Nazari, H., Jackson, J.A., Ghorashi, M., and Walker, R., 2005, Surface ruptures and building damage of the 2003 Bam, Iran, earthquake mapped by satellite synthetic aperture radar interferometric correlation: J. Geophys. Res., v. 110, p. B03302, doi:10.1029/2004JB003299.

Fielding, E.J., Wright, T.J., Muller, J., Parsons, B.E., and Walker, R., 2004, Aseismic deformation of a fold-and-thrust belt imaged by synthetic aperture radar interferometry near Shahdad, southeast Iran: Geology, v. 32, p. 577-580.

Funning, G.J., Parsons, B.E., Wright, T.J., Jackson, J.A., and Fielding, E.J., 2005, Surface displacements and source parameters of the 2003 Bam (Iran) earthquake from Envisat advanced synthetic aperture radar imagery: J. Geophys. Res., v. 110, p. B09406,doi:10.1029/2004JB003338.

Jackson, J.A., Bouchon, M., Fielding, E.J., Funning, G.J., Ghorashi, M., Hatzfeld, D., Nazari, H., Parsons, B., Priestley, K., Talebian, M., Tatar, M., Walker, R., and Wright, T.J., 2006, Seismotectonic, rupture-process, and earthquake-hazard aspects of the 26 December 2003 Bam, Iran, earthquake: Geophys J Int, v. 166, p. 1270-1292.

Massonnet, D., Rossi, M., Carmona, C., Adragna, F., Peltzer, G., Feigl, K., and Rabaute, T., 1993, The displacement field of the Landers earthquake mapped by radar interferometry: Nature, v. 364, p. 138–142.

Parsons, B., Wright, T., Rowe, P., Andrews, J., Jackson, J., Walker, R., Khatib, M., Talebian, M., Bergman, E., and Engdahl, E.R., 2006, The 1994 Sefidabeh(eastern Iran) earthquakes revisited: new evidence from satellite radar interferometry and carbonate dating about the growth of an active fold above a blind thrust fault: Geophysical Journal International, v. 164, p. 202-217.

Talebian, M., Fielding, E.J., Funning, G.J., Jackson, J.A., Nazari, H., Parsons, B.E., Priestley, K., Ghorashi, M., Rosen, P.A., Walker, R., and Wright, T.J., 2004, The 2003 Bam (Iran) earthquake: rupture of a blind fault: Geophys. Res. Lett, v. 31, p. L11611, doi:10.1029/2004GL020058.

Wang, R., Xia, Y., Grosser, H., Wetzel, H.U., Kaufmann, H., and Zschau, J., 2004, The 2003 Bam (SE Iran) earthquake: precise source parameters from satellite radar interferometry: Geophysical Journal International, v. 159, p. 917-922.

SIMULATION OF GROUND MOTION TIME-HISTORIES

Sanaz Rezaeian[1] and Armen Der Kiureghian[2]
[1] Doctoral student, University of California, Berkeley, CA, USA. sanazr@berkeley.edu
[2] Taisei Professor of Civil Eng., University of California, Berkeley, CA, USA. adk@ce.berkeley.edu

ABSTRACT

A method for generating an ensemble of artificial ground motion time-histories that are compatible with a given set of earthquake and site characteristics is presented. Acceleration time-histories are modeled by a stochastic process that is high-pass filtered. The stochastic model captures the main features of recorded ground motions, including the evolutionary intensity and the time-varying predominant frequency and bandwidth. The high-pass filtering assures zero residual velocity and displacement of the motion, as well as realistic response spectral values at long periods. Based on investigation of many recorded ground motions, predictive relations are constructed that empirically link the ground motion model parameters to selected earthquake and site characteristics. These predictive relations facilitate random generation of the model parameters, which is the key to realistically representing the natural variability of ground motions, for a given set of earthquake and site characteristics.
Keywords: earthquake, stochastic simulation, ground motions for time-history dynamic analysis

INTRODUCTION

In seismic design and analysis of structures, development of ground motions is a crucial step because even with the most sophisticated and accurate methods of structural analysis, the validity of predicted structural responses is in the mercy of the selected ground motions. Several levels of ground motions are commonly considered for seismic assessment of a structure.

For motions with low intensity levels, where the structure is expected to remain elastic, response spectrum analysis is usually sufficient. This type of analysis only requires knowledge of the ground motion spectral values. One of the most practical approaches to obtain these values is to use empirically based ground motion prediction equations (GMPEs), also known as attenuation relations. Many GMPEs have been developed that predict the median and standard deviation of ground motion spectral values for a range of spectral periods; the most recent of them is the Next Generation Attenuation (NGA) relations [1]. These GMPEs have been calibrated against observed data and are commonly used in practice.

For motions with high intensity levels, where nonlinear structural behavior is likely, time-history dynamic analysis is necessary. This type of analysis requires knowledge of acceleration time-histories. Prediction of future ground motion time-histories is not an easy task because many factors, some unknown, contribute to the attenuation of the seismic waves from their source of generation to the site of interest. Several seismological-based methods are available for generating artificial ground motions (see, e.g., [2]-[3] for recently improved methods); however, these tend to be too complicated for use in practice and require information that may not be available to the designer. As a result, it is common practice to use real motions that were recorded during a previous earthquake, even though it is unlikely for a future ground motion to

be exactly the same as a previous one. In using previously recorded motions, difficulties arise because ground motion properties vary for different earthquake and site characteristics, and recorded motions are not available for all types of earthquakes in all regions. As a result, engineers are forced to select ground motions recorded at locations other than the site of interest and they modify them to represent the design response spectrum of the project site. Many controversies exist on methods of selecting and modifying real records, which could result in unrealistic ground motion properties. One solution to this problem is to use simulated time-histories in conjunction or in the place of real records when lack of recorded motions becomes a problem. The purpose of this study is to provide a method of generating an appropriate suite of simulated time-histories for a given set of earthquake and site characteristics that are commonly available to a design engineer.

To achieve this goal, a stochastic process that is high-pass filtered is used to model acceleration time-histories. This model was developed in a previous study and the details can be found in [4]. The model employs six parameters that are related to the physical features of the ground motion and their values can be identified for a given accelerogram. Parameter identification is done by matching certain statistical characteristics of the model and the target accelerogram, which are representatives of the time-varying intensity, frequency and bandwidth of an acceleration time-history. The model parameters are identified for a large number of recorded accelerograms with known earthquake and site characteristics. The resulting observational data are used to construct predictive relations for the model parameters in terms of earthquake and site characteristics by the means of regression analysis. These predictive relations allow random generation of the model parameters for a given set of earthquake and site characteristics. Each set of randomly generated model parameters is used to simulate a ground motion time-history. Variation among these simulated ground motions resembles the natural variability of recorded ground motions and is an important advantage of the presented method. The adequacy of simulated acceleration, velocity, and displacement time-histories are illustrated through an example. Furthermore, as a validation measure, it is shown that the resulting elastic response spectra accurately capture both the median and the variability of response spectra of recorded ground motions as reflected in the NGA GMPEs.

This procedure was partially presented in [5] and is briefly summarized in this paper. More details in regards to the procedure and the predictive relations are presented in [6].

STOCHASTIC GROUND MOTION MODEL

Earthquake ground motions have nonstationary characteristics both in time and frequency domains. Variation of the ground motion intensity in time is referred to as the temporal nonstationarity. Variation of the frequency content of the ground motion in time is referred to as the spectral nonstationarity. To simulate ground motions, a fully nonstationary stochastic model is developed that is based on time-modulating a filtered white-noise process with the filter having time-varying parameters. Whereas the time-modulation provides temporal nonstationarity, the variation of filter parameters over time achieves spectral nonstationarity. The model is mathematically defined by

$$x(t) = q(t, \boldsymbol{\alpha}) \left\{ \frac{1}{\sigma_h(t)} \int_{-\infty}^{t} h[t - \tau, \boldsymbol{\lambda}(\tau)] w(\tau) d\tau \right\} \quad (1)$$

where $x(t)$ represents acceleration as a function of time, which can be interpreted as the superposition of filter responses to a sequence of pulses with the time of application τ. In this expression, $q(t, \boldsymbol{\alpha})$ is the time-modulating function with parameters $\boldsymbol{\alpha}$; $w(\tau)$ is a white-noise process; the integral inside the curled brackets is a filtered white-noise process with $h[t - \tau, \boldsymbol{\lambda}(\tau)]$ denoting the impulse response function (IRF) of a linear filter with time-varying parameters $\boldsymbol{\lambda}(\tau)$; and $\sigma_h(t)$ is the standard deviation of the process represented by the integral inside the curled brackets. For more detail on discretization and implementation of this model see [4]. Due to the normalization by $\sigma_h(t)$, the process inside the curled brackets has unit variance so that $q(t, \boldsymbol{\alpha})$ represents the standard deviation of $x(t)$ and thus completely defines the temporal nonstationarity of the process, while the spectral nonstationarity is defined separately by the unit-variance process inside the curled brackets.

In this study, $q(t, \boldsymbol{\alpha})$ is selected to be a "gamma" function: $\alpha_1 t^{\alpha_2 - 1} \exp(-\alpha_3 t)$, with $\boldsymbol{\alpha} = (\alpha_1, \alpha_2, \alpha_3)$, where $0 < \alpha_1, \alpha_3$ and $1 < \alpha_2$. This functional form is chosen due to its flexibility and ease of relating its parameters to physical properties of accelerograms. For the filter, an IRF is selected that corresponds to the pseudo-acceleration response of a single-degree-of-freedom linear oscillator with $\boldsymbol{\lambda}(\tau) = (\omega_f(\tau), \zeta_f(\tau))$, where $\omega_f(\tau)$ represents the filter frequency and $\zeta_f(\tau)$ represents the damping ratio of the filter. Both of these parameters depend on the time of application of the pulse (see [4] for more details).

The simulated process in (1) is high-pass filtered to assure zero residual velocity and displacement of the motion, as well as realistic response spectral values at long periods. Without such filtering, stochastically generated ground motions tend to overestimate response spectral values in the long period range (usually greater than 2 seconds). A critically damped oscillator is selected as the high-pass filter. The corrected acceleration record, denoted $z''(t)$, is obtained as the solution of the differential equation

$$z''(t) + 2\omega_c z'(t) + \omega_c^2 z(t) = x(t) \quad (2)$$

where ω_c is the frequency of the high-pass filter (also referred to as the corner frequency in [4]). It is noted that this filtering has insignificant influence on the statistical characteristics representing the evolutionary intensity and frequency content of the acceleration process.

Model Parameters

The stochastic model in (1) is defined in terms of a set of parameters. These parameters are divided into two groups: modulating function parameters and filter parameters, which respectively characterize the time modulation and the evolutionary frequency content of the acceleration time-history.

As mentioned previously, the modulating function parameters $(\alpha_1, \alpha_2, \alpha_3)$, are related to three variables that directly represent the physical properties of an accelerogram (I_a, D_{5-95}, t_{mid}). I_a represents the expected Arias intensity, a measure of the total energy defined as $\int_0^{t_n} x(t)^2 dt$ where t_n denotes the total duration of motion. D_{5-95} represents the effective duration of motion

defined as the time interval between the instants at which the 5% and 95% levels of I_a are reached. t_{mid} represents the time at the middle of the strong shaking phase of the motion, which in this study is assumed to occur at the 45% level of I_a. This assumption is based on the observation that the time it takes to rise from zero to the strong shaking phase of an accelerogram is usually shorter that the time it takes to fall from the strong shaking phase back to zero. Relations that allow estimation of $(\alpha_1, \alpha_2, \alpha_3)$ from (I_a, D_{5-95}, t_{mid}) are based on the fact that the selected functional form for $q(t, \boldsymbol{\alpha})$ is proportional to the gamma probability distribution function (for more details see [5] or [6]).

After investigation of many accelerograms, appropriate functional forms were selected for the filter parameters. The filter frequency is represented by a linear function: $\omega_f(\tau) = \omega_{mid} + \omega'(\tau - t_{mid})$, where ω_{mid} denotes the filter frequency at the middle of the strong shaking phase and ω' denotes the rate of change of the filter frequency over time. Due to the observed insignificant change in the damping ratio during the effective duration of motion, the filter damping is simply represented by a constant factor: $\zeta_f(\tau) = \zeta_f$.

In summary, the physically-based parameters (I_a, D_{5-95}, t_{mid}) and $(\omega_{mid}, \omega', \zeta_f)$ completely define the time modulation and the evolutionary frequency content of the nonstationary ground motion model. Our simulation procedure is based on generating samples of these parameters for given earthquake and site characteristics.

Identification of Model Parameters

The six model parameters can be identified for a target recorded acceleration time-history by matching the characteristics of the ground motion model to those of the given accelerogram. The complete separation of the temporal and spectral nonstationary characteristics of the process facilitates parameter identification by allowing the modulating function parameters to be identified prior to and independently of the filter parameters.

The modulating function parameters (I_a, D_{5-95}, t_{mid}), that control the evolving intensity of the process are naturally matched with the corresponding measures of Arias intensity, effective duration, and the time at the middle of the strong shaking phase (taken as time to the 45% level of Arias intensity) of the target accelerogram.

Then, the filter parameters $(\omega_{mid}, \omega', \zeta_f)$ that control the evolving predominant frequency and bandwidth of the process are identified. This is done by matching the statistical characteristics of the process including the cumulative mean number of zero-level up-crossings (as a surrogate measure of the predominant frequency) and the mean rate of negative maxima and positive minima (as a surrogate measure of the bandwidth) to the corresponding measures of the target accelerogram (see [4]-[6]).

The six model parameters are identified for many recorded ground motions in order to obtain observational data. These data are then used to construct predictive equations, by the means of regression analysis that allow random generation of the model parameters for a given set of earthquake and site characteristics.

STRONG MOTION DATABASE

The strong motion database used in this study is a subset of the ground motions used in the development of Campbell-Bozorgnia NGA (CB-NGA) model [1]. The accelerograms in the database are representative of "free-field" ground motions recorded in shallow crustal events in tectonically active regions. Four variables (F, M, R_{rup}, V_{s30}), commonly available to a design engineer, are selected to represent earthquake and site characteristics. These variables respectively represent the faulting mechanism, the moment magnitude, the closest distance from the site to the ruptured area, and the shear wave velocity at the top 30 meters of the site. F assumes values of 0 and 1 for strike-slip and reverse types of faulting. The selected earthquakes in the database have $6.0 \leq M$, $10km \leq R_{rup} \leq 100km$, and $600m/s \leq V_{s30}$. These limitations were enforced for the database to represent motions that are capable of producing nonlinear behavior in structures, and also to exclude the effects of near-fault ground motions and soil nonlinearity. As a result, the database contains 31 pairs of horizontal recordings from 12 earthquakes for strike-slip type of faulting, and 72 pairs of horizontal recordings from 7 earthquakes for reverse type of faulting. Figure 1 demonstrates a good magnitude-distance distribution of the data.

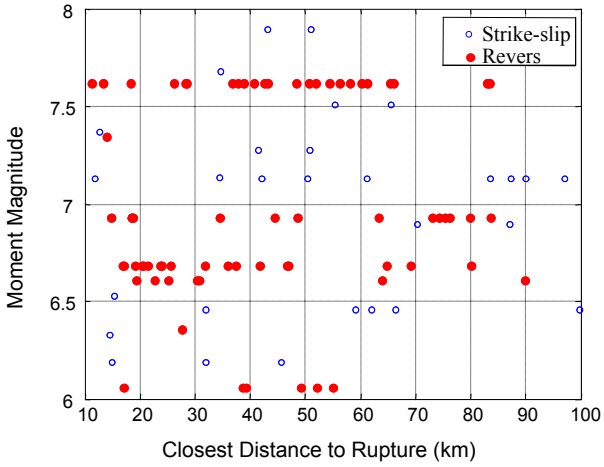

Fig. 1. Distribution of magnitude and distance of the records in the database.

PREDICTIVE RELATIONS FOR THE MODEL PARAMETERS

As mentioned previously, sample observations of the model parameters are obtained by fitting the stochastic ground motion model to the recorded motions in the database in terms of their time-varying intensity and their evolutionary frequency content. After obtaining these observational data, regression is used to construct empirical prediction equations for each parameter in terms of earthquake and site characteristics. This procedure results in six predictive models of the form

$$\Phi^{-1}[F_\theta(\theta)] = \mu\left(F, M, R_{rup}, V_{s30}, \boldsymbol{\beta}\right) + \eta + \epsilon \tag{3}$$

where θ represents a model parameter, $\Phi^{-1}[.]$ is the inverse of the standard normal cumulative distribution function and $F\theta\,[.]$ is the cumulative distribution function of θ. As a result, the left hand side of (3) satisfies the normality criterion required for the response variable in regression

analysis. To identify $F_{\theta}[.]$ probability distributions are assigned to the model parameters by the method of moments and maximum likelihood estimation. Figure 2 shows the assigned distributions (see [6] for more details on the distribution boundaries and parameters).

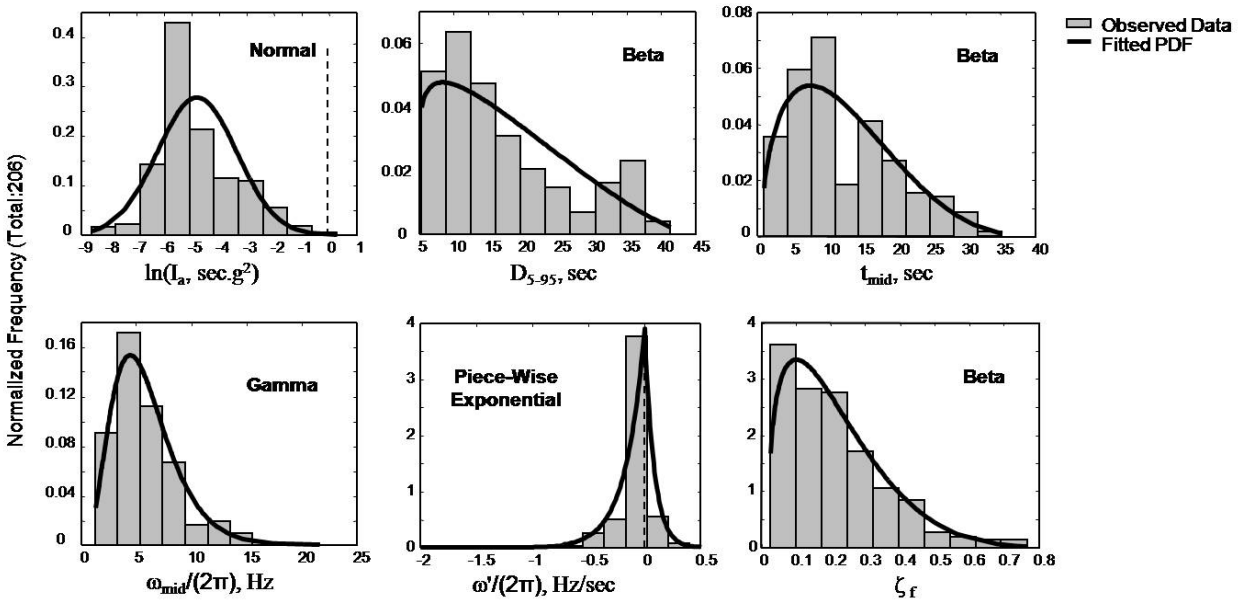

Fig. 2. Assigned probability density functions (PDFs) superimposed on observed normalized frequency diagrams of model parameters.

In (3), the function μ represents the predicted mean of θ conditioned on earthquake and site characteristics and involving the set of regression coefficients β. The summation of η and ε represents the total regression error defined as the difference between the observed and predicted values of the model parameter. The regression error is divided into two terms because the database contains different number of recordings for different earthquakes. Therefore, to account for the specific effects of individual earthquakes on the database (since this effect is random among earthquakes, this type of regression is usually referred to as the random-effect modeling), η denotes the inter-event error (error among data belonging to different earthquakes), and ε denotes the intra-event error (error among the data belonging to records of an individual earthquake). η and ε are independent zero-mean normally distributed random variables whose variances must be identified based on observed data.

Regression coefficients and variances of the error terms, which are different for each model parameter, are identified by calibrating each regression model against data using maximum likelihood estimation (MLE) methods. Possible dependencies among the model parameters are then captured by identifying the cross correlations between their errors. Detailed regression results are presented in [6].

SIMULATION OF A SUITE OF GROUND MOTIONS

Given a design scenario that specifies the earthquake and site characteristics (*F, M,* R_{rup}*,* V_{s30}), jointly normal inter-event errors, η, and jointly normal intra-event errors, ϵ, are randomly simulated for the set of model parameters and are used in the empirical prediction equations to generate an ensemble of possible values for the model parameters. This process properly accounts for the cross-correlations between the model parameters. Each set of six model parameters is then used to generate an artificial accelerogram that represents a possible future ground motion for the specified design scenario.

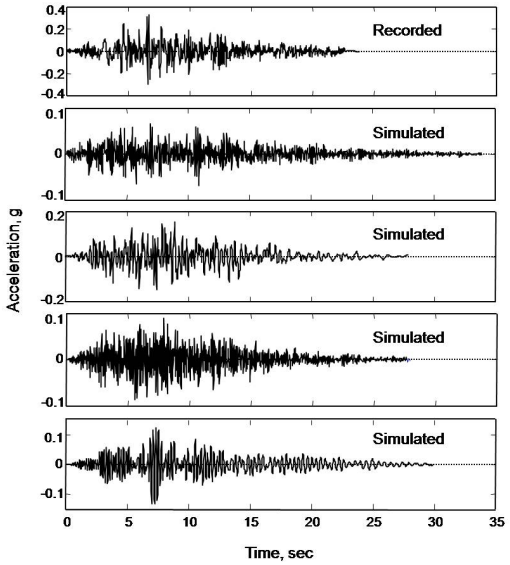

Realizations of model parameters:					
I_a $(sec.g^2)$	D_{5-95} (sec)	t_{mid} (sec)	$\frac{\omega_{mid}}{2\pi}$ (Hz)	$\frac{\omega'}{2\pi}$ $\left(\frac{Hz}{\text{sec}}\right)$	ζ_f
0.0924	12.30	6.78	5.90	0.12	0.26
0.0076	17.23	6.27	6.88	−0.01	0.14
0.0348	14.22	7.22	4.48	−0.16	0.38
0.0091	14.07	6.31	10.75	−0.24	0.26
0.0230	14.87	8.32	4.36	−0.15	0.03

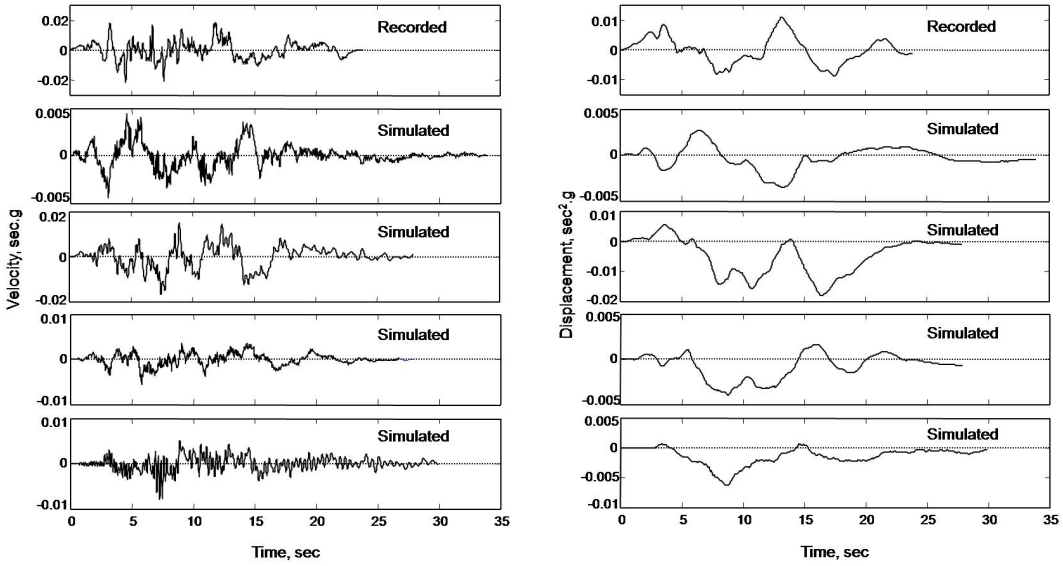

Fig. 3. Acceleration, velocity, and displacement time-histories of one recorded and four simulated motions corresponding to the design scenario earthquake.

Figure 3 shows four simulated and one real recording for a given design scenario of $F = 1$, $M = 7.35$, R_{rup}, $= 14$ km and V_{s30} =660 m/s. Observe how different the shape and properties of the ground motions can be among the time-histories representing a future event. Figure 3 also demonstrates that the overall features of the resulting suite of acceleration, velocity, and displacement time-histories compare well with real recorded motions.

ELASTIC RESPONSE SPECTRUM

As a validation measure for the presented method of ground motion simulation, elastic 5% damped response spectra of many simulated motions for various design scenarios were generated and their statistics were compared to existing GMPEs. In general, the median and variability of the acceleration and displacement response spectra of simulated motions compare well against their corresponding predicted values by the NGA models (for more details and limitations on spectral periods and earthquake and site characteristics refer to [6]). Figure 4 shows this comparison against CB-NGA model for $F = 0$, $M = 7.5$, R_{rup}, $= 20$ km and V_{s30} =760 m/s.

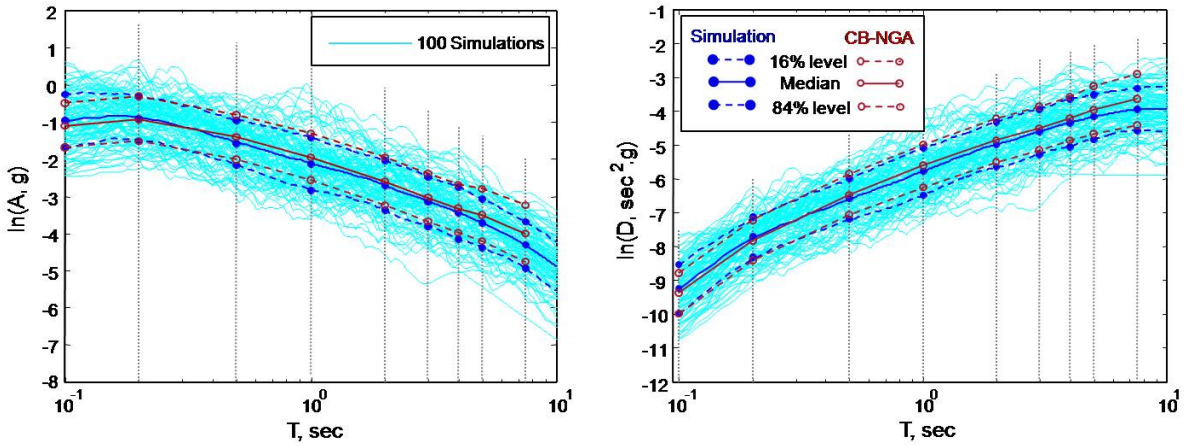

Fig. 4. Natural logarithm of acceleration (left) and displacement (right) response spectrum (5% damped). 16%, median, and 84% levels of 100 simulations are compared to their corresponding values predicted by CB-NGA model.

CONCLUDING REMARKS

A new method for simulating an ensemble of far field strong ground motions on firm ground for a given set of earthquake and site characteristics is presented. An important achievement of the proposed method is that, by random generation of the model parameters, it provides a realistic representation of the natural variability of ground motions. This variability is comparable with the variability observed in existing ground motion prediction equations for response spectrum that are based on the NGA database.

ACKNOWLEDGEMENT

This work was supported by the State of California through the Transportation Systems Research Program of the Pacific Earthquake Engineering Research Center (PEER). Any opinions, findings and conclusions or recommendations expressed in this material are those of the authors and do not necessarily reflect those of the funding agency. The support and guidance of Dr. Yousef Bozorgnia, associate director of PEER, is appreciated.

REFERENCES

[1] Campbell, K.W. and Y. Bozorgnia (2007). Campbell-Bozorgnia NGA Ground Motion Relations for the Geometric Mean Horizontal Component of Peak and Spectral Ground Motion Parameters. *PEER 2007/02 Report, Pacific Earthquake Eng. Research Center (PEER)*, University of California, Berkeley, CA.

[2] Frankel, A. (2009). A constant stress-drop model for producing broadband synthetic seismograms: Comparison with the Next Generation Attenuation relations. *Bulletin of the Seismological Society of America,* **99:** 664-680.

[3] Causse, M., F. Cotton, C. Cornou and P. Bard (2008). Calibrating median and uncertainty estimates for a practical use of Empirical Green's Functions technique. *Bulletin of the Seismological Society of America*, **98:** 344-353.

[4] Rezaeian, S. and A. Der Kiureghian (2008). A stochastic ground motion model with separable temporal and spectral nonstationarities. *Journal of Earthquake Engineering and Structural Dynamics*, **37:** 1565-1584.

[5] Rezaeian, S., A. Der Kiureghian and Y. Bozorgnia (2008). Stochastic ground motion model with time-varying intensity, frequency and bandwidth characteristics. *14th World Conference on Earthquake Engineering (14WCEE) Proceedings,* Beijing, China, Paper No. 03-03-0033.

[6] Rezaeian, S. and A. Der Kiureghian (2009). Simulation of synthetic ground motions for specified earthquake and site characteristics. Under preparation.

CRUCIAL ROLE OF COORDINATED MULTIDISCIPLINARY SEISMIC RESEARCH

Yousef Bozorgnia
Associate Director, Pacific Earthquake Engineering Research Center (PEER),
University of California, Berkeley, CA 94720

ABSTRACT

This paper discusses the crucial role and various elements of coordinated multidisciplinary seismic research. As an example, a multidisciplinary earthquake center, Pacific Earthquake Engineering Research Center (PEER), is briefly overviewed. PEER is a national engineering research center with initial multi-year funding from the US National Science Foundation (NSF). PEER is now a self-sufficient center with research funding from various Federal agencies, the State of California, and private industry. Within PEER, two well-coordinated multidisciplinary seismic research programs are also exemplified. The first example is the Next Generation Attenuation (NGA) models. The NGA program is a mega research program at PEER with numerous coordinated sub-projects. NGA has two major phases: (a) ground motion models for shallow crustal earthquakes in active tectonic regions (NGA-West), and (b) development of ground motion prediction equations (GMPEs) for stable continental regions such as the central & eastern US (NGA-East). The NGA-West has had major impacts on almost all seismic hazard analysis on the West Coast of the US and in similar tectonic regions of the world. The NGA-East is in its early development, and will be completed in a few years. The second example of a multidisciplinary program within PEER is the Tall Buildings Initiative (TBI), which is another well-coordinated research activity with the goal of providing guidelines for seismic analysis and the design of tall buildings close to active faults. TBI has numerous sub-projects ranging from ground motion issues, soil-structure interaction, case study buildings, to socio-economic aspects of the seismic design of tall buildings.

INTRODUCTION

Earthquake engineering and science are fundamentally multidisciplinary activities. Such a multidisciplinary emphasis is evident in the goal of earthquake engineering "*to reduce seismic risks to a socio-economically acceptable level*" (Bertero and Bozorgnia, 2004). In this definition, various multiple disciplines have to be coordinated to quantify the ground motion hazard, estimate the exiting seismic risk on the built environment, assess the socio-economic impacts of earthquakes, and measure risk reduction through various mitigation and prevention measures. Such multidisciplinary efforts require integration of a wide spectrum of expertise ranging from geology and seismology, to various engineering disciplines, to social and economic analyses. However, advances in each of such disciplines are necessary but not sufficient conditions for progress towards complex real-world solutions of reducing seismic risks.

For example, for estimation of financial losses in a future earthquake it is important to predict median ground motion and its uncertainties, as well as structural and non-structural fragilities. That is, we need data and analysis from fault rupture all the way to structural and non-structural damage assessments.

Another example is performance-based earthquake engineering (Krawinkler and Miranda, 2004), which requires progress and interaction among several disciplines from earth science to those that examine socio-economic decision variables.

On the research aspects of earthquake engineering and science, any national or international research center with a goal of understanding and providing solutions to complex impacts of earthquakes on the society, should address issues in various disciplines such as: geology, seismology; ground motion hazard analysis; geotechnical engineering; structural engineering; lifelines; and social and financial aspects of earthquakes. A coordinated interaction among such disciplines is crucial. This is a challenging effort in both academia and the practicing sector. For example, the traditional legacy in academic research is more disciplinary than multidisciplinary, and removing such barriers may take an enormous amount of careful planning and implementation.

In the following sections, background on the NSF multidisciplinary Engineering Research Centers (ERCs) is provided; followed by a brief overview of the Pacific Earthquake Engineering Research Center (PEER). Two examples of multidisciplinary research programs at PEER will also be presented to show the necessity, and fruitful outcome, of well-coordinated seismic research.

NSF ENGINEERING RESEARCH CENTERS

In 1985, the US National Science Foundation (NSF) initiated a national program to form Engineering Research Centers (ERCs). The ERC program was designed to create long-term collaborations between universities and industry, create new industry-relevant knowledge at the intersections of the traditional disciplines, and prepare a new generation of engineering leaders who are more capable of engaging successfully in team-based, cross-disciplinary engineering practice (NSF ERC, 1997). The ERC Program grew out of concern expressed in the early 1980s by the US National Academy of Engineering and NSF that: (1) rapid technological advances were occurring at the intersection of engineering and other disciplines, requiring a cross-disciplinary approach to engineering that had not been incorporated into engineering research or practice; and (2) a mismatch had developed between the way engineering was carried out in industry and the way students were being trained in universities.

Since 1985, numerous multidisciplinary ERCs have been funded by the NSF. The NSF requires a well-established management organization for such ERCs. For example, the centers should have a director, associate Director, a research committee, defined research areas, a Business and Industry Partnership (BIP) program, etc. The ERCs are also strongly encouraged to interact with private industry and state governments, and to attract other extramural funding in addition to that from the NSF. The centers are funded by the NSF for a finite duration, and they are envisioned to be self-sustaining beyond the NSF's funding period. One such ERC has been the Pacific Earthquake Engineering Research Center (PEER).

PACIFIC EARTHQUAKE ENGINEERING RESEARCH CENTER (PEER)

PEER was established in 1997 by the NSF, with headquarters at the University of California, Berkeley. The seismic research projects are coordinated over nine universities: University of California (UC), Berkeley; Caltech; Stanford; UC Davis; UC Irvine; UCLA; UC San Diego;

USC; and the University of Washington at Seattle. Besides the core universities, investigators from numerous other universities and consulting companies conduct research in earthquake-related geohazard assessment, geotechnical and structural engineering, risk management, and public policy. PEER organizes its research around the concept of performance-based earthquake engineering. This new technology enables earthquake professionals to design facilities to meet the specific seismic performance needs of owners and other stakeholders, including considerations such as safety, cost, and post-earthquake functionality. PEER's research defines appropriate performance targets, and develops engineering tools and criteria that can be used by practicing professionals to achieve those targets. PEER also conducts education and outreach programs to reach students, policy makers, and others interested in earthquake issues.

In 2007, PEER "graduated" as a NSF-ERC, and is now a self-sufficient earthquake engineering research center with growing funding from the Federal government, State of California, and private industry. In January 2009, PEER and UC Berkeley's Earthquake Engineering Research Center (EERC) merged and the combined organization is now called PEER. The new components of the new PEER include the earthquake simulator (shaking table) laboratories, and the National Information Service for Earthquake Engineering (NISEE).

PEER has several "Mega Research Programs". These are large multidisciplinary research programs with numerous research sub-projects under each. The sub-projects are integrated by PEER to solve complex multidisciplinary seismic issues that the society is facing. Examples of Mega Research Programs are the Next Generation Attenuation (NGA) models; Tall Buildings Initiative; Transportation Systems Research Program; Seismic Performance of Lifelines; Seismic Performance of Older Non-Ductile Concrete Buildings, etc. In the following sections, two examples of such Mega Research Projects are briefly overviewed.

NEXT GENERATION ATTENUATION (NGA) PROGRAM

The NGA is a Mega Research Program coordinated by PEER. The NGA program has two phases: (a) development of ground motion prediction equation (GMPE) for shallow crustal earthquakes in active tectonic regions (NGA-West); and (b) an on-going follow up program to develop GMPEs for Stable Continental Regions (SCRs), similar to the Central Eastern US (NGA-East).

The NGA-West program represents a major advancement in ground motion prediction. The advancements in GMPE are made possible by an extensive update of the PEER strong motion database together with supporting research studies sponsored by the NGA program (Power *et al.*, 2008; Campbell and Bozorgnia, 2007, 2008). The NGA-West database is one of the largest uniformly processed ground motion databases in the world. The database is a collection of ground motion data recorded worldwide in active tectonic regions, and it includes more than 10,000 recorded free-field motions. Selected key advancements of the NGA-West GMPEs include their ability to predict:

- ✓ Median and fractile elastic response spectra up to a period of 10 sec. Previous ground motion prediction equations were valid to a much shorter maximum period (e.g., 3-5 seconds)
- ✓ Ground motions for moment magnitude range 5 to 8+
- ✓ Ground motions for distance range 0-200 km

- ✓ Inclusion of average shear-wave velocity in top 30-m of soil (V_{S30}) in most of NGA-West models for site classification.

Figure 1 presents an example of NGA-West result by Campbell and Bozorgnia (2008) for peak ground acceleration (PGA) for magnitude 5 to 8. Effects of magnitude and distance saturations are evident in this figure.

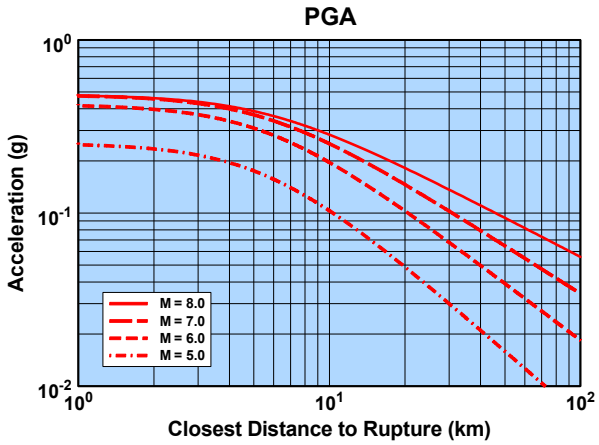

Fig. 1. Example result of Campbell and Bozorgnia (2008) NGA-West ground motion prediction equation.

Figure 2 shows the median pseudo-acceleration response spectra up to a period of 10 sec, predicted by the Campbell and Bozorgnia (2007, 2008) NGA-West ground motion model for different magnitudes and source-to-site distances. The predicted median *displacement* response spectra presented in Figure 3 clearly show the predicted behavior at long periods. The ability of NGA-West models to predict long-period ground motions is a major advancement in both deterministic and probabilistic seismic hazard analyses.

It should be noted that the aleatory standard deviations in the NGA-West models are dependent on period. As shown in Figure 4, generally the standard deviation increases with increasing the period. Therefore, the uncertainty of seismic hazard prediction for flexible systems (e.g., tall buildings and seismically isolated structures) is higher than that for short-period structures. The effect of such a larger aleatory uncertainty can be pronounced in a probabilistic seismic hazard analysis when ground motions at long return periods are required.

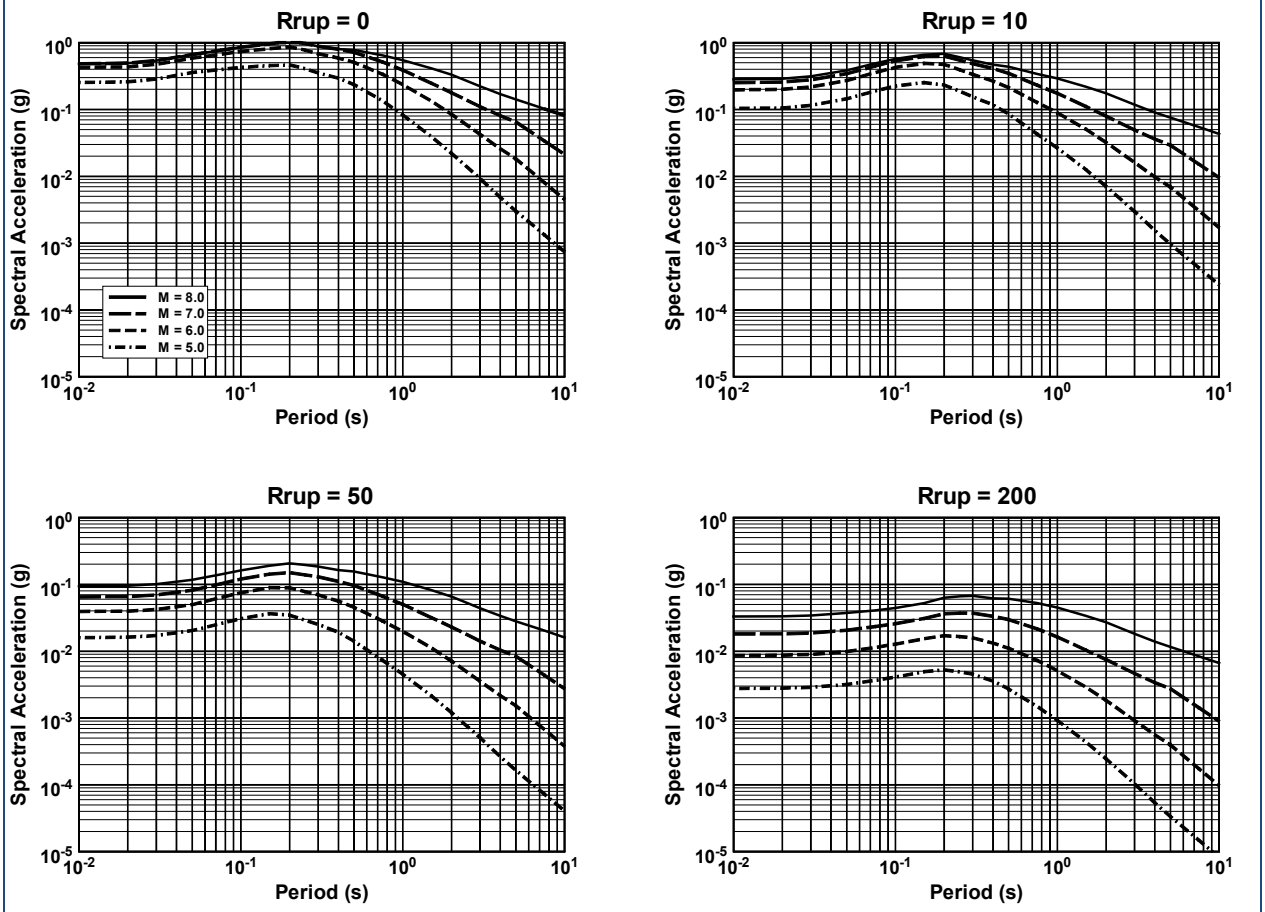

Fig. 2. Campbell-Bozorgnia NGA ground motion model prediction for 5% damped elastic pseudo-acceleration response spectra. The ground motion model is evaluated for magnitudes M = 5.0, 6.0, 7.0 and 8.0; rupture distances $R_{RUP} = 0$, 10, 50 and 200 km; strike-slip faulting; a 30-m shear-wave velocity of $V_{S30} = 760$ m/s; and a basin depth of $Z_{2.5} = 2$ km (Campbell and Bozorgnia, 2007).

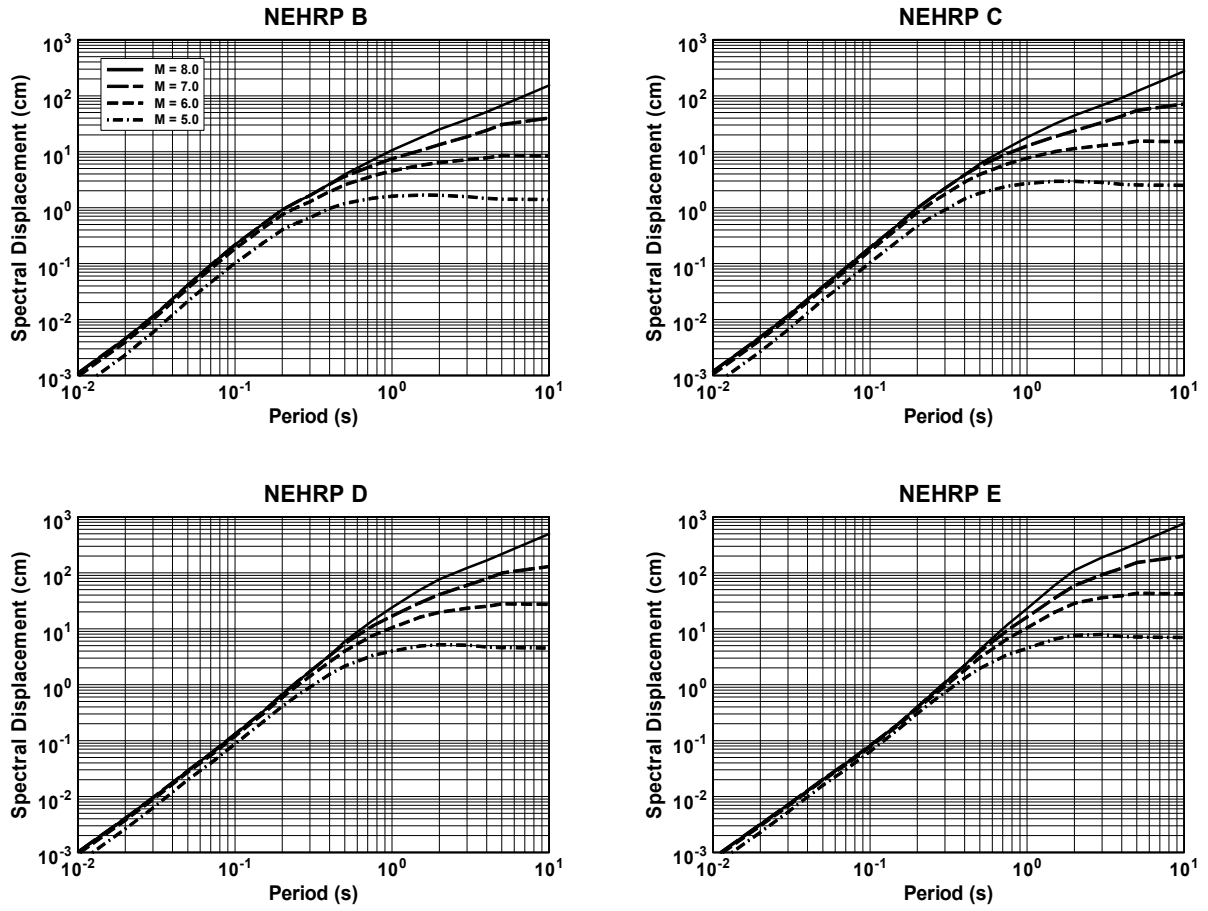

Fig. 3. Campbell-Bozorgnia NGA-West ground motion model prediction for 5% damped relative displacement response spectra The ground motion model is evaluated for magnitude of M = 5.0, 6.0, 7.0 and 8.0; $V_{S30} = 1070$ m/s (NEHRP B), $V_{S30} = 525$ m/s (NEHRP C), $V_{S30} = 255$ m/s (NEHRP D) and $V_{S30} = 150$ m/s (NEHRP E); a rupture distances of $R_{RUP} = 0$; strike-slip faulting, and a basin depth of $Z_{2.5} = 2$ km (Campbell and Bozorgnia, 2007, 2008).

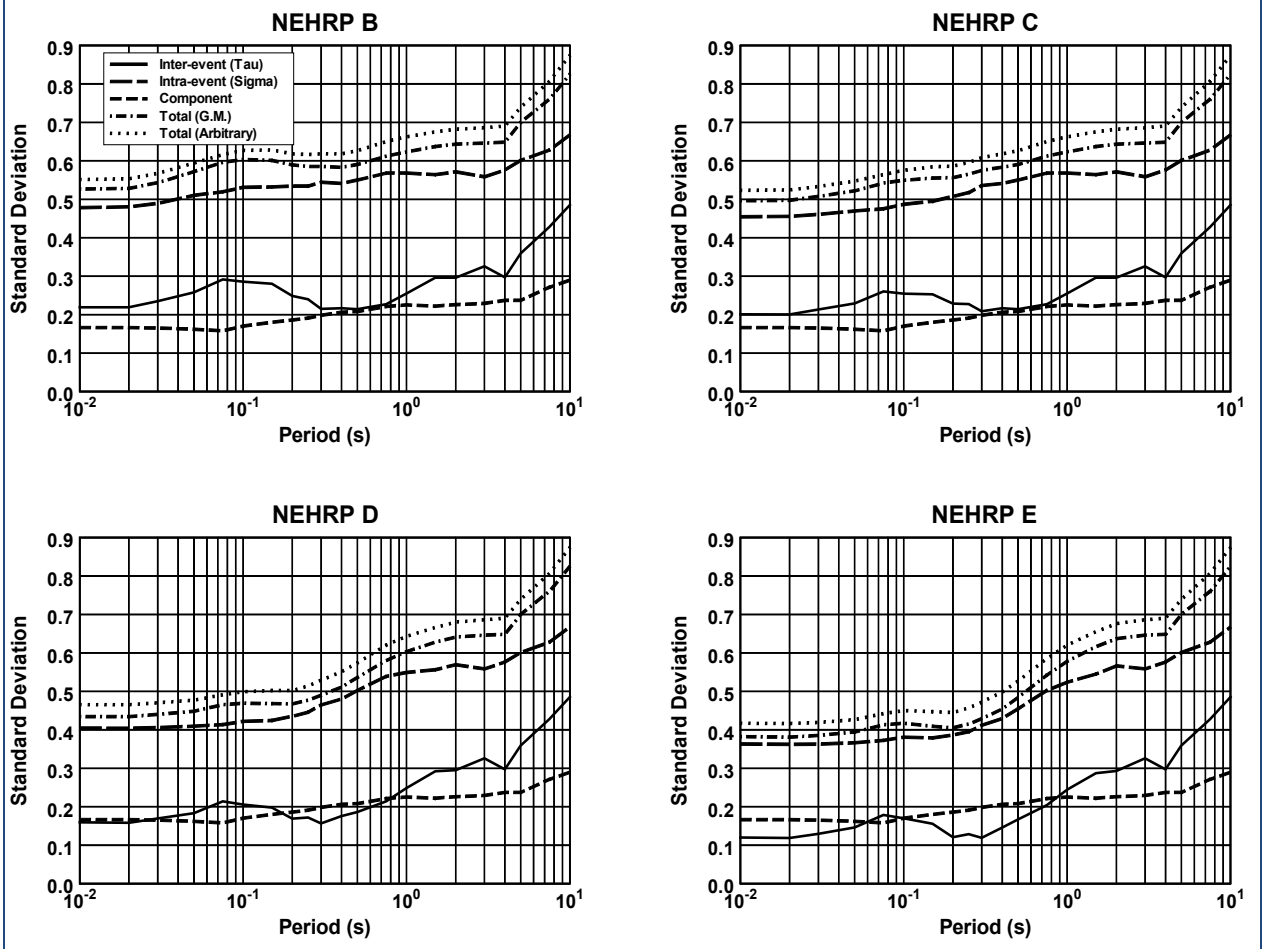

Fig. 4. Campbell-Bozorgnia NGA-West standard deviation scaling with oscillator period for a magnitude of $M = 7.0$ and a rupture distance of $R_{RUP} = 10$ km for different NEHRP site classifications (Campbell and Bozorgnia, 2007, 2008).

The standard deviation of the predicted ground motions is also a function of the orientation and type of the horizontal component as well as on the nonlinearity of the site response (see Figure 4). Therefore, it is important that the users of the NGA-West models implement the full formulation of the standard deviation as a function of various input parameters and site conditions.

The NGA-West models were extensively reviewed by the US Geological Survey (USGS) and were adopted for the development of the 2008 US National Hazard Maps. Figure 5 presents a sample of the 2008 national hazard map for the western US for 10% probability of exceedance in 50 years at period 1.0 sec. The national hazard maps are used as the basis for seismic design and analysis of almost entire civil engineering facilities in the US.

Other on-going related research projects include the development of GMPEs for other ground motion intensity measures such as inelastic response spectra (e.g., Bozorgnia and Campbell, 2004; Bozorgnia, *et al.,* 2010).

Recently PEER started the NGA-East program. This is another multi-year multidisciplinary program that includes geologists, seismologists, geotechnical engineers, structural engineers, and end users. The goal is to develop GMPEs for lower seismicity Stable Continental Regions such as the Central & Eastern US. The impact of NGA-East will also be monumental, as it will affect most regions in the US. The NGA-East program has several large research topics and each in turn has numerous sub-projects underneath. Examples of the research topics are: development of a comprehensive database of recorded ground motions in Stable Continental Regions; seismic source characterization; site response studies; ground motion simulations; and development of GMPEs. Similar to the NGA-West, there will be numerous invitational and public workshops to disseminate the preliminary findings and collect comments and feedback from the earthquake community.

NGA is an excellent example of a major well-coordinated multidisciplinary research program with a wide range of impacts over a large region. Various supporting research projects under NGA are coordinated to achieve a larger goal of developing high-quality robust ground motion models. Without such multidisciplinary research coordination, the same individual researchers working alone could not produce the same high-quality products as they did in the NGA program.

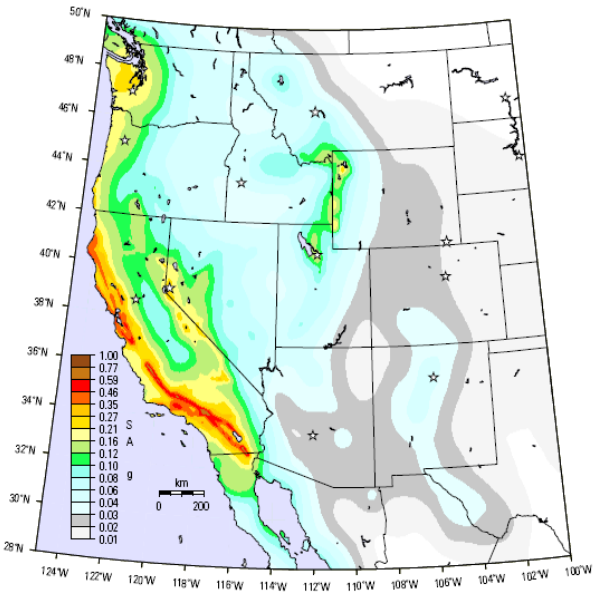

Fig. 5. Map of 1-sec spectral acceleration for 10-percent probability of exceedance in 50 years in the Western United States in standard gravity, g (Petersen, *et al.*, 2008).

Another example of a successful coordinated multidisciplinary research is the PEER Tall Buildings Initiative (TBI). The new generation of tall buildings in high seismic areas of the US feature framing systems, materials, heights, and dynamic properties not envisioned by the current building code prescriptive provisions. Rather than force these buildings to conform, many jurisdictions are allowing these new designs to proceed under the alternative procedures provision of the building code, which allows alternative lateral-force procedures using rational analyses based on well-established principles of mechanics in lieu of the prescriptive provisions (Moehle, *et al.,* 2007). Most designs are opting for a *performance-based* approach in which a rational analysis demonstrates serviceability and safety equivalent to that intended by the code prescriptive provisions. Figure 6 shows an example of a tall building in California which was designed according to performance-based design (PBD) principles.

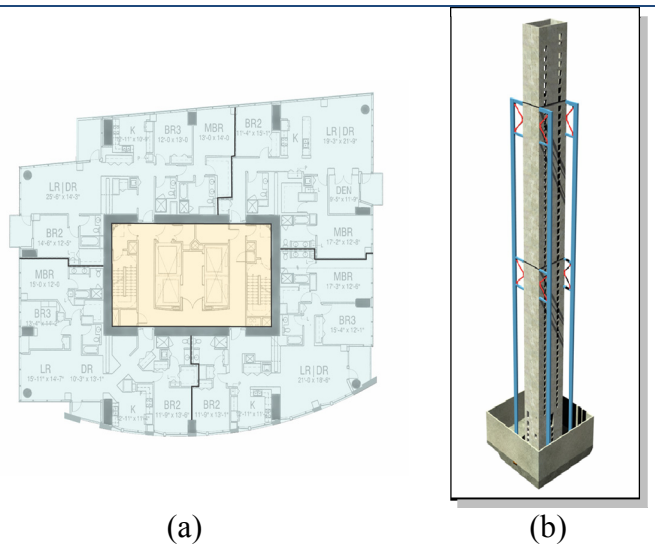

Fig. 6. (a) Plan view of a core-wall tall building in California; and (b) the core-wall lateral-load resisting system (Moehle, *et al.*, 2007).

The *Tall Buildings Initiative* is a Mega Research Program coordinated by PEER to address complex seismic issues for the analysis and design of the new generation of tall buildings. This Mega Research Program has several sub-projects; a few of them are mentioned below.

✓ *Sensitivity analysis to ground motions*. In this project, several realistic computer models of tall buildings in California are analyzed. The models are subjected to numerous scaled and un-scaled input ground motions. The sensitivities of various *Engineering Demand Parameters* (*EDP*s; structural response in this case), with respect to building and ground motion characteristics are investigated. For example, Figure 7 shows a sample result of story shear forces for various input motions for a tall building located in San Francisco.

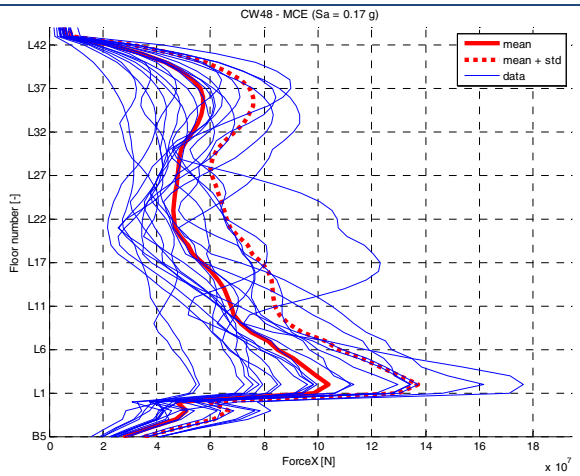

Fig. 7. Story shears in a case study core-wall building, from nonlinear response history analysis, for ground motions scaled so the first-mode spectral acceleration matches the uniform hazard level value at the MCE hazard level (Moehle, *et al.*, 2007).

✓ *Synthetically generated ground motions and comparison with recorded motions.* In this task, the differences between simulated and recorded ground motions are investigated. Special attention is focused on long period motions, which are more relevant to tall buildings. However, comparison also includes short period motions for their influence on higher modes of tall buildings. Examples of comparisons between the characteristics of simulated and recorded ground motions (as manifested by the NGA-West models) are shown in Figure 8. This figure presents inter-event residuals between the NGA models and ground motions simulated for the Puente Hills Blind Thrust fault in Los Angeles (Stewart, *et al.*, 2008).

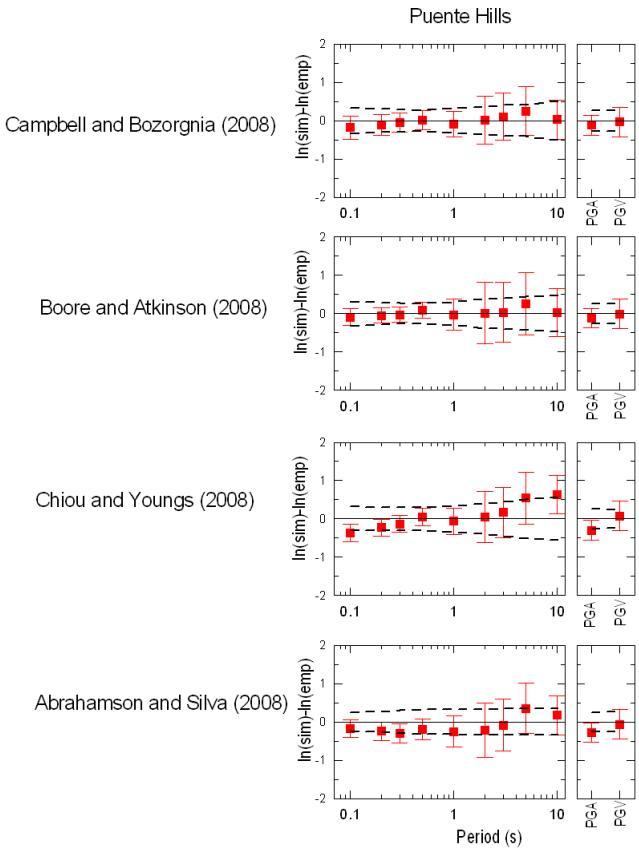

Fig. 8. Inter-event residuals between NGA models and ground motions simulated for the Puente Hills Blind Thrust fault in Los Angeles (Stewart, *et al.*, 2008).

The results shown in Figure 9 are for spectral accelerations at several periods ranging from 0.1 to 10 sec. The dashed lines in this figure indicate ± one inter-event standard deviation. The simulation event terms generally fall within a reasonable range, mostly within one standard deviation (Stewart, *et al.,* 2008). Figure 9 presents the intra-event residual (versus distance) between the Puente Hills simulated ground motions and Campbell & Bozorgnia (2008) NGA-West empirical model. This figure shows faster distance-attenuation of the simulated data relative to the NGA model (Stewart, *et al.,* 2008). The apparent bias in the distance scaling of simulated motions is much smaller for the Puente Hills event than for a previously investigated large magnitude rupture of the southern San Andreas Fault.

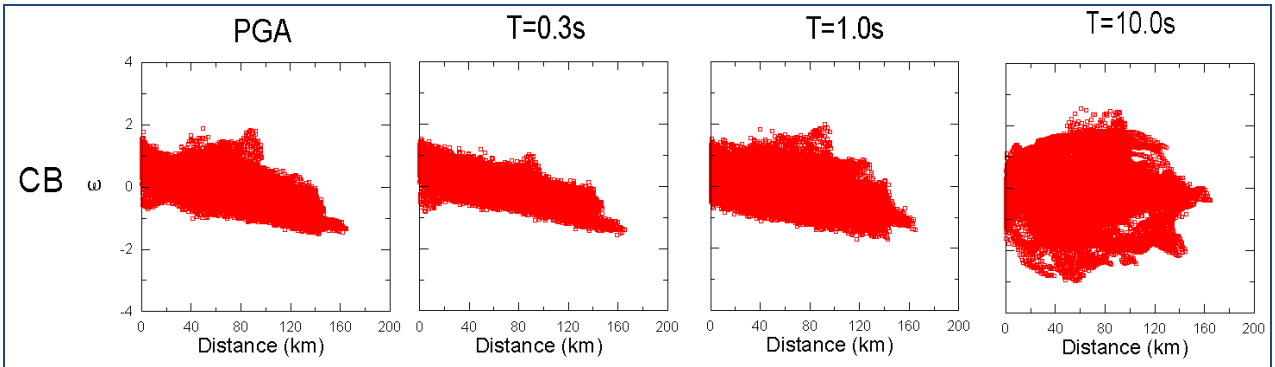

Fig. 9. The intra-event residuals of the Puente Hills simulated motions relative to the Campbell & Bozorgnia (2008) NGA model for PGA and spectral ordinates at periods *T*=0.3, 1.0, and 10.0 sec versus rupture distance (Stewart, *et al.*, 2008).

✓ *Guidelines on modeling and acceptance criteria.* A report is being prepared to document various computer modeling acceptance criteria. This is a joint effort between PEER and the Applied Technology Council (ATC).

✓ *Input ground motions for tall buildings with subterranean levels.*

✓ *Guidelines for seismic design of tall buildings.* Comprehensive seismic design guidelines for PBD of new tall buildings are being written. The seismic design guidelines document includes recommendations on a range of PBD seismic issues including: input ground motions, soil-structure-interactions, serviceability checks, acceptance criteria for Maximum Considered Earthquake, among others. PEER has collected comments and feedback from the community and is finalizing the seismic design guidelines. One of the strengths of the seismic design guidelines document is that it is drafted by both academicians and practitioners with a diverse range of expertise.

✓ *Quantification of seismic performance levels*. In this sub-project, three tall buildings are deigned and their seismic responses are compared. The characteristics of the three buildings are as follows:

- Concrete core wall system (48 stories)
- Concrete dual system (48 stories)
- Steel frame with buckling-restrained braces (BRB)
- Located in Los Angeles, California
- Having fundamental period of ~ 5sec
- Each building is designed based on:
  - Building code provisions (except height limit)
  - Performance-based design (PBD), per the 2008 Los Angeles Tall Buildings Structural Design Council (LATBSDC) design criteria
  - "PBD+", a higher performance than PBD; to be proposed by the designer, and approved by TBI.

TBI is another example of a well-coordinated research program bringing together engineering seismologists, geotechnical engineers, structural engineers and other stakeholders to solve a complicated set of technical issues with an enormous regional impact.

CONCLUDING REMARKS

The quantification and reduction of seismic risks are the goals of earthquake engineering and to achieve these goals the earthquake community is facing complex multidisciplinary challenges. From a seismic research perspective, a key challenge is the coordination and integration of individual research projects in diverse disciplines ranging from geology, seismology, ground motion hazards, geotechnical engineering, structural and non-structural engineering, to the socio-economic sciences. A parallel interaction should also be coordinated between researchers and practitioners. Researchers need input from practitioners about the real-world challenging issues and constraints; and practitioners need to know the emerging research findings, methodologies and tools to improve practice.

In this paper, PEER, as an example of a national research center with a record of accomplishment of coordinating large complex multidisciplinary research programs, was briefly overviewed. Examples of two fruitful multidisciplinary research programs at PEER, with wide impacts on the quantification and reduction of seismic risks, were also discussed.

For other countries such as Iran, the role of a coordinated national seismic research program is even more crucial. Such an integrated seismic research program would minimize duplication of research efforts, and accelerate the process of transferring research ideas to practice.

International scientific collaborations also play a crucial role in reducing seismic risks globally as earthquakes do not recognize political borders. A good example of such a successful international cooperation was the US-UK-Iran scientific collaboration after the 2003 Bam, Iran, earthquake which resulted in the discovery of a previously unknown buried fault in Bam. On December 26, 2003, in less than 20 seconds of strong ground shaking, Bam lost the vast majority of its buildings, and consequently tens of thousands of Iranians lost their lives.

ACKNOWLEDGEMENTS

The US-Iran Seismic Workshop, held in Irvine, California, was sponsored by the US National Academy of Sciences (NAS). The support of the NAS and participation of both US and Iranian earthquake engineers and scientists in the seismic workshop is gratefully appreciated.

REFERENCES

Bertero, V.V., and Bozorgnia, Y. (2004). *Early years of earthquake engineering and its modern goal*, Chapter 1, in *Earthquake Engineering: From Engineering Seismology to Performance-Based Engineering*, Bozorgnia and Bertero (Eds.), CRC Press, Florida.

Bozorgnia, Y., and Campbell, K.W. (2004). *Engineering Characterization of Ground Motion,* Chapter 5, in *Earthquake Engineering: From Engineering Seismology to Performance-Based Engineering*, Bozorgnia and Bertero (Eds.), CRC Press, Florida.

Bozorgnia, Y., Hachem, M., and Campbell, K.W. (2010). "Ground motion prediction equation ("attenuation relationship") for inelastic response spectra", *Earthquake Spectra*, in-print, February 2010.

Campbell, K.W. , and Bozorgnia, Y. (2008). NGA ground motion model for the geometric mean horizontal component of PGA, PGV, PGD and 5% damped linear elastic response spectra for periods ranging from 0.01 to 10 s, *Earthquake Spectra*, **24**, No. 1, 139-171.

Campbell, K.W. and Bozorgnia, Y. (2007). *Campbell-Bozorgnia NGA Ground Motion Relations for the Geometric Mean Horizontal Component of Peak and Spectral Ground Motion Parameters*, *Report PEER 2007/02*, Pacific Earthquake Engineering Research Center (PEER), University of California, Berkeley, May 2007.

Krawinkler, H., and Miranda, E. (2004). *Performance-Based Earthquake Engineering,* Chapter 9, in *Earthquake Engineering: From Engineering Seismology to Performance-Based Engineering*, Bozorgnia and Bertero (Eds.), CRC Press, Florida.

Moehle, J.P., Bozorgnia, Y., and Yang, T. (2007). The tall buildings initiatives, *Proceedings of the Convention of the Structural Engineers Association of California*, Lake Tahoe, California.

NSF ERC (1997). *Background: ERC Program*, National Science Foundation, *http://www.nsf.gov/pubs/1998/nsf9840/nsf9840.htm?org=NSF#II*

Petersen, M.D., Frankel, A.D., Harmsen, S.C., Mueller, C.S., Haller, K.M., Wheeler, R.L., Wesson, R.L., Zeng, Y., Boyd, O.S., Perkins, D.M., Luco, N., Field, E.H., Wills, C.J., and Rukstales, K.S., 2008. *Documentation for the 2008 update of the United States national seismic hazard maps*, *USGS Open-File Report 2008-1128*.

Power, M., Chiou, B., Abrahamson, N.A., Roblee, C., Bozorgnia, Y. and Shantz, T. (2008). An introduction to NGA. *Earthquake Spectra*, **24**, 3-21.

Stewart, J.P., Star, L.M., and Graves, R.W. (2008). *Validation against NGA empirical model of simulated motions for M7.15 rupture of Puente Hills Fault*, *Final Report* to Pacific Earthquake Engineering Research Center (PEER), University of California, Berkeley.

SEISMIC RISK REDUCTION: A COMMUNITY BASED APPROACH

Maziar Hosseini (Ph.D., P.E.)
Tehran Disaster Mitigation and Management Organization
(hosseini@tdmmo.ir)
Kambod Amini Hosseini (Ph.D.)
International Institute of Earthquake Engineering and Seismology

ABSTRACT

Risk reduction without active participation of communities and people at risk is almost impossible, even if the local governments have appropriate plans for this purpose. The residents should take necessary measures for strengthening their own buildings, co-operate in the improvement of their neighborhood, improve their preparedness for response and increase their skill for confronting a potential earthquake. Moreover other activities in risk reduction and disaster management such as insurance and land-use planning cannot be properly implemented without willing local residents. In order to increase public participation in risk reduction activities, it is essential to work on promoting public awareness to change attitudes about hazards and risk reduction. For this purpose it is essential to use the existing infrastructures and facilities at the community level and provide necessary training in different areas of risk reduction. This paper considers the master plan of risk reduction and the recent activities carried out for involving communities in risk reduction activities.

1. INTRODUCTION

Nowadays, the importance of public awareness and participation in risk reduction programs is clear for all of the stakeholders around the world. Residents have important roles in different areas of risk reduction and disaster management. For example, in mitigation activities, ordinary people should be engaged in retrofitting their own vulnerable structures or co-operate in the improvement of infrastructures. In preparedness plans, they should be properly trained for self rescue and relief activities (considering that during the first hours after an event, the residents themselves are the main bodies who can save the lives of other residents). In addition, success in risk reduction policies (such as insurance) needs public participation to have proper results. Also in the response stage, without public participation in related activities the golden hours for saving residents cannot be properly managed. Finally in the reconstruction stage, it is essential to involve local communities for planning and implementation activities to have proper results.

Thus Community-Based Disaster Management should be developed and organized at local levels to have successful results in disaster management activities. This issue has been considered by the Tehran City Council and Tehran Disaster Management Organization as a key element in planning and implementation activities which has been also reflected into the Tehran Risk Reduction Program that will be discussed in the following parts.

2. SEISMIC RISK REDUCTION PROGRAM

The city of Tehran, the Capital of the Islamic Republic of Iran, is located in a seismic prone area in an active part of the Alpine-Himalayan Orogenic belt (Alborz Mountain Range) and is surrounded by some active faults; thus a strong earthquake could be expected in this area in the future based on existing studies (figure 1).

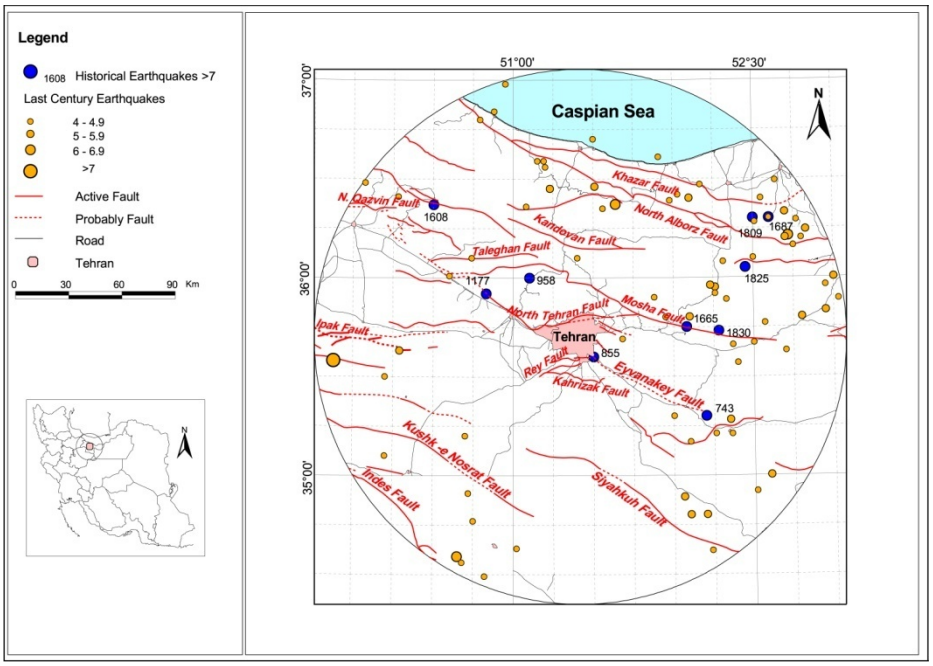

Fig. 1. Main faults around Tehran and the location of historical and recent earthquakes around the city in 150 km radius.

The existing conditions show the importance of mitigation and preparedness planning before the occurrence of a destructive event to reduce its effects to an acceptable level. For this purpose the Tehran Seismic Risk Reduction Program has been prepared by the Tehran City Council and is under implementation by the Tehran municipality. The main components of this plan are shown in figure (2). Figure (3) also depicts the main branches of different components of this plan.

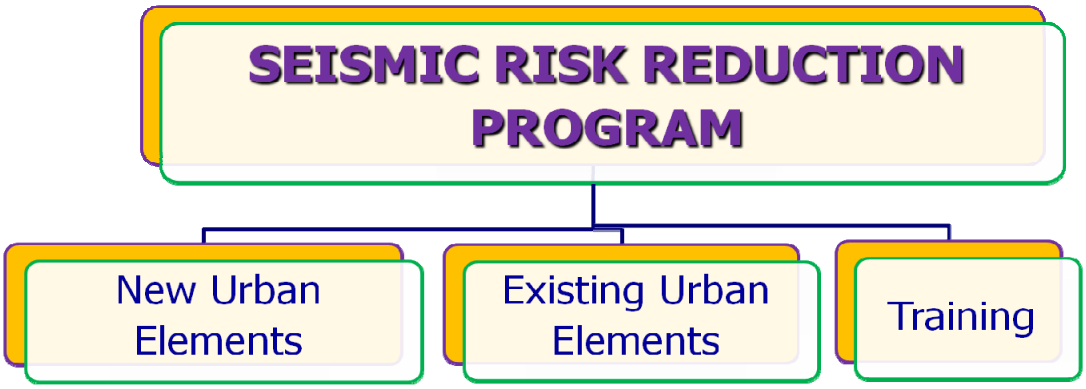

Fig. 2. Main components of seismic risk reduction program of Tehran.

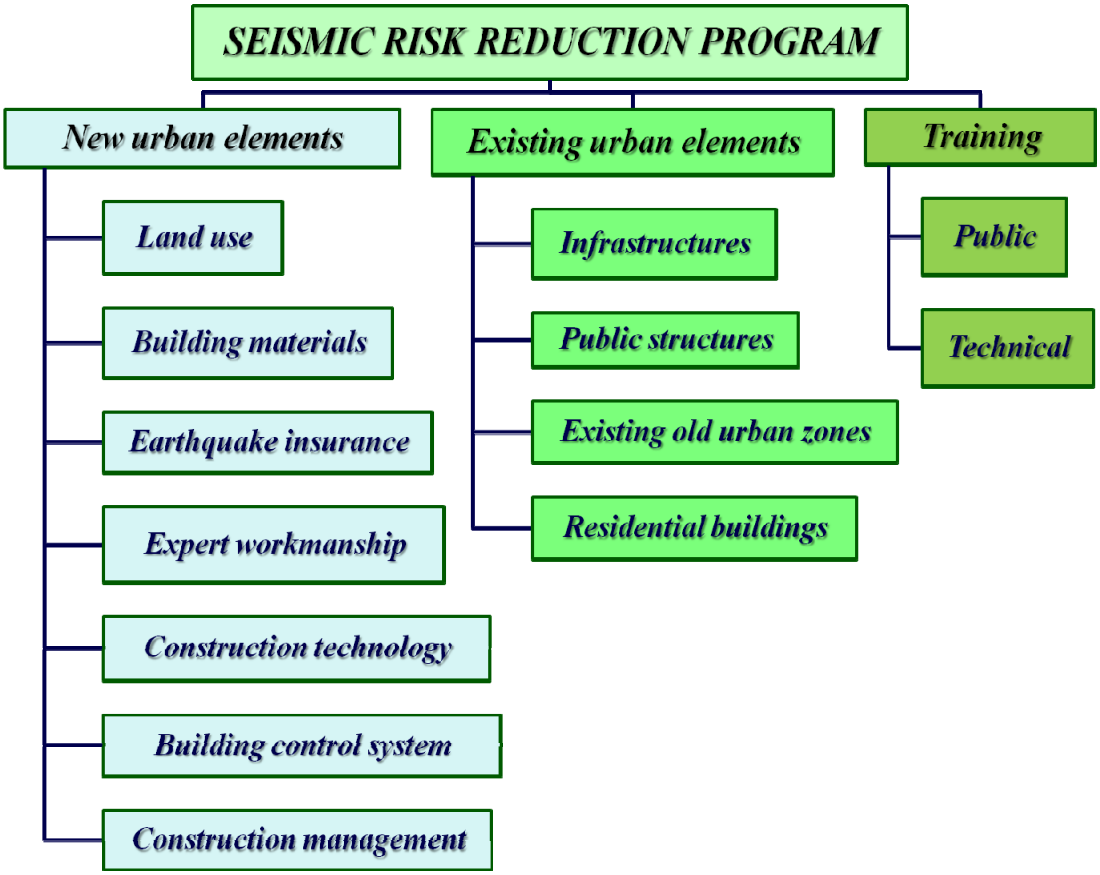

Fig. 3. The main branches of components of seismic risk reduction program of Tehran.

The definitions of these branches will be presented briefly in the following sections.

2.1. New Urban Elements

Land use: Land-use planning improves location selection, which, in turn reduces exposure to earthquake risk and so it can reduce damage potential and save lives in times of earthquake. So in this phase of the subprogram, it is necessary to revise existing plans and define suitable land use plans for urban development.

Building materials: In order to improve the construction quality of city elements, it is necessary to upgrade the technical specification of building materials. So building material standards in the production, distribution and installation phases must be revised and controlled effectively.

Earthquake insurance: Earthquake insurance regulations is a cornerstone of comprehensive risk management and by promotion of it, besides covering the economic losses caused by earthquakes, it can be linked to preventive activities that overtime will reduce risk. For

example, with lower earthquake insurance premiums for less vulnerable buildings, people are encouraged to seek more earthquake resistant construction and so seismic risk is reduced.

Expert workmanship: The goal of this item is to create coordination between the designed structure and the constructed structure. In this case, it is necessary to train unprofessional building workmen and the grade of workmanship warrant must be controlled.

Construction technology: Currently most of the city elements of Tehran are built based on the traditional construction methods. So the modern construction technology must be introduced and by encouraging policies such as low profit loans, the contractors should be equipped to use those modern technologies.

Building control system: Building control system is ensuring that the building design and construction satisfies the minimum standards of health and safety. This is done by checking and approving submitted plans for compliance with the regulations and inspecting the work during construction. Since one of the most obvious ways to reduce vulnerability is to increase the quality of buildings, it is necessary to modify the control system of building construction.

Construction management: In order to improve the quality of construction and to optimize the time and cost of construction, it is necessary to upgrade the existing construction management.

2.2. Existing Urban Elements

Infrastructures: Infrastructures and lifelines are basic necessities to prevent expansion of disaster scale. Therefore, strengthening or rehabilitation of existing facilities must be expedited.

Public structures: The importance of public structures such as hospitals, schools, fire stations, police stations in disaster management is obvious, thus the strengthening or rehabilitation of these existing structures must be expedited.

Existing old urban zones: These areas normally have dense a population, old and weak structures and narrow streets. The programs for improvement include recognition of the existing old urban zones, preparation of site design plans and renewal of these zones by contributions from the local people.

Residential buildings: The programs for strengthening of residential buildings include presenting the simple type retrofitting systems for residential buildings and to encourage policies such as low bank profit loans.

2.3. Training

Training in seismic risk reduction can be categorized into public and technical training. It is very important that the people have the general knowledge of site hazard, vulnerability and strength of their buildings and to know how to respond during and after an earthquake. Naturally the trained part is ready to provide the gained knowledge and ability for disasters mitigation and share the gained knowledge with neighbors, which will be an opportunity to build the resilience of nation and communities to disasters, in support of sustainable development. Also along this line, the role of mass media is important because the way the media report and comment on earthquakes

will, in a good measure, shape the way in which the community reacts in the face of a disaster, before, during and after its occurrence.

In the following parts and based on what was mentioned regarding the seismic risk reduction program, some activities carried out in Tehran to train residents about the necessary activities for preparedness for a potential earthquake and improve public awareness will be summarized.

3. COMMUNITY BASED ACTIVITIES IN RISK REDUCTION AND DISASTER MANAGEMENT

As mentioned above, the active participation of residents in risk reduction plans is a key point for success of these activities. In order to encourage people to consider this issue, at first it is essential to promote public awareness about risk reduction and then increase public education and willingness to make buildings safer. These activities should be planned in different ways by using the existing communities or other means such as the media. A summery about the recent activities for promoting public awareness and participation in earthquake risk reduction activities in Tehran will be presented and discussed briefly in the following parts and some of the projects carried out in this line will be explained. These activities can be classified into 2 main groups as follows.

3.1. Public Participation in Seismic Risk Reduction and Disaster Management

In order to promote the community based activities in residential areas, several parameters should be considered from legal and institutional arrangement up to providing necessary training and tools for potential use at the time of earthquake. The most important progress in this regard in Tehran will be discussed in this part.

3.1.1. Legal and Institutional Arrangement

The legal framework for promoting public participation in disaster management activities in Iran have been established at different levels during the recent years including:

1- National level: Several plans and policies have been prepared and approved at the highest levels (Expediency Council) to governmental and Islamic Assembly levels. In most of these policies, the role of residents in risk reduction has been considered directly or indirectly.

2- Tehran level: Tehran City Council has also ratified some specific rules and regulation for promoting community level disaster management and Tehran Disaster Management organization (TDMMO) was assigned to establish the necessary infrastructures and provide necessary assistance in the related areas.

3.1.2. Promoting Disaster Management in Residential Places

In order to develop the community based disaster management at local level the first step was to define different zones (Mahalleh) and neighborhood units and then select related boundaries of the Mahalleh. A sample is shown in figure 4:

Fig. 4. Selecting boundaries of Mahalleh and neighborhood.

At the next stage the appropriate places for disaster management information exchange and setting communication center were identified and the method of managing these local organizations were developed. For this purpose some key persons at the neigbourhood and Mahalleh level were selected including influential people like the elderly, elected delegates, etc. In selecting these key persons several interviews in schools and mosques and local councils were carried out and by evaluating the gathered questionnaires and documents, they have been selected. These people then were informed about the purpose of the project and were assigned as leader of these tasks at each neighbourhood and Mahalleh.

Then the necessary training was provided by disaster mangement experts, construction experts (for providing information about the safety of the buildings), urban planners, etc. for the selected groups in each neighbourhood/Mahalleh. Moreover diagnosis maps and evacuation maps were prepared for some Mahalleh and distributed among residents. Also in these Mahalleh, some drills were carried out to improve public awareness about evacuation. Figures 5 and 6 depicts some sample maps (diagnosis map and evacuation map) prepared for one of the mahalleh of Tehran.

Fig. 5. A sample of Diagnosis Map prepared for one of the Mahalleh in Tehran.

Fig. 6. A sample Evacuation Map prepared for one of the Mahalleh of Tehran.

The next activity in this process is related to improving the communication and interaction levels among residents by doing public participation drills and development of interaction between residents and the municipality by using flyers, bulletins, etc. The following centers and groups were considered to build appropriate bridges between responsible organizations and residents:

1. Residential Complex Management notice boards;
2. Sub-districts' Associations (Shora Yari);
3. Public Buildings (administrative offices, Mosques, …);
4. Educational institutions: School, universities …;
5. Cultural Centers;
6. Health and Medical Service Centers;
7. Sport Centers;
8. NGOs;
9. Red Crescent Organization;

In figure 7, some photos of implemented evacuation drills carried out in one Mahalleh of Tehran are shown.

Fig. 7. Public participation in evacuation drills.

3.1.3. Organizing Volunteer Groups (DAVAM)

Another important step in the process of raising public cooperation is organizing a neighbourhood emergency response volunteer program (DAVAM) at the Mahalleh level. The Purpose of the DAVAM project is to reduce the risk of injury and loss of life or property by strengthening the capacity of the local community to prepare for, respond to, and recover from disasters. The best method for this purpose was to organize the volunteers to coordinate the emergency response activities in a more effective manner. The Criteria for selecting the volunteers could be summarized as follows:

- Age between 18 to 55 Years;
- Good physical and mental health (no heart disease, no allergy, proper height and Weight);
- Being resident of the District (Minimum residency of 2 Years);
- Intending to live in that District for a Long Period of Time;
- Not being a member of other related responsible organizations (Fire Brigade, Army, Hospitals, etc);

- Not having any criminal record;
- Holding the minimum educational certificate of intermediate School (diploma).

These groups will be supported by the Tehran Municipality (TDMMO) by providing the necessary training, funds, tools and facilities for disaster management or emergency response.

3.2. Improvement of Public Awareness

As mentioned above one of the main duties of the disaster management authorities is rising public awareness through educational works such as preparing books and providing programs for different target groups. For this purpose several education materials have been developed in Tehran. For example, a multimedia CD and book was prepared and distributed in Tehran to more than 1.000.000 persons. In this CD basic information about natural hazards and means of preparedness against them is explained by using movies, pictures and multimedia effects. Other activities for promoting public awareness are as follows:

- Using billboards in public places for encouraging building safety works for wide-spread information dissemination (figure 8);

Fig. 8. Some billboard and placards for promoting public awareness.

- Distributing posters among the communities that describe safety issues for encouragement of people to reduce the disasters' impacts and promoting preparedness (figure 9);
- Holding exhibitions on earthquakes safety and training (figure 10).

Fig. 9. A sample of posters distributed among residents.

Fig. 10. Some samples of exhibition and trainings.

4. CONCLUSION

This paper presents some of the activities carried out for promoting public participation in earthquake risk reduction in Tehran. These programs consist of identifying earthquake phenomena, hazard level and benefits of seismic resistant buildings and other necessary information for preparedness. The trained part of the population will be ready to provide the gained knowledge and ability for disaster mitigation and share the gained knowledge with neighbors, which will be an opportunity to build the resilience of the nation and communities to earthquake disaster. Of course there are still a lot of things to do to make safe communities in whole areas of the city. Future necessary steps for increasing public awareness and participation include:

- Facilitating legal frameworks for establishment of Community Disaster Management Organization;
- Strengthening neighborhood units through collaborative methods defined by sociologists, urban designers and cultural experts;
- Encouraging people to participate in the activities of these units;
- Formulating a systematic structural plan for the centers' operation;
- Enhancing bottom – up approaches in the process;
- Establishing a network among the individual units mentioned above.

REFERENCES

1. Amberaseys, N. N. and Melville, C. P. (1982) A History of Persian Earthquakes, *Cambridge University Press*, London.
2. Seismic Risk Reduction Program, (2008) Tehran City Council, Tehran.
3. Hosseini, M. (2008) Disaster Management, TDMMO and Shahr Press, Tehran, Iran.
4. Amini Hosseini, K. and Hosseini, M. (2007) Evaluation of old urban structures and emergency road networks vulnerabilities to a potential earthquake in Tehran, Proceeding of 5th International Conference of Seismology and Earthquake Engineering (SEE5), Tehran, Iran.
5. Maheri, M. R., Naeim, F. and Mehrain (2005) Performance of adobe residential buildings in the 2003 bam, Iran, Earthquake, *Earthquake Spectra*, Volume 21, No. S1, Pages S125-S136, EERI.
6. Nateghi, F. A. (2001) Earthquake scenario for mega-city of Tehran, *Disaster Prevention and Management*, Volume 10, No. 2, Pages 95-100.

SEISMIC VULNERABILITY ASSESSMENT OF UNREINFORCED MASONRY BUILDINGS: A GUIDELINE

Hamzeh Shakib
Professor, Department of Civil Engineering, Tarbiat Modares University, Tehran, Iran

ABSTRACT

In this study, a guideline for seismic vulnerability assessment of unreinforced masonry buildings is reviewed. A brief discussion is made on the qualitative and the quantitative approaches to assessing the vulnerability of masonry buildings.

INTRODUCTION

A high percentage of Iranian buildings are unreinforced masonry buildings. Construction of unreinforced masonry buildings in Iran dates back to more than 2000 years ago. During this time, a number of destructive earthquakes have occurred during which many buildings collapsed completely. The existing masonry buildings in Iran are largely the structures constructed in the past 100 years. Since the types of units, mortars, and construction methods changed during this time, knowing the age of a masonry building may be useful in identifying the characteristics of its construction. Although structural properties cannot be inferred solely from age, some background on typical materials and methods for a given period can help to improve the engineering judgment and provide some directions in the assessment of an existing building. Mechanical properties for masonry materials and components shall be based on available construction documents and as-built conditions for a particular building. Where such information fails to provide adequate data to quantify material properties, it needs to be supplemented by material tests and assessments of existing conditions. On account of the research development and new findings on the seismic behavior of unreinforced masonry buildings it is necessary to redefine the seismic assessment procedure of this type of building. In this study, a few comments are made on the guidelines previously proposed by the author.

QUALITATIVE PROCEDURES

In the first step, the qualitative procedures are developed. Here, two methods are introduced. In the first method 10 questions are designed and weighed in relation to their seismic resistant contributions. In the second method, a detailed qualitative assessment is carried out to assess the degree of vulnerability. These methods, specifically the former, help the natural disaster programmers to screen the existing buildings.

QUANTITATIVE PROCEDURES

Based on the field visits to the earthquake stricken area in Iran, experimental tests, and by referring to some guidelines, the quantitative procedure is adapted. The main changes are made in the expected and lower bound lateral strength of unreinforced masonry walls and piers. The bed-joint sliding and the diagonal tension are selected as the failure modes. Among the four usual modes of failure the other two modes named as rocking and toes crashing have not been considered in this guideline. The construction techniques in Iran are such that the last two modes

of failure do not usually happen as observed in the field visit. The selected two modes of failure are shown in figure 1.

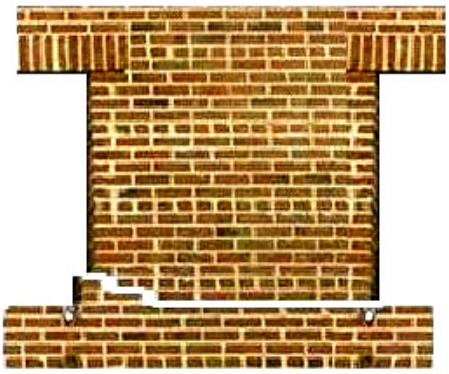

Fig. 1-a. Bed-joint sliding.

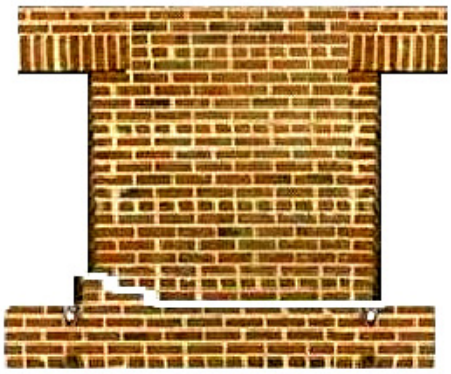

Fig. 1-b. Diagonal tension.

The lateral strength of existing and enhanced URM walls or pier components shall be the lesser of the expected lateral strength, Q_{CE} , based on bed-joint sliding shear strength, calculated in accordance with equation-1:

$$Q_{CE} = V_{bjs} = v_{me} A_n \quad (1)$$

Or the lower bound lateral strength, Q_{CL}, based on diagonal tension stress calculated in accordance with equation-2:

$$Q_{CL} = V_{dt} = f'_{dt} A_n \left(\frac{L}{h_{eff}}\right) \sqrt{1 + \frac{f_a}{f'_{dt}}} \quad (2)$$

Where, A_n = area of net mortared/grouted section; L = length of wall or pier; h_{eff} = height to resultant of lateral force; v_{me} = expected bed-joint sliding shear strength; V_{bjs} = expected shear strength of wall or pier based on bed-joint sliding shear strength; f_a = axial compressive stress due to gravity loads; f'_{dt} = lower bound masonry diagonal tension strength; V_{dt} = lower bound shear strength based on diagonal tension stress for wall or pier.

For unreinforced masonry components, the expected masonry shear strength, v_{me}, shall be measured using an approved in-place shear test. Expected shear strength shall be determined in accordance with Equation-3:

$$v_{me} = 0.56\, v_{te} + 0.75 \frac{P_D}{A_n} \quad (3)$$

P_D = gravity compressive force applied to a wall or pier component; v_{te} = Average bed-joint shear strength; Individual bed joint shear strength test values, v_{to}, shall be determined in accordance with Equation-4:

$$v_{to} = \frac{V_{test}}{A_b} - \sigma_{D+L} \quad (4)$$

V_{test} = Test load at first movement of a masonry unit; A_b = Sum of net mortared area of bed joints above and below the test unit; σ_{D+L} = Stress due to gravity loads at the test location.

ACCEPTANCE CRITERIA

The acceptance criteria shall be applied to building systems including any combination of existing masonry walls, masonry walls enhanced for seismic rehabilitation, and new walls added to an existing building for seismic rehabilitation. Actions in a structure shall be classified as being either deformation-controlled or force-controlled.

Whenever the lateral strength is the lesser value of the expected lateral strength, Q_{CE}, compared to lower bound lateral strength, Q_{CL}, the lateral behavior of wall and piers is taken to be deformation-control. Otherwise, the lateral behavior of wall or pier is taken to be force-control. The behavior of axial compressive of walls or piers is always taken to be force-control.
In linear methods, for the lateral behavior of walls and piers when they are deformation-controlled, the following relation should be satisfied.

$$m\kappa Q_{CE} \geq Q_{UD} \quad (5)$$

In which m is taken from table 1.However, in linear method, for the lateral behavior of walls and piers when they are force-controlled, the following relation should be satisfied.

$$\kappa Q_{CL} \geq Q_{UF} \quad (6)$$

Table 1. Coefficient m for linear analysis.

Acceptance criteria / Behavioral mode	IO	Primary member		Secondary member	
		LS	*CP*	LS	*CP*
Bed-Joint Sliding for buildings with ties	*1*	*3*	*4*	*6*	*8*
Bed-Joint Sliding for buildings without ties	*1*	*1.5*	*2*	*3*	*4*

Where design actions are determined using nonlinear procedures, component force deformation response shall be represented by nonlinear force-deformation relations. Force-deformation relations shall be based on experimental evidence or the generalized force-deformation relation shown in Figure 2, with parameters *c*, *d*, and *e* as defined in Table 2.

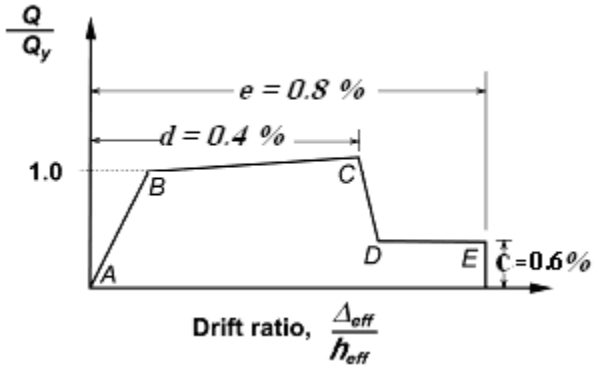

Fig. 2. Force-deformation relation for masonry elements or components.

Component drift ratios are the ratio of differential displacement, Δ_{eff}, between each end of the component over the effective height, h_{eff}, of the component. Depending on the geometry of the wall or pier configuration, the elevations at which these parameters are determined may vary within the same wall element.

In Nonlinear Static Procedure for deformation controlled components, nonlinear deformations shall not exceed the values given in table 2. Variables *d* and *e*, representing nonlinear deformation capacities for primary and secondary components, shall be expressed in terms of drift ratio percentages as defined in Figure 2. For force controlled components lower bound strengths shall not be less than the maximum design forces as mention in equation 6.

Table 2. Force-deflection relations parameters in nonlinear static procedure.

	Deformation parameters			**Acceptance Criteria; Performance Level**				
					Primary member		**Secondary member**	
Masonry Behavioral Mode	***c*** **%**	***d*** **%**	***e*** **%**	**IO %**	**LS %**	**CP %**	**LS %**	**CP %**
Bed-Joint Sliding	0.6	0.4	0.8	0.1	0.3	0.4	0.6	0.8

OUT-OF-PLANE UNREINFORCED MASONRY WALLS

Unreinforced masonry walls shall be evaluated for out-of-plane inertial forces as isolated components spanning between floor levels, and/or spanning horizontally between columns or pilasters. Unreinforced masonry walls shall not be analyzed out-of-plane with the Linear or Nonlinear Static Procedures. The out-of-plane unreinforced masonry walls shall be controlled by using table-3.

Table 3. Limitation to h/t ratio for wall.

Wall position	**A≥0.35g**	**A<0.35g**
Wall on the top floor	10	14
Wall on the other floor	15	15

CONCLUSION

The following conclusions are drawn from this study:

- Compared to the other two unreinforced masonry building instructions available in Iran, this guideline has a performance-based design and can be used to assess the masonry buildings for different performance and earthquake levels.
- The qualitative procedures presented in this guideline are highly functional for screening the existing masonry building.
- The quantitative procedures adopted in this guideline are based on two failure modes: the bed-joint sliding and the diagonal tension modes.

REFERENCES

1. Instruction for seismic rehabilitation of existing unreinforced masonry buildings, No:376, Management and planning organization, Islamic Republic of Iran, 2007.
2. ASCE 31-03-Seismic evaluation of existing buildings, American of Civil Engineering, 2003.
3. FEMA 356 “Seismic rehabilitation prestandard”, Federal Emergency Management Agency, US, 2000.
4. Seismic evaluation and strengthening of existing buildings, Final draft, Indian Institute of Technology, Kanpur, India, 2004.

DISASTER RECOVERY THEORY, MODELS, AND MEASURES: INSIGHTS FROM THE LAST 20 YEARS

Laurie A. Johnson, Ph.D. AICP[1]

INTRODUCTION

Recovery is a return to normalcy after a disrupting event, such as a disaster. But even a simple definition raises critical questions: What was "normal" before the disaster? Is restoring or replacing that which existed before the disaster really wise? When is the process completed? This paper briefly addresses the status of three challenges in disaster recovery: developing a theory of disaster recovery, establishing a process for effectively managing recovery, and establishing principles to improve recovery policy, programs, and management.

This year marks the 20th anniversary of the M6.9 Loma Prieta earthquake that struck Northern California in 1989, taking 63 lives and causing up to $10 billion in property losses (USGS 2009). Heavy damage in Santa Cruz County and the cities of Santa Cruz and Watsonville, as well as neighborhoods and major transportation projects in San Francisco and Oakland, required redevelopment plans and sustained financial and public intervention for many years for a return to normalcy to be fully realized. But, at the time, disaster recovery was a poorly understood and one of the least researched areas of disaster management. There had been little study of the long-term management of recovery activities following disasters, and even fewer that involved modern, urban settings. There was also only a limited amount of learning from really large, urban disasters, and many of the studies were inconsistent in their temporal coverage or limited in their technical focus.

This paper reports on the progress made in disaster recovery research over the previous decades with an emphasis on constructing theories on disaster recovery and recovery management, and modeling and measuring the recovery process and outcomes. It draws substantially from the author's dissertation, entitled "Developing a Management Framework for Local Disaster Recovery: A study of the U.S. disaster recovery management system and the management processes and outcomes of disaster recovery in 3 U.S. cities," submitted in partial fulfillment of the doctoral degree, School of Informatics, Kyoto University in March 2009 (Johnson 2009).

PROGRESSION OF DISASTER RECOVERY RESEARCH

In the 20 years since the 1989 Loma Prieta earthquake, there has been substantial learning from a considerable number of disasters that have had a protracted recovery effort. Long-term studies that have contributed to the significantly growing body of disaster literature devoted to recovery-related topics include studies on over a dozen major earthquakes, such as the M7.4 Manjil Iran (1990); M6.7 Northridge CA (1994); M6.9 Kobe Japan (1995); M7.6 and M7.2 Turkey (1999); M7.7 Chi-Chi Taiwan (1999); M7.7 Gujurat India (2001); M6.6 Bam Iran (2003); M9 Sumatra

[1] Principal, Laurie Johnson Consulting, 2550 Gough St. #6 San Francisco, CA 94123 Tel: (415)614-1438 Email: laurie@lauriejohnsonconsulting.com

and tsunami (2004); M6.6 Niigata Japan (2004); M6.8 Niigata Japan (2007); and M7.8 Sichuan China (2008) (cites).Some of the other non-seismic disasters that have been the focus of recovery research include: Hurricane Hugo (1989); the Oakland Firestorm (1991); Hurricane Andrew (1992); Midwest Floods (1993); North Dakota Floods (1997); Hurricane Floyd & India Cyclone (1999); World Trade Center (2001); Hurricanes Fabian, Isabel, and Typhoon Maemi (2003); the four Florida Hurricanes (2004); Hurricanes Katrina, Rita, and Wilma (2005); and, Hurricanes Gustav and Ike (2007).

Some of the key studies of recovery following major earthquakes looked at the restoration and rebuilding processes following the 1906 San Francisco, California; 1923 Tokyo, Japan; 1963 Skopje, Yugoslavia; 1964 Anchorage, Alaska; 1968 Guatemala City, Guatemala; 1972 Managua, Nicaragua; 1976 Friuli, Italy; 1976 Tangshan, China; 1980 El Asnam, Algeria; 1985 Mexico City, Mexico; and, 1988 Spitak, Armenia (Haas, Kates, and Bowden 1977; William Spangle and Associates et al. 1980; William Spangle and Associates 1991; Arnold 1993). Some other non-seismic disasters that had a protracted recovery process which was studied and documented included several early-20th century U.S. hurricanes and post-World War II reconstruction in Europe and Japan.

Early research gave structure to the physical process of recovery. *Reconstruction Following Disaster* was the first U.S.-funded research study to take a comprehensive, longer-term view of disaster recovery (Haas, Kates, and Bowden 1977). Based upon case studies that included the rebuilding following the 1906 San Francisco, 1964 Alaska and 1972 Managua earthquakes, Haas et al described "recovery" as an "ordered, knowable, and predictable process" in which there is a strong community desire to "return to normalcy" following a disastrous event (Haas, Kates, and Bowden 1977, xxvi). They also found that cities almost always rebuild on the same site, and it usually looks familiar to its residents, an insight that has been confirmed by subsequent studies of post-disaster reconstruction planning (Haas, Kates, and Bowden 1977, xxv; William Spangle and Associates et al. 1980; Arnold 1993; Olshansky, Johnson, and Topping 2006). Their work is characteristic of the recovery research of the 1970s and 1980s which emphasized understanding the physical aspects of rebuilding.

Challenges of managing and modeling the recovery process. *Community Recovery* was the first U.S. study that carefully examined governmental organization and recovery processes at a community-level (Rubin 1985). This study looked at 14 disasters throughout the U.S caused by an array of agents. In contrast to the Haas et al study, none of these were catastrophic disasters and all the communities eventually recovered (Rubin 1985, 55). Rubin et al. stressed that "recovery encompasses all domains of community life" – residential, business, public services and facilities, general population, and mitigation (Rubin 1985, 15). They also observed that recovery is more complicated than Haas' sequential model with an ill-defined endpoint and no agreed upon measure of success. Along with many other studies around this time, they also attempted to model the recovery process, but were unable to determine how to measure "effective recovery" and outcomes (Rubin 1985, 12-13). Instead, they proposed a series of characteristics and actions found in the recovery processes, organized around 3 elements – personal leadership, ability to act, and knowledge of what to do; furthermore, they found that leadership is the most critical of these elements (Rubin 1985, 37).

Post-disaster recovery is an opportune time for mitigation and betterment. In the context of modern, industrialized cities, more recent research suggests that recovery is never a return to the status quo ex ante – or the conditions as they were before the event (Alesch 2005; Daniels, Kettl, and Kunreuther 2006; Olshansky, Johnson, and Topping 2006). Catastrophes, in particular, tend to offer opportunities for large-scale redevelopment, as Arnold describes in Tangshan, Spitak, and parts of Tokyo (Arnold 1993). In the 1990s and 2000s, many researchers reported on the importance of post-disaster recovery in the disaster cycle since it provides significant opportunities for mitigation and thereby helping to break the cycle (William Spangle and Associates 1991; Berke, Kartez, and Wenger 1993; Eadie and Johnson 1997; Schwab 1998; Mileti 1999; Smith and Wenger 2007). Of the 3 primary levels of governance in the U.S. – local, state, and national, individual local governments face the greatest public pressure to provide a quick return to normalcy, while also having potentially one of the most opportune times, post-disaster, to rebuild stronger, change land use patterns, reduce development in hazardous areas, and also reshape social, political and economic pre-existing conditions. The desire to return to normalcy also competes with the value choices to 'reduce future community vulnerability' or 'seize opportunities for community betterment,' such as improved efficiency, equity or amenity.

Social and economic dimensions of recovery can present long-lasting challenges. Research following some of the more recent, large-scale urban disasters – starting with the 1985 Mexico City earthquake and including the 1989 Loma Prieta earthquake, 1992 Hurricane Andrew, 1994 Northridge and 1995 Kobe earthquakes, 2004 Tsunami, and 2005 Hurricane Katrina – acknowledged the complexities of the recovery process extending well beyond physical and organizational dimensions of recovery, into social, emotional, economic, financial, institutional, and environmental realms as well (Hayashi 2007; Olshansky and Chang 2009).

Most of the sociological research on recovery has focused on family and household recovery (Mileti 1999). Noteworthy is the work of Tamura, Tatsuki and others, who tracked the speed and quality of personal and family recovery for a decade after the 1995 Kobe, Japan earthquake (Tamura 2007; Tatsuki 2007). They identified "seven elements of life recovery," of which housing was identified as the most important, followed closely by social ties (Tamura 2007). Land use planning was the third and a markedly lower element, followed closely by physical/mental health, preparedness, economic and financial situations, and relation to government (Tamura 2007). This survey data, along with an expanded 2005 survey of Kobe area victims and surveys of victims of the 2004 Niigata earthquake, was also used to construct a recovery and reconstruction calendar that illustrates the differential rates and extended timeframes for key elements of post-disaster social recovery (Kimura 2007).

Studies of the long-term economic effects of disasters have focused primarily on individual businesses or economic sectors. One survey of over 1,000 businesses following the 1994 Northridge earthquake found that the "more post-disaster operational problems a business encountered, the lower its probability of recovering (Dahlhamer and Tierney 1998, 132). In separate studies, Chang and Nagamatsu found contrasting evidence in Kobe's economy following the 1995 earthquake. Chang's investigation of specific economic sectors, such as the Port of Kobe, revealed long-term structural change (Chang 2001). Nagamatsu found that Kobe's post-disaster economy suffered from both the earthquake damage and macroeconomic depression; the situation was so severe that the city had a negative growth rate for 2 years after the earthquake (Nagamatsu 2007).

Observing long-term recovery in Japan following the 1995 Kobe earthquake, Hayashi (2007) considered how the various elements of recovery can influence each other. He concluded that the significant investment of Japan's national government in infrastructure and physical restoration may have been a disincentive in stimulating new or emerging economic development in the impacted area (Hayashi 2007, 415). In looking at Kobe's recovery, the physical recovery was completed within 5 years, while elements of economic and life recovery had still not been achieved by 2006 – 11 years after the earthquake (Hayashi 2007, 414).

CONSTRUCTING THEORIES ON DISASTER RECOVERY AND DISASTER RECOVERY MANAGEMENT

In January 2005, the 1st International Conference on Urban Disaster Reduction, held in Kobe, Japan, designated an entire conference track to the development of a "Theory of Disaster Recovery." The session participants concurred that, as of yet, there is no theory or even consensus definitions about what "recovery" means, how it should be modeled or measured, or what constitutes "successful" or "effective" recovery (Olshansky and Murao 2005). As one participant put it (Alesch 2005): "Few things are as practical as good theory; few activities are as risky as implementing policies or taking irrevocable actions on the basis of faulty or nonexistent theory."

One of the difficulties in producing a comprehensive theory of disaster recovery is that "it must integrate current findings with theoretical concepts" that bridge across levels of social units (e.g. households, neighborhoods, community, region, and society) (Smith and Wenger 2007). While there have been a few quantitative attempts at modeling the recovery process and measuring its outcomes, the vast majority of recovery-related research has been mostly qualitative in nature; and qualitative recovery research is subject to both factual and perceptual errors or variations (Rubin 1985; Alesch and Holly 2007). Comparable disaster situations are infrequent happenings; post-disaster decisions and actions are occurring in many instances under duress; documentation is sometimes limited; and, with the passage of time, perceptions and recollections change. There are still formidable challenges that theoretical development efforts have to overcome.

A decision-based theory of recovery and recovery management. "Disaster recovery" is a complex process that encompasses both short-term and long-term activities and involves all elements of modern urban settings (i.e. physical, social, economic and institutional). The process works to achieve a stable state across all these elements, and is not necessarily a return to what existed before; it has no clear end point. The "disaster recovery process happens with the many decisions made, and resulting actions taken, by individuals, businesses and institutions, both directly and indirectly impacted, as they determine whether to do nothing, essentially restore what was lost, or try to improve beyond what existed before the disaster" (Johnson 2009).

"Disaster recovery management is also a decision process that involves planning, organizing, leading and controlling a comprehensive recovery vision, and influencing the many simultaneous decision-actions required to achieve it as effectively and efficiently as possible" (Johnson 2009). Key influences are vision – often in the form of leadership and plans – and resources, most importantly money (Rubin 1985; Johnson 2009). But, without a comprehensive understanding of the needs or a recovery vision, bureaucratic management approaches tend to be reactive, inflexible, and inefficient. Flexible and forward-thinking approaches – similar to decentralized

models used in crisis management – can provide the capacity needed to influence these "decision-actions" while also keeping pace with the compressed timeframes of recovery (Johnson 2009).

Tensions of time compression in recovery. Recovery and its management processes occur in an extreme environment where time is compressed due to the pressures to restore normalcy (Johnson 2009; Olshansky and Chang 2009). The urban setting which might have taken decades or more to construct, must, post-disaster, be repaired or rebuilt in a much shorter time; and decision making must go faster than information, knowledge, and planning generally flows. Yet, rebuilding needs time to be accomplished thoughtfully and to allow for proper deliberation and public discourse on how to achieve risk reduction and betterments, such as improved efficiency, equity or amenity as part of the process. Citizen participation is essential, to determine vision, provide communication, and ensure community support (Olshansky, Johnson, and Topping 2006).

Optimizing the flow of money in recovery. Disaster recovery also requires some portion of the total funds spent over decades or longer to construct urban environments. However, post-disaster, the amount and flow of money needs to match the compressed pace of recovery. Knowing how much money is needed and where it is needed are major challenges in a post-disaster environment. It may be obvious when there is too little money or it comes too slowly; however, "too much" or "too fast" has problems too. Recovery funding also comes from many sources: insurers; local, state, and national governments; foundations; investors; victims' savings; international aid organizations. All of these sources are vital to successful recovery. But, getting it from the source to the "need" also has many challenges (i.e. distribution, accountability, capacity). Setting priorities for use of limited funds is a challenge, and the process is not usually a rational one. Flexibility of funding is also important since post-disaster needs change with time.

MODELING AND MEASURING THE RECOVERY PROCESS AND OUTCOMES

Along with better theory, researchers also acknowledge the need for better models and measures of disaster recovery and recovery management processes, as well as consistent methods to track and record recovery and develop recovery archives over time (Olshansky and Murao 2005; Smith and Wenger 2007; Olshansky and Chang 2009). With infrequent disaster events, there has been an inherent lack of systematic study to develop quantitative data as well as qualitative indicators of recovery, such as plans, processes, key actors and institutions (Miles and Chang 2006). Researchers are challenged to "overcome the tendency to build up knowledge one disaster at a time and focus more on what disasters… of all types have in common with respect to origins, dynamics, and outcomes" (Tierney 2007, 520).

While Haas, Spangle and others have agreed that recovery and reconstruction can take up to 10 years to complete, we still lack an understanding of how to define and describe recovery across multiple sectors, the endpoint of recovery, what has been achieved with recovery. As Comerio succinctly summarized, the degree of success in recovery will depend upon the measures made at (Comerio 2005):

- At the different scales (e.g. individual, household, neighborhood, community, city or region)
- Over what length of time (e.g. days, months, years, or decades)

- From the perspective of the evaluator (e.g. individual recipient of assistance, local community, funding provider, independent evaluator).

Hayashi (2007) proposes that successful recovery requires coordination among 3 recovery goals – economic, physical and life recovery; and, furthermore, that economic recovery should be the top priority and guiding force in recovery; but life recovery for all disaster victims is the ultimate goal (Hayashi 2007, 416). Hayashi regards physical recovery as a tool for economic development and upgrading social infrastructure to achieve future sustainable development; he also proposes that personal and family recovery should be viewed as a direct result of economic recovery (Hayashi 2007, 416).

Karatani and Hayashi (2007) analyzed statistical data published monthly by the city of Kobe, Japan for over a decade following the 1995 earthquake, to develop a concept and scheme of recovery indices based upon time series analysis. They propose setting standardized benchmarks of 100% for the value during the last month prior to the earthquake, in order to make data dimensionless and comparable across fields (Karatani and Hayashi 2007, 455). They developed equations based upon time series analysis to determine and extract trends, periodic variations (i.e. season variations), and noise (random variation) in the data. Finally, they entered in a 120 items from the Kobe city statistics which spanned 13 years, or 154 months, from April 1992 to January 2005. Data items included: population, household consumption and retail sales, bankruptcies and outstanding bank loans, new housing and job starts, and railway ridership (Karatani and Hayashi 2007, 457). Karatani and Hayashi's work provides one of the most comprehensive methodologies for collecting and analyzing recovery outcomes when data is available. Additional accumulation and analysis of data from other locations and disasters are needed in order to generalize the Kobe city analysis into a recovery model.

Notably distinct from all other research is the work of Miles and Chang (2006) to develop and refine a more holistic model that looks at linkages between sectors, scales and processes, and anticipates recovery trajectories across the sectors. Their conceptual model of recovery is comprised of an object model, dynamic model and functional model, which together describe the real-world system (Miles and Chang 2006, 444). The object types in the model include the community, neighborhoods, households, businesses, and lifelines. Each object type has attributes and engages in behaviors that have influences on the outcomes. The functional model describes 5 principal types of interrelated recovery influences: (1) the dynamic effects of changes over time; (2) agent-attribute effects that may influence its recovery, such as demand for a business' product; (3) interaction effects; (4) spatial effects; and (5) policy or decision effects (Miles and Chang 2006, 449). They have tested and calibrated the model against the 1994 Northridge and 1995 Kobe earthquakes and shown that agent recovery timepaths are interdependent (e.g. households consume business products, while businesses provide households with income) (Olshansky and Chang 2009). Their future research is focused on determining what factors most strongly influence recovery and how certain policy and planning intervention can affect recovery capabilities and therefore community resilience (Olshansky and Chang 2009).

Even with such advances, the field of disaster recovery research still lacks a robust set of qualitative descriptors, and even much less quantitative measures of recovery progress and outcomes. By distilling the research literature, which was remarkably consistent, Johnson (2009) derived a set of 38 qualitative descriptors of physical, social, economic, and institutional

outcomes that can be used to assess the outcomes of recovery from multiple perspectives; see Table 1. A portion are defined as "restoration" indicators since they are more related to direct products or outcomes of the process of recovery (i.e. numbers of houses repaired or rebuilt). Also, indicators of "resilience" are also defined to describe how future disruption has been minimized, flexibility and adaptability have been added, and other improvements have been made as part of the recovery process (Bruneau et al. 2003; Vale and Campanella 2005; Smith and Wenger 2007). It is proposed that these indicators can be used to develop a more holistic recovery policy and also track and measure its post-disaster effectiveness (Johnson 2009).

Table 1. Compilation of restoration and resilience indicators derived from recent recovery research studies (source: Johnson 2009).

	Restoration	Resilience
Physical (11)	•Rebuilt damaged residential units •Rebuilt damaged commercial/ industrial properties •Utilities restored and rebuilt infrastructure •Rebuilt public facilities •Visual evidence of disaster gone	•Mitigation improvements to residential units •Mitigation of commercial/ industrial units •Mitigation of public facilities infrastructure •Environmental recovery and improvements
Social (8)	•Population and resident retention/growth •Schools resumed and educational opportunities •Satisfaction of basic human needs/ daily life •Mental and physical health maintained/ restored	•Affordable and ample residential housing supply •Neighborhood condition improvements •Social and geographic equity •Social networks resilience and self-reliance
Economic (6)	•Jobs resumed/retention •Business resumption/retention •Cultural/historic/recreation/tourist amenities	•Affordable and ample commercial/industry space •Economic diversity and business/market/job growth •Wealth recovery/sustainability improvement
Institutional (13)	•Timely recovery action/ reconstruction completion •Leadership, innovation, creativity and vision •Use of high-quality information in decisionmaking •Robust stakeholder representation, decisionmaking •Ample resources and ability to leverage them •Resident/business satisfaction with outcomes •Positive external reputation/perception	•Institution routines, redundancy, sustainable capacity •Intergovernmental collaboration, institutional equity •Institutionalized/strengthened/sustainable planning •Fiscal recovery/sustainability/improvement •Political recovery/sustainability/improvement •Risk management/preparedness commitment

SUMMARY

Over the past 20 years, researchers have developed a more multi-disciplinary understanding of the disaster recovery process; yet, disaster recovery is still a relatively new field of research and there are still many challenges in constructing theories of recovery and recovery management, as well as models and measures of the process and outcomes. Research following the 1994 Northridge and 1995 Kobe earthquakes has been critical to advancing the field. Still, none of the major earthquake megacity scenarios that we have been planning for have yet happened, such as Beijing, Cairo, Kathmandu, Los Angeles, Mexico City, San Francisco/Oakland, Taipei, Tehran, and Tokyo.

Recovery and recovery management are decision processes. Government institutions can best influence the many decision-actions with vision (i.e. leadership and plans) and resources (i.e. money). One distinguishing characteristic of recovery is time compression and its affect on urban development and decision processes. Flexible, forward-thinking management approaches – similar to the decentralized models used in crisis management – can help develop a

comprehensive understanding of the post-disaster needs as well as a unified vision. They can also provide the necessary capacity to influence the many decision-actions, while keeping pace with time compression in recovery.

Flexible funding flows are also needed to better match the dynamic and compressed pace of recovery. Finally, a more holistic understanding of the desired outcomes – both in restoring what has been lost and improving urban resilience – is needed to improve our recovery policy, programs, and management.

REFERENCES

Alesch, Daniel. 2005. Complex Urban Systems and Extreme Events: Toward a Theory of Disaster Recovery. In *1st International Conference on Urban Disaster Reduction*. Kobe, Japan, January 18.

Alesch, Daniel, and James Holly. 2007. *Long-term Community Disaster Recovery: Managing in the Aftermath (DRAFT MANUSCRIPT)*. Fairfax, VA: Public Entity Risk Institute.

Arnold, Christopher. 1993. *Reconstruction After Earthquakes: Issues, Urban Design, and Case Studies*. Report to the National Science Foundation. San Mateo, CA: Building Systems Development, Inc.

Berke, Philip, Jack Kartez, and Dennis Wenger. 1993. Recovery After Disaster: Achieving sustainable development, mitigation and equity. *Disasters* 17, no. 2: 93-109.

Bruneau, Michel, Stephanie E. Chang, Ronald T. Eguchi, George C. Lee, Thomas D. O'Rourke, Andrei M. Reinhorn, Masanobu Shinozuka, Kathleen Tierney, William A. Wallace, and Detlof von Winterfeldt. 2003. A Framework to Quantitatively Assess and Enhance the Seismic Resilience of Communities. *Earthquake Spectra* 19, no. 4 (November): 733-752.

Chang, Stephanie E. 2001. Structural Change in Urban Economies: Recovery and Long-Term Impacts in the 1995 Kobe Earthquake. *The Kokumin Keizai Zasshing (Journal of Economics and Business Administration)* 183, no. 1, Special issue on the Great Hanshin Earthquake: Economic Analysis of the Disaster and the Recovery: 47-66.

Comerio, Mary. 2005. Key Elements in a Comprehensive Theory of Disaster Recovery. In *1st International Conference on Urban Disaster Reduction*. Kobe, Japan, January 18.

Dahlhamer, James M., and Kathleen Tierney. 1998. Rebounding from Disruptive Events: Business Recovery following the Northridge Earthquake. *Sociological Spectrum* 18: 121-141.

Daniels, Ronald, Donald Kettl, and Howard Kunreuther, eds. 2006. *On Risk and Disaster: Lessons from Hurricane Katrina*. Philadelphia, PA: University of Pennsylvania Press.

Eadie, Charles, and Laurie A. Johnson. 1997. Recovery and Reconstruction: A Status Report from Recent U.S. Earthquake on Organization Issues, Land Use Policy, Redevelopment and Urban Design. In , 97-A:91-102. Vol. 97. Pasadena, CA: Earthquake Engineering Research Institute, August.

Haas, J. Eugene, Robert Kates, and Martyn Bowden, eds. 1977. *Reconstruction Following Disaster*. Cambridge, MA and London, England: The MIT Press.

Hayashi, Haruo. 2007. Long-term Recovery from Recent Disasters in Japan and the United States. *Journal of Disaster Research* 2, no. 6: 413-418.

Johnson, Laurie A. 2009. Developing a Management Framework for Local Disaster Recovery: A study of the U.S. disaster recovery management system and the management processes and outcomes of disaster recovery in 3 U.S. cities. Dissertation submitted in partial fulfillment of the Doctoral Degree, School of Informatics, Kyoto University. March.

Karatani, Yuka, and Haruo Hayashi. 2007. Quantitative Evaluation of Recovery Process in Disaster-Stricken Areas Using Statistical Data. *Journal of Disaster Research* 2, no. 6: 453-464.

Kimura, Reo. 2007. Recovery and Reconstruction Calendar. *Journal of Disaster Research* 2, no. 6: 465-474.

Miles, S., and Stephanie E. Chang. 2006. Modeling Community Recovery from Earthquakes. *Earthquake Spectra* 22, no. 2 (May): 439-458.

Mileti, Dennis S. 1999. *Disaster by Design: A Reassessment of Natural Hazards in the United States*. An Activity of the International Decade for Natural Disaster Reduction. Washington D.C.: Joseph Henry Press.

Nagamatsu, Shingo. 2007. Economic Problems During Recovery from the 1995 Great Hanshin-Awaji Earthquake. *Journal of Disaster Research* Volume 2, no. 5: 372-380.

Olshansky, Robert, Laurie Johnson, and Kenneth Topping. 2006. Rebuilding Communities Following Disaster: Lessons from Kobe and Los Angeles. *Built Environment* 32, no. 4. Lessons from Urban Disasters: Planning for Resilient Cities: 354-374.

Olshansky, Robert, and Osamu Murao. 2005. Toward a Comprehensive Theory of Disaster Recovery presented at the 1st International Conference on Urban Disaster Reduction, January 20, Kobe.

Olshansky, Robert B., and Stephanie E. Chang. 2009. Planning for Disaster Recovery: Emerging Research Needs and Challenges. *Progress in Planning*. Special Issue on Emerging Research Agendas in Urban Planning (In press): (Manuscript provisionally accepted).

Rubin, Claire. 1985. *Community Recovery from a Major Natural Disaster*. Monograph No. 41. Boulder, Colorado: Program on Environment and Behavior, Institute of Behavioral Science, University of Colorado.

Schwab, Jim. 1998. *Planning for Post-Disaster Recovery and Reconstruction*. Planning Advisory Service Report Number 483/484. Chicago, IL: American Planning Association, December.

Smith, G., and Dennis Wenger. 2007. Chapter 14, Sustainable Disaster Recovery: Operationalizing An Existing Agenda. In *Handbook of Disaster Research*, 234-257. Handbooks of Sociology and Social Research. New York, NY: Springer. www.springer.com.

Tamura, Keiko. 2007. Defining Recovery: 7-Element Model. *Journal of Disaster Research* 2, no. 6: 475-483.

Tatsuki, Shigeo. 2007. Long-term Life Recovery Processes Among Survivors of the 1995 Kobe Earthquake: 1999, 2001, 2003, and 2005 Life Recovery Social Survey Results. *Journal of Disaster Research* 2, no. 6: 484-501.

Tierney, Kathleen J. 2007. From the Margins to the Mainstream? Disaster Research at the Crossroads. *Annual Review of Sociology* 3: 503-525.

USGS, U.S. Geological Survey. 2009. Progress Toward a Safer Future Since the 1989 Loma Prieta Earthquake. USGS Fact Sheet 151-99, Online Version 1.0. http://pubs.usgs.gov/fs/1999/fs151-99/.

Vale, Lawrence, and Thomas Campanella, eds. 2005. *The Resilient City: How Modern Cities Recover from Disaster*. New York, NY: Oxford University Press. www.oup.com.

William Spangle and Associates. 1991. *Rebuilding After Earthquakes: Lessons From Planners*. Portola Valley, CA: William Spangle and Associates, Inc.

William Spangle and Associates, Earth Science Associates, H. J. Degenkolb & Associates, George S. Duggar, and Norman Williams. 1980. *Land Use Planning After Earthquakes*. Portola Valley, CA: William Spangle and Associates, Inc. www.spangleassociates.com.

A PROPOSAL FOR US-IRANIAN COLLABORATION: IMPROVING SCHOOL EARTHQUAKE SAFETY IN CENTRAL ASIA

Brian E. Tucker
GeoHazards International
Palo Alto, California 94301

OBJECTIVE

Our objective is for US and Iranian specialists in earthquake engineering, seismology, public policy and school administration to collaborate on a project that would improve school earthquake safety in the ten countries comprising the Economic Cooperation Organization (ECO). The project would accomplish this by establishing region-wide policy norms and building capacity within ECO and its members. The Iranian and U.S. specialists would work with colleagues from all ECO countries.

PROBLEM

There are two problems. The most obvious is the disaster waiting to happen in schools in Central Asia. In the October 8, 2005 earthquake in northern Pakistan, over 8,000 schools were either destroyed or damaged beyond repair. Over 17,000 school age children perished and over 20,000 suffered serious injuries including amputations. Many of the schools in ECO member nations are equally vulnerable to earthquakes. Millions of children are at risk every day. The second problem is that many ECO countries lack a school earthquake safety policy framework and the capacity to implement such a policy. This lack of policy and capacity makes it impossible to sustain the systematic long-term effort needed to improve school earthquake safety and thus avoid future disasters in ECO countries.

THE ECONOMIC COOPERATION ORGANIZATION

The Economic Cooperation Organization (ECO) is an intergovernmental regional organization established in 1985 by Iran, Pakistan, and Turkey for the purpose of promoting economic, technical, and cultural cooperation among the member states. The current members are the Islamic State of Afghanistan, Azerbaijan Republic, Islamic Republic of Iran, Republic of Kazakhstan, Kyrgyz Republic, Islamic Republic of Pakistan, Republic of Tajikistan, Republic of Turkey, Turkmenistan and Republic of Uzbekistan. Its secretariat is located in Tehran, Iran. See www.ecosecretariat.org. ECO and GHI have worked together over several years on school earthquake safety, for example, co-hosting a workshop in June 2006 with OECD, that described the ECO region's school earthquake risk and mitigation options and, most recently, meeting in December 2008 to decide how best to address that risk. This proposal is the outcome of that meeting.

APPROACH

The Iranian and U.S. specialists would work with the ECO Secretariat to host a series of meetings in Tehran followed by assessments of the school earthquake safety programs of 3 ECO countries. GHI has worked with the Organization for Economic Cooperation and Development (OECD) to develop guidelines for effective national school earthquake safety programs for OECD member countries; this work is described in *Keeping Schools Safe in Earthquakes* (OECD, 2004). Specialists from Iran, the United States, other ECO countries and OECD would develop, using the OECD guidelines as a starting point, guidelines for effective school earthquake programs for ECO countries. Policy discussions would provide an opportunity to transfer earthquake risk and risk reduction knowledge making concepts more transparent, build capacity within the participating organizations, and create mutually supporting efforts and personal relationships. These factors make the policy easier to implement and sustain. Officials and engineers from nations with active school earthquake safety programs such as Iran, Turkey and the United States where the California school earthquake safety program is 75-years old, would share their experience and knowledge.

The project would have three phases.

1. **Policy Development and Capacity Building.** The ECO members would develop an ECO school earthquake safety policy, an assessment protocol and an action plan for implementation appropriate for ECO countries. The OECD Recommendation Concerning Guidelines on Earthquake Safety in Schools would be the starting point. Representatives of the ECO member nations and invited experts would discuss how the OECD guidelines could be adapted to the needs of ECO countries. The ECO Council of Ministers would consider these guidelines for possible adoption.
2. **National Assessments**. Three ECO nations, to be named later, would conduct national self-assessments of current school earthquake safety policies using the protocol adopted as part of Phase 1. ECO and regional earthquake professionals would assist with these assessments.
3. **Demonstration Projects**. ECO, GHI and regional earthquake professionals would conduct implementation projects in each of the nations undertaking Phase 2 assessments to demonstrate the feasibility of measures included in the guidelines prepared in Phase 1. These projects would engage responsible parties from the host nations, and build capacity among their representatives and within ECO. These projects would address elements in the policy that call for vulnerability analysis and retrofitting, awareness, preparedness plans, reducing falling hazards and teaching about earthquakes.

RESULTS

- Earthquake professionals from the United States, Iran and other countries from the ECO region will have worked together to improve the school earthquake safety of the ECO countries;
- The ECO Secretariat will have become a center of excellence for school earthquake safety;
- A school earthquake safety policy will have been considered for adoption by the ECO Council of Ministers and member nations;
- An assessment protocol and action plan will have been written for ECO nations;
- Three nations will have assessed their conformance with the ECO policy and the results will have been used to encourage assessments in other nations;
- Two projects implementing the policy recommendations will have demonstrated the feasibility of mitigation to ECO nations; and
- Earthquake safety experts and education administrators within the United States, Iran and other ECO nations will have built new professional relationships.

EARTHQUAKE RISK LOSS ASSESSMENT

Mohsen Rahnama, Patricia Grossi, and Mary Lou Zoback

Risk Management Solutions, Newark, CA, USA
Email: mohsen.rahnama@rms.com

ABSTRACT

This paper reviews the history of insured catastrophe losses and the development of earthquake risk loss assessment models, illustrating the buildings blocks of models and the assessment of risk for insurance purposes. The paper concludes with the latest state-of-the-art models developed by Risk Management Solutions, highlighting the current challenges faced by risk modelers and the role of models in reducing the impacts of earthquake hazards worldwide.

INTRODUCTION

The growing number of people who live in locations exposed to natural perils such as earthquakes, floods, and tropical cyclones, along with higher concentrations of value and the increased vulnerability of infrastructure, has led to a rapid rise in worldwide exposure to losses from natural catastrophes.

The role of catastrophe insurance in protecting societies from the effects of disasters varies by country and peril. In general, insurance is more widely available for wind perils than for earthquake risks. For example, the 1994 Northridge Earthquake in the United States caused total economic losses of US$45 billion with insured losses at approximately US$18.5 billion (in 2008 dollars). The 1995 Great Hanshin Earthquake in Japan caused even more damage. Total economic losses have been estimated at over US$100 billion, but insured losses only covered 3% of the loss due to limited payout rates from Japan's residential insurance at that time. By contrast, insurance claims for windstorms Lothar and Martin in Western Europe in 1999 are estimated to have paid for more than 50% of the total economic losses. Following Hurricane Katrina in 2005, approximately US$70 billion in insurance payments—close to 55% of the economic loss—were made to residents and businesses in coastal Louisiana and Mississippi, including payouts from the U.S. National Flood Insurance Program (NFIP), to help rebuild and recover.

As Figure 1 shows, both economic and insured losses from natural disasters are increasing. In addition, if one considers the number of fatalities resulting from natural disaster events—particularly for earthquake events in regions with non-engineered buildings—there has been little progress over time in reducing casualties. For example, the Wenchuan Earthquake, which struck on May 12, 2008 and caused 70,000 casualties, was the highest casualty event since the 1976 Tangshan Earthquake. Moreover, the L'Aquila Earthquake, which occurred on April 6, 2009, caused 300 casualties but was a reminder of the vulnerability of the building stock. In essence, there is a need to manage and mitigate the

risk from future disasters and earthquake loss assessment or catastrophe models are extremely useful in gaining a better understanding and management of risk.

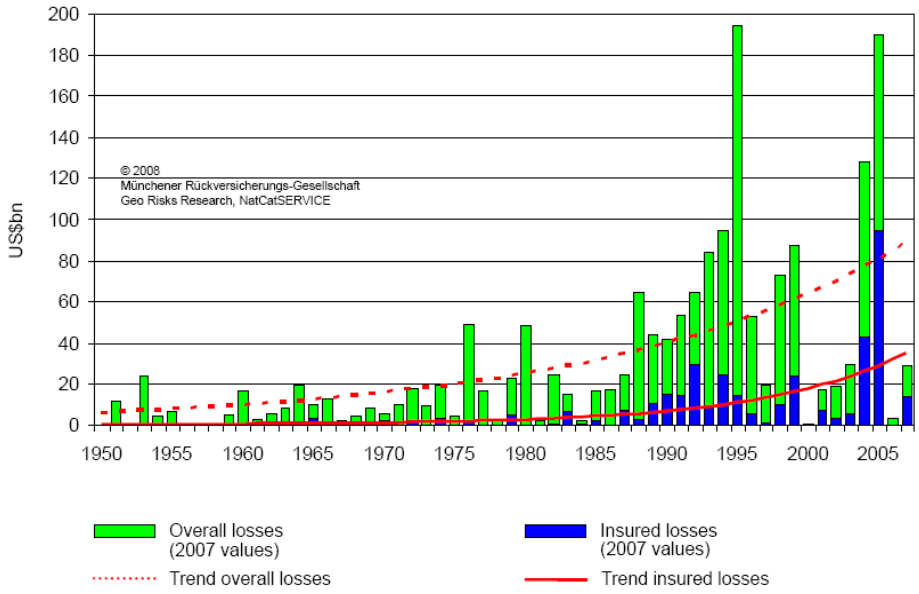

Fig. 1. Overall and insured losses from global natural disasters from 1950 to 2007 (Source: Munich Re, 2008).

CATASTROPHE MODELS

Roots of Modeling

Catastrophe modeling is not rooted in one field or discipline. The science of assessing and managing catastrophe risk originates in the fields of property insurance and the science of natural hazards. Insurers may well argue that catastrophe modeling's history lies in the earliest days of property insurance coverage for fire and lightning. In the 1800s, residential insurers managed their risk by mapping the structures that they covered. Not having access to the Geographic Information Systems (GIS) software of today, they used tacks on a wall-hung map to indicate their concentration of exposure. This crude technique served insurers well and limited their risk in the fire-prone urban areas.

On the other hand, a seismologist or meteorologist may well argue that the origin of catastrophe modeling lies in the modern science of understanding the nature and impact of natural hazards. In particular, the common practice of measuring an earthquake's magnitude and a hurricane's intensity is one of the key ingredients in catastrophe modeling. A standard set of metrics for a given hazard must be established so that risks can be assessed and managed. This measurement began in the 1800s, when the first modern seismograph (measuring earthquake ground motion) was invented and modern versions of the anemometer (measuring wind speed) gained widespread usage.

In the first part of the twentieth century, scientific measures of natural hazards advanced rapidly. By the 1970's, studies theorizing on the source and frequency of events were published. These developments led U.S. researchers to compile hazard and loss studies, estimating the impact of earthquakes, hurricanes, floods, and other natural disasters.[1] These two separate developments–mapping risk and measuring hazard–came together in a definitive way in the late 1980's and early 1990's, in the first generation of catastrophe models.

These models then gained widespread attention until after Hurricane Andrew hit southern Florida in August of 1992. Nine insurers became insolvent as a result of their losses from the hurricane and many others suffered 'larger than expected' losses based on actuarial principles employed for risk management at the time. After the 1994 Northridge and 1995 Kobe earthquakes, insurers and reinsurers further realized that, in order to reduce the likelihood of a very severe loss relative to their surplus, they needed to estimate and manage their natural hazard risk more precisely. Many companies turned to the modelers of catastrophe risk for decision support.

Since this time, the catastrophe modeling business has grown considerably. In 2009, catastrophe models are in widespread usage throughout the insurance industry, assisting insurers, reinsurers and other stakeholders to manage their risk from natural disaster events in the U.S. and other regions of the world.

Framework for Earthquake Risk Modeling

The basic framework for modeling earthquake risk is an engineering-based model, which assumes that losses are a consequence of the direct action of the hazard (e.g. the earthquake ground motion) on the exposure. The exposure—the building or facility and its contents—is subject to damage, which takes some predefined cost to repair or replace. Damaged buildings tend to be individual and separate; the damage is discrete. Damage at a commercial or industrial facility can result in the interruption of business activities, which will further add to the losses. Where residential properties are badly damaged, people may incur additional costs if they relocate while their property is being repaired. Therefore, the cost is the sum of all the individual elements of damage and loss, and these elements are largely independent of each other.[2] This is the engineering-based model understanding of a catastrophe, in which the total loss is the sum of the hazard multiplied by the exposure multiplied by the vulnerability at each location (For more information, see Grossi and Kunreuther, 2005).

If one would describe this approach in a step-by-step process, the five steps in a probabilistic catastrophe model for earthquake hazard are illustrated in Figure 2. These include: (1) generating the stochastic earthquake events; (i.e., defining the hazard); (2) assessing the earthquake ground motion; (3) developing the exposure at risk (e.g., characterization of the property at risk, including its vulnerability to damage); (4)

[1] For more information on the developments of earthquake risk modeling, see Grossi et al., 2008.
[2] When calculating net losses to an insurance portfolio, losses at property locations in close proximity to each other are highly spatially correlated.

calculating the damage to the exposure at risk; and (5) quantifying the direct and indirect financial loss, including allocating losses to the stakeholders at risk (e.g., property owner, insurer, reinsurer as applicable).

Fig. 2. Catastrophe modeling framework for earthquake risk.

Limitations of Models

Each step in the process shown in Figure 2 is critical to the overall loss estimate. For any model, recognizing the importance of input data is essential. The "garbage in, garbage out" principle holds irrespective of how advanced or state-of-the-art a model may be. Partial information on a property's characteristics can result in an inaccurate measure of risk. For example, is a residential structure coded as masonry when in fact it is wood frame? Is a commercial structure in fact a petrochemical refinery when it is coded as a chemicals processing plant? Are the structures' and contents values underestimated? This type of misinformation in the underwriting process results in inaccurate measures of risk.

Models are central to critical decisions that range from the pricing and underwriting of individuals accounts to the management and allocation of capital on a global scale, and when appropriately used, are essential tools for making informed judgment. But it is important to properly understand the limitations of models in order to fully appreciate uncertainty behind any one decision. In recent years, major catastrophes—Hurricanes Charley, Frances, Ivan, and Jeanne in 2004 and Hurricane Katrina in 2005, in particular—had a major impact on how catastrophe models are viewed and being utilized by the insurance industry. Insurers are taking a closer look at their own underwriting practices and taking a more comprehensive approach to understanding and managing risk. In essence, the science and impact of natural hazards are not completely understood and lead to uncertainty in estimating catastrophe risk. By recognizing the uncertainty associated with catastrophe models, insurers are more disciplined about managing their exposure and are beginning to take steps to protect themselves against losses that they may not have foreseen.

STATE-OF-THE-ART IN EARTHQUAKE RISK MODELING AND MANAGEMENT

One of the primary responsibilities of a catastrophe modeler is to continually remain abreast of and incorporate relevant new science in a timely fashion to ensure the models provide the best possible quantification of risk. Risk Management Solutions remains committed to this responsibility, incorporating the latest understanding of science into its 2009 models for earthquake risk in both North and South Americas. This section explores the latest science—and accompanying inherent uncertainty—in the RMS® North America Earthquake Model. In addition, an ongoing project at RMS, analyzing the humanitarian impacts of future earthquakes on six of the most at-risk South American capital cities, is presented, illustrating the application of the RMS® South America Earthquake model to mitigate risk.

Uncertainty in Earthquake Ground Motion

The foundation of the seismic source models for the RMS North America Earthquake regions in the United States is a database of earthquake sources produced by the U.S. Geological Survey for use in the National Seismic Hazard Maps (Petersen et al., 2008). For all earthquake regions in the contiguous U.S., the seismic source model is based on the 2008 version of the National Seismic Hazard Mapping Project (NSHMP). The RMS model also incorporates the new scientific results of the NSHMP, most notably the Next Generation Attenuation (NGA) relationships. The attenuation relationships model ground motions for shallow crustal events in the western parts of North America. This suite of attenuations includes three published models: Boore and Atkinson (2008), Campbell and Bozorgnia (2008), and Chiou and Youngs (2008).

These ground motion models were developed based on the same ground motion data but with different underlying assumptions. As a result, there are differences between the ground motions predicted by these models. While the largest differences are observed for the larger (>7.25) magnitude events, there are differences along the range of magnitude events. For this reason, it is important to explore the differences in loss due to the different assumptions in ground motion modeling. In Figure 3, the normalized loss cost ratios, defined as the average annual loss (AAL) per $1,000 in exposure, for the three attenuation relationships are illustrated. In general, the Chiou and Youngs relationship generates the highest loss costs (on right in Figure 3) with the lowest costs generated by the Campbell and Bozorgnia relationship (in middle of Figure 3).

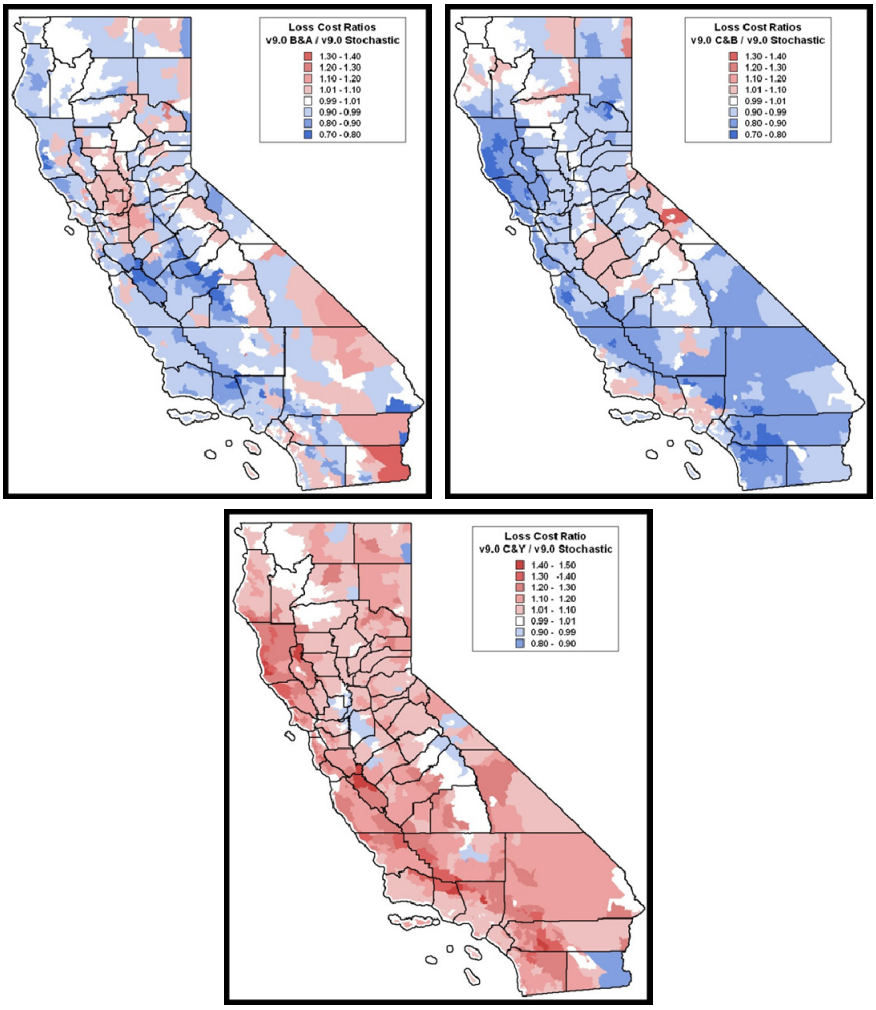

Fig. 3: Comparison of normalized loss cost ratios (average annual insured loss per $1,000 in exposure) in California, assuming the Boore and Atkinson attenuation relationship (left), the Campbell and Bozorgnia attenuation (center), and the Chiou and Youngs attenuation (right).

Seismic Vulnerability of South America Capital Cities

Researchers at RMS are currently developing a study to address the humanitarian impacts of future earthquakes on six of the most at-risk South American capital cities. One objective of the study is to quantify the humanitarian and economic risk for each of the capital cities, utilizing the RMS earthquake model for South America and developing a new class of exposure at risk, representing the most at-risk populations. The project focuses on the capital cities along South America's western and northern margins that sit astride active plate boundaries and hence face the highest seismic hazard: Caracas, Venezuela; Bogotá, Colombia; Quito, Ecuador; Lima, Perú; La Paz, Bolivia; and Santiago, Chile.

Results from the RMS suite of catastrophe models indicate that capital cities of South America face considerable seismic risk when considered in a global context (Figure 4).

The loss costs in Figure 4 represent the normalized risk to residential structures and are defined as the insured average annual loss (AAL) per $1000 of exposure for each city. The high loss costs for South American capitals—particularly for Lima, Quito, Santiago, and Bogotá—are due to a combination of a high-level of exposure to seismic hazard and a relatively high vulnerability of typical construction.

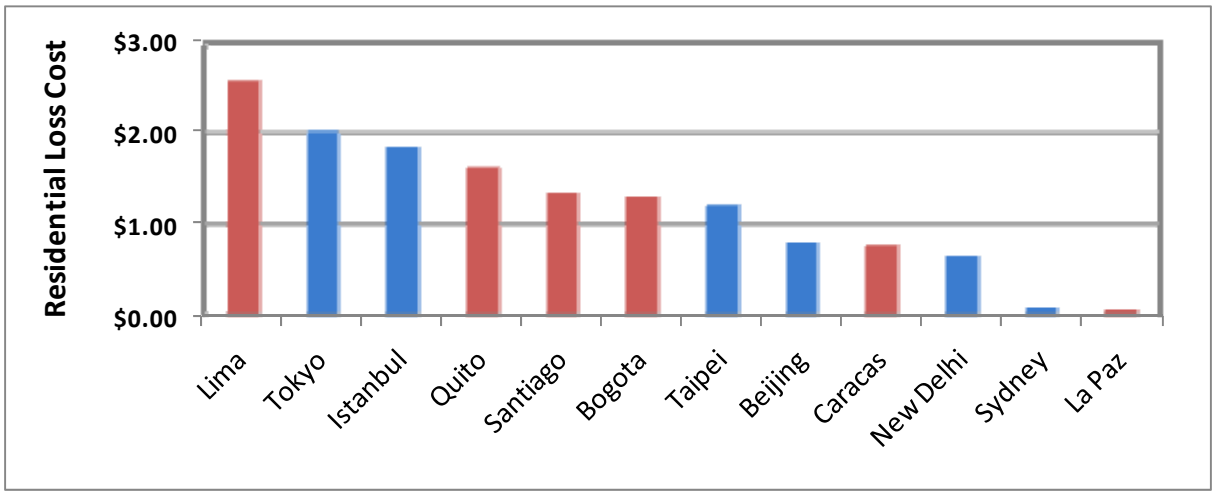

Fig. 4. Residential economic loss costs (Average Annual Loss/$1000 exposure value) for a number of major global cities, South American capital cities highlighted in red.

As the RMS catastrophe models are generally geared towards insurance industry requirements, they do not capture the complete exposure of uninsured marginal populations, such as the informal structures housing urban poor. For this reason, in this project, efforts are focused on accurately characterizing the complete population distribution, as well as the inventory and vulnerability of the informal structures in the capital cities.

Although an entire city will be impacted by an earthquake, the high-density shanty districts that have developed on the margins of capital cities face particularly high risk because they consist largely of substandard and seismically fragile construction and they are often built on slopes that are prone to landslides. Unfortunately, as the occupants have ”improved” these dwellings from their original wood, cardboard, and corrugated tin construction to structures created out of concrete and brick, their vulnerability to earthquake damage and casualties has substantially increased. These shanty areas in the six capital cities are home to millions of people. Typically, the construction is informal, using cheap, readily available materials. These neighborhoods are largely unplanned and the density of structures is extremely high, often with footpaths instead of roads. Limited access to these areas is expected to compound emergency response efforts (Figure 5).

Fig. 5. Shanties on a hillside in Caracas (Source: http://21stcenturysocialism.com/article/alba_latin_ americas_anti-imperialist_economic_project_01110.html).

The project's goal is to focus attention on this increasing problem throughout South America and much of the developing world. In a later phase of the project, the implementation of mitigation solutions are planned, through partnerships with public agencies, NGOs and other local stakeholders to promote mitigation actions that lead to life safety and reduce future losses and suffering.

CONCLUSION

Natural hazard catastrophe modeling has evolved considerably from the days when actuarial methods relying on past loss experience were used for risk assessment and management. Catastrophe modeling is now part of the landscape of tools used by the insurance industry for a better understanding and management of risk, as it provides the means for incorporating additional information from a wide array of disciplines as it becomes available. Catastrophe modeling also provides a unified platform for decision makers to quantify the uncertainty associated with risk and incomplete information.

As the insurance industry relies more heavily on catastrophe modeling, there is more demand and greater challenges facing those that develop models. Modelers must devise methodologies for assessing and improving data quality. They must develop approaches that incorporate new scientific information and new ways to efficiently model uncertainties within each component of the model. They must quantify modeling uncertainties in ways that can be used by stakeholders who rely on these models.

Insured losses from catastrophic events have increased over the past 25 years, in part due to an increase in population and exposure in areas susceptible to catastrophic events. One thing is certain—this trend in losses and the associated global catastrophic risk will continue into the future. The modelers of catastrophe risk must face the challenges posed by the insurance industry to help mitigate and manage this risk.

REFERENCES

Boore, D.M., and Atkinson, G.M. (2008). Ground-motion prediction equations for the average horizontal component of PGA, PGV, and 5%-damped PSA at spectral periods between 0.01 s and 10.0 s. *Earthquake Spectra*, 24(1).

Campbell, K.W., and Bozorgnia, Y. (2008). Ground motion model for the geometric mean horizontal component of PGA, PGV, PGD and 5% damped linear elastic response spectra for periods ranging from 0.01 to 10.0 s. *Earthquake Spectra*, 24(1).

Chiou, B., and Youngs, R. (2008). A NGA model for the average horizontal component of peak ground motion and response spectra. *Earthquake Spectra*, 24(1).

Grossi, P. and Kunreuther, H. (2005). *Catastrophe Modeling: A New Approach to Managing Risk*, Springer, New York.

Grossi, P., Dong, W., and Boissonnade, A. (2008). *Evolution of Earthquake Risk Modeling*. Proceedings of the 14th World Conference on Earthquake Engineering, October 2008, Beijing, China.

Munich Re (2008). Great natural disasters 1950–2007: overall and insured losses, Geo Risks Research, NatCatSERVICE, http://www.munichre.com/en/ts/geo_risks/natcatservice/default.aspx

Petersen, Mark D., Frankel, Arthur D., Harmsen, Stephen C., Mueller, Charles S., Haller, Kathleen M., Wheeler, Russell L., Wesson, Robert L., Zeng, Yuehua, Boyd, Oliver S., Perkins, David M., Luco, Nicolas, Field, Edward H., Wills, Chris J., and Rukstales, Kenneth S. (2008). Documentation for the 2008 Update of the United States National Seismic Hazard Maps. U.S. Geological Survey Open-File Report 2008–1128.

EARTHQUAKE RESISTANCE OF MODERN REINFORCED MASONRY CONSTRUCTION

Richard E. Klingner[1], P. Benson Shing[2], W. Mark McGinley[3], David I. McLean[4], Hussein Okail[5], and Seongwoo Jo[6]

For the past two and one-half years, the masonry industry has been working with university researchers under the National Science Foundation's NEES program to develop performance-based design provisions for masonry and masonry veneer. In January 2009, a full-size wood-stud frame with clay masonry veneer was tested on the NEES large outdoor shaking table of the University of California at San Diego. In March 2009, a load-bearing concrete masonry structure with clay masonry veneer was tested at the same facility. These structures are shown in Fig. 1 and Fig. 2, respectively.

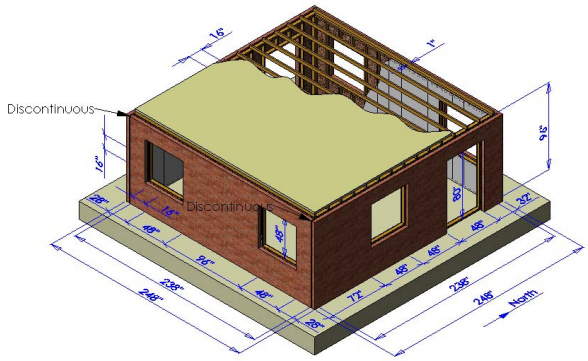

Fig. 1. Full-size, wood-stud frame structure with sheathing, ties and clay masonry veneer, interior gypsum wallboard.

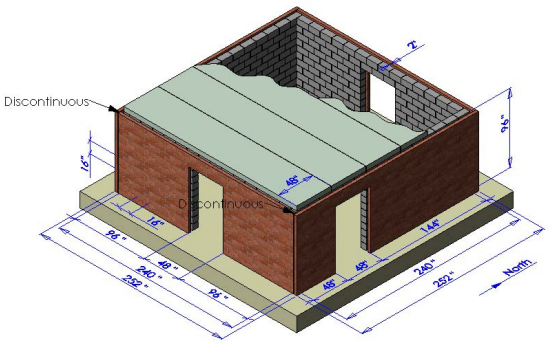

Fig. 2. Full-size concrete masonry structure with clay masonry veneer.

Both specimens are designed and detailed according to current requirements of the Masonry Standards Joint Committee (MSJC) Code and Specification, and provide valuable information on the performance of modern masonry and masonry veneer in zones of high seismic risk.

The wood-stud structure tested different types of veneer connectors and joint reinforcement. The most important finding from the January testing was that masonry veneer can help the seismic performance of wood-stud frames, and should not be considered as mass only in the seismic design of those frames. Veneer connected with screw-mounted rigid ties performed better than veneer connected with nail-mounted flexible ties, and veneer with joint reinforcement did not

[1] L. P. Gilvin Professor in Civil Engineering, The University of Texas at Austin, Austin, Texas 78712, USA.
[2] Professor, Dept. of Structural Engineering, the University of California at San Diego, La Jolla, California 92093, USA.
[3] Professor and Endowed Chair for Infrastructure Research Civil and Environmental Engineering, University of Louisville, Louisville, KY 40292.
[4] Professor, Department of Civil and Environmental Engineering, Washington State University, Pullman, WA 99164-2910.
[5] Graduate Research Assistant, Dept. of Structural Engineering, the University of California at San Diego, La Jolla, CA 92093.
[6] Graduate Research Assistant, The University of Texas at Austin, Austin, TX 78712.

perform differently from veneer without joint reinforcement. Based on these results, researchers will propose refinements to current seismic design approaches for wood-stud frames with masonry veneer, and to current MSJC design provisions for masonry veneer over wood-stud frames.

The concrete masonry structure tested different types of shear reinforcement and different types of veneer connectors. All walls used deformed reinforcement in bond beams. The structure's north side had bond beams at the bottom course, while its south side had the first bond beam at the required spacing above the top of the foundation. Its east and north walls used tri-wire joint reinforcement and veneer connectors spaced at 16 in. vertically. Its west and south walls used double eye-and-pintle connectors spaced at 16 in. horizontally and vertically, with no joint reinforcement.

In January and March 2009, colleagues from around the world were invited to join researchers and masonry industry colleagues (Table 1) as each structure was tested.

- Before the test, participants and observers received background information on the specimen and its expected behavior.
- During the test, participants attended an on-site briefing and tour of the specimen and shaking-table facility.
- During the test, participants and observers evaluated many aspects of specimen performance. These included a global assessment of the seismic performance of masonry and masonry veneer designed using current MSJC requirements; a comparison of the performance in seismic shear of bed-joint reinforcement versus bond beams with deformed reinforcement; and a comparison of the seismic performance of veneer with and without bed-joint reinforcement.

Table 1. Masonry industry partners on NSF NEES masonry project.

NSF NEES INDUSTRY PARTICIPANTS			
NAME	**TITLE**	**AFFILIATION**	**EXPERTISE**
J. Gregg Borchelt	Vice President, Engineering and Research	Brick Industry Association, Reston, VA	masonry veneer, masonry structures, earthquake engineering
John Chrysler	Executive Director	Masonry Institute of America, Torrance, CA	masonry veneer, earthquake engineering, masonry constructability
Jamie Farny	Program Manager, Masonry and Special Products	Portland Cement Association, Skokie, IL	masonry mortar, masonry standards
Eric Johnson	Director of Engineering	Brick Industry Association Southeast Region, Charlotte, NC	masonry veneer
Rashod Johnson	President	The Roderick Group, Chicago, IL	masonry structures, masonry constructability
John Melander	Director of Product Standards and Technology	Portland Cement Association, Skokie, IL	masonry mortar, masonry standards
Robert Thomas	President	National Concrete Masonry Association, Herndon, VA	masonry structures, masonry testing
Diane Throop	Director of Engineering	International Masonry Institute, Annapolis, MD	masonry structures and masonry constructability
Jason Thompson	Director of Engineering	National Concrete Masonry Association, Herndon, VA	masonry structures, earthquake engineering, masonry testing

OVERALL TEST RESULTS FOR CONCRETE MASONRY BUILDING WITH MASONRY VENEER

Fig. 3 below shows the concrete masonry building with masonry veneer, essentially undamaged after four incredible earthquake. *Fig. 4* below shows the same building after the fifth incredible earthquake, which caused damage to the clay masonry veneer and the reinforced concrete masonry backup system.

Fig. 3. Reinforced concrete masonry building, essentially undamaged after four incredible earthquakes.

Fig. 4. Reinforced concrete masonry building, showing damage after the fifth incredible earthquake.

Even the best structure, shaken hard enough, can be damaged. To understand how well this modern masonry structure performed, look at the simulated earthquakes that it resisted:

- several low-level earthquakes;
- a so-called "design level earthquake," which is expected about every 500 years, with ground shaking of about 0.67 g (67% of the acceleration of gravity);
- a so-called "maximum considered earthquake," which is expected about every 2500 years, with ground shaking of about 1 g.
- three repetitions to levels higher than the maximum considered earthquake, including one shake to almost 3 g, stronger than any known earthquake; and
- one final shake at almost 3 g, stronger than any known earthquake.

WHAT THE TESTS SHOWED

1. Low-rise masonry buildings with reinforced CMU back-up and clay masonry veneer, designed and constructed according to the requirements of the 2008 MSJC Code and Specification for Seismic Design Category D (highly seismic zones of the US), can resist earthquakes above the Maximum Considered Earthquake (MCE) without collapse.
2. These buildings perform as expected:
   (a) Response is controlled by the reinforced concrete masonry shear walls, which may yield at their bases and then begin to slide above MCE.
   (b) Clay masonry veneer, designed and constructed according to the requirements of the 2008 MSJC Code and Specification, experienced only minor cracking and stayed fully connected to the CMU walls, up to 1.75 MCE.
3. The seismic behavior of low-rise masonry buildings with reinforced CMU back-up and clay masonry veneer is well predicted by nonlinear dynamic analysis and static design tools.

ACKNOWLEDGEMENTS

This NEES small group project is supported by the US National Science Foundation's Network for Earthquake Engineering Simulation (NEES), whose program director is Dr. Joy Pauschke. The project is led by The University of Texas at Austin. The shaking-table work is being conducted at the NSF NEES equipment site at the University of California at San Diego, whose help and cooperation are gratefully acknowledged. The Council for Masonry Research, the Portland Cement Association, and the Brick Industry Association have provided direct financial support for this work. They and other masonry industry groups have provided materials, testing services and in-kind support. The work described here represents the individual and collective contributions of the researchers and graduate research assistants noted here.

SEISMIC PERFORMANCE OF EXISTING AND RETROFITTED DOME-ROOF ADOBE HOUSES IN IRAN USING SHAKING TABLE TESTS

Ali Bakhshi, Mohammad Ali Ghannad, Mohammad Yekrangnia, and Hamid Masaeli
Civil Engineering Department, Sharif University of Technology, Tehran, Iran

ABSTRACT

This paper presents a summary report of shake table tests conducted on two 2:3 scale models representing conventional dome-roof adobe houses of Iran. The first model, constructed by common practice, is designed to evaluate seismic performance and vulnerability of dome-roof adobe houses. The second model is exactly duplicating of first one and then retrofitted with an appropriate method, based on results obtained from first model tests and the improvement in seismic behavior of the structure. Zarand 2005 earthquake (Chatrood station) has been selected as the input excitation at 25%, 100%, 125%. 150% and 175% levels consecutively. Several instrumentations including acceleration, and displacement transducers have been taken to capture response time histories of both models, in addition to few strain gauges for recording of steel rod responses in the second structure. In first model, the roof panels collapsed due to walls' rocking action and imbalanced forces, at 125% excitation level. The second model has been retrofitted with 8 horizontal rods drilled into the walls and bolted on the opposite wall surfaces. To improve walls in-plane strength, welded steel mesh, covered less than a half area of walls on one side of the walls is used. The retrofitted model tolerated even peak acceleration of 0.61g, almost without any serious damage.

INTRODUCTION

Construction of brick masonry and clay adobe houses was the most typical construction technique in Iran and many other countries. About 95 percent of almost 4 million rural houses of Iran, housing more than 20 million people, have no lateral load bearing elements and are vulnerable to earthquake [1]. The condition is almost same for masonry houses, specifically built prior to practice of Iranian seismic provision. The reason for construction of these kinds of materials is undeniably their low cost, ease of construction and availability for both rural and urban areas. However, these traditional construction materials have little resistance, i.e. strength and ductility, to withstand earthquake-induced forces.

The collapse of adobe constructions has been and still remains as one of the main cause of loss of human lives and of economic devastation following strong earthquakes, especially in developing countries [2]. In Iran one of the most dramatic examples is the 2003 Bam earthquake, when more than 40,000 people were buried under heavy masonry and adobe ruins. Although many years of research have succeeded in developing improved construction techniques and the adobe code for building design and construction has been adopted in some courtiers like Peru, these efforts are not directly applicable to existing adobe constructions, which represent a real seismic risk [3].

Therefore, it is imperative to find low cost retrofitting alternatives, capable of providing these buildings with sufficient confinement and integrity as to withstand a severe earthquake without collapse. In response to this demand, a project was defined at Sharif University of Technology under the title "Seismic vulnerability study of rural houses in Iran". The first

phase of this research included gathering structural information and classification of rural houses based on their seismic behavior and presenting the dominant types of the rural houses [4]. The second phase was dedicated to computer modeling of the indicated types of houses in the first phase and investigating dynamic properties using ambient vibration tests on different types of actual rural houses [5-6]. The third phase encompasses two shaking table tests on a typical adobe building, i.e. a single story dome-roof, in conventional and retrofitted states. This paper summaries part of results of two shaking table tests conducted at Earthquake Simulation Laboratory, Sharif University of Technology.

PAST RESEARCH ON SEISMIC BEHAVIOR AND STRENGTHENING OF ADOBE BUILDINGS

Retrofit measures significantly improve seismic performance when they provide overall structural continuity, prevent instability, and provide restraint to reduce the relative displacements of cracked wall sections [7]. According to these facts and considering adobe buildings behavior during past earthquakes, retrofit strategy focuses on two main parts: maintaining structural integrity by keeping the walls together and guaranteeing box-like behavior, and enhancing walls in-plane shear strength.

Bond Beam

Perhaps the most widely proposed method of strengthening adobe houses is the placement of bond beam in the upper perimeter of the walls. Garcia et al. [9] preformed shaking table tests to evaluate the effectiveness of adding tie beam and FRP reinforcement on adobe buildings. There are several shaking table tests concerning the role of bond beams in these buildings [10-11].The main drawback of bond beams (besides the top belt confining the walls) is that this procedure does not work properly for adjacent dwellings without distinct separate walls, see Figure 1. Additionally, this method requires intervention and causing some damages to the existing buildings.

Fig. 1. Rural houses configuration in arid regions of Iran.

Mesh

Reinforcing adobe walls with mesh grids has proved a good retrofit technique over the past earthquakes and by many shaking table tests, as well [12 to 19].

Strap and Center Core Rod

Using vertical and horizontal rubber or steel strips and straps on masonry walls in order to tie the discrete masonry blocks together can be regarded as another solution for seismic rehabilitation of these structures. Drilling the walls from the top at subsequent distances and filling the holes with rods and grout greatly increases shear strength of the system. The rods can be in the form of steel bars, cane or bamboo. Some studies on the aforementioned retrofit systems are [7] and [20 to 22].

TEST PROGRAM

Two 2:3 scaled adobe buildings with polygonal (tetradome) roof were tested on the shaking table at Earthquake Simulation Laboratory, Sharif University of Technology. The models weighed about 24ton and had a square plan of 3.60*3.60m. They were made of raw adobe blocks 20*20*4.5 cm with mud mortar in walls and mud-gypsum mortar in roof with 1cm of thickness. The thickness of 2.5-wythe walls and single wythe roof was 52cm and 12 cm, respectively. The walls and roof height were 2m and 1m, respectively. Four different types of walls were considered to investigate the effect of openings on the behavior of the walls and torsion on the overall behavior of the building, for instance, wall without opening, wall with a large window, wall with a large niche or corbel, wall with a small window and a door, as shown in Figure 2. All openings were constructed as having upper arch-shape, very similar to prototype construction in several provinces.

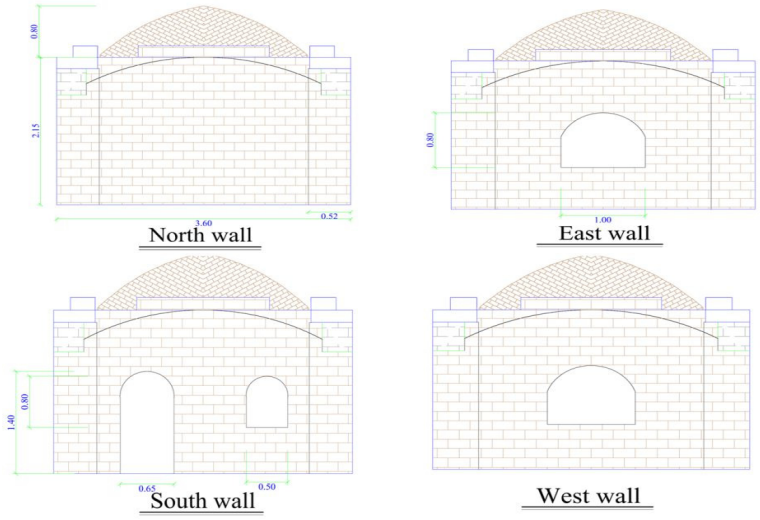

Fig. 2. Geometrical configuration of the model building.

Zarand earthquake, 2005 (Chatrood station) was selected as the input motion which was the excitation record of four full-scaled masonry buildings tested beforehand. The dominant frequency of this record is about 10 Hz which is close to natural frequency of these types of buildings. Since the scaling method was gravity-forces-neglected, the time is compressed to 66.7% and the acceleration was amplified to 150%, in accordance with similitude law. As illustrated in Figure 3, the P.G.A. of both records in horizontal directions was scaled to 0.35g, entitled 100% as of design earthquake hereafter [23].

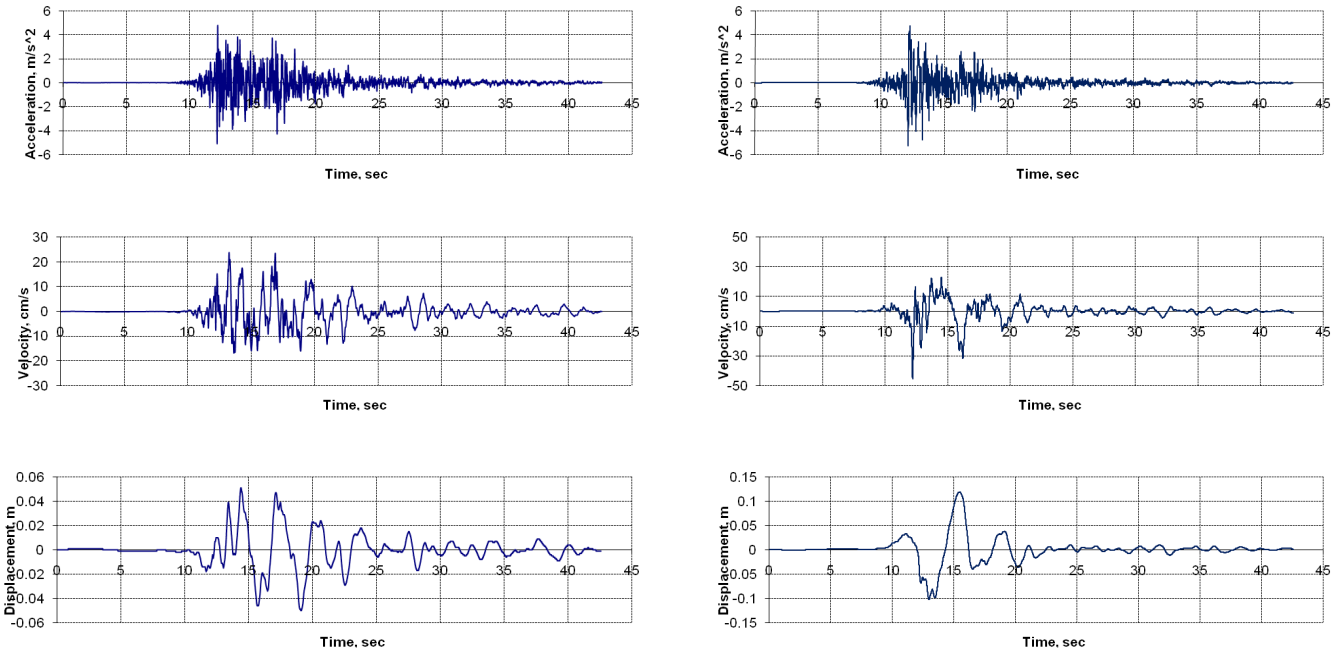

(a) E-W direction (b) N-S direction

Fig. 3. Input excitation in both horizontal directions (scaled and nominated as 100%).

Data Acquisition and Response Recording

In order to investigate the global and local response of the system, 12 accelerometers and 4 displacement transducers were installed to record the response of the walls and the dome in several test steps. The schematic arrangement of the sensors is depicted in Figure 4, in which circles and triangles represent acceleration and displacement transducers, respectively. As can be seen in this figure, all displacement transducers and some accelerometers were located at the wall corners to capture the global behavior of the model structure which is associated with the walls in-plane response. The dominant natural frequency of the models in each step is determined based on these accelerometers data. On the other hand, one accelerometer was placed at the mid-length of each wall to record the corresponding out-of-plane motions. Also two accelerometers captured the domes response in two perpendicular horizontal directions. In addition, to measure the steel rod response forces during excitation in the retrofitted model, all rods were mobilized to strain gages. It is worth mentioning that the qualitative behavior of the both models was recorded by means of 13 high-speed cameras including inside the room.

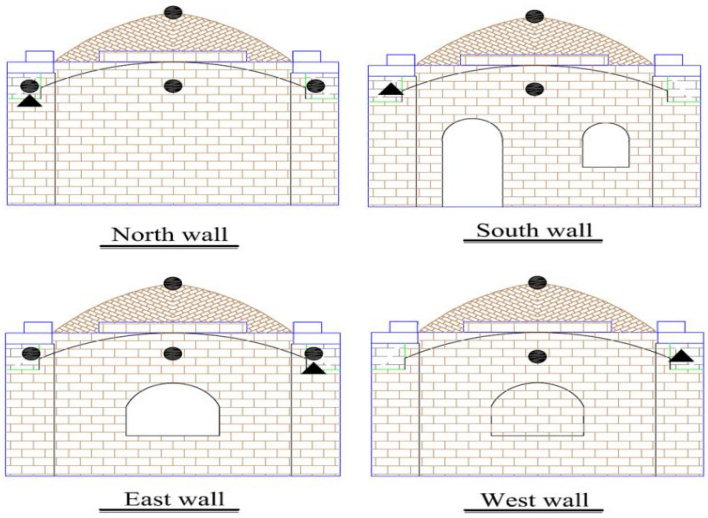

Fig. 4. Schematic view of sensor configuration.

It should be noted that the displacement transducers were removed in the sever test steps because of high possibility of building collapse (100% and 150% in the unretrofitted and retrofitted models, respectively). Instead, displacements given by gradient papers placed on the walls and top of the dome were recorded using high sensitive cameras.

Seismic Performance of Conventional Model Structure

The model experienced almost no serious damage in 100% level of excitation. However, as indicated in Figure 5, sequential pictures captured during 125% level of excitation, the roof panels overturned subsequently due to walls' rocking action and imbalanced forces among damaged roof panels. No major in-plane cracks were observed thanks to low slenderness ratio of walls. Only southern wall showed some crack propagation, as expected. The northern wall (the strongest) deflected out-of-plane in the 1st mode shape of a cantilever column, as demonstrated in Figure 6. Some bed joint sliding also occurred but in out-of-plane direction. Cracks were oriented upwards above openings, not 45 degrees from their corners. No adobe block fell on the ground,

hence proving the effectiveness of arch action, see Figure 7. It is worth noting that almost identical reaction for arched opening was observed in shaking table test and real houses subjected to Zarand 2005 earthquake ecitation, as compared in Figure 7.

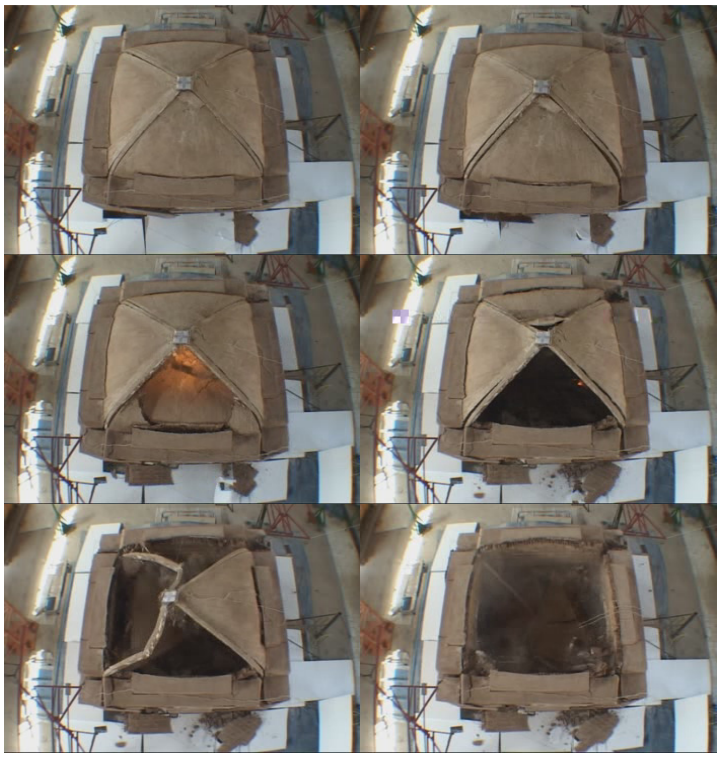

Fig. 5. Conventional model failure at 125% level of excitation.

Fig. 6. Overturned walls.

Fig. 7. Effective reaction of arched openings.

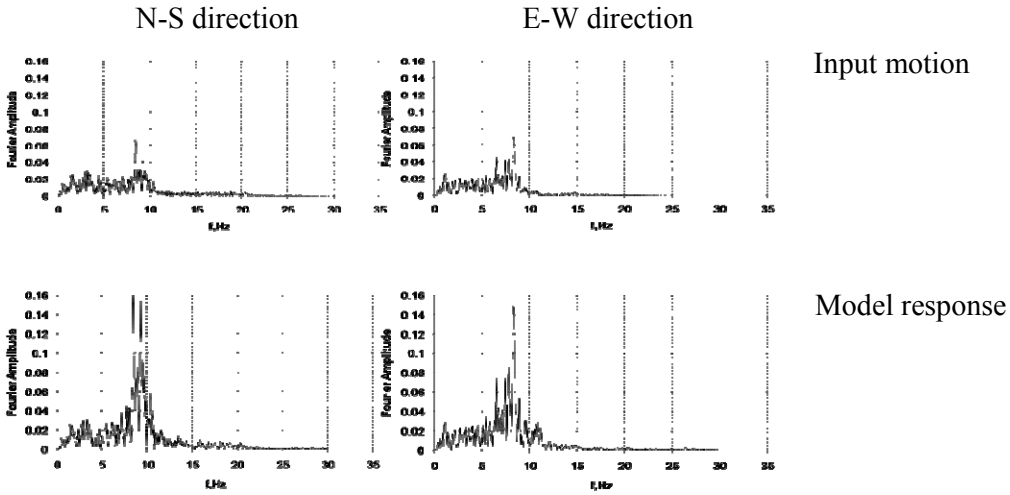

Fig. 8. Fourier spectra of the input motion and the in-plane wall response of the models, at the level of 25% excitation.

This model experienced some serious damages during consecutive steps. The damage was in the form of visible cracks in the walls and decrease in the natural frequency. Figure 8 shows the acceleration Fourier spectra of the input motion and the in-plane wall response of the both models at the step 1, i.e. 25% level. As illustrated in the figure, fundamental frequency of the model structure in both directions stands at the range of 8 to 10 Hz, for elastic response. This is consistent with the results measured in actual buildings using ambient vibration tests [6].

Seismic Performance of Retrofitted Model Structure

The second model was retrofitted with 8 horizontal rods drilled into the walls and bolted on the opposite wall surfaces. The expected function of these rods is tying parallel walls and preventing them from outward overturning. Moreover, to improve walls in-plane strength, welded steel mesh was put on one side of the walls (outside). The mesh covered less than a half area of walls and connected to them by some shear keys drilled through walls at the most appropriate locations, as shown in Figures 9(a) and 9(b).

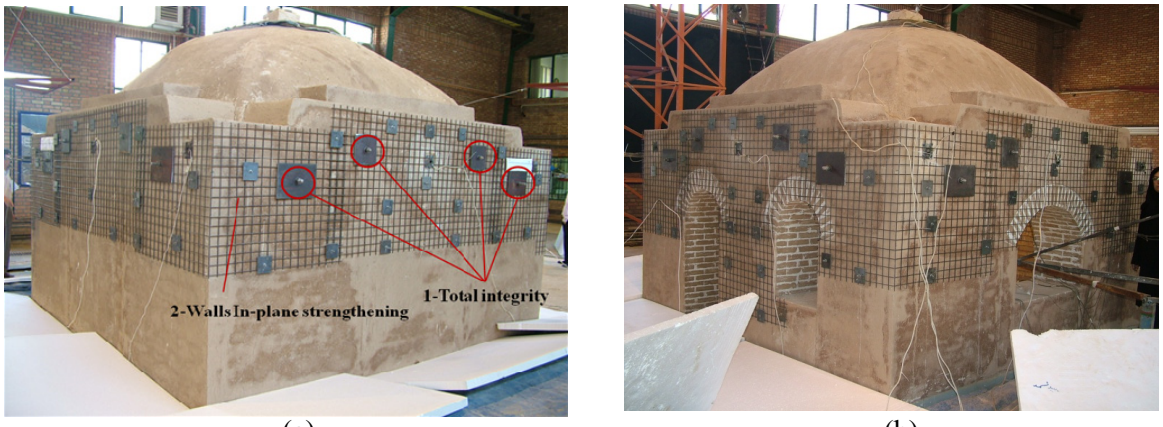

(a) (b)

Fig. 9. Retrofitted model structure from different views.

The model reacted well to the subsequent excitations and did not collapse at the final stage of 175% level of the Zarand motion. The severity of damages in the model was C(2) to D(3), according to EERI standardized damage states [24]. As can be observed in Figures 10 and 11, the main mode of failure of the building was torsion at the wall bases. This mechanism is preferable because bed joint sliding (in in-plane and out-of-plane directions) is considered as a good energy dissipating behavior in hysteresis curves; although has little ductility. The main cracks were transformed to the lower levels of walls, hence almost all the walls shear capacity were interacted without walls separation at the corners. Some local detachments and crushing were observed at the large opening corners, but no serious danger to the building overall stability has been detected. (Fig. 12)

Fig. 10. Shear cracks at the base of door.

Fig. 11. Shear cracks at the corner.

Fig. 12. Shear-due-to-torsion crack at eastern wall.

As mentioned earlier, the main cause of failure in the model building is attributed to torsion. This phenomenon is explained below. According to FEMA356 C7-1 the stiffness of cantilever masonry piers can be considered as [25]:

$$K = \frac{1}{\frac{h^3_{eff}}{3E_m I_g} + \frac{h_{eff}}{A_v G_m}} \quad (1)$$

in which

h_{eff} = Wall height

A_v = Shear area

I_g = Moment of inertia for the gross section representing uncracked behavior

E_m = Masonry elastic modulus

G_m = Masonry shear modulus

This formula gives the natural period of the system in both directions $T_{W-E} = 0.10s, T_{N-S} = 0.14s$ which is a good assessment according to structural response at level 25%. It is noteworthy that there is 1.2m distance in the N-S direction between center of mass and center of rigidity of the system. This causes a considerable torsion in the model which is shown in Figure 13. It should be emphasized that the base shear of the model was considered equal in both directions.

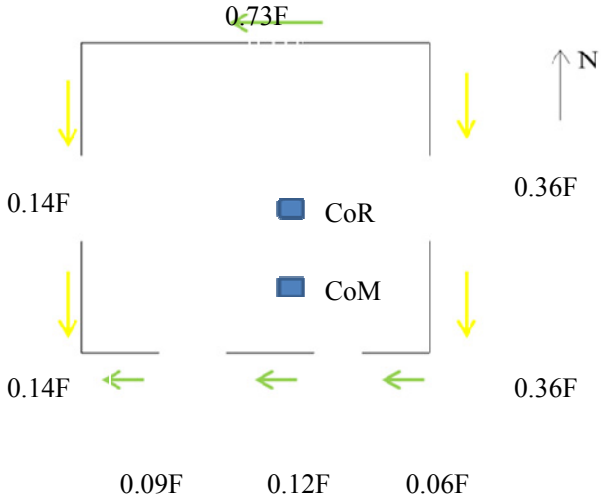

Fig. 13. Load bearing distribution in the model piers.

As can be seen in the above figure based on the ratio of load to capacity, the eastern wall bears the highest chance to crack. This situation is depicted in Tables 1 in which the shear capacity of each wall is associated with its length. The ratio of the created force and capacity of the eastern wall is the highest.

Table 1. Ratio of created force to shear capacity of various wall.

wall	load	capacity	Load/capacity
North wall	0.73F	3.6L	20.2
East wall	0.36F	1.3L	27.7
West wall	0.14F	1.3L	10.8
South-E wall	0.06F	0.7L	0.9
South wall	0.12F	0.9L	1.3
South-W wall	0.09F	0.8L	1.1

Figure 14 represents the sequential damage in terms of dominant behavioral frequency in the retrofitted model in the steps of 25%, 100%, 125% and 150% levels.

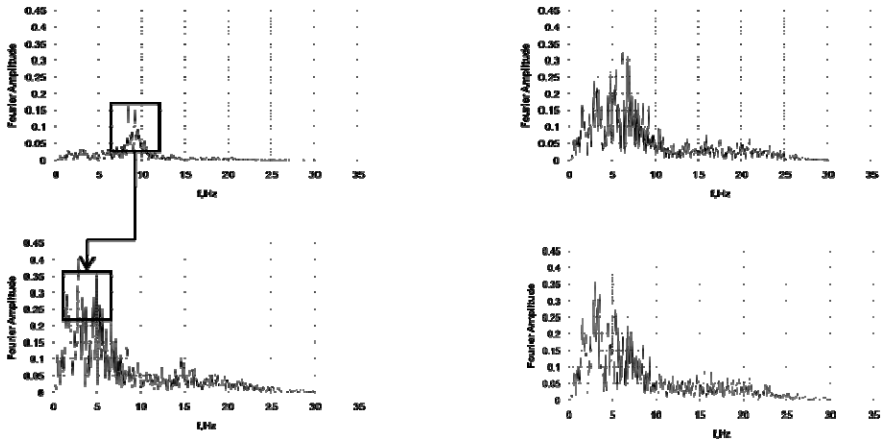

Fig. 14. Fourier spectra of the top of the out-of-plane southern wall of the retrofitted model at the steps 25%, 100%, 125% and 150%.

It should be noted that the response of the west and east walls (walls with niche and window opening) were almost the same up to the step 125%. After this step, the west wall responded a little intensely, but the Fourier spectra of both responses were virtually identical. Also the behavior of the top of the walls and the dome roof were congruous in the retrofitted model up to step 125%. In the next steps, the dome exhibited very high amplifications in its peak response, though the amplifications were restricted to very short time span.

Considering linear distribution of the induced acceleration across the wall, the resultant acting force equals $F_0 = M_e(\frac{gt}{h})$ in which M_e is the active wall mass in the first mode: $M_e = \frac{3}{4}M$. The resultant acting force acts at 2/3 wall's height. By taking moment at the wall's toe, the rod's necessary diameter is calculated. It is noteworthy that it was decided to use four rods in each direction. The schematic representation of the steel rods is shown in Figure 15.

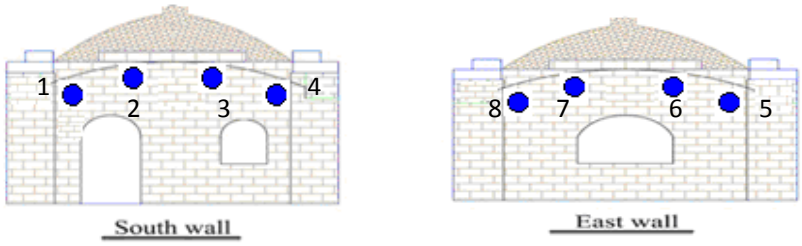

Fig. 15. Schematic representation of the steel rods and their code numbers.

Figure 16 depicts the ratio of strain time history to yielding strain in the steel rods coded as of 7 and 8 in the final test step, i.e. 175% level. As can be seen in this figure, rod 8 experienced the largest strains. Since for reliability purposes, 22mm rods were used instead of 14mm, this ratio is

low (about 30%) even in the step 175%. From the peak strains and also residual strains in the rods, it is obvious that these elements are the main reason for preventing walls detachment and guaranteeing "box-like" behavior.

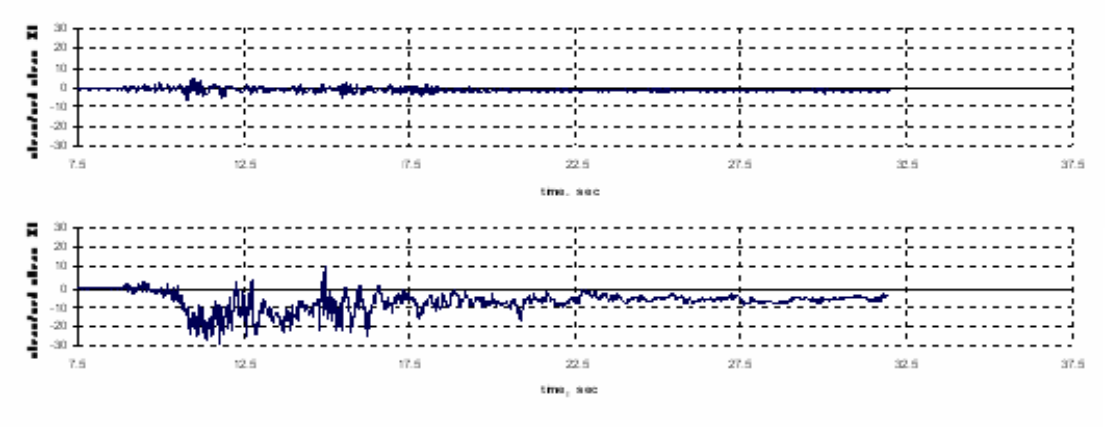

Fig. 16. Time history of the rod strain to yield strain ratios in the steel rods 7 and 8.

Figure 17 shows the ration of absolute peak strains in the rods to the yield strain in different test steps. It is obvious from this figure that response of Rod 8 is quite different with others which implies further investigation needed. This figure shows that maximum forces induced in rods coded 1 to 7 played a crucial role in enhancing the models overall stability.

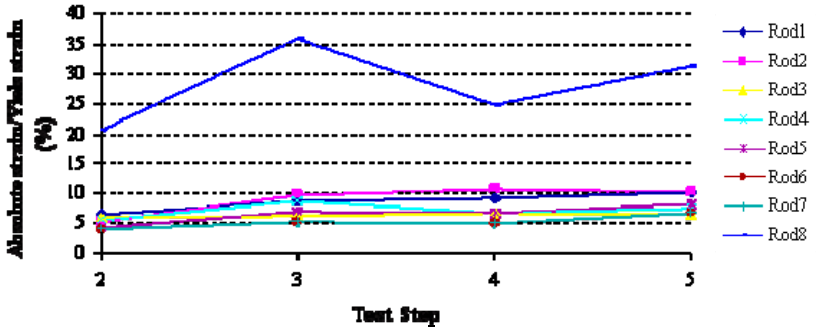

Fig. 17. Ratio of absolute peak strains in the rods to the yield strain in different test steps.

Response Comparison

Figure 18 shows the dominant frequency and the absolute peak accelerations in the sensors installed on both models at different test steps. It is obvious that trend of frequency reduction in both models happened accordingly. As demonstrated also in this figure, the unretrofitted model experienced severe damages in the step 100% (step 3), however, in the retrofitted model (step2 – corresponding to 100%) no obvious alternation in the dominant frequency is observed. Meanwhile response accelerations in the unretrofitted model were more intense in comparison with the retrofitted model in the same test step.

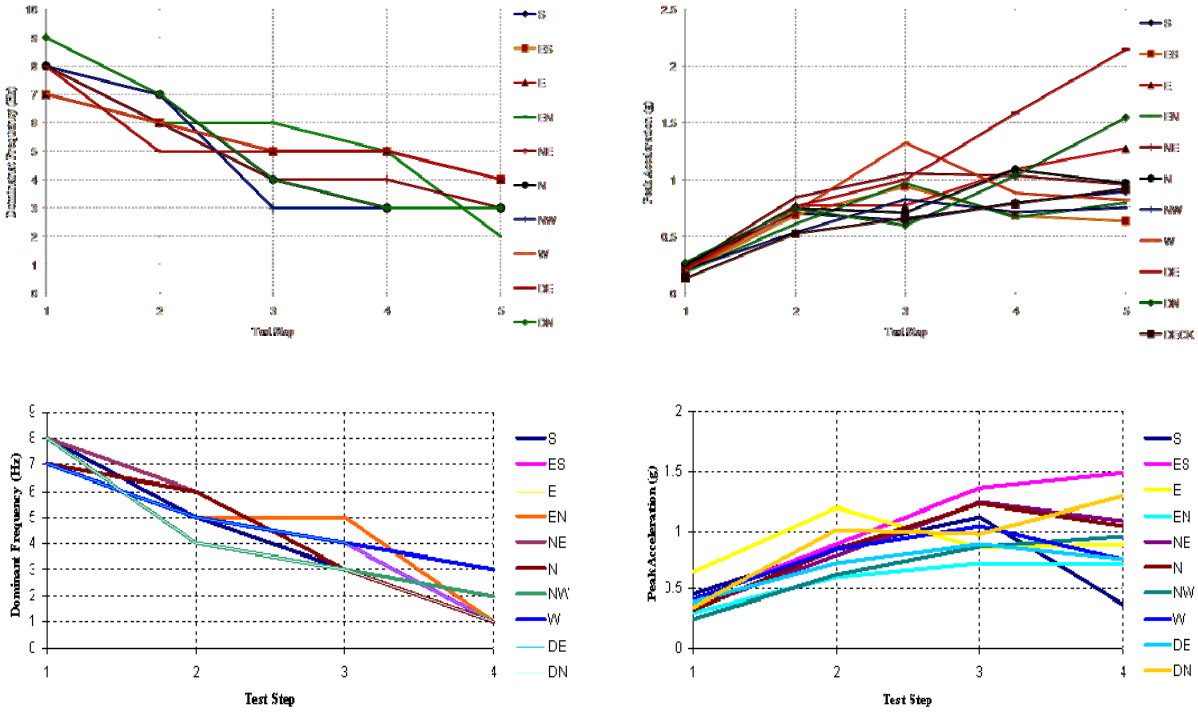

Fig. 18. Dominant frequencies and absolute peak accelerations of the responses for retrofitted and unretrofitted models in different test steps.

SUMMARY AND CONCLUSIONS

Adobe buildings generally have thick, low walls and their slenderness ratio is smaller than masonry walls. Hence they potentially can bear great amounts of shear forces; since many adobe structures experience premature collapse, i.e. detachment of perpendicular walls from each other, their capacity cannot be taken advantage of. The main focus of the retrofit system in this study was tying the parallel walls and guaranteeing the "box-like" behavior of the structure. In this manner, it was expected that other failure modes of the building be activated; chief among them in-plane shear and tensile cracks in the walls. Considering walls heavy weight which results in great resistance in the lower parts of the walls, the upper level of the walls was given higher priority. The retrofit technique consisted of horizontal steel rods and the steel welded mesh with thru-wall connections proved very satisfactory in enhancing the structural behavior in earthquakes. The conventional model collapsed in the test step having peak acceleration of 0.44g; while the retrofitted model tolerated even peak acceleration of 0.61g, almost without any serious damage. It is noteworthy that the cost of retrofit per square area of the walls and plan of the building is less than 10USD and 20USD, respectively. Therefore not only the proposed retrofit system can fulfill the most essential requirements of adobe building, but also its feasibility and economical advantages put this system as an appropriate choice in retrofitting dome-roof adobe buildings throughout the country.

REFERENCES

1. Housing Foundation of Iran (2003), Rural Houses Specifications Count.
2. Kuroiwa J. "A Regional Earthquake Scenario in Southern Peru." Proceeding of the 11th WCEE, Acapulco, Mexico. Paper no. 2167 . Oxford:Pergamon, 1996.
3. Giesecke A, Zegarra L, San Bartolomé A, Quiun D. "Reconditioning of Existing Adobe Houses to Mitigate Earthquake Effects." Proceeding of the 11th WCEE, Acapulco, Mexico. Paper no. 666. Oxford:Pergamon, 1996.
4. Ghannad M.A., Bakhshi A., Mousavi Eshkiki S.E., Khosravifar A., Bozorgnia Y., Taheri Behbahani A.A., A Study on Seismic Vulnerability of Rural Houses in Iran, First European Conference on Earthquake Engineering and Seismology, Geneva, Switzerland, 3-8 September 2006
5. Dehghan Banadaki A., Ghannad M.A., Bakhshi A., Lotfalipour M., A Numerical Study on Seismic Behavior of a Typical Rural House of Iran, The 14th World Conference on Earthquake Engineering, October 12-17, 2008, Beijing, China
6. Lotfalipour M., Dehghan A., Bakhshi A., and Ghannad M.A., "Dynamic Characteristics of Rural Adobe Houses in Iran Using Ambient Vibration Measurements", Proceedings of the 14th World Conference on Earthquake Engineering, Beijing, China, 2008.
7. Tolles E.L., Kimbro E.E. and Ginell W.S., "Planning and Engineering Guidelines for the Seismic Retrofitting of Historic Adobe Structures", The Getty conservation institute, Scientific Reports Series, Los Angeles, California, 2002.
8. Tolles E.L. and Krawinkler H., "Seismic Testing on Small Scale Models of Adobe Houses", Proceedings of the 9th World Conference on Earthquake Engineering, Tokyo-Kyoto, Japan, 1988.
9. Garcia G. Villa, Ginocchio F., Tumialan G. and Nanni A., Reinforcing of Adobe Structures with FRP Bars
10. Blondet M., Ginocchio F., Marsh C., Ottazzi G., Villa Garcia G. & Yep J. 'Shaking Table Test of Improved Adobe Masonry Houses'. Proc. 9th World Conference on Earthquake Engineering. Tokyo-Kyoto, Japan, 1988.
11. Bayülke N., Gençer Ö., Başyiğit C., Terzi S., Impulse Table Test of a "Bimblock" Masonry Structure
12. Meli R., Hernandez O., Padilla M. Strengthening of Adobe Houses for Seismic Actions, Proceeding of the 7th WCEE, Istanbul, Turkey. Vol. IV: 465-72, 1980.
13. Soforonie R.A., Crisan R., Toanchina M., Retrofitting the Masonry of Cultural Heritage Buildings, Fifth National Conference on Earthquake Engineering, 26-30 May 2003, Istanbul, Turkey
14. Juh´asov´a E., Sofronie R., Bairr˜ao R., Stone Masonry in Historical Buildings—Ways to Increase Their Resistance and Durability, Engineering and Structures (2007)
15. San Bartolome A., Quiun D. and Zegarra L., Effective System for Seismic Reinforcement of Adobe Houses, 13th World Conference on Earthquake Engineering, Vancouver, B.C., Canada
16. Yamin L. E., Phillips C.A., Reyes J.C., Ruiz D.M., Seismic Behavior and Rehabilitation Alternatives for Adobe and Rammed Earth Buildings, 13th World Conference on Earthquake Engineering, Vancouver, B.C., Canada
17. Meguro K., Mayorca P., Guragain R., Shathiparan N., Nesheli N., Shaking Table Experiment on Masonry Buildings and Effectiveness of PP- Band Retrofitting Technique.
18. Blondet M., Villa Garcia G., Earthquake Resistant Earthen Buildings, 13th World Conference on Earthquake Engineering Vancouver, B.C., Canada, August 1-6, 2004, Paper No. 2447
19. Blondet M., Torrealva D., Vargas J., Velasquez J. and Tarque N., Seismic Reinforcement of Adobe Houses Using External Polymer Mesh, First European Conference on Earthquake Engineering and Seismology (a joint event of the 13th ECEE & 30th General Assembly of the ESC) Geneva, Switzerland, 3-8 September 2006 Paper Number: 632
20. Turer A., Korkmaz S.Z. and Korkmaz H.H., Performance Improvement Studies of Masonry Houses Using Elastic Post-tensioning Straps, Earthquake Eng. Struct. Dyn. 2007; 36:683–705
21. Abrams d., Smith T., Lynch J. and Franklin S., Effectiveness of Rehabilitation on Seismic Behavior of Masonry Piers, Journal of Structural Engineering, Vol. 133, No. 1, January 1, 2007
22. Dowling, D.M., Samali, B., Low-cost, Low-tech Means of Improving the Earthquake Resistance of Adobe-mud Brick Houses, International Conference on Earthquake Engineering (ICEE 2006), 8-9 September 2006, Lahore, Pakistan.
23. Iranian code of Practice for Seismic Resistant Design of Buildings, Standard No. 2800, 3rd Edition (2005)
24. EERI (1995), Northridge Earthquake Reconnaissance, Vol. 1, Supplement C to Volume 11 of Earthquake Spectra, Earthquake Engineering Research Institute, Oakland, California
25. FEMA 356, FEDERAL EMERGENCY MANAGEMENT AGENCY, November 2000

SEISMIC PERFORMANCE OF PARTIALLY GROUTED REINFORCED CONCRETE MASONRY BUILDINGS

Ahmad A. Hamid
Civil, Architectural and Environmental Engineering Department, Drexel University
Philadelphia, USA, hamidaa@drexel.edu

ABSTRACT

Historically, the challenges to masonry construction posed by seismic provisions have been limited to western states. However, with the recent adoption of the International Building Code (IBC 2003) throughout the nation, seismic provisions are now negatively impacting the economy of masonry structures in the eastern US. The new IBC seismic provisions are particularly harmful to masonry construction, thus passively promoting the use of competing systems. There is little, if any, basis for such claims in the literature, as masonry bearing wall buildings remain one of the least studied structural systems. This is particularly true for partially grouted reinforced masonry buildings which is a common building system in the eastern US. This paper presents a review of past research and challenges in performance-based design of partially reinforced concrete masonry. Past and current research on partially grouted masonry assemblages and wall component at Drexel University are briefly presented. Test results of assemblages and walls indicates that the behavior of partially grouted reinforced masonry walls are different from that for fully grouted walls and that the shear strength of partially grouted walls are significantly less than that of similar fully grouted walls. Future research at Drexel will include testing of 1/3 scale two story partially grouted reinforced masonry wall-bearing masonry building. This building test will allow investigating the effect of flanges, wall openings and interaction between perpendicular walls. It is hoped that the proposed system-level research will provide a realistic prediction of the seismic performance and will lead to a more accurate seismic codes' design provisions for reinforced masonry shear wall buildings.

MOTIVES AND OBJECTIVE

Historically, the challenges to masonry construction posed by seismic provisions have been limited to western states. However, with the recent adoption of the International Building Code (IBC 2003) throughout the nation, seismic provisions are now negatively impacting the economy of masonry structures in the eastern US. While it is widely postulated among the masonry industry that the IBC provisions are particularly harmful to masonry construction (thus passively promoting the use of competing systems) there is little, if any, basis for such claims in the literature, as masonry bearing wall buildings remain one of the least studied structural systems. Consequently, the masonry industry finds itself at a crossroads: it can continue to support targeted material or component-level research in a fragmented manner, and continue to expect incremental gains; or it can form partnerships among the many industry organizations and pool funds towards more meaningful, system-level research capable of clearly identifying areas of excessive conservatism and affecting appropriate code changes.

The overarching goal of current and future masonry research at Drexel is to argue for the latter, and to illustrate the opportunity at hand to begin to emphasize the many positive attributes of

masonry bearing wall systems. A new vision for masonry research will be articulated founded on the identified gaps and the authors' experiences, and aimed at uncovering current conservatism to develop more appropriate seismic provisions for partially grouted reinforced concrete masonry, particularly for the eastern US.

IBC SEISMIC PROVISIONS-THE CHALLENGE

In 1997 the International Code Council (ICC) initiated an effort to draft a comprehensive building code consistent with and inclusive of the existing model codes. This effort resulted in the development of the International Building Code (IBC) in 2000, which is now maintained and updated every three years. A consequence of this unification is that provisions developed for one region now influence the entire country.

For masonry buildings, current seismic provisions define five lateral force resisting systems and their corresponding detailing requirements, and provide limitations on their use based on the SDC, see Table 1. (Note in Table 1, NL refers to not limited, NP refers to not permitted, and numerical values represent height limitations). Schematics of the various types of reinforced masonry shear walls are shown in Figure 1(a). In addition to the reinforcement and grout shown, several provisions prescribe the required connection details between orthogonal walls and diaphragms. To provide a perspective on this discussion, Figure 1(b) shows a map of approximate SDCs to illustrate the influence of the IBC seismic design provisions throughout the eastern US.

In general, there are two critical aspects of these provisions that represent the core challenge to masonry bearing-wall construction. First, the limitation placed on the lateral force resisting systems for masonry is quite severe and results in significant cost increases. Although objective, quantitative cost data is difficult to come by, it is clear that the required increase in reinforcement and grout, and the corresponding labor for SDC C through F significantly impacts cost (especially when one considers that construction of plain masonry in the eastern US has been the norm for centuries).

The second primary challenge posed by the IBC seismic provisions relates to the response modification coefficients (R-factors) shown in Table 1. These R-factors represent a measure of a system's inherent robustness and ductility and serve to decrease the seismic demand that must be considered in design (i.e. the higher the R-factor, the lower the demand that must be designed for). As can be seen from Table 1, the masonry system R-factors are lower than some competing systems. For example, if we compare an ordinary reinforced masonry shear wall (R = 2½) with ordinary steel braced frames in light-frame construction (R = 4), it is apparent that the masonry system must be designed to resist 60% more lateral force. Whether these R-factors are justified by system-level response attributes is still open to much debate.

While many believe that the IBC seismic provisions do not meet these goals in the case of masonry, it must be recognized that without demonstrated proof of system behavior, such as in the case of many masonry systems, conservatism must be leveraged to ensure the most fundamental responsibility of the code - to protect life safety - is achieved.

Throughout the second half of the 20th Century RM structures were constructed in high seismic regions and, for the most part, performed reasonably well in earthquakes. Unfortunately, the

initial approach to RM design -- a mixture of empirical rules based on heuristics and a working stress (elastic) design methodology -- ultimately proved incapable of reliably satisfying the ductility and strength requirements of seismic design. By the late 1970s it was clear that RM was falling behind competing structural materials such as concrete and steel, and was becoming increasingly rare in high seismic regions.

To combat this, in the mid-1980s the US National Science Foundation (NSF) and the corresponding agency in Japan funded the "US-Japan Coordinated Program for Masonry Research" [1]. To organize the US portion of the program the NSF formed the Technical Coordinating Committee for Masonry Research (TCCMAR). The broad goal of this initiative was to jump start the transition of masonry codes and standards to a more rational limit state design methodology in the hopes of improving the economy of RM construction to stimulate competition and foster lower building costs. However, due to limited resources, TCCMAR recognized early on that this effort could not be comprehensive, but rather should be aimed to provide a body of knowledge and framework for future development. Given this limitation, it was decided to focus on RM for high seismic regions (i.e. consistent with a fully-grouted special reinforced masonry shear wall system). Therefore, the MSJC design provisions [2] are based on testing fully grouted (FG) heavily reinforced masonry shear walls [3, 4] and sub-system [5]. The applicability of these provisions to partially grouted (PG) masonry is questionable.

Given the description above, it is clear that masonry research conducted to date has focused on the extremes of masonry construction: either heavily reinforced, fully grouted masonry or URM. As a result, there is little information about the response of lightly reinforced, partially-grouted masonry construction that is likely appropriate for the higher seismic regions in the eastern US.

Aside from technical considerations, this vision provides the only means to develop a persuasive rebuttal to the current seismic provisions that are challenging masonry construction in the eastern US. To that end, a research program aimed at bridging the knowledge-gap associated with the system-level performance of lightly reinforced partially grouted masonry shear wall systems has been initiated in 2007 at Drexel University. The overarching goal of this research is to investigate the response of lightly reinforced, low-rise masonry buildings and to identify system-level mechanisms that contribute to displacement and force capacity. It is envisioned that such an effort will clearly uncover any sources of excessive conservatism within current seismic provisions and inform future seismic provisions regarding the limitation of masonry structural systems and masonry system R-factors.

Table 1. Basic seismic force resisting system limitation and response modification coefficients based on SDC (IBC 2003).

BASIC SEISMIC-FORCE-RESISTING SYSTEM	RESPONSE MODIFICATION COEFFICIENT, R^a	SYSTEM LIMITATIONS AND BUILDING HEIGHT LIMITATIONS (FEET) BY SEISMIC DESIGN CATEGORY AS DETERMINED IN SECTION 1616.3[c]				
		A or B	C	D[d]	E[e]	F[e]
1. Bearing Wall Systems						
A. Ordinary steel braced frames in light-frame construction	4	NL	NL	65	65	65
B. Special reinforced concrete shear walls	$5^1/_2$	NL	NL	160	160	100
C. Ordinary reinforced concrete shear walls	$4^1/_2$	NL	NL	NP	NP	NP
D. Detailed plain concrete shear walls	$2^1/_2$	NL	NP	NP	NP	NP
E. Ordinary plain concrete shear walls	$1^1/_2$	NL	NP	NP	NP	NP
F. Special reinforced masonry shear walls	5	NL	NL	160	160	100
G. Intermediate reinforced masonry shear walls	$3^1/_2$	NL	NL	NP	NP	NP
H. Ordinary reinforced masonry shear walls	$2^1/_2$	NL	160	NP	NP	NP
I. Detailed plain masonry shear walls	2	NL	NP	NP	NP	NP
J. Ordinary plain masonry shear walls	$1^1/_2$	NL	NP	NP	NP	NP
K. Light frame walls with shear panels—wood structural panels/sheet steel panels	$6^1/_2$	NL	NL	65	65	65

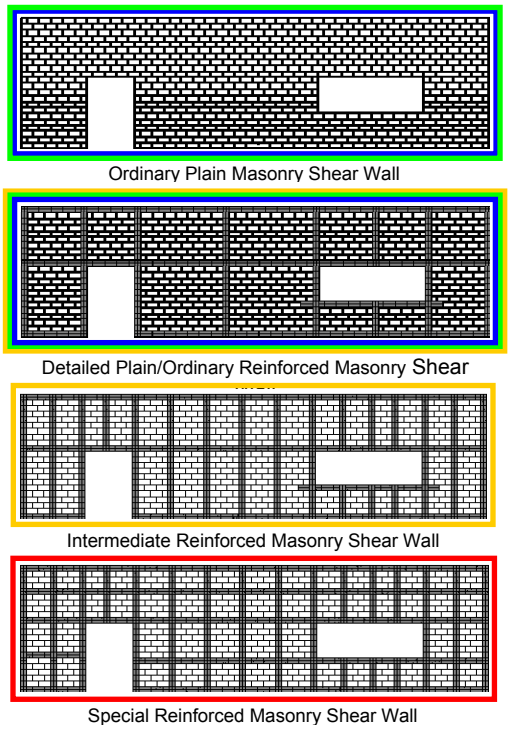

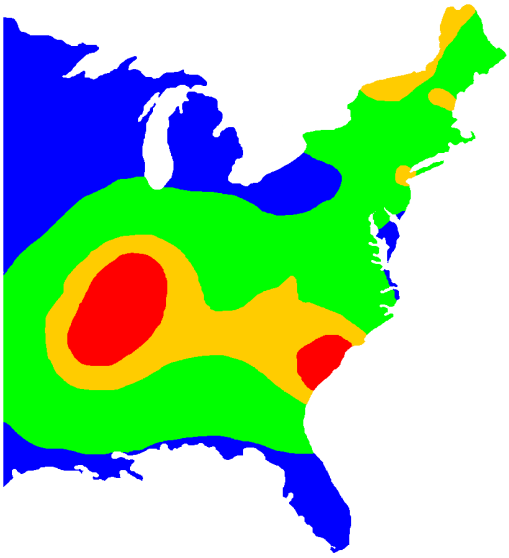

Fig. 1. (a) Schematic of the IBC reinforced masonry shear walls and (b) SDC of the Eastern US for soil condition C (IBC 2003 [6]).

PAST AND CURRENT RESEARCH ON PARTIALLY GROUTED REINFORCED MASONRY SHEAR WALLS AT DREXEL

In 1992, Ghanem et al. [7] conducted 1/3 scale tests of partially grouted concrete masonry cantilever shear walls under monotonic lateral load. Three different reinforcement arrangements were used, see Figure 2. Vertical and horizontal steel reinforcement percentages were kept constant for the three walls. The spacing of reinforcement and extend of grouting (only at the cells containing steel reinforcement) were the main variables. Figure 3 presents the load-displacement curves for the three walls. As shown, stiffness, strength and post-peak response are different for the three walls. It was concluded that the behavior of partially reinforced masonry is strongly dependent on the distribution of reinforcement. As the reinforcement is more uniformly distributed, both the strength and deformation capacity of the walls increased. In addition, the distribution of reinforcement had a marked effect of wall failure mode. As the reinforcement went from being concentrated in local areas (SWA) to being more uniformly distributed (SWC), the failure modes switched from shear to shear/flexure to flexure. Finally, it was concluded that in order to avoid brittle shear failure the horizontal reinforcement should be distributed; however, to enhance flexural strength the vertical steel should be concentrated at the ends of the wall.

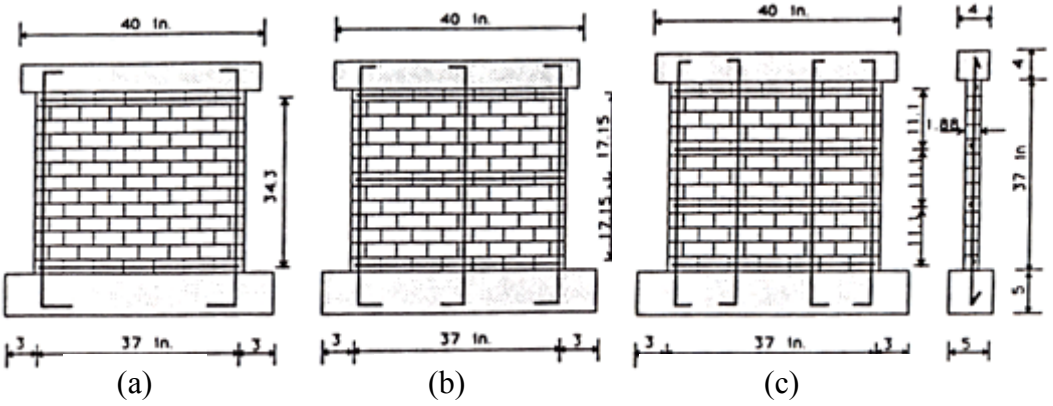

Fig. 2. Reinforcement configuration for (a) Wall SWA, (b) Wall SWB, and (c) Wall SWC (taken from Ref. 7).

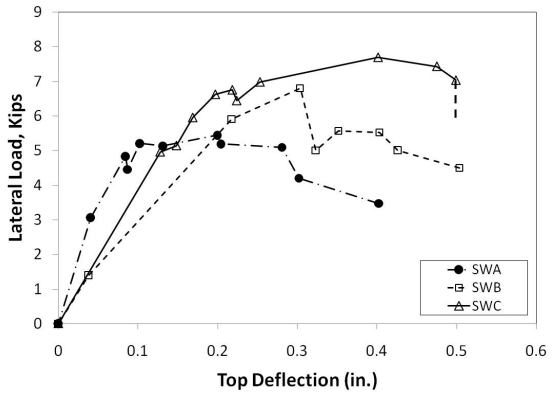

Fig. 3. Monotonic force-displacement response of Wall SWA, Wall SWB, and Wall SWC (Redrawn from [7]).

In 2007, a comprehensive research study was initiated to investigate the seismic response of partially grouted concrete masonry at the assemblages [8] and wall components [9] levels. The main goal is to determine the effect of partial grouting on shear wall cyclic response. Figure 4 shows a schematic of the shear wall test setup. With the two displacement-controlled vertical actuators it was possible to control the rotation at the top of the specimen to create fixed-fixed boundary conditions.

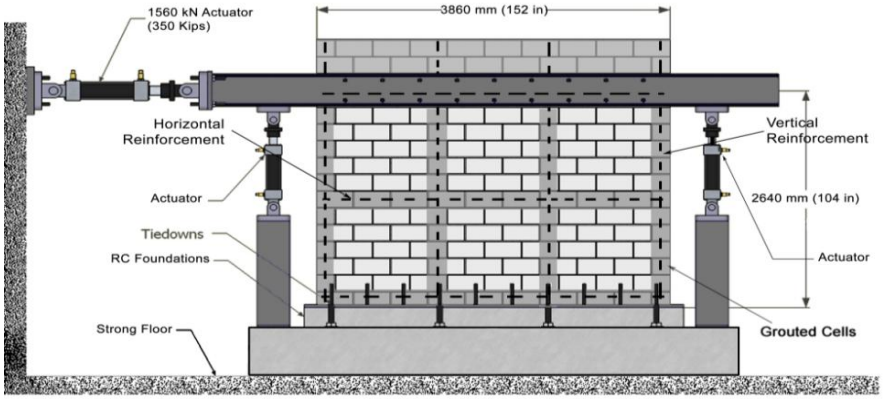

Fig. 4. Shear wall test setup [9].

Fig. 5. Cracking and failure mode of partially grouted walls [9].

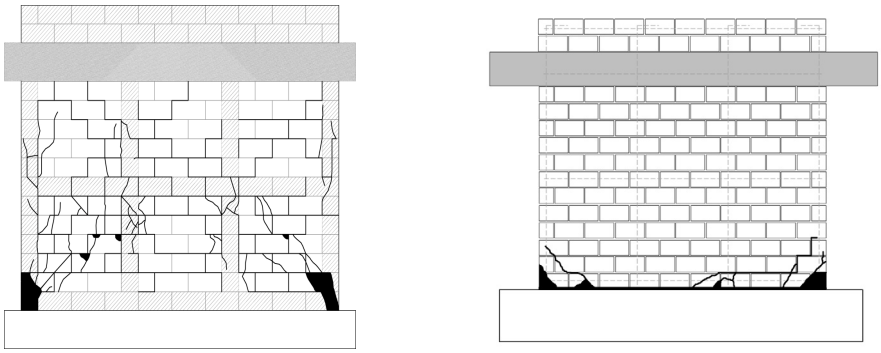

(a) PG Wall (b) FG Wall

Fig. 6. Wall cracking and failure modes of partially and fully grouted walls [9].

Tests indicated a distinct difference in behavior of partially and fully grouted walls with similar reinforcement. The behavior of partially grouted shear walls is similar to that of masonry in-filled frames. As shown in Figure 7 the shear strength of partially grouted wall is significantly

less than that of fully grouted wall with the same reinforcement. Based on the experimental data from this research program and past researches, the MSJC code is non-conservative in predicting the strength of partially grouted shear walls.

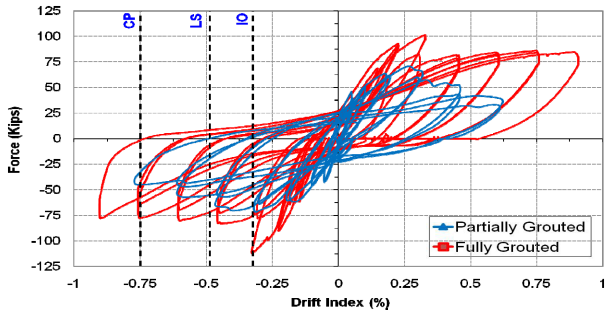

Fig. 7. Cyclic load-displacement curves for partially and fully grouted walls [9].

FUTURE SYSTEM-LEVEL MASONRY RESEARCH AT DREXEL

To fill this knowledge-gap and to identify and reduce any excessive conservatism it may be sustaining, investigations into system-level performance must become the norm for masonry research. While the behavior of structural systems such as frames may be reasonably approximated by investigating the response of primary components (e.g. columns and beams), this is not the case for bearing-wall systems. Such systems are highly indeterminate and interconnected, which precludes the accurate a priori identification of continuity conditions and force-resisting mechanisms that affect individual component response. As a result, component-level investigations of such systems are hampered by considerable levels of epistemic uncertainty. Faced with this challenge, past researchers have been forced to employ conservatism by isolating individual components and neglecting poorly understood system-level mechanisms. Such studies implicitly ignore the many desirable attributes of bearing-wall systems and are prone to providing overly conservative results.

In order to perform such an investigation with the limited resources likely available, this effort will leverage the established field of reduced-scale structural modelling [10]. Small-scale modelling of concrete masonry has been successfully used at Drexel University in the past 25 years.

The salient tasks for the proposed investigation are listed in the following and shown schematically in Figure 8.

With funding from the masonry industry (NCMA, PCA and IMI) a 1/3 scale two story partially grouted reinforced masonry wall-bearing masonry building with configuration shown in Figure 9 will be constructed with 1/3 scale blocks produced in-house using the shown block-making machine (Figure10) and rigid concrete diaphragms. This test will allow investigating the effect of flanges, wall openings and interaction between perpendicular walls. Two displacement-controlled actuators at each floor level will impose equal cyclic displacements to the in-plane walls and the restoring force will be measured. Load-displaced hysteretic curves will be drawn to determine wall stiffness, strength and ductility.

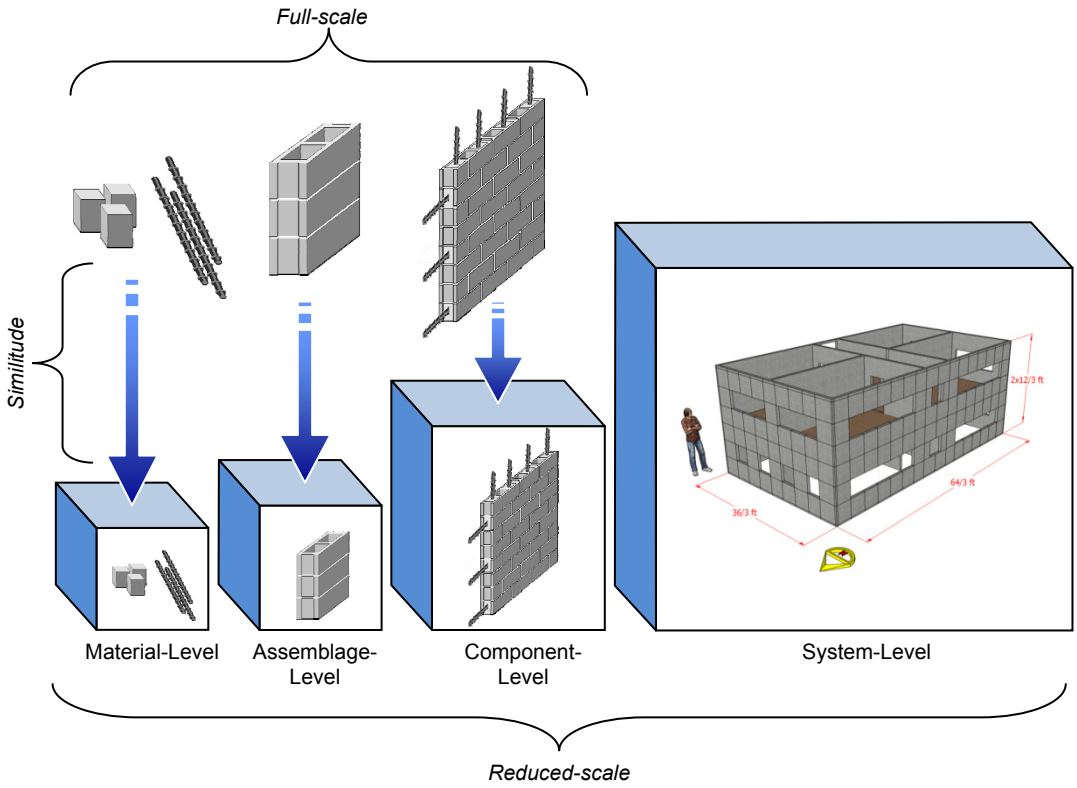

Fig. 8. Overview of small-scale validation at the material-, assemblage-, and component-levels building to reduced scale experiments of complete masonry bearing-wall systems.

The building configuration (Figure 9) was carefully selected to represent typical construction details of masonry buildings and to be able to capture effect of key parameters on the building response including:

a. Interaction of in-plane and out-of-plane walls
b. Effect of plan and elevation irregularities
c. Effect of wall perforations on failure mode, strength and deformation capacity
d. Effect of pier's aspect ratios and level of axial load due to overturning moment

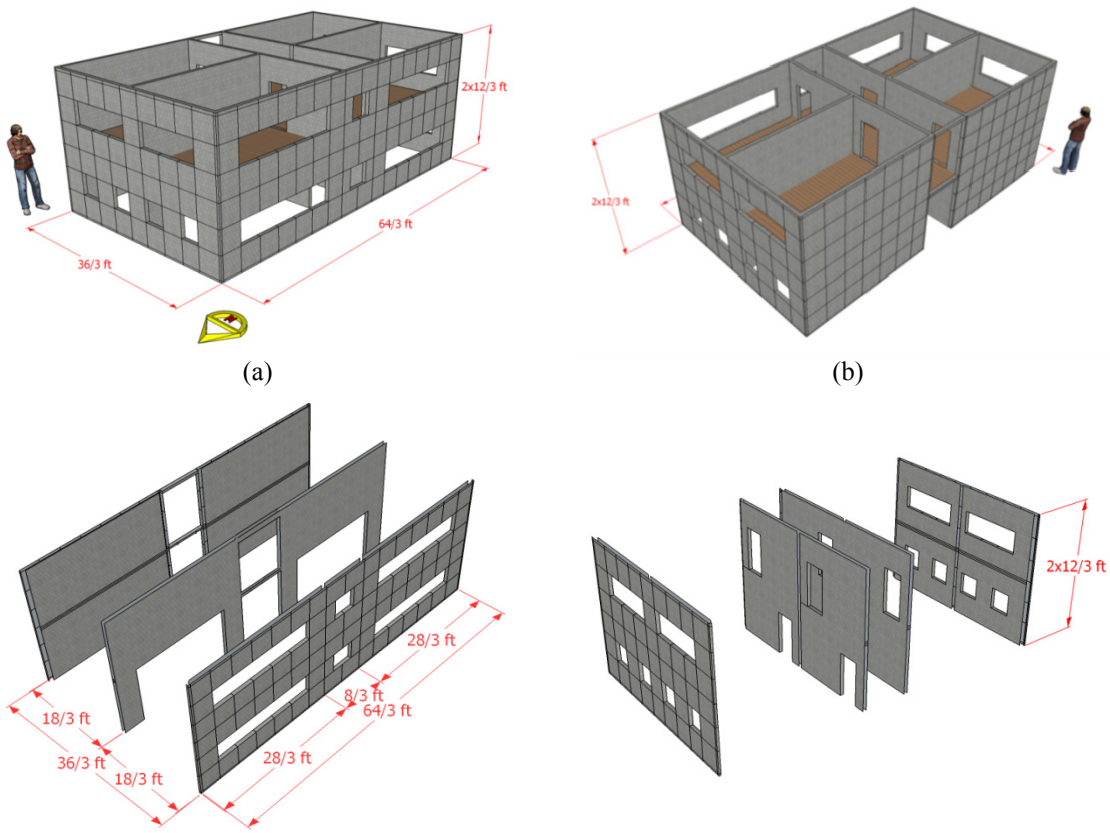

Fig. 9. Proposed building configuration (a) north view, (b) south view, and lateral load bearing system in (c) north-south direction, and (d) east-west direction.

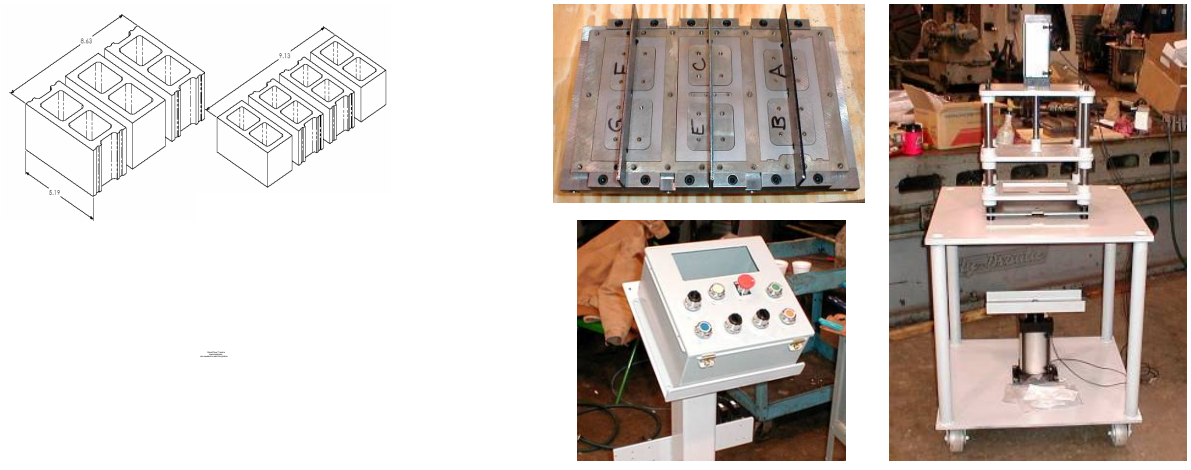

Fig. 10. Small-scale blocks produced in-house at the Masonry Research Lab of Drexel University.

SUMMARY AND CONCLUSIONS

Current American codes' provisions are based on testing fully grouted masonry. Past and current wall tests demonstrate that partial grouting reduces wall strength and deformation/ductility capacity. Current codes' shear strength predictions are un-conservative. There is an urgent need for system-level research to accurately predict the capacity and ductility of partially grouted masonry buildings. It is hoped that the on-going system-level research at Drexel will help developing realistic seismic design provisions for reinforced partially grouted concrete masonry buildings.

REFERENCES

1. Noland, J.L. (1988) "A review of the U.S. coordinated program for masonry building research," Proceedings of the Fourth North American Masonry Conference, UCLA
2. Masonry Standards Joint Committee (MSJC) (2008) "Building Code Requirements for Masonry Structures," ACI 530/ASCE 5, TMS 402, American Concrete Institute, American Society of Civil Engineers, and The Masonry Society, Detroit, New York, Boulder
3. Shing, P.B., J.L. Noland, H. Spaeh, and E. Klamerus (1988) "Inelastic behavior of masonry wall panels under in-plane cyclic loads," Proceedings of the Fourth North American Masonry Conference, UCLA
4. Merryman, M., G. Leiva, N. Antrobus, and R.E. Klingner (1990) "In-plane seismic resistance of two-story coupled concrete masonry walls," ASTM Special Technical Publication, No. 1063, pp. 378-393
5. Seible, F, M.J.N. Priestley, G.R. Kingsley, and A.G. Kurkchubasche (1994) "Seismic response of full-scale five-story reinforced-masonry building," ASCE Journal of Structural Engineering, Vol. 120, No. 3, pp 925-946
6. Ghanem, G. M., A. S. Essawy, and A. A. Hamid (1992) "Effect of Steel Distribution on the Behavior of Partially Reinforced Masonry Shear Walls," Proceedings of the 6th Canadian Masonry Symposium, University of Saskatchewan, Saskatoon, Canada.
7. IBC 2003, "International Building Code," 2nd Edition, International Code Council, Inc, USA
8. Mota M.C., Minaie E., Golecki T., Holly E., Moon F.L., and Hamid A.A. (2007) "Diagonal Tension Strength of Partially Grouted Concrete Masonry Assemblages," Proceedings of the 10th North American Masonry Conference, St. Louis, Missouri, June 3-6, 2007
9. Minaie E., Salama M., d'Hermillon B., Dulka J., Moon F. L., Hamid A. A. (2008), "Shear Strength of Partially Grouted Reinforced Masonry Shear Walls subjected to In-plane Loading", Proceedings of the 6th Annual Meeting of NEES, Portland, Oregon, June 2008
10. Harris, H. G. and Sabnis, G. M. (1999) "Structural Modeling and Experimental Techniques," 2nd Edition, CRC Press, Boca Raton

INNOVATIVE SEISMIC RISK MITIGATION FOR MASONRY BUILDINGS

Daniel P. Abrams
Willett Professor of Engineering
University of Illinois at Urbana-Champaign
email: d-abrams@illinois.edu

PREFACE

Seismic assessment and rehabilitation schemes for unreinforced masonry buildings have largely followed traditional methods of structural engineering over the last five decades. Simple approaches of strengthening have been employed, which are based on principles previously developed for design to resist static gravity loads. Structural capacity in the form of strength has been added to meet demands that are expressed in terms of forces. An essentially nonlinear dynamic action has been represented with an equivalent set of forces using force reduction factors that approximate the ductility or deformation capacity. Because seismic response is viewed through the lens of these equivalent forces, engineers typically view mitigation as strengthening. However, this does not need to be the case even for unreinforced masonry buildings, which have been shown to deform with considerable displacement capacity. What needs to be changed is the way of thinking. Old technologies for simplifying this problem can be abandoned in lieu of new computational approaches that exploit advanced simulation methods used in related fields of structural mechanics. No longer does seismic response of unreinforced masonry buildings need to be represented with simplified, force-based static models since technologies for structural analysis have changed and will continue to improve in the future.

TRADITION VS. INNOVATION

This paper presents an introspective look at how traditional engineering methods can be changed so that future risk mitigation strategies for masonry buildings can be improved. Traditional approaches are contrasted with innovative schemes, methods and solutions that are possible with current advanced technologies. Such innovations include displacement-based approaches for seismic assessment and rehabilitation, and advanced computational simulations of three-dimensional building response using high capacity computers. With the combination of these two advancements, notions of structural capacity can be represented in terms of displacements or deformations rather than forces and stresses. Mitigation of seismic damage can be achieved by thinking of ways to enhance deformability by recognizing displacement-controlled actions. This concept is somewhat new for unreinforced masonry buildings but is not unrealistic considering rocking and sliding mechanisms.

Seismic response of masonry buildings no longer needs to be analyzed using overly simple and approximate planar models. Finite element methods are currently available for representing three-dimensional behavior of orthogonal walls and floor diaphragms. These models can be extended further to include nonlinear mechanisms representing the post-cracking range of response and foundation effects. With new computational tools such advanced analytical models can be a reality.

NEW TOOLS

Since advancements in computational technologies have been made at rates far exceeding that of masonry engineering, much capability can be exploited. The most recent benchmark in computing capability will be reached in 2011 when the Blue Waters project goes online at the University of Illinois. This new NSF-sponsored computer will deliver sustained performance of one petaflop (1 quadrillion calculations per second). With this capability, seismic response of complete populations of buildings and other civil structures can be modeled across an urban area including spatial distributions of ground motions. Such analyses will not only enhance mitigation efforts for individual buildings, but will provide scenarios for emergency response planning for an entire region. It is time that earthquake engineers accelerate development of simulation models so that they can take advantage of these new computational capabilities. One example of an ongoing effort along these lines is the MAEviz software application developed at the Mid-America Earthquake Center.

LIMITATIONS OF CURRENT METHODS

One may ask why should we bother with such far-reaching new developments when we have seismic codes and guidelines that adequately address assessment and rehabilitation of unreinforced masonry buildings. The answer to this question is that present methods have severe limitations because of their simplifying assumptions. Such limitations are addressed in this presentation and including the following: (a) accuracy of force reduction factors used with the equivalent lateral force procedure, (b) modeling the distribution of lateral story shear to individual piers in a perforated shear wall, (c) modeling interaction effects from orthogonal planar elements meeting at a corner of a building, (d) modeling of the coupling between walls of disparate stiffness, and (e) neglecting displacement controlled actions such as rocking and sliding. Examples illustrating new options for displacement-based retrofit are given to suggest how new modeling approaches may result in safer or more economical solutions.

INTERNATIONAL COLLABORATION

The need for innovation in seismic hazard mitigation is best expressed for a common and wide category of unreinforced masonry buildings used across the globe – that being public school buildings. School buildings were the most heavily affected type of building structure during the great Wenchuan earthquake of May 2008. Student and teacher populations suffered heavy losses of life with over 70,000 deaths and nearly 400,000 injuries in total. Complete collapse of schools buildings has occurred in many other parts of the world, including the 2001 Bhuj earthquake in India. Researchers have postulated that 7300 schools in Japan face a high risk of collapse if a strong earthquake was to occur, and that over 40,000 school buildings have insufficient strength and should be retrofitted. Similar risks exist in Iran where a concerted national effort is underway to retrofit masonry school buildings. With this common high-risk problem of masonry school fragilities, extended multi-lateral efforts would make a significant impact across the globe that would increase seismic safety for future generations. Exploitation of advanced computational technologies and adoption of displacement-based methods of seismic rehabilitation, as discussed earlier, may be a means towards achievement of this goal.

CONCLUDING REMARKS

In summary, innovation in structural engineering related to modeling of seismic response for masonry buildings should be accentuated and accelerated rather than continuing to extrapolate at a slow pace from traditional methods of the past. New computational methods should be developed for assessing and visualizing seismic response and behavior of complete nonlinear building systems in three dimensions rather than a series of planar elements. Displacement-based concepts should be embraced since they will yield much different results than force-based concepts for masonry buildings, which are commonly thought to be quite stiff and brittle. This new way of thinking will result in safer construction at a reduced mitigation cost and thus reduce seismic risk and save lives.

The purpose of the presentation is to intrigue participates from Iran and the United States to pursue collaborative efforts that will ultimately mitigate risk and save lives as a result of vulnerability of unreinforced masonry school buildings to seismic actions.

ROLE OF SEISMIC RETROFITTING OF BUILDINGS IN EARTHQUAKE RISK MITIGATION FOR IRAN

A. S. Moghadam
International Institute of Earthquake Engineering and Seismology (IIEES), Tehran, Iran
e-mails: moghadam@iiees.ac.ir

ABSTRACT

Earthquakes have caused major disasters in Iran. There are different options to reduce the devastating effects of this natural phenomenon. To effectively reduce the risk much effort should be directed toward identifying the seismic vulnerability of buildings and retrofitting them. If the building found to be seismically vulnerable, different retrofitting options should be carefully studied. Improper selection of retrofitting scheme causes waste of much needed financial resources and risks the lives of inhabitants in earthquake prone regions. Therefore, there is an urgent need to a guideline for identifying the best retrofitting scheme that can be used by an engineer in seismic retrofitting projects. This paper has four parts. In the first part the role and importance of seismic retrofitting of buildings are identified within the earthquake risk mitigation and disaster planning for Iran. A summary of challenges that should be dealt are presented in the second part of the paper. Then, some case studies of application of seismic retrofitting techniques in recent years are introduced in the third part of the paper. Finally, in the fourth part of the paper, based on experiences in the last decade some techniques for identifying the best seismic retrofitting option are offered.

1. INTRODUCTION

This paper reviews some experiences gained and challenges faced regarding seismic retrofitting of buildings in Iran during the last decade. First, the role and importance of seismic retrofitting of buildings are identified within the earthquake risk mitigation for Iran. A summary of challenges that should be dealt are presented later. Then, some case studies of application of seismic retrofitting techniques in recent years are introduced. Finally, some techniques to improve the approach to seismic retrofitting are offered.

2. ROLE OF SEISMIC RETROFITTING IN EARTHQUAKE RISK MITIGATION FOR IRAN

Earthquakes have caused major disasters in some parts of the world. Countries in those regions face different challenges to reduce the devastating effects of this natural phenomenon. Improving earthquake prediction procedures, establishing early warning systems and developing disaster management programs are taken seriously in some hazardous countries.

However to reduce risk effectively in countries such as Iran, much effort should be directed toward identifying the seismic vulnerability of buildings and retrofitting them as focus of every risk mitigation program. Damage to structural and non-structural elements of buildings has been the main source of risk in earthquakes (Figures 1 and 2).

Fig. 1. A building damaged in Bam (2003) earthquake.

Fig. 2. Damage to non-structural elements in Silakhor (2006) earthquake.

3. CHALLENGES OF SEISMIC RETROFITTING IN IRAN

Seismic retrofitting has a history more than thirty years in Iran. However, in the last ten years it has grown substantially due to large amount of funding by governmental agencies. The first Iranian guideline on seismic retrofitting of existing buildings was developed in 2002 by International Institute of Earthquake Engineering and Seismology (IIEES). This document made an important contribution to familiarize the engineering community to new concepts of seismic evaluation and retrofitting. It has been taught as short courses to engineers and as graduate courses to university students.

The next milestone has been the initiation of schools retrofitting program in 2004 that has increased the momentum of involvement of professional engineers in seismic retrofitting of existing building in different towns and cities. However at that time, the capacity of the engineering community was far less than what was needed to study a large number of vulnerable school buildings in short period of time. Therefore less than expected output from the school retrofitting program in a period of four years caused the main challenge that seismic retrofitting movement faces in Iran. Different methods to accelerate the retrofitting process is being suggested and investigated by parties involved.

4. SOME OF SEISMIC RETROFITTING CASES IN IRAN

Seismic retrofitting in the past ten years was mainly focused on important public and governmental buildings such as schools, hospitals and public services offices in Iran. Most of schools studied were one to three story masonry buildings. However some of taller buildings are also studied that are among the largest seismic retrofitting projects in the world.

Fig. 3. A Retrofitted 56-Story reinforced concrete building.

5. A PROCEDURE TO HELP SELECTING THE OPTIMUM RETROFITTING OPTION

Guidelines such as FEMA 356 (ASCE, 2000), provide standardized approaches for analytical modeling of different types of buildings to investigate the performance of their structural and non-structural elements in a specific earthquake level. If the building found to be seismically vulnerable, different retrofitting options should be carefully studied. In order to use guidelines, Experience of the designer is the most important parameter in leading to an optimum retrofitting scheme. Improper selection of retrofitting scheme causes waste of much needed financial resources and risks the lives of inhabitants in earthquake prone regions. Besides higher cost, improper selection of retrofitting scheme usually causes trouble in executing the scheme such as disturbing the performance of the building for a longer period of time. Such problems sometimes lead the authorities to believe that the only solution for seismically deficient buildings is to demolish the existing building and rebuild it. The author of this paper has many experiences in this regard with authorities of “Housing Foundation of Iran” after 2003 Bam and 2006 Silakhor earthquakes on the subject of earthquake damaged buildings and with authorities of “School

Board of Iran" about existing deficient school buildings. Therefore, to reduce the seismic loss by retrofitting poor designed or constructed buildings there is an urgent need to a guideline for identifying the best retrofitting scheme that can be used by an experienced engineer in seismic retrofitting projects.

Seismic retrofitting technique selection has been subject of some researches. Smyth et. al (2004) conducted comparative evaluation of seismic retrofitting measures through economical fragility based analysis. Kafali and Grigoria (2005) developed a method to identify an optimal retrofitting technique for structural and nonstructural systems using both capacity and cost analyses. Porter et. al (2006) employed the assembly based vulnerability method to estimate the cost-effectiveness of retrofitting options for wood frame buildings in terms of benefit-cost ratio. Alanne and Klobut (2003) develop a multi-criteria evaluation in accordance to use of energy in the retrofitting process. Thomson et al. (2003) represent value delivery in design stages by incorporating design quality indicator and Mc Cormack and Rad (1997) present a methodology to estimate earthquake expected loss.

The main purpose of present study is to develop a measurable procedure for selecting the most appropriate technique in seismic retrofitting of a vulnerable building and provide helpful tool for clients and decision-makers to make a suitable selection. Basically, by identification of the most adequate factors related to seismic rehabilitation of structures, the important parameters involved in the technique selection of the retrofitting process are introduced and classified.

6. DEVELOPMENT OF THE PROPOSED METHODOLOGY

Four main issues are involved in evaluation of a proposed rehabilitation program for strengthening an existing building. First of all, is the engineering method employed in evaluation of that retrofitting technique that is a technical problem of code requirements, design approach, materials and construction techniques. The second one and the most critical issue, is the cost of strengthening. This, primarily consist of the cost of construction but also involves design costs, possible costs of testing and cost of permits and approvals and cost of construction financing. Third, there are indirect costs associated with strengthening which in many ways are analogous to the indirect costs of earthquake damage and finally, is the question of the effectiveness of the strengthening in reducing damages (FEMA-174, 1989 and FEMA-356, 2000).

Seismic damages directly related to structural specifications of building. Among them are; building and foundation material (strength, weight …); height; structural framing; design method; expected life of building; building shape in plan and elevation (Regular & Irregular) and proximity to other buildings (ATC-13, 1985).

To indicate the necessity of building to rehabilitate, first need to consider the building specification. The building owner or code official shall select the seismic retrofitting objective that consists of the selection of a target building performance level in an anticipated earthquake hazard level, such as basic safety level that expected the building to experience little damage from relatively frequent, moderate earthquakes. (FEMA-356, 2000) Then the building status quo such as its type, detailing, connectivity, material strength and condition of the structural elements should be studied. Most often when all alternatives are considered, the options of modifying the building to reduce the risk of damage should also be studied. By using engineering judgment and

analysis, the effects of rehabilitation on stiffness, strength and deformability of building are evaluated in the analytical model to reliably accept the rehabilitation scheme.

The proposed procedure of this paper is developed in three steps as a multi-criteria method which is discussed in the following sections. There are many parameters affect in rehabilitation process of a building. Clients need to be familiar with the most effective parameters to schedule suitable plan for assign resources. The procedure summarized in three parts. First, different parameters influencing effectiveness and efficiency of a retrofitting technique are recognized and categorized. Then, a quantitative approach is developed to measure the relative advantages of different retrofitting options. Finally, a survey program is conducted and opinions of some leading authorities, both from academia and profession, are used to calibrate the factors embedded in the method. This pattern help the decision-makers to select the most appropriate retrofitting option which all of the parameters spotted in the process.

6.1 Parameters Determining the Effectiveness of a Retrofitting Technique

There are many different parameters that are potentially important in seismic rehabilitation of a building. These important parameters are summarized in Appendix A and are explained in the following. *The type of structural system* is definitely affects the proper technique. There are some retrofitting techniques that are naturally used for steel buildings, such as bracing. However, this technique is less common in concrete or masonry buildings. *Building geometry* such as its shape, size or height is also important. A sole concrete core can be a good solution for a small building; however for a large building without a rigid diaphragm, a more distributed lateral load resisting system in plan could be preferable. *Construction quality* of the existing building is usually important in selecting the technique. For a poor quality building, sometimes it is better to employ a method that reduces the transferred seismic force to the building rather than designing a huge new system for it. The *building occupancy* usually defines the set of constraints that the design engineer should be deal with. For a residential building, it may be possible to select a scheme that takes some time to apply, but for an educational building it is important that the retrofitting scheme take no longer than a summer time to apply. The intensity of seismic risk, the importance of different geotechnical hazards such as liquefaction site effects, even the soil type in the site depends on *the building location*.

The *constructional aspects* include those parameters which can be significant in the executing process. With respect to different types of occupancy of building, *Construction duration* and *construction difficulty* can change the final decision. Some plans have limited time and area to execute. Also, *Availability of Constructional Guideline* can be useful for low-experienced contractors to be aware of executing process.

The *economical characteristics* of retrofitting schemes are also among the most important parameters, specifically for clients that should be considered in selecting the best retrofitting option. The simplest approach is to estimate the direct cost of each option by summing up the cost of items that each scheme is made of. It includes a series of items from the cost of removing the existing finishing to the cost of adding new material or elements and providing a new finishing. Usually this cost is compared with the *replacement cost of the building to* assess the retrofitting scheme. The value of retrofitting costs, including cost of designers, labors and materials are compared with the benefit of performing strengthening plan.

The technical characteristics of retrofitting schemes are among the most important parameters that should be considered in selecting the best retrofitting option. A scheme which *adds less weight* besides improving the level of performance is more desirable. However, explicit comparison of technical characteristics of retrofitting options is usually conducted by performing linear or nonlinear analyses of the retrofitted building to check the acceptance criteria for structural, non structural and equipments. A scheme that can be applied while the people can still use the building is often preferred. The *sensitivity of performance* of each scheme to the *technical and constructional errors*, also the availability of information on *performance of such schemes in previous earthquakes* is much useful.

6.2 Quantifying the Selection Process

6.2.1 Categorizing the Items

By classification of the aforementioned parameters indicated in section 6.1, designers are enabled to systematically deal with the problem. Those parameters that are recognized as potentially important in seismic rehabilitation of a building are classified into five key groups: Building Characteristics, Constructional Aspects, Economical Aspects, Technical Aspects and Architectural Aspects.

6.2.2 Development of Scoring Algorithm

A weighting factor of $\underline{BC}$ is used for Building Characteristics key group. Weighting factors $\underline{CA}$, $\underline{EA}$, $\underline{TA}$ and $\underline{AA}$ are used for Constructional Aspects, Economical Aspects, Technical Aspects and Architectural Aspects key groups respectively. Other weighting factors used for the sub-divisions of the key groups.

In accordance with categorizing the most appropriate parameters, the values of each component need to be considered. A scoring system has been established by survey to characterize weighting factors assigned to the key groups and their sub-divisions. Each factor is assigned a value. The format of the form is designed to compare three retrofitting options, Alternative A, Alternative B and Alternative C. The user has to assign a grade for each alternative. The partial score of the Alternative (A) derived from the Building Characteristics key group is calculated as:

$$EP_{(1)} = (BC)\times\begin{bmatrix}(BC_S)\times\left[(BC_S)_t\times(A_S)_t\right]+\left[(BC_G)\times\left[(BC_G)_h\times(A_G)_h+(BC_G)_d\times(A_G)_d\right]\right]+\\(BC_C)\times\left[(BC_C)_c\times(A_C)_c+(BC_C)_d\times(A_C)_d\right]\end{bmatrix} \quad (1)$$

The partial score of the Alternative (A) derived from the Constructional Aspects key group is calculated as:

$$EP_{(2)} = (CA)\times\begin{bmatrix}(CA_{DU})\times(A_{DU})+(CA_{DI})\times(A_{DI})+(CA_T)\times(A_T)+(CA_M)\times(A_M)+(CA_P)\times(A_P)+\\(CA_G)\times(A_G)+(CA_E)\times(A_E)\end{bmatrix} \quad (2)$$

The partial score of the Alternative A derived from the Economical Aspects key group is calculated as:

$$EP_{(3)} = (EA)\times\left[(EA_{LR})\times(A_{LR})+(EA_C)\times(A_C)+(EA_L)\times(A_L)+(EA_V)\times(A_V)+(EA_P)\times(A_P)\right] \quad (3)$$

The partial score of the Alternative A derived from the Technical Aspects key group is calculated as:

$$EP_{(4)} = (TA)\times\left[\begin{array}{l}(TA_R)\times(A_R)+(TA_W)\times(A_W)+(TA_P)\times(A_P)+(TA_N)\times(A_N)+(TA_C)\times(A_C)+\\(TA_F)\times(A_F)+(TA_{DU})\times(A_{DU})+(TA_E)\times(A_E)+(TA_{DE})\times(A_{DE})+\\(TA_M)\times\left[\begin{array}{l}(TA_M)_t\times(A_M)_t+(TA_M)_{pi}\times(A_M)_{pi}+(TA_M)_{hi}\times(A_M)_{hi}+\\(TA_M)_s\times(A_M)_s+(TA_M)_p\times(A_M)_p+(TA_M)_c\times(A_M)_c\end{array}\right]\end{array}\right] \quad (4)$$

The partial score of the Alternative A derived from the Architectural Aspects key group is the calculated as:

$$EP_{(5)} = (AA)\times(A) \quad (5)$$

Finally, the total score for the Alternative A is summed up as:

$$EP_{T(A)} = \sum_{i=1}^{5}(EP)_i \quad (6)$$

6.3 Calibrating the Coefficients of the Scoring Algorithm Using Expert Opinion

Professional judgment and expert opinion is the most widely useful tools in estimating the relative importance of different factors and prioritizing them. It is a common method with many practical applications such as developing building code formulas. According to Canter and Sadler (1997), for comparison of alternatives with qualitative or quantitative information on each alternative, methods such as checklists, expert opinions, mass balance calculation, matrices and also decision analysis such as Analytical Hierarchy Process (AHP) are commonly used. This approach has been used for consideration of damage probability matrices for the sake of evaluating damage factor for 78 facility classes (ATC-13, 1985). It is also has been used in developing the score-based analysis to evaluate the basic structural hazard of different types of buildings (ATC-21, 1996). Previous studies in this area mainly deal with application of benefits and costs method in retrofitting of structure for an earthquake hazard level (Grossi, 1998), and housing performance evaluation model for multi family residential buildings using the AHP analysis (Sun-Sook K. et al. 2005).

The main goal of the study presented in this paper was to develop a framework to quantify the retrofitting option selection for experienced engineers to apply for their clients to decide suitable selection. In this study, surveys were conducted to gather information from experts to develop weighting functions of the key groups and their members. For this purpose, a group, consists of twenty structural engineers and leading authorities in the area of seismic retrofitting are selected, both from academia and profession, to rank each parameter in relative values on scale of 1 to 9 (low to high), by using the proposed form. The exact grade for each parameter is the mean value provided by experts.

Based on experts' opinion and their engineering-judgment a model is developed for choosing the best option among three alternatives by comparing their attributes. For the evaluation of each alternative among the others one needs to provide information of building and performing analyses to obtain the level of expected performance. Then the scores for each alternative will be modified in equations 1 to 6 by weighting functions which lead to its final score.

Based on expert's opinions the most important item in Building Characteristics Aspects key group is considered as “building condition”, meaning the quality of design and construction of the building is more important than even structural system in this regard. The most important item of Constructional Aspects key group is considered as “level of experience needed for contractors and labors, then “availability of constructional guideline”. It shows a tendency toward traditional retrofitting techniques that enjoy widely available construction details and guidelines, also experienced contractors familiar with those. The most important item in Economical Aspects key group is considered as rehabilitation “effect on loss reduction”. It seems for professionals in seismic retrofitting field, what is not lost economically (“Effect in Loss Reduction” item) is more important than what is paid (“Cost of Retrofitting” item) or even what is gained (“Effect in Value of Building” item). The most important item of Technical Aspects key group is considered as “Effect in building ductility” and also “Availability of Design Codes”. Therefore, the preference technically is the retrofitting option that enhances the ductile behavior of the building and protects it against brittle modes of failure and also, the retrofitting technique with standardized design procedure is preferred.

Accordingly, general comparison of five key groups shows the order of their importance as, Economical, Technical and Constructional Aspects, then Building Characteristics, and finally, Architectural Aspects respectively.

7. CONCLUSIONS

This paper presents the outline of a methodology based on expert judgment to evaluate the most effective parameters in selecting the optimum option for seismic rehabilitation project. Through a simple quantifying process, the procedure enables an engineer to determine the optimum retrofitting option. The most important parameters are identified and classified so presented result can bring out a suitable plan in optimizing selection process for retrofitting projects and supports decision-makers in choosing the most adequate technique for rehabilitating a vulnerable building. Of course due to complexity of task and numerous parameters involved, a lot more research is needed to complete and generalized the method.

ACKNOWLEDGEMENT

The author would like to thank Mr. Behnam M. Azmoodeh for his contribution in sections 5 and 6 of this paper.

APPENDIX A: Effective Parameters in Seismic Rehabilitation of Buildings

Building Characteristics	Type of Structural System	Steel	
		Concrete	
		Masonary	
	Building Geometry	Height	
		Plan	
	Building Location	Seismically Activity	
		Soil Profile	
		Liquefaction	
	Building Occupancy	Residential	
		Educational	
		Commercial	
		Industrial	
		Critical Facility*	
		Lifeline Facility*	
	Building condition	Design and Construct Quality	
		Age of building	
		Configuration	
		Structural Framing	
Constructional Aspects	Construction Duration		
	Construction Difficulties		
	Construction Technology		
	Availability of Materials		
	Automation Possibility		
	Availability of Constructional Guideline		
	Level of Experience needed for Contractors and Labors		
Economical Aspects	Residential	Building Square Footage	
		Probable Damage	Physical Damage
			Human Loss
		Relocation Cost	
		Number of Occupants	
		Type and Value of Facility Content	
		Presence of Occupants in Time of Rehabilitation	
	Commercial	Loss of Income	
		Recovering Time	
		Loss of Function	
	Effect in Loss Reduction		
	Current Value of Building		
	Cost of Labors (Variable in Different Locations)		
	Benefit-Cost Analysis**	Benefit of Rehabilitation	
		Cost of Retrofitting	
		Discount Rate	
		Time Horizon	
		Value of Human Life	
		Replacement Value	
	Improving Performance	Rehabilitation Objects	
		Ground Shaking Intensity	
	Effects on building seismic response		
	Effects on building weight		
	Past experiences in earthquakes		

Technical Aspects	Seismic Rehabilitating of Past Earthquake from Performance of Building	
	Using Maximum Structural Capacity	
	Minimum Strengthening in Foundation	
	Demands and Expected Behavior of Building	
	Structural and Non-Structural Component Interaction	
	Sensitivity of Performance to Technical and Constructional Errors	
	Availability of Design Codes	
	Reducing negative effects on performance	Reducing in Torsion
		Reducing in Plan Irregularity
		Reducing in Height Irregularity
		Reducing in Soft Story
		Reducing in Pounding
		Reducing in Short Column
Affecting of Scheme(s) on Architecture of Building		

(*) Structures such as communication towers, utilities (electrical/water/natural gas/telephone), waterfront structures, bridges, pipelines, storage tanks, often require more experience and attention in selecting the appropriate rehabilitation technique

(**) Benefit-Cost analysis is a systematic rational decision-making which is often used in economical justifying projects

REFERENCES

Alanne, K., Klobut. K., A Decision-making tool to support integration of sustainable technologies in refurbishment projects, *Eighth international IBPSA conference*, Netherland, August 2003

American Society of Civil Engineers (ASCE), *Prestandard and Commentary for the Seismic Rehabilitation of Buildings*, Report FEMA 356, Reston V.A., American Society of Civil Engineers, 2000

ATC-13,*Earthquake Damage Evaluation Data for California*, Applied Technology Council, Redwood city California, FEMA contract No. EMW-C-0912,1985

ATC-21,*Rapid Visual Screening for Potential Seismic* Hazards*: A Handbook Applied Technology Council*, Redwood city California, FEMA-154,1988

Canter, L., Sadler, B., *A tool kit for effective EIA practice review of the methods and perspectives on their application*, university of Oklahoma, A supplementary report of the international study of the effectiveness of environmental assessment,1997

FEMA-174, *Establishing Programs and Priorities for the Seismic Rehabilitation of Buildings (Handbook),* 1989

FEMA-356*, Prestandard and commentary for the seismic rehabilitation of buildings*, Federal Emergency Management Agency, Washington DC,2000

Grossi, P.A., Assessing the Benefits and Costs of Earthquake Mitigation, *Financial Institution Center*, 1998, The Wharton school-University of Pennsylvania

Kafali, C., Grigoriu, M., Rehabilitation decision analysis, *in the proceeding of the international conference on structural safety and reliability*, 2005

Mc Cormack, T.C., Rad, F.N., An earthquake loss estimation methodology for buildings based on ATC-13 and ATC-21, Earthquake Spectra, Volume 13, No. 4, P.P 605-621, November 1997

Porter, K.A., Scawthorn, C.R., Beck, J.L., Cost effectiveness of stronger woodframe buildings, earthquake spectra, 2006, VOL 22, issue 1, P.P 239-266

Smyth, A.W., Gulay, A., Deodatis, G., Erdik, M., Franco, G., Gulkan, P., Kunreuther, H., Lus, H., Mete, E., Seeber, N., Yuzugullu, O., Probabilistic benefit-cost analysis for earthquake damage mitigation: Evaluating measures for apartment in turkey, Earthquake spectra, 2004, VOL 20, NO 1., P.P 171-203

Sun-Sook, K., In-Ho, Y., Myoung-Souk, Y., Kwang-Woo, K., Development of a housing performance evaluation model for multi-family residential buildings in Korea, journal of Building and Environment, Vol 40, issue 8, P.P 1103-1116, August 2005

Thomson, D.S., Austin, S.A., Devine-Wright, H., Mills, G.R., Managing value and quality in design; building research & information; volume 31,issue 5, pages 334-345, 2003

CALIFORNIA MISSION CHURCH SEISMIC ANALYSIS PROJECT — A PROGRESS REPORT

Fred Webster
Fred Webster Associates
Menlo Park, CA 94025

ABSTRACT

The structural system of some of the old churches of the Spanish missions of California is unique. Their massive adobe walls, (5-feet or more in thickness, 30-feet or more in height), and wood-framed roofs and ceilings enclose long narrow spaces, often more than 100-feet in length and 30-feet or less in width. There are at least five[1] of these mission buildings in California that have not been strengthened for earthquake hazard reduction, and others for which it may be appropriate to consider additional strengthening.

Because of their adobe walls, mission church buildings are included in the class of unreinforced masonry (URM) bearing wall buildings. In the State of California URM buildings have been identified as hazardous in earthquake shaking. The State has mandated that city and county jurisdictions require that seismic hazards posed by URM buildings be mitigated. However, model ordinances (such as the International Existing Building Code) that are intended to regulate the strengthening of URM buildings are not applicable to buildings with very massive adobe walls enclosing long narrow spaces.

The typical URM building addressed by the model ordinances has relatively thin walls braced by a flexible roof diaphragm that spans across the building, and braced at each end by shear walls perpendicular to the diaphragm span. The principal structural element controlling the typical URM building is the roof diaphragm. The stiffness of the diaphragm that would be required to brace the massive adobe walls by the rules of these model ordinances would be far beyond that of a conventional diaphragm. By contrast, the principal structural elements controlling seismic response of mission church buildings are the massive adobe walls rocking on their foundations. In these buildings, the diaphragms are expected to have a secondary role in the seismic response.

The Getty Seismic Adobe Project shake table testing program of the 1990s developed a very promising seismic stabilizing methodology for historical adobe building systems, variations of which have been tested on shake tables at several facilities, including:. Stanford University's John Blume Center, U.C. Berkeley's Richmond Field Station, the Institute for Earthquake Engineering and Engineering Seismology in Skopje, Macedonia, the Pontifica Universidad Catolica in Lima, Peru, and recently the Sharif University of Technology, Tehran, Iran. However, due to the limitations of model size that can practically fit on these tables, alternative seismic analysis methodologies are required to realistically account for the soil-structure interaction of the massive walls on their foundations, as well as the interaction of the walls with flexible diaphragms.

1 San Luis Rey, San Miguel, San Antonio, San Juan Bautista, and possibly Santa Inez; San Francisco de Asis (Mission Dolores) may have already been strengthened; Santa Barbara and San Luis Obispo have been strengthened.

A team of Structural Engineers[2] is currently investigating the nature of this seismic analysis problem. Preliminary calculations indicate that the walls, as they rock on their foundations, probably remain stable during shaking of expected intensity. However, if the walls are not adequately braced at the top, the displacements of the rocking walls will likely be excessive, resulting in damage at the building corners as the displacing longitudinal walls attempt to separate from the perpendicular bracing walls. A relatively flexible conventional wood diaphragm at the tops of the walls may provide enough restraint to control displacement of the rocking wall. This is in contrast to the likely performance resulting from the installation of the very rigid, high-strength diaphragm that would be required for compliance with the currently used model ordinances. Such a diaphragm would likely cause heavy shear damage in the bracing end walls.

The Getty Conservation Institute is sponsoring the development of a non-linear lumped parameter computer (LPM) analysis of the Mission San Miguel, Arcángel church building in San Miguel, California as part of their Earthen Architecture Initiative. Walls, diaphragm and soil foundation are modeled using LPM/I Ver.102, a computer program for non-linear dynamic analysis of lumped parameter models by Ewing / Kariotis / Engelkirk & Hart – sponsored by the National Science Foundation. Site specific input characteristics of the massive masonry walls, the roof or ceiling diaphragm as a restraining element coupled to the adobe end shear walls, and elasto-plastic foundation soil springs are all part of the investigation. Input ground motion will be scaled to the ASCE 7-05 required response spectrum using two ground shaking records – one record in which short-period shaking is dominant; one in which long-period shaking is dominant.

The purpose of these non-linear analyses will be to determine the "least" diaphragm stiffness that keeps the tall adobe walls stable during expected earthquake shaking. The output data will also be used to determine wall anchorage forces, diaphragm end-shear anchor forces and shear wall design loading. Upon completion of the LPM model analysis for the Mission San Miguel site, the program and mission church modeling approach will be used to complete a sensitivity evaluation based on the variability and uncertainty of the input characteristics and input ground motion. Further, it is anticipated that the LPM program and church model will be available for use on other mission churches of other sites in California as they go through the seismic upgrade requirements for URM buildings. If the data from a number of churches are analyzed in this way, it is anticipated that patterns will emerge that would allow a simplified analysis procedure to be developed that would not require use of the LPM model.

2 Structural Engineers Michael Krakower, John Kariotis, Alex Mustapha, Nels Roselund and Fred Webster.

THE EFFECT OF SOIL ON SEISMIC PERFORMANCE OF STRUCTURES

Mohammad Ali Ghannad
Department of Civil Engineering, Sharif University of Technology, P.O. Box 11155-9313, Tehran, Iran

ABSTRACT

This paper presents a brief summary of recent research on soil-structure-interaction (SSI) effects on elastic and inelastic response of structures carried out at the Department of Civil Engineering at Sharif University of Technology. Soil-structure systems with both surface and embedded foundations are studied. This is carried out through a comprehensive parametric study for a wide range of representative non-dimensional parameters. As the model, a simplified single degree of freedom system with idealized bilinear behavior is used for the structure. The soil beneath the structure is considered as a homogeneous half-space and is modeled by a discrete model based on the concept of Cone Models. The total soil-structure model is analyzed by direct step-by-step integration in time domain subjected to a suit of 24 selected accelerograms recorded on alluvium deposits. The results are used to investigate the effect of selected non-dimensional parameters on the structural ductility and strength demands. It is concluded that SSI is generally beneficial for structures with surface foundations except for the rare case of short period slender structures. Also, it is shown that foundation embedment may increase the structural demands for slender buildings with large embedment ratios especially for the case of relatively soft soils. Comparing the results with and without inclusion of kinematic interaction reveals that the rocking input motion, due to kinematic interaction, plays the main role in this phenomenon. Moreover, the NEHRP-2003 provisions for considering SSI effect in design are assessed. It is concluded that using these provisions may lead to higher ductility demands in the structure, especially for the case of short period buildings located on soft soils.

1. INTRODUCTION

It is about four decades that the soil-structure interaction (SSI) effect has been known for engineers and researchers. During this period, many researchers have estimated the SSI effects on seismic design of structures. SSI phenomenon has two main effects. First, the difference between stiffness of the foundation and the surrounding soil causes the motion experienced by the essentially rigid foundation, i.e., the Foundation Input Motion (FIM), to differ from the Free-Field Motion (FFM) due to Kinematic Interaction (KI) effect. Second, the flexibility of soil affects the response of the structure subjected to FIM. In fact, the soil-structure system behaves as a new system with different dynamic properties, i.e., longer natural period and usually higher damping. The latter is usually called Inertial Interaction (II) effect [1]. The general effects of SSI on elastic response of structures were the subject of numerous studies in 1970s [2-8]. More specifically, the pioneering works by Veletsos and his co-workers [6-8] led to the tentative provisions in ATC3-06 [9], which is in fact the basis for modern regulations on seismic design of soil-structure systems [10]. The SSI effect on the response of nonlinear structures, however, was not studied in detail. On the other hand, the current seismic design philosophy is based on inelastic behavior of buildings during moderate and strong earthquakes. The SSI effect on inelastic demands of structures thus deserves special attention. The earliest studies on inelastic soil-structure systems were made by Veletsos and Vebric [11] and Bielak [12]. Later, Müller

and Keintzel [13] studied the ductility requirements of soil-structure systems. They brought to light the fact that the ductility demand of structures, as a part of the soil-structure system, could be different than that of the equivalent single degree of freedom system. In recent years, by development of performance based design philosophy, the SSI effect on inelastic response of structures has attracted much more attention [14-22]. Here, a summary of recent works on SSI effect on inelastic response of structures done at Department of Civil Engineering of Sharif University of Technology [17-20] is presented.

2. SOIL-STRUCTURE MODEL

Figure 1a shows the soil-structure system considered in this study. The soil under the structure is considered as a homogeneous half-space where the super-structure is modeled as a single-degree of freedom system with height h, mass m and mass moment of inertia I. These parameters may be considered as the effective values for the first mode of vibration of a real multi degree of freedom system. The foundation is considered to be rigid with embedment depth e and mass and mass of inertia m_f and I_f, respectively. The basic model for such a soil-structure system is shown in Figure 1b in which the structure is replaced by an elasto-plastic spring along with a dashpot with coefficients k and c, respectively. The soil is considered to be in full contact with the foundation and is modeled as a discrete model based on the concept of Cone Models for embedded foundations [23]. Two degrees of freedom are introduced in this model for the foundation, namely sway, u_f, and rocking, φ. Consequently, by considering an additional internal degree of freedom for the soil model, φ_1, a 4-degree of freedom model is formed for the whole soil-structure system as shown in Figure 1b. The internal degree of freedom allows the frequency dependency of the soil stiffness also to be taken into account while all the coefficients in the model are frequency independent. The coefficients in the model are defined as follows:

$$k_{0h} = \frac{8\rho V_s^2 r}{2-\nu}\left(1+\frac{e}{r}\right) \quad , \quad c_{0h} = \frac{r}{V_s}\gamma_{0h}k_{0h} \tag{1a}$$

$$k_{0r} = \frac{8\rho V_s^2 r^3}{3(1-\nu)}\left[1+2.3\frac{e}{r}+0.58\left(\frac{e}{r}\right)^3\right] \quad , \quad c_{0r} = \frac{r}{V_s}\gamma_{0r}k_{0r} \tag{1b}$$

$$c_{1r} = \frac{r}{V_s}\gamma_{1r}k_r \quad , \quad I_{1r} = \left(\frac{r}{V_s}\right)^2 \mu_{1r}k_{0r} \tag{1c}$$

where ρ, ν, V_s, and r are the specific mass, Poisson's ratio, shear wave velocity of the soil, and the radius of the cylindrical foundation, respectively. Besides, γ_{0h}, γ_{0r}, γ_{1r}, and μ_{1r} are non-dimensional coefficients of the discrete model in terms of e/r and are calculated using the following formulae:

$$\gamma_{0h} = 0.68+0.57\sqrt{\frac{e}{r}} \qquad \gamma_{0r} = 0.15631\frac{e}{r}-0.08906\left(\frac{e}{r}\right)^2-0.00874\left(\frac{e}{r}\right)^3 \tag{2a}$$

$$\gamma_{1r} = 0.4+0.03\left(\frac{e}{r}\right)^2 \qquad \mu_{1r} = 0.33+0.1\left(\frac{e}{r}\right)^2 \tag{2b}$$

Sway springs and dashpots are connected to the superstructure model with the following eccentricities in order to account for the coupling terms between the sway and rocking degrees of freedom in the stiffness matrix of the embedded foundation:

$$f_k = 0.25e \tag{3a}$$

$$f_c = 0.32e + 0.03e\left(\frac{e}{r}\right)^2 \tag{3b}$$

Using the Correspondence Principle [1], the soil material damping can be introduced into the model by adding a dashpot or a mass to every spring or dashpot, respectively. The model is then subjected to sway and rocking components of FIM, u_g and φ_g as shown in the figure. More details can be found in at [20].

The introduced soil-structure model has the capability of being used directly in a time domain analysis. This allows conducting inelastic dynamic analysis of soil-structure systems. Here, Elasto-plastic behavior is considered for the structure while all the soil representative springs behave elastically. The effect of soil nonlinearity, however, may be approximately introduced into the model through equivalent linear approach in which a degraded shear wave velocity, consistent with the estimated strain level in soil, is used for the soil medium [24]. This is the same approach used in current regulations such as NEHRP 2003 [10] and ASCE41 [25] where the strain level in soil is implicitly related to the peak ground acceleration.

It is shown that there are three key non-dimensional parameters which control the soil-structure response while the other parameters may be set to some typical values [26]. These parameters are defined as follows.

1. A non-dimensional frequency as an index for the structure to soil stiffness ratio defined as:
$$a_0 = \frac{\omega h}{v_S} \tag{4}$$
where ω is the natural circular frequency of the fixed base structure. It can be shown that the practical range of a_0 for ordinary building type structures is from zero for the fixed-base structure to about 2 for cases with predominant SSI effect [26].
2. Aspect ratio of the building defined as *h/r*.
3. Embedment ratio of the foundation defined as *e/r*.

3. DUCTILITY AND STRENGTH DEMANDS OF STRUCTURES WITH SURFACE FOUNDATION

In this section, inelastic response of soil-structure systems with surface foundations is studied. As input ground motions, 24 free-field strong motions recorded on alluvium deposits are used. This is done by step by step integration of equation of motions using the Newmark β method. Details of the selected ground motions are listed in Table 1. It is supposed that the ground motions are mainly the result of vertically propagating shear waves, which leads to no kinematic interaction for surface foundations. As a result, the horizontal component of FIM equals FFM while the rotational component vanishes. Different soil-structure systems having 100 different

fixed-base periods and different values of defined key parameters are considered. In each case, the model is analyzed to reach different levels of ductility in the structure in addition to the elastic analysis.

A certain procedure is followed to investigate the SSI effect on the ductility demand of the structure. For each soil-structure model, first the yield strength demand of the super-structure in the fixed-base state, i.e., ignoring the soil effect is calculated. This is done to reach specific ductility level when subjected to any specified free-field ground motion. Then, the ductility demand of the structure, as a part of the soil-structure system, is calculated for soil-structure systems with different values of a_0 and h/r, providing the same yield strength for the structure as calculated in the fixed-base state. This is done for all ground motions listed in Table 1 and the averaged results are plotted in Figure 2. The results are depicted in the form of ductility demand spectrum where the abscissa is the fixed-base natural period of the structure, T_{fix}. The figure shows the results for soil-structure systems with a_0=1,2 and h/r=1,3,5 for presumed fixed-base target ductility, μ_{fix}, of 6. The soil-structure system with a_0=2 is the representative of cases with substantial SSI effect. As shown, for squat buildings with h/r=1the ductility demand of soil-structure systems is equal or smaller than the presumed fixed-base value of 6 in almost entire range of period. For slender structures with h/r=3 and 5, however, there is a threshold period before which the flexible-base ductility is greater than that of the fixed-base one; afterwards, the trend is reversed. The larger the non-dimensional frequency a_0, the greater is the difference between ductility demands of the flexible-base and the fixed-base models. However, considering that slender structures usually have periods longer than the observed threshold period, one may conclude that SSI generally reduces ductility demand of structures except for short period squat buildings.

From another point of view, Figure 3 shows the elastic and inelastic strength demands of the structure for different soil-structure systems. The results have been normalized by the product of mass of structure and peak ground acceleration (PGA) for each record before average. Figure 3a shows the SSI effect on elastic strength demand of the structure, i.e., the strength required to maintain the structure in elastic range. Again, the results are shown for models with two different aspect ratios, h/r=1,3 as the representatives of squat and slender buildings and for two different values of non-dimensional frequency a_0=1,3 in addition to the fixed-base structure (a_0=0). As mentioned before, a_0 is an index of structure-to-soil stiffness ratio that controls the severity of soil-structure phenomenon. The value of a_0=3 is representative of systems with severe SSI effect for conventional building type structures [26]. The effect of SSI on inelastic strength demand of structures undergoing two different ductility levels, μ =2,6, is also shown in parts b and c of the figure. The results show a general trend of lower strength demands for soil-structure systems in comparison to the fixed-base structures. The only exception is the rare case of short period buildings with aspect ratio h/r=3. This trend is clearer for the case of a_0=3 where SSI effect is predominant. Again, considering that slender buildings usually don't have such short periods, one may conclude that generally, SSI reduces the structural strength demands. Also, it is clearly observed that the SSI effect becomes less important as the structure undergoes more inelastic deformations, leading to almost the same inelastic strength demands for the case of μ =6. It means that SSI affects the elastic and inelastic strength demands of structure in different ways. Consequently, it is concluded that response modification coefficients, which is defined as the ratio of elastic and inelastic strength demands, are apparently different for the fixed-base structure and soil-structure systems. It means that using the fixed-base response modification

coefficients for soil-structure systems, as implicitly suggested by current seismic codes, leads to different levels of ductility demand in the structure. This issue is investigated in detail in the next section.

4. ASSESSMENT OF NEHRP2003 PROVISIONS

The optional provisions of NEHRP2003 [10] for SSI effect allows the designer to reduce the design base shear up to 30 percent. The procedure to calculate the reduction rate is simple and is based on the idea of replacing the soil-structure system with an equivalent single degree of freedom oscillator. This idea was originally proposed by Veletsos and his co-workers [6-8] in order to estimate the effect of SSI on elastic response of structures. Considering the same response modification coefficient, R, for the fixed- and flexible-base structures, the provisions extend the idea to inelastic response of soil-structure systems. In fact, the provisions implicitly suppose that SSI affects elastic and inelastic demands in the same way. However, as discussed in the previous section this is not true and SSI generally affects inelastic demands less than elastic demands. Therefore, smaller values of response modification coefficients should be used for soil-structure systems to find inelastic strength demands from elastic demands. A detailed study on response modification coefficient, also known as strength reduction factor, of soil-structure systems is found in [18].

As a result of the above discussion, one may expect higher ductility demands for soil-structure systems designed base on NEHRP2003 recommendations. To explore the problem, three different systems as shown in Figure 4 are examined. System 'A' is considered as a single degree of freedom fixed-base structure designed based on NEHRP2003 provisions with design base shear, V. System 'B' represents a soil-structure system consisting of the same structure as in System 'A' located on surface of flexible soil - as happens in the reality. Finally, System 'C' is the same as system 'B' but having a reduced design base shear, $\tilde{V}$, computed according to SSI section of NEHRP2003 provisions. The period and damping ratio of the structure in all three systems are considered to be the same. In fact, System 'A' represents the ideal model, which is usually used in the analysis and design of structures as well as in seismic performance evaluation of existing structures. System 'B' is a more realistic model for predicting the response of structures designed based on the conventional design procedures, i.e., without considering the SSI effect in design. The superstructure is exactly the same in Systems 'A' and 'B'. However, the response of the structure would be different for two systems by virtue of SSI effect in System 'B'. Ductility demands of System 'B' can be more or less than those of System 'A' based on the period of the structure and type of excitation. On the other hand, ductility demands of System 'C' are usually higher than System 'B' because of lower strength of the structure in System 'C'. Thus, it is expected that using the optional SSI related provisions in design may lead to higher ductility demands in the structure. Comparison of the response of Systems 'A', 'B', and 'C' reflects the difference between the expected performance levels which are implicitly considered in the provisions for structures designed with and without considering the SSI effect. Such a comparison is made in Figure 5 for a presumed ductility demand of 6 for System 'A'. The details of the procedure to calculate the results shown in this figure can be found in [17]. Results are provided for a_0=1,2 and h/r=1,3. Except for short period slender structures, the results show a small difference between ductility demands of Systems 'B' and 'A'. However, there is a considerable difference between ductility demands of System 'C' and those of Systems 'A' or 'B' especially for short period structures. This can be explained by the fact that ductility demand

of short period structures is more sensitive to response modification coefficient [27]. It means that the ductility demand of short period structures could be very large even if their strength is only slightly below that required for the system to remain elastic. This effect is seen more clearly for the case of a_0=2 where the response modification coefficient is more affected by SSI. It means that using current provisions for considering SSI effect in design may lead to higher ductility demand in the structure, especially for the case of short period structures located on soft soils. Obviously, this is inconsistent with the prevalent expectation that all options provided by seismic codes should result in comparable levels of safety.

5. THE EFFECT OF FOUNDATION EMBEDMENT

Foundation embedment has two main effects: changing the dynamic stiffness of soil and changing the input motion. The first effect is directly introduced in the model of Figure 1b through parameter e, which indicates the embedment depth. The latter effect, which is the result of KI effect, must be considered separately. Generally, as the result of KI, two different FIM components are produced: Horizontal FIM, u_g, and Rocking FIM, φ_g. Horizontal FIM component generally decreases in comparison to FFM especially for more embedment depths; however, rocking FIM amplitude increases as the depth of embedment increases. These components are in fact the input motion to the soil-structure model introduced in Figure 1b. Here, the method proposed by Meek and Wolf [28], which is based on the concept of double-cone models, is used to evaluate FIM components. Details on application of this method can be found at [20].

The same study as done on ductility demand of structures with surface foundations, in Figure 2, is conducted here for the case of embedded foundations. Figure 6 shows the results for two embedment ratios e/r=1 and 2. As seen, SSI has a different effect on ductility demand of the structure with embedded foundation. Although the foundation embedment generally reduces ductility demands of squat buildings, with h/r=1, it results in higher demands for slender buildings with aspect ratios h/r=3 and 5. The increase in ductility demands is not significant for embedment ratios up to e/r=1. However, for deeper foundations the ductility demand can be much higher than expected. This is true almost in the whole range of demonstrated period. So, one may conclude that foundation embedment is, in general, beneficial for squat structures while it may increase ductility demands in slender structures having deep embedded foundations. Obviously, the trend is intensified by increasing the non-dimensional frequency a_0. As explained by Mahsuli and Ghannad [20], KI plays the main role in this phenomenon, which is discussed next. Figure 7 demonstrates the ductility demand curves evaluated both with and without inclusion of KI effect for soil-structure systems with a presumed fixed-base target ductility of 6. In the other words, it presents the response of the soil-structure system once with the use of FFM as the input motion and once by subjecting the system to FIM components. Again, the curves show the average of the results for 24 ground motions listed in Table 1. As seen, for squat structures, with h/r=1, inclusion of KI effect generally reduces the flexible-base ductility demand. In fact, the ductility demand of soil-structure systems without KI effect is very close to 6, i.e., the presumed fixed-base target ductility, for almost the whole range of period. It means that KI plays the main role in reducing ductility demands. This trend is observed more clearly in the case of a_0=2. For slender structures, with h/r=3, however, the role of KI effect depends on the embedment ratio. For shallow foundations, with e/r=0.5, the effect of KI is negligible. In contrast, by increasing the embedment ratio, KI affects the ductility demand more considerably

leading to a significant effect for e/r=2. In the other words, the FIM is considered as a more severe input motion than the original FFM in such cases.

6. CONCLUSIONS

The effect of SSI on inelastic strength and ductility demands was investigated. This is done through an extensive parametric study for a wide range of non-dimensional parameters, which control the problem. Both cases with surface and embedded foundations were studied. Based on the model and the ground motions used, it was concluded that SSI is generally beneficial for structures with surface foundations except for the rare case of short period slender structures. Also, it was concluded that foundation embedment is, in general, beneficial for squat structures while it may increase ductility demands for the case of slender buildings. Such increase in ductility demands is not significant for shallow foundations with embedment ratios up to e/r=1. However, for deeply embedded structures, the ductility demand can be much higher than expected. The effect is intensified for structures located on relatively soft soils, i.e. for larger values of non-dimensional frequency, a_0. Comparing the results with and without inclusion of KI effect reveals that the rocking input motion due to KI plays the main role in this phenomenon. Moreover, the NEHRP2003 provisions for considering SSI effect in design are assessed. It is concluded that using these provisions, which allows reducing base shear due to SSI, may lead to higher ductility demands in the structure, especially for the case of short period buildings located on soft soils. Based on the results presented here and other valuable researches done by other researchers it is believed that the subject deserves much more attention.

ACKNOWLEDGEMENTS

The material presented in this paper is a brief summary of recent SSI research carried out at the Department of Civil Engineering at Sharif University of Technology. The following graduate students were actively involved in this research during the last few years: Mr. Alireza Ahmadnia, Mr. Hossein Jahankhah, Mr. Amir Hossein Jafarieh, Mr. Mojtaba Mahsuli and Mr. Mofid Nakhaei. The sincere and dedicated efforts of these individuals are greatly appreciated. Also, the partial financial support of Sharif University of Technology is gratefully acknowledged.

REFERENCES

1. Wolf JP. *Dynamic Soil-Structure Interaction*. Prentice-Hall, Englewood Cliffs, New Jersey, 1985.
2. Perelman DS, Parmelee RA, Lee SL. Seismic response of single-storey interaction system. *Journal of Structural Division* (ASCE) 1968; **94**(ST11): 2597-2608.
3. Sarrazin MA, Roesset JM, Whittman RV. Dynamic soil-structure interaction. *Journal of Structural Division* (ASCE) 1972; **98**(ST7): 1525-1544.
4. Jennings PC, Bielak J. Dynamics of buildings-soil interaction. *Bulletin of Seismological Society of America* 1973; **63**(1): 9-48.
5. Chopra AK, Gutierrez JA. Earthquake response analysis of multistory buildings including foundation interaction. *Earthquake Engineering and Structural Dynamics* 1974; **3**(1): 65-77.
6. Veletsos AS, Meek JW. Dynamic behavior of building-foundation system. *Earthquake Engineering and Structural Dynamics* 1974; **3**(2): 121-138.
7. Veletsos AS, Nair VVD. Seismic interaction of structures on hysteretic foundations. *Journal of the Structural Division* (ASCE) 1975; **101**(1): 109-129.
8. Veletsos AS. Dynamics of structure-foundation systems. *Structural and Geotechnical Mechanics*, A Volume Honoring N. M. Newmark (Editor: W. J. Hall), Prentice-Hall, Englewood Cliffs, New Jersey, 1977; 333-361.

9. Applied Technology Council. *Tentative Provisions for the Development of Seismic Regulations for Buildings*. ATC-3-06, California, 1978.
10. Building Seismic Safety Council (BSSC). *NEHRP Recommended Provisions for Seismic Regulations for New Buildings and Other Structures*. Federal Emergency Management Agency, Washington DC, 2003.
11. Veletsos AS, Verbic B. Dynamics of elastic and yielding structure- foundation systems. *Proceedings of the 5th World Conference on Earthquake Engineering*, Rome, 1974.
12. Bielak J., Dynamic response of non- linear building- foundation systems. *Earthquake Engineering and Structural Dynamics*, 1978; **6**: 17–30.
13. Muller F.P. and Keintzel E., Ductility requirements for flexibly supported antiseismic structures, *Proceedings of the Seventh European Conference on Earthquake Engineering*. 1982; **3**: 27-34.
14. Rodriguez ME, Montes R. Seismic response and damage analysis of buildings supported on flexible soils. *Earthquake Engineering and Structural Dynamics* 2000; **29**(5): 647-665.
15. Youssef A, Bernal D. Soil-structure interaction effects on inelastic design. *7th National Conference on Earthquake Engineering*, Boston, July 21-25, 2002.
16. Aviles J, Perez-Rocha L. Soil-structure interaction in yielding systems. *Earthquake Engineering and Structural Dynamics* 2003; **32**(11): 1749-1771.
17. Ghannad MA, Ahmadnia A. The effect of soil-structure interaction on inelastic structural demands. *European Earthquake Engineering* 2006; **20**(1): 23-35.
18. Ghannad MA, Jahankhah H. Site dependent strength reduction factors for soil-structure systems. *Soil Dynamics and Earthquake Engineering* 2007; **27**(2): 99-110.
19. Nakhaei M, Ghannad MA. The effect of soil-structure interaction on damage index of buildings. *Engineering Structures* 2007; **30**(6): 1491-1499.
20. Mahsouli M, Ghannad MA. The Effect of Foundation Embedment on Inelastic Response of Structures. *Earthquake Engineering and Structural Dynamics* 2008; **38**(2), pp. 423–437.
21. Lin YY, Miranda E. Kinematic soil-structure interaction effects on maximum inelastic displacement demands of SDOF systems. *Bulletin of Earthquake Engineering* 2008; **6**(2): 241–259.
22. Stewart JP, Comartin C, Moehle JP. Implementation of soil-structure interaction models in performance based design procedures. *Proceedings Third UJNR Workshop on Soil-Structure Interaction,* Menlo Park, California, USA, March 29-30, 2004.
23. Wolf JP. *Foundation Vibration Analysis Using Simple Physical Models*. Prentice-Hall, Englewood Cliffs, New Jersey, 1994.
24. Kramer SL. *Geotechnical Earthquake Engineering.* Prentice Hall, NJ, 1996.
25. ASCE/SEI 41-06, *Seismic Rehabilitation of Existing Buildings*, American Society of Civil Engineers, 2007.
26. Ghannad MA, Fukuwa N, Nishizaka R. A study on the frequency and damping of soil-structure systems using a simplified model. *Journal of Structural Engineering*, Architectural Institute of Japan (AIJ) 1998; **44**(B): 85-93.
27. Chopra AK, *Dynamics of structures, Theory and Applications to Earthquake Engineering*, Prentice Hall, New jersey 1995.
28. Meek JW, Wolf JP. Cone models for embedded foundation. *Journal of Geotechnical Engineering Division* (ASCE) 1994; **120**(1): 60–80.

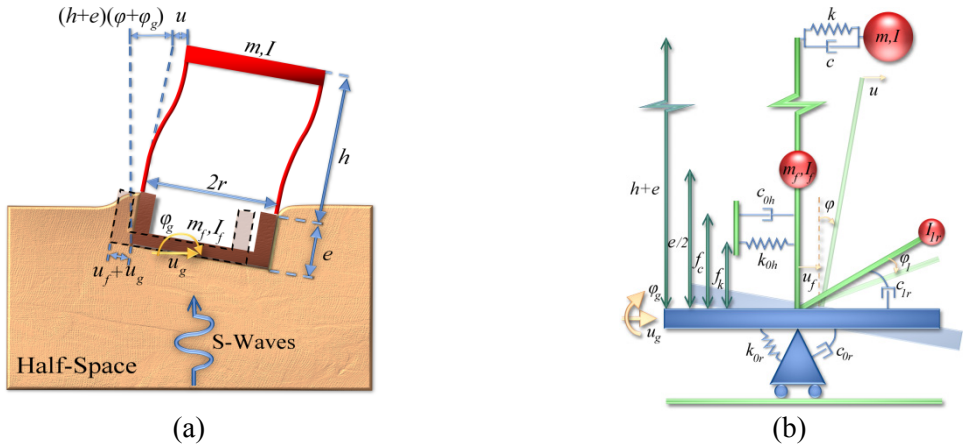

Fig. 1. (a) The soil-structure system; (b) the basic soil-structure model.

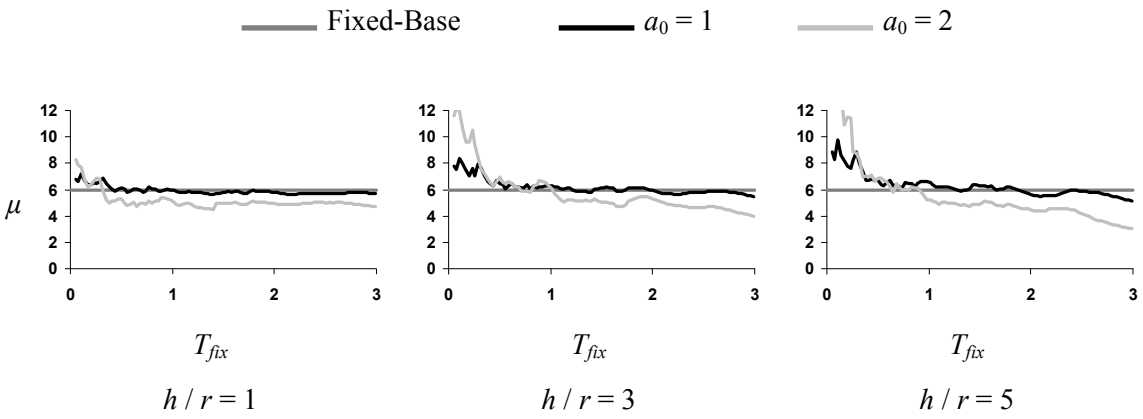

Fig. 2. Averaged ductility demand for different soil-structure systems with surface foundation subjected to ground motions listed in Table 1 (μ_{fix}=6). [20].

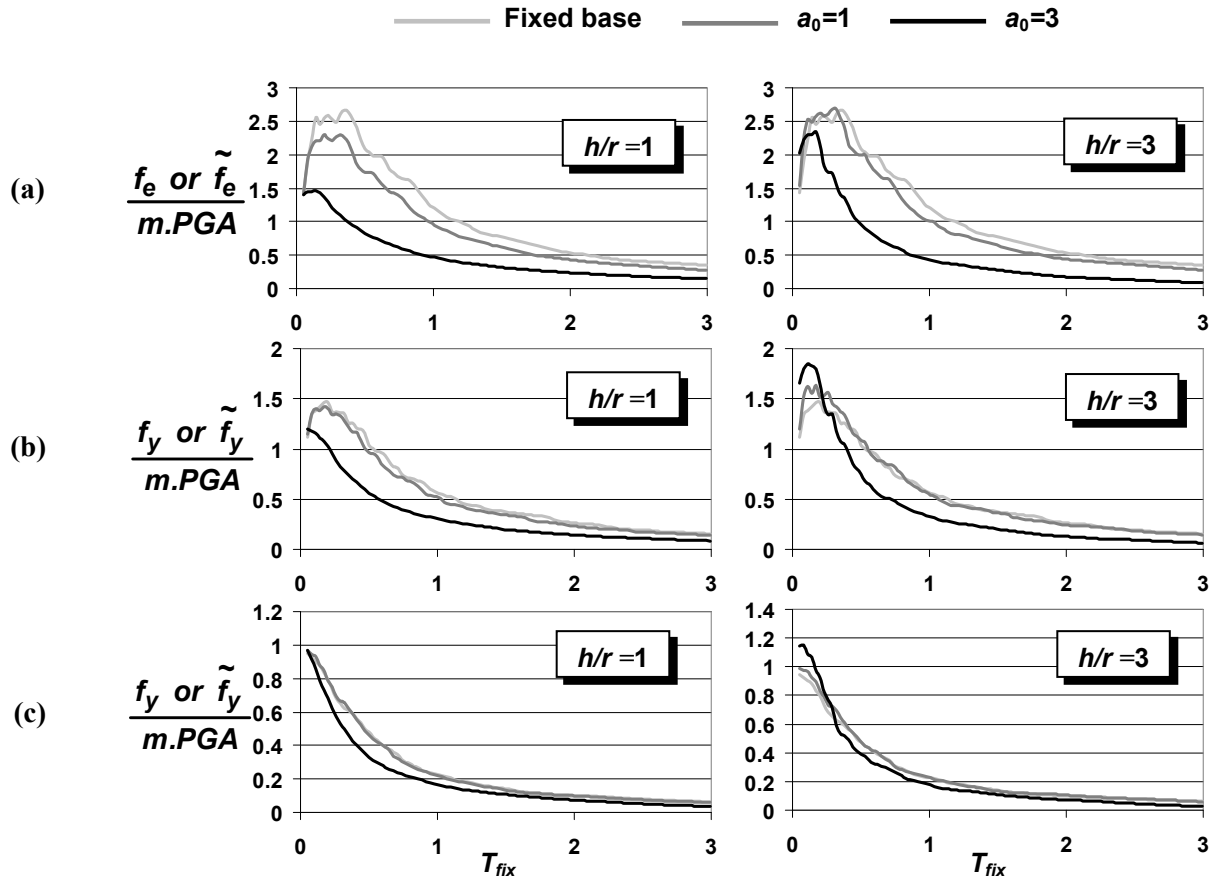

Fig. 3. Normalized average elastic and inelastic strength demand spectra for ground motions listed in Table 1: (a) μ_{fix}=1 (b) μ_{fix}=2 and (c) μ_{fix}=6. [18].

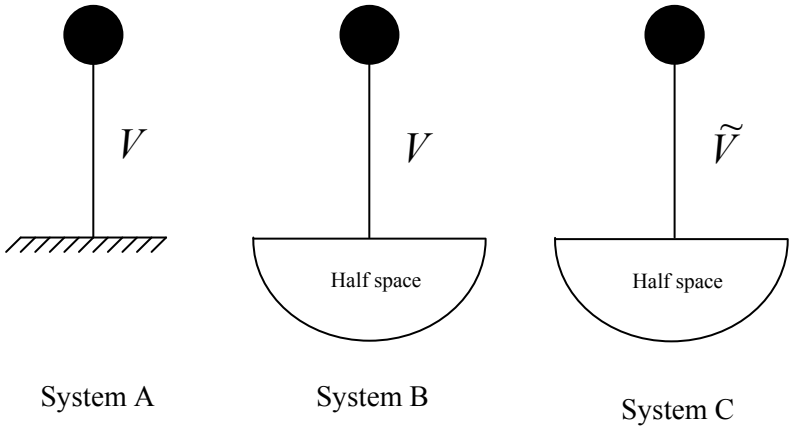

Fig. 4. Systems 'A', 'B' and 'C' considered for evaluating NEHRP2003 provisions.

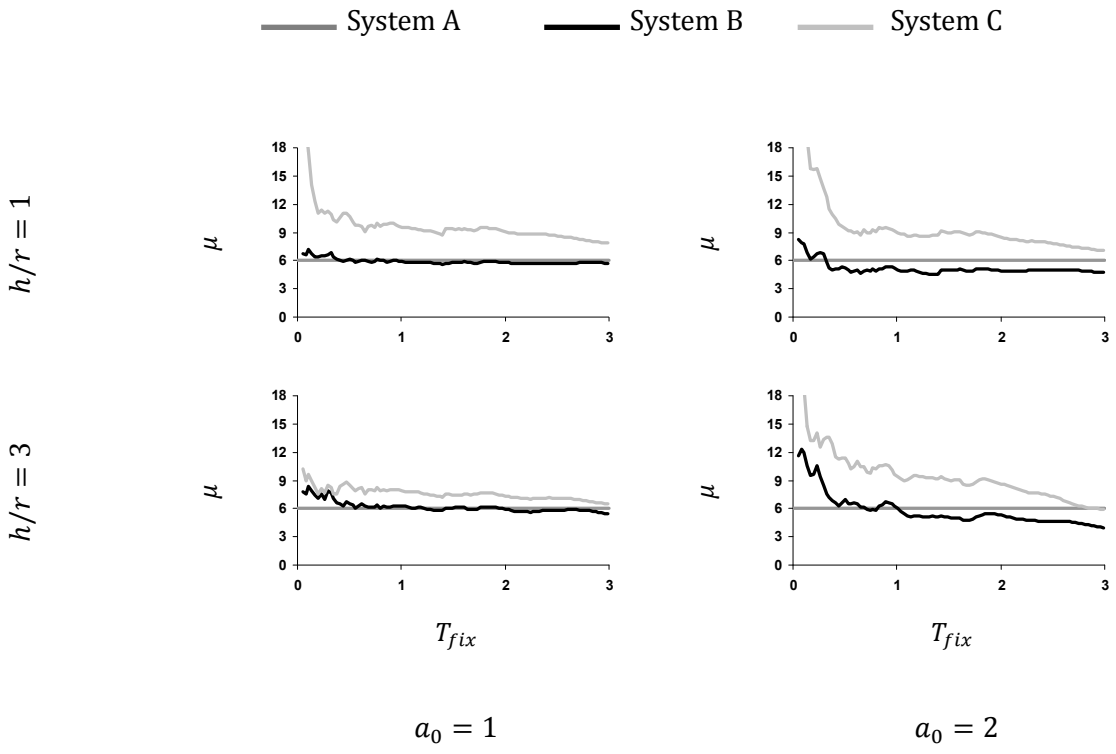

Fig. 5. Comparison of the ductility demand of Systems 'B' and 'C' with a presumed ductility demand of 6 for System 'A'.

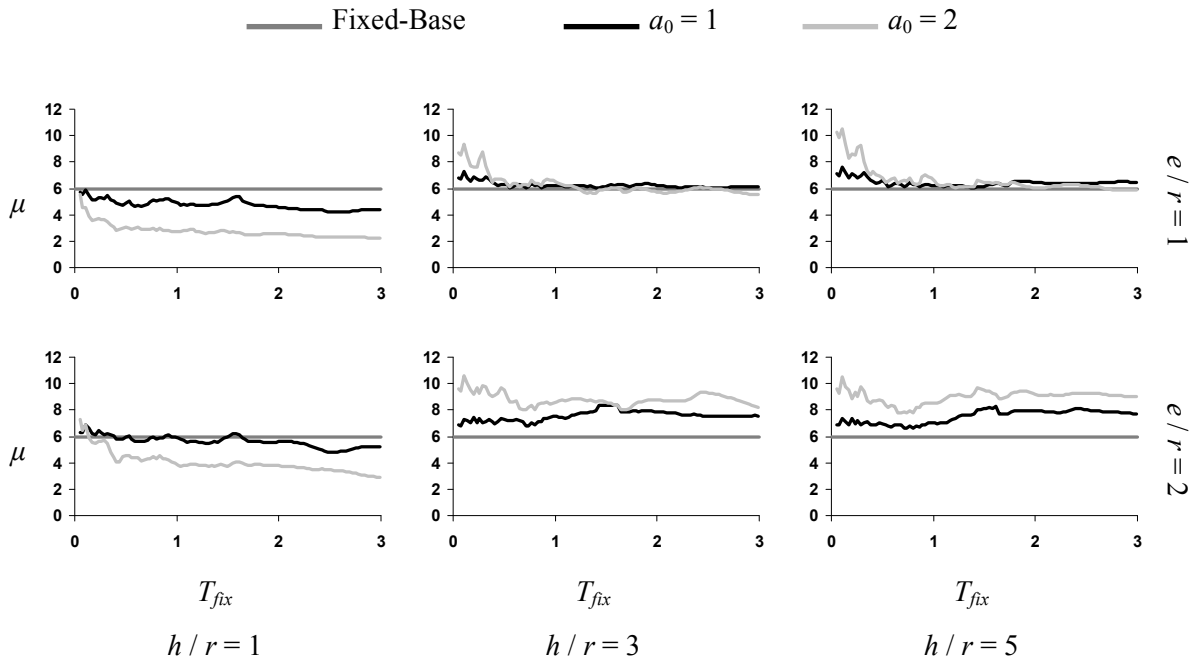

Fig. 6. Averaged ductility demand for different soil-structure systems with embedded foundation subjected to ground motions listed in Table 1 (μ_{fix}=6). [20].

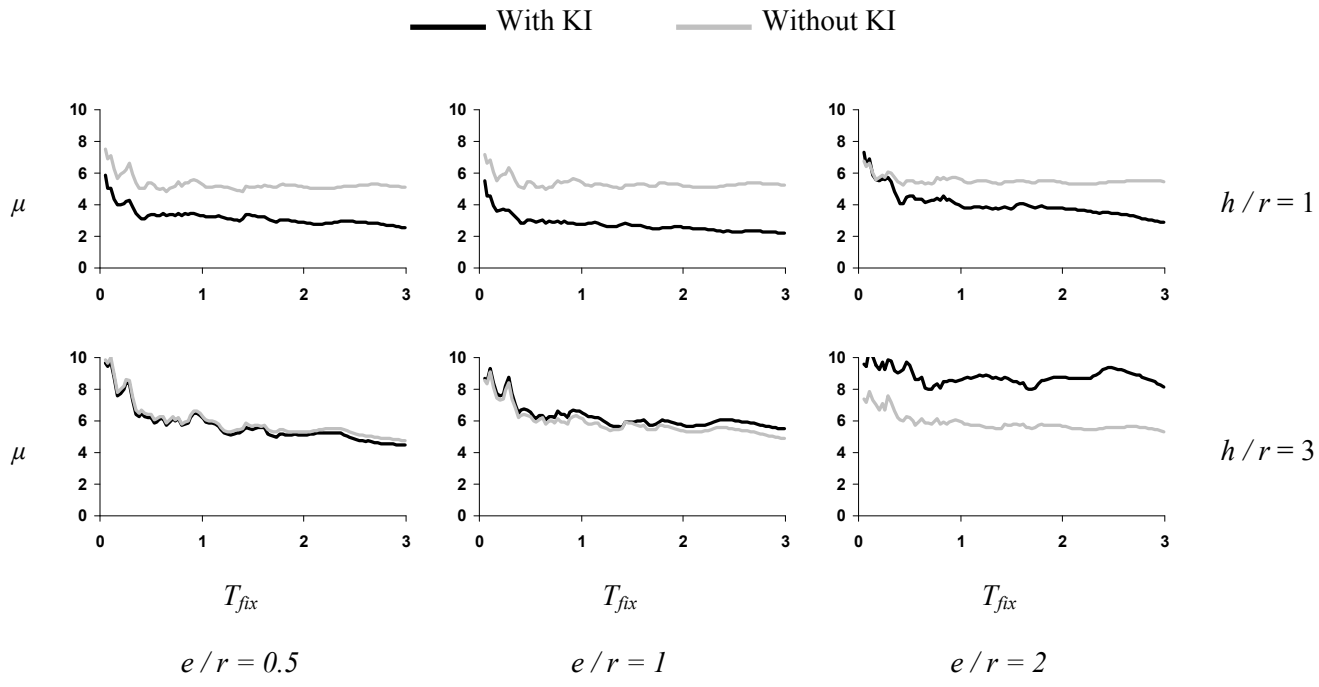

Fig. 7. Averaged ductility demand for different soil-structure systems with embedded foundation subjected to ground motions listed in Table 1 with and without inclusion of KI effect (μ_{fix}=6 , a_0=2). [20].

Table 1. Selected ground motions recorded at alluvium sites.

Station	Geology	Earthquake Date	Magnitude	Epicentral Distance (km)	Component	PGA (g)
El Centro - Irrigation Distinct	Alluvium	Imperial Valley, May 18, 1940	6.3 (M_L)	8	S90W, S00E	0.21, 0.31
Taft - Lincoln School Tunnel	Alluvium	Kern County, July 21, 1952	7.7 (M_S)	56	308, 218	0.15, 0.18
Figueroa - 445 Figueroa St.	Alluvium	San Fernando, February 9, 1971	6.5 (M_L)	41	N52E, S38W	0.14, 0.12
Ave. of the Stars - 1901 Ave. of the Stars	Silt and Sand Layers	San Fernando, February 9, 1971	6.5 (M_L)	38	N46W, S44W	0.14, 0.15
Meloland- Interstate 8 Overpass	Alluvium	Imperial Valley, October 15, 1979	6.6 (M_L)	21	36, 270	0.31, 0.30
Bond Corner - Highways 98 and 115	Alluvium	Imperial Valley, October 15, 1979	6.6 (M_L)	3	14, 230	0.51, 0.78
Alhambra - Freemont School	Alluvium	Whittier - Narrows, October 1, 1987	6.1 (M_L)	7	27, 180	0.41, 0.30
Altadena - Eaton Canyon Park	Alluvium	Whittier - Narrows, October 1, 1987	6.1 (M_L)	13	90, 360	0.15, 0.30
Burbank - California Federal Saving Building	Alluvium	Whittier - Narrows, October 1, 1987	6.1 (M_L)	26	250, 340	0.23, 0.19
Los Angeles - Baldwin Hills	Alluvium over Shale	Whittier - Narrows, October 1, 1987	6.1 (M_L)	27	90, 360	0.06, 0.13
Capitola - Fire Station	Alluvium	Loma Prieta, October 17, 1989	7.1 (M_S)	9	90, 360	0.44, 0.53
Hollister - South and Pine	Alluvium	Loma Prieta, October 17, 1989	7.1 (M_S)	48	90, 180	0.25, 0.21

ON THE OPTIMUM PERFORMANCE-BASED DESIGN OF STRUCTURES

H. Moghaddam
Department of Civil Engineering, Sharif University of Technology, Tehran, Iran

ABSTRACT

In conventional seismic design provisions, the preliminary design of most buildings is based on equivalent static forces. Historically, the height wise distribution of these static forces seems to have been chosen arbitrarily by engineering judgment. However, as the design basis is being shifted from strength to deformation in modern performance-based design codes, these conventional load patterns need to be rationalized. This paper examines the adequacy of equivalent static forces in the general context of performance based design. Further, it introduces a new method for optimum performance design against seismic excitations. This method is based on the concept of uniform distribution of deformation. In this approach, the structural properties are modified so that inefficient material is gradually shifted from strong to weak areas of a structure. This process is continued until a state of uniform deformation is achieved. It is shown that the seismic performance of such a structure is optimal, and behaves generally better than those designed by conventional methods. This method has been employed for optimum design of various structural forms such as shear buildings, moment resisting frames, concentrically braced frames, and RC frames, and the results are discussed.
Keywords: Ductility demand; Multi-degree of freedom systems; Optimum strength and stiffness distribution; Seismic codes; Performance-based design.

1. INTRODUCTION

Seismic design is currently based on force rather than displacement, essentially as a consequence of the historical developments of an understanding of structural dynamics and, more specifically, of the response of structures to seismic actions and the progressive modifications and improvement of seismic codes worldwide. Although design procedures have become more rigorous in their application, this basic force-based approach has not changed significantly since its inception in the early 1900s. Consequently, the seismic codes are generally regarding the seismic effects as lateral inertia forces. The height wise distribution of these static forces (and therefore, stiffness and strength) seems to be based implicitly on the elastic vibration modes (Green, 1981; Hart, 2000).

Recent design guidelines, such as FEMA 356 and SEAOC Vision 2000, place limits on acceptable values of response parameters, implying that exceeding of these acceptable values represent violation of a performance objective. Further modifications to the preliminary design, aiming to satisfy the Performance Objectives could lead to some alterations of the original distribution pattern of structural properties. As structures exceed their elastic limits in severe earthquakes, the use of inertia forces corresponding to elastic modes may not lead to the optimum distribution of structural properties. Many experimental and analytical studies have been carried out to investigate the validity of the distribution of lateral forces according to seismic codes. Lee and Goel (2001) analyzed a series of 2 to 20 story frame models subjected to various earthquake excitations. They showed that in general there is a discrepancy between the

earthquake induced shear forces and the forces determined by assuming distribution patterns. The consequences of using the code patterns on seismic performance have been investigated during the last decade (Anderson et al., 1991; Gilmore and Bertero, 1993; Martinelli et al., 2000). Chopra (2001) evaluated the ductility demands of several shear-building models subjected to the El- Centro Earthquake of 1940. The relative story yield strength of these models was chosen in accordance with the distribution patterns of the earthquake forces specified in the Uniform Building Code (UBC). It was concluded that this distribution pattern does not lead to equal ductility demand in all stories, and that in most cases the ductility demand in the first story is the largest of all stories. The first author (1995, 1999) proportioned the relative story yield strength of a number of shear building models in accordance with some arbitrarily chosen distribution patterns as well as the distribution pattern suggested by the UBC1997. It is concluded that: (a) the pattern suggested by the code does not lead to a uniform distribution of ductility, and (b) a rather uniform distribution of ductility with a relatively smaller maximum ductility demand can be obtained from other patterns. These findings have been confirmed by further investigations (Moghaddam et al., 2003; Moghaddam and Hajirasouliha, 2004; Karami et. al., 2004), and led to the development of a new concept: optimum distribution pattern for seismic performance that is discussed in this paper. An effective optimization algorithm is developed to find more rational criteria for determination of design earthquake forces. It is shown that using adequate load patterns could result in a reduction of ductility demands and a more uniform distribution of deformations.

2. MODELING AND ASSUMPTIONS

Among the wide diversity of structural models that are used to estimate the non-linear seismic response of building frames, the shear-beam is the one most frequently adopted. In spite of some drawbacks, it is widely used to study the seismic response of multi-story buildings because of simplicity and low computer time consumption (Diaz et al., 1994). Lai et al. (1992) have investigated the reliability and accuracy of such shear-beam models.

120 shear-building models of ten-story structures with fundamental period varying from 0.1 sec to 3 sec, and target ductility demand equal to 1, 1.5, 2, 3, 4, 5, 6 and 8 have been used in the present study. It should be noted that the range of the fundamental period considered in this study is wider than that of the real structures to cover all possibilities. In the present shear-building models, each floor is assumed as a lumped mass that is connected by perfect elastic-plastic shear springs. The total mass of the structure is distributed uniformly over its height as shown in Figure 1. The Rayleigh damping is adopted with a constant damping ratio 0.05 for the first few effective modes. In all MDOF models, lateral stiffness is assumed as proportional to shear strength at each story, which is obtained in accordance with the selected lateral load pattern.

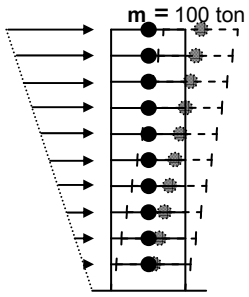

Fig. 1. Typical 10-story shear building model.

Twenty selected strong ground motion records are used for input excitation as listed in Table 1. All of these excitations correspond to the sites of soil profiles similar to the S_D type of UBC 1997 and are recorded in a low to moderate distance from the epicenter (less than 45 km) with rather high local magnitudes (i.e., M>6). Due to the high intensities demonstrated in the records, they are used directly without being scaled.

The above-mentioned models are, then, subjected to the seismic excitations and non-linear dynamic analyses are conducted utilizing the computer program DRAIN-2DX (Prakash et al., 1992). For each earthquake excitation, the dynamic response of models with various fundamental periods and target ductility demands is calculated.

Table 1. Strong ground motion characteristics.

	Earthquake	Station	M	PGA (g)	USGS Soil
1	Imperial Valley 1979	H-E04140	6.5	0.49	C
2	Imperial Valley 1979	H-E04230	6.5	0.36	C
3	Imperial Valley 1979	H-E05140	6.5	0.52	C
4	Imperial Valley 1979	H-E05230	6.5	0.44	C
5	Imperial Valley 1979	H-E08140	6.5	0.45	C
6	Imperial Valley 1979	H-EDA360	6.5	0.48	C
7	Northridge 1994	CNP196	6.7	0.42	C
8	Northridge 1994	JEN022	6.7	0.42	C
9	Northridge 1994	JEN292	6.7	0.59	C
10	Northridge 1994	NWH360	6.7	0.59	C
11	Northridge 1994	RRS228	6.7	0.84	C
12	Northridge 1994	RRS318	6.7	0.47	C
13	Northridge 1994	SCE288	6.7	0.49	C
14	Northridge 1994	SCS052	6.7	0.61	C
15	Northridge 1994	STC180	6.7	0.48	C
16	Cape Mendocino 1992	PET000	7.1	0.59	C
17	Duzce 1999	DZC270	7.1	0.54	C
18	Lander 1992	YER270	7.3	0.25	C
19	Parkfield 1966	C02065	6.1	0.48	C
20	Tabas 1978	TAB-TR	7.4	0.85	C

3. CONVENTIONAL LATERAL LOADING PATTERNS

In most seismic building codes (Uniform Building Code, 1997; NEHRP Recommended Provisions, 1994; ATC-3-06 Report, 1987; ANSI-ASCE 7-95, 1996; Iranian Seismic Code, 1999), the height wise distribution of lateral forces is to be determined from the following typical relationship:

$$F_i = \frac{w_i h_i^k}{\sum_{j=1}^{N} w_j h_j^k} \cdot V. \tag{1}$$

where w_i and h_i are the weight and height of the i^{th} floor above the base, respectively; N is the number of stories; and k is the power that differs from one seismic code to another. In some provisions such as NEHRP-94 and ANSI/ASCE 7-95, k increases from 1 to 2 as period varies from 0.5 to 2.5 second. However, in some codes such as UBC-97 and Iranian Seismic Code (1999), the force at the top floor (or roof) computed from Equation (1) is increased by adding an additional force $F_t=0.07TV$ for a fundamental period T of greater than 0.7 second. In such a case, the base shear V in Equation (1) is replaced by $(V-F_t)$.

Next we investigate the adequacy of conventional loading patterns concerning the fundamental period of the structures and ductility demand imposed by the ground motion.

4. ADEQUACY OF CONVENTIONAL LOADING PATTERNS

It is generally endeavored to induce a status of uniform deformation throughout the structure to obtain an optimum design as in Gantes et al. (2000). Karami et al. (2004) showed that for a given earthquake, the weight of seismic resistant system required to reach to the prescribed target ductility is correlated with the *cov*, the coefficient of variation, of the story ductility demands and the two minimize simultaneously. Therefore, they concluded that the *cov* of ductilities could be used as a means of assessing the adequacy of design load patterns to optimum use of material.

To investigate the efficiency of conventional loading patterns to lead to the equal ductility demands in all stories, shear-building models with various periods and ductility demands are subjected to 20 selected ground motions (Table 1). In each case, strength and stiffness are distributed within the stories according to the lateral load pattern suggested by UBC 1997. Subsequently, the stiffness pattern is scaled to adjust the prescribed fundamental period. Maximum ductility demand is then calculated by performing non-linear dynamic analysis for the given exaction. By an iterative procedure, the total strength of the model is scaled (without changing it's distribution pattern) until maximum ductility demand gets to the target value with less than 1 % error. Finally, *cov* of the story ductility demands is calculated for each case. Figure 2 illustrates the average of *cov* obtained in 20 earthquakes versus fundamental period and for various target ductility demands. Based on the results presented in Figure 2, it is concluded that:

1. Using the strength pattern suggested by UBC 1997 leads to an almost uniform distribution of ductility demands for the structures within the linear range of behaviour. However, the adequacy of conventional load patterns is reduced in non-linear ranges of vibration. It is shown that increasing the target ductility is always accompanied by increasing in *cov* of story ductility demands.
2. The *cov* of story ductility demands are especially large in the structures with both short fundamental period and large target ductility demand. It implies that using the

conventional loading patterns to design this type of structures do not lead to the satisfactory use of material incorporated in the building construction.

3. In the structures with long fundamental period (i.e. greater than 0.5 sec), *cov* of ductilities is more dependent on the maximum ductility demand than the fundamental period of the structure. However, seismic loading patterns suggested by most seismic codes are not a function of the target ductility.
4. When the structures behave linearly or nearly linearly (i.e. ductilities smaller than two), increasing in the fundamental period is generally accompanied by increasing in the *cov* of story ductility demands. This could be explained by increasing the influence of higher modes as the period of vibration increases.

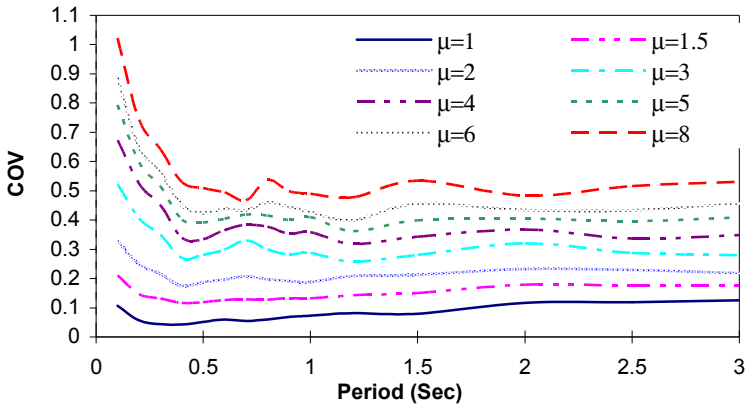

Fig. 2. *Cov* of story ductility demands, average of 20 earthquakes.

5. CONCEPT OF THEORY OF UNIFORM DEFORMATION

As discussed before, the use of distribution patterns for lateral seismic forces suggested by codes does not guarantee the optimum performance of structures. Current study indicates that during strong earthquakes the deformation demand in structures does not vary uniformly. Therefore, it can be concluded that in some parts of the structure, the deformation demand does not reach the allowable level of seismic capacity, and therefore, the material is not fully exploited. If the strength of these strong parts decreases, the deformation would be expected to increase (Riddell et al., 1989; Vidic et al., 1994). Hence, if the strength decreases incrementally, we should eventually obtain a status of uniform deformation. At this point the material capacity is fully exploited. As the decrease of strength is normally obtained by the decrease of material, a structure becomes relatively lighter as deformation is distributed more uniformly. Therefore, in general it can be concluded that a status of uniform deformation is a direct consequence of the optimum use of material. This is considered as the *Theory of Uniform Deformations* (Moghaddam and Hajirasouliha, 2004 & 2005). This theory is the basis of the studies presented in this paper.

6. OPTIMUM DISTRIBUTION OF DESIGN SEISMIC FORCES

The theory of uniform deformation can be easily adapted for evaluation of optimum patterns for shear buildings. It should be noted that there is a unique relation between the distribution pattern of lateral seismic forces and the distribution of strength (as the strength at each floor is obtained

from the corresponding story shear force). Hence, for shear buildings, we can determine the optimum pattern for distribution of seismic lateral loads instead of distribution of strength. Let's assume that we want to evaluate the most appropriate lateral load pattern to design a 10-story shear building (Figure 1) with a fundamental period of 1 sec, so that it can sustain the Northridge earthquake 1994 (CNP196) without exceeding a maximum story ductility demand of 4. The following optimization procedure is used:

1. Arbitrary primary patterns are assumed for height wise distribution of strength and stiffness. However, for shear building models we can assume that these two patterns are similar, and therefore, an identical pattern is assumed for both strength and stiffness. Here, the uniform pattern is chosen for the primary distribution of strength and stiffness.
2. The stiffness pattern is scaled to attain a fundamental period of 1 sec.
3. The structure is subjected to the given excitation, and the maximum story ductility is calculated, and compared with the target value. Consequently, the strength is scaled (without changing the primary pattern) until the maximum deformation demand reaches the target value. This pattern is regarded as a feasible answer, and referred to as the first acceptable pattern. For the above example, story strength and maximum story ductility corresponding to the first feasible answer are given in Table 2.
4. The *cov* (coefficient of variation) of story ductility distribution within the structure is calculated. The procedure continues until *cov* decreases down to an acceptable level. The *cov* of the first feasible pattern was determined as 0.719. The cov is high, and the analysis continues.
5. At this stage the distribution pattern is modified. Using the theory of uniform deformation, the inefficient material should be reduced to obtain an optimum structure. To accomplish this, stories where the ductility demand is less than the target values are identified and weakened by reducing strength and stiffness. Experience shows that this alteration should be applied incrementally to obtain convergence in numerical calculations. Hence, the following equation is used in the present studies:

$$[V_i]_{n+1} = [V_i]_n \left[\frac{\mu_i}{\mu_t} \right]^{\alpha} \tag{2}$$

where μ_i is the ductility demand at i^{th} story, and μ_t is the target ductility assumed as equal to 4 for all stories. V_i is the shear strength of the i^{th} story. n denotes the step number. α is the convergence coefficient ranging from 0 to 1. For the above example, an acceptable convergence has been obtained for a value of 0.2 for α. Now, a new pattern for height wise distribution of strength and stiffness is obtained. The procedure is repeated from step 2 until a new feasible pattern is obtained. It is expected that the *cov* of ductility distribution for this pattern is smaller than the corresponding *cov* for the previous pattern. This procedure is iterated until *cov* becomes small enough, and a status of rather uniform ductility demand prevails. The final pattern is considered as practically optimum.

Table 2. The preliminary and final arrangement of strength and stiffness.

Story	Preliminary Arrangement		Final Arrangement	
	Story Strength (ton.f)	Story Ductility	Story Strength (ton.f)	Story Ductility
1	1753	4	1435	3.98
2	1753	2.46	1351	3.99
3	1753	1.78	1229	3.99
4	1753	1.41	1089	4.00
5	1753	1.38	953	4.00
6	1753	1.19	808	3.99
7	1753	0.98	662	3.99
8	1753	0.82	512	3.99
9	1753	0.59	371	3.97
10	1753	0.31	204	3.99
Cov		0.719		0.002
Total Strength	17532		8614	

Cov: Coefficient of variation

Story ductility pattern for preliminary and final answers are compared in Table 2. According to the results, the efficiency of utilizing this method to reach to the structure with uniform ductility demand distribution is emphasized. Figure 3 illustrates the variation of *cov* and total strength from first feasible answer toward the final answer. Figure 3 shows the efficiency of the proposed method that resulted in reduction of total strength by 41% in only five steps. It is also shown in this figure that proposed method has good capability to convergence to the optimum answer without any oscillation. It can be noted from Figure 3 that decreasing in *cov* is always accompanied by a decreasing in total strength. Here the total strength is in proportion to the total weight of the seismic resisting system. These results are in agreement with the *Theory of Uniform Deformation*.

Table 2 shows the results of analysis for the first and final step. The height wise distribution of strength can be converted to the height wise distribution of lateral forces. Such pattern may be regarded as the optimum pattern of seismic forces for the given earthquake. As shown in Figure 4, this would enable the comparison of this optimum pattern with the conventional lateral loading patterns suggested by seismic design codes. The results indicate that to improve the performance under this specific earthquake, the frame should be designed in compliance with a new load pattern different from the conventional UBC pattern.

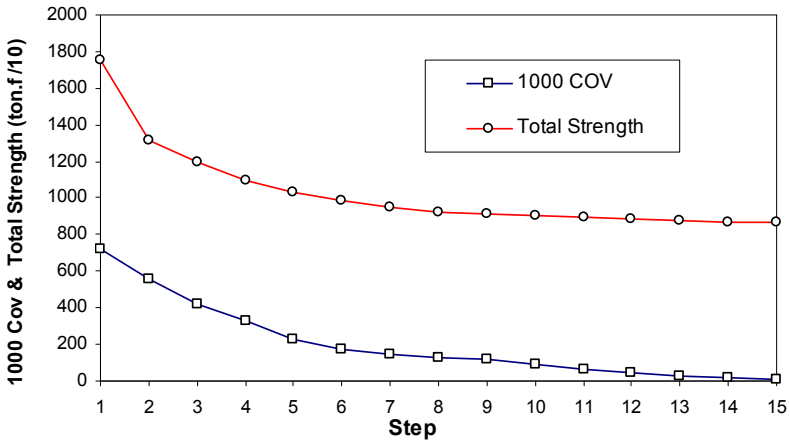

Fig. 3. *Cov* of story ductility demands and total story strength for feasible answers, 10-story shear building with T=1 Sec and μ_t=4, Northridge 1994 (CNP196).

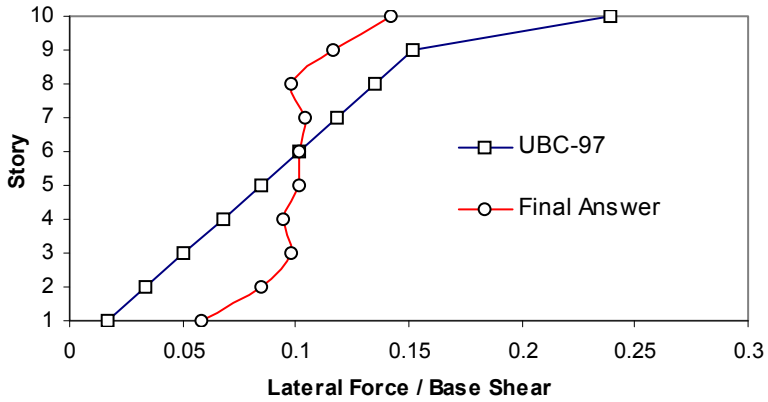

Fig. 4. Comparison of UBC-97 & optimum lateral force distribution, 10-story shear building with T=1 Sec and μ_{ti}=4, Northridge 1994 (CNP196).

As described before, an initial strength distribution is necessary to begin the optimization algorithm. In order to investigate the effect of this initial load (or strength) pattern on the final result, for the previous example four different initial load patterns have been considered:

1. A concentrated load at the roof level
2. Triangular distribution similar to the UBC code of 1997
3. Rectangular distribution
4. An inverted triangular distribution with the maximum lateral load at the first floor and the minimum lateral load at the roof level

For each case, the optimum lateral load pattern was derived for Northridge 1994 (CNP196) event. The comparison of the optimum lateral load pattern of each case is depicted in Figure 5. As shown in this figure, the optimum load pattern is not dependent on the initial strength pattern; however the speed of convergence is to some extent dependant on the initial strength pattern. This phenomenon has been confirmed by further analyses on different models and ground motions.

This leads to a very significant conclusion**:** The optimum design is unique, and does not depend on analysis path, and therefore, the analysis can be started off from any assumed initial design.

Using this optimization method, the adequacy of optimum loading patterns to reduce required structural weight is examined.

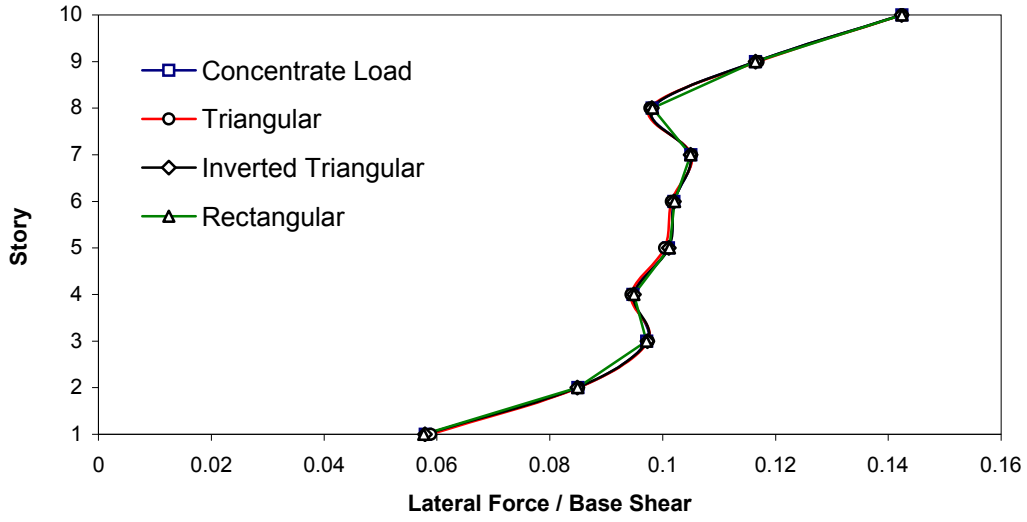

Fig. 5. Optimum load pattern for different initial strength distributions, 10-story shear building with T=1 Sec and μ_t=4, Northridge 1994 (CNP196)

7. ADEQUACY OF OPTIMUM LOADING PATTERNS

To investigate the validity and accuracy of the proposed optimization method, the foregoing procedure has been applied to find the optimum pattern for 120 shear-building models with different fundamental periods and target ductility demands subjected to 20 selected earthquakes. In this study, the maximum story ductility is considered as the failure criterion, implying that exceeding of the target ductility represents violation of the performance objective. Therefore, according to the *Theory of Uniform Deformation,* it is expected that seismic performance be improved by a uniform distribution of ductility demands. It is demonstrated in previous section that the proposed method is very efficient to reach to the uniform distribution of ductility demands.

To evaluate the weight of the seismic resistant system for MDOF structures, it is assumed that the weight of lateral-load-resisting system at each story, W_{Ei}, is proportional to the story shear strength, V_i. Therefore, the total weight of the seismic resistant system, W_E, can be calculated as:

$$W_E = \sum_{i=1}^{n} W_{Ei} = \sum_{i=1}^{n} \lambda \cdot V_i = \lambda \cdot \sum_{i=1}^{n} V_i \qquad (3)$$

where λ is the proportioning coefficient. According to Equation 3, the ratio of total structural weight for the UBS designed models to the optimum models, $(W_E)_{UBC/}$ $(W_E)_{opt,}$ has been calculated for all cases. Figure 6 shows the mean values of $(W_E)_{UBC/}$ $(W_E)_{opt,}$ as a function of ductility demand and for different fundamental periods. This period has been obtained by averaging the responses of 20 earthquakes.

According to the results illustrated in Figure 6, it is concluded that:

1. Having the same period and ductility demand, structures designed according to the optimum load pattern always have less structural weight compare to those designed conventionally. Therefore, the adequacy of optimum loading patterns is emphasised.
2. In the elastic range of vibration (μ=1), the total structural weights required for the models designed according to the UBC load pattern are in average 10% above the optimum value. Hence, it can be concluded that for practical purposes, using the conventional loading patterns is satisfying within the linear range of vibrations.
3. Increasing the ductility demand is generally accompanied by increasing in the structural weight required for the conventionally designed models compare to the optimum ones. This implies that conventional loading patterns loose their efficiency in non-linear ranges of vibration. It is illustrated that for conventionally designed structures with high levels of ductility demand, the required structural weight could be more than 50% above the optimum weight.

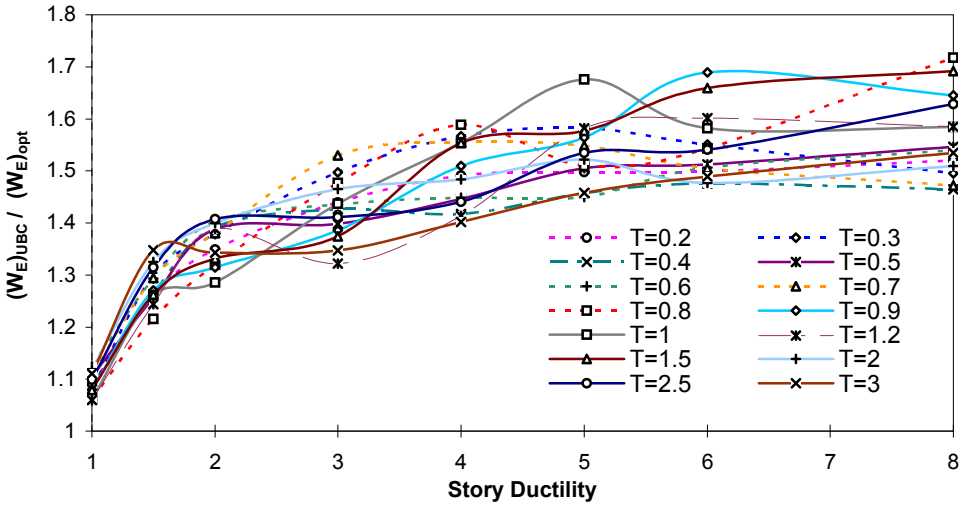

Fig. 6. The ratio of total structural weight for the UBC designed models to the optimum models, $(W_E)_{UBC} / (W_E)_{opt}$, Average of 20 earthquakes.

8. MORE ADEQUATE LOADING PATTERNS

It is well known that there are many uncertainties in seismic loading and seismic design of structures. One of the most random parameters is the seismic event that might occur in a place; therefore, the selection of a ground motion for seismic design of a structure might be at great task. As described before, to improve the performance under a specific earthquake, structure should be designed in compliance with an optimum load pattern different from the conventional patterns. This optimum pattern depends on the earthquake, and therefore, it varies from one earthquake to another. However, there is no guarantee that the frame will experience seismic events, which are the same as the design ground motion. While each of the future events will have its own signature, it is generally acceptable that they have relatively similar characteristics. Accordingly, it seems that the model designed with optimum load pattern is capable to reduce the maximum ductility experienced by the model after similar ground motions. It can be concluded that for general design proposes, the design earthquakes must be classified for each structural performance category and then more adequate loading patterns must be found by

averaging optimum patterns corresponding to every one of the earthquakes in each group. To verify this assumption, 20 strong ground motion records with the similar characteristics, as listed in Table 1, were selected. Time history analyses have been performed for all earthquakes and the corresponding optimum pattern has been found for shear-building models with different fundamental periods and target ductility demands. Consequently, 2400 optimum load patterns have been determined at this stage. For each fundamental period and ductility demand a specific matching load distribution has been obtained by averaging the results for all earthquakes. These average distribution patterns were used to design the given shear building models. Then the response of the designed models to each of the 20 earthquakes was calculated. In Figure 7, the ratio of required structural weight to the optimum weight, (W_E) / $(W_E)_{opt}$, for the models designed with the average pattern is compared with those designed conventionally. This figure has been obtained by averaging the responses of shear-building models with fundamental period of 0.1 sec to 3 sec, subjected to 20 earthquake ground motions. It is illustrated in Figure 7, having the same period and ductility demand, structures designed according to the average of optimum load patterns require less structural weight compare to those designed conventionally. The efficiency of the average load pattern is more obvious for the models with high ductility demand. As shown in Figure 7, using this pattern in high levels of ductility demand resulted in more than 30% reduction in the total structural weight compared with conventionally designed models. It can be concluded that the proposed approach can be utilized efficiently for any set of earthquakes with similar characteristics.

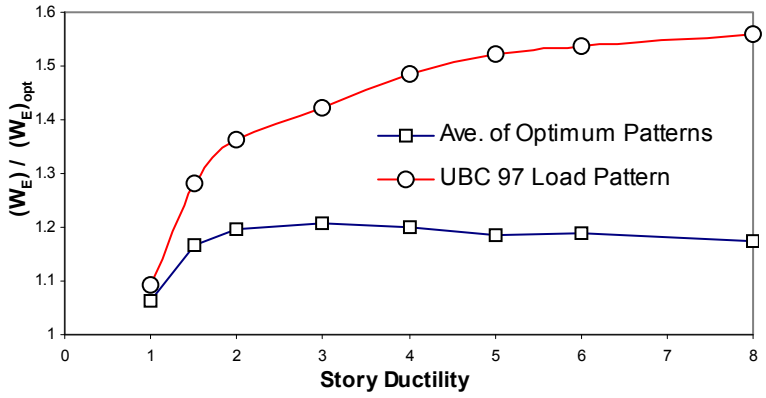

Fig. 7. The ratio of required structural weight to the optimum weight, (W_E) / $(W_E)_{opt}$, for the models designed with the average pattern and those designed conventionally, Average of 20 earthquakes.

It was shown that using the average of the optimum load patterns results in a better seismic performance in comparison with the conventional patterns. Such a load pattern is designated as 'more adequate load pattern'. At present, the seismic load patterns suggested by most seismic codes do not depend on the ductility. However, the present study shows that more adequate loading patterns are a function of both the period of the structure and the target ductility demand. According to the results of this study, more adequate loading patterns could be illustrated in four different categories as follows:

Triangular Load Pattern

As described before, triangular load pattern is suggested by most of the seismic building codes. It is shown in Figure 8, in average, this load pattern is close to the optimum pattern corresponding to the models with elastic behavior and fundamental period shorter than 1 sec. This conclusion is also in agreement with the results shown in Figure 2. It can be noted from Figure 8 that, in general, increasing the fundamental period results in increasing the loads at the top stories. This could be explained by increasing the influence of higher modes as the period of vibration increases.

Trapezoid Load Pattern

As shown in Figure 9, trapezoid load pattern is appropriate for models with fundamental period shorter than 0.5 sec and small target ductility demand (i.e. $\mu_t \leq 3$). It can be noted from Figure 9 that increasing the ductility demand results in decreasing the loads at the top stories and increasing the loads at the lower stories. It is also shown in Figure 9 that increasing the fundamental period is generally accompanied by increasing the loads at the top stories. By increasing the ductility demand, this load pattern converts to the parabolic pattern.

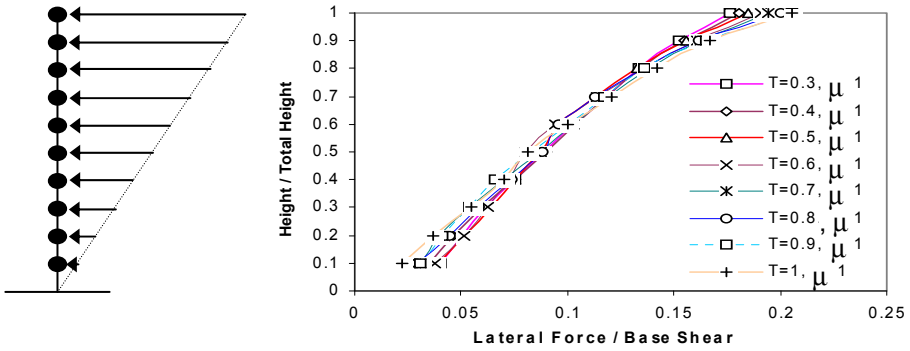

Fig. 8. Triangular load patterns.

Parabolic Load Pattern

According to the results of this study, more adequate load patterns are in parabolic shape for a wide range of periods and ductility demands. It seems that the rectangular pattern accompanied by a concentrated force at the top floor, which is suggested by Karami et al. (2004), also belongs to this category. As shown in Figure 10, in general, parabolic load patterns are appropriate to design three categories of structures:

- Structures with fundamental period shorter than 0.5 sec and high ductility demand ($\mu_t \geq 3$)
- Structures with fundamental period longer than 1 sec and small ductility demand ($\mu_t \leq 3$)
- Structures with fundamental period varying from 0.5 sec to 1 sec

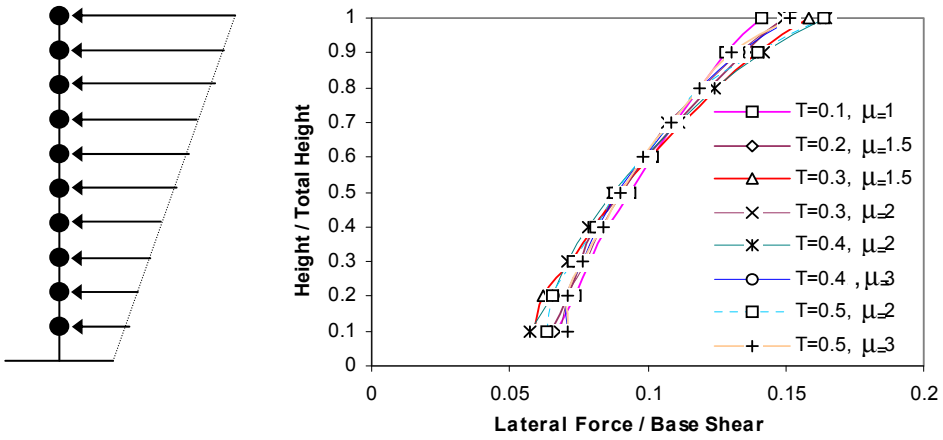

Fig. 9. Trapezoid load patterns.

As Figure 10 indicates, for the same ductility demand, loads at the top stories are increasing as the fundamental period of the structure increases. It is also shown in Figure 10 that increasing the ductility demand results in decreasing the loads at the top stories and increasing the loads at the lower stories. For higher levels of ductility demand, optimum load patterns corresponding to the models with fundamental period longer than 1 sec, move toward the hyperbolic pattern.

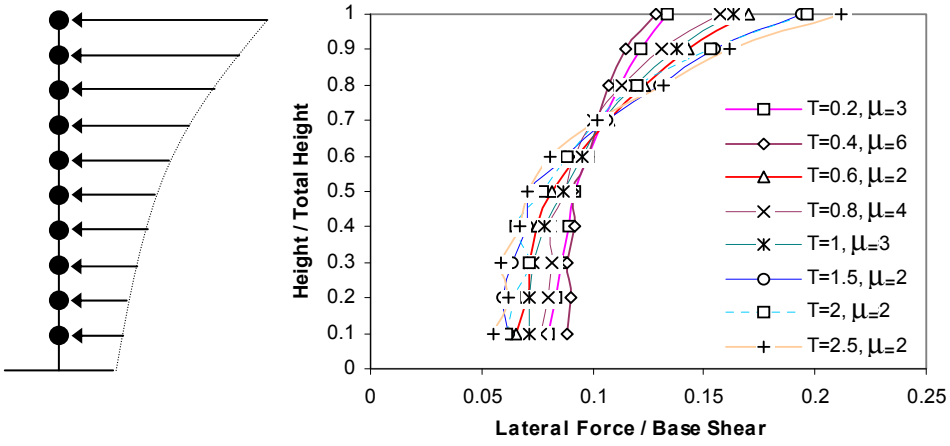

Fig. 10. Parabolic load patterns.

Hyperbolic Load Pattern

As illustrated in Figure 11, more adequate load patterns are in hyperbolic shape for structures with high levels of ductility demand ($\mu_t \geq 3$) and fundamental period longer than 1 sec. It is also shown in this figure that increasing the ductility demand results in decreasing the loads at the top stories and increasing the loads at the lower stories.

It can be noted from Figure 11 that for the optimum loading patterns corresponding to the structures with long periods and high levels of ductility demand ($T \geq 2.5$ sec and $\mu_t \geq 5$), loads assigned to the lower stories could be greater than those assigned to the top stories. Therefore in this case, optimum loading patterns are completely different with the lateral loading patterns suggested by the seismic codes (e.g. triangular pattern). However, it should be mentioned that this condition is beyond the most practical designs.

While more adequate load patterns could be very different in their shape, it is possible to establish some general rules. According to the illustrated results, increasing the fundamental period is usually accompanied by increasing the loads at the top stories caused by the higher mode effects. On the other hand, in general, increasing the ductility demand results in decreasing the loads at the top stories and increasing the loads at the lower stories. By changing both the fundamental period of the structure and the target ductility demand, these two contrary effects are combined with each other. It should be noted that there is not a definite boundary between different categories of more adequate load patterns and they convert to each other very smoothly.

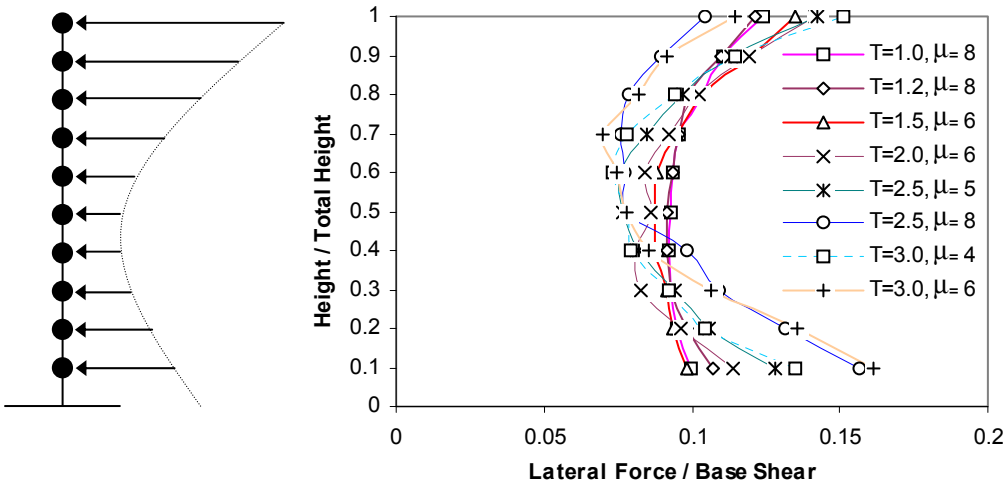

Fig. 11. Hyperbolic load pattern.

Table 3. More adequate load patterns with respect to the target ductility demand and the fundamental period of the structure.

	$0.1 \leq T \leq 0.5$	$0.5 \leq T \leq 1$	$1 \leq T \leq 3$
$\mu_t = 1$	Triangular	Triangular	Parabolic
$1 < \mu_t \leq 3$	Trapezoid	Parabolic	Parabolic
$3 \leq \mu_t \leq 8$	Parabolic	Parabolic	Hyperbolic

To summarize the above discussions, more adequate load patterns are presented in Table 3 with respect to the fundamental period of the structure and the target ductility demand. More adequate load patterns introduced in this paper are based on the 20 selected earthquakes, as listed in Table 1. However, discussed observations are fundamental and similar conclusions have been obtained

by further analyses on different models and ground motions (Hajirasouliha, 2004). However, it should be noted that the results cannot be directly applied to shear walls, as they behave substantially different from shear-building type of structures. The optimization method proposed in this paper, can be used for any set of earthquakes, and can provide an efficient optimum performance-based seismic design method for building structures. As we know, In performance based design we consider multiple limit states (e.g. service event, rare event, very rare event). However, different events (earthquakes) would result in different optimum load distributions. It seems rational to consider the very rare event as the governing criterion for preliminary design, and control the design for other events.

9. BASICS OF OPTIMUM PERFORMANCE DESIGN

In the foregoing sections, it was shown that the theory of uniform deformation can be adapted for evaluation of optimum patterns for shear buildings. Now consider case, the structure in Fig. 12 is subjected to dynamic forces $\overline{\mathbf{P}}(\mathbf{t})$, and excitations $\overline{\ddot{\mathbf{g}}}(\mathbf{t})$.

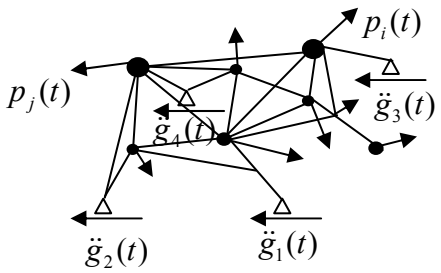

Fig. 12. Dynamic force and excitations.

As shown in the figure, the support excitations can be generally different. This can be the case for seismic excitation of the supports in structures of large dimensions. The dynamic forces $P_i(t)$ are applied to various points in different directions. The performance design method requires that the structure stays within the deformation acceptance criteria when subjected to the given force and excitations. For ordinary buildings that are like a vertical cantilever, it was shown that a conventional load pattern can be considered as rather adequate. However, the question is that what would be the conventional loading pattern for static design of this structure, if it is to experience nonlinear excursions of deformation during the loading. Indeed, aforementioned patterns such as triangular and hyperbolic seem irrelevant. Even if we consider combining the first few modes, we need to have a preliminary design before conducting a dynamic analysis. However, as it was indicated in section 6, the optimum design is unique, and does not depend on the analysis path, and therefore, the analysis can be started off from any assumed initial design. This greatly eases the design.

Let's consider a conceptual example shown in Figure 13. The objective is to design a truss-like structure for sustaining four masses M1 to M4 by using any number of stud members connecting these masses to each other, and to the supports A to E. The acceptance criterion is assumed as a member ductility of 4 when subjected to the horizontal component of the Northridge Earthquake of 1994 (CNP196). Masses M1 to M4 are assumed to be 20, 5, 10, and 5 tons, respectively.

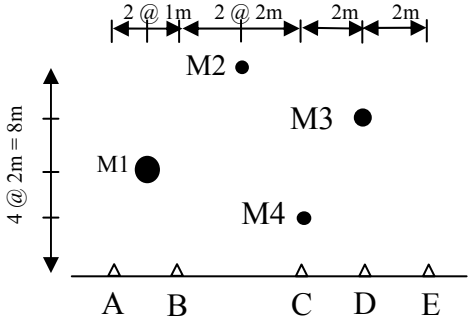

Fig. 13. The position of masses and supports.

At the starting point, a very general arrangement is chosen by considering all possible connections as shown in Figure 14. In the first step, an identical area of cross section of 1 cm^2 is assumed for all members. It is also assumed that the strength of each member is equal to (Af_y) in both tension and compression. The structure is subjected to the seismic excitation, and the ductility demand is calculated for all members. Subsequently, the area of cross section of all members is scaled until the maximum ductility demand reaches the acceptance criterion of 4.

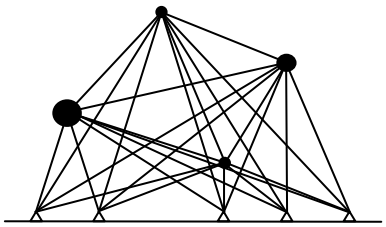

Fig. 14. Preliminary arrangement of members.

The distribution of material and ductility demand at this stage is shown in Table 4. These results indicate that some members undergo much less deformation than others. This implies that the material is not fully exploited in some members.

Table 4. The preliminary and final arrangement of members.

Members	Preliminary Arrangement		Final Arrangement	
	Cross Section (cm^2)	Member Ductility	Cross Section (cm^2)	Member Ductility
1	1243.6	4.009	2363.8	3.998
2	1243.6	2.303	0.0	---
3	1243.6	1.077	3246.9	4.001
4	1243.6	1.173	0.0	---
5	1243.6	1.129	0.0	---
6	1243.6	1.735	0.0	---
7	1243.6	0.453	0.0	---
8	1243.6	0.580	0.0	---
9	1243.6	0.484	140.1	4.002
10	1243.6	0.650	0.0	---
11	1243.6	0.209	522.2	3.999
12	1243.6	0.764	330.0	4.001
13	1243.6	0.623	0.0	---
14	1243.6	0.485	0.0	---
15	1243.6	0.273	0.0	---
16	1243.6	1.191	691.2	4.000
17	1243.6	1.123	818.6	4.000
18	1243.6	0.189	0.0	---
19	1243.6	0.940	0.0	---
20	1243.6	1.800	1146.6	3.999
21	1243.6	0.457	10.9	3.997
22	1243.6	1.517	581.6	4.000
23	1243.6	1.233	0.0	---
24	1243.6	0.226	0.0	---
25	1243.6	0.690	0.0	---
26	1243.6	1.057	629.6	4.001
Cov		0.785		0.001
Weight	162.3 ton		52.7 ton	

Considering the *theory of uniform deformation*, it should be attempted to move towards a uniform ductility distribution demand to obtain a lighter structure. To accomplish this, the optimization procedure in Section 6 is employed:

1. An arbitrary primary pattern is assumed for the distribution of structural properties that control the response of structure (such as strength, stiffness, and damping). Here, the cross section area is the only controlling parameter. Hence, as mentioned before, a uniform pattern is chosen.
2. The structure is subjected to the excitation, and the maximum deformation is calculated, and compared with the acceptance criterion. The structural properties are then scaled, without changing the primary pattern, until the maximum deformation demand reaches the acceptance value. This pattern is regarded as a feasible answer, and referred to as the first acceptable pattern. For the above example, member ductility represents the deformation demand, and the results of the first and the final steps are presented in Table 4.
3. The coefficient of variation cov of deformation distribution within the structure is calculated. If the cov is considered to be small enough, we can stop, and consider the pattern as practically optimum. Otherwise the analysis continues. The cov of the first acceptable pattern was determined as 0.785. It is decided that the cov is high, and the analysis should continue.

4. At this stage the distribution pattern of structural properties is modified. Using the *Theory of Uniform Deformation*, the inefficient material is reduced until an optimum structure is obtained. To accomplish this, the positions where the deformation is less than the acceptance value are identified, and the material is reduced accordingly. As emphasized before, this alteration should be applied incrementally in order to achieve convergence in the numerical calculations. Hence, the following equation is used in the present studies:

$$[(p_{sc})_i]_{n+1} = [(p_{sc})_i]_n \left[\frac{d_i}{d_{ti}}\right]^{\alpha} \tag{4}$$

where d_i and d_{ti} are demand and acceptance deformations at position i. $(P_{sc})_i$ is the structural control parameter, relating to position i. n denotes the step number. α is the convergence coefficient ranging from 0 to 1. For the above example, as acceptable convergence was obtained for a value of α=0.2. Considering the cross-section area, Ai, as the structural control parameter and member ductility, μ_i, as the deformation demand and substituting 4 as the acceptance deformation for all members, the following equation is obtained.

$$[(A)_i]_{n+1} = [(A)_i]_n \left[\frac{\mu_i}{4}\right]^{0.2} \tag{5}$$

Using these modified cross sections, the procedure is repeated from step 2, until a new feasible pattern is obtained. It is expected that the cov of deformation distribution for the new pattern is smaller than the corresponding cov for the previous pattern. This procedure is iterated until cov becomes small enough, and a status of rather uniform deformation prevails. Starting from a cov of 0.785, we reach a cov of 0.001 at the final step. A comparison of the results of primary and final steps in Table 4 leads to the following conclusions:

1. The weight of total material has decreased from 162.3 ton to 52.7 ton.
2. Member ductility demands in the final step have become remarkably uniform.
3. The method has been able to recognize and eliminate the redundant and inefficient members. Out of 26 members in the primary arrangement in Figure 14 only 11 members remain in the final step as shown in Figure 15.

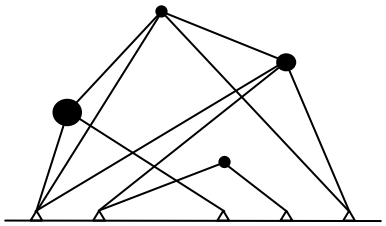

Fig. 15. Final arrangement of members.

10. EFFECT OF ACCEPTANCE CRITERION

In the previous section, it was shown that in the optimum procedure it is attempted to close the gap between the demand deformation and acceptance criterion. This inevitably makes the design quite sensible to variations in design parameters such as the type and magnitude of ground motion, and the mechanical properties of structural members. As shown in the foregoing section, to obtain the optimum design it can be assumed all possible links between the given masses, and let the optimum procedure eliminate the redundant members. However, in practice this may be dangerous as the structure could fail due to a minor change in the presumptions. To investigate the effect of presumed deformation capacity on the final design shown in Fig. 15, the optimization analysis was repeated for different acceptance criteria. The results are illustrated in Fig. 16. The figure indicates that the design depends on the acceptance criterion. Thus, it seems reasonable to carry out the optimum analysis for a range of design parameters, and determine the final design as the envelope of the individual designs as shown in Fig. 16.b.

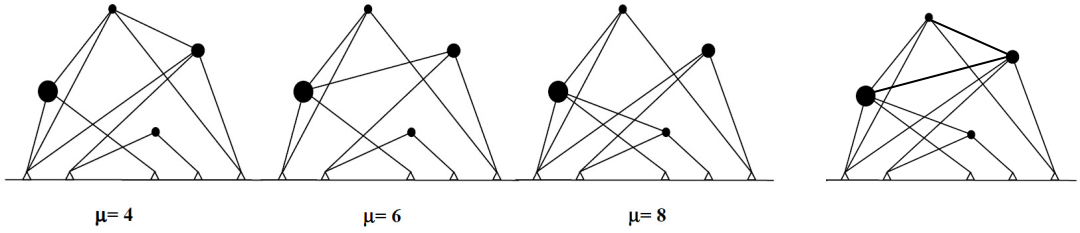

a. individual designs b. envelope design

Fig. 16. Optimum design for various acceptance criteria.

11. MOMENT RESISTING FRAMES

The optimum analysis discussed in Section 6 has been extended, and used for various structural systems. For a moment resisting frame, the acceptance criteria are assumed in accordance with FEMA 356 in which, the acceptable nonlinear rotation of beams and columns are given. In accordance with the rules set for optimum design in Section 6, the analysis consists of the following steps.

1. An arbitrary initial design is assumed.
2. The frame is subjected to the excitation and maximum plastic rotations of hinges are calculated.
3. The *COV* of maximum plastic rotations with respect to the acceptance limits is determined from the following equation.

$$COV = \frac{\sqrt{\sum_{i=1}^{n} (\theta_{mpi} - \theta_{ui})^2}}{\theta_{ave}} \quad , \tag{6}$$

Where

$$\theta_{ave} = \frac{1}{n} \sum_{i=1}^{n} \theta_{mpi}$$

where θui is the ultimate permissible rotation, and θmpi is the maximum plastic rotation of ith joint, respectively. If the *COV* is considered to be small enough, the procedure stops, and the frame is considered as practically optimum. Otherwise the procedure continues.

4. The distribution of structural properties is modified using the following equation.

$$[(SN)_{el}]_{k+1} = [(SN)_{el}]_k \left[\frac{\theta_{maxel}}{\theta_{ui}}\right]^{\alpha} \tag{7}$$

Where $[(SN)_{el}]_k$ and $[(SN)_{el}]_{k+1}$ are the cross section areas of the element, correspondingly, at steps k and $k+1$., and α is the convergence coefficient ranging from 0 to 1. For frames, a value of about α =0.02 was found to be convenient. $\theta maxel$ is the absolute maximum plastic rotation of hinges in the element *el* occurring during the analysis.

5. The frame is analyzed under gravity forces, and the stability is checked. For failing members, the strength increases to become stable. The analysis is iterated until *COV* becomes small enough and a status of rather uniform deformation prevails.

The details of this procedure are discussed in Moghaddam et al 2007. For example, the results of optimum analysis of the frames shown in Fig. 17 subjected to 5 different earthquakes are demonstrated in Fig. 18. It can be seen that in all cases, total weight of the frame is smoothly reduced and correspondingly, *COV* is also reduced. This indicates that the plastic rotations of hinges are approaching the ultimate permissible rotation. The *COV* does not reach zero (i.e. plastic rotations do not touch the ultimate permissible rotations) because of the limitation imposed on frame to sustain gravity forces. If this constraint was not present, many of the plastic rotations could reach the acceptance criterion, and *COV* could become zero.

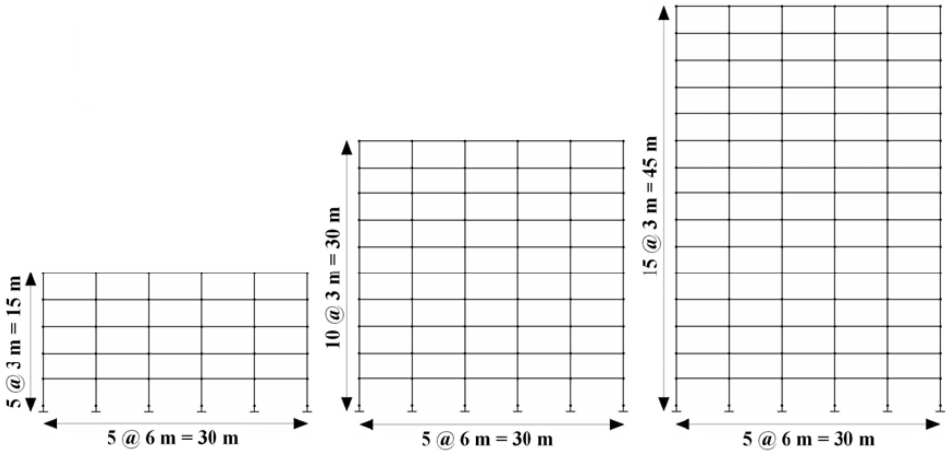

Fig. 17. Typical geometry of moment resisting frame*s*

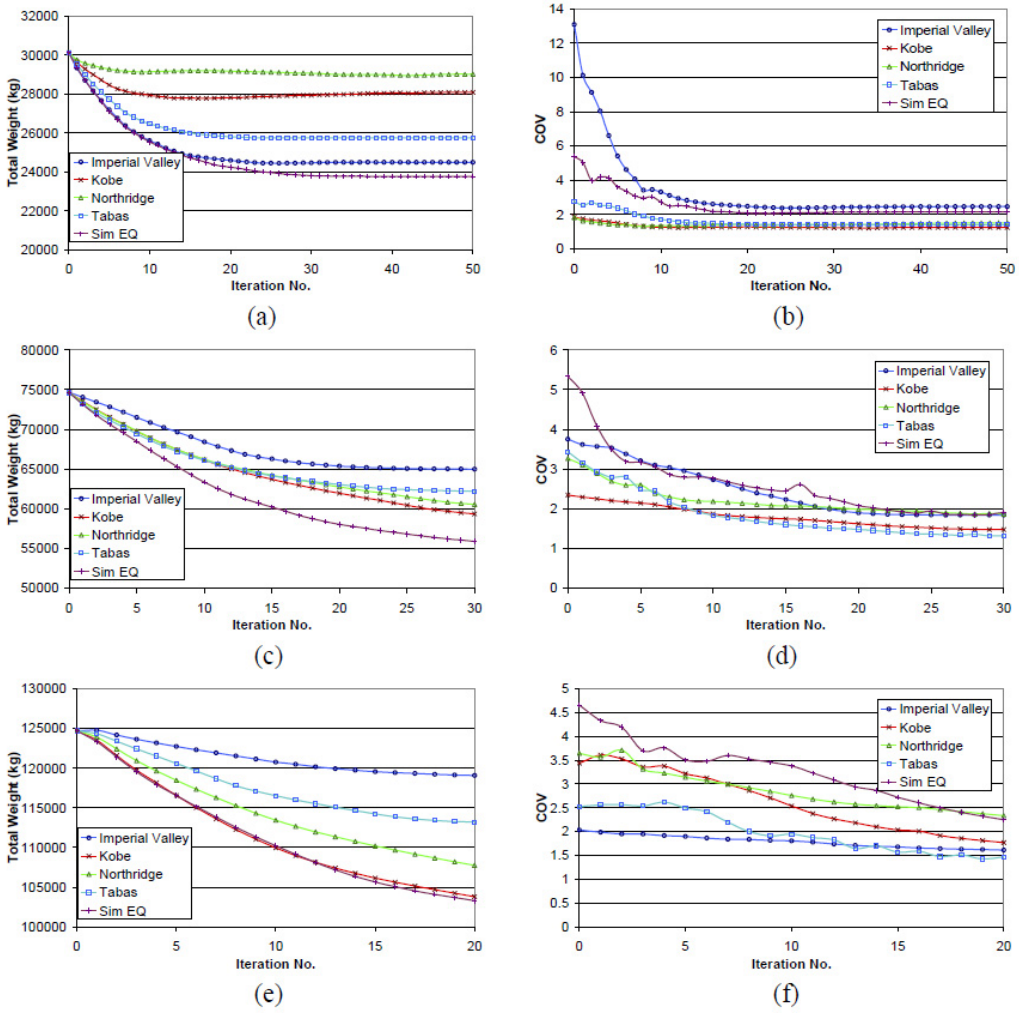

Fig. 18. (a), (c) and (e) Total weight reduction for 5, 10 and 15 story frames, respectively in 5 earthquakes (b), (d) and (f) COV variation for 5, 10 and 15 story frames, respectively in 5 earthquakes.

12. CONCENTRICALLY BRACED FRAMES

Optimum analysis in Section 6 was used for concentrically braced frames (Moghaddam et al, 2004).

As an example, a 15-story model designed in accordance to the Uniform Building Code (UBC) 1997, as shown in Figure 19, is considered to be laterally loaded for the Northridge earthquake 1994 (CNP196). The yield capacity in tension is set equal to the nominal tensile resistance, while the yield capacity in compression is set equal to 0.28 times the nominal compressive resistance as suggested by Jain et al 1980. The story drift is assumed as the acceptance criterion. The following conditions are also stipulated:

(a) The cross sections of beams and columns are not regarded as variables in the optimization procedures, and therefore they remain unchanged.

(b) All columns are checked for stability under the combination of gravitational loads and the dynamic seismic forces.

To obtain the optimum distribution of bracings, the evolutionary optimization method discussed in Section 6 is adapted as follows:

1. The model is already designed for gravitational and any arbitrary lateral load pattern for seismic loads. Here, the cross section area of bracings is assumed to be the only key parameter controlling the structural seismic behavior. However, as mentioned before, the columns have to be checked for stability. This is indeed a stipulating condition for the optimization program.
2. The structure is subjected to the given excitation, the peak values of inter-story drifts, $(\Delta)_i$, and the average of those values, Δ_{avg}, are determined. Consequently, the *COV* of inter-story drifts is calculated. If *COV* is small enough, distribution of bracing strength in each story can be considered as practically optimum. The *COV* of the first pattern is determined as 0.42. It is decided that the *COV* is high, and the analysis should be continued.
3. At this step the distribution of bracing cross section areas, as a parameter monotonically proportion to the shear strength of each story and hence to the total strength of the story, is modified. Using the *Theory of Uniform Deformations*, the inefficient material should be shifted from strong parts to the weak parts to obtain an optimum structure. To accomplish this, the cross section of bracings should be increased in the stories with peak inter-story drift greater than the average of peak drifts, Δ_{avg}, and should be decreased in the stories where peak inter-story drift is less than the average. The total cross section areas of all bracings in the frame is kept unchanged in order for the structural weight of the frame to be constant. This alteration should be applied incrementally to obtain convergence in numerical calculations. Hence, the following equation was used in the present work

$$[(A_b)_i]_{n+1} = [(A_b)_i]_n \left[\frac{(\Delta)_i}{\Delta_{avg}} \right]^{\alpha} \tag{8}$$

   where $(A_b)_i$ is the total cross section area of bracings at i^{th} story, n denotes the step number. As explained before, α is the convergence coefficient ranging from 0 to 1. For the above example, an acceptable convergence has been obtained for a value of α equals 0.2. Consequently, cross section areas of the bracings are scaled so that the total structural weight remains constant. Using these modified cross sections; the procedure is repeated from step 2. It is expected that the *COV* of peak inter-story drifts for this pattern is smaller than the corresponding *COV* for the previous pattern. This procedure is iterated until *COV* becomes small enough, and a state of rather uniform inter-story drift prevails.

Figure 20, illustrates the evolution of inter-story drift distribution from the UBC 97 Uniform Building Code (UBC) 1997 model toward the final optimum distribution. As it is shown in this figure, inter-story drifts in the final step have become remarkably uniform and the maximum inter-story drift has been decreased from 4.8 *cm* to 2.8 *cm*.

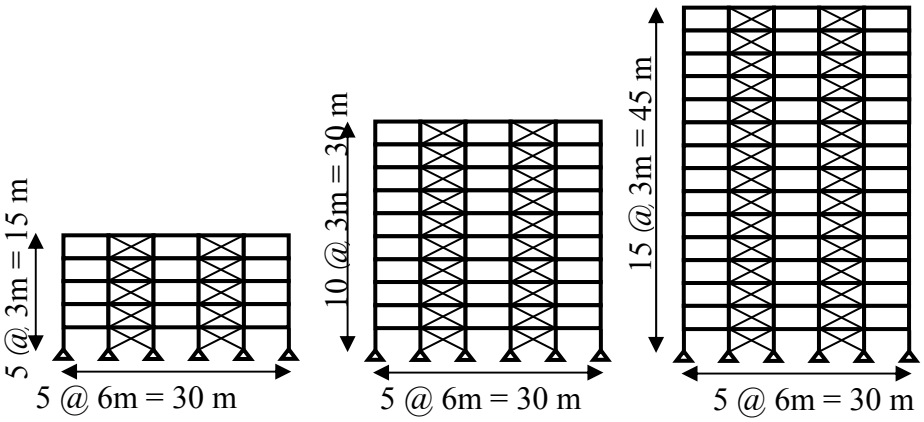

Fig. 19. Typical geometry of concentric braced frame.

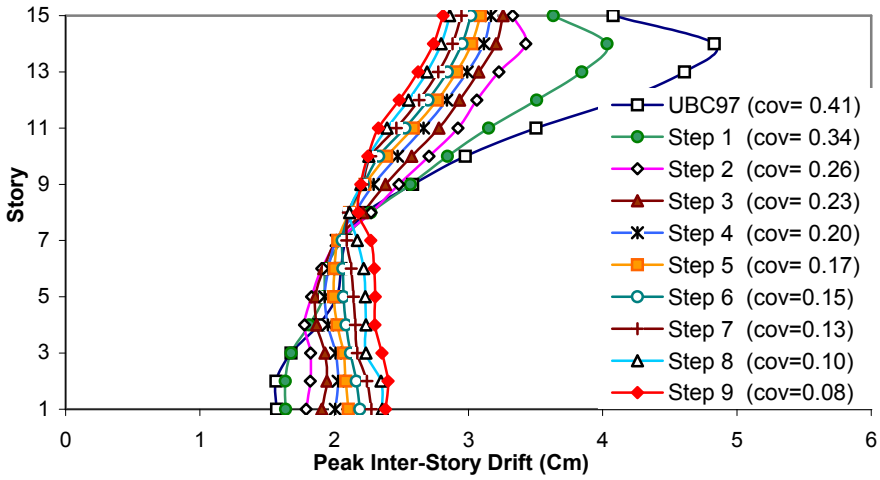

Fig. 20. Peak Inter-story drift distribution from UBC97 designed model toward the Final answer, 15 story braced frame, Northridge 1994 (CNP196).

13. RC FRAMES

The optimum analysis in Section 6 has been employed to evaluate the optimum longitudinal reinforcement pattern of RC frames (Moghaddam, Hajirasouliha, and Asadi 2007). The optimization target can be one of the damage indexes (*DI*) which is generally used to evaluate the performance of RC structures. In this study, Park and Ang damage index is employed for the global damage induced to the RC frames subjected to the seismic excitation. This damage index is based on scaled values of ductility and dissipated energy of the local element during the seismic excitation. Steel reinforcement, as compared with concrete materials, appears to be the more cost-effective material, which can be effectively used to control the damage in RC buildings. In this study, steel reinforcement ratios are taken as the design variables during the design optimization process. Park and Ang damage index, and Demand to Capacity Ratio (*DCR*) have been considered as damage index parameter for beams and column respectively. Since the

columns in the considered RC frames are mostly force control elements, Park and Ang damage index is not an appropriate indicator for their efficiency to carry earthquake loads. Considering the *Theory of Uniform Deformation*, it should be attempted to move toward a uniform damage distribution in all structural elements. For this purpose, the longitudinal reinforcements should be shifted from elements with lower damage index to the elements which experience higher damage subjected to the design seismic excitation. At this stage, the material strength capacity is fully exploited. To accomplish this, the following optimization procedure has been employed:

1. An arbitrary chosen frame is assumed as initial model.
2. The frame is subjected to the seismic excitation, and Park and Ang damage indexes for beams, and demand to capacity ratios, for columns are calculated.
3. The Coefficient of Variation (*COV*) of damage indexes for beams and columns is calculated. If the *COV* is small enough, the procedure stops, and the frame can be considered practically optimum. Otherwise the procedure continues.
4. At this stage the distribution of structural properties is modified. Experience has shown that this alteration should be applied incrementally in order to achieve convergence in the numerical calculations. Hence, the following modification factors are used in the present study:

$$k_{1i} = \left(\frac{d_i}{d_{ave}} \right)^{\alpha} \tag{9}$$

$$k_{2j} = \left(\frac{DCR_j}{DCR_{ave}} \right)^{\beta} \tag{10}$$

where d_i is the local damage index of the i^{th} beam and d_{ave} is the average of these values for all beams. Similarly, DCR_j is demand to capacity ratio for j^{th} column and DCR_{ave} is the average of these values for all columns. α and β are the convergence coefficients ranging from 0 to 1. Based on the results of this study, for RC frames, a value of 0.01 is convenient for both α and β. Subsequently, the longitudinal reinforcements in beams and columns are modified using the following equations:

$$\left[(A_{sbeam})_i \right]_{n+1} = \left[k_{1i} \right]_n \left[(A_{sbeam})_i \right]_n \tag{11}$$

$$\left[(A_{scol})_j \right]_{n+1} = \left[k_{2j} \right]_n \left[(A_{scol})_j \right]_n \tag{12}$$

where n denotes the step number, and A_{sbeam} and A_{scol} are cross section area of longitudinal reinforcements in beams and columns respectively. Subsequently, all of the longitudinal reinforcements are scaled such that the total reinforcement weight remains unchanged. The frame is then analyzed under gravitational forces to ensure that the frame can sustain the gravity loads. If any member fails, its longitudinal reinforcement is increased accordingly. The procedure is iterated until *COV* of damage indexes for beams and columns becomes small enough, and a status of rather uniform damage distribution prevails.

Five strong ground motion records were used to evaluate the seismic performance of the RC frames:

- Northridge (0.64g); Kobe (0.82g); Landers (0.25g); Cape Mendocino (0.66g) and a synthetic earthquake
- record generated using the SIMQKE program (Vanmarke 1976) to have a target spectrum close to that of
- the UBC 1997 code with a PGA of 0.44 g. All of these excitations correspond to the sites of soil profiles
- similar to the design site soil, SD, of UBC. The comparison between artificially generated spectra and the
- UBC 1997 design spectra is shown in Fig 21.

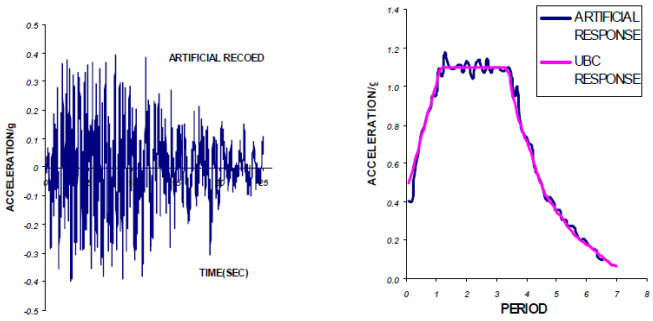

Fig. 21. A comparison of the UBC design spectrum with the synthetic earthquake.

5, 10 and 15 stories RC frames were optimized using the proposed method subjected to five selected earthquake events. The geometry and gravity loadings of the frames are assumed as identical to the steel frames in Fig. 17. The initial frames were designed according to UBC 1997 Code. Story damage distributions of the initial and optimum models are compared in Fig. 22.

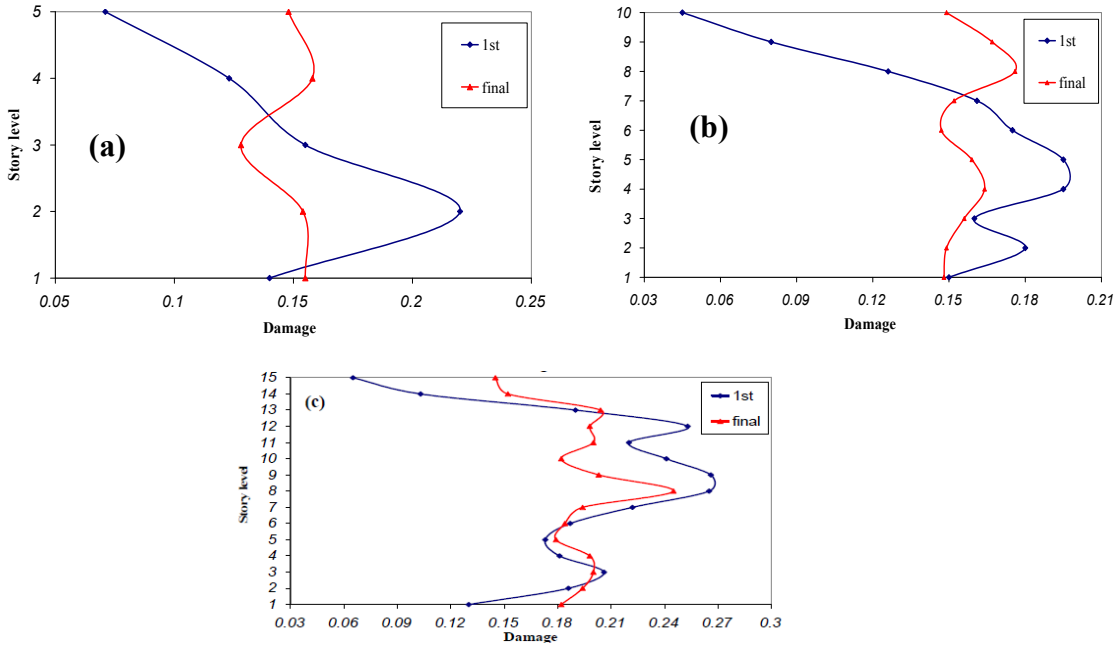

Fig. 22. Story damage distributions of the initial and optimum models subjected to the synthetic earthquake, (a): 5 story model; (b): 10 story model; (c): 15 story model.

This figure indicates that using the proposed optimization method leads to an almost uniform distribution of damage indexes within the structures. The global *DI* and *COV* of story damage indexes for the initial and optimum models are compared in Table 5. It is shown that having the same longitudinal reinforcement weight, the global *DI* has been considerably decreased in the optimum models compared to the conventional ones. The efficiency of the proposed optimization method has been emphasized by conducting the algorithm on different models and earthquake ground motions (Moghaddam, Hajirasouliha & Asadi 2007). Story damage distributions of the initial and optimum 10 story models are illustrated in Fig. 23 for different earthquake records.

Table 5.Comparison of Global *DI* and *COV* of story damage indexes for the initial and optimum models subjected to the synthetic earthquake.

MODEL	Global *DI* at 1st step	*COV* of Story Damage Indexes at 1st step	Global *DI* at Final step	*COV* of Story Damage Indexes at Final step
5	0.134	0.0206	0.108	0.0010
10	0.136	0.0168	0.122	0.0006
15	0.115	0.0182	0.109	0.0040

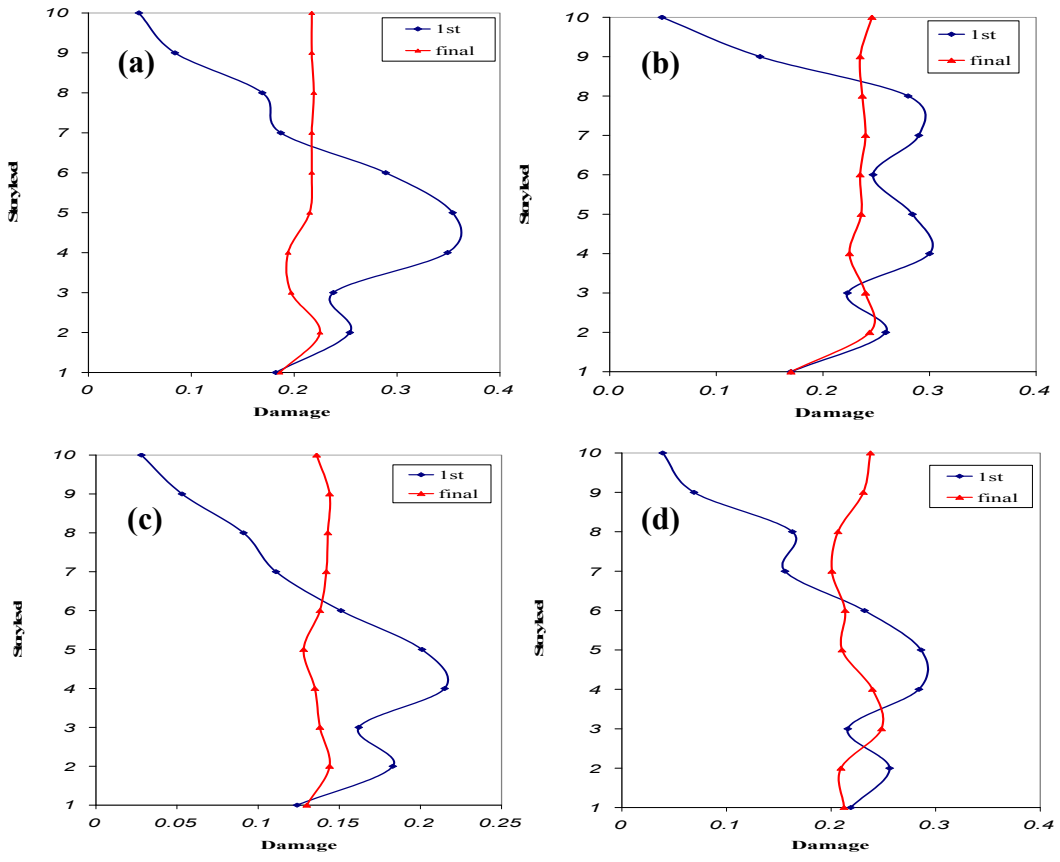

Fig. 23. Story damage distributions of the initial and optimum 10 story models subjected to (a) Northridge; (b) Kobe; (c) Landers; (d) Cape Mendocino.

14. CONCLUSIONS

1. This paper presents a new method for optimization of dynamic response of structures subjected to seismic excitation. This method is based on the concept of uniform distribution of deformation.
2. It is shown that using the load pattern suggested by seismic codes does not lead to a uniform distribution of deformation demand, and, it is possible to obtain uniform deformation by shifting the material from strong to weak parts. It has been shown that the seismic performance of such structure is optimal. Hence, it can be concluded that the condition of uniform deformation results in optimum use of material. This has been denoted as the *Theory of Uniform Deformation.*
3. By introducing an iterative method, *Theory of Uniform Deformation* has been adapted for optimum seismic design of shear buildings. It is concluded that this can efficiently provide an optimum design. It has been demonstrated that there is generally a unique optimum distribution of structural properties, which is independent of the seismic load pattern used for initial design.
4. For a set of earthquakes with similar characteristics, the optimum load-patterns were determined for a wide range of fundamental periods and target ductility demands. It is shown that, having the same story ductility demand, models designed according to the average of optimum load patterns have relatively less structural weight in comparison with those designed conventionally.
5. Considering the average of optimum patterns, more adequate load patterns have been introduced with respect to the fundamental period of the structure and the target ductility demand. The proposed patterns are illustrated in four categories including triangular pattern, trapezoid pattern, parabolic pattern and hyperbolic pattern. It is shown that, increasing the fundamental period is usually accompanied by increasing the loads at the top stories caused by the higher mode effects. Alternatively, increasing the ductility demand results in decreasing the loads at the top stories and increasing the loads at the lower stories.
6. This optimization method has also been used for performance based design of moment resisting frames, and concentrically braced frames, and RC frames. The results indicate that for each case, a unique optimum design can be obtained which is independent of the assumed initial design.
7. It has been demonstrated that in general an optimum design is affected by the amount of uncertainty in the parameters that control the design, such as the deformation capacity of the structural members.
8. It is shown that the constraint imposed to sustain stability for gravity loads, results in a slight increase of the structural weight as compared with an optimum design where this constraint is removed.

REFERENCES

Anderson, J.C., Miranda, E., Bertero, V.V., Kajima Research Team, 1991. Evaluation of the seismic performance of a thirty-story RC building, UCB/EERC-91/16, Berkeley: Earthquake Engineering Research Center, University of California.

ANSI-ASCE 7-95, 1996. Minimum Design Loads for Building and other Structures.

ATC-3-06 Report, Tentative provisions for the development of seismic regulations for buildings, San Francisco, California.

Chopra, A. K., 2001. Dynamics of structures: theory and applications to earthquake engineering, 2nd Edition, Prentice Hall Inc., London.

Diaz, O., Mendoza E., Esteva, L., 1994. Seismic ductility demands predicted by alternate models of building frames, Earthquake Spectra, Vol. 10, No.3, pp. 465-487.

FEMA 356, 2000. Prestandard and commentary for the seismic rehabilitation of buildings. Washington, DC: Federal Emergency Management Agency.

Gantes, C.J., Vayas, I., Spiliopoulos, A., 2000. Optimum Bending and Shear Stiffness Distribution for Performance Based Design of Rigid and Braced Multi-Story Steel Frames, Behavior of Steel Structures in Seismic Areas, pp 585-592.

Gilmore, T.A., Bertero, V.V., 1993. Seismic performance of a 30-story building located on soft soil and designed according to UBC 1991, UCB/EERC-93/04, Berkeley: Earthquake Engineering Research Center, University of California.

Green, N. B., 1981. Earthquake resistant building design and construction, 2nd Edition, Van Nostrand Reinhold Company, New York.

Hajirasouliha, I., 2004. Optimum strength distribution for seismic design of structures, D.Phil. thesis. Sharif University of Technology, Tehran, Iran.

Hart, G.C., 2000. Earthquake forces for the lateral force code, The Structural Design of Tall Buildings, pp. 49-64.

Iranian Code for Seismic Resistant Design of Buildings, 1999. 1st Ed., Building and Housing Research Center, Tehran.

Jain, A.K., Goel, S.C. and Hanson, R.D., 1980, "Hysteretic cycles of axially loaded steel members", *Journal of Structural Division*, ASCE, VOL.106, No.8, pp.1777-1795.

Karami Mohammadi, R., El Naggar, M.H., Moghaddam, H., 2004. Optimum strength distribution for seismic resistant shear buildings, International Journal of Solids and Structures, 41, pp. 6597-6612.

Lai, M. ,Li, Y., Zhang, Ch., 1992. Analysis method of multi-rigid-body model for earthquake responses of shear-type structure, WCEE 10th Conf., Madrid, Spain, pp.4013-4018.

Lee, S.S., Goel, S.C., 2001. Performance based seismic design of structures using target drift and yield mechanism, U.S Japan Seminar on Advanced Stability and Seismicity Concept for Performance Based Design of Steel and Composite Structures, Kyoto, Japan.

Martinelli, L., Perotti, F., Bozzi, A., 2000. Seismic design and response of a 14-story concentrically braced steel building, Behaviour of Steel Structures in Seismic Areas, pp 327-335.

Moghaddam, H., 1995. Earthquake Engineering, RTRC Publications, 1st Edition, Tehran, 1995 (in Persian).

Moghaddam, H., Esmailzadeh Hakimi, B., 1999. On the optimum seismic loading of multistory structures, 3rd International Conference on seismology and earthquake engineering, Tehran, Iran, pp.669-676.

Moghaddam, H., Hajirasouliha, I., 2004. A new approach for optimum design of structures under dynamic excitation, Asian Journal of Civil Engineering, Vol.5, pp. 69-84.

Moghaddam, H., Hajirasouliha, I., Doostan, A., 2003. On the optimum strength distribution in seismic design of structures, Response of Structures to Extreme Loading (XL2003), Canada, Toronto.

Moghaddam, H., Hajirasouliha, I., Doostan, A., 2004, Optimum seismic design of concentrically braced frames: concepts and design procedures, Journal of Constructional Steel Research, Vol 61/2, pp 151-166.

Moghaddam, H, Hajirasouliha, I, 2005, Fundamentals of Optimum performance-based design for dynamic excitations, Journal of Scientica Iranica, Vol 12, No. 4.

Moghaddam, H, Hajirasouliha, I., Rahemi M.A., 2007, Optimum Performance-based Design of Steel Moment Resistant Frames for seismic excitations. 5th inter national Conference on Seismology & Earthquake Engineering . May. Tehran . Iran

Moghaddam, H, Hajirasouliha, I., Asadi,P., 2007, Optimal design of reinforced concrete frames under seismic excitation., 5th international Conference on Seismology & Earthquake Engineering, May, Tehran . Iran

NEHRP, 1994. Recommended Provisions for the Development of Seismic Regulation for New Buildings, Building Seismic Safety Council, Washington, DC.

Prakash, V., Powell, G.H., Filippou, F.C., 1992. DRAIN-2DX: Base program user guide, Report No. UCB/SEMM-92/29.

Riddell, R., Hidalgo, P., Cruz, E., 1989. Response modification factors for earthquake resistant design of short period buildings, Earthquake Spectra, Vol 5, No. 3, pp. 571-590.

SEAOC. Vision 2000, 1995. Performance based seismic engineering for buildings. Sacramento, CA: Structural Engineers Association of California.

Uniform Building Code (UBC) 1997. International Conference of Building Officials, vol. 2.

Vidic, T, Fajfar, P, Fischinger, M., 1994. Consistent inelastic design spectra: strength and displacement, Journal of Earthquake Engineering and Structural Dynamics, Vol 23, pp. 507-521.

ENDURANCE TIME METHOD: FROM IDEATION TO APPLICATION

Homayoon E. Estekanchi[1], Abolhassan Vafai[2], and H. T. Riahi[3]

SUMMARY

Endurance Time (ET) method is an innovative dynamic pushover procedure in which structures are subjected to a gradually intensifying acceleration function and their performance is assessed based on their response at different excitation levels according to the specified performance objectives. The concept of the ET method is somewhat analogous to the exercise test used by cardiologists for assessing cardiovascular status of heart patients or athletes. Standard intensifying acceleration functions for ET analysis have been produced using numerical procedures and optimization techniques. For quantitative comparisons, the acceleration functions have been calibrated in such a way that their response spectrum remains proportional to a template spectrum with a linearly increasing proportionality factor. Thus, induced accelerations and displacements increase linearly with time. It has been shown that by using the average of three acceleration functions, acceptable convergence and accuracy can been achieved for linear SDOF and MDOF systems. Consistency of the results with codified procedures has been discussed. It is shown that nonlinear response of moment frames can also be estimated with reasonable accuracy by this method.

Keywords: Dynamic Pushover, Endurance Time Analysis, Performance Based Design, Response History Analysis

1. INTRODUCTION

The common philosophy of seismic design codes is to achieve the dual goal of keeping the non structural damage to a minimum in the case of service level earthquakes and ,also, to prevent structural failure in the case of collapse level earthquakes [Newmark, 1971]. Apparent shortcomings in traditional seismic design methods, along with remarkable developments in the field of information technology and the availability of vastly improved analytical tools, has encouraged researchers and engineers to seek for more rational and consistent methods for seismic resistant design of structures. There have been remarkable developments in this area in recent years. Nonlinear pushover and time-history analyses are becoming standard practice in engineering design offices. Various procedures are now available to predict nonlinear response of the structure through a pushover analysis [Chopra and Goel, 1999, 2003]. Incremental dynamic procedure is another alternative to predict realistic dynamic seismic behaviour of structures [Vamvatsikos and Cornell, 2003, 2005]. Extensive research is currently underway in the direction of realization of Performance Based Seismic Engineering objectives [Bozorgnia and Bertero, 2004; Bertero and Bertero, 2002]. Thanks to these recent developments, it has become possible for the structural analyst to incorporate the most significant nonlinear material and geometric behaviour into the model and perform a more realistic analysis of structural behaviour during seismic events [Chopra, 1995; FEMA, 2005]. Based on recent developments, it can be predicted that design procedures based on nonlinear time-history analysis will become more popular in near future. This is mostly due to the fact that time-history analysis is the only

[1] *Associate Professor, Sharif University of Technology, Tehran, Email : stkanchi@sharif.edu*
[2] *Professor, Sharif University of Technology, Tehran, Email: vafai@sharif.edu*
[3] *PhD candidate, Department of Civil Engineering, Sharif University of Technology, Tehran, Email: h_tajmir@yahoo.com*

procedure that allows direct incorporation of nearly all types of nonlinear and time dependant effects in the analysis.

In this paper, an innovative dynamic pushover procedure for seismic analysis and evaluation of structures that is based on time-history analysis is presented. The concept of the method, called Endurance Time (ET) method [Estekanchi et. al, 2004], can be explained by a hypothetical shaking table experiment. It is assumed that three model buildings with unknown dynamic properties are to be investigated with reference to their performance against seismic type dynamic loading. Let's consider that these models are put on a shaking table and fixed to it as shown in Figure 1. The experiment starts by subjecting the buildings into a dynamic excitation with very low amplitude and then gradually increasing the intensity. As the amplitude of vibration is increased with time (say, at t=8 sec), a point is reached when one of the buildings collapses. Assume that this happens to be model "A" in Figure 1. As time passes and the vibration amplitude is further increased (say, at t=13 sec), the second structure fails. Assume this to be building "C" in Figure 1. Further, consider that building "B" happens to be the last building to fail in this hypothetical experiment (at t=18 sec). Now, based on this experiment, it is concluded that building "B", which endured longer, has the best performance, while building "A", which failed soonest, performed the worst. Note that the judgment is based on the evident performance of each structure, which in this case turns out to be the maximum time during which each building remained stable, without any direct reference to the building strength or stiffness or other dynamic characteristics. If the goal was to evaluate the building's resistance to collapse, then, such experiment seems to show a relevant measure [Estekanchi et. al. 2008].

In ET method, seismic resistance is investigated based on the response to an intensifying excitation as a continuous function of time. The idea of the Endurance Time method is similar to the method used by cardiologists to evaluate the cardiovascular condition of the heart patients, known as exercise test (or stress test). In exercise test, the patient is asked to walk on a tread-mill with a variable slope and speed. The test starts with a low slope and low speed condition. During the test, the slope and speed are increased gradually, while the physical and biological condition of the patient, such as blood pressure, heart beat rate, etc are monitored. The test is commenced until signs of distress or abnormal conditions are observed. The cardiovascular condition is then judged on the basis of the speed and slope level that could be tolerated [Stewart, Kittelson, and Kay, 2000].

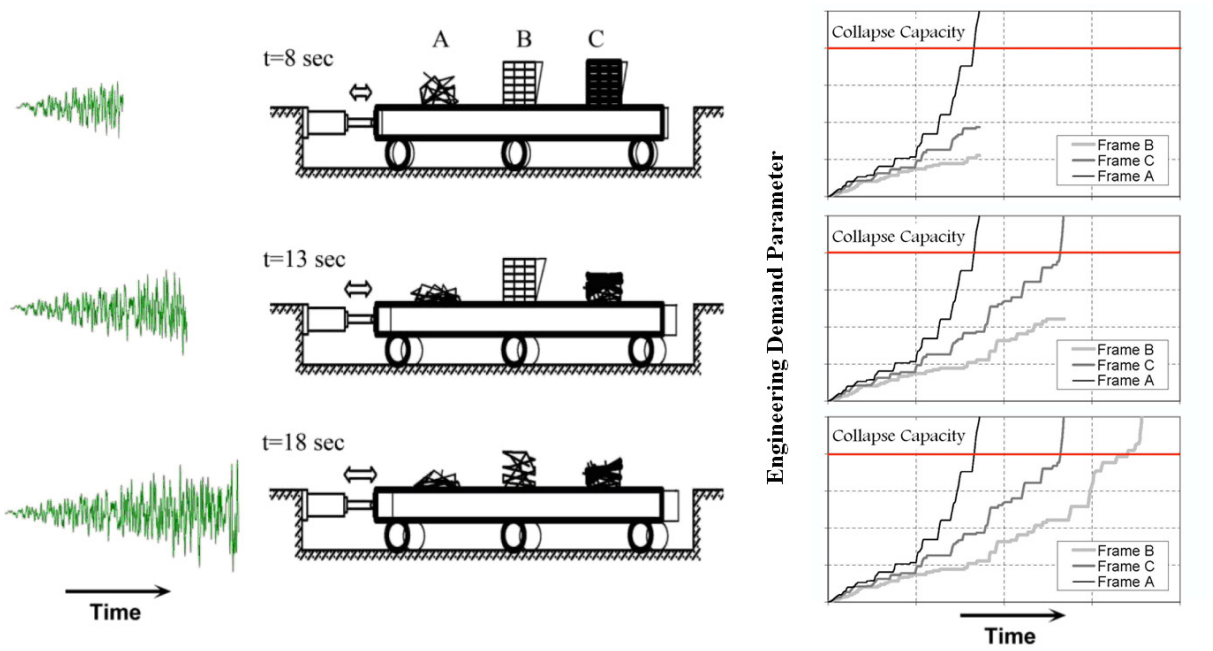

Fig. 1. ET hypothetical test on shaking table.

In the Endurance Time method, nearly the same concept is applied. The idea behind ET method is roughly to put the structure on a ramp-like acceleration function and see how far it can go. The structure is subjected to a specially designed acceleration function with intensifying dynamic demand. The relevant performance indexes such as maximum stresses, displacements, plastic hinge rotations, etc, are monitored until they reach a limiting value. The performance of the structure is judged on the basis of the time when the damage limit is exceeded. Various damage indexes and structural criteria can be considered simultaneously in order to reach more conclusive results. The big question here is weather an intensifying acceleration function can be designed in such a way that the results from such a test or analysis can be useful in practice. In other words, how well can we expect the results from such analysis or test to be correlated to seismic analysis results? In this paper, the basic concepts and practical application of ET method has been explained.

2. ET ACCELERATION FUNCTIONS

The choice of an appropriate dynamic input is fundamental to the successful implementation of the ET concept. The ideal input function is the one that results in highest consistency and best correlation between the endurance time analysis results and the actual or well known performance characteristics of the structures subjected to ground motions scaled according to desired return periods.

2.1 Intensifying Acceleration Functions

By using numerical optimization techniques, ET acceleration functions with the property of having a response spectrum that while remaining compatible to a desired template response spectrum, proportionally intensifies with time are created. This implies that the response

spectrum of any window of these acceleration functions from t_0=0 to t_1=t resembles that of the pre-specified response spectrum with a scale factor that increases linearly with time (t). The response spectrum of the Iranian National Building Code (INBC) standard 2800 [BHRC, 2005], considering soil type II (relatively stiff soil, Vs=375~750 m/s, T_0=0.1 sec, T_s=0.5 sec) and a very high seismicity area (A=0.35g), has been considered as a basis for calculating a set of ET acceleration functions. This design spectrum is given by formulas (1).

$$\begin{cases} B = 1 + S(\dfrac{T}{T_0}) & T < T_0 \\ B = 1 + S & T_0 \le T < T_s \\ B = (1+S)(\dfrac{T_s}{T})^{\frac{2}{3}} & T_s \le T \end{cases} \qquad S_{aC} = \frac{ABI}{R_c} \tag{1}$$

where T is period of free vibration, T_0 and T_s are soil factors, S is 1.5 and B is building response factor. Importance factor (I) and response reduction factor (R_c) have not been applied (assumed equal to 1.0) in generating the acceleration functions.

ET acceleration functions are designed so that at some predefined time, t_{Target}, their scale factor relative to the template codified spectrum reaches unity. Therefore, structures that satisfy the code requirement up to $t = t_{Target}$ can be considered as code compliant. A major difference between an ET acceleration function and an ordinary response spectrum compliant accelerogram is that in an ET acceleration function, time is a significant dimension that indicates the amplitude of excitation. Based on engineering judgment and until more research has been done, a linear intensification with time will be applied to the spectrum of ET acceleration functions. The response spectrum for ET acceleration functions is defined as follows:

$$\begin{aligned} S_u(T,t) &= \max(|u(\tau)|) \quad \tau \in [0,t] \\ S_a(T,t) &= \max(|a(\tau)|) \quad \tau \in [0,t] \end{aligned} \tag{2}$$

where u is displacement, a is acceleration and t is time. Time proportionality of the ET acceleration functions response spectra can be described by formulas (3) as follows:

$$\begin{aligned} S_{aC}(T,t) &= \frac{t}{t_{Target}} S_{aC}(T) \\ S_{uC}(T,t) &= \frac{t}{t_{Target}} S_{aC}(T) \times \frac{T^2}{4\pi^2} \end{aligned} \tag{3}$$

where T represents periods of free vibration, t_{Target} is target time (equal to 10 seconds in this study) and S_{aC} is codified acceleration spectrum. Analytical approaches to find acceleration functions that satisfy conditions stated in equations 3 are formidably complicated. The problem has been formulated as an optimization problem as follows:

$$\text{Minimize } F(a_g) = \int_0^{T_{\max}} \int_0^{t_{\max}} \{[S_a(T,t) - S_{aC}(T,t)]^2 + \alpha[S_u(T,t) - S_{uC}(T,t)]^2\} dt\, dT \tag{4}$$

Acceleration data points have been considered as the variables and the problem is solved considering 200 different periods distributed in the range of 0.0 to 5.0 seconds. Three acceleration functions have been generated using this procedure. These are named ETA20a01-03, respectively. Figure 2 shows a typical ET acceleration function obtained in this manner.

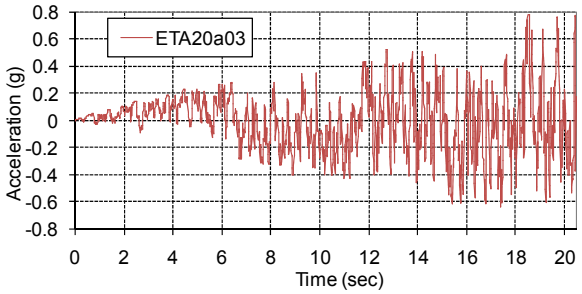

Fig. 2. A typical intensifying acceleration function (ETA20a03).

The response spectra of ETA20a01-03 at various specified times are depicted in Figure 3. It is interesting to note that the convergence of solutions in the optimization problem has been quite satisfactory and the response spectrum intensifies in a uniform manner with time, as desired.

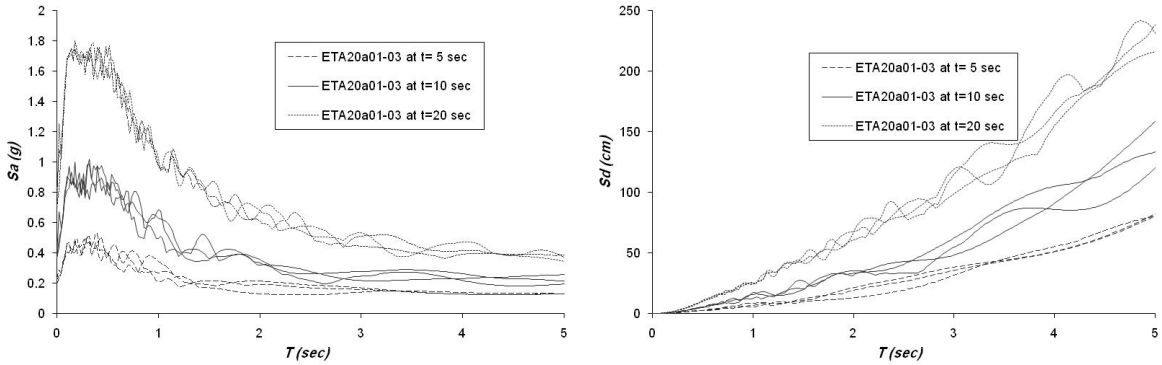

Fig. 3. Response spectrum of ETA20a01-03 at various times (ξ=5%).

3. LINEAR ANALYSIS OF STEEL FRAMES

Various model frames have been designed according to the AISC-ASD specifications. Typical frame geometry and section properties are depicted in Figure 4.

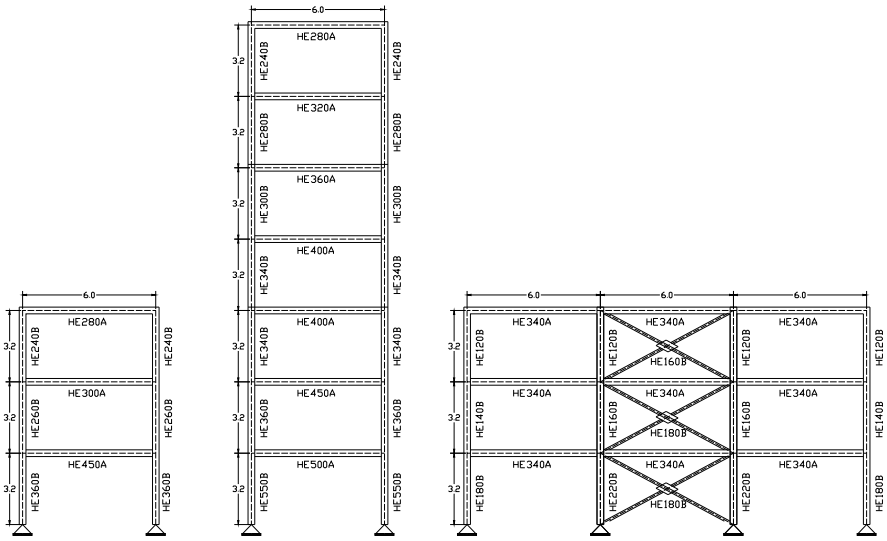

Fig. 4. Typical moment and braced steel frames.

In Figure 5, maximum drifts from three ET analyses, along with their averages at t=10s, are compared to static and response spectrum analysis results. As the number of stories increase, the results start to diverge from each other. However, even in the case of taller frames, maximum differences are below 10%. In general, where response spectrum analysis results tend to diverge from static analysis results, ET analysis results are more compliant with the response spectrum results. This could be expected considering the fact that ET and response spectrum analyses are both of a dynamic nature and can better predict the behaviour of tall frames where the effect of higher modes becomes significant [Estekanchi et. al., 2007].

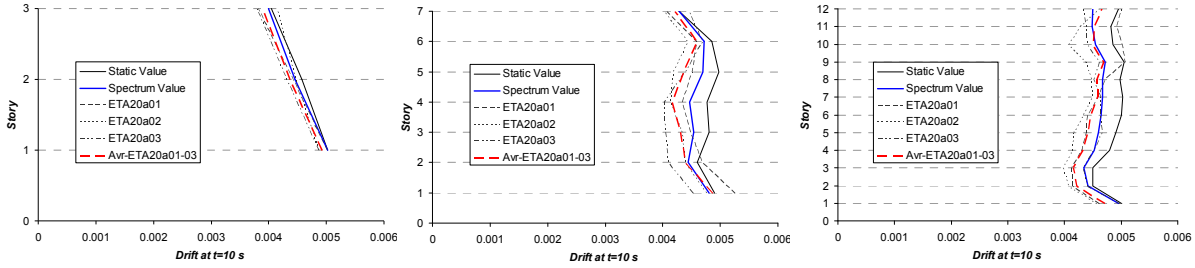

Fig. 5. Story drift at target time t=10 sec, (a) FM03B1 (b) FM07B1 (c) FM12B3.

3.1 Calibration for Codified Application

Response Spectrum (RS) analysis is a well known procedure for structures that are categorized as irregular by the code. Even in case of regular structures, the response spectrum analysis is considered superior as compared to equivalent static procedure. When ET acceleration functions that are compatible with code specified design spectrum are used in ET analysis, the analysis results of this procedure can be directly related to the results from RS analysis. When the template spectrum of the ET acceleration functions are matched with the same design spectrum, a single scaling factor can be applied to the set of acceleration functions as shown in Figure 6.

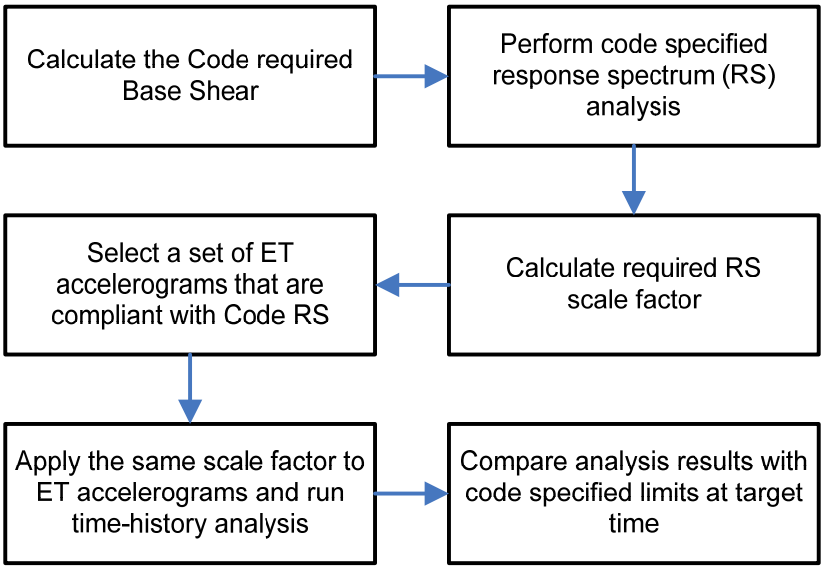

Fig. 6. Code compliant linear ET analysis.

A typical plot of design ratio of a column has been depicted in Figure 7. In the first three seconds, the Dead + Live load combination case has dominated the resulting maximum ratio and, therefore, this part of the curve has remained horizontal. After that, the ratio obtained through ET analysis follows a linearly increasing path. It can be seen that the design ratio exceeds 1.0 at about 10.5s considering the average of the ET analyses. The design ratio from static analysis has been about 0.87 and has been exceeded at about t=9.5s, the theoretical value for this being t=10s. It should also be noted that the design ratio for the same member, when using response spectrum analysis results with a scaled base shear of V_{static}, is about 1.05. This increase over the static value is due to the assumption of moments being applied with a similar sign, i.e. single curvature bending [Estekanchi et. al., 2007].

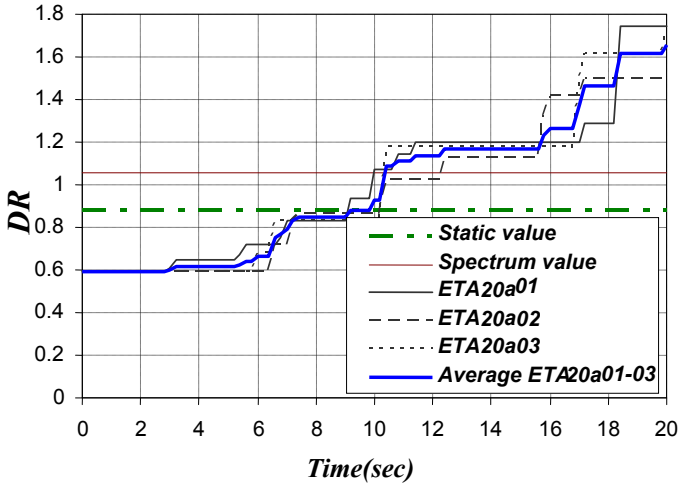

Fig. 7. Design ratio of FM07B4_S4.

4. APPLICATION TO NON-LINEAR ANALYSIS

The ET method can be readily applied to the case of nonlinear analysis with no significant complication. ET analysis can be considered as a dynamic pushover procedure, where the applied accelerogram is an increasing function of time. Three ET acceleration functions used in this part (ETA20f set) are generated in such a way that their response spectra remains proportional to that of the average of seven ground motions recorded on a stiff soil condition [Riahi and Estekanchi, 2006]. The average response spectrum is smoothed and used for generation of ETA20f set (Figure 8). Characteristics of the selected ground motions are shown in Table 1.

Table 1. Characteristics of 7 ground motions used in this study.

Date	*Earthquake Name*	*Magnitude (Ms)*	*Station Number*	*Component (deg)*	*PGA (cm/s^2)*
06/28/92	Landers	7.5	12149	0	167.8
10/17/89	Loma Prieta	7.1	58065	0	494.5
10/17/89	Loma Prieta	7.1	47006	67	349.1
10/17/89	Loma Prieta	7.1	58135	360	433.1
10/17/89	Loma Prieta	7.1	1652	270	239.4
04/24/84	Morgan Hill	6.1	57383	90	280.4
01/17/94	Northridge	6.8	24278	360	504.2

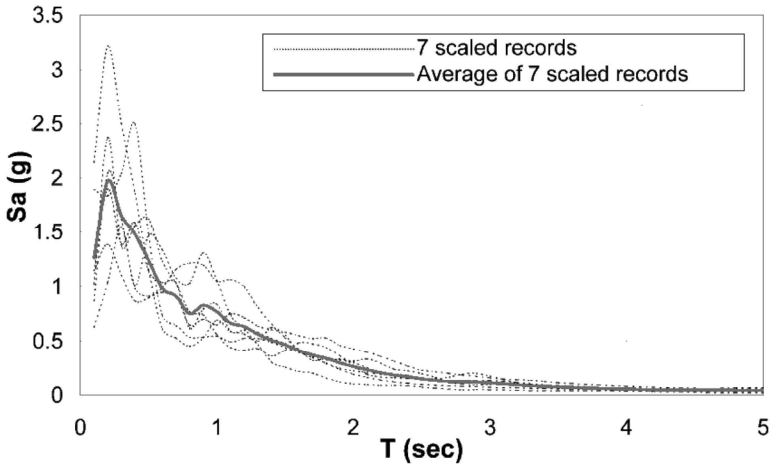

Fig. 8. Average response spectrum from selected ground motions (ξ=5%).

The response spectrum of any window of ETA20f set of acceleration functions from t_0=0 to t_1=t resembles that of the average response spectrum of seven ground motions with a scale factor that is proportional with time (t) as shown in Figure 9. This scale factor is equal to 1.0 for t_{Target}=10 sec in this study [Riahi et. al. 2009].

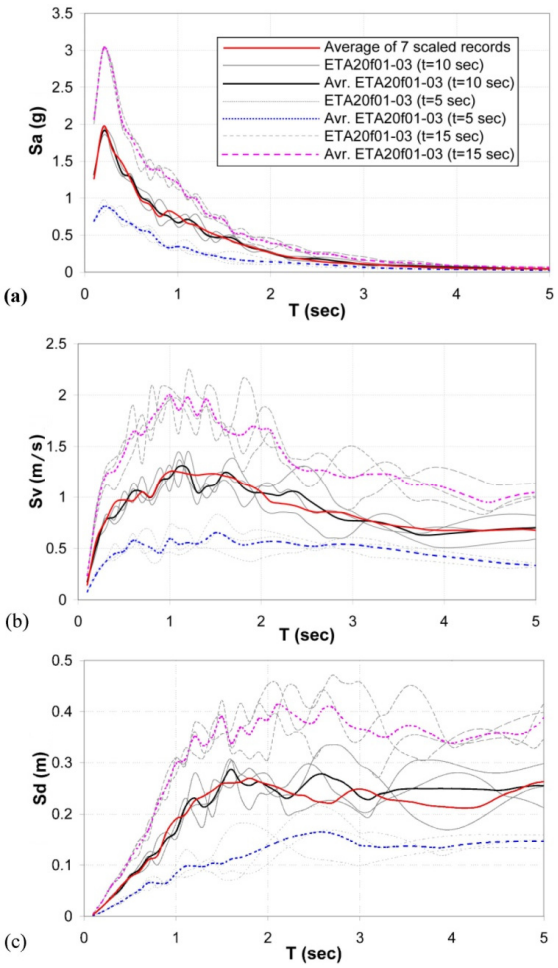

Fig. 9. Response spectra of ETA20f series acceleration functions for ξ=5% at different time. a) total acceleration. b) velocity response c) displacement response.

Average acceleration response spectra for scaled accelerograms are compared with the average of total acceleration spectra for ETA20f series for different strength ratio (R) values in Figure 10. Results show the acceptable compatibility between these acceleration functions and ground motions in nonlinear range. There are some differences between the results of ET acceleration functions and real records but a systematic difference is not significant [Riahi et. al. 2009].

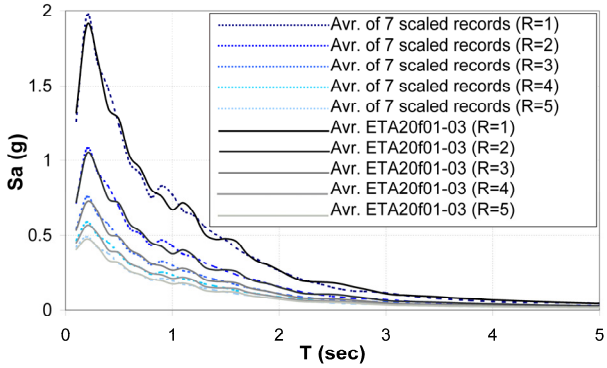

Fig. 10. Comparison of average of total acceleration spectra for 7 scaled accelerograms and ETA20f series for different R values (ξ=5%.).

In order to verify the results of ET analysis in the nonlinear range, a set of steel frames consisting of two-dimensional regular generic frames with 3, 7 and 12 stories that have a single bay or three bays are investigated. Generic frames of this study are adopted from the models developed by Estekanchi et al. (2007). These frames are designed according to Iranian National Building Code (INBC) that is almost identical with AISC ASD design recommendations. Each frame is designed in three alternatives regarding the intensity levels of design lateral loads. Standard frames (S) match codified base shear, under-designed (W) frames are designed based on one half of the codified base shear and overdesigned frames (O) have been designed for twice the codified base shear. Frame masses are assumed to be the same for these three kinds of frames for ease of comparison. In standard and overdesigned frames, story drift was the controlling design criteria but in underdesigned frames, element forces control the design. Some major dynamic properties of these frames are shown in Table 2 [Riahi et. al. 2009].

Table 2. Specifications of the frames.

Frames	Number of Stories	Number of Bays	Total Mass ($KN.sec^2/m$)	Mass participation Mode 1	Period of free vibration (sec)	Design base shear (KN)
FM03B1RGW	3	1	81.47	90.98%	1.20	59.7
FM03B1RGS	3	1	81.47	88.03%	0.89	116.32
FM03B1RGO	3	1	81.47	85.15%	0.60	244.92
FM03B3RGW	3	3	244.40	88.57%	1.25	179.3
FM03B3RGS	3	3	244.40	85.71%	0.89	362.17
FM03B3RGO	3	3	244.40	85.64%	0.61	729.26
FM07B1RGW	7	1	190.09	81.18%	2.03	101.38
FM07B1RGS	7	1	190.09	80.60%	1.43	204.78
FM07B1RGO	7	1	190.09	80.56%	0.99	414.92
FM07B3RGW	7	3	570.28	81.25%	2.05	302.34
FM07B3RGS	7	3	570.28	80.92%	1.44	609.77
FM07B3RGO	7	3	570.28	80.40%	0.97	1233.41
FM12B3RGW	12	3	977.61	79.32%	2.89	399.2
FM12B3RGS	12	3	977.61	78.43%	2.05	804.38
FM12B3RGO	12	3	977.61	75.17%	1.30	1631.52

Figure 11 compares the maximum interstory drift ratio at each story level obtained by ET, standard pushover and time history analyses for FM07B3RGS, FM07B3RGW, FM12B3RGS and FM12B3RGW frames. Maximum interstory drift ratios of pushover analysis are taken from the deformed shape of the frame when it reaches its target displacement. Although results of ET analysis and time history analysis have some differences but predictions of these two methods are mostly close together.

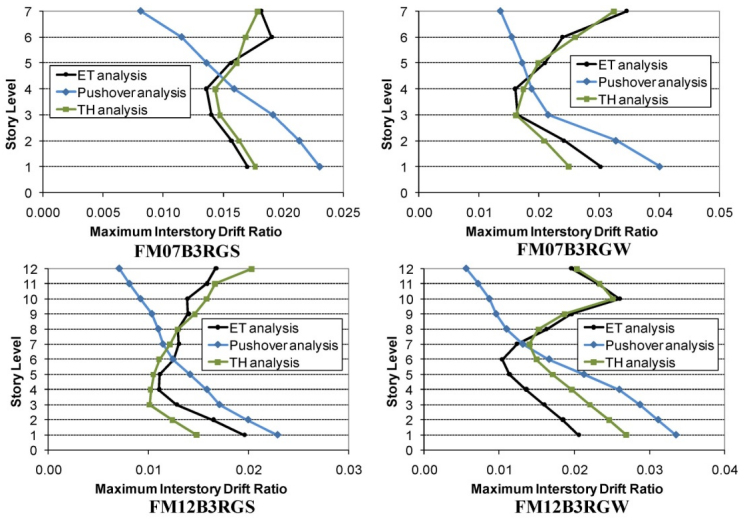

Fig. 11. Comparison of maximum interstory drift ratios of FM07B3RGS, FM07B3RGW, FM12B3RGS and FM12B3RGW frames at different story levels obtained by ET, pushover and time history analyses.

Figure 12 shows maximum plastic hinge rotations of FM07B3RGS frame from three methods. Size of the circles is proportional to the value of plastic rotation. As can be seen, ET analysis has predicted plastic hinge rotations at top stories with reasonable accuracy.

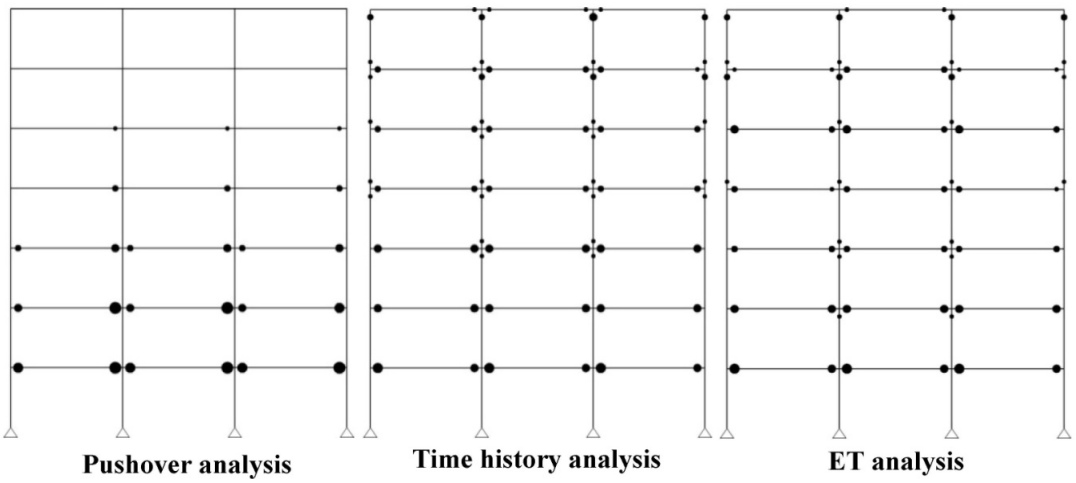

Fig. 12. Comparison of maximum plastic hinge rotation in time history analysis, ET analysis and pushover analysis for FM07B3RGS frame.

Correlation between maximum interstory drift ratios calculated from ET method and time history analysis at different IMs is shown in Figure 13. This figure summarizes the results of 630 nonlinear time history analyses and 45 ET analyses. The coefficient of determination (R squared value=0.95) is near unity and it shows fine correlation between the results. In addition, the linear relation with coefficient near one (0.96) shows that ET acceleration functions keep their intensifying trend with time in nonlinear states with acceptable accuracy. By increasing IMs, Engineering Demand Parameters obtained by the methods are increased and their differences

with linear trend line are increased. For underdesigned frames that experience more nonlinearity, maximum difference between correlation points and linear trend line can be observed.

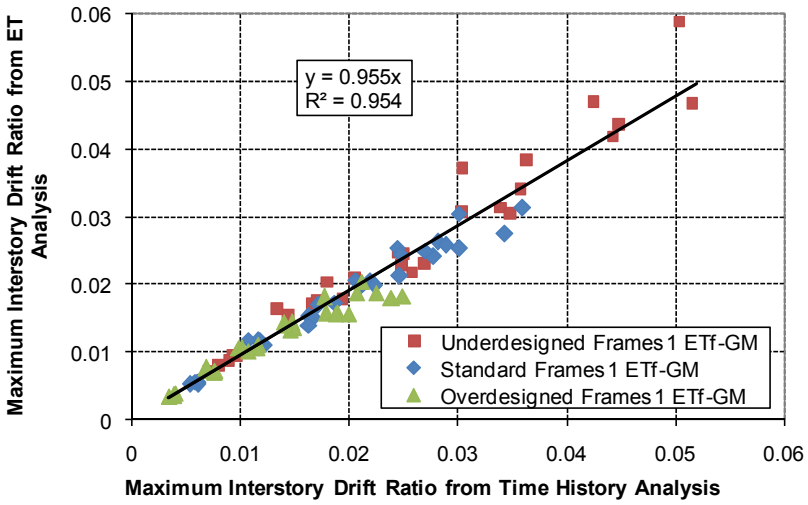

Fig. 13. Correlation between maximum interstory drift ratios obtained from ET analysis and time history analysis for different frames at different IMs (ETA20f and GM1 sets).

5. SUMMARY AND CONCLUSIONS

In Endurance Time (ET) method structures are subjected to a gradually intensifying acceleration function and their performance is judged based on their dynamic response at various intensity levels. The basic concept of the ET method is very similar to the exercise test used by cardiologists for assessing the condition of heart patients and athletes. Analysis results from two sets of intensifying acceleration functions are used in this paper in order to demonstrate the application of ET analysis. In these acceleration functions, the response spectrum of each window of the acceleration function from t=0 to t=t_1, while remaining proportional with a template spectrum, magnifies linearly with time. In the first set, the template spectrum has been driven from seismic code specifications, while in the second set used for nonlinear comparative study, the smoothed average response spectrum of selected ground motions is used as template. Different design criteria can be considered in ET analysis based on the design objective. The results of ET analysis are shown to be consistent with response spectrum procedure. A method for calibration of ET analysis results to meet code requirements has been proposed. ET method can be extended for application in nonlinear analysis of various structures. Results from nonlinear response analysis of steel moment frames show acceptable accuracy in predicting response history analysis results from ground motions. It can be concluded that when a time-history base analysis seems to be most appropriate method, i.e. when various sources of complicated nonlinear behavior are to be investigated, the ET method can be considered as an alternative analysis procedure. Application of ET method in seismic analysis of non-building structures such as reservoirs, dams, shell structures and bridges is currently underway by the authors. By reducing the number of required response history analyses and bridging the gap between static and complete response history procedures, ET method has a potential to pave the way towards practical performance based design of structures using nonlinear response history analysis. This advantage of ET method also makes it a good candidate for application in experimental seismic analysis, were the number of required experiments is a critical factor.

However, more research in this area is required before ET method can be recommended in practical applications.

ACKNOWLEDGEMENT

The authors would like to thank the Sharif University of Technology Research Council, and the Structures and Earthquake Engineering Center of Excellence (SECE) for their support of this research.

REFERENCES

Behfar, K., Estekanchi, H. E., and Vafai, A. (2004). "An analytical approach for generating design response spectra compatible accelerograms." The Seventh International Conference on Computational Structures Technology, Lisbon, Portugal 7-9 Sep, 2004

Bertero, R. D. and Bertero, V. V. (2002). "Performance-based seismic engineering: the need for a reliable conceptual comprehensive approach", Earthquake Engineering and Structural Dynamics, 31, 3, Mar. 2002, pages 627-652

BHRC (2005). Iranian code of practice for seismic resistant design of buildings, standard No. 2800-05, 3rd edition, Building and Housing Research Center, Tehran.

Bozorgnia Y. and Bertero V. V. (2004). Earthquake engineering: from engineering seismology to performance-based engineering, CRC Press, USA.

Chopra A. K. and Goel, R. K. (2003), "A modal pushover analysis procedure to estimate seismic demands for buildings: Summary and Evaluation", Fifth national conference on Earthquake Engineering, 26-30 May 2003, Istanbul, Turkey

Chopra A. K., Goel R. K. (1999), "capacity_demand-diagram methods for estimating seismic deformation of inelastic structures: SDF systems", Report No. PEER-1999/02 Pacific earthquake engineering research center, college of engineering, University of California, Berkeley

Chopra A. K. (1995), "Dynamics of structures: theory and applications to earthquake engineering", Prentice Hall International Series in Civil Engineering and Engineering Mechanics, Prentice Hall, Englewood Cliffs, New Jersey, 1995

Estekanchi, H. E., Vafai, A. and Sadeghazar, M. (2004). "Endurance time method for seismic analysis and design of structures", Scientia Iranica, Vol. 11, No. 4, pp 361-370

Estekanchi, H.E., Riahi, H.T. and Vafai, A (2006), "Endurance Time Method: A Dynamic Pushover Procedure for Seismic Evaluation of Structures", First European Conference on Earthquake Engineering and Seismology, Geneva, Switzerland, 3-8 September 2006, Paper Number: 443

Estekanchi, H.E., Valamanesh, V. and Vafai, A. (2007), "Application of Endurance Time Method in Linear Seismic Analysis", Engineering Structures, Vol. 29, No. 10, pp 2551-2562

Estekanchi H.E., Riahi H.T. and Vafai A., (2008) "Endurance Time Method: Exercise Test for Seismic Assessment of Structures" 14th World Conference on Earthquake Engineering, Beijing.

Estekanchi, H. E., Arjomandi, K and Vafai, A. (2008), "Estimating Structural Damage of Steel Moment Frames by Endurance Time Method", Journal of Constructional Steel Research, Vol. 64, No. 2, pp 145-15

FEMA, (2005). Improvement of nonlinear static seismic analysis procedures, FEMA-440, Federal Emergency Management Agency, Washington DC.

Newmark, N. M. (1971), Fundamentals of Earthquake Engineering, Prentice-Hall, Englewood Cliffs

Riahi, H.T. and Estekanchi, H.E., (2006), "Application of Endurance Time Method for Estimating Maximum Deformation Demands of Structures", First European Conference on Earthquake Engineering and Seismology, Geneva, Switzerland, 3-8 September 2006, Paper Number: 872

Riahi, H.T., Estekanchi, H.E., and Vafai, A., (2009) "Endurance Time Method - Application in Nonlinear Seismic Analysis of SDOF Systems". Journal of Applied Sciences, 9 (10): 1817-1832, 2009.

Riahi H.T., Estekanchi H.E. and Vafai A. (2009), "Estimates of average inelastic deformation demands for regular steel frames by Endurance Time method", To appear in the journal of Scientia Iranica (Accepted)

Stewart R.A., Kittelson, J., and Kay I. P. (2000). "Statistical methods to improve the precision of the treadmill exercise test". J. Am. Coll. Cardiol. Oct; 36(4):1274-9

Vamvatsikos, D., and Cornell, C. A. (2005). Seismic performance, capacity and reliability of structures as seen through incremental dynamic analysis, The John. A Blume earthquake engineering center, Stanford University

Vamvatsikos, D., and Cornell, C. A. (2003). "Incremental dynamic analysis". Earthquake Engineering and Structural Dynamics 31, 491–514.

DESIGN FOR COLLAPSE SAFETY

F. Zareian[1], H. Krawinkler[2], and L.F. Ibarra[3]

[1]Assistant Professor, Department of Civil and Environmental Engineering, UC - Irvine, USA
[2]Professor, Department of Civil and Environmental Engineering, Stanford University, USA
[3]Senior Research Engineer, Southwest Research Institute, USA
zareian@uci.edu, krawinkler@stanford.edu, libarra@cnwra.swri.edu

ABSTRACT

Collapse prevention is a major constraint in the design decision process. Because of shortcomings in analytical modeling, collapse usually is assumed to be associated with an acceptable story drift. Recently, the introduction of realistic deterioration models has made it possible to predict structural response close to collapse. Evaluation of collapse capacity can be based on a measure called *relative intensity*, which is defined as the ratio of ground motion intensity to a structure strength parameter. Using this measure, the proposed approach for design for collapse safety consists of (a) specifying performance targets (e.g., tolerable probability of collapse at certain hazard level, mean annual frequency of collapse), and (b) deriving engineering parameters for system selection, using the relatively simple design decision support tools discussed in this paper. The proposed approach addresses the effects of aleatory and epistemic uncertainties on these engineering parameters. Application of this approach is illustrated through examples and discussions provided in the paper.

1. INTRODUCTION

Collapse in earthquake engineering implies loss of vertical (gravity) load carrying capacity of the structure during and after ground shaking. In modern structures in which brittle failure modes are prevented, collapse is usually triggered by large interstory drifts that are amplified by P-Δ effects (Bernal 1992, Gupta and Krawinkler 1999) and deterioration in strength and stiffness of structural elements (Ibarra 2003). In performance assessment, an already selected and proportioned structural system can be evaluated for its ability to resist ground motions without collapse, provided that reliable analytical models are available to predict behavior in the inelastic range up to collapse.

Design is different from performance assessment, by virtue of the fact that the building and its structural components and system first have to be created. Good designs are based on concepts that incorporate performance targets *up front* in the conceptual design process, so that subsequent performance assessment becomes more of a verification process of an efficient design rather than a design improvement process that may require radical changes.

Collapse prevention is one of the major constraints in the design decision process. Because of shortcomings in analytical modeling, collapse is usually assumed to be associated with an acceptable story drift. This approach does not permit redistribution of damage and does not account for the ability of the structural system to sustain deformations without collapse that are

significantly larger than those associated with loss in resistance of individual elements. Ibarra (2003) has developed a methodology for evaluating structural collapse capacity for deteriorating structural systems. In Ibarra's study, the evaluation of collapse capacity is based on a measure called *relative intensity*, which is defined as the ratio of ground motion intensity to a structure strength parameter. The same measure will be used throughout this paper to address design for collapse safety.

This paper is concerned with conceptual design for collapse safety. The first task is to identify structural parameters that significantly affect the structure's collapse capacity and develop collapse capacity fragility curves associated with different combinations of these structural properties. The second task is to address the effects of uncertainties, both aleatory and epistemic, on the collapse capacity. The final task is to develop a process for estimating suitable structural properties that satisfy specified collapse performance targets. Conceptual design for collapse safety is greatly facilitated by focusing on discrete performance targets associated with discrete hazard levels, similar to the way it is being practiced in most of the performance-based guidelines presently in use. A more general approach is to define the performance target in the form of a tolerable mean annual frequency of collapse. Both options are pursued in the following discussion.

2. DOMAINS THAT CONTROL DESIGN FOR COLLAPSE SAFETY

Design for collapse safety comprises two domains; the *Hazard Domain*, and the *Structural System Domain* as illustrated in Figure 1. In conceptual design for collapse safety, the objective is to search for effective solutions at a time at which the details of the structural system are yet to be determined. In the following discussion the content of the two domains is summarized.

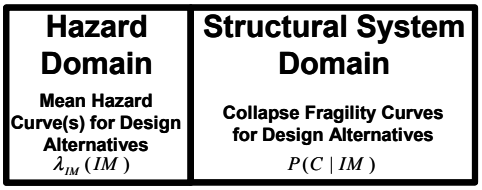

Fig. 1. Domains controlling design for collapse safety.

2.1 Hazard Domain

The hazard domain contains the return period dependent description of the ground motion intensity plus associated time history records. The intensity measure could be a scalar or a vector quantity (Baker and Cornell 2004), with the latter being of particular importance in the case of near-fault ground motions. In the numerical example presented later the spectral acceleration at the first mode period of the structural system ($S_a(T_1)$) is used as *IM*. The process of developing hazard curves involves many scientific assumptions (Kramer 1996). This means that there is *epistemic* uncertainty in the evaluation of a hazard curve. It has been shown by Jalayer (2003) that the *epistemic* uncertainty in the hazard is dealt with by using the *mean* hazard curve, denoted as $\bar{\lambda}_{IM}(IM)$, which reflects directly the *epistemic* uncertainty involved the process of developing hazard curves. It is important to note that the mean hazard curve changes with the first mode period of the explored structural system.

The records selected to represent the seismic input for specific *IM* values affect the collapse fragility curves contained in the structural system domain discussed in Section 2.2. The associated issues of ground motion scaling and near-fault effects have been and still are the subject of research and are not discussed further in this paper.

2.2 Structural System Domain

This domain contains collapse fragility curves, which portray, for a given structural system, the probability of collapse as a function of the intensity measure ($P(C|IM)$). Such curves can be obtained by subjecting deteriorating structural systems of specific properties to sets of ground motions representative of the range of *IMs* in which collapse is expected. If all component deterioration modes are adequately presented in the analytical model, it should be feasible to analytically trace structures until collapse by incrementing the *IM* of the ground motion until a minute increment in *IM* leads to a very large increment in a global engineering demand parameter, *EDP* (such as maximum interstory drift), indicating dynamic instability.

Research has been performed recently on the "collapse capacity" of moment resisting frames, utilizing component hysteresis models that account for strength deterioration in the backbone curve (see Figure 2) and for cyclic deterioration in strength and stiffness (Ibarra 2003). The collapse capacity is defined as that value of the "relative intensity", defined here as $[S_a(T_1)/g]/\gamma$ (γ= base shear strength coefficient V_y/W) at which dynamic instability occurs due to deterioration and P-Δ effects. It is noted that $[S_a(T_1)/g]/\gamma$ is equivalent to the ductility dependent strength reduction factor R_μ. The probability density function (assuming a lognormal distribution) of the collapse capacity is obtained as illustrated in Figure 3, and the corresponding cumulative distribution function represents the collapse fragility curve, $P(C|IM)$. Collapse fragility curves of the type shown in Figure 4 have been derived for regular and soft story frames subjected to a set of 40 ground motions. It has been concluded that the collapse fragility depends primarily on the component ductility capacity δ_c/δ_y (which is assumed to be the same for all components in the structure), the post-capping stiffness ratio α_c (see Figure 2), and the cyclic deterioration parameter $\gamma_{s,c,k,a}$. These parameters, together with the fundamental period T_1 and the base shear strength parameter $\gamma = V_y/W$, control the design for collapse safety.

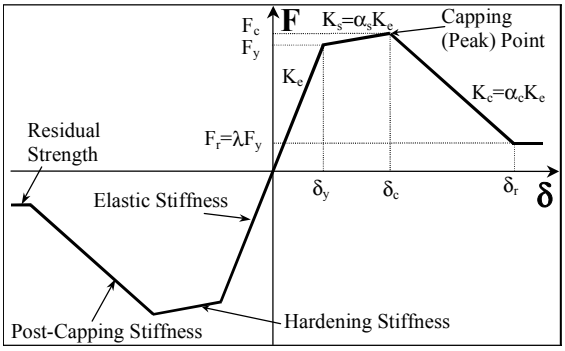

Fig. 2. Backbone curve for deteriorating component hysteresis models (after Ibarra 2003).

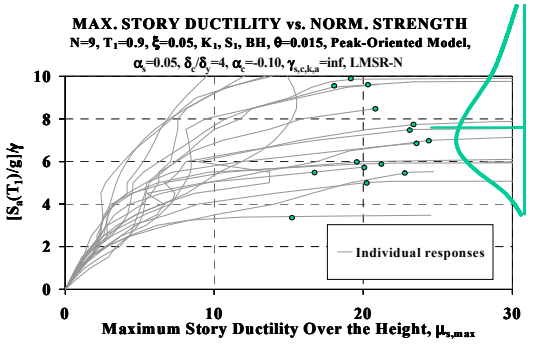

Fig. 3. *IDAs* until collapse and distribution of collapse capacity (after Ibarra 2003).

The *aleatory* uncertainty due to the record-to-record variability is represented in the collapse fragility curve. If a lognormal distribution is considered for the probability of $[S_a(T_1)/g]/\gamma$ associated with collapse, it's measure of dispersion (which is the standard deviation of the log of the data), β_{RC} ("Randomness in collapse Capacity"), is the representation of *aleatory* uncertainty. The *epistemic* uncertainty, which has a number of sources, with lack of knowledge about the exact structural properties and inaccurate structural modeling being two major ones, affects the median estimate of $[S_a(T_1)/g]/\gamma$ associated with collapse but it is assumed to have no effect on β_{RC}. In other words, the lognormal distribution that was considered for collapse fragility curves has a random median value and a constant dispersion of β_{RC}. Detailed representation of *epistemic* uncertainty is discussed in Section 3.2.

3. DECISION SUPPORT IN CONCEPTUAL DESIGN FOR COLLAPSE SAFETY

3.1 Design for Tolerable Probability of Collapse at a Specific Hazard Level

In most codes and guidelines it is assumed that adequate collapse safety is provided by limiting the maximum story drift at the design earthquake level to a specific value (e.g., a drift limit of 0.02 at the 10/50 hazard level). The drift at this hazard level is estimated from either an elastic analysis or an inelastic time history analysis. But the latter usually is executed with the use of component hysteresis models that do not account for strength and stiffness deterioration. Thus, these *EDP* predictions provide no insight into the probability of collapse. With the advent of deterioration models that do account for important aspects of deterioration it is becoming possible to trace the response of structures to collapse (Ibarra 2003, Sivaselvan and Reinhorn 2000, Song and Pincheira 2000) and to be specific about a collapse performance target. Such a target could be expressed as a tolerable probability of collapse at a specific hazard level (say, 10% at the 2/50 hazard level), which could include a confidence statement (say, 10% at the 2/50 hazard level with 90% confidence) if epistemic uncertainty is accounted for. Figure 5 illustrates the design for collapse safety for a specific hazard level. The intersection of the line denoting the *IM* value at the specified hazard level with the line denoting the tolerable probability of collapse divides the design alternatives into a feasible and an unfeasible solution space.

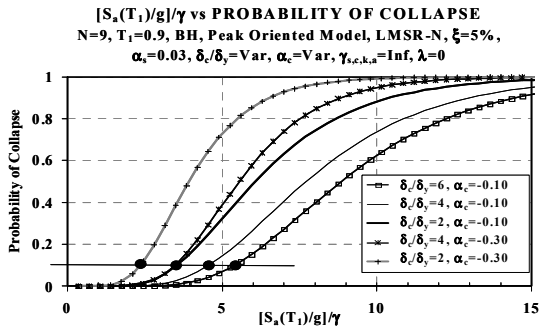

Fig. 4. Collapse fragility curves for 9-story frame structures with T_1 = 0.9 s (after Ibarra 2003).

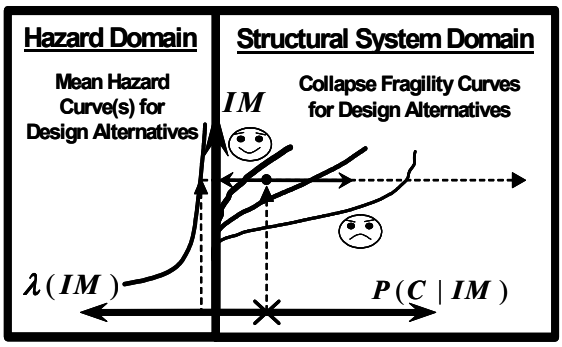

Fig. 5. Conceptual design for collapse safety at discrete hazard levels.

3.2 Design for Tolerable Mean Annual Frequency of Collapse

A different way to express desired collapse performance is to target a tolerable mean annual frequency (MAF) of collapse. If *epistemic* uncertainty is considered, a confidence level should be associated with the MAF, which now can be expressed as λ_C^x (e.g., tolerable mean annual frequency of collapse of 0.0004 with 90% confidence, $\lambda_C^{90\%} = 0.0004$. This performance target is more general (it permits the estimation of the probability of collapse over an expected life time), but it is more difficult to implement because the "accurate" computation of a MAF requires integration over the S_a hazard curve:

$$\lambda_C^x = \int_{Sa} P^x(C \mid sa) \left| d\overline{\lambda}_{Sa}(sa) \right| \tag{1}$$

In Equation 1, $P^x(C \mid sa)$ is probability distribution function of $Sa(T_1)$, or simply *Sa*, associated with collapse for confidence level *x*. The uncertainty in the probability distribution function of *Sa* associated with collapse, $P(C \mid sa)$ (which has been accounted for in the calculation of MAF of collapse by introducing a confidence level *x*) is due to *epistemic* uncertainty. The other source of uncertainty is the *aleatory* uncertainty which has been discussed in Section 2.2. The *epistemic* uncertainty affects the estimate of the median of *Sa* associated with collapse, $\hat{\eta}_C$, and it is assumed that it has no effect on β_{RC}. The effect of *epistemic* uncertainty on $\hat{\eta}_C$ is described by β_{UC} ("Uncertainty in collapse Capacity") which is the dispersion of the lognormal distribution fitted to the median estimates of $\hat{\eta}_C$. Jalayer (2003) has introduced a closed form solution, Equation 2, to estimate λ_C^x :

$$\lambda_C^x = \int_{Sa} P^x(C \mid sa) \left| d\overline{\lambda}_{Sa}(sa) \right| = \left[\overline{\lambda}_{Sa}(\hat{\eta}_C) \right] \left[\exp\left(\frac{1}{2} k^2 \beta_{RC}{}^2 \right) \right] \left[\exp[K_x(k\beta_{UC})] \right] \tag{2}$$

The simplified expression on the right-hand side contains the MAF of the spectral acceleration associated with the 50% probability of collapse, $\overline{\lambda}_{Sa}(\hat{\eta}_C)$, and two terms that account, in an approximate manner, for the uncertainties inherent in the computation of the collapse "capacity" (the $[S_a(T_1)/g]/\gamma$value causing collapse). The second term on the right hand side of Equation

(2) accounts for the *aleatory* uncertainty and contains the slope of the hazard curve, k, at the referenced spectral acceleration value, and the dispersion, β_{RC}, due to record to record variability in the collapse fragility curve.. The dispersion β_{RC} in Equation (2) is found to be on the order of 0.4 to 0.5 (except for long period structures for which it is smaller because of the dominance of P-delta effects). The third term on the right hand side of Equation (2) accounts for the *epistemic* uncertainty. Pilot studies have shown that the dispersion due to *epistemic* uncertainties in the collapse fragility curve, β_{UC}, may be as large as or larger than that due to *aleatory* uncertainties (Ibarra 2003). For this reason, it is assumed that β_{UC} is equal to 0.4 in the example described below. K_x is the standardized Gaussian variate associated with probability x of not being exceeded, and x is the confidence level that is sought for design.

4. EXAMPLE IMPLEMENTATION OF DECISION SUPPORT FOR COLLAPSE SAFETY

Providing collapse safety implies adherence to capacity design concepts, and it implies design for ductility. The latter is implicitly considered in present design approaches with the judgmental response modification (R) factor or behavior (q) factor. These factors are tied to component detailing (ductility) requirements, and in the design process they are used to reduce the strength design level to a fraction of the elastic demand associated with the spectral acceleration at the first mode period. To this date it is not known whether or not this R (or q) based design process provides a quantifiable, or for that matter even remotely consistent, factor of safety against collapse. Provided one can develop confidence in the collapse fragility curves of the type illustrated in Figure 3, the process illustrated conceptually in Section 3 can be utilized to perform designs that target a specific tolerable probability of collapse. This is illustrated next with an example.

The example addresses a 9-story office building, located in Southern California. Desired performance at the collapse prevention level could be expressed in terms of a tolerable probability of collapse at a specified hazard level or alternatively, a tolerable mean annual frequency of collapse. These two alternatives implicitly consider the *aleatory* uncertainty involved in the estimation of collapse capacity. The *epistemic* uncertainty can be dealt with by introducing confidence levels for design targets. These design targets could be expressed as a tolerable probability of collapse at a specified hazard level with a certain confidence statement, or a tolerable mean annual frequency of collapse with a certain confidence level.

4.1 Design for Tolerable Probability of Collapse at a Specific Hazard Level

In the example it was decided to use reinforced concrete moment-resisting frames as the primary structural system. Because of space constraints, only moment frames with T_1 = 0.9 and 1.8 sec. and with a base shear strength coefficient $\gamma = V_y/W$ = 0.1, 0.2, and 0.3 are considered as alternatives. For the same reason the effect of *epistemic* uncertainty, which may be expressed in terms of a confidence statement, is ignored in this section. The site specific spectral acceleration hazard curves for the period of 0.9 sec. and 1.8 sec. are shown in the left portion of Figure 6. At the 2/50 hazard level, the collapse fragility curves for the structures with T_1 = 0.9 sec. and γ= 0.1, 0.2, 0.3, and T_1 = 1.8 sec. and γ= 0.1, 0.2, shown in the right portion of Figure 6 (which is magnified at the left hand side of the figure), indicate that the actual probability of collapse is greater than 0.1, rendering these solutions undesirable for collapse safety. Only for

the T_1 = 1.8 sec. and γ= 0.3 structure, the collapse fragility curve in the right portion of Figure 6 indicates that the actual probability of collapse is smaller than 0.1 at 2/50 hazard level, rendering this solution desirable for collapse safety.

One could inspect collapse fragility curves for stronger structures, or, perhaps better from the perspective of behavior, take advantage of collapse spectra of the type shown in Figures 7 and 8 (Ibarra 2003). These spectra show the relative intensity $[S_a(T_1)/g]/\gamma$ associated with a certain probability of collapse (10% in Figure 7, and 50% in Figure 8) for frame structures with $T_1 = 0.1N$ (N = number of stories) and several combinations of system parameters (see Figure 2). The spectra illustrate the effect of component ductility capacity (δ_c/δ_y) on the relative intensity, assuming α_c = -0.1 and no cyclic deterioration ($\gamma_{s,c,k,a} = \infty$). For a tolerable probability of collapse of 10% in a 2/50 event, data of the type shown in Figure 7 provides the necessary design decision support (similar spectra are available for other combinations of system parameters). For instance, if T_1 is selected as 0.9 sec. and the component ductility capacity is 4.0, the $[S_a(T_1)/g]/\gamma$value for a 10% probability of collapse is 4.6, which for the 2/50 hazard of the example problem ($S_a(0.9)$ = 1.7g) results in a required base shear strength coefficient of γ= 1.7/4.6 = 0.37. A larger ductility capacity (better detailing) or a more flexible structure can reduce the required strength. For instance, for T_1 = 0.9 sec. and δ_c/δ_y = 6, the $[S_a(T_1)/g]/\gamma$value is 5.4, which would result in γ= 1.7/5.4 = 0.31. Alternatively, a more flexible structure could be selected. For T_1 = 1.8 sec. and δ_c/δ_y = 4, the $[S_a(T_1)/g]/\gamma$value is 3.5, which for the 2/50 S_a value of 0.86g at 1.8 sec. results in a required base shear strength coefficient of γ= 0.86/3.5 = 0.25.

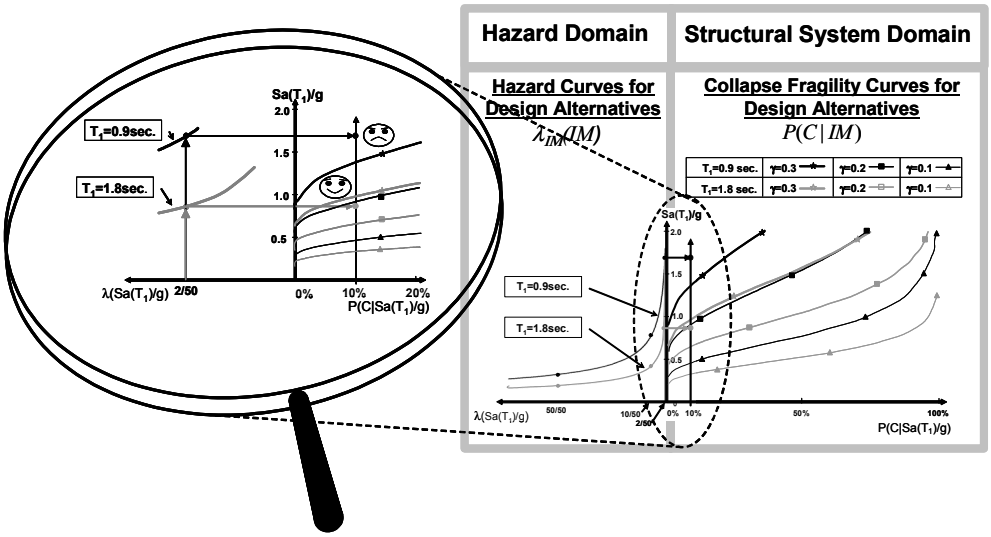

Fig. 6. Example of conceptual design for collapse safety at discrete hazard levels.

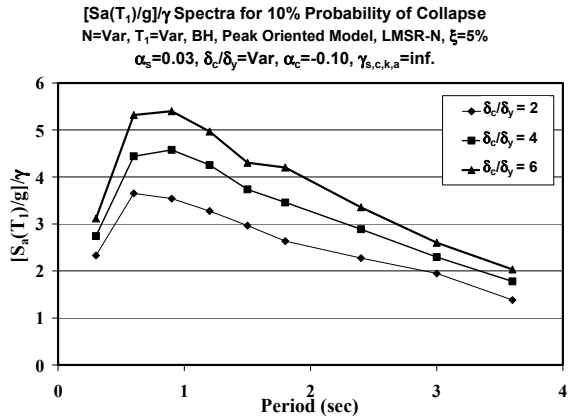

Fig. 7. [Sa(T1)/g]/γ spectra for Beam-Hinge models associated with 10% probability of collapse.

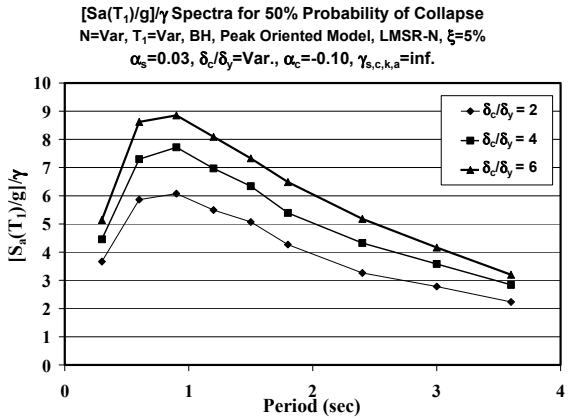

Fig. 8. [Sa(T1)/g]/γ spectra for Beam-Hinge models associated with 50% probability of collapse.

These are the kind of trade-offs that can be evaluated through the use of collapse probability spectra of the type shown in Figure 6, presuming that a tolerable probability of collapse is specified at a specific hazard level. It is important to note that the benefits of component ductility capacity and of flexibility are much smaller than anticipated from code design procedures. An increase in δ_c/δ_y by 50% (from 4 to 6) only led to a decrease in required base shear strength coefficient γ from 0.37 to 0.31, and an increase in T_1 from 0.9 to 1.8 sec. only led to a decrease in required base shear strength coefficient γ from 0.37 to 0.25 even though the elastic strength demands would differ by a factor of 2.0 in the constant velocity region of design spectra.

4.2 Design for Tolerable Mean Annual Frequency of Collapse

Continuing the above example, let us target a tolerable mean annual frequency of collapse of 0.0002 (i.e., a tolerable probability of collapse of approximately 0.0002x50 = 0.01 in a 50 year life span) and for the time being ignore the *epistemic* uncertainty by not specifying a confidence level of this design target. For this case, Equation 2 reduces to

$$\lambda_C = \left[\overline{\lambda}_{Sa}(\hat{\eta}_C)\right]\left[\exp\left(\frac{1}{2}k^2\beta_{RC}{}^2\right)\right] \tag{3}$$

The above collapse safety criterion could be used, together with $[S_a(T_1)/g]/\gamma$ spectra for a 50% probability of collapse (see Figure8), to arrive at effective design solutions. Again using the example of the 9-story frame structure, the following design alternatives could be explored. If a period of 0.9 sec. and a component ductility capacity of δ_c/δ_y = 4 are targeted, then the median $[S_a(T_1)/g]/\gamma$ value from Figure 8 is 7.7. For the site specific hazard curve the slope of the S_a hazard curve in the neighborhood of a MAF of 0.0001 to 0.0004 is about 2.2, and the β_{RC} value is about 0.4 (Ibarra 2003). Thus, from Equation (3) the MAF of the S_a associated with the 50% probability of collapse, $\overline{\lambda}_{Sa}(\hat{\eta}_C)$, is equal to $0.0002/\exp(0.5\text{x}2.2^2\text{x}0.4^2) = 0.000136$. From the S_a hazard curve for the site of the example problem, the corresponding S_a is 2.8g, and the corresponding γ value is 2.8/7.7 = 0.36. Alternatives are to increase the component ductility

capacity (if it is increased from 4 to 6, $[S_a(T_1)/g]/\gamma$ is 8.9, and for the same $\bar{\lambda}_{S_a}(\hat{\eta}_C)$ of 0.000136 the γ value becomes 2.8/8.9 = 0.31), or to increase the structure period. If, for instance, T_1 is 1.8 sec., the $[S_a(T_1)/g]/\gamma$ value from Figure 8 is 5.4 (for $\delta_c/\delta_y = 4$), and, using the site specific k value of 2.4 for the T = 1.8 sec. hazard curve, $\bar{\lambda}_{S_a}(\hat{\eta}_C)$ becomes 0.000126, the S_a value for this MAF is 1.4g, and the base shear strength parameter γ becomes 1.4/5.4 = 0.26.

By including the *epistemic* uncertainty, one could target, for instance, a 90% confidence level for a mean annual frequency of collapse of 0.0004 (2% in 50 years). Using the process illustrated previously, if a period of 0.9 sec. and a component ductility capacity of $\delta_c/\delta_y = 4$ are assumed, then the median $[S_a(T_1)/g]/\gamma$ value from Figure 8 is 7.7. For the site specific hazard curve the slope of the S_a hazard curve in the neighborhood of a MAF of 0.001 to 0.004 is about 2.2, and the β_{RC} value is about 0.4. For the 90% confidence level, the K_x value is 1.28. Using $\beta_{UC} = 0.4$, the MAF of S_a at the median collapse capacity, $\bar{\lambda}_{S_a}(\hat{\eta}_C)$, is computed from Equation (2) as 0.0004/[exp(0.5x2.22x0.42).exp(1.28x2.2x0.4)] = 0.000088. From the S_a hazard curve the corresponding S_a is 3.4g, and the corresponding γ value is 3.4/7.7 = 0.44. This is a large value that would control strength design. As before, alternatives are to increase the component ductility capacity (if it is increased from 4 to 6, $[S_a(T_1)/g]/\gamma$ is 8.9, and for the same $\bar{\lambda}_{S_a}(\hat{\eta}_C)$ of 0.000088 [presuming that both β_{RC} & β_{UC} are insensitive to the ductility change] the γ value becomes 3.4/8.9 = 0.38), or to increase the structure period. If, for instance, T_1 is 1.8 sec., the $[S_a(T_1)/g]/\gamma$ value from Figure 8 is 5.4 (for $\delta_c/\delta_y = 4$), and, presuming that k is also about 2.4 for the T = 1.8 sec. hazard curve, the S_a value for a MAF of 0.000074 becomes 1.8g, and the base shear strength parameter γ becomes 1.8/5.4 = 0.33.

The importance of including *epistemic* uncertainty and an associated confidence level can be quantified by computing the base shear strength coefficient γ for a targeted mean annual frequency of collapse of 0.0004 from Equation (3), i.e., by ignoring the *epistemic* uncertainty. In this case γ becomes 0.26 for $T_1 = 0.9$ sec. and $\delta_c/\delta_y = 4$, as compared to the value of 0.44 for the case including epistemic uncertainty and a high confidence level of 90%. This example demonstrates that epistemic uncertainty together with a high confidence level can indeed have a large effect on the target design strength of frame structures (the assumed value of $\beta_{UC} = 0.4$ is believed to be realistic).

5. CONCLUSIONS

This paper proposes two approaches to accomplish effective design for collapse safety and illustrates them conceptually and through examples. Conceptual design for collapse safety implies a decision process that leads to the selection of one or several effective design alternatives based on either a tolerable probability of collapse at discrete hazard levels or a tolerable mean annual frequency of collapse with or without a confidence statement, depending on the incorporation or exclusion of *epistemic* uncertainties. The implementation challenges are to identify structural parameters that significantly affect the structure's collapse capacity, to develop collapse fragility curves associated with different combinations of these structural properties, to quantify the effects of uncertainties, both *aleatory* and *epistemic*, on collapse fragility curves, and to develop a process for estimating structural properties that meet specified collapse performance targets. It was shown by example that increasing the flexibility (choosing a structure with larger natural period) or increasing the ductility capacity of structural members reduces the required strength for collapse safety – but by a smaller amount than anticipated based

on present code design concepts. Uncertainties, both *aleatory* and *epistemic*, have a significant effect on the outcome of the conceptual design for collapse safety.

ACKNOWLEDGEMENTS

This research was carried out as part of a comprehensive effort at Stanford's John A. Blume Earthquake Engineering Center to develop basic concepts for PBEE and supporting data on seismic demands and capacities. This effort is supported by the NSF sponsored Pacific Earthquake Engineering Research (PEER) Center.

REFERENCES

Bernal, D. (1992), "Instability of Buildings Subjected to Earthquakes," *Journal of Structural Engineering*, **118**(8), 2239-2260.

Gupta, A. and Krawinkler, H. (1999), "Seismic Demands for Performance Evaluation of Steel Moment Resting Frame Structures," Report 132. John A. Blume EERC, Stanford University.

Ibarra, L.F. (2003), "Global Collapse of Frame Structures Under Seismic Excitations," *Ph.D. Dissertation*, Department of Civil Engineering, Stanford University.

Cornell, A. and Krawinkler, H. (2000), "Progress and Challenges in Seismic Performance Assessment," *PEER News*, April 2000.

Deierlein G. (2004), "Overview of a Comprehensive Framework for Earthquake Performance Assessment. *Proc. Int'l Workshop on Performance-Based Seismic Design – Concepts and Implementation,* Bled, Slovenia, 15-26.

Krawinkler, H. and Miranda, E. (2004), "Performance-Based Earthquake Engineering," Chapter 9 of *Earthquake Engineering: From Engineering Seismology to Performance-based Engineering*, CRC Press.

Jalayer, F. (2003), "Direct Probabilistic Seismic Analysis: Implementing Nonlinear Dynamic Assessments," *PhD. Dissertation,* Department of Civil Engineering, Stanford University.

Baker, J. and Cornell, C. A. (2004), "Choice of a Vector of Ground Motion Intensity Measures for Seismic Demand Hazard Analysis," *Proceedings of 13th WCEE*, Vancouver, Canada, Paper No. 3384.

Kramer, S. L. (1996), "Geotechnical Earthquake Engineering," *Prentice Hall*.

Sivaselvan, M.V. and Reinhorn, A.M. (2000), "Hysteretic Models for Deteriorating Inelastic Structures," *Journal of Engineering Mechanics*, American Society of Civil Engineers, **126**(6), 633-640.

Song, J. and Pincheira, J. (2000), "Spectral Displacement Demands of Stiffness and Strength Degrading Systems," *Earthquake Spectra*, **16**(4), 817-851.

Cornell, C.A. (1996), "Calculating Building Seismic Performance Reliability; A Basis for Multi-Level Design Norms," *Proc. 11th WCEE*, Acapulco, Mexico.

VM, SHEAR-FLEXURAL, LINK ELEMENT FOR SEISMIC ANALYSIS OF STEEL FRAMES

M. T. Kazemi[1], S. Erfani [2], and M. Hoseinzadeh Asl[3]

ABSTRACT

This paper represents a summary of recently introduced mixed shear-flexural, VM, link element, and its application in eccentrically braced frames and special girder moment frames. It is shown that the mixed VM link element may be used to address the experimental and the finite element analytical results. The element considers shear- flexural interaction and provides modeling of flexural yielding, shear yielding and their interaction in frames subjected to the monotonic or cyclic loadings. The inelastic shear and flexural deformations and tangential stiffness are considered by using the multi-surface approach with dissimilar yield surfaces and by a stiffness matrix with nonzero off-diagonal components. A modified VM link element is also introduced, which has the additional capabilities of modeling softening and damage.

1. INTRODUCTION

Inelastic analysis and design of structures has made great progress due to the rapid development of computer hardware and software in recent decades (Jirasek and Bazant, 2002). The common approach of modeling inelastic behavior of a frame element is to adopt inelastic hinge formation. A generalized plastic hinge, with zero length, accounting for interaction of axial, torsional and biaxial bending moments, based on multi-surfaces plasticity concept, was presented by Powell and Chen (1986). Krenk et al. (1993), using a piecewise linearized yield surface and linear kinematic hardening rule, developed a formulation for displacement discontinuities with extension and rotation components. A method for modeling the members with yielding under combined flexure and axial force in steel frames subjected to earthquake ground motions was presented by Kim and Engelhardt (2000). Their method had the capability of modeling plastic axial deformation and changes in axial stiffness based on isotropic and kinematic strain-hardening defined in axial-flexural space. Liew and Tang (2000) used the two surface plasticity concept for considering the inelastic interaction between axial force and bending moment, but the effect of shear force was ignored. Ricles and Popov (1994), developed a formulation for modeling link elements in eccentrically braced frames (EBFs), based on multi-surfaces plasticity concept. In their work, the link beam has a nonlinear hinge at each end, and each hinge consists of uncoupled shear and flexural nonlinear sub hinges. Ramadan and Ghobarah (1995), using the separate shear and flexural nonlinear hinges, also investigated the link element of EBFs.

In the present research, the model proposed by Kazemi and Erfani (2007a) and Erfani and Kazemi (2007), is presented. A general VM link element (indicating a mixed shear-flexural element), with optional zero or nonzero length, is introduced in locations where shear-flexural interaction is anticipated. The VM link element has the capability for modeling of flexural yielding, shear yielding, as well as combined shear-flexural yielding. The multi-surfaces concept with dissimilar yield surfaces and off diagonal components in flexibility matrixes is used. Elastic

[1] *Associate Professor, Civil Engineering Department, Sharif University of Technology, Tehran, Iran. Email: kazemi@sharif.edu*
[2] *Assistant Professor, Civil Engineering Department, Amirkabir University of Technology, Tehran, Iran. Email: sderfani@aut.ac.ir*
[3] *Ph.D. Candidate, Civil Engineering Department, Sharif University of Technology, Tehran, Iran. Email: hosinzadeh@mehr.sharif.ir*

and inelastic shear distortion and flexural rotation are considered. It is shown that the mixed VM link results have good agreement with the experimental, as well as, finite element analytical results (Kazemi and Erfani 2007b; Kazemi and Erfani 2009). An improved mixed shear-flexural element is introduced, which has the additional capabilities of modeling strength softening and stiffness degradation, which could make it more suitable for seismic evaluation of the existing frames.

2. DEFINITION OF VM LINK ELEMENT

The VM link element (Kazemi and Erfani 2007a; Erfani and Kazemi 2007) is consisted of one inner inelastic combined shear-flexural hinge with zero length and two rigid parts with zero or nonzero lengths in two sides of it. Geometrical presentation of this element has been shown in Figure 1, where i and j are the outer nodes and h is the inner hinge. The inner hinge has arbitrary location. The lengths of two rigid parts are Li and Lj, and L= Li+ Lj is the total length of the element. The element will be more representative of inelastic zone if we take L equal to the length of inelastic zone.

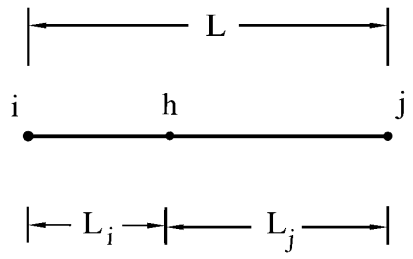

Fig. 1. Configuration of the VM link element.

The properties of the VM link element are defined such that relative deformations between two ends of it are equal to the relative deformations between two ends of inelastic zone in reality. The element's end forces and displacements in the element local coordinate system are presented in Figure 2a. Figure 2b shows the element's internal forces and deformations in the inner inelastic hinge node.

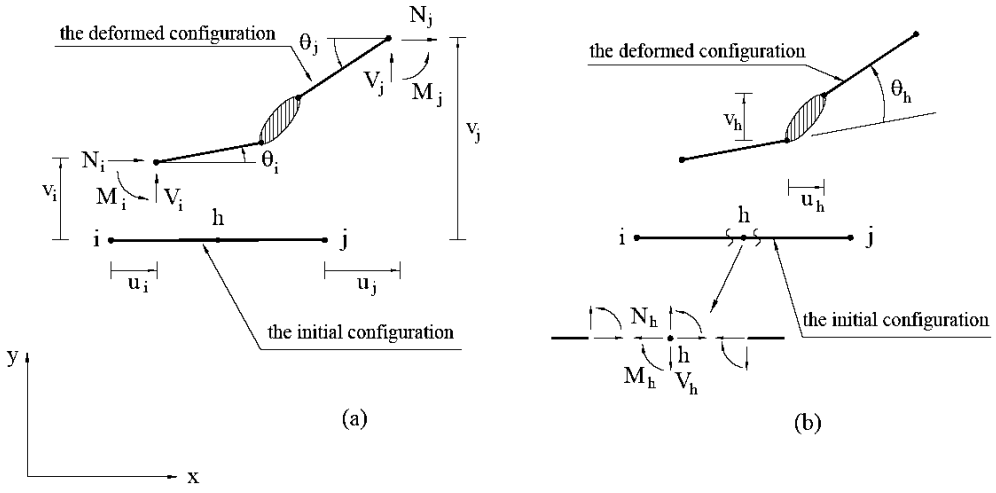

Fig. 2. (a) The element's end forces and displacements, (b) The element's internal forces and deformations.

If the element's end forces and displacements are described as column vectors of **P** and **U**, respectively, and the element's internal forces and deformations in the inner inelastic hinge node are defined as column vectors $\mathbf{P}_h$ and $\mathbf{U}_h$, respectively, then one could write:

$$\mathbf{P} = \mathbf{A}\mathbf{P}_h \qquad \mathbf{U}_h = \mathbf{A}^T\mathbf{U} \quad , \tag{1}$$

where, **A** is the transformation matrix and its components depend only on lengths of rigid parts of the element and are as follows:

$$\mathbf{A} = \begin{bmatrix} \mathbf{A}_i \\ \mathbf{A}_j \end{bmatrix} \quad , \quad \mathbf{A}_i = \begin{bmatrix} -1 & 0 & 0 \\ 0 & -1 & 0 \\ 0 & -L_i & -1 \end{bmatrix} \quad , \quad \mathbf{A}_j = \begin{bmatrix} 1 & 0 & 0 \\ 0 & 1 & 0 \\ 0 & -L_j & 1 \end{bmatrix} \tag{2}$$

Considering the above relationships, the element's tangential stiffness matrix **K** can be written as follows:

$$\mathbf{K} = \mathbf{A}\mathbf{K}_h\mathbf{A}^T = \mathbf{A}\mathbf{F}_h^{-1}\mathbf{A}^T \tag{3}$$

where, $\mathbf{K}_h$ and $\mathbf{F}_h$ are the tangential stiffness and flexibility matrixes of the inner hinge, respectively.

By calculating the inner hinge's tangential flexibility matrix, $\mathbf{F}_h$, and then inversing it, the tangential stiffness matrix, $\mathbf{K}_h$, is obtained. For small deformation, $\mathbf{F}_h$ can be decomposed as:

$$\mathbf{F}_h = \mathbf{F}_h^e + \mathbf{F}_h^p \tag{4}$$

where, $\mathbf{F}_h^e$ and $\mathbf{F}_h^p$ are the inner hinge's elastic and plastic tangential flexibility matrices, respectively. For definition of $\mathbf{F}_h^p$, a flow rule is used:

$$\mathbf{F}_h^p = \mathbf{m}_V\mathbf{F}_{hV}^p + \mathbf{m}_M\mathbf{F}_{hM}^p \tag{5}$$

In which, m_v and m_M are the components of **m** vector in VM space, which is the unit location vector of action point as in figure 3. $\mathbf{F}_{hV}^p$ and $\mathbf{F}_{hM}^p$ are the flexibility matrixes related to the pure shear and the pure flexural loadings, respectively. In a pure loading, only the related internal force at the inner hinge is nonzero, and the other internal forces are zero.

To consider interaction between shear and flexure the multi surface concept in shear-flexural, VM, space is used. This concept, which was originally defined in stress space (Khan and Huang 1995; Mroz 1969), was adapted with some modifications for the resultant forces space for frame elements (Powell and Chen 1986; Ricles and Popov 1994; Kim and Engelhardt 2000). In the VM link element, with considering piecewise dissimilar yield surfaces, polygonal shape as shown in Figure 3, the shear-flexural interaction is considered more realistically. To prevent intersection of yield surfaces, the corresponding sides of all yield surfaces should be parallel with each other and the length of any side of any yield surface should be smaller than the length of corresponding side of outer yield surfaces.

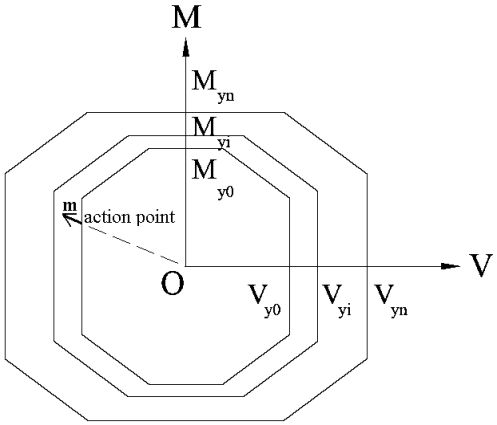

Fig. 3. Typical piecewise dissimilar yield surfaces.

In the several recent works (Powell and Chen 1986; Krenk et al. 1993; Ricles and Popov 1994; Kim and Engelhardt 2000), the element formulation is based on combined kinematic and isotopic hardening for shear force, and only kinematic hardening for flexure. In this paper, only kinematic hardening is used for both shear and flexure, although the isotropic hardening could be implemented as well. To manage the dissimilar yield surfaces, a new kinematic hardening rule is developed (Kazemi and Erfani 2007a).

3. ANALYSIS OF ECCENTRICALLY BRACED FRAMES

The capability of the VM link element for modeling of shear links in EBFs was investigated by Kazemi and Erfani (2009). The medium size shear link tested by Kasai and Popov (1986), and analyzed by Ricles and Popov (1994) was reinvestigated. The link element consisted of a W8 × 10 section with a length of L = 368 mm. The shear capacity of the element's section was Vp = 205·5 kN and the flexural capacity was Mp = 56·3 kN.m. The element was subjected to cyclically symmetric deformations. Experimental (Kasai and Popov 1986) and analytical (Kazemi and Erfani 2009) results are compared in Figure 4. The horizontal axes indicate the relative shear deformation between two ends of the link beam. As shown, the special VM link results are in good agreement with the test results.

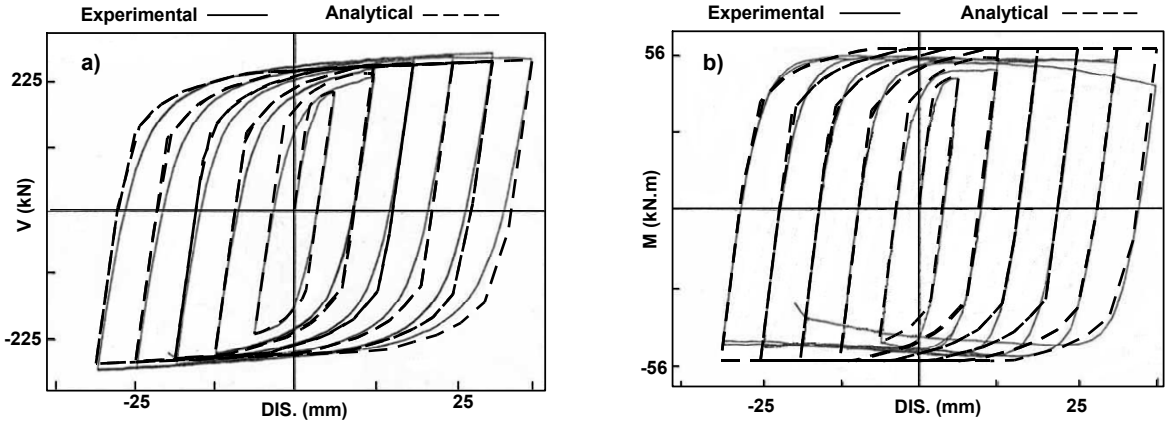

Fig. 4. Experimental measurements and analytical results of the link beam with a short length: (a) shear displacement; (b) moment displacement.

To examine the effects of shear–flexural interaction on structural response, a four-storey eccentrically braced steel frame (EBF) subjected to the El Centro earthquake was studied. The record was scaled up by a factor of 1.5 to a peak ground acceleration of 0.5 *g*. The sections of the members and dimensions of the EBF are summarized in Figure 5. All of the connections and supports are assumed to be rigid, except the connections between bracings and the other elements, which are assumed to have a pin connection.

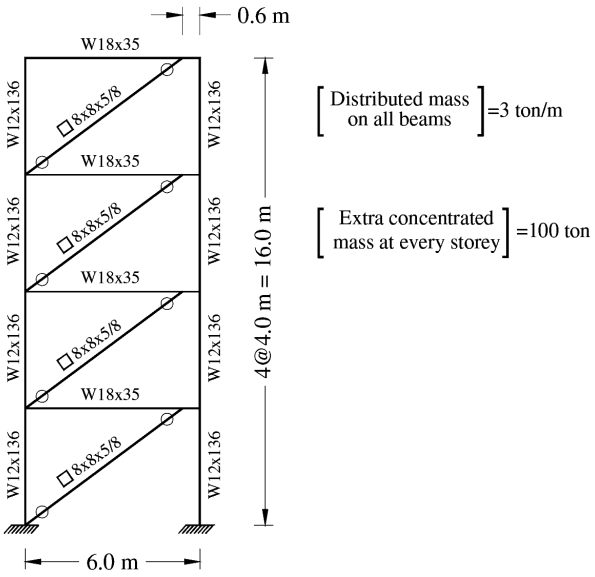

Fig. 5. Configuration of the four-storey eccentrically braced frame (EBF).

Three models for the link beams were used. In the first model, indicated by VM, the proposed special VM link element was employed for modeling the links. In the second model, called SP, separate multi-linear shear and flexural springs were used for the modeling of the link beams. In the third model, named RC, the link beams were modeled by using the VM link element, but with rectangular yield surfaces and flow rule. The results indicated that there are significant differences in the predicted values obtained from the three models. It is interesting to note that the directions of the lateral displacements are completely different for these models.

4. ANALYSIS OF SPECIAL GIRDER MOMENT FRAMES

Kazemi and Erfani (2007b) studied the seismic behavior of a four story building frame by the use of VM link element. Three cases are considered. In the first case, the frame is assumed to be ordinary moment frame (OMF) with ordinary girders in all stories. The ordinary girders are regular plate girders. In the second case, referred to as SGMF4, the frames are assumed to be special girder moment frames (SGMF) with special girders in the all floors. The special girders are the same as the ordinary girders but with a hole in the middle. The geometrical configuration of the special girder is presented in Figure 6. The column type and configuration is the same as those in the OMF.

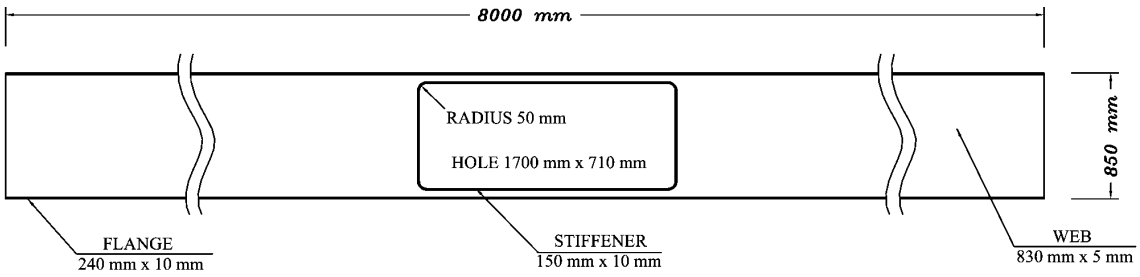

Fig. 6. Geometrical configuration of special girder.

In the third case, referred to as SGMF3, the frames have special girders in the three lower stories and ordinary girders in the roof. They concluded that in an overall comparison of the three model frames, SGMF 3 has the best seismic performance.

5. NEW ADVANCES IN THE VM LINK ELEMENT

The introduced VM element is unable to model the softening and stiffness degradation of existing frames. The modified VM link element has the capability of modeling combined flexural (rotational) and shear (lateral deformation) yielding, and damage (stiffness and strength degradations). The multi-surfaces concept with dissimilar yield surfaces is used for considering inelastic lateral and rotational deformations. The yield surfaces are defined in the deformation space. Modeling of softening behavior can be easily achieved by defining negative values for the flexibility matrix. For the inner hinge one could write:

$$\dot{\mathbf{U}}_h = \mathbf{F}_h \dot{\mathbf{P}}_h = (\mathbf{D}^f \mathbf{F}_h^e + \mathbf{F}_h^p)\dot{\mathbf{P}}_h \tag{6}$$

$\dot{\mathbf{U}}_h$ and $\dot{\mathbf{P}}_h$ are the rates of deformations and internal forces in the inner hinge of the element. $\mathbf{F}_h^e$ and $\mathbf{F}_h^p$ have been defined previously. D^f is the flexibility degradation (damage) matrix, which will be explained in more details later. The components of $\mathbf{F}_h^e$ may be obtained from classic analyses or formulas. It is assumed that the components corresponding to axial deformation in flexibility matrix remain elastic and constant.

For definition of $\mathbf{F}_h^p$ a flow rule is used:

$$\mathbf{F}_h^p = \mathbf{m}_v \mathbf{F}_{hv}^p + \mathbf{m}_\theta \mathbf{F}_{h\theta}^p \tag{7}$$

In which, m_v and m_θ are the components of **m** vector in modified VM space, which is the unit location vector of action point. $\mathbf{F}_{hv}^p$ and $\mathbf{F}_{h\theta}^p$ are the flexibility matrixes related to the pure lateral deformation and the pure rotation, respectively. For considering interaction between lateral deformation and rotation, the multi surface concept in modified VM space is used (Figure 7).

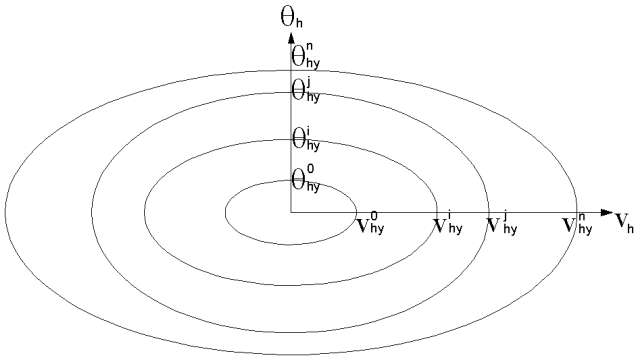

Fig. 7. Typical yield surfaces in the modified VM space.

Often, it is assumed that in the modified VM space the yield surface i is similar to the yield surface j, then we will have

$$\frac{v_{hy}^{i}}{v_{hy}^{j}} = \frac{\theta_{hy}^{i}}{\theta_{hy}^{j}} \tag{8}$$

Where v_{hy}^{i}, v_{hy}^{j}, θ_{hy}^{i}, and θ_{hy}^{j} are pure lateral deformation and pure rotation points on i and j yield surfaces (see Figure 7). In general, this may not be a good assumption. In the present study, the surfaces are dissimilar. When the inner surface i interacts with the yield surface j, it is assumed that the border of inner surface is cut by the outer surface in the interaction region (Figure 8-a). As the inner surface i moves back inwards, it changes to its initial shape as shown in Figure 8-b.

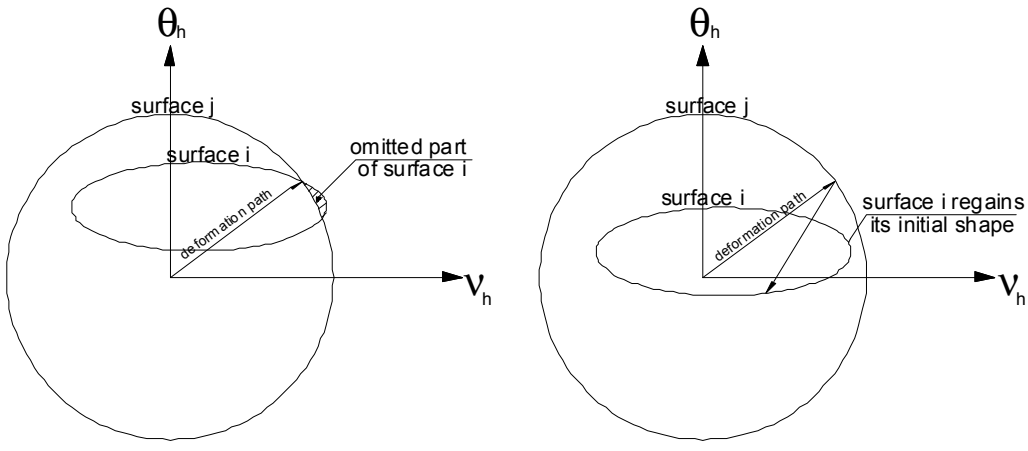

Fig. 8. Interaction of the yield surfaces, a) the border of inner surface *i*, is cut by the outer surface in the interaction region, b) the inner surface regains its initial shape.

The yield function of surface "i" is assumed to be as:

$$\left(\frac{v_{h}^{i}}{v_{hy}^{i}}\right)^{S^{v}} + \left(\frac{\theta_{h}^{i}}{\theta_{hy}^{i}}\right)^{S^{\theta}} = 1 \qquad S^{v}, S^{\theta} \geq 1 \tag{9}$$

where, S^v and S^θ are member dependent parameters of surface i, and will be determined based on test or finite element results. By taking larger values for S^v and S^θ parameters, the interaction between the rotational and lateral deformation of the member reduces. Different values of S^v and S^θ can be assumed for different yield surfaces.

The element formulation is based on combined kinematic and isotropic hardening. Here, only kinematic hardening is used for both shear and flexure. The hardening rule is similar to the one introduced by Kazemi and Erfani (2007a). The yield function is defined as:

$$\varphi_i(\mathbf{U}_h - \boldsymbol{\alpha}_i, \mathbf{H}_i) = 0 \tag{10}$$

Where, φ_i is the ith yield function of the inner hinge, $\mathbf{U}_h$ is the action vector of inner hinge, α_i presents the ith yield function center, and $\mathbf{H}_i$ is the expansion matrix of the ith yield surface and is defined as:

$$\mathbf{H}_i = \mathbf{D}^S \mathbf{S}_i \tag{11}$$

where, $\mathbf{D}^S$ is the strength degradation matrix of ith yield surface, which is explained in more details below. $\mathbf{S}_i$ is the scaling matrix of the ith yield surface for the consideration of isotropic hardening. Here only kinematic hardening is used and the matrix $\mathbf{S}_i$ is a unit matrix.

It is well known from experimental evidence that any material deteriorates as a function of the loading history. Every inelastic excursion causes damage and the damage accumulates as the number of excursions increases. Therefore it is necessary to include degradation effects in the modeling of hysteretic behavior. Two types of degradation are included in modified VM element: flexibility degradation and strength degradation.

Flexibility degradation refers to the increase of flexibility (decrease of stiffness) as a function of the deformation history. In order to consider the increase in flexibility the elastic flexibility matrix is pre-multiplied by flexibility degradation matrix, $\mathbf{D}^f$ as in the eq. [6]. Where:

$$\mathbf{D}^f = \begin{bmatrix} 1 & 0 & 0 \\ 0 & \dfrac{1}{\left(1-d_v^f\right)^2} & \dfrac{1}{\left(1-d_v^f\right)\left(1-d_\theta^f\right)} \\ 0 & \dfrac{1}{\left(1-d_v^f\right)\left(1-d_\theta^f\right)} & \dfrac{1}{\left(1-d_\theta^f\right)^2} \end{bmatrix} \tag{12}$$

d_v^f and d_θ^f are associated to the damage due to the lateral deformation and rotation, respectively. These variables can take values between 0 (no damage) and 1(total damage) and are equal to:

$$d_i^f = (1 - \exp(-f_i^j p_i)) \qquad 0 \le d_i^f < 1 \tag{13}$$

where p_i represents the i component of accumulated plastic deformation of the hinge (i.e., $p_v = \int \left| du_v^p \right|; p_\theta = \int \left| du_\theta^p \right|$). f_i^j is the stiffness degradation parameter, which is determined

based on the experimental or finite element results. i stands for component of deformation and j stands for the most outer yield surface number, which have been passed by deformation history. For each yield surface, two pairs of the stiffness degradation parameters, one for lateral deformation and the other for rotational deformation, shall be defined.

Strength degradation refers to the decrease of the yield strength values as a function of the deformation history. In order to consider the decrease in yield strength the isotropic scaling matrix, $\mathbf{S}_i$, is pre-multiplied by strength degradation matrix, $\mathbf{D}_i^S$, as in the eq. 11. Where:

$$\mathbf{D}^S = \begin{bmatrix} 1 & 0 & 0 \\ 0 & 1-d_v^s & 0 \\ 0 & 0 & 1-d_\theta^s \end{bmatrix} \tag{14}$$

d_v^S and d_θ^S are associated to the damage due to the lateral deformation and rotation, respectively. These variables can take values between 0 (no damage) and 1 (total damage) and are equal to:

$$d_i^S = (1-\exp(-s_i^j p_i)) \qquad 0 \le d_i^S < 1 \tag{15}$$

where p_i represents the i component of accumulated plastic deformation of the hinge. s_i^j is the strength degradation parameters, i standing for the component of deformation and j standing for the most outer yield surface number, which has been passed by deformation history. For each yield surface, two pairs of the strength degradation parameters, one for lateral deformation and the other for rotational deformation, shall be defined.

When the members suffer lateral torsional buckling, they may show post yield softening behavior. This may also happen when members have non-compact section elements and local buckling of section elements is governing. The existing version of the model cannot predict, properly, those and other similar cases. The new version, which was introduced in this section, is under development and will be employed for the hinges with softening and damage.

6. CONCLUSION

In this paper, the mixed shear-flexural, VM, link element was described. Multi-surfaces plasticity concept was used for modeling of the mixed hinge element by proposing of dissimilar yield surfaces and a new non associated flow rule. The VM link element was examined for shear link beams in eccentrically braced frames and also in special girder moment frames. The analytical results with existing test results were compared and good agreements were observed. Finally, a new modified VM link element is introduced, which has the additional capabilities of modeling softening and damage. This new version is under process of verification.

REFERENCES

Erfani, S. and Kazemi, M.T. (2007). Shear-flexural interaction analysis of reduced web section beams using VM link element, International Journal of Engineering, Vol. 20 (1), pp. 23-35.

Jirasek, M. and Bazant, Z. P. (2002). Inelastic Analysis of Structures. New York, John Wiley & Sons, LTD.

Kasai, K.S.M. and Popov, E.P. (1986). General behavior of WF steel shear link beams, Journal of Structural Engineering, Vol. 12 (2), pp. 362-382.

Kazemi, M.T. and Erfani, S. (2007a). Mixed shear-flexural (VM) hinge element and its applications, Scientia Iranica, Vol. 14 (3), pp. 193-204.

Kazemi, M.T. and Erfani, S. (2007b). Analytical study of special girder moment frames using a mixed shear-flexural link element, Canadian Journal of Civil Engineering, Vol. 34, pp. 1119-1130.

Kazemi, M.T. and Erfani, S. (2009). Special VM link element for modeling of shear–flexural interaction in frames, The Structural Design of Tall and Special Buildings, Vol. 18, pp. 119-135.

Khan, A. S. and Huang, S. (1995). Continuum Theory of Plasticity. New York, John Wiley & Sons. Inc.

Kim, K.D. and Engelhardt, M.D. (2000). Beam-column element for nonlinear seismic analysis of steel frames, ASCE Journal of Structural Engineering, Vol. 126 (8), pp. 916-925.

Krenk, S., Vissing, S., and Vissing-J., C. (1993). A finite step updating method for elastoplastic analysis of frames, ASCE Journal of Engineering Mechanics, Vol. 119 (12), pp. 2478-2495.

Liew, J.Y.R. and Tang, L.K. (2000). Advanced plastic hinge analysis for the design of tubular space frames, Engineering Structures, Vol. 22 (7), pp. 769-783.

Mroz, Z. (1969). An attempt to describe the behavior of metals under cyclic loads using a more general work hardening model, Acta Mechanica, Vol. 7 (2-3), pp. 199-212.

Powell, G.H. and Chen P.F.S. (1986). 3D beam-column element with generalized plastic hinges, ASCE Journal of Engineering Mechanics, Vol. 112 (7), pp. 627-641.

Ramadan, T. and Ghobarah, A. (1995). Analytical model for shear-link behavior, Journal of Structural Engineering, Vol. 121 (11), pp. 1574-1580.

Ricles, J.M. and Popov, E.P. (1994). Inelastic link element for EBF seismic analysis. ASCE Journal of Structural Engineering, Vol. 120 (2), pp. 441-463.

SUT–DAM 3D: AN INTEGRATED SOFTWARE ENVIRONMENT FOR MULTI-DISCIPLINARY GEOTECHNICAL ENGINEERING

A. R. Khoei*, H. Moslemi , M. Anahid, S. A. Gharehbaghi, O. R. Barani, and T. Mohamadnejad

Center of Excellence in Structural and Earthquake Engineering, Department of Civil Engineering, Sharif University of Technology, P.O. Box. 11365-9313, Tehran, Iran

ABSTRACT

As computer simulation increasingly supports engineering design, the requirement for a computer software environment providing an integration platform for computational engineering software increases. In this paper, an integrated software environment is demonstrated for multi-disciplinary computational modeling of structural and geotechnical problems. The SUT–DAM 3D is designed in both popularity and functionality with the development of user-friendly pre- and post-processing software. In SUT–DAM 3D, a numerical model is developed based on a Lagrangian finite element formulation for large deformation dynamic analysis of saturated and partially saturated soils. An adaptive FEM strategy is used into the large displacement finite element formulation by employing an error estimator, adaptive mesh refinement, and data transfer operator. The SUT–DAM 3D supports different yield criteria, including classical and advanced constitutive models, such as the Pastor-Zienkiewicz and cap plasticity models. The paper presents details of the environment and includes an example of the integration of application software.

Keywords: FE software, Pre-processing, Post-processing, Adaptive strategy, Unsaturated soils, P-Z model, Cap plasticity.

1. INTRODUCTION

The finite element method has become a very important analysis tool in many engineering problems as a result of the increase in computer power and the progress in numerical computation technologies. It provides a powerful procedure to mathematically model physical phenomena. The technique is numerically formulated and is effectively used on a broad range of computers. The method has increased in both popularity and functionality with the development of user-friendly pre- and post-processing software. Effective use of the method was enhanced with the introduction of low cost computer graphics systems that provided the means to both automate the generation of the mathematical model and visually display both the model and the computed results. The procedure used to automate the generation of the numerical definition of the model is named finite element pre-processing and that used to visualize the results is named post-processing. Computer simulation methods for structural, flow and thermal analysis are well developed and have been used in design for many years. Many software packages are now available which provide an advanced capability. However, they are not designed for nonlinear adaptive FE modeling of geotechnical problems associated with saturated and unsaturated soils.

* Corresponding author. Tel. +98 (21) 6600 5818, Fax. +98 (21) 6601 4828
Email address: arkhoei@sharif.edu (A.R. Khoei

Porous media is a composition of particles of different size and shape constituting the solid skeleton together with at least one fluid medium filling the remaining pores. The mechanical behavior of the fully or partially saturated porous medium and in particular of soils, is governed largely by the interaction of their solid skeleton with the pore fluid, generally water, present in the pore structure. This interaction is particularly strong in dynamic problems and may lead to liquefaction due to large pore pressure build up, which frequently occurs under earthquakes. Thereby, coupled problems of fluid flow and deformation of the solid skeleton are typically encountered. A one-dimensional theory of consolidation was first proposed by Terzaghi [1] in 1943 and then extended to three-dimensional cases by Biot [2–4]. Although these first attempts were restricted to linear elastic soil skeleton and fluid flow through the solid phase governed by the Darcy law, they have been the basis for a lot of subsequent works in geophysics, soil and rock mechanics. The first numerical solution was made by Ghaboussi and Wilson [5] and then used by Zienkiewicz and Bettess [6] and Zienkiewicz and Shiomi [7] for low frequency phenomena, such are associated with earthquakes a formulation based only on soil displacements and pore pressures. De Boer and Kowalski [8] developed this theory on material non-linearity behavior of the soil skeleton, which has been included in the Terzaghi-Biot framework. Zienkiewicz *et al*. [9] derived a generalized incremental form which includes large deformation and nonlinear material behavior for liquefaction analysis of soil structures.

The subject of unsaturated soils has been receiving attention increasingly for the last few decades. In early works, attempts had been made to modify Biot's consolidation theory which was initially developed for saturated soils, for solving unsaturated soil problems. Fredlund and Morgenstern [10] and Chang and Duncan [11] postulated the pore water and pore air as a homogeneous and compressible fluid. They expressed the compressibility of the homogeneous fluid as functions of different parameters, such as pore water pressure and degree of saturation. A simple extension of two phase formulation to semi-saturated problems was proposed by Zienkiewicz *et al*. [12] based on the assumption of the air or gas present in the pores remaining at atmospheric pressure. They employed their extended formulation for the dynamic analysis of a semi-saturated dam under earthquake loading. Coupled formulations that involve the air and water phases in soils have been also presented by Alonso *et al*. [13] and Gawin *et al*. [14]. However, because of the great complexity of the three-phase models, extensive and specially designed soil testing is required to determine the properties of the soil-air-water mixture. An extension of Zienkiewicz's theory was employed by Khoei *et al*. [15] for solving geotechnical problems associated with unsaturated soils.

In this paper, the computer software SUT̃DAM 3D is demonstrated for computational simulation of geotechnical problems associated with unsaturated soils. A finite element model is developed based on the Lagrangian formulation for large deformation simulation of static and dynamic analyses of saturated and unsaturated soils. An adaptive strategy is employed into the large deformation FE formulation by applying an error estimator, adaptive mesh refinement, and data transfer operator. The adaptive strategy consists in defining new appropriate finite element mesh within the updated, deformed geometry and interpolating (mapping) the pertinent variables from one mesh to another in order to continue the analysis. Different yield criteria are incorporated into the software to describe the nonlinear behavior of the material, including classical and advanced constitutive models, such as the Pastor-Zienkiewicz and cap plasticity models. The software is designed in both popularity and functionality with the development of user-friendly pre- and post-processing software. Pre-processing software is used to create the model, generate

an appropriate finite element grid, apply the appropriate boundary conditions, and view the total model. Post-processing provides visualization of the computed results. It is attempted to summarize work directed at exploring the concepts of an integrated software environment for nonlinear adaptive FE modeling of geotechnical problems associated with saturated and unsaturated soils. It reviews the capabilities that are provided by pre- and post-processing and suggests enhancements and new features that will likely be developed in the near future.

2. OVERVIEW OF THE SOFTWARE ENVIRONMENT

In order to design the software environment SUTDAM 3D, several technical requirements have been considered [16, 17]. These requirements are as follows; the object-oriented programming, C++ programming language, graphic engine, exception handling, data structure, and the input and output phases.

Object-oriented programming: The object-oriented programming is one of the most important techniques in the design of an integrated software environment, which models the real-world objects using software counterparts. It takes the advantage of class relationships where the objects of a certain class have similar characteristics. It also takes the advantage of *inheritance* relationships, and *multiple inheritance* relationships. The object-oriented programming gives a more natural and intuitive way to view the programming process by *modeling* the real-world objects, their behaviors and their attributes, and *creating* communication between the objects. It *encapsulates* the data (attributes) and functions (behavior) into packages called *objects;* the data and functions of an object are intimately tied together. Objects have the property of *information hiding.* This means that although objects may know how to communicate with one another across well-defined *interfaces,* objects normally are not allowed to know how other objects are implemented.

C++ programming language: C++ is a powerful computer programming language. It supports all characteristics of the object-oriented programming and includes many important capabilities not involved in an object-oriented system, such as: function overloading, operator overloading, templates and exception handling. SUTDAM 3D has been written in C++, in order to perform different aspects of these characteristics and capabilities.

Graphic engine: Inheritance is one of the most important characteristics in object-oriented programming, which is proposed in SUTDAM 3D. It is developed by a set of valuable graphical features, which are independent of computer hardware. Those graphical objects perform the graphical tasks in a wide range from drawing a simple line to supporting three-dimensional tasks. SUTDAM 3D can simply handle all of those functions in a simple way because of the object-oriented capabilities.

Exception handling: The extensibility of C++ increases substantially the number and kinds of errors that can occur. Exception handling enables programmers to write clearer, more robust and more fault-tolerant programs. The new exception handling features of C++ enable the programmer to remove the error handling code from the ‘main line’ of a program's execution. This improves program readability and modifiability. With the C++ style of exception handling it is possible to catch all kinds of exceptions, to catch all exceptions of a certain type or to catch all exceptions of related types. In SUTDAM 3D, three major types of exceptions have been

designed. The first two types are the hardware and software exceptions, which are supported by Integrated Development Environment (IDE). The third one is a set of additional exception classes declared by SUTDAM 3D. These additional exceptions are used to guarantee the stability of SUTDAM 3D in critical situations.

Data structure: SUTDAM 3D needs to store and retrieve all information of a problem, such as: nodes, elements, boundaries, loadings, *etc*. Data structures are used to store those information in an easy-to-use manner. Data structures are classified as either linear or nonlinear. In a linear data structure, the elements form a sequence, or a linear list. There are two basic ways of representing such linear structures in memory. One way is to have the linear relationship between the elements represented by means of sequential memory locations, called *arrays*. Another way of storing a list in memory is to have each element in the list contain a field, called a *link* or *pointer*, which contains the address of the next element in the list. There is another list structure which has been applied in SUTDAM 3D, called a two-way list, and can be traversed in two directions; in the usual forward direction from the beginning of the list to the end, or in the backward direction from the end of the list to the beginning.

The input and output phases: SUTDAM 3D is designed to define the input data in two different manners. One option is based on the standard Win32 dialog box by defining the data through out a text file. In another option, the input data can be defined by using the graphical tools, and selecting the nodes, elements, boundaries and other objects, directly. Furthermore, two different options have been also designed to present the output results in SUTDAM 3D; text file and graphical options. The software also supports other special formats for output data, which can be used for importing the results into other commercial software.

3. THE ANALYSIS UTILITY ENVIRONMENT

3.1. Mathematical Model for Pore Fluid Soil Skeleton Interaction

The essence of mathematical theory governing the behavior of porous media with a single pore fluid was first established by Biot [24]. This theory was extended by Zienkiewicz *et al*. [7, 9] to deal with nonlinear behavior of materials. Assuming that the size of solid grains and pores are very small compared with the dimensions in macroscopic scale, the use of averaged variables for total stress σ_{ij}, solid matrix displacement u_i, and the mean flow velocity relative to the solid phase v_i are allowed. The effective stress is an essential concept defining the stresses, which control strength and constitutive behavior of porous material. The concept of effective stress can be considered based on the division of the total stress between the part carried by the solid skeleton and the fluid pressure, in which the strength and deformation of the soil skeleton is only dependent on the stress part. Considering σ_{ij} as the total stress vector, δ_{ij} as the Kronecker delta and p as the pore fluid pressure with positive value in compression, the effective stress σ'_{ij} can be computed as $\sigma'_{ij} = \sigma_{ij} + \alpha\delta_{ij} p$, where α depends on the material type defined by $\alpha = 1 - K_{av}/K_s$, with K_s denoting the bulk modulus of solid particles and K_{av} the average bulk modulus of the solid skeleton. α is taken to be unity for soils.

The governing equations of saturated porous media, particularly soils, with a single fluid phase, generally water are presented based on the total equilibrium for soil-pore fluid mixture, the equilibrium equation for the pore fluid, called the generalized Darcy's equation, the mass

balance of flow equation, the concept of effective stress, and the constitutive model for the nonlinear behavior of saturated soil [7, 9]. The overall equilibrium equations for the soil-fluid mixture can be written as

$$\sigma_{ij,j} + \rho\ddot{u}_i + \underline{\rho_f[\dot{v}_i + v_j v_{i,j}]} - \rho b_i = 0 \tag{1}$$

$$p_{,i} + V_i^D + \rho_f \ddot{u}_i + \underline{\rho_f[\dot{v}_i + v_j v_{i,j}]/n} - \rho_f b_i = 0 \tag{2}$$

$$-v_{i,i} + \dot{\varepsilon}_{ii} + \frac{n\dot{p}}{K_f} + \frac{(1-n)\dot{p}}{K_s} - \frac{K_{av}}{K_s}(\dot{\varepsilon}_{ii} + \frac{\dot{p}}{K_s}) + n\underline{\frac{\dot{\rho}_f}{\rho_f}} + \dot{\theta} = 0 \tag{3}$$

where b_i is the body force per unit mass, ρ_f is the fluid density and ρ is the density of total composite, defined by $\rho = n\rho_f + (1-n)\rho_s$, with n denoting the porosity and ρ_s the density of solid particles. V_i^D represents the viscose drag force, which can be obtained from the Darcy seepage law by $v_i = k_{ij}V_j^D$, where k_{ij} is the dynamic permeability. In above equations, ε_{ij} are the total strains, K_f is the fluid bulk modulus and $\dot{\theta}$ is the rate of volume expansion of the solid in the case of thermal changes. In equation (1), the underlined term is the effect of fluid relative acceleration to the solid particles and convective terms of this acceleration. Equation (2) ensures the momentum balance for the fluid phase and equation (3) indicates the mass balance of the fluid flow. In equation (3), the fluid flow divergence is balanced by the change of pores volume in the control volume. First term is the fluid flow divergence, second is the volume change due to change in strains, third is the additional storage volume due to compression of fluid under its pressure, fourth is the additional storage volume due to compression of solid particle under fluid pressure, and fifth is the volume change of solid particles under their effective inter-granular stress. The last two terms are corresponding to change of fluid density and volume change of solid particles in the case of thermal changes and in general are negligible.

The definition of the combined compressibility of the fluid and solid phases can be presented by $C = nC_f + (\alpha - n)C_s$, where C_f is the compressibility of fluid defined by $C_f = 1/K_f$, and C_s is the compressibility of solid particles defined as $C_s = 1/K_s$. Substituting α and C into equation (3) and omitting the negligible terms, lead to

$$-v_{i,i} + \alpha\dot{\varepsilon}_{ii} + \dot{p}C = 0 \tag{4}$$

Equations (1), (2) and (4) present the behavior of porous media in both static and dynamic conditions, with considering the interaction of its solid skeleton with the pore fluid. The pore fluid pressure p, the relative velocity of fluid flow to solid phase v_i and the displacement of solid skeleton u_i are the unknown variables in these equations system. When the acceleration frequencies are low, as in the case of earthquake motions, the underlined terms in equations (1) and (2) are not important and can be omitted as shown by Zienkiewicz *et al*. [18]. By omitting these terms, the variable v_i can be eliminated from the equations, so the simplified governing equation, which contain two independent variables u_i and p, can be achieved as

$$\sigma_{ij,j} + \rho\ddot{u}_i - \rho b_i = 0 \tag{5}$$

Combining equations (2) and (4) and omitting the negligible terms, the second governing equation will be obtained as

$$\left[k_{ij}\left(p_{,j}+\rho_f \ddot{u}_j-\rho_f b_j\right)\right]_{,i}+\alpha\dot{\varepsilon}_{ii}+\dot{p}C=0 \tag{6}$$

Equations (5) and (6) together form the $\mathbf{u}-p$ formulation, which must be solved in a coupled manner. In order to solve these equations, the initial and boundary conditions are necessary. For the total momentum balance on the part of boundary Γ_t, the total traction $\mathbf{t}$ is specified, while for Γ_u, the displacement $\mathbf{u}$ is given. For the fluid phase, the value of p is specified on Γ_p.

3.2. Governing Equations for Unsaturated Conditions

In order to develop the governing equations in unsaturated cases, some modifications must be implemented. In unsaturated conditions, the voids of porous media are filled partly by water and partly by air. For simplicity, Zienkiewicz *et al*. [12] assumed that the air pressure is zero $(p_a=0)$. In this study, the soil is taken as porous media and the pores are filled partly by water and partly by air. Considering the degrees of water and air saturation by S_w and S_a, respectively, in which $S_w+S_a=1$, the density of soil-pore fluid mixture can be modified as $\rho=nS_w\rho_w+nS_a\rho_a+(1-n)\rho_s$. Furthermore, the definition of effective stress can be modified based on the average pore pressure by applying the well known Bishop's law [19]. The average pore pressure is defined as $p_{av}=\chi\, p_w+(1-\chi)p_a$, where χ is the Bishop's parameter depends on the degree of water saturation. A good approximation of χ can be given by the degree of water saturation S_w. For simplicity, consider the value of air pressure zero, the average pore pressure can be then approximated by $p_{av}=S_w p_w+(1-S_w)p_a$.

In order to modify the mass balance equation of fluid flow, given in equation (3), the divergence of fluid flow is balanced by the change of pores volume in the control volume. Considering the effect of water saturation along with a new term which take these changes into account, lead to

$$-v_{i,i}+\dot{\varepsilon}_{ii}+S_w\left(\frac{n\,\dot{p}_w}{K_f}+\frac{(1-n)\dot{p}_w}{K_s}\right)-\frac{K_{av}}{K_s}(\dot{\varepsilon}_{ii}+\frac{\dot{p}}{K_s})+n\frac{\dot{\rho}_w}{\rho_w}+\dot{\theta}+n\,\dot{S}_w=0 \tag{7}$$

A modified definition of the combined compressibility C can be written as $C=S_w\left(nC_f+(\alpha-n)C_s\right)+n\left(\dot{S}_w/\dot{p}_w\right)$. Applying the material parameter α and the new definition of combined compressibility C and then, omitting the negligible terms in equation (7), we will obtain

$$-v_{i,i}+\alpha\,\dot{\varepsilon}_{ii}+\dot{p}_w C+n\,S_w\frac{\dot{\rho}_w}{\rho_w}=0 \tag{8}$$

in which the relation between the degree of saturation and permeability and also, the degree of saturation and water pressure must be taken into account.

Finally, the modified $\mathbf{u}-p$ formulation, including the total equilibrium of soil mixture and the continuity and mass balance equation, for static and dynamic behavior of saturated and unsaturated soils can be rewritten as

$$\sigma_{ij,j} + \rho\ddot{u}_i - \rho b_i = 0 \tag{9}$$

$$\left[k\left(p_{w,j} + S_w\rho_f\ddot{u}_j - S_w\rho_f b_j\right)\right]_{,i} + \alpha\dot{\varepsilon}_{ii} + \dot{p}_w C = 0 \tag{10}$$

The above equations have been implemented into the computer software SUT–DAM 3D to model two-dimensional and axisymmetric applications of saturated–unsaturated soils. In addition, it can deal with static and dynamic analysis of drained and undrained soils, as shown in Figure 1.

3.3. FE Formulation of Governing Equations

In order to obtain a numerical solution of the governing equations of saturated-unsaturated porous media, presented in previous sections, a suitable discretization process is necessary for both spatial and time discretization. The spatial discretization can be achieved by suitable shape functions for two variables u_i and p_w, defined as $\mathbf{u} = \mathbf{N}^u\overline{\mathbf{u}}$ and $p_w = \mathbf{N}^p\overline{p}_w$, where $\mathbf{N}^u$ and $\mathbf{N}^p$ are the shape functions. The governing equations can now be transformed into a set of algebraic equations in space by the use of an appropriate Galerkin method. The discretization of first equation in space can be achieved by pre-multiplying equation (9) by $(\mathbf{N}^u)^{\mathrm{T}}$ and integrating over the spatial domain, as

$$\mathbf{M}\ddot{\overline{\mathbf{u}}} + \int_\Omega \mathbf{B}^{\mathrm{T}}\boldsymbol{\sigma}' d\Omega - \mathbf{Q}\overline{p} - \mathbf{f}^{(1)} = 0 \tag{11}$$

where the mass matrix $\mathbf{M}$, the coupling matrix $\mathbf{Q}$, and the load vector $\mathbf{f}^{(1)}$ are defined as

$$\mathbf{M} = \int_\Omega (\mathbf{N}^u)^{\mathrm{T}}\rho\mathbf{N}^u d\Omega$$

$$\mathbf{Q} = \int_\Omega \mathbf{B}^{\mathrm{T}} S_w \mathbf{m}\mathbf{N}^p d\Omega \tag{12}$$

$$\mathbf{f}^{(1)} = \int_\Omega (\mathbf{N}^u)^{\mathrm{T}}\rho\mathbf{b} d\Omega + \int_{\Gamma_t} (\mathbf{N}^u)^{\mathrm{T}}\bar{\mathbf{t}} d\Gamma$$

In equation (11), the constitutive relation is taken into account by $d\boldsymbol{\sigma}' = \mathbf{D}d\boldsymbol{\varepsilon} = \mathbf{D}\mathbf{B}d\overline{\mathbf{u}}$, where $\mathbf{B}$ is the matrix relating the increments of strain and displacements. For geometrically nonlinear behavior, we can select either a total or an updated Lagrangian coordinate system in SUT–DAM 3D, as shown in Figure 1. A Lagrangian description is used which describes the material behavior with respect to either the original domain in the case of a total Lagrangian frame or the domain at the previous calculation step in the case of an updated Lagrangian scheme [20]. The non-linear strain displacement relationship is defined in terms of the infinitesimal and large

displacement components by $\boldsymbol{\varepsilon} = \boldsymbol{\varepsilon}_L + \boldsymbol{\varepsilon}_{NL}$, with $\boldsymbol{\varepsilon}_L$ and $\boldsymbol{\varepsilon}_{NL}$ denoting the linear and nonlinear strains. Thus, we can write $\mathbf{B}$ in terms of the linear and nonlinear strain-displacement matrix as

$$\mathbf{B} = \mathbf{B}_L + \mathbf{B}_{NL}(\bar{\mathbf{u}}) \tag{13}$$

where $\mathbf{B}_L$ is the same matrix as in a linear infinitesimal strain analysis and only $\mathbf{B}_{NL}$ depends on the displacement.

In a similar manner the second discretized equation is derived by pre-multiplying equation (10) by $(\mathbf{N}^p)^{\mathrm{T}}$ and integrating over the spatial domain as

$$\mathbf{Q}\dot{\bar{\mathbf{u}}} + \mathbf{H}\bar{p} + \mathbf{G}\dot{\bar{p}} - \mathbf{f}^{(2)} = 0 \tag{14}$$

where

$$\mathbf{H} = \int_\Omega (\nabla \mathbf{N}^p)^{\mathrm{T}} k \nabla \mathbf{N}^p d\Omega$$

$$\mathbf{G} = \int_\Omega \mathbf{N}^p C\, \mathbf{N}^p d\Omega \tag{15}$$

$$\mathbf{f}^{(2)} = -\int_\Omega (\mathbf{N}^p)^{\mathrm{T}} \nabla^{\mathrm{T}} (\mathbf{k} S_w \rho_f \mathbf{b}) d\Omega$$

In order to complete the numerical solution, it is necessary to integrate the differential equations (11) and (14) in time. In the present study, the generalized Newmark *GN22* method is considered for the displacement parameter and *GN11* method for the pressure parameter. In this method, it is assumed that the variables are known at time t^n and must be evaluated at time $t^{n+1} = t^n + \Delta t$, in which the only unknown variables are $\Delta\ddot{\bar{\mathbf{u}}}_n$ and $\Delta\dot{\bar{p}}_n$. Applying time discretization into equations (11) and (14) lead to

$$\mathbf{M}^{n+1}\Delta\ddot{\bar{\mathbf{u}}}^n + \mathbf{P}(\bar{\mathbf{u}}^{n+1}) - \mathbf{Q}^{n+1}\bar{\beta}_1 \Delta t \Delta\dot{\bar{p}}^n - \mathbf{f}_1^{n+1} = \mathbf{0} \tag{16}$$

$$\left(\mathbf{Q}^{\mathrm{T}}\right)^{n+1}\beta_1 \Delta t \Delta\ddot{\bar{\mathbf{u}}}^n + \mathbf{H}^{n+1}\bar{\beta}_1 \Delta t \Delta\dot{\bar{p}}^n + \mathbf{G}_{n+1}\dot{\bar{p}}^n - \mathbf{f}_2^{n+1} = \mathbf{0} \tag{17}$$

where $\mathbf{P}(\bar{\mathbf{u}}^{n+1}) = \int_\Omega \mathbf{B}^{\mathrm{T}} \boldsymbol{\sigma}'^{n+1} d\Omega$. Parameters β_1 and $\bar{\beta}_1$ are in the range of 0 to 1 and for unconditional stability of the solution process, $\beta_1 \geq 0.5$ and $\bar{\beta}_1 \geq 0.5$. The nonlinear coupled equations (16) and (17) are solved employing the Newton Raphson procedure.

In SUT–DAM 3D, the direct implicit algorithm based on the generalized Newmark scheme is used for the time integration and an automatic time step control facility is provided (Figure 2). For non-linear iteration, choices among fully or modified Newton-Raphson method and quasi-Newton method, using the initial stiffness method, Davidon inverse method or BFGS inverse method, are possible, as shown in Figure 2. For solving the linear algebraic equations, a symmetric core profile direct solver or Preconditioned Conjugate Gradient iterative solvers can be used. The software uses dynamic arrays, vectors, and maps from Standard Template Library

of C++ language. All input information, such as: nodes, elements, boundaries, material properties, *etc* are stored and retrieved using the Standard Template Library. It guarantees the compatibility of the source code with other compilers supporting STL. Both triangular and quadrilateral elements are available in the element library, including 3, 6, 7 noded triangles, 4, 8, 9 noded quadrilaterals, 4, 10 noded tetrahedrals, and 8, 20 noded hexahedrals.

3.4. Adaptive FE strategy

The objective of adaptive techniques is to obtain a mesh which is optimal in the sense that the computational costs involved are minimal under the constraint that the error in the finite element solution is acceptable within a certain limit. Since the computational effort can be linked to the number of unknowns of the finite element mesh the task is to find a mesh with a minimum number of unknowns, or nodes, for a given error tolerance. To obtain an optimal mesh, in the sense of an equal solution quality, it is desirable to design the mesh such that the error contributions of the elements are equally distributed over the mesh. In a practical scheme for an adaptive analysis in plasticity, the mesh must be changed when the error is more than a prescribed value. After changing the mesh, all state variables must be transferred to the integration points of the new mesh. Since, in a conventional displacement formulation of FEM, the state variables are stored at these integration points, then the transfer of these values from the old integration points to the new ones can be carried out by using nodal points as the reference points to store the information. In the case that nodal points are used as reference points, the variables at any arbitrary point can be evaluated by interpolation. In general, the procedure described above can be executed in three parts; an error indicator, an adaptive mesh refinement, and the mapping of variables [21].

3.4.1. Error Indicator

Discontinuity and failure of elasto-plastic solids is very frequently accompanied by development of surfaces or bands at which high gradients of displacement are present. Thus, if we refine the element size h in a manner ensuring that

$$h\left|\frac{\partial \varphi}{\partial x}\right| = C \tag{18}$$

where C is a predetermined constant and φ is a scalar variable of the absolute displacement, i.e., $\varphi = (\mathbf{u}^{\mathrm{T}}\mathbf{u})^{1/2}$, with $\mathbf{u}$ denoting the displacement vector. By ensuring that the mesh is generated so that the quantity C is constant throughout all elements, we achieve a solution which captures well all local discontinuities and which is efficient in achieving the progression which gives overall accuracy. In 2D/3D contexts, the refinement criterion of (18) provides a useful indicator and leads to a successful capture of discontinuities. Of course now, the maximum gradient of the scalar function φ is used and h refers to the minimum element size. Thus, the error can be estimated based on the maximum gradient of absolute displacements as

$$e = \varphi - \varphi^h \;\le\; \tilde{e} = ch\left|\frac{\partial \varphi^h}{\partial \tilde{x}}\right|_{\max} \tag{19}$$

where φ^h is the absolute value of displacements for the finite element solution, $\tilde{x}$ is any direction chosen, h is the element size, c is a positive constant and the displacement gradient is computed from the numerical solution. In order to indicate the amount of elongation, the curvatures will be considered by two orthogonal directions, maximum and minimum values, in which the element will be elongated in the direction of the minimum curvature. Thus, if in any element the principal second derivatives and their directions can be found, then the element could be stretched with sizes

$$s = \frac{h_{\max}}{h_{\min}} = \left(\left| \frac{\partial^2 \varphi^h}{\partial \tilde{x}^2} \right|_{\max} \Big/ \left| \frac{\partial^2 \varphi^h}{\partial \tilde{x}^2} \right|_{\min} \right)^{1/2} \tag{20}$$

3.4.2. Adaptive Mesh Refinement

Adaptive remeshing of finite element solutions refers to improving the quality of the solutions by enriching the approximation in some manner so as to achieve the best solution for a given computational effort. An adaptive process is actually a feedback approach, which is optimal with respect to clearly defined objectives. In practical applications, we shall try to devise a procedure in which the error indicator in each element is reduced to, or below, a specified value. For this purpose, a solution including displacements and its first and second derivatives will be obtained from an initial mesh. As the constant c in equation (18) is not known a priori and the specification of maximum levels for the error indicators $\tilde{e}$ is not easy, the maximum value of r will be computed in the whole domain by

$$r = h_{old} \left| \frac{\partial \varphi^h}{\partial \tilde{x}} \right|_{\max} \tag{21}$$

The new mesh size will be obtained by choosing an appropriate value for r in the new mesh. The new value of r can be considered to be proportional to the absolute maximum value of it in the old mesh, i.e. $r = \beta r_{\max}$, thus

$$h_{\text{new}} = (\beta r_{\max}) \Big/ \left(\left| \frac{\partial \varphi^h}{\partial \tilde{x}} \right|_{\max} \right) \tag{22}$$

where β is a prescribed value which is suggested to be between 0.1–0.4.

After indicating the minimum size of elements from equation (22) and determining the elongation s and its direction by expression (20), a mesh satisfying the requirements will be finally generated by an efficient mesh generator which allows the new mesh to be constructed according to a predetermined size and elongation distribution. Figure 3 presents the designed interfaces for the adaptive strategy in SUT–DAM 3D.

3.4.3. Mapping of Variables

Once a new mesh is generated, state and internal variables need to be mapped from the old finite element mesh to the new one. The mapping of state and internal variables between two finite element meshes is the essential part of any adaptive strategy that is employed in simulation of history-dependent material processes on evolving general unstructured meshes. The state variables consist of the nodal displacements and the internal variables include the Cauchy stress tensor, the strain tensor, the plastic strain tensor and a vector of internal variables. Several important aspects of the mapping process have to be addressed, i.e.,

(i) consistency with the constitutive equations,
(ii) requirement of equilibrium,
(iii) compatibility of the history-dependent internal variables transfer with the displacement field on the new mesh,
(iv) compatibility with evolving boundary conditions,
(vi) minimization of the numerical diffusion of the transferred state fields.

Let $\boldsymbol{u}_n^{\text{old}}, \boldsymbol{\varepsilon}_n^{\text{old}}, (\boldsymbol{\varepsilon}_n^p)^{\text{old}}, \boldsymbol{\sigma}_n^{\text{old}}, \boldsymbol{q}_n^{\text{old}}$ denote the values of displacement, strain tensor, plastic strain tensor, stress tensor and a vector of internal variables at time t_n for the mesh h. For simplicity of notation, we define a state array $\boldsymbol{\Lambda}_n^{\text{old}} = \left(\boldsymbol{u}_n^{\text{old}}, \boldsymbol{\varepsilon}_n^{\text{old}}, (\boldsymbol{\varepsilon}_n^p)^{\text{old}}, \boldsymbol{\sigma}_n^{\text{old}}, \boldsymbol{q}_n^{\text{old}}\right)$. Furthermore, assume that the estimated error of the solution $\boldsymbol{\Lambda}_n^{\text{old}}$ respects the prescribed criteria, while these are violated by the solution $\boldsymbol{\Lambda}_{n+1}^{\text{old}}$. In this case, a new mesh $h+1$ is generated and a new solution $\boldsymbol{\Lambda}_{n+1}^{\text{new}}$ is computed by evaluating the plastic strain $(\boldsymbol{\varepsilon}_n^p)^{\text{new}}$ and the internal variables $\boldsymbol{q}_n^{\text{new}}$ for a new mesh $h+1$ at time step t_n. In this way, the state array $\widehat{\boldsymbol{\Lambda}}_n^{\text{new}} = \left((\boldsymbol{\varepsilon}_n^p)^{\text{new}}, \boldsymbol{q}_n^{\text{new}}\right)$ is constructed, where $\widehat{\boldsymbol{\Lambda}}$ is used to denote a reduced state array. It must be noted that the state array $\widehat{\boldsymbol{\Lambda}}$ characterizes the history of the material and provides sufficient information for computation of a new solution $\boldsymbol{\Lambda}_{n+1}^{\text{new}}$. The mapping of internal variables is denoted by the transfer operator $\mathcal{T}_1$. In addition, a transfer operator is employed that transfers the state variables, i.e. displacement field, from the old to a new mesh. In the context of the backward Euler scheme where solution is sought at time step t_{n+1}, this transfer provides a trial solution. The mapping of state variables is denoted by the transfer operator $\mathcal{T}_2$.

The mapping process of displacement field is stated using the transfer operator $\mathcal{T}_2$ as

$$\boldsymbol{u}^{\text{old}}(\Omega) \rightarrow \boldsymbol{u}^{\text{new}}(\Omega) \tag{23}$$

where $\boldsymbol{u}^{\text{old}}$ and $\boldsymbol{u}^{\text{new}}$ denote the displacement fields given by the old and new finite element meshes, respectively, where both finite element models occupy the same domain Ω. The mapping process for the internal variables can be stated in a similar manner using the transfer operator $\mathcal{T}_1$ as

$$\boldsymbol{I}^{\text{old}}(\Omega) \rightarrow \boldsymbol{I}^{\text{new}}(\Omega) \tag{24}$$

where $\boldsymbol{I}^{\text{old}}(\Omega)$ and $\boldsymbol{I}^{\text{new}}(\Omega)$ are the list of internal variables of the old and new finite element meshes.

Before the solution variables can be transferred from the integration points of the old finite element mesh to the nodal points of the new finite element mesh, we must first determine which element in the old mesh contains the node *n* in the new finite element mesh. Since this task has to be performed for every nodal and integration point in the new finite element mesh, it is important that a reliable and computationally efficient procedure be used. In this study, we have employed the 'superconvergent patch recovery' SPR method to project the values from the old Gauss points to the old nodal points. In this case, we first obtain the smoothed nodal point values for each of the variables in the list $\boldsymbol{I}^{\text{old}}$, then use the inverse mapping technique to transfer these variables to the nodal points of the new finite element mesh and finally the corresponding values at the new Gauss points can be calculated using interpolation functions in the new finite element mesh. In Figure 4, the adaptive mesh refinement is shown for a slope at three different stages in SUT−DAM 3D. The results display that the adapted meshes improve significantly the shear band zone and the reaction become close between these meshes.

3.5. Soil Constitutive Models

In order to adequately reproduce soil behaviour under cyclic loading, as a sequence of loading/ unloading/ reloading, modifications have to be introduced to the classical constitutive models. The success for an elasto-plastic solution of the nonlinear coupled equations (16) and (17) depends on; firstly, a reasonable elasto-plastic constitutive model which can reproduce soil behaviour under complicated loading conditions and secondly, an accurate and stable integration algorithm for elasto-plastic constitutive relation. It is however imperative that the proposed model includes two characteristics. It must be in terms of effective stresses to show the failure when a residual angle of friction is reached and, it must be history dependent to show an accumulation of negative volumetric strain which results in pore pressure increases and hence strength degradation which is the essence of liquefaction. Furthermore, it needs to reproduce as accurately as possible stress-strain paths observed in laboratory experiments and make this with a relatively small number of parameters. In SUT−DAM 3D, the nonlinear behaviour of soil is simulated using the Pastor-Zienkiewicz and cap plasticity models for the description of cyclic loading. In addition, the software supports other yield criteria, including: Tresca, von-Mices, Mohr-Coulomb and Drucker-Prager models, as shown in Figure 5.

3.5.1. Pastor-Zienkiewicz Model

A generalized plasticity model was first developed by Pastor and Zienkiewicz to predict the basic phenomena encountered in dynamic loading of fully saturated porous media such as the accumulation of plastic strain and pore pressure build-up during the loading process. The main advantage of theory is that neither yield surface nor plastic potential surface needs to be explicitly defined. In generalized plasticity theory, the elasto-plastic constitutive matrix in loading $\mathbf{D}_L$ differs from constitutive matrix in unloading $\mathbf{D}_U$. In fact, at each point of the stress space, a direction tensor is specified to distinguish between loading and unloading. The constitutive matrix can be defined as

$$\mathbf{D}_L = \mathbf{D}_e - \frac{\mathbf{D}_e.\mathbf{n}_{gL}.\mathbf{n}^T.\mathbf{D}_e}{H_L + \mathbf{n}^T.\mathbf{D}_e.\mathbf{n}_{gL}}, \qquad \mathbf{D}_U = \mathbf{D}_e - \frac{\mathbf{D}_e.\mathbf{n}_{gU}.\mathbf{n}^T.\mathbf{D}_e}{H_U + \mathbf{n}^T.\mathbf{D}_e.\mathbf{n}_{gU}} \tag{25}$$

where H_L and H_U are the plastic hardening/softening modulus in loading and unloading and $\mathbf{n}_{gL}$ and $\mathbf{n}_{gU}$ are the normal vector to plastic potential in loading and unloading conditions. In this frame work, all necessary components of elasto-plastic constitutive matrix depend on the current state of stress and loading/unloading condition. In this theory, parameters $\mathbf{n}_g$, $\mathbf{n}$ and $H_{L/U}$ can be obtained without referring to plastic potential, or yield surfaces. However, the yield and potential surfaces, f and g, can be defined using the normal directions to these surfaces. In order to introduce the parameters of the model, a triaxial compression test may be applied. Considering $p' = J_1/3$, $q = \sqrt{3J_{2D}}$ and their work-associated strains invariants ε_v^p and ε_s^p, with J_1 and J_{2D} denoting the first invariant of effective stress tensor and second invariant of deviatoric effective stress tensor, respectively, it can be shown that the dilatancy d_g can be approximated from the stress ratio $\eta = p'/q$ by $d_g = d\varepsilon_v^p / d\varepsilon_s^p$, or $d_g = (1+\alpha)(M_g - \eta)$, where α is a material parameter and M_g denotes the slope of critical state line. The normal vectors to the plastic potential and yield surfaces can be determined by

$$\mathbf{n}_g^T = (n_{gv}, n_{gs}) = \left(d_g, 1\right) \Big/ \sqrt{1 + d_g^2} \tag{26}$$

$$\mathbf{n}^T = (n_v, n_s) = \left(d_f, 1\right) \Big/ \sqrt{1 + d_f^2} \tag{27}$$

where d_f is defined in a similar manner to d_g as $d_f = (1+\alpha)(M_f - \eta)$, where M_g / M_f is approximately equal to relative density. In the case of $d_f = d_g$, the plasticity relationship is associated.

The plastic modulus H_L for the loading condition is defined by

$$H_L = H_0 p' H_f \left(H_v + H_s\right) H_{DM} \tag{28}$$

where

$$H_f = \left(1 - \eta/\eta_f\right)^4 \tag{29}$$

$$H_s = \beta_0 \beta_1 \exp(-\beta_0 \xi) \tag{30}$$

$$H_v = \left(1 - \eta/M_g\right) \tag{31}$$

$$H_{DM} = \left(\zeta_{\max}/\zeta\right)^\gamma \tag{32}$$

In above $\eta_f = \left(1 + 1/\alpha\right) M_f$, $\zeta = p' \left[1 - \left((1+\alpha)/\alpha\right)\left(\eta/M_g\right)\right]^{1/\alpha}$, and $\zeta_{\max}$ is the maximum value of ζ. H_0, β_0 and β_1 are the material parameters obtained from experiments, and ξ is defined as $\xi = \int (d\mathbf{e}^{pT} d\mathbf{e}^p)^{1/2}$. The plastic modulus H_U for unloading condition is defined by

$$H_U = H_{U0}\left(M_g/\eta_U\right)^{\gamma_U} \quad \text{for } \left|M_g/\eta_U\right| > 1$$
$$H_{U0} \quad \text{for } \left|M_g/\eta_U\right| \le 1 \tag{33}$$

where H_{U0} is the material parameter and η_U is the stress ratio of p'/q from which unloading takes place. The vector $\mathbf{n}_{gU}$ is defined as

$$\mathbf{n}_{gU} = (n_{gUv}, n_{gUs})^T = (-abs(n_{gv}), +n_{gs})^T \tag{34}$$

3.5.2. Cap Plasticity Model

The cap models are based on the concept of continuous yielding of materials, but they are expressed in terms of a three-dimensional state of stress and are formulated on the basis of consistent mechanics principles [15]. The yield surface of this elasto-plastic model has a moving cap, intersecting the hydrostatic loading line, whose position is a function of plastic volumetric strain. The main features of the cap model include a failure surface and an elliptical yield cap which closes the open space between the failure surface and the hydrostatic axis. The cap surface expands in the stress space according to a specified hardening rule. The functional forms for these surfaces are

$$f_1 = \sqrt{J_{2D}} - \theta J_1 + \gamma e^{-\beta J_1} - \alpha = 0 \tag{35}$$

$$f_2 = R^2 J_{2D} + (J_1 - L)^2 - R^2 b^2 = 0 \tag{36}$$

$$f_3 = J_1 - T = 0 \tag{37}$$

where α, β, γ and θ are the parameters of fixed yield surface f_1, which controls the deviatoric stress limits. The fixed yield surface f_1 is defined by an exponential function and in reality is consist of two different Drucker-Prager yield surfaces. The cap yield surface f_2 is an elliptical function, with R denoting the ratio of two elliptical cap's diameters. The function f_3 indicates the tension cutoff zone, with T denoting the material's tension limit.

The hardening rule for moving cap is related to the volumetric plastic strain ε_v^p as

$$X(\kappa) = X(\varepsilon_v^p) = \frac{-1}{D} \ln\left(\frac{1-\varepsilon_v^p}{W}\right) + X_0 \tag{38}$$

where D and W are material parameters and X_0 refers to the position of initial cap surface. The plastic hardening/softening modulus H is zero for f_1 and f_3.

In order to compute the elasto-plastic constitutive matrix, we need to calculate the plastic hardening/softening modulus and flow direction vector.

$$H = -\left(\frac{\partial f_2}{\partial \kappa}\right)\left(\frac{\partial \kappa}{\partial \boldsymbol{\varepsilon}}\right)^T \mathbf{n}_g \tag{39}$$

$$\frac{\partial F}{\partial \boldsymbol{\sigma}} = C_1 \frac{\partial J_1}{\partial \boldsymbol{\sigma}} + C_2 \frac{\partial (J_{2D})^{1/2}}{\partial \boldsymbol{\sigma}} + C_3 \frac{\partial J_{3D}}{\partial \boldsymbol{\sigma}} \tag{40}$$

where $C_1 = \partial F / \partial \boldsymbol{\sigma}$, $C_2 = \partial F / \partial (J_{2D})^{1/2}$ and $C_3 = \partial F / \partial J_{3D}$.

For the fixed yield surface, the values of constants C_1, C_2 and C_3 in the case of associated flow rule are as follows; $C_1 = -\theta - \beta\gamma e^{-\beta J_1}$, $C_2 = 1$ and $C_3 = 0$. It can be seen that the value of C_1 is less than zero. It means that the normal vector to the plastic potential surface is in opposite direction of $J_1 -$axis. On the other hand, the associated flow rule results in dilation of material (increase of volume) and the stress state lays on the fixed yield surface at the ultimate shear stress. As the ultimate shear stress shows no volume changes in material, the non-associated flow rule can be therefore utilized, in which the normal vector to the plastic potential surface is perpendicular to $J_1 -$axis. Thus, the values of constants C_1, C_2 and C_3 for plastic flow vector $\mathbf{n}_g$ are $C_1 = 0$, $C_2 = 1$ and $C_3 = 0$.

In order to calculate the values of constants C_1, C_2 and C_3 for moving cap surface, the values of constants C_i in flow direction vector can be obtained using function f_2 in equation (36) as

$$C_1 = \frac{J_1 - L}{\sqrt{R^2 J_{2D} + (J_1 - L)^2}}, \quad C_2 = \frac{R^2 \sqrt{J_{2D}}}{\sqrt{R^2 J_{2D} + (J_1 - L)^2}}, \quad C_3 = 0 \tag{41}$$

The plastic hardening/softening modulus for moving cap surface can be determined by equation (39). Considering the hardening parameter κ equal to ε_v^p, it leads to

$$H = -\left(\frac{\partial f_2}{\partial \varepsilon_v^p}\right)\left(\frac{\partial \varepsilon_v^p}{\partial \boldsymbol{\varepsilon}}\right)^T \mathbf{n}_g = -\left(\frac{\partial f_2}{\partial \varepsilon_v^p}\right)\left(n_{g\,ii}\right) \tag{42}$$

where

$$\frac{\partial f_2}{\partial \varepsilon_v^p} = \frac{\partial f_2}{\partial L}\frac{\partial L}{\partial \varepsilon_v^p} + \frac{\partial f_2}{\partial b}\frac{\partial b}{\partial \varepsilon_v^p} \tag{43}$$

where $\partial f_2 / \partial L = 2(J_1 - L)$ and $\partial f_2 / \partial b = -2R^2 b$. From the definition of moving cap surface, we have $L = X - Rb$, $b = \theta L - \gamma e^{-\beta L} + \alpha$ and then, $L(1 + R\theta) - R\gamma e^{-\beta L} + R\alpha = X$. By taking derivative from these relations, we will obtain

$$\frac{\partial L}{\partial \varepsilon_v^p} = \frac{1}{D(W - \varepsilon_v^p)} \frac{1}{1 + R\theta + R\beta\gamma e^{-\beta L}} \tag{44}$$

$$\frac{\partial b}{\partial \varepsilon_v^p} = \frac{1}{R}\left(\frac{\partial X}{\partial \varepsilon_v^p} - \frac{\partial L}{\partial \varepsilon_v^p}\right) \tag{45}$$

Finally, the values of constants C_1, C_2 and C_3 for the tension cut-off yield surface can be simply calculated according to equation (37) as $C_1 = -1.0$, $C_2 = 0$ and $C_3 = 0$, and the plastic hardening/softening modulus for tension cut-off surface is assumed to be zero.

4. NUMERICAL SIMULATION RESULTS IN SUT–DAM 3D

This example demonstrates the performance of SUT–DAM 3D by employing the Pastor-Zienkiewicz plasticity model in elasto-plastic dynamic analysis of saturated and unsaturated earth dam. The analyses are carried out to simulate the lower San Fernando dam, which collapsed during the earthquake of February 9, 1971. Although the earthquake lasted for about 15 s, failure of dam occurred at about 60 s after beginning of the earthquake. Seed *et al*. [22] illustrated this failure, as shown in Figure 6(a). They found that the time difference between the failure and end of the earthquake was due to important pore pressure build-up, as a result of cyclic loading, first in the central portion of the dam and then, the migration of this excess pore pressure in the post earthquake period to the regions closer to the upstream slope of the dam, and so the failure occurred at about 60s after beginning of the earthquake.

The finite element mesh used in this analysis for both solid and fluid phases is shown in Figure 6(b). Also presented in Figure 6(c) is the geometry, material zones and boundary conditions of the dam. The general material properties of the dam are given in Table 1 for different zones. The material parameters of Pastor-Zienkiewicz model are listed in Table 2. The distribution of pore pressure in the dam body at steady state condition is presented in Figure 7(a). As can be observed, the negative pore pressure exists in dam crest and downstream slope in unsaturated zones. Without this suction the preliminary computations indicates that immediate local failure develops in dry material due to shaking. Figure 7(b) shows the distribution of effective vertical stress in the dam body at steady state condition. In order to illustrate the mechanism of the failure in the dam body, the distribution of excess pore water pressure, the effective stress contours and the distribution of first invariant of effective stress are presented in Figure 8 at 60 s after beginning of the earthquake using the Pastor-Zienkiewicz model. According to this figure, there is a region with large portion of excess water pressure in the center of the dam at the end of earthquake. Also presented in this figure is the minimum values of the effective vertical stress and first invariant of effective stress in the upstream slope region, which is similar to failure surface illustrated in Figure 6(a). These results demonstrate that there is a good agreement between the predicted failure using the Pastor-Zienkiewicz model and those reported by Seed *et al*. [22].

5. CONCLUSION

In the present paper, an integrated software environment was demonstrated for multi-disciplinary computational modeling of structural and geotechnical problems. The SUT–DAM 3D was designed in both popularity and functionality with the development of user-friendly pre- and post-processing software. Pre-processing software was used to create the model, generate an appropriate finite element grid, apply the appropriate boundary conditions, and view the total

model. Post-processing provided visualization of the computed results. In SUT–DAM 3D, a numerical model was developed based on a Lagrangian finite element formulation for large deformation dynamic analysis of saturated and unsaturated soils. An adaptive FEM strategy was used into the large displacement finite element formulation by employing an error estimator, adaptive mesh refinement, and data transfer operator. Different yield criteria, including classical and advanced constitutive models, such as the Pastor-Zienkiewicz and cap plasticity models were implemented in SUT–DAM 3D. It was attempted to summarize work directed at exploring the concepts of an integrated software environment for simulation of powder forming processes. Finally, the performance of SUT–DAM 3D was illustrated in modeling of the failure of lower San Fernando dam under the 1971 earthquake. The numerical simulation illustrates the performance of the SUT–DAM 3D in simulating the mechanism of failure and indicating the motion along the failure surfaces.

ACKNOWLEDGEMENTS

The authors gratefully acknowledge the financial support of the Ministry of Energy, particularly Iran Water Resource Management Organization (IWRMO) through Grant No. 82/571/152 awarded to Sharif University of Technology.

REFERENCES

1. K. Terzaghi, Theoretical Soil Mechanics, *Wiley*, New York, 1943.
2. M.A. Biot, General theory of three dimensional consolidation, *J. Appl. Phys.*, **12** (1941) 155-164.
3. M.A. Biot, Theory of propagation of elastic waves in a fluid-saturated porous solid, *J. Acous. Soc. America*, **28** (1956) 168-191.
4. M.A. Biot, Mechanics of deformation and acoustic propagation in porous media, *J. Appl. Phys.*, **33** (1962) 1482-1498.
5. J. Ghaboussi and E.L. Wilson, Flow of compressible fluid in porous elastic media, *Int. J. Numer. Meth. Engng.*, **5** (1973) 419-442.
6. O.C. Zienkiewicz and P. Bettess, Soils and other saturated media under transient dynamic conditions; General formulation and the validity of various simplifying assumptions, *Soil Mechanics- Transient and Cyclic Loads* (Eds. G.N. Pande and O.C. Zienkiewicz) , Ch. **1**, 1982.
7. O.C. Zienkiewicz and T. Shiomi, Dynamic behavior of saturated porous media; The generalized Biot formulation and It's numerical solution, *Int. J. Numer. Analyt. Meth. Geomech.*, **8** (1984) 71-96.
8. R. de Boer and S.J. Kowalski, A plasticity theory for fluid saturated porous media, *Int. J. Eng. Sci.*, 21 (1983) 11-16.
9. O.C. Zienkiewicz, A.H.C. Chan, M. Pastor, D.K. Paul and T. Shiomi, Static and dynamic behavior of soils; A rational approach to quantitative solution. I. Fully saturated problems, *Proc. R. Soc. Lond.*. (1990) 285-309.
10. D.G. Fredlund and N.R. Morgenstern, Stress state variables for unsaturated soils, *J. Geotech. Engng. Div. ASCE*, **103** (1977) 447-466.
11. C.S. Chang and J.M. Duncan, Consolidation analysis for partly saturated clay by using an elastic-plastic effective stress-strain model, *Int. J. Numer. Anal. Meth. Geomech.*, **7** (1983) 39-55.
12. O.C. Zienkiewicz, Y.M. Xie, B.A. Schrefler, A. Ledesma and N. Bicanic, Static and dynamic behavior of soils; A rational approach to quantitative solution. II. Semi-saturated problems, *Proc. R. Soc. Lond.*, (1990) 311-321.
13. E.E. Alonso, A. Gens and A. Josa, A constitutive model for partially saturated soils, *Geotechnique*, **40** (1990) 405-430.
14. D. Gawin, L. Simoni and B.A. Schrefler, Numerical model for hydro-mechanical behaviour in deformable porous media: a benchmark problem, *Proc. 9th Int. Conf. on Computer Methods and Advances in Geomechanics*, **2** (1997) 1143-1148.
15. A.R. Khoei, A.R. Azami and S.M. Haeri, Implementation of plasticity based models in dynamic analysis of earth and rockfill dams; A comparison of Pastor-Zienkiewicz and cap models, *Comput. Geotechnics,* **31** (2004) 385-410.

16. A.R. Khoei, An integrated software environment for finite element simulation of powder compaction processes, *J. Mater. Proc. Tech.*, **130-131** (2002) 171-177.
17. A.R. Khoei, PCS_SUT: A finite element software for simulation of powder forming processes, *J. Mater. Proc. Tech.*, **125-126** (2002) 602-607.
18. O.C. Zienkiewicz, A.H.C. Chan, M. Pastor, B.A. Schrefler and T. Shiomi, Computational Geomechanics with Special Reference to Earthquake Engineering, *Wiley*, 1999.
19. A.W. Bishop and G.E. Blight, Some aspects of effective stress in saturated and partially saturated soils, *Geotechnique*, **13** (1963) 177-197.
20. A.R. Khoei, Computational Plasticity in Powder Forming Processes, *Elsevier*, UK, 2005.
21. A.R. Khoei, A.R. Tabarraie and S.A. Gharehbaghi, H-adaptive mesh refinement for shear band localization in elasto-plasticity Cosserat continuum, *Commun. Nonlinear Sci. Numer. Simul.,* **10** (2005) 253-286.
22. H.B. Seed, Consideration in the earthquake resistant design of earth and rockfill dams, *Geotechnique*, **29** (1979) 215-263.

Table 1. The San Fernando dam; the general material properties.

Zone	$E\,(Pa)$	υ	$K_s\,(Pa)$	$K_w\,(Pa)$	$\rho_s\ (kg/m^3)$	n	$k\,(m/s)$
1	1.53e+8	0.2857	1.0e+22	2.0e+9	2756	0.375	0.001
2	0.89e+8	0.2857	1.0e+22	2.0e+9	2756	0.375	0.01
3	1.02e+8	0.2857	1.0e+22	2.0e+9	2756	0.375	0.001
4	0.98e+8	0.2857	1.0e+22	2.0e+9	2756	0.375	0.01

Table 2. The San Fernando dam; the parameters of Pastor-Zienkiewicz model.

Zone	K_0	G_0	M_g	M_f	α_g, α_f	β_0	β_1	H_0	$H_{U0}\,(Pa)$	γ, γ_U
1	120	180	1.55	1.400	0.45	4.2	0.2	700.0	6.00e+7	2.0
2	70	105	1.51	0.755	0.45	4.2	0.2	408.3	3.50e+7	2.0
3	80	120	1.51	1.133	0.45	4.2	0.2	467.0	4.00e+7	2.0
4	75	112	1.51	0.906	0.45	4.2	0.2	408.3	3.75e+7	2.0

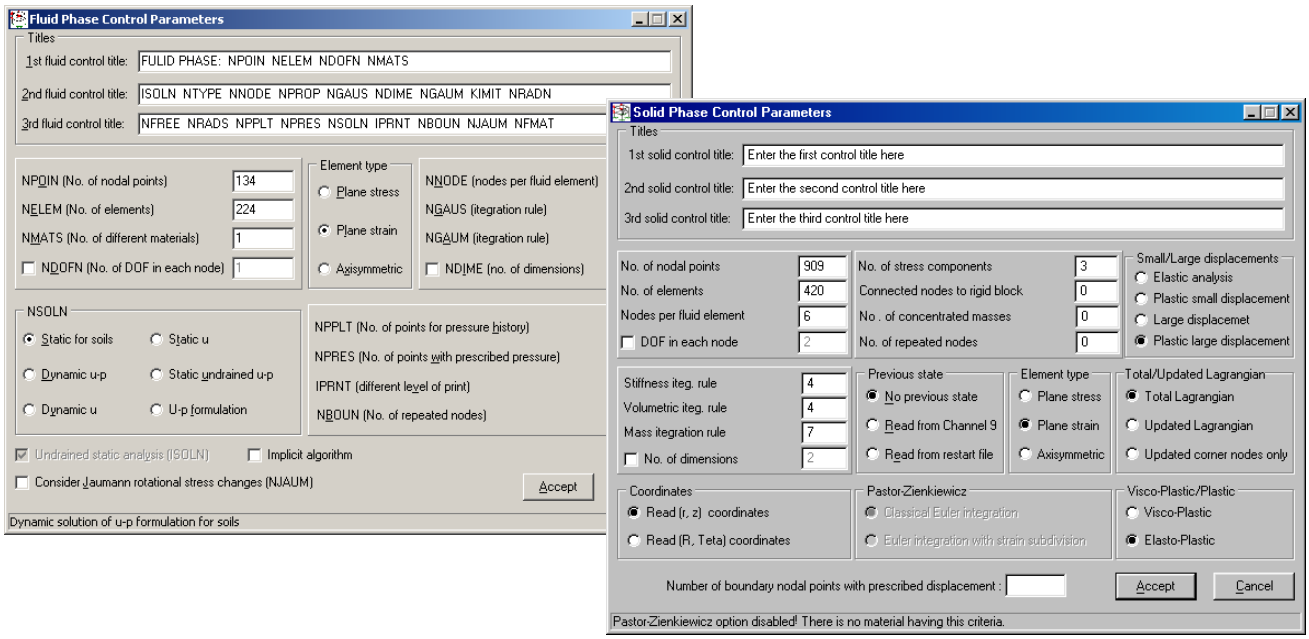

Fig. 1. Definition of fluid and solid phase parameters in SUT–DAM 3D.

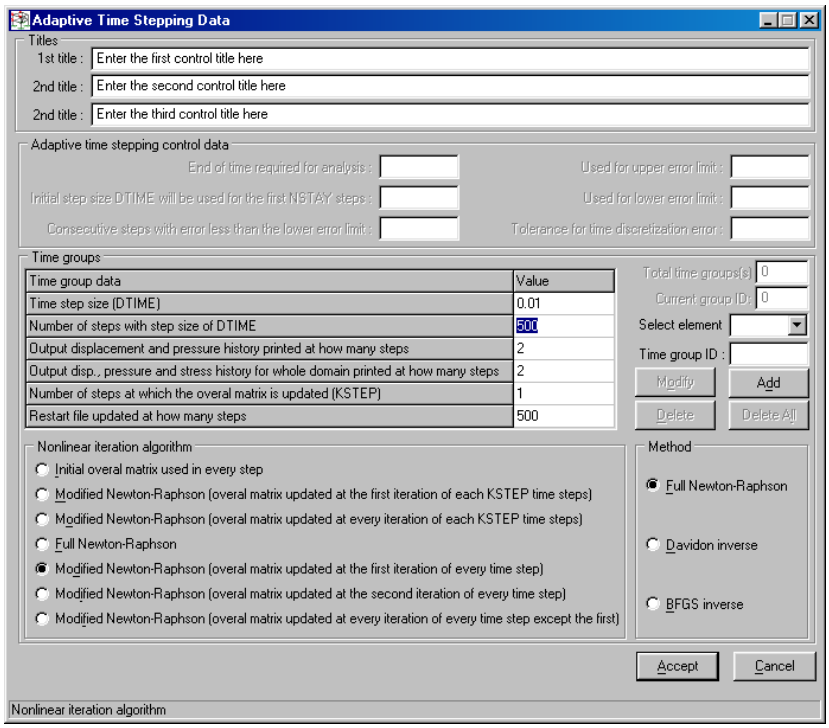

Fig. 2. Definition of time integration and non-linear iteration algorithms in SUT–DAM 3D.

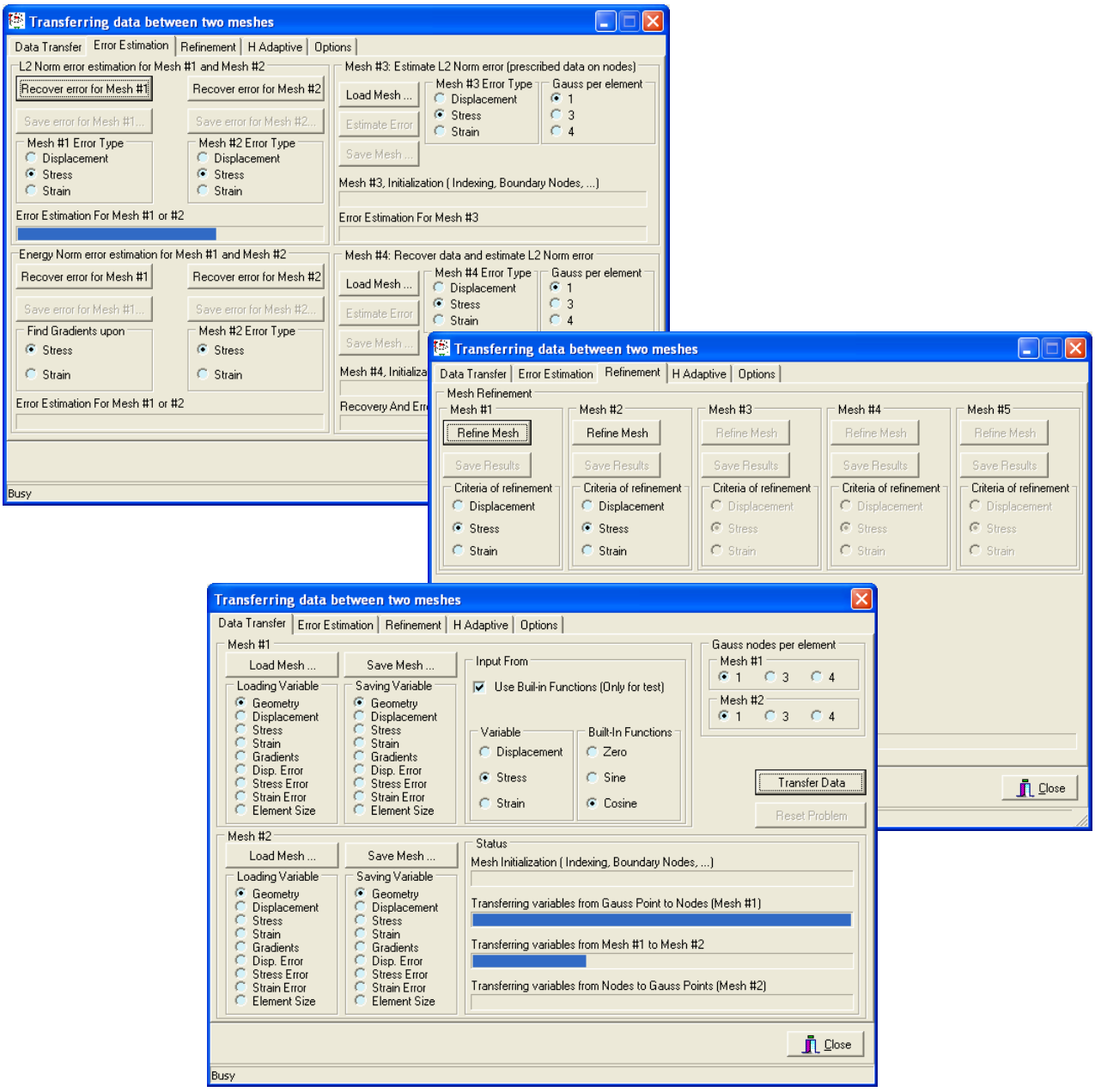

Fig. 3. Adaptive FEM strategy in SUT–DAM 3D; error estimation, adaptive mesh refinement, and data transfer operator.

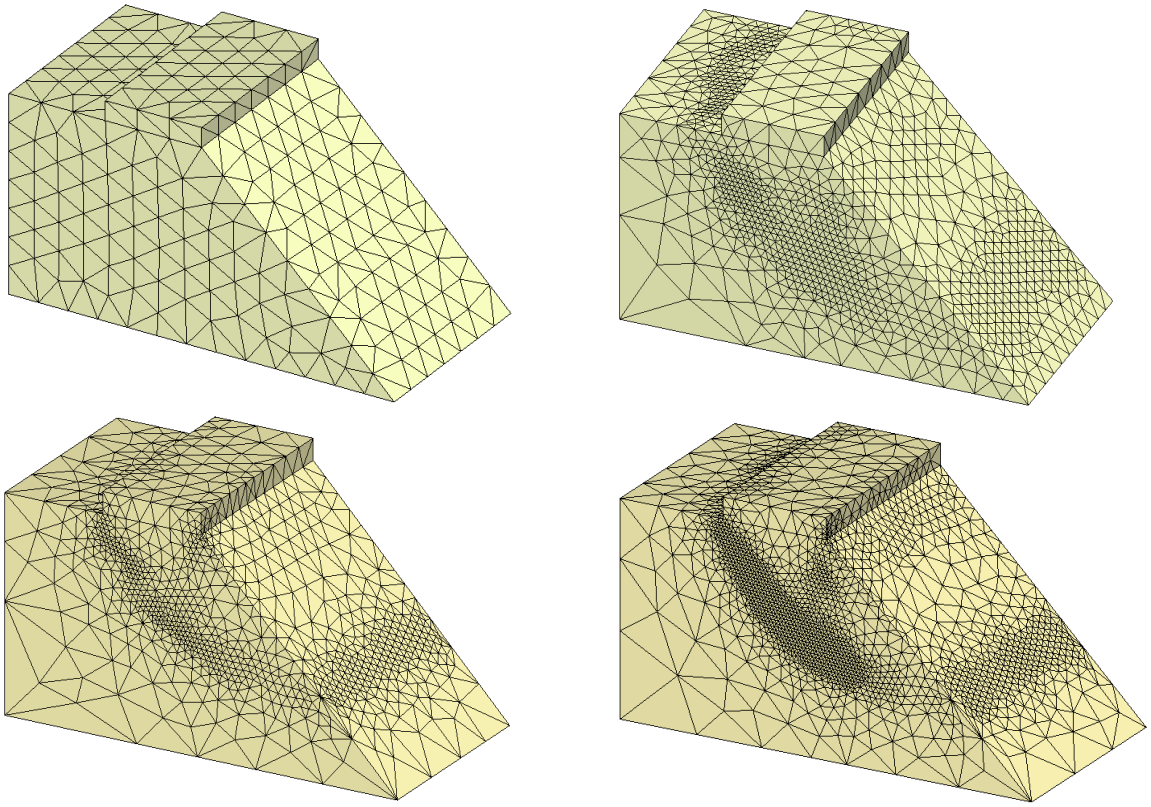

Fig. 4. Adaptive remeshing for a slope in SUT–DAM 3D.

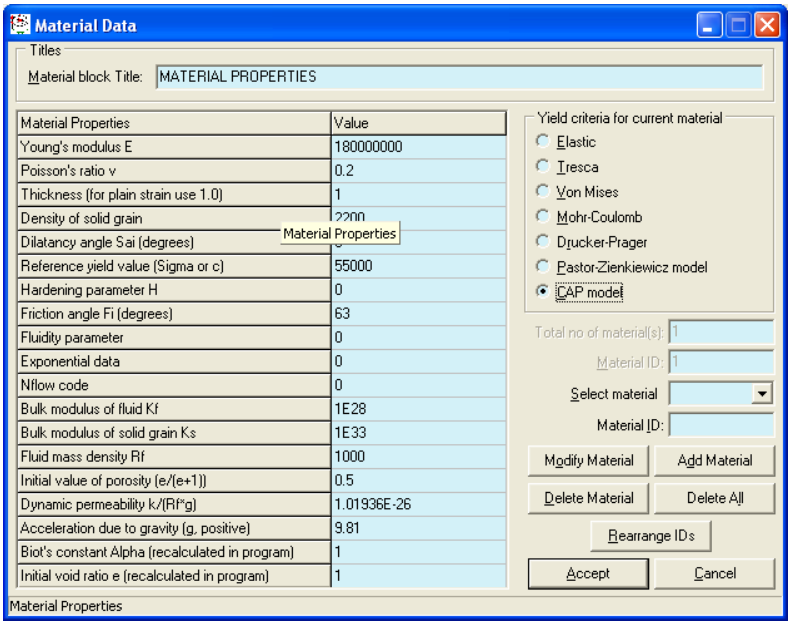

Fig. 5. Definition of the material parameters in SUT–DAM 3D.

(a)

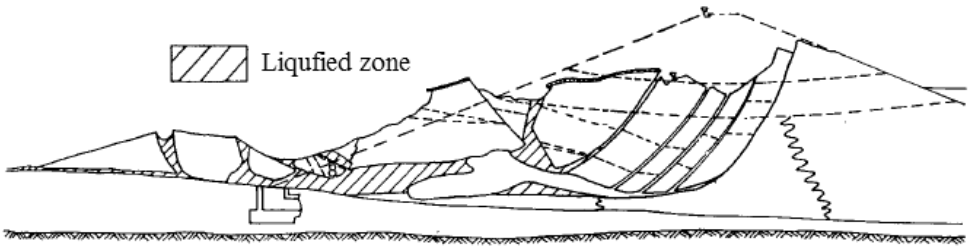

(b)

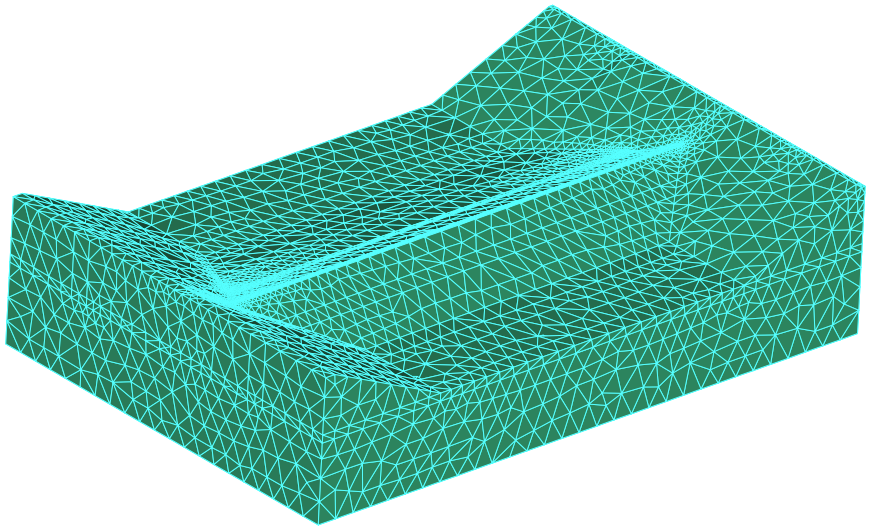

(c)

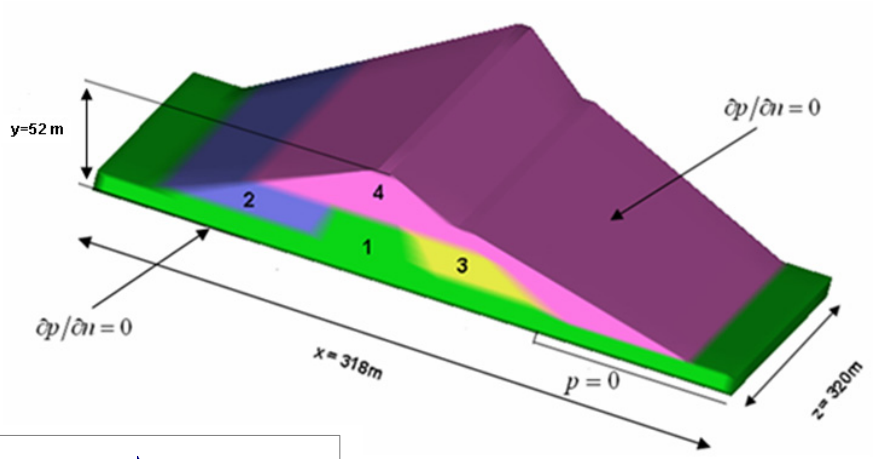

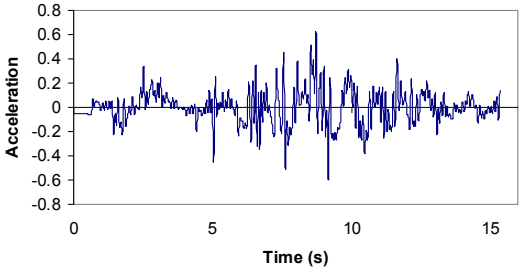

Fig. 6. The lower San Fernando dam; (a) the mechanism of the failure (Seed *et al.* [32]),(b) the finite element mesh, (c) the material zones, boundary conditions and earthquake.

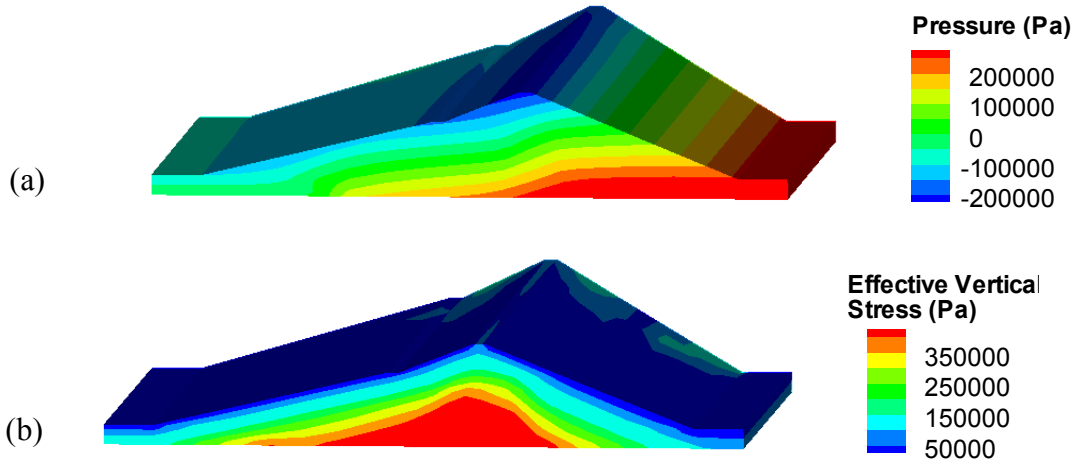

Fig. 7. The steady state condition; (a) The distribution of pore pressure, (b) the distribution of effective vertical stress.

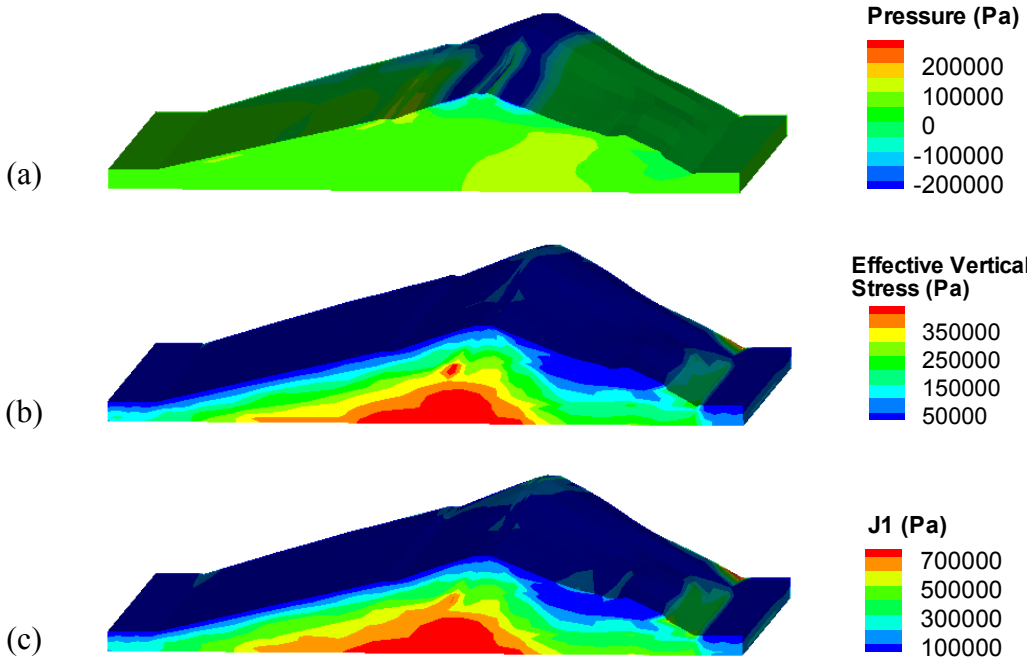

Fig. 8. Numerical simulation results at 60 s after beginning of the earthquake using Pastor-Zienkiewicz model; (a) The distribution of excess pore water pressure,(b) The distribution of effective vertical stress, (c) The distribution of the first invariant of effective stress.

PERFORMANCE-BASED EARTHQUAKE ENGINEERING APPLIED TO A BRIDGE IN LIQUEFIED AND LATERALLY SPREADING GROUND

Scott J. Brandenberg[1)], and Pirooz Kashighandi[2)]

1) Assistant Professor, Dept. of Civil and Env. Engineering, University of California, Los Angeles, United States

2) Graduate Student, Dept. of Civil and Env. Engineering, University of California, Los Angeles, United States

sjbrandenberg@ucla.edu, pirooz@ucla.edu

Abstract: Fragility functions developed for liquefaction and lateral spreading against typical classes of bridges are integrated with a probabilistic lateral spreading ground displacement methodology in a performance-based earthquake engineering example problem. A site near UCLA is selected and a probabilistic seismic hazard analysis is performed to obtain a hazard curve expressing mean annual rate of exceedance of peak ground acceleration. The disaggregation of the seismic hazard curve is also computed. A liquefiable soil profile is selected, and hazard curve expressing mean annual rate of non-exceedance of factor of safety against liquefaction is computed from the seismic hazard curve and disaggregation. A hazard curve expressing mean annual rate of exceedance of lateral spreading ground displacement is then computed using a semi-empirical probabilistic framework. The ground displacement hazard curve is compared with a typical approach wherein a probabilistic ground motion is selected and the engineering calculations are performed deterministically. Finally, the fragility functions are applied and a hazard curve is computed that expresses the mean annual rate of exceedance of various engineering demand parameters. This example problem shows how performance-based earthquake engineering can be applied to liquefaction problems to better communicate uncertainty and risk to decision- and policy- makers.

1. INTRODUCTION

As of 2008, more than half of the earth's population lives in cities. Growth of our urban centers has placed a premium on sites with marginal or poor quality soils that had previously been considered inappropriate for development. This problem is particularly pertinent to geotechnical earthquake engineering because (1) a large fraction of the world's urban centers are in seismically active regions, (2) loose or soft soils have exhibited poor behavior due to cyclic failure and liquefaction in past earthquakes, causing death and billions of dollars in economic damages, and (3) our understanding of the seismic behavior of these soils is not well calibrated with meaningful experience because (thankfully) earthquakes are rare occurrences and few designers live to see how design-level shaking affects their projects. Geotechnical engineers strive to learn as much as possible from earthquakes as they occur around the world, but our evaluation procedures remain fraught with uncertainty. Considering how much uncertainty

geotechnical engineers encounter, an outsider would be justified in assuming that we are experts at quantifying and communicating risk to our clients. After all, other related fields with similar levels of uncertainty have embraced probabilistic methods. For example, consider the widespread adoption of probabilistic seismic hazard analysis in building codes. However, we have been reticent to adopt probabilistic methods in geotechnical engineering in large part because (1) there is a poor understanding of risk assessment among our community, and (2) we haven't automated our engineering evaluation procedures to permit the large number of realizations often required to integrate uncertainty in our calculations. As a result we are overly-reliant on "engineering judgment" that is not adequately calibrated with meaningful experience for earthquake applications, and we don't fully understand the risk associated with our design recommendations.

Liquefaction-induced lateral spreading and its effect on bridges is a geotechnical topic where statistical methods can help us quantify uncertainty and make better decisions. Lateral spreading occurs in gentle slopes or near a free face where soil is under a static driving shear stress, and an earthquake induces liquefaction in the loose saturated soil deposit and ground displacements accumulate in the direction of static driving shear stress during shaking. Ground displacements are often in the range of tens of centimeters to meters. When the static driving shear stress exceeds the undrained strength of the liquefied material, a flow slide occurs and the ground deformations can be very large (e.g., on the order of tens of meters). Lateral spreading hazard is particularly pertinent for bridges that often cross bodies of water where liquefiable soil deposits are prevalent. Fig. 1 shows the Showa Bridge, which collapsed due to unseating of the simply supported spans caused by liquefaction and lateral spreading of the soils in which the piles were founded. Other bridges have performed reasonably well in lateral spreads. For example, the Landing Road Bridge suffered only moderate, repairable damage as a result of 2m of lateral spreading of the adjacent soil (Berrill et al. 2001), and several bridges were only slightly damaged due to tens of centimeters of ground displacements during the 2007 Niigata Ken Chuetsu-Oki earthquake (Kayen et al. 2007). This range of performance levels underscores the need for improved methodologies for predicting how much damage is anticipated due to liquefaction.

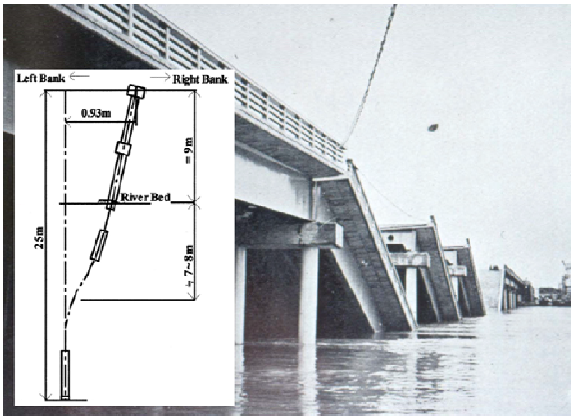

Figure 1: Collapse of Showa Bridge due to liquefaction and lateral spreading during 1964 Niigata earthquake (Yasuda and Berrill 2000).

This paper demonstrates how the performance-based earthquake engineering can be applied to predict liquefaction-induced damage to bridges. An example problem consisting of a site with a corresponding seismic hazard curve and disaggregation is combined with a liquefiable soil profile to compute a hazard curve defining mean annual rate of exceedance of lateral spreading ground displacement. The ground displacement hazard curve is combined with recently-developed fragility functions to compute mean annual rate of exceedance of various bridge engineering demand parameters due to liquefaction and lateral spreading.

2. SITE AND SEISMIC HAZARD ANALYSIS

A site in Santa Monica, CA, (118.492°W, 34.015°N) was selected for this example problem. This is the same Santa Monica site analyzed by Kramer and Mayfield (2007), which provides a convenient means of validating the liquefaction hazard curve with their results. A probabilistic seismic hazard analysis was performed using OpenSHA (Field et al. 2003), with Vs_{30} = 300 m/s. The seismic hazard curve and magnitude disaggregation are shown in Figs. 2 and 3. The soil profile at the site consists of a $2m$ thick nonliquefied crust with unit weight γ = 18 kN/m^3 lies over a clean liquefiable sand with $(N_1)_{60}$ = 10. The ground gently slopes at an angle of $\beta = 2°$ and can be reasonably represented as an infinite slope.

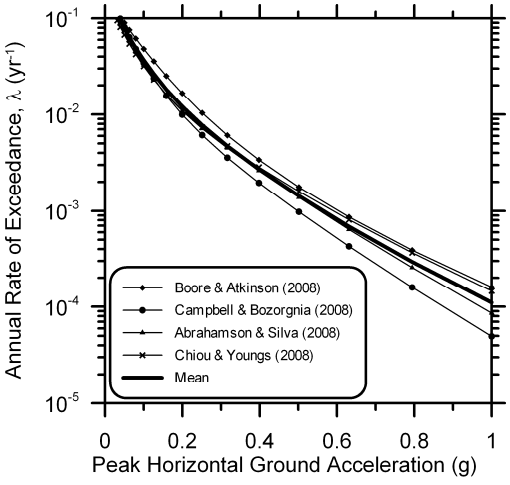

Figure 2: Hazard curves from probabilistic seismic hazard analysis of Santa Monica site.

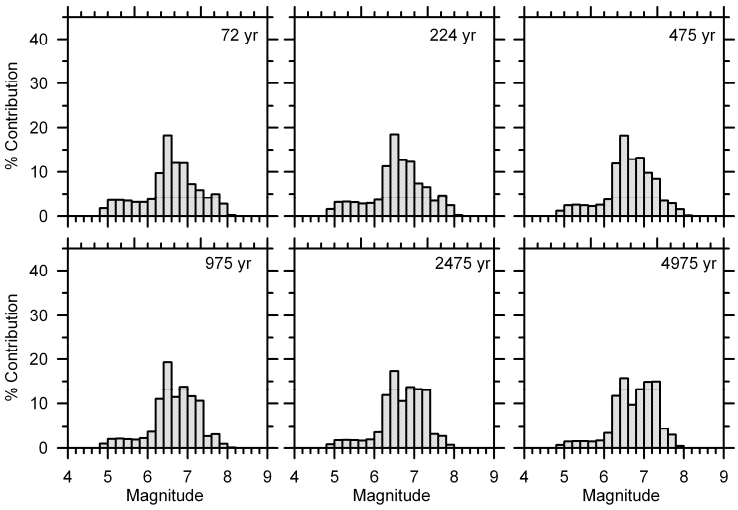

Figure 3: Distributions of magnitude contributions to seismic haz-

3. LIQUEFACTION TRIGGERING EVALUATION

The next step in the analysis is computing the annual rate of exceedance of triggering of liquefaction. To simplify, the mean hazard curve from Fig. 2 will be used. Kramer and Mayfield (2007) outlined a framework for computing annual rate of non-exceedance of liquefaction that is adopted in this study. The approach is based on the probabilistic liquefaction triggering framework developed by Cetin et al. (2004), using the regression constants that account for measurement/estimation errors. Eq. 1 defines probability of factor of safety against liquefaction (FS_L) dropping below a value (FS_L^*) given $(N_1)_{60}$, fines content FC cyclic stress ratio CSR_{eq} moment magnitude M_w and vertical effective stress σ_{vo}'. The cyclic stress ratio is defined as $CSR_{eq} = 0.65(PGA/g)(\sigma_v/\sigma_{vo}')r_d$, where the stress reduction factor r_d was treated deterministically (Golesorkhi 1989). Uncertainty in r_d is anticipated to have negligible effect on the hazard analysis since the site is so shallow and r_d is near unity.

$$P\left[FS_L < FS_L^* \mid PGA, M_w\right] = \Phi\left[-\frac{(N_1)_{60}(1+0.004FC) - 13.79\ln CSR_{eq} - 29.06\ln M_w - 3.82\ln(\sigma_{vo}'/p_a) + 0.06FC + 15.25}{4.21}\right] \quad (1)$$

$$\Lambda_{FS_L^*} = \sum_{j=1}^{N_{M_w}} \sum_{i=1}^{N_{PGA}} P\left[FS_L < FS_L^* \mid PGA_i, M_{w_j}\right] \Delta\lambda_{PGA,M_w} \quad (2)$$

Peak horizontal ground acceleration (PGA) is not sufficient to characterize liquefaction triggering, and magnitude appears as well due to the influence of duration and frequency content. Hence, the hazard calculation must be integrated over PGA and M_w, which requires the disaggregation shown in Fig. 3. Eq. 2 defines the probability of non-exceedance of factor of safety against liquefaction, where the summations indicate discrete numerical integration over an adequate range of PGA and M_w values using the binning method wherein the probability density functions are divided into small slices for numerical integration (after Kramer and Mayfield 2007). Fig. 4 shows the mean annual rate of non-exceedance of factor of safety against liquefaction, which is similar to the Santa Monica site presented by Kramer and Mayfield (see Fig. 9 in their paper). The return period for $FS_L<1$ is about 100 years (i.e. $\Lambda=0.01$ yr^{-1}).

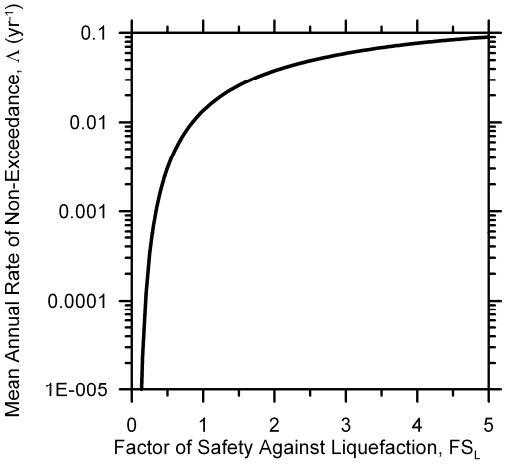

Fig. 4: Liquefaction triggering hazard curve.

4. GROUND DISPLACEMENT EVALUATION

The next step in the procedure is computing the mean annual rate of exceedance of lateral spreading ground displacement for this site. A number of methods for estimating lateral spreading displacements exist, and including multiple approaches is important for quantifying the effects of epistemic uncertainty. However, for simplicity only a single approach is utilized in this paper, though the methodology can easily be extended to other methods. The approach by Bray and Travasarou (2007) for computing permanent ground displacements is combined with the approach by Olson and Stark (2002) for estimating undrained residual strength of liquefied sand. For $(N_1)_{60} = 10$, the mean value of $s_r/\sigma_v' = 0.1$ based on the Olson and Stark suggestion, hence $\mu_{sr} = 0.1(2m)(18kN/m^3) = 3.6kPa$. Furthermore, the standard deviation is $\sigma_{sr} = 0.025(2m)(18kN/m^3) = 0.9kPa$. The static driving shear stress is $\tau_{stat} = (2m)(18kN/m^3)\sin(2°) = 1.3kPa$. If the static driving shear stress exceeds the undrained residual strength, then a flow slide occurs and ground displacement is large. Assuming that s_r is log-normally distributed, the probability of a flow slide can be computed using Eq. 3, where Φ is the standard normal cumulative distribution function.

$$P\left[Flow\ Slide \mid Liq\right] = \Phi\left[\frac{\ln \tau_{stat} - \ln s_r}{\sqrt{1 - \frac{\sigma_{sr}^2}{\mu_{sr}^2}}}\right] \quad (3)$$

For cases when a flow slide does not occur, the lateral spreading ground displacement is be computed using the methodology of Bray and Travasarou (2007) defined in Eqs. 4, where k_y is the yield acceleration. For an infinite slope, $k_y = (s_r - \tau_{stat})/\gamma H\cos\beta$.

The probability of lateral spreading ground displacement exceeding some value, *d*, conditioned on the occurrence of liquefaction is given in Eq. 5, where the summation indicates numerical integration by the

$$
\begin{aligned}
&P(D=0) = 1-\Phi\left(-1.76-3.22\ln(k_y)+3.52\ln(PGA)\right)\\
&P(D>d\mid D>0) = 1-\Phi\left(\frac{\ln(d)-\ln(\hat{d})}{0.66}\right)\\
&\ln(\hat{d}) = -0.22-2.83\ln(k_y)-0.333(\ln(k_y))^2+0.566\ln(k_y)\ln(PGA)\\
&\qquad +3.04\ln(PGA)-0.244(\ln(PGA))^2+0.278(M_w-7)
\end{aligned}
\tag{4}
$$

$$
P(D>d\mid Liq) = \sum_{i=1}^{N_{k_y}}\left[1-P(D=0)\right]\left[P(D>d\mid D>0)\right]\left[1-P(FlowSlide\mid Liq)\right]\Delta k_y + P(FlowSlide\mid Liq) \tag{5}
$$

binning method over the random variable k_y, which depends on random variable s_r.

The mean annual rate of exceedance of free-field lateral spreading ground displacement is computed by inserting the conditional probability defined in Eq. 5 in the hazard integral, as defined in Eq. 6.

$$
\lambda_D = \sum_{j=1}^{N_M}\sum_{i=1}^{N_{PGA}} P(D>d\mid Liq)P(Liq\mid PGA,M_w)\Delta\lambda_{PGA,M_w} \tag{6}
$$

Fig. 5 shows the lateral spreading ground displacement hazard curve for the example problem, which was computed using 30 bins for PGA and k_y, and 17 bins for magnitude, for a total of 15,300 computations. Also shown in Fig. 5 are several values of ground displacement computed deterministically by taking the PGA associated with some hazard level combined with the modal magnitude (M_w = 6.5 in this case), mean k_y value, and mean lateral spreading displacement value computed using Eq. 4. In this case the deterministic approach underestimates the true ground displacement hazard primarily because (1) the modal magnitude was used and higher magnitudes contribute to larger displacements according to a nonlinear relation, and (2) the mean value of the liquefied undrained strength was used and lower undrained strengths produce larger displacements according to a nonlinear relation. Kramer and Mayfield (2007) also showed how inconsistencies between the probabilistic and deterministic approaches to liquefaction triggering evaluation arise due to nonlinearities in the equations, and the mismatch depends on the slope of the hazard curve. These observations indicate that the return period associated with a design level ground motion may not be the same as the return period for a deterministically-computed engineering response parameter, and utilizing the performance-based approach is the only way to provide consistency.

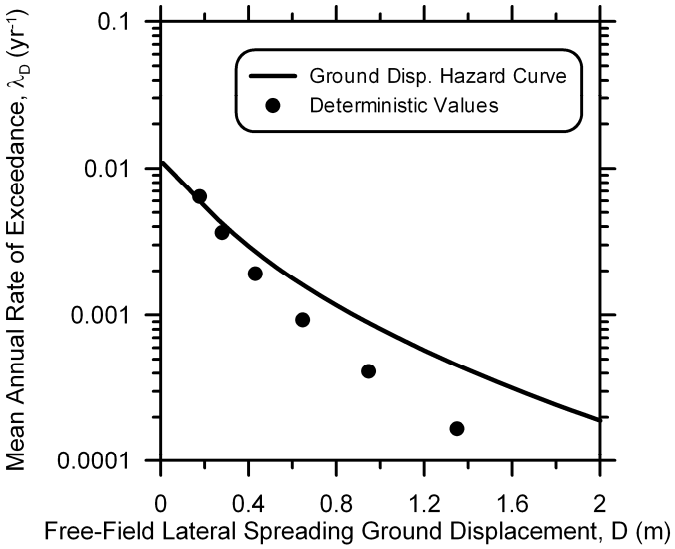

Fig. 5: Free-field lateral spreading ground displacement haz-

5. BRIDGE ENGINEERING DEMAND PARAMETER EVALUATION

Co-author Kashighandi recently defended his Ph.D. dissertation, which will be filed in the next few months. The topic of his dissertation was developing fragility functions for bridges in liquefied and laterally spreading ground to be used as a screening tool for identifying which set of Caltrans bridges is most susceptible to liquefaction. He developed demand fragility surfaces that define probability of exceeding some engineering demand parameter (EDP) (e.g., pier column curvature ductility, pile cap displacement, abutment displacement) as a function of free-field lateral spreading ground displacement. The fragility functions were developed using equivalent static global analysis, and the details are beyond the scope of this paper. Example demand fragility surfaces are shown in Fig. 6 for bridges constructed after 1971 with simply-supported spans, seat-type abutments, and 24" Cast in Drilled Hole deep foundations supporting the pile caps and abutments.

The conditional probabilities defined in the demand fragility surfaces were inserted into the hazard integral to define the mean annual rate of exceedance of the three EDP values (Eq. 7). The EDP hazard curves are plotted in Fig. 7. The 10% in 50 year EDP values ($\lambda = 2.1\text{x}10^{-3}$ yr^{-1} and return period = 475yr) are pile cap displacement = 0.18*m*, the pier column remains elastic, and abutment displacement = 0.15*m*. These EDP hazard curves provide for better decision-making compared with the standard-of-practice approach of selecting a probabilistic ground motion and performing engineering calculations deterministically.

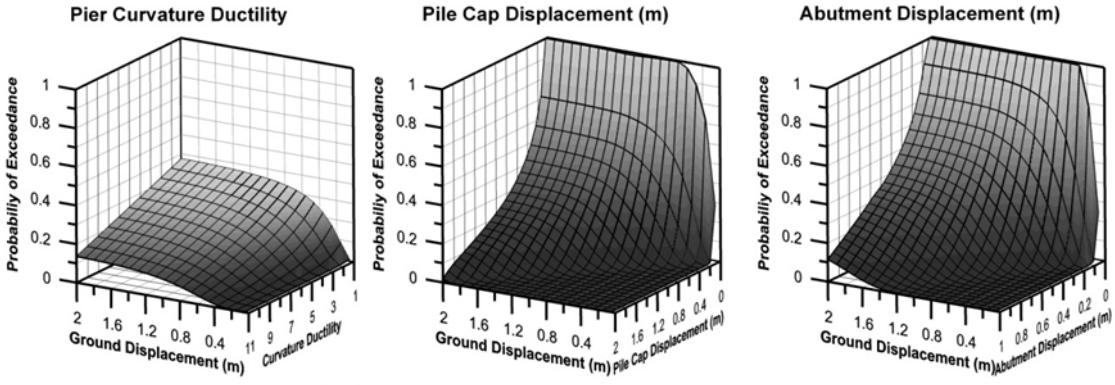

Fig. 6: Demand fragility surfaces for post-1971 bridges with simply-supported spans, seat-type abutments, and 24" CIDH piles.

$$\lambda_{EDP} = \sum_{j=1}^{N_M} \sum_{i=1}^{N_{PGA}} P(EDP > edp \mid D) P(D > d \mid Liq) P(Liq \mid PGA, M_w) \Delta\lambda_{PGA,M_w} \tag{7}$$

6. CONCLUSIONS

In this paper, a seismic hazard curve was integrated to obtain mean annual rate of non-exceedance of factor of safety against liquefaction, mean annual rate of exceedance of free-field lateral spreading ground displacement, and mean annual rate of exceedance of several engineering demand parameters that are meaningful for bridges. The procedure could be taken further, as defined in the framework of the Pacific Earthquake Engineering Research Center, to define a damage measure based on the engineering demand

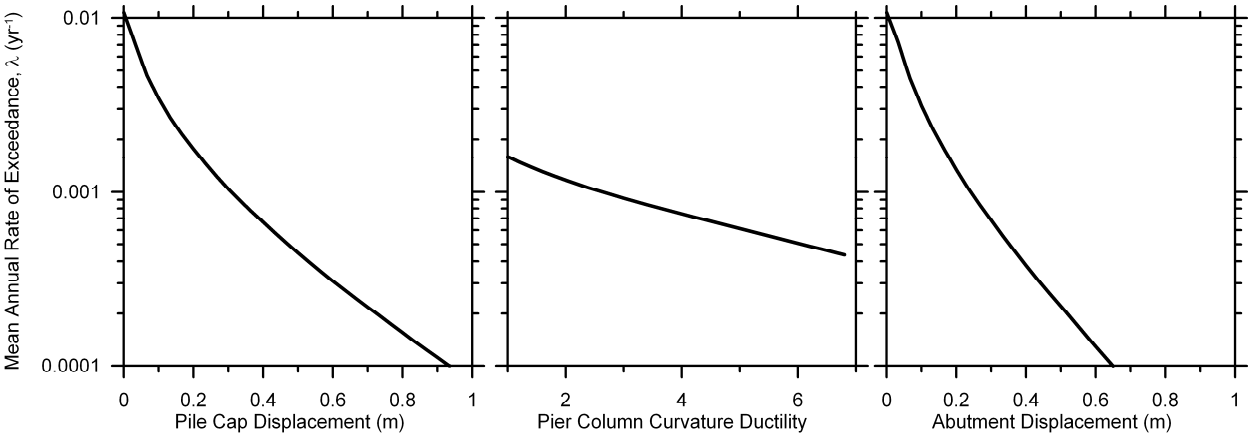

Fig. 7: Mean annual rate of exceedance of pile cap displacement, pier column curvature ductility, and abutment displacement.

parameters (e.g., exceeding a pier column curvature ductility of 7 results in total damage of the pier column), and a decision variable based on the damage measure (e.g., the cost of replacing a totally damage pier column is $X). Decisions could then be made based on mean annual rate of exceedance of dollar loss, which is a much more intuitive decision tool compared with making decisions based on mean annual rate of exceedance of PGA, lateral spreading displacement, or EDP's.

7. ACKNOWLEDGEMENTS

Funding for this work was provided by the California Department of Transportation and the National Science Foundation through the Pacific Earthquake Engineering Research Center under project no. SA5407:1 (Caltrans) and SA5258 (NSF). Tom Shantz was the contract coordinator. The contents of this paper do not necessarily represent a policy of either agency or endorsement by the state or federal government.

8. REFERENCES

Abrahamson, N., and Silva, W. (2008). "Summary of the Abrahamson & Silva NGA ground motion relations." *Earthquake Spectra*, EERI, 24(1), 67-98.

Berrill, J.B., Christensen, S.A., Keenan, R.P., Okada, W., and Pettinga, J.R. (2001). "Case study of lateral spreading forces on a piled foundation." Geotechnique, 51(6). 501-517.

Boore, D.M., and Atkinson, G.M. (2008). "Ground-motion prediction equations for the average horizontal component of PGA, PGV, and 5%-damped PSA at spectral periods between 0.01 s and 10.0 s." *Earthquake Spectra*, EERI, 24(1), 99-138.

Bray, J.D., and Travasarou, T. (2007). "Simplified procedure for estimating earthquake-induced deviatoric slope displacements." *J. Geotech. Geoenviron. Eng.*, ASCE, 133(4), 381-392.

Campbell, K.W., and Bozorgnia, Y. (2008). "NGA ground motion model for the geometric mean

horizontal component of PGA, PGV, PGD and 5% damped linear elastic response spectra for periods ranging from 0.01 to 10 s." *Earthquake Spectra*, EERI, 24(1), 139-172.

Cetin, K.O., Seed, R.B., Der Kiureghian, A., Tokimatsu, K., Harder, L.F. Jr., Kayen, R.E., and Moss, R.E.S. (2004). "Standard penetration test-based probabilistic and deterministic assessment of seismic soil liquefaction potential." *J. Geotech. Geoenviron. Eng.*, ASCE, 130(12), 1314-1340.

Chiou, B.S.-J., and Youngs, R.R. (2008). "An NGA model for the average horizontal component of peak ground motion and response spectra." *Earthquake Spectra*, EERI, 24(1), 173-216.

Field, E.H., T.H. Jordan, and C.A. Cornell (2003). OpenSHA: A Developing Community-Modeling Environment for Seismic Hazard Analysis", Seismological Research Letters Volume 74, Number 4, pages 406-419.

Golesorkhi, R. (1989). "Factors influencing the computational determination of earthquake-induced shear stresses in sandy soils." PhD. Dissertation, Univ. of California, Berkeley, Calif.

Kayen, R., Collins, B., Abrahamson, N., Ashford, S., Brandenberg, S.J., Cluff, L., Dickenson, S., Johnson, L., Tanaka, Y., Tokimatsu, K., Kabeyasawa, T., Kawamata, Y., Koumoto, H., Marubashi, N., Pujol, S., Steele, C., Sun, J. I., Tsai, B., Yanev, P., Yashinsky, M., and Yousok, K. (2007). Investigation of the M6.6 Niigata-Chuetsu Oki, Japan, earthquake of July 16, 2007: U.S. Geological Survey Open-File Report 2007-1365, 230 p.

Kramer, S.L., and Mayfield, R.T. (2007). "Return period of soil liquefaction." *J. Geotech. Geoenviron. Eng.*, ASCE, 133(7), 802-813.

Olson, S.M. and Stark, T.D. (2002). "Liquefied strength ratio from liquefaction case histories." *Canadian Geotechnical Journal*, 39, 629-647.

AN OVERVIEW ON THE GEOTECHNICAL EARTHQUAKE ENGINEERING RESEARCHES AT CIVIL ENGINEERING DEPARTMENT OF SHARIF UNIVERSITY OF TECHNOLOGY

S. Mohsen Haeri, Ph.D., DIC
Professor, Civil Engineering Department,
Sharif University of Technology, Tehran, Iran

1. INTRODUCTON

Several subjects on Geotechnical Earthquake Engineering have been under study at Civil Engineering Department of Sharif University of Technology since 1990.
These studies can be categorized in the following heading:

1. Land instabilities such as liquefaction, landslides and rock falls.
2. Local site effects on the earthquake characteristics and seismic microzonation of urban areas.
3. Dynamic characterization of cemented gravelly sands.
4. Dynamic behavior of earth and rockfill dam especially Concrete Faced Rockfill Dams (CFRD)

In the following sections, these topics would be discussed briefly in some detail.

2. LAND INSTABILITIES DUE TO EARTHQUAKE

Land instabilities due to earthquakes have been a major cause for destruction or damage to assets and lives in the world including Iran. In this line land instabilities caused by earthquakes has been one of the main concerns of geotechnical and earthquake engineers in Iran. The main aspects of land instabilities due to earthquakes are liquefaction and landslide. The researches on these two subjects which have been carried out at Civil Engineering Department of Sharif University of Technology are explained below.

2.1. Landslide

Landslides can turn to one of the most distractive phenomena induced by earthquakes in mountainous area. The epicenter of the Manjil (1990) earthquake with a magnitude of $M_s = 7.3$ was located in a mountainous area and therefore massive landslides and vast rock falls took place during or just after the main earthquake shaking. A campaign was initiated to study these landslides in detail. Some of the studies on these landslides are listed below:

- Reconnaissance of the major landslides induced by Manjil 1990 earthquake with a completed survey of the geographical, geometrical and geotechnical information for these landslides. Tables including the data and the maps including the location and size of the landslides are prepared for more than 76 massive landslides, induced by Manjil (1990) earthquake [1]. The number of landslides was much more, however, the details of 76 landslides with a dimension of 100m was collected only.
- Landslide Hazard zonation for the affected area by Manjil 1990 earthquake, and modification of the methods recommended by TC4. The proposed modification was materialized by calibration of the landslide zonation maps with the mapped landslides [2]

- The detailed study and back analysis of a number of massive landslides due to Manjil 1990 earthquake. One of the landslides is named Galdian Landslide with dimensions of $(2500^m L \times 400^m W \times 40^m D)$ that moved more than 250^m and destroyed olive gardens and a number of houses in Rudbar city located in the epicenter. The detailed study of this landslide included undisturbed sampling and testing, geophysical profiling, and detailed surveying. Based on such a data back analysis of the landslide was performed and the reason for triggering of the landslide was discussed. Some other landslides with different mechanism also went under detailed study, such as Giash landslide [4].

We have also conducted comprehensive researches on landslide hazard zonation of Mazandaran province. One of the by products of this study was the proposal of a new method for landslide hazard zonation [5]. The method has been widely used in Iran by researchers and engineers.

2.2. Liquefaction

Liquefaction induced by Manjil 1990 earthquake was extensively observed in the town of Astaneh and its suburbs, located in north Iran [6]. This was the starting point for the research on liquefaction at SUT. Many activities under the subject of liquefaction have been going on during last 18 years at SUT. The studies can be divided in to four different fields: site investigation and microzonation, laboratory studies, soft computing, and the effect of lateral spreading on deep foundations.

2.2.1. Site Investigation and Liquefaction Microzonation

Site investigation including boring, sampling and standard penetration testing (SPT) were performed at Astaneh, where liquefaction was overwhelming due to the Manjil 1990 earthquake; and the reasons for the occurrence or non occurrence of the liquefaction in different sections of the town were investigated [7,8]. In this line a method was proposed for the prediction of the level ground damage induced by liquefaction [9].
The damages due to the liquefaction induced by Manjil (1990) earthquake made some warning for the cities in Gilan province. This fact led us to the liquefaction microzonation of the Gilan plain for different levels of earthquakes intensities [10].
As part of an earthquake microzonation for the mega city of Tehran, the liquefaction potential in south Tehran was studied using SPT and a liquefaction microzonation map was prepared for this section of the city [11].

2.2.2. Laboratory Studies

A variety of laboratory studies have been conducted on the liquefaction phenomena using monotonic and cyclic tests on soil elements. The main studies can be introduced as follows:

- Monotonic testing on gravelly sand of Tehran to recognize the liquefaction potential of the uncemented section of the alluvial deposit of Tehran and to find steady state characteristics of that material [12, 13].
- Monotonic testing on silty sands to study the effect of the amount and shape of fines on the liquefaction characteristics of the sands [14].
- Cyclic testing on gravelly sand of Tehran to study the cyclic behavior of the uncemented section of the alluvial deposit of Tehran [15].

- Cyclic tests on an Iranian standard sand (Babolsar sand) to study the effect of initial static shear stress on the liquefaction potential of the sands using both cyclic triaxial tests and simple shear test [16,17].
- Monotonic stress path study on Bobolsar sand using Hollow Cylinder Apparatus with special emphasis on the effect of medium principal stress (σ_2), rotation of principal stress (α) and fine contents on the characteristics of these sands. This study is underway and no document is yet published.

2.2.3. Soft Computing

Soft computing including Neural Network, Fuzzy systems, and Neuro-fuzzy systems can predict or explain liquefaction phenomena very well. The SUT studies on this subject are as follows:

- Use of Neural Network for the perdition of liquefaction potential [18].
- Implementation of Neuro-fuzzy to predict lateral spreading due to the liquefaction [19].

2.2.4. Effect of Lateral Spreading on Deep Foundation

Lateral spreading due to liquefaction can damage the deep foundations of the structures. Study on this subject is vital especially for the harbor facilities in Iran. Therefore, the following activities have recently been started at SUT:

- Study of the effect of lateral spreading on single and group piles using Open Seas code. No publications have yet been prepared on this subject.
- Study of the effect of lateral spreading on pile groups using physical modeling. A pile group located in a $3.5^m \times 1.1^m \times 2^m$ box is going to be tested on a $4^m \times 4^m$ shaking table. This study is underway and no result has yet been prepared.

3. LOCAL SITE EFFECTS ON THE EARTHQUAKE CHARACTERISTICS

Studies under this subject have been conducted for four cities in Iran: Rasht [20], Tabriz [21], Qazvin [22] and Kermanshah [23]. The methodology used for these studies are described below:

- Dynamic characterization of the deposits based on the subsurface geological and geotechnical data. Some new geotechnical investigations are conducted to verify or complete the data.
- 1D wave propagation analysis and the study of the effect of deposit on earthquake characteristic. The studied parameters are the peak ground acceleration, dynamic amplification, predominant period, and spectral amplification for different period ranges.
- Producing microzonation maps for the preceding characteristics.
- Producing design spectra for different sections of each city, based on the microzonation.

In addition microtremor measurements and analysis are conducted for verification of the calculated predominant periods. Based on the micrometer measurements in the city of Tabriz a method was proposed for the estimation of the natural period of the deposits for vertical component of the earthquake [24].

4. DYNAMIC CHARACTERIZATION OF CEMENTED GRAVELLY SANDS

Tehran alluvium is mainly cemented gravelly sand to sandy gravel. Also Tehran is prone to earthquakes. Therefore the study on the dynamic characteristics and liquefaction potential of this soil is vital. The static and dynamic behavior of this deposit has been a major topic being worked on at SUT for more than a decade. Different types of cementation including natural and artificial cementation have been implemented. Calcite is the natural cementation of the deposit and therefore it was desired to prepare artificially cemented samples with calcite. However, it is very difficult to crystallize the calcite as a cementing agent between the sand and gravel particles. The technique finally became successful, taking about one year time. It is worthwhile to mention that taking undisturbed cylindrical samples from natural soil is almost impossible and therefore the use of artificially cemented samples is a need for understanding of the behavior of this soil.

Having prepared the artificially cemented samples, they have gone under undrained cyclic loading and the dynamic characteristics and liquefaction potential of the deposit have been investigated and evaluated by conducting cyclic triaxial tests on representative samples [25].

5. EFFECT OF EARTHQUAKE ON EARTH AND ROCKFILL DAMS WITH ESPECIAL EMPHASIS ON CONCRETE FACED ROCFILL DAM (CFRD)

It is more than 14 year that we are working on the effect of earthquakes on Concrete Forced Rockfill Dams. These activities started from scratch with writing a program in C^{++} environment. The program could solve 2D problem with elastic and nonlinear elastic material behavior for the rockfill [26]. The refinements and enhancement of the solutions for the problem included the following improvements:

5.1. Two Dimensional Analysis

- Consideration of Elasto-Plastic behavior for the rockfill material.
- Study on the effect of reservoir elevation on the response of the CFRD to earthquakes with special emphasis on the forces in the face slabs [27].

5.2. Three Dimensional Analysis

The above problem was solved in three dimensions [28] and a number of graduate students have worked on different aspects of the problem as follows:

- Study on the effect of spatial variation of ground motion and out of phase movement of the abutments on CFRDs during earthquakes. This problem was solved [29] for the body waves (P, SV and SH).
- Effect of Dam- Abutment- Foundation Interaction (DAFI) was also studied. This effect can compensate the accelerated effects of scattering [30].
- In a further development the effect of reservoir elevation on 3D response of CFRD with consideration of Spatial Variation of Ground Motion (SVGM) and (DAFI) is studied [31].
- The problem of SVGM for a Rayleigh wave approaching a trapezoidal valley was solved [32] and the response of the CFRD to an scattered motion for Rayleigh wave was also studied [33] considering both SVGM and DAFI.

- The effect of reservoir elevation on the response of CFRD with consideration of SVGM and DAFI. was finally studied [3].

ACKNOWLEDGMENT

The researches reported in this paper have been supported by various organizations including vice president for research of Sharif University of Technology, UNDP, Housing Foundation, Ministry of Energy, Ministry of Road and Transportation. All supports are gratefully acknowledged.

REFERENCES

[1] Haeri, S.M. (1994), "Earthquake Induced Landslides with Emphasis on Large Landslides Induced by Manjil Earthquake", Tehran, Iran. (P)

[2] Haeri, S.M. and Samiee, A.H. (1994), "Some Methods of Landslide Microzonation" Proc. of 10 ECEE, vol. 2, pp 95-10., Wien, Austria, Balkema, Rotterdam

[3] Haeri, S.M., Sattari, M.H. & Ishihara, K.(1994), "Galdian Landslide Induced by Manjil Earthquake" 13th International Conf. On Soil Mech & Found Eng. (ICSMFE), New Dehli.

[4] Haeri, S.M. & Samiee, A.H. (1995), "Study on Giash Landslide Induced by Manjil Earthquake, Iran", IS-Tokyo 95, Earthquake Geotechnical Engineering, Ishihara (ed.) Balkema, Rotterdam, pp 1031-1036

[5] Haeri, S.M. and Samiee A.H.(1997), "A New Method for Landslide Microzonation with Emphasis on Mazandaran Province Landslide Microzonation" Jr. of Geo Sciences, Scientific Quarterly Journal, Bulletin of Geological Survey of Iran., vol 6, No 23-24, pp 2-15, Tehran, Iran. (P)

[6] Ishihara, K., Haeri, S.M., Moinfar, A.A., Towhata, I, & Tsnjino, S. (1992), "Geotechnical Aspects of the June 20, 1990, Manjil Earthquake, in Iran", Soils & Foundations, Jr. of Japanese Geotechnical Society, Vol. 32, No. 3, 61-78, Sept.

[7] Haeri, S.M.(1991), "Liquefaction Associated With 20 June 1990, Manjil Earthquake, Iran." SDEE-91 Conference, Karlsruhe, Germany, pp 129-134. Balkema, Rotterdam

[8] Haeri, S.M. & Zolfaghaari, M.R. (1992), "On the Earthquake Induced Liquefaction in Astaneh, Iran" Proc. of 10 WCEE, Madrid, Spain, Vol. I, pp 129-134

[9] Haeri, S.M. & Yasrebi, S.S. (1997), "A New Method for Evaluation of Liquefaction Damage on the Ground Surface" 4th Int. Conf on Civil Eng. Tehran, Iran. (P

[10] Haeri, S.M.(1992), "Microzonation of Gilan Plane for Liquefaction with Emphasis on Astaneh", Workshop on Seismic Zoning Methodologies for Geotechnical Hazards, LNEC, Lisbon, Portugal

[11] Haeri, S.M. & Hamidi, A. (2000), "Liquefaction Studies in South Tehran by Steady State Method" Proc. of 5th Int. Conf. on Civil Eng., Mashhad, Iran. (P)

[12] Haeri, S.M., and Hamidi, A. (2004) "Steady State and Liquefaction Characteristics of Gravely Sands" International Journal of Geotechnical & Geological Engineering, Springer Publisher, Germany, Vol 23, pp 141-156

[13] Hamidi, A., and Haeri, S.M. (2005), "A New Correlation Between Steady State Strength and SPT N-value for Gravely Sands", 58th Canadian Geotechnical Engineering Conference, Quebec, Canada

[14] Haeri, S.M. & Yasrebi S.S. (1999), "Effect of Amount and Angularity of Particles on Undrained Behavior of Silty Sands", Scientia Iranica, International Journal of Science and Technology, Vol. 6, No 3 & 4, pp 188-195.

[15] Haeri, S.M., Shakeri, M.R. & Shahcheraghi, S.A. (2008), "Dynamic Strength of Gravely Sand with Emphasis on Membrane Compliance" Proc. of the World Conference on Earthquake Engineering, 12-17 October, Beijing, China

[16] Haeri, S.M., and Khoshghalb, A., (2006), "Effect of Initial Static Shear Stress on Liquefaction Resistance of a Uniform Sand" Proc. of 1st ECEES and 13th ECEE, Geneva, Switzerland

[17] Haeri, S.M. & Pouragha, M., (2009) "The Effect of Initial Static Shear Stress on the Liquefaction Resistance of Babolsar Sand using Cyclic Simple Shear Tests" Proc. of 8th Int. Congress on Civil Engineering, Shiraz, Iran

[18] Haeri, S.M. & Karimi, M. (1999), "Evaluation of Liquefaction Potential Using Neural Network", Amir Kabir, Journal of Science and Technology, Vol. 11, No. 42, pp 108-119 (P)

[19] Haeri, S.M., Khalili, A. and Sadati, N., (2006), "A Neuro Fuzzy Model for Prediction of Liquefaction Induced Lateral Spreading" 8 NCEE, San Francisco, USA

[20] Haeri, S.M. and Kholafaee, M. (1994), "Local Site Effects in the City of Rasht During Manjil Earthquake of June 20 1990, Iran" Proc, of 2nd Int. Conf. On Earthquake Resistance Construction and Design, pp 109-116, Balkema, Rotterdam
[21] Haeri, S.M. and Hajialilu M., (2000), "Seismic Microzonation of the City of Tabriz in Iran" Asian Journal of Civil Engineering, Vol 1, No 3, pp 63-70, BHRC, Iran
[22] Haeri, S.M., Poursharifi, J and Orumiehe, M.A. (1998), "Site Effect Studies and Microzonation of the City of Qazvin", Seminar on Earthquake and Educational Spaces, Shiraz. (P)
[23] Sharafi, H. and Haeri, S.M. (2006), "Seismic Microzonation of the City of Kermanshah", 7th International Conference on Civil Engineering. Tehran, Iran (P)
[24] Haeri, S.M. & Hajialilu M. (1999), "Vertical and Horizontal Seismic Microzonation by Microtremor Measurement" Proc. 2nd Int. Conf. On Earthquake Geotechnical Engineering, pp 249-254, Lisbon, Portugal
[25] Haeri, S.M., Shakeri, M.R. & Ghayomi, M., (2007), "Dynamic Properties of a Limy Cemented Gravely Sand", Proc. of 4th International Conference on Earthquake Geotechnical Engineering, Thessaloniki, Greece
[26] Haeri, S.M. & Keyhani, R. (1999), "Dynamic Analysis of Concrete Faced Rockfill Dams" Proc. SEE-3 Vol 3 pp 95-106, Tehran (P)
[27] Haeri, S.M., and Esfehani, M. (2004), "Effect of Reservoir Elevation on the Response of CFRD to Earthquakes", Sharif Journal of Science and Technology, SUT, Tehran, Iran, Vol 20, No.27 pp 3-9 (P)
[28] Haeri, S.M. , Esmaeeli, S.S. , Esfehani, M. (2003), "Dynamic Analysis of Concrete Faced Rockfill Dams in 2D and 3D Conditions". 4th International Conference on Seismology and Earthquake Engineering, Tehran. (P)
[29] Haeri, S.M. & Karimi, M. (2004) "3D Dynamic Analysis of Concrete Faced rockfill Dams, with Spatial Variable Ground Motion" International Journal of Dam Engineering, Vol .XIV, Issue 4, pp 255-291
[30] Haeri, S.M. & Karimi, M., (2006), "Three Dimensional Response of Concrete Faced Rockfill Dam to Strong Earthquakes Considering Dam-Foundation Interaction and Spatial Variable Ground Motion" Proc. of 1st ECEES and 13th ECEE, Geneva, Switzerland
[31] Haeri, S.M., Ghadimi, B. & Bahmanpour, A., (2007), "Scattering of Rayleigh Waves by a Trapezoidal Canyon" 18th Engineering Mechanics Division Conference (EMD2007), ASCE, USA
[32] Haeri, S.M. Ghadimi, B. & Bahmanpour, A., (2007) "Effect of Reservoir Elevation on 3D Dynamic Response of a Typical Concrete Faced Rockfill Dam with consideration of Dam Foundation Interaction and Spatial Variation of Ground Motion" 18th Engineering Mechanics Division conference (EMD2007) , ASCE, USA
[33] Haeri, S.M. & Seiphoori A., (2009), "Response of Concrete Faced Rock-Fill Dam to Rayleigh Waves Considering Dam-foundation Interaction and Spatial Variability of Earthquake Ground Motion" Proc. of 8th Int. Congress on Civil Engineering, Shiraz, Iran

* (P) = (in Persian)

EVALUATING THE EFFECTIVENESS OF SOIL DENSIFICATION FOR MITIGATING LIQUEFACTION-INDUCED SETTLEMENT OF BUILDINGS

Ali Pak and Hadi Shahir
Department of Civil Engineering
Sharif University of Technology, Tehran, Iran

ABSTRACT

Liquefaction is one of the destructive phenomena that occurs in loosely deposited saturated sands during earthquakes. This phenomenon may sometimes cause a general failure of structures because of the loss of foundation bearing capacity. In other situations it causes a wide range of structural damages such as settlement and tilt of the buildings. For a performance-based design approach estimating the amount of liquefaction-induced settlement of buildings during various levels of earthquake intensities is of prime importance. In this research numerical modeling is used as a tool for determining the possibility of liquefaction occurrence and estimating the amount of liquefaction-induced settlement. The response of shallow foundations on liquefied sand during earthquake is studied using a 3D fully coupled hydro mechanical dynamic analysis. A well-calibrated critical state two-surface plasticity model has been used in the numerical analysis which is capable of accounting for the volumetric shear response of soil skeleton in a wide range of densities and confining pressures. In this research variation of soil permeability during liquefaction and its effects on soil seismic response is investigated. A variable permeability function is proposed which relates the permeability coefficient to the excess pore pressure ratio. The OpenSees platform is used to conduct the numerical simulations. After implementing the proposed function to OpenSees, the numerical tool was verified by simulating centrifuge experiments and the analysis results were compared with the experimental measurement.

Mitigating the hazards caused by liquefaction using soil improvement methods such as compaction have been numerically studied. A comprehensive parametric study is carried out in order to get insight into the complex interactive behavior of footing, superstructure, and treated (densified) or untreated soil layers under seismic loads. A new relationship for estimating liquefaction-induced settlement of shallow foundations has been developed. This relationship provides the required values for performance-based design of building foundations.

1. INTRODUCTION

Liquefaction takes place because of the pore water pressure accumulation in loose saturated sand deposits under earthquake loading, which causes a substantial reduction in the strength of the underlying soils.

Liquefaction phenomenon due to earthquake is usually accompanied by a large amount of settlement and/or tilt of structures. Based on the observations made in the past earthquakes, ground improvement by densification is one of the most useful methods that can be used to mitigate the liquefaction hazards.

The effectiveness of densification in mitigating the effects of liquefaction can be demonstrated by reviewing the low level of damage of buildings constructed on densified ground during major seismic events as far back as the 1964 Nigata earthquake (1).

Current design practice regarding the use of densification as a liquefaction resistance measure is mostly based on preventing the liquefaction triggering by a reasonable safety margin. In this design procedure, the amount of reduction of foundation settlement under earthquake loading is unknown. Currently there is no standard design procedure for evaluating the amount of foundation settlement considering soil improvement measures employed to mitigate liquefaction.

Evaluation of liquefaction-induced settlement and tilting requires modeling the process of liquefaction and subsequent consolidation and their effects on the behavior of shallow foundations. Quantitative analysis of liquefaction can only be accomplished by considering the coupled hydro-mechanical interaction of the soil skeleton and of the pore fluid. For this purpose, a suitable formulation for simulating the behavior of the two-phase continuum and a proper constitutive model are required. On the other hand, in most of the studies the effects of the variation of soil permeability during liquefaction has not been properly considered. Experimental investigations clearly show that the permeability of soil drastically increases due to liquefaction (1-2). To properly simulate the post liquefaction settlement, it is important to take the variation of permeability into account.

In this research, a 3D. fully coupled dynamic finite element analysis with a well-calibrated constitutive model is introduced for simulating the seismic response of shallow foundations on treated (densified) and untreated saturated granular soil strata. OpenSEES platform has been used, with the required modifications applied to it, to conduct the numerical simulations. A series of centrifuge experiments are simulated to show the model capability in capturing the important aspects of the dynamic response of footings on liquefiable and densified subsoils. After verification of the numerical model, based on a comprehensive parametric study, a general relationship for estimation of liquefaction-induced settlement of shallow foundations is proposed.

2. PREVIOUS STUDIES

Previous works on the topic can be classified in three broad categories. The first category belongs to field works and observations made after real earthquakes. Some failures and damages of buildings due to liquefaction have been observed and recorded during 1964 Niigata, Japan earthquake (Ishihara, 1981) [3]. Adachi et al. (1990) [4] reported the liquefaction-induced settlement of buildings after Luzon, Philippine earthquake. A number of papers have been published after 1990 Manjil, Iran earthquake [5] and 1999 Kocaeli, Turkey earthquake [6]. The observations made during previous earthquakes have shown that dimensions of the foundations and surcharge pressure as well as the type of structure affects the amount of settlement due to liquefaction. Although bearing capacity failure due to subsoil liquefaction has occasionally occurred, many of buildings have experienced a certain amount of permanent settlement and / or tilt. Based on the observations, some investigators have proposed empirical relations for estimating the amount of liquefaction induced settlement [7,8]. However, no relationship has been proposed so for, to account for the effect of soil improvement on the settlement of shallow foundations.

The second category of previous investigations belongs to laboratory experiments. For evaluating the dynamic response of shallow foundations on saturated sand strata during earthquake both shaking table and centrifuge tests have been used. Here only a number of them are mentioned since it is not intended to be an exhaustive review of the literature.

Hatanaka et al. (1987) [9], and Liu & Qiao (1984) [10] carried out physical modeling on the subject using shaking table. Whitman & Lambe (1988), [11] Liu (1992) [12], and Gutierrez (1998) [13] conducted centrifuge experiments to study the behavior of footing on liquefiable soils, while Hatanaka et al. (1987), Liu & Dobry (1997) [15], and Haussler (2002) [16] used the centrifuge experiments to study of the behavior of footings on improved subsoils. They studied the effects of foundation width, surcharge pressure, and soil characteristics on the amount of settlement of rigid footings on liquefiable soils. In case of improved subsoil, the effects of depth and width of improvement, soil relative density, etc. have been studied.

Numerical simulation of the dynamic behavior of shallow footings during liquefaction is the third category that is mentioned here. Although a number of numerical modelings have considered separate mechanisms for pore pressure generation and soil deformation, most of them have used a coupled procedure in which the interactive effects of soil deformation and fluid flow are taken into account in the analysis.

In some numerical investigations, the influence of soil liquefaction on the soil-structure interaction has been studied [17]. These modelings generally consist of simulation of the dynamic interaction between a homogeneous liquefying soil layer and a structure resting on the ground surface using a 2D. coupled finite element analysis; but dynamic response of shallow foundations on improved ground has not yet been investigated using numerical simulation.

3. GENERAL FORMULATION OF THE NUMERICAL MODEL

In this study, OpenSees has been used to conduct the numerical simulation. As for the geomechanics modules, a number of elements, algorithms and material models from University of California, Davis computational geomechanics toolset have been employed [18]. In the following, the general formulation of the numerical model is presented.

For a fully coupled hydromechanical analysis, the u-p formulation in which the displacement of solid phase (u) and pressure of fluid phase (p) are unknowns; is used:

$$M\ddot{U} + \int_V B^T \sigma' dV - QP - f^{(s)} = 0 \tag{1a}$$

$$Q^T \dot{U} + HP + S\dot{P} - f^{(p)} = 0 \tag{1b}$$

where M is the mass matrix, U is the solid displacement vector, B is the strain-displacement matrix, σ' is the effective stress tensor, Q indicates the discrete gradient operator coupling the motion and flow equations, P is the pore pressure vector, S is the compressibility matrix, and H is the permeability matrix. The vectors $f^{(s)}$ and $f^{(p)}$ include the effects of body forces and external loads, and fluid fluxes respectively.

A plasticity constitutive model developed by Dafalias & Manzari [19] was employed for modeling of the behavior of sand. A schematic representation of this model in the π-plane is shown in Figure 1.

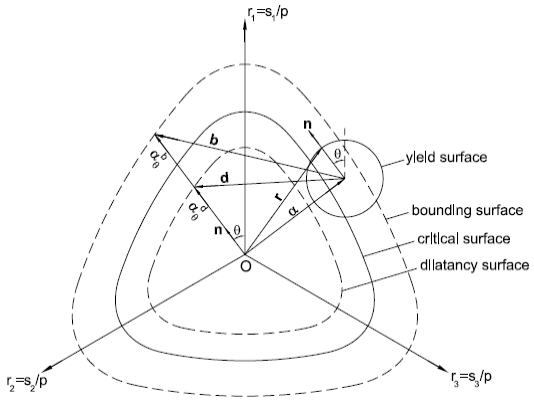

Fig. 1. Schematic representation of the two-surface model in the π-plane [19].

In this model, the isotropic hypoelasticity assumption is adopted with the elastic moduli as functions of current pressure and void ratio. The yield surface is a circular cone with its apex at the origin. The size of yield surface is normally considered a constant (no isotropic hardening) and rather small value in most applications. This model includes three other surfaces namely: bounding (peak), dilatancy, and critical surfaces. The critical surface is in direct correspondence to the critical stress ratio in the triaxial space. The critical state of a soil [20] is attained when the stress ratio $\eta = q/p$ equals the critical stress ratio (M), which is a material constant. In the current model, the bounding and dilatancy stress ratios are related to the critical stress ratio by way of the "state parameter" as follows:

$$M^b = M\exp(-n^b\psi)\ ;\ M^d = M\exp(-n^d\psi) \tag{2}$$

where M^b and M^d are peak and dilatancy stress ratios and n^b and n^d are positive material constants. $\psi = e - e_c$ is the "state parameter" proposed by Been and Jefferies [21], where e is the current void ratio of the soil element and e_c is the critical void ratio corresponding to the existing confining stress. The following power relation defines the Critical State Line (CSL):

$$e_c = e_0 - \lambda_c\left(\frac{p_c}{p_{at}}\right)^{\xi} \tag{3}$$

where e_0, λ_c and ξ are critical state constants.

The plastic modulus (K_p) and dilatancy coefficient (D) are related to the distance from the bounding and dilatancy surfaces as follows:

$$K_p = \frac{2}{3}ph\mathbf{b}:\mathbf{n} \tag{4}$$

$$D = A_d\mathbf{d}:\mathbf{n} \tag{5}$$

The vectors $\mathbf{b}$ and $\mathbf{d}$ shown in Figure 1, are defined as the vectors connecting the current stress state to its image on the bounding and dilatancy surfaces, respectively. p is the mean effective stress and h is a positive scalar-valued function. A_d is a function including the effects of "fabric change phenomenon" arisen during stress increment reversal after occurrence of a dilative plastic volumetric strain.

The constants of Dafalias and Manzari model were calibrated for Nevada sand by Shahir et al. [22] which is shown in Table 1. The model has 15 constants divided into 6 categories based on their functions. One of the main features of this constitutive model is its applicability to all densities and confining pressures with the same set of material constants.

Table 1. Material parameters of the critical state two-surface plasticity model for Nevada sand [5].

Constant	Variable	Value	Constant	Variable	Value
Elasticity	G_0	150	Plastic modulus	h_0	9.7
	ν	0.05		c_h	1.02
Critical state	M	1.14		n^b	2.56
	c	0.78	Dilatancy	A_0	0.81
	λ_c	0.027		n^d	1.05
	e_0	0.83	Fabric-dilatancy tensor	$z_{\max}$	5
	ξ	0.45		c_z	800
Yield surface	m	0.02			

4. VARIABLE PERMEABILITY FUNCTION

Numerical studies of liquefaction in which a variation in permeability has been considered are rare. Manzari and Arulanandan [23] used findings of Arulanandan and Sybico [1], and employed a variable permeability (as a function of time) for simulation of VELACS model No. 1. Their proposed permeability function gives a sudden increase to the permeability value only for the first seconds of liquefaction initiation, although the measured excess pore pressure ratios during the centrifuge experiment indicated that the liquefaction state is sustained for a long period. Also, in their analysis a unique permeability function was considered for all elements while different pore pressure responses were recorded along the soil column. They reported that by using their proposed permeability function, the measured settlement was simulated well. However, both rates of build-up and dissipation of pore pressure were overestimated when compared to the experimental measurements.

According to the study performed by Shahir, et al. [22], the variation of permeability coefficient in all pore pressure build-up, liquefaction, and dissipation phases can be expressed as a function of the excess pore pressure ratio. They proposed the following function for taking the variation of permeability into account in the numerical simulation of liquefaction:

$$\frac{k}{ki}=\begin{cases}1+(\alpha-1)\times r_u^{\beta_1} & in\,build-up\,phase\,(r_u<1)\\ \alpha & in\,liquefied\,state\,(r_u=1)\\ 1+(\alpha-1)\times r_u^{\beta_2} & in\,dissipatio\,n\,phase\,(r_u<1)\end{cases} \tag{6}$$

where k is the soil permeability coefficient during the process of liquefaction, k_i is initial (at-rest) permeability coefficient before shaking and α, β_1, and β_2 are positive material constants. r_u is the excess pore pressure ratio defined as follows:

$$r_u=\frac{\Delta u}{\sigma'_{v0}} \tag{7}$$

where Δu is the excess pore water pressure and σ'_{vo} is the initial vertical effective stress.

The above formulation was implemented into OpenSees for updating the coefficient of permeability at the end of each time step during seismic analysis, and applied to simulate the behavior of a saturated sand layer subjected to earthquake loading in the centrifuge experiment. By comparing the numerical results with centrifuge experiment records on Nevada sand, the constants were calibrated as $\alpha = 20$, $\beta_1 = 1.0$, and $\beta_2 = 8.9$.

The obtained value for α parameter basically means that the permeability coefficient increases up to 20 times during the initial liquefaction. This value is larger than the reported values by Arulanandan and Sybico [1] and Jafarzadeh and Yanagisawa [2], but it is consistent with the reported value by Balakrishnan [24]. From the practical viewpoint, the permeability coefficient is difficult to measure. So, the value of α may alter due to the inaccuracy involved in the measurement of initial permeability value.

5. VERIFICATION OF THE NUMERICAL MODEL

The coupled numerical model, which uses the calibrated values mentioned in Table 1 and variable permeability function explained in section 4, has been verified firstly against centrifuge experiment that was accomplished by Gonzalez et al. [25] at Rensselaer Polytechnic Institute to study the liquefaction of a uniform saturated sand. In this experiment a steel plate has been put on the surface of sand that was placed in a laminar box. No foundation was used in this experiment and the effect of surcharge on the behavior of sand was simulated by a steel plate. The details of the verification of this centrifuge experiment can be found in Shahir and Pak (2009) [26].

6. BEHAVIOR OF FOOTING RESTING ON LIQUEFIABLE AND DENSIFIED SOILS

Next, for verification of the numerical model in simulating the behavior of footings resting on liquefiable and densified soil, the centrifuge experiments conducted by Hausler [16] were considered. This verification is explained here in more detail.

Hausler [16] carried out several centrifuge experiments to study the effects of ground improvement on the response of shallow footings under different conditions. Four centrifuge experiments were selected for numerical modeling in which the effects of improvement depth on the foundation settlement and other responses were studied.

The centrifuge model 1 consisted of a square rigid structure rested on approximately 20 meters of liquefiable Nevada sand with initial relative density (D_r) of 30% which was placed in a flexible container. A sketch of the geometry of the experiments is presented in Figure 2. In models 2 to 4, the soil beneath the structure was compacted up to a relative density of 85% with different depths of 6 m (0.3H improved), 14 m (0.7H improved) and 20 m (Full depth improved). The initial relative density of the surrounding unimproved soil was 30%. The improved zone was square in plan and symmetric around the foundation axis, and the width of improvement zone was approximately twice the foundation width. The structure is a cubic rigid block with the same dimension of 8 meters in all directions and a bearing pressure of 96 kPa embedded 1.0 m in the top dry soil.

The pore fluid used in the experiments had a viscosity 10 times greater than that of water and the model was spun up to a centrifuge acceleration of 40g. Considering the scaling laws in centrifuge

modeling, this experiment simulates a soil deposit with a permeability coefficient 4 times greater than that of Nevada sand in prototype scale.

All models were shaken with a sequence of three scaled (small, large and medium) versions of the 83m depth, N-S component of 1995 Kobe Port Island earthquake. In this paper, only the small scale event with a peak ground acceleration of 0.15g which was applied prior to other shakings was analyzed. The prototype time history of the input motion is shown in Figure 3.

6.1. Description of the Numerical Model

Numerical modeling of the centrifuge experiments were performed in prototype scale. A three-dimensional mesh with 1960 8-node cubic elements was used in the analyses as shown in Figure 4. Table 2 lists the properties of Nevada sand used in the analyses. To consider the effect of laminar box in the numerical simulation, the lateral boundaries perpendicular to the direction of shaking were constrained together to have the same displacement in the direction of shaking. The displacements of lateral boundaries parallel to the direction of shaking were tied in the direction perpendicular to shaking. The bottom boundary was assumed fixed. Full dissipation of pore pressure was allowed through the surface of sand layer and the lateral and bottom boundaries were supposed to be impervious. The structure was modeled by rigid brick elements connected rigidly to the adjacent soil nodes. The Young's modulus for the structure is chosen large enough (2×10^7 kPa) so that the structure can be considered rigid.

Analyses were carried out in three steps. First, a static analysis was performed to apply the gravitational forces due to self weight of the soil and also weight of the structure. After this step, the resultant displacement, velocity, and acceleration vectors were zeroed, and the initial effective stresses and pore water pressures were stored. Then, the earthquake loading was applied as a prescribed acceleration time history at the bottom boundary. During seismic analysis, the variation of permeability function was incorporated in the analysis using Eq. (6). After ending of earthquake loading, the consolidation phase to allow the redistribution and dissipation of the developed excess pore pressures was analyzed.

The above mentioned three steps of analysis were performed for each of the 4 models, i.e. 0.0, 0.3H, 0.7H, and 1.0H soil improvement depths.

6.2. Results and Discussion

Excess Pore Pressure

Figures 5 and 6 display the predicted and measured maximum excess pore pressure ratios along the soil depth at free field and under the foundation centerline, respectively. It is noted that the maximum excess pore pressure ratios at all elevations do not occur at the same time. The maximum excess pore pressure ratios were presented in tabular format by Hausler [16] and the digital data of the centrifuge experiments was not available. Thus, the time history of excess pore pressures could not be compared and the maximum excess pore pressure ratios were used for comparison.

As shown in Figure 5, the occurrence of liquefaction ($r_u = 1.0$) up to the depth of about 12.0 m in the free field was accurately predicted by the numerical model. The zero depth represents foundation bottom level. In deeper strata, both numerical simulation and experimental model

indicate that the condition of zero effective stress or initial liquefaction state did not occur. The predicted pore pressure ratios in the free field from all four models are nearly the same and match well with the measured values. At the bottom of the soil layer the predicted pore pressure ratio is somewhat greater than the measured one (Figure 5).

The predicted excess pore pressure ratios presented in Figure 6 are generally in good agreement with the experimental measurements. According to the experimental measurements as well as simulation results, densification had a major influence in the reduction of the developed excess pore pressure ratio beneath the foundation. The average excess pore pressure ratios under the foundation in model (4) are about 65% of model (1). It is noted that even in model (1) in which no ground improvement was made and the developed excess pore pressure under foundation is higher than other improved models, the initial liquefaction state was not observed beneath the foundation. Contrary to the observed behavior in the free field, the experimental and numerical results in all of four models show that the minimum excess pore pressure ratio occurs at shallow depths beneath the foundation and increases gradually downward. The maximum excess pore pressure ratio, however, does not occur at the bottom of the models, but rather at some intermediate depths.

The difference between the pattern of excess pore pressure ratio in the free field and beneath the foundation is mainly attributed to difference between the initial vertical effective stresses. The initial vertical effective stress used for calculating the excess pore pressure ratio (Eq. 7) is due to the effective weight of the soil layers in the free field. However, under the foundation the effect of foundation load also contributes to the excess pore pressure. Therefore, the values of excess pore pressure ratio under the foundation are substantially lower than those in the free field.

Structure Settlement

The measured and predicted foundation settlements in all experiments are presented versus normalized compaction depth in Figure 7(a). Figure 7(b) shows the foundation settlement normalized to the free field soil settlement. The measured free field settlement in the experiments varies between 20 to 25 cm and the predicted value for the free field settlement is about 20 cm in all numerical models. In Figure 7(b) the influence of different free field settlements has been removed by normalization of foundation settlement. As seen in this figure, the predicted settlements are in good agreement with the experimental observations.

The normalized foundation settlement has decreased from 2.13 in the experiment without compaction to 0.43 in the experiment with full depth compaction, i.e. the foundation settlement has decreased about 5 times due to densification. This indicates the effectiveness of densification in mitigation of the liquefaction induced settlement. As observed in Figure 7, there is a rather negligible reduction in the foundation settlement in the case of superficial compaction up to depth of 0.3H (H: total soil depth). The major reduction in foundation settlement is achieved when the improved zone extends through 0.7H. Further compaction below the depth of 0.7H has a minor effect on reducing the amount of foundation settlement. It is noted that the obtained values may not be generalized for other situations and more research is warranted considering a wide range of soils, foundations, and shaking parameters.

The simulation results indicate that the values of excess pore pressure ratio under the foundation are substantially less than those in the free field owing to the effects of the structure surcharge,

and so contrary to the free field, the liquefaction state is not observed beneath the foundation. Soil densification proved to have a major effect in reducing the developed excess pore pressure ratio beneath the foundation.

The effectiveness of densification in the reduction of the liquefaction-induced settlement has been simulated well. The simulation results as well as experimental measurements reveal that further compaction below the depth of 0.7H has a minor effect on reducing the amount of foundation settlement. The results also indicate that the optimum value for width of the improved zone around the foundation is equal to the foundation width plus depth of soil liquefaction. This optimum value is independent of the foundation width.

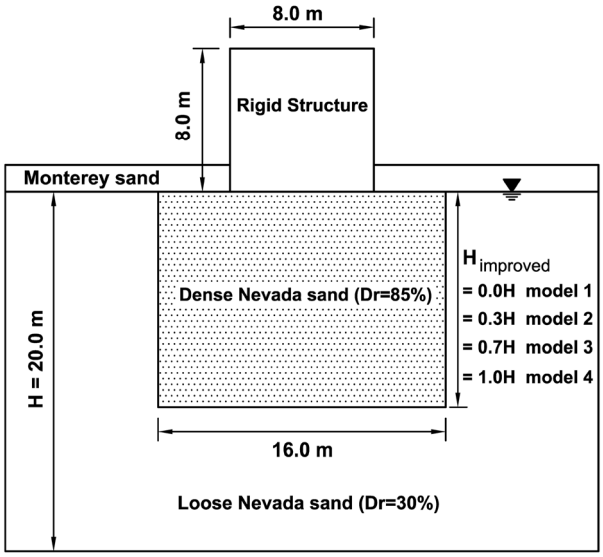

Fig. 2. Geometry of the centrifuge experiments [2].

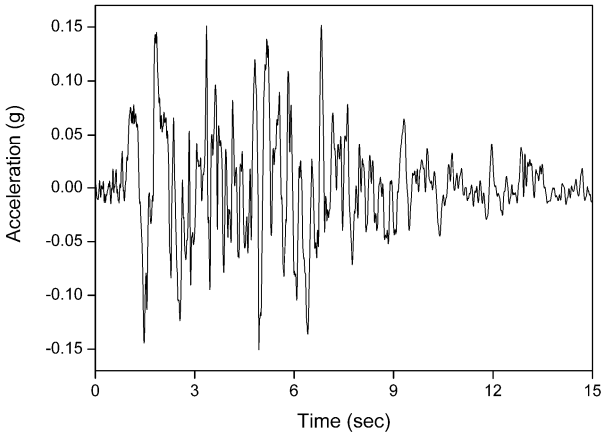

Fig. 3. Prototype time history of the input motion.

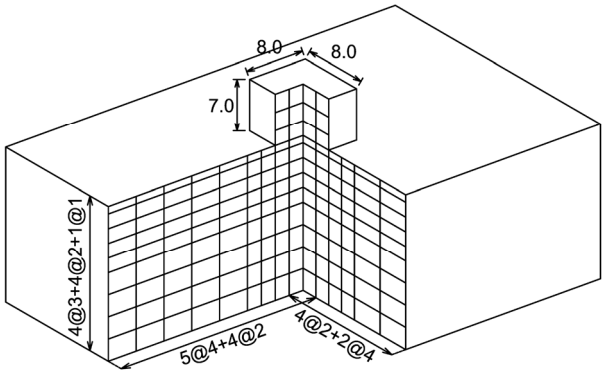

Fig. 4. Cross section of the 3D Finite element mesh (all dimensions are in m).

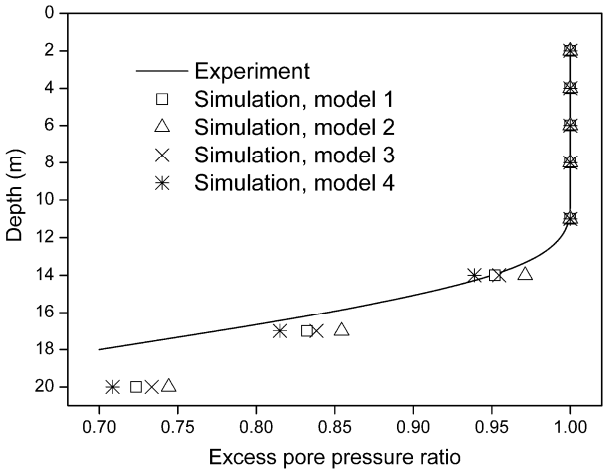

Fig. 5. Distribution of excess pore pressure ratio along the soil depth at free field.

Table 2. Properties of Nevada sand used in the analyses [16].

Parameter	Value at D_r=30%	Value at D_r=85%
Void ratio	0.781	0.586
Saturated unit weight	19.0 kN/m^3	20.15 kN/m^3
Water permeability	4.0×10^{-5} m/sec	2.5×10^{-5} m/sec
Prototype permeability	1.6×10^{-4} m/sec	1.0×10^{-4} m/sec

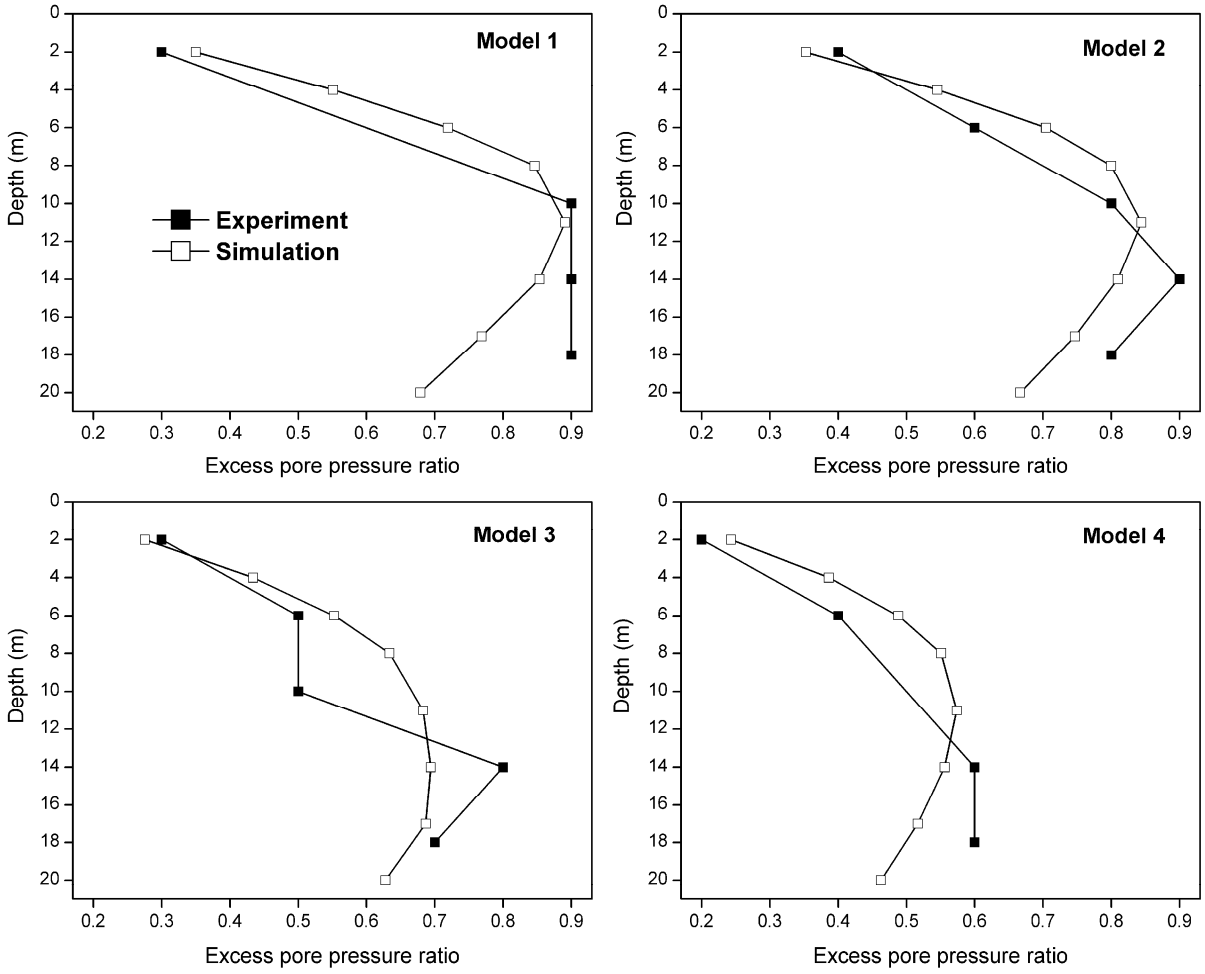

Fig. 6. Distribution of excess pore pressure ratio along the soil depth under the foundation.

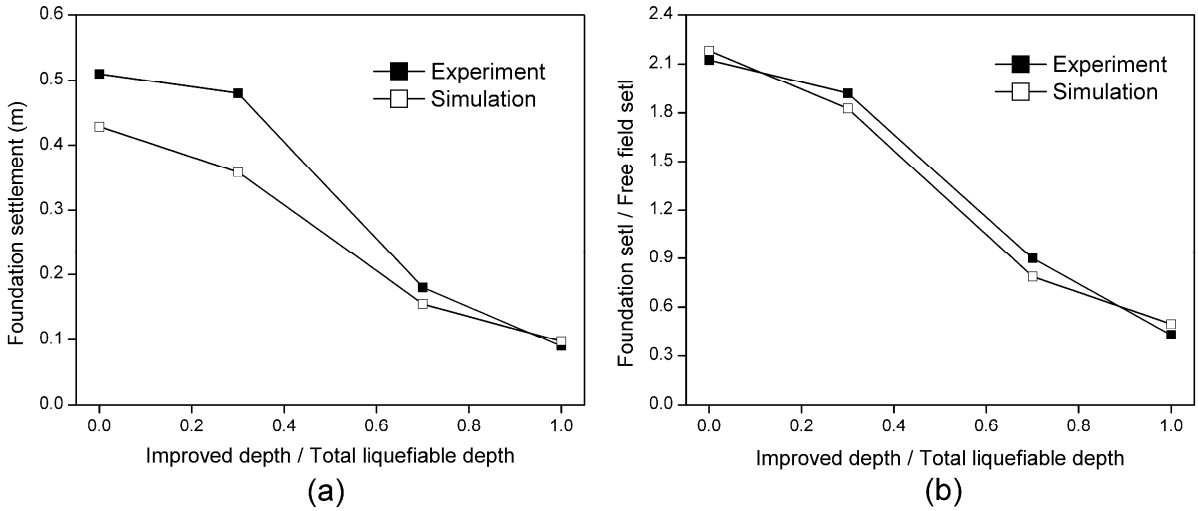

Fig. 7. Foundation settlement versus normalized compaction depth (a) absolute amounts of settlement (b) Normalized values.

7. A NEW RELATIONSHIP FOR ESTIMATING LIQUEFACTION-INDUCED SETTLEMENT OF SHALLOW FOUNDATIONS

Development of a general relationship for determining the liquefaction-induced settlement of shallow foundation is rather complex due to two main reasons: firstly non-uniform stress field in the soil layers beneath the structure and soil-water interaction effects that causes an extremely complicated behavior of foundation on the liquefied subsoil, and secondly, variety of influencing factors relevant to soil, foundation, and input motion that cause broad variations in the results.

However, having a suitable relationship for the liquefaction-induced settlement of shallow foundations is very important from the practical viewpoint. This relationship can be used to assess the seismic performance of shallow foundations resting upon liquefiable subsoil and its effects on the overall performance of structure. In this regard, the numerical model which was verified through simulation of a number of centrifuge experiments, has been employed for conducting a comprehensive parametric study including various combinations of the soil, foundation, and excitation characteristics.

Similar to the centrifuge experiment used for verification, in the parametric analyses the structure was considered as a rigid block embedded 1 m in the top dry soil. Also, the ground water table was considered at the bottom of structure. To be well-matched with real situations, in the current analyses the soil permeability was considered equal to the Nevada sand permeability. The variable parameters in the course of parametric study were soil height, soil relative density, footing width, footing bearing pressure, and peak ground acceleration. The range of variation of each parameter in the parametric study is presented in Table (2). For different soil heights, the foundation width was considered in a manner that the width ratio varies in the range of 0.2 to 5.0. In all analyses, the ratio of the height to the width of the structure (aspect ratio) was considered equal to 0.5.

After completion of a number of analyses and interpretation of the results, it was found that the trend of results for the cases that the total height of the soil is liquefied is different from that of the cases with partial liquefied height. Thus, the results of the analyses for these two cases are presented separately.

7.1. The Models with Entirely Liquefied Height

In the first step, soil relative density, net footing pressure, and peak ground acceleration are supposed to be 30%, 80 kPa, and 0.3g, respectively and the effects of soil height and the foundation width are studied. By analyzing a soil column, the maximum liquefaction depth in this condition was obtained 21.4 m. Thus, for having an entirely liquefied condition, soil height was considered in the range of 5 to 20 m.

In Figure 8, the results of the analysis for the models with entirely liquefied height are presented in the form of settlement ratio versus width ratio. The settlement ratio and the width ratio are ratios of foundation settlement and width to the thickness of liquefied soil, respectively. As observed, the simulation results show a consistent trend. For the small width ratios, the numerical results show that the settlement ratio increases with the width ratio, while for the large width ratios the settlement ratio decreases gently with increasing of the width ratio. In Figure 8,

an exponential curve which best describes the simulation results, was fitted to the data points. In the curve fitting procedure, the point at which the trend of variation is reversed was found at the width ratio equal to 0.9. The equation of the fitted curve is as follows:

$$\frac{S_f}{Z_l} = 0.018 \exp\left(-0.5\frac{B_f}{Z_l}\right) - 0.029 \exp\left(-3.0\frac{B_f}{Z_l}\right) + 0.019 \quad (8)$$

where S_f is the average settlement of foundation, B_f is the foundation width, and Z_l is the thickness of liquefaction.

The observed behavior can be explained by examination of the effect of variation of foundation width on two components of the settlement, i.e. volumetric compaction and shear deformation. The results of analyses indicate that by widening of foundation, somewhat more excess pore pressure is developed beneath the center of foundation, which can be attributed to the increased confinement provided by a wider foundation. The volumetric compaction of the soil is a function of the developed excess pore pressure. However, in this case the percent of increase in developed excess pore pressure is not significant and therefore, its effect on the volumetric compaction of soil underneath the foundation is not considerable. For determination of the influence of the foundation width on lateral movement of the liquefiable soil below the foundation (shear deformation), it should be noted that in the classical soil mechanics, the depth of influence for calculation of static settlement of a square footing is usually considered equal to its width. Therefore, for the width ratio less than one, the depth of influence of foundation is less than the liquefiable soil height and so, similar to a footing on a homogeneous soil layer (in undrained condition with no volume change), footing settlement increases by increasing of footing width.

For the width ratio greater than one, the depth of influence of foundation is greater than the liquefiable soil height and the current problem is similar to a footing resting on a deformable layer with finite thickness overlaying rigid bedrock. In this case, by increasing the foundation width, the zone influenced by the foundation pressure becomes greater comparing to the liquefied soil thickness, hence the effect of the liquefied soil layer on the foundation settlement becomes smaller, and consequently the foundation settlement decreases.

In order to display the effect of soil relative density, peak ground acceleration, and footing bearing pressure on the liquefaction-induced settlement of footings, several analyses with variation of these parameters were carried out. The results of the analyses are presented in Figure 9(a) and compared with the initial case. As observed, the footing settlement increases by decreasing of soil relative density, increasing of peak ground acceleration, and increasing of bearing pressure. These results match well with the observations during the shaking table and centrifuge model tests (Yoshimi and Tokimatsu, 1977[9], Liu and Qiao, 1984 [10], Liu, 1992 [12], Gutierrez, 1998)[13].

In an endeavor to develop a unique relationship, it was found that the effect of relative density and peak ground acceleration can be eliminated by dividing the settlement ratio by square root of maximum thicknesses of liquefaction. Maximum thickness of liquefaction ($Z_{l,m}$) is defined as the thickness of liquefaction in a homogeneous sand layer with infinite depth in the free field.

For elimination of the bearing pressure effect, dividing by the $q_{net}^{0.4}$ (q_{net}: net bearing pressure) can be used. In Figure 9(b) the normalized curves are shown. As observed, the normalized curves

are fairly matching. Thus, the proposed factors reasonably eliminate the influence of the relative density, peak ground acceleration, and bearing pressure and can be used for development of a unique relationship.

In Figure 10, the results of all analyses in the form of settlement ratio divided by the two factors were plotted versus width ratio. As can be observed, the analyses results fall in a narrow band and so, an exponential curve can be fitted to the data with good accuracy. The fitted curve is shown in Figure 10 and its equation is as follows:

$$\frac{S_f / Z_l}{Z_{l,m}^{0.5} \times q_{net}^{0.4}} = 0.0007 \exp\left(-0.5 \frac{B_f}{Z_l}\right) - 0.0012 \exp\left(-3.1 \frac{B_f}{Z_l}\right) + 0.0007 \quad (9)$$

where $Z_{l,m}$ is the maximum thickness of liquefaction in m and q_{net} is net bearing pressure in kPa.

Regarding the definition of Z_l and $Z_{l,m}$, the following relations hold between these two parameters:

$$Z_l = \begin{cases} H_t & if \ \ H_t \le Z_{l,m} \\ Z_{l,m} & if \ \ H_t > Z_{l,m} \end{cases} \quad (10)$$

where H_t is the total soil height.

7.2. The Models with Partially Liquefied Height

As mentioned above, the Equation (9) is valid only for the cases where the total height of the free field soil is liquefied under the earthquake loading. However, for the deep layers of medium dense sand subjected to low to medium intensity shakings, the total height of the soil may not liquefy. In other words, the thickness of the soil layer is greater than the maximum thickness of liquefaction.

In this case, the total foundation settlement can be divided into two parts: settlement due to subsidence of upper liquefied layer and settlement due to subsidence of lower unliquefied layer. The part of foundation settlement, which is related to the upper liquefied layer, can be estimated using Eq. (9). The results of the conducted analyses for estimation of the settlement of the lower unliquefied layer are discussed in the following.

Simulation of various partially liquefied height models with different combinations of soil, foundation, and input motion parameters revealed that the settlement of the soil stratum below the maximum thickness of liquefaction is independent of the footing characteristics and its value in the free field and under the foundation is almost the same. This result indicates that the settlement of the soil stratum below the maximum thickness of liquefaction is mainly due the volumetric compaction of the soil mass and the amount of shear deformation in this layer is negligible. This can be attributed to the fact that below the maximum thickness of liquefaction the adjacent soil layers in the free field have not been liquefied, so they have enough shear strength not to allow the soil below the foundation to spread outwards.

By normalizing the settlement of soil layer below the maximum thickness of liquefaction and the total soil height by the thickness of liquefaction, the analyses results show a definite relationship with minor scatter, as shown in Figure 11. The equation of the fitted curve is as follows:

$$\frac{S_1}{Z_l} = 0.0144 \ln\left(\frac{H_t}{Z_l}\right) \tag{11}$$

where S_1 is the settlement of soil layer below the maximum thickness of liquefaction.

In the case of entire liquefied depth, the Equation 13 gives zero value for S_1. Therefore, by adding Equations 9 and 11, a general equation applicable for all of the above mentioned cases, can be obtained as follows:

$$\frac{S_f}{Z_l} = Z_{l,m}^{0.5} \times q_{net}^{0.4} \times \left[0.0007 \exp\left(-0.5\frac{B_f}{Z_l}\right) - 0.0012 \exp\left(-3.1\frac{B_f}{Z_l}\right) + 0.0007\right] + 0.0144 \ln\left(\frac{H_t}{Z_l}\right) \tag{12}$$

This equation is a general relationship for estimation of liquefaction-induced settlement of a square rigid footing (or a rigid structure with low aspect ratio) founded on top of a homogeneous saturated fine-grained sand layer. It is notable that this relationship is valid only if bearing capacity failure does not take place.

A key parameter in this equation is the thickness of liquefaction. This parameter is a well-known engineering parameter and several empirical methods have been proposed for its estimation.

Thus, the proposed equation is simply applicable to practical purposes.

Table 3. Range of variations of each parameter in the parametric study.

Parameter	Minimum value	Maximum value
Total soil height (m)	5	50
Soil relative density (%)	30	50
Footing width (m)	3	60
Net footing bearing pressure (kPa)	40	120
Peak ground acceleration	0.15g	0.3g

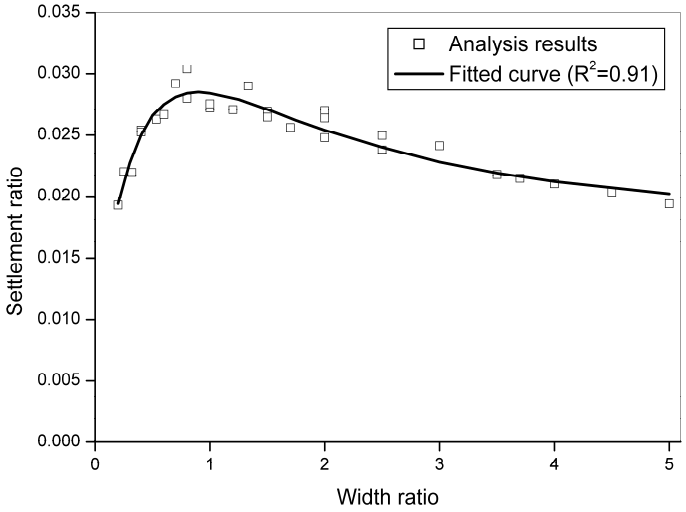

Fig. 8. Settlement ratio versus width ratio for analyses with D_r=30%, PGA=0.3g, and q_{net}=80 kPa.

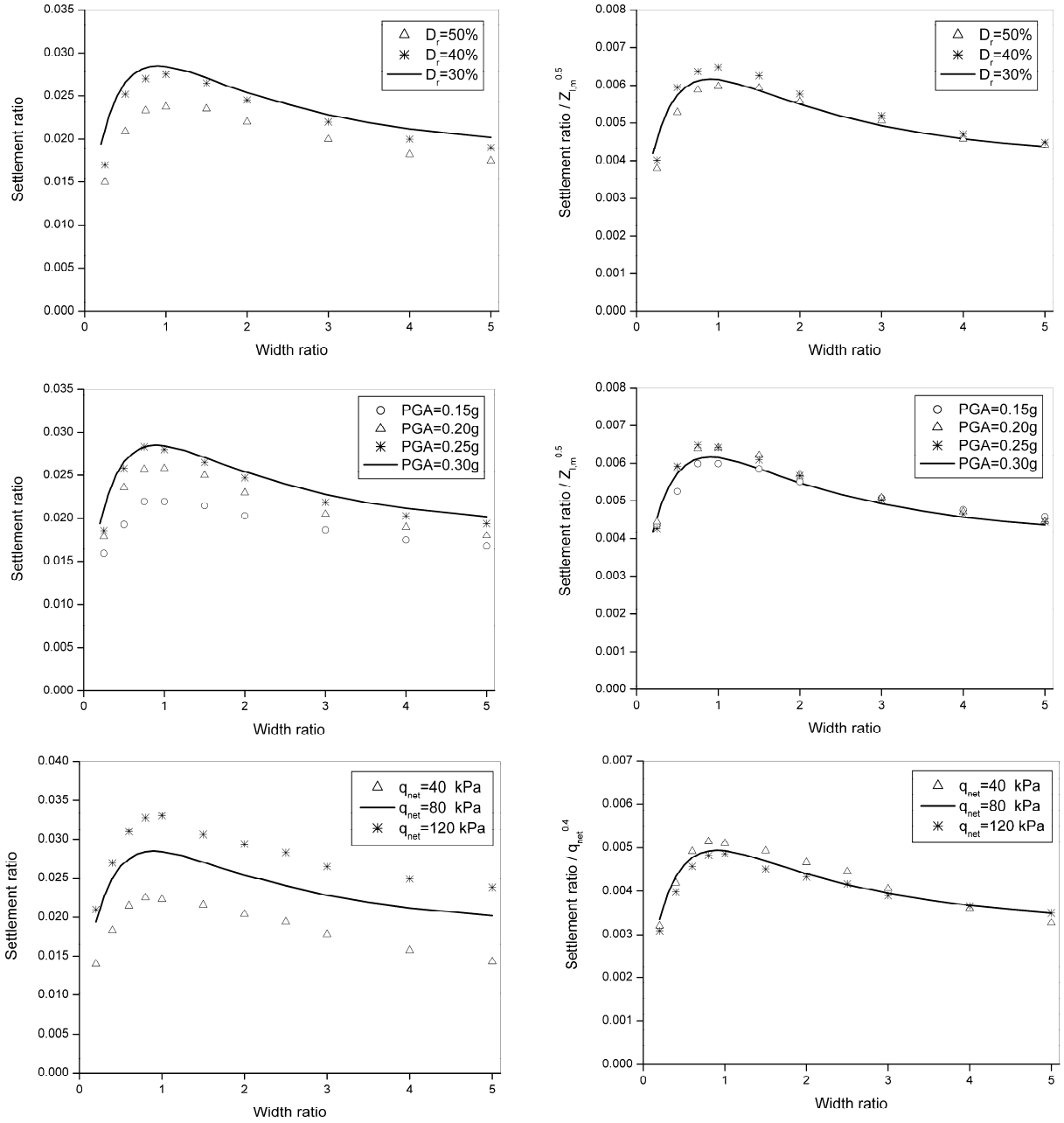

(a) (b)

Fig. 9. (a) Effects of variations in peak ground acceleration, subsoil relative density, and net bearing pressure (b) Normalized curves.

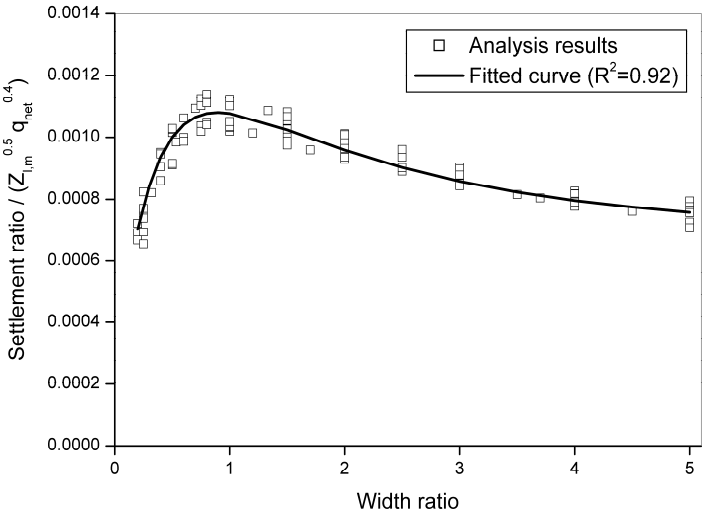

Fig. 10. Results of all analyses.

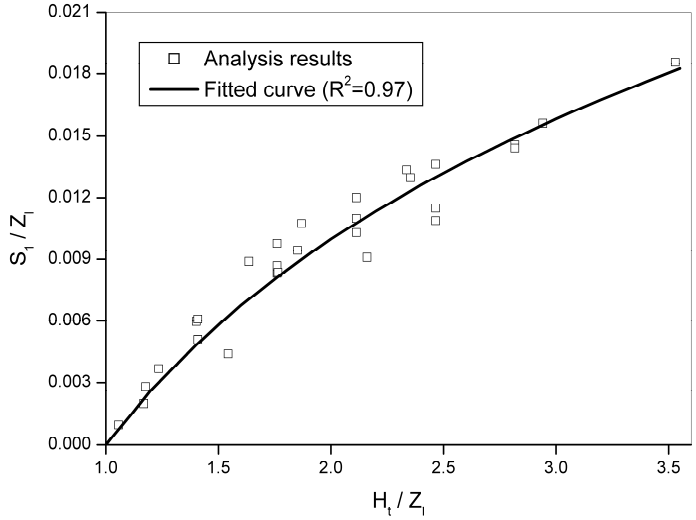

Fig. 11. Settlement of soil layer below the maximum thickness of liquefaction.

8. CONCLUSIONS

In this paper an overview of the results of a research on the behavior of shallow foundations on saturated loose sandy deposits that are prone to liquefaction due to earthquake was presented.

Numerical simulation was used as a tool for this research. Three dimensional dynamic coupled hydro-mechanical finite element analysis has been employed. An advanced critical state two-surface plasticity model has been used for simulating the complicated contractive behavior of saturated loose sand subjected to seismic loading. The model parameters have been exclusively calibrated for this research. For properly modeling the settlement and/or tilt of the structures built on the liquefiable sand layers, an important phenomenon that occurs during liquefaction i.e. variation of soil permeability has been taken into account in the course of numerical study by introducing a variable permeability function.

One of the main purposes of the research was obtaining a design procedure for optimizing the process of ground improvement by densification methods in order to mitigate the earthquake hazards that are associated with liquefaction. From this research the following conclusions are obtained:

1. Attempting to model a complicated interactive phenomenon such as seismic behavior of shallow foundations on liquefiable ground, requires employing an advanced constitutive model and a variable permeability function for soil incorporated in a numerical code that is capable of conducting dynamic fully coupled hydro mechanical analysis in saturated porous media.
2. Determining the behavior of shallow foundations on liquefiable ground is possible through estimation of settlement and/or tilt of the structure due to liquefaction. The values that are obtained for settlement / tilt are used for a performance-based design approach that improves our engineering design standards to reduce the risk, and mitigate the hazards that are associated with liquefaction.
3. Soil improvement by densification methods, greatly reduces the amount of settlement and tilt of the structure. The major reduction in the foundation settlement is achieved when the depth of the improved zone extends up to 70% of the total liquefiable soil depth. Below this depth the amount of settlement reduction is small.
4. The optimum value for width of the improved zone around the building foundation has been found to be equal to the foundation width plus the depth of soil liquefaction.
5. A new relationship has been proposed for estimating the foundation settlement resting on totally or partially liquefiable medium sand layers.
6. A design procedure has been developed for densification of the ground in order to reduce the liquefaction hazards for the structure economically.

REFERENCES

1. Arulanandan, K. and Sybico, J.Jr., (1992), “Post-liquefaction settlement of sand,” Proc. of the Wroth Memorial Symposium, Oxford University, England.
2. Jafarzadeh, F. and Yanagisawa, E., (1995), “Settlement of sand models under unidirectional shaking,” Proc. of First International Conference on Earthquake Geotechnical Engineering, IS-Tokyo, pp 693-698.
3. Ishihara, K., Kaya, Y., "Case studies of liquefaction in the 1964 Niigata earthquake", soils and foundations, 1981, 21(3): 35-52.
4. Adachi, T., Iwai, S., Yasui, M. and sato, Y. "Settlement and inclination of reinforced concrete buildings in Dagupan city due to liquefaction during 1990 Philippine earthquake. In: proceedings of 10th world conference on Earthquake Engineering A.A. Balkema, Rotterdam, the Nether lands, vol. (2), 1992, p 147-152.
5. Ishihara, K., Haeri, S.M., Moinfar, A.A., Towhata, I, & Tsnjino, S. (1992), “Geotechnical Aspects of the June 20, 1990, Manjil Earthquake, in Iran”, Soils & Foundations, Jr. of Japanese Geotechnical Society, Vol. 32, No. 3, 61-78, Sept.
6. Japanese Geotechnical society (JGS). Report on the investigations of the 1999 Kocaeli earthquake, Turkey, 2000 (in Japanese).
7. Ishii, Y., Tokimatsu, K., "Simplified procedures for evaluation of settlements of structures during earthquakes". In: proceedings of he qth world conference on Earthquake Engineering, Tokyo, Japan, Vol. III, 1988, p. 95-102.
8. Liu, H. "An Empirical Formula for evaluation of building settlement due to earthquake liquefaction. In: proceedings of 3rd international conference on recent advance in geotechnical earthquake engineering and soil dynamics, St, Louis, Missouri, vol. I, 1995, p. 289-293.
9. Hatanaka, M. Suzuki, Y., Miyaki, M., and Tsukuni, S. (1987) “Some Factors Affecting the Settlement of Structures due to Sand Liquefaction in Shaking Table Tests”, Soils and Foundations, 27 (1), 94-101
10. Liu, H., and Qiao, T., "Liquefaction potential of saturated sand deposits underlying foundation of structure", In: proceedings of 8th World Conference on Earthquake Engineering, San Fransisco, vol. 3, 1984, p 199-206.

11. Whitman, R.V. and Lambe, P.C., "Earthquake like shaking of structure founded on saturated sand. In Corte J.F. (editor), Proceedings of International conference on Geotechnical centrifuge modeling, "A.A. Balkema, Rotterdam, The Netherlands, 1988, p. 529-538.
12. Liu, L. "Centrifuge earthquake modeling of liquefaction and its effect on shallow foundations, ph. D. Thesis, Department of civil and Environmental Engineering, reseller polytechnic institute, Troy, New York, 1992.
13. Gutierrez, A.M., "Centrifuge modeling of surface structure on normally consolidated silty sand deposited in layers under water and subjected to seismic excitation". Ph. D. thesis, Department of civil and environmental engineering, Rensselaer polytechnic Institute, Troy, New York, 1998.
14. Yoshimi, Y., Tokimatsu, K., "Settlement of buildings on saturated sand during earthquakes, soils and foundations, 1977: 17(1): 23-28.
15. Liu, L., and Dobry, R. (1997) "Seismic Response of Shallow Foundation on Liquefiable Sand", J. Geot. and Geoenv. Engrg., ASCE, 123(6), 557-567
16. Hausler, E.A., "Influence of Ground Improvement on settlement and liquefaction: A study based on field case history evidence and dynamic geotechnical centrifuge tests, ph. D. Dissertation, University of California, Berkeley, 2002.
17. Lopez- Caballero, F., Modaressi farahmand – Razavi, A., "Numerical simulation of liquefaction effects on seismic SSI", soil dynamics and Earthquake engineering, 28, pp. 85-98 (2008)
18. Jeremic, B. and Sture, S., (1998), "Tensor data objects in finite element programming," International Journal for Numerical Methods in Engineering, 41, pp 113–126.
19. Dafalias, Y.F. and Manzari, M.T., (2004), "Simple plasticity sand model accounting for fabric change effects," Journal of Engineering Mechanics, 130(6), pp 622-634.
20. Schofield, A.N. and Wroth, C.P., (1968), "Critical state soil mechanics," McGraw-Hill, New York.
21. Been, K. and Jefferies, M.G., (1985), "A state parameter for sands," Geotechnique, **35**(2), pp 99-112.
22. Shahir, H., Pak, A., Taiebat, M. and Jeremic, B., "Evaluation of variation of permeability in liquefiable soil under earthquake loading," submitted to Soil Dynamics and Earthquake Engineering.
23. Manzari, M.T. and Arulanandan, K., (1993), "Numerical predictions for Model No. 1," Proc. of Verification of Numerical Procedures for the Analysis of Soil Liquefaction Problems, A.A. Balkema, Rotterdam, pp 179-185.
24. Balakrishnan, A., (2000), "Liquefaction remediation at a bridge site," PhD Dissertation, University of California, Davis.
25. Gonzalez, L., Abdoun, T. and Sharp, M.K., (2002), "Modeling of seismically induced liquefaction under high confining stress," International Journal of Physical Modeling in Geotechnics, **2**(3), pp 1-15.
26. Shahir, H. and Pak, A. (2009), "Numerical Investigation of the effects of Soil Densification on the Reduction of Liquefaction-induced settlement of Shallow Foundations", Scientica Iranica, In Press

ASSESSMENT OF SEISMIC RISK IN LIFELINE SYSTEMS

by

M. Shinozuka
University of California, Irvine

ABSTRACT

The primary objective of this paper is to summarize the simulation-based probabilistic methodology for evaluation of performance of spatially distributed systems serving urban population centers under operational and extreme event conditions. The methodology is multidisciplinary involving disciplines of engineering, economics, natural and social sciences. The methodology promotes the system design based on robustness, resilience and sustainability. Critical infrastructures typically include utility and transportation networks which are operationally and functionally interdependent and interactive. The system performance is defined in terms of robustness, resilience and sustainability. This presentation focuses on analysis of system robustness and resilience and makes some observations with respect to sustainability. For the purpose of clearly demonstrating the methodology, this paper deals with a model developed for the Los Angeles Department of Water and Power's (LADWP's) power system as part of the Western Electricity Coordinating Council (WECC) grid, and the model is used to simulate its robustness and resilience under a set of scenario earthquakes consistent with the regional seismic hazard defined by USGS. The result of the simulation agreed with the robustness and resilience actually demonstrated by the system under the Northridge earthquake. In addition, by employing the model of the entire WECC grid, it is possible to analyze the power flow status within the grid under various component disablements.

SEISMIC DESIGN AND RETROFIT OF CALIFORNIA BRIDGES

Mark S. Mahan[1]

ABSTRACT

Bridge engineering in California, particularly seismic design, has evolved greatly due to the lessons learned from major earthquakes. The San Fernando earthquake of 1971, the Loma Prieta earthquake of 1989, and the Northridge earthquake all have been instrumental in shaping the California practice. The establishment of the Caltrans' Seismic Design Criteria (SDC) is the outcome of this evolution. The California practice is further spreading to other states through the newly approved AASHTO Guide Specification for LRFD Seismic Bridge Design (referred to as LRFD Seismic Guide Spec), July 2007. In particular, the most critical Seismic Design Category "D", within the LRFD Seismic Guide Spec, has the same design requirements as in Caltrans' practice. It is expected that more of the California detailing of seismic-critical components will appear in other parts of US. The concepts of "Confinement", "Continuity", and "Balance" in bridges are presented here within the context of acceptable bridge damage. Plastic hinging in seismic critical elements, capacity protected components, and post earthquake performance of bridges are all covered within the California practice. The preferred California bridge system of Cast-In-Place Post Tensioned Box Girder Bridge has proven itself in seismic conditions. The use of Pre-Cast (PC) Bridge systems is increasing due to the requirements of "Accelerated Bridge Construction" in California. Examples of both alternatives with special seismic detailing are presented here.

INTRODUCTION

The AASHTO Guide Specifications for LRFD Seismic Bridge Design (referred to as LRFD Seismic Guide Spec) was approved in July 2007. In this document the US has been subdivided into four Seismic Design Categories A, B, C, and D. The state of California is mostly designated as Seismic Design Category D, or SDC D for short. It must be noted that the term SDC in the LRFD Seismic Guide Spec is different than the Caltrans' Seismic Design Criteria (SDC). The SDC D is the most demanding category within the Guide Spec and the requirements for this category are very similar to the Caltrans' SDC. All references made to one of these two codes imply that the other code is similar.

In Caltrans' seismic design practice all bridges are expected to meet three fundamental performance requirements of "Confinement", "Continuity", and "Balance". The LRFD Guide Spec has similar requirements that lead the designers towards the same outcome, particularly for LRFD SDC C and D. It could be argued that a major earthquake in California dictated each of these requirements from 1971 to present. Therefore, a brief review of three major earthquakes of 1971 San Fernando, 1989 Loma Prieta, and 1994 Northridge is presented in the next section.

The bridge design and construction practice has evolved from event to event. Some changes have come slowly and some have been very fast paced, due to public demand. Quick fixes have been obvious but some major changes have come slowly that one needs to search deep into

[1] Senior Bridge Engineer, California Department of Transportation, Sacramento, CA

Caltrans' practice to identify. A case study in a completed Pre-Cast project will be presented to highlight the slow changes and what may be coming in future.

POST EARTHQUAKE EVALUATION OF BRIDGES

It is a standard practice at Caltrans to dispatch a team of engineers to survey the damage following an earthquake and to prepare a report to include the lessons learned from that earthquake. The team is called Post Earthquake Investigation Team, PEQIT for short. The study of the three PEQIT reports following the earthquakes of 1971, 1989, and 1994 clearly shows their influence in seismic codes and practice of Caltrans.

The 1971 San Fernando earthquake revealed "Confinement" problems. Route 5/405 Separation structure, a two-span Cast-In-Place (CIP) post tensioned box girder collapsed due to the minimal confinement of No. 4 reinforcement ties spaced at 12 inches in the 4' by 5' rectangular columns. The rectangular ties were closed with a lap splice. The failure of this and several other bridges prompted Caltrans to use column cores with spirals and hoops. In addition, Caltrans installed cable restrainers for Pre-Cast and steel girders in conjunction with support seat enlargements.

The 1989 Loma Prieta earthquake proved that Caltrans needed to do more with the "Continuity" of structures. Massive failures, mostly on older bridges, questioned the entire Caltrans practice. The limited seat of only 5 inches for the San Francisco-Oakland Bay Bridge (SFOBB) caused the collapse of one segment of upper deck onto the lower deck. The old two-level Cypress viaduct with many pins in its structural system collapsed. The piles supporting the slab bridge near Watsonville sheared and punched through the deck. Even though the problem of seat width at intermediate hinges was identified in the 1971 earthquake, the lack of "Continuity" in the structural systems was one of the major findings of the 1989 earthquake.

The 1994 Northridge earthquake affected some older retrofitted bridges and some of the newer generation of bridges. At the I-5/SR-14 interchange lack of "Balance" was evident in the failure of the ramp. The column at bent 2 was much shorter than the columns at bents 3 and 4. The shear demand at bent 2 was extremely large causing a complete shear failure of this bent.

The experience associated to these major earthquakes is well reflected in the current Caltrans Seismic Design Criteria (SDC) and the LRFD Seismic Guide Spec.

DESIGN CODES AND VARIOUS BRIDGE SYSTEMS

A close study of Bridge Design Codes including the seismic codes reveals that the emphasis is on specific category of bridges. In other words, codes are written with specific bridge systems in mind. As an example, Caltrans' SDC is written with an emphasis on the Cast-In-Place (CIP) Post-Tensioned Box Girders. Most of the discussion regarding the "Confinement", "Continuity", and "Balance" assumes that the bridge has a ductile framing system. The LRFD Seismic Guide Spec has a list of Earthquake Resisting Systems (ERSs) [table 3.3-1a] and Earthquake Resisting Elements (EREs) [table 3.3-1b]. This emphasis in the code is to encourage the design engineers to practice with proven components and systems. These lists have been carefully collected based on years of laboratory testing and post earthquake observations.

EXPECTED BRIDGE PERFORMANCE

Both Caltrans' SDC and the LRFD Guide Spec require "no collapse" for ordinary standard bridges. This is a very simple performance criteria because the more complicated bridge performance criteria requires bridge specific laboratory testing which is only justified for special bridges. California Toll bridges each have their own performance criteria, which include "Safety" and "Functionality" definitions.

A closer look at the list of all EREs mentioned above and a study of the latest seismic design practice shows that only a certain combinations of EREs are placed in a specific bridge. For example, Plastic Hinges in columns and shafts are not usually mixed with the isolation devices and energy dissipaters. On the other hand, the abutment backfill soil can be mixed with any other ERE. Some EREs are preferred for new bridges and some are preferred for old bridges. Rocking of the bridge foundation is very rarely used in new bridges and it is mostly appropriate for retrofit strategies.

CALTRANS' PREFERENCE OF ERES

As mentioned earlier, Caltrans has adopted the Plastic Hinges (PH) in columns and shafts as the main ERE with the abutment backfill mobilization as the preferred ERS in Ordinary Standard bridges. This is clearly different than other States within the US where Pre-Cast systems are in abundance. This choice is based on testing of many columns performed by various universities for Caltrans, following the 1989 Loma Prieta earthquake. Figures 1, 2, and 3 show the deflected shape of the column and the condition of the PH for the 6' diameter column/shaft test at UCLA. Similar columns are expected to perform to drift levels well beyond 5% in a bridge.

Many design engineers at Caltrans use the column/shaft combination to design bridges similar to the bridge shown in Figures 4. Multi-column bridges supported on shafts also add an element of redundancy and enhance the seismic performance of the bridge by providing two Plastic Hinges per column/shaft. This doubles the energy dissipation capacity of the bridge (see Figure 5).

SEISMIC PERFORMANCE OF PRE-CAST BRIDGE SYSTEMS

In traditional Pre-Cast (PC) bridge systems the PC girders are stacked on top of the substructure and the bridge does not have the same robust framing characteristic as in the Cast-In-Place (CIP), Post Tensioned bridges. The problem typically is present at the sub-structure to super-structure interface. PC girders are placed on top of the bent cap beams and the bridge does not resist bending moments in the longitudinal direction.

For a long PC bridge supported on single-column bents the engineer must identify a proper ERS requiring a fixed-based column. Such sub-structure is comparable in cost to the CIP bridges. However, for a long PC bridge supported on multi-column bents the engineer needs fixed-based columns, while a CIP bridge can perform well with pin-based columns. The cost difference between the two systems is considerable, indicating the advantages of the CIP system. Therefore, CIP and PC alternatives are not equal in many situations; however, the project engineer is required to provide equal performance.

Given all of the above considerations one design team at Caltrans designed a PC system to compete with CIP, particularly in regards to seismic response of this major structure described below.

SAN MATEO – HAYWARD PRE-CAST (PC) BRIDGE

A 4.46-mile portion of the San Mateo - Hayward Bridge (see Figure 6) was designed as mostly PC elements crossing the San Francisco Bay. This is the low-rise segment of this major bay crossing. The design engineer provided several options, from which the contractor bid on the 42-inch PC shell piling with 90-foot PC girders, mixed with partially PC bent cap beam and partially PC deck.

Initially, three 42-inch diameter PC shell piles where driven through the bay mud to obtain adequate bearing with cut-offs at proper elevation above water (see Figure 7). Then collars were placed around each pile at the top to support a partially PC "bath tub" cap beam (see Figure 8). Partially PC bent cap beam (Figure 9) was supported on the collars (Figure 10) at proper elevation. Then the longitudinal girders were placed in bent cap beam cavities (see Figures 11, 12 and 13). The bottom steel extending from the girder ends were connected using mechanical couplers (see Figures 14 and 15) to provide the continuity and framing action in the longitudinal direction. Reinforcement cages were placed in the hollow pile extensions to frame them into the cap beam. Then concrete was poured into the cap beam simulating a CIP construction (see Figure 16). Later, the longitudinal deck reinforcement would complete the column-cap-girder framing as if all were a part of CIP system (see Figure 17).

With all complexity to this PC Bridge design the contractor was able to build 270 feet of bridge per week (see Figure 18). The additional complexity of this bridge system should be judged relative to the enhanced seismic performance of such system.

CONCLUSIONS

Seismic design codes have been traditionally updated due to major failures following devastating earthquakes. The Caltrans' Seismic Design Criteria has been improving through three decades of seismic practice and it has greatly influenced the national LRFD Seismic Guide Spec.

Seismic codes are usually written with specific seismic bridge systems and components in mind. The Cast-In-Place, Post-Tensioned Box Girder bridges are the primary choice at Caltrans with Plastic Hinging in columns and shafts. The abutment soil could be used as a energy dissipating mechanism. The LRFD Seismic Guide Spec includes these elements in addition to a more comprehensive list of specific Earthquake Resisting Systems (ERSs) and Earthquake Resisting Elements (EREs).

Pre-Cast (PC) bridge systems can be detailed, at an extra cost, to simulate the CIP systems under seismic demands. Such PC systems have higher component cost and demand longer construction schedules. However, It is estimated that the post-earthquake repair cost will be lower and they could be back in service faster.

REFERENCES

AASHTO Guide Specification for LRFD Seismic Bridge Design (LRFD Seismic Guide Spec), July 2007.
California Department of Transportation, Caltrans Seismic Design Criteria, SDC version 1.4, June 2006.
California Department of Transportation, The San Fernando Earthquake, Field Investigation of Bridge Damage, 1971.
California Department of Transportation, The Loma Prieta Earthquake, Post Earthquake Investigation Team (PEQIT) report, October 17, 1989.
California Department of Transportation, The Northridge Earthquake, Post Earthquake Investigation Team (PEQIT) report, January 17, 1994.

Conversion Table

1 mile = 5280 feet
1 foot = 12 inches
No. 4 US Reinforcement = No. 13 Metric Reinforcement
1 inch = 25.4 mm

Fig. 1. Six-foot diameter column/shaft test at UCLA.

Fig. 2.- Plastic hinge below ground.

Fig. 3. Hoop fracture at maximum ductility.

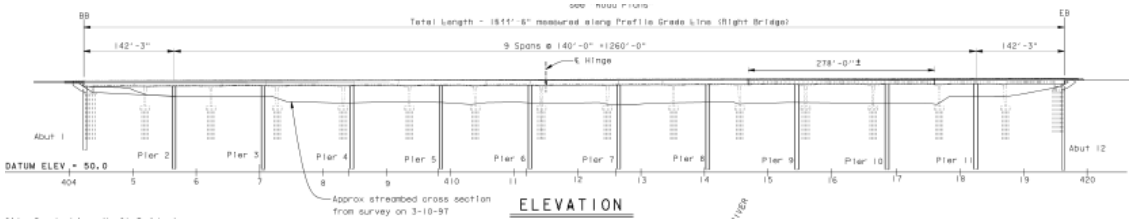

Fig. 4. Salinas River bridge, 1550-foot cast-in-place post tensioned box girder bridge.

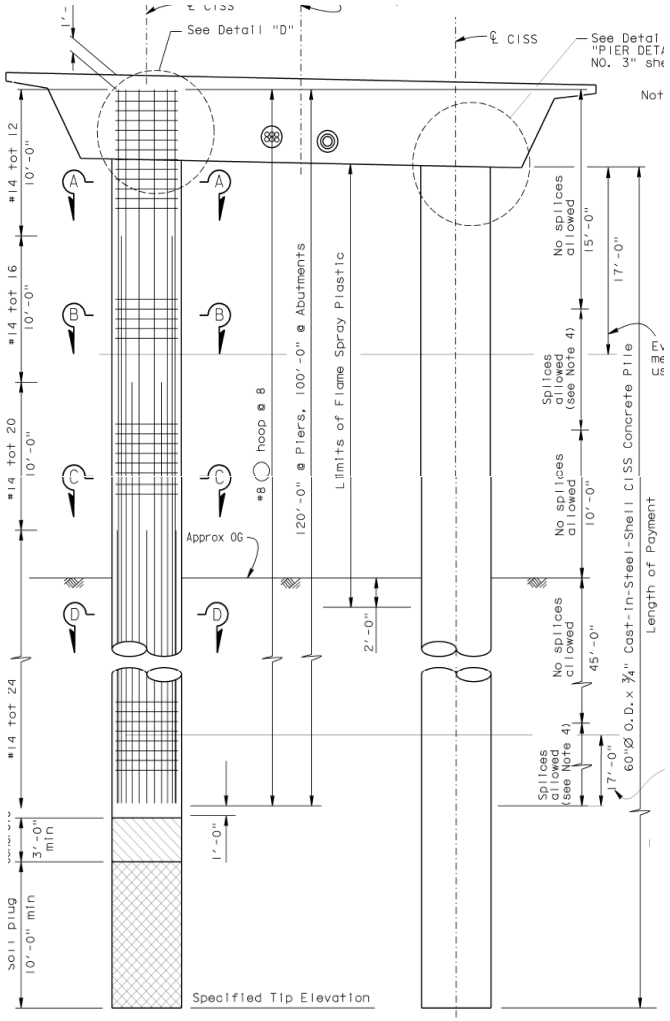

Fig. 5. Two-column bent supported on shafts.

Fig. 6. San Mateo – Hayward bridge.

Fig. 7. 42-inch hollow shell column/shaft driving operation.

Fig. 8. Collar placed at top of column to support pre-cast bent cap beam.

Fig. 9. Pre-cast portion of the bent cap beam.

Fig. 10. Pre-cast bent cap beam supported on shaft extensions.

Fig. 11. Pre-cast girders placed in cap beam openings.

Fig. 12. All pre-cast elements placed in designated openings.

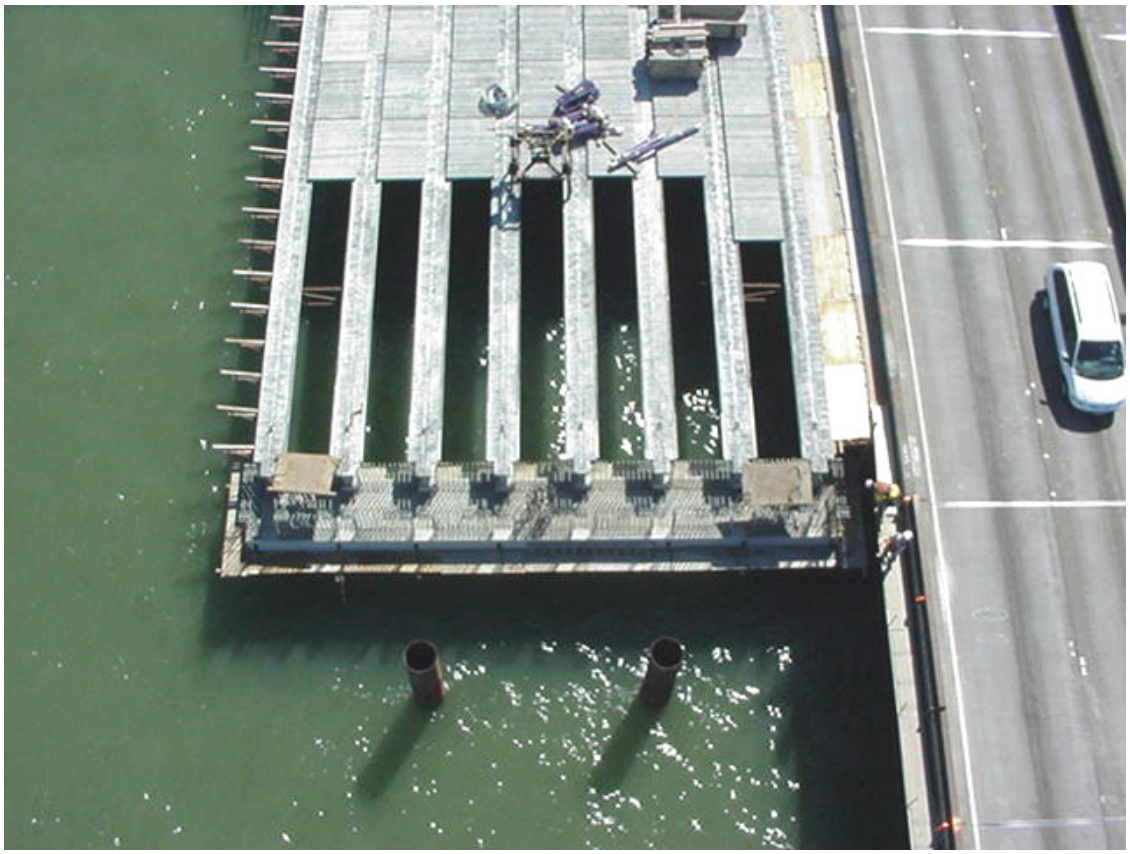

Fig. 13. Top view of pre-cast bridge components.

Fig. 14. Cast-in-place portion of bent cap beam ready for concrete pour.

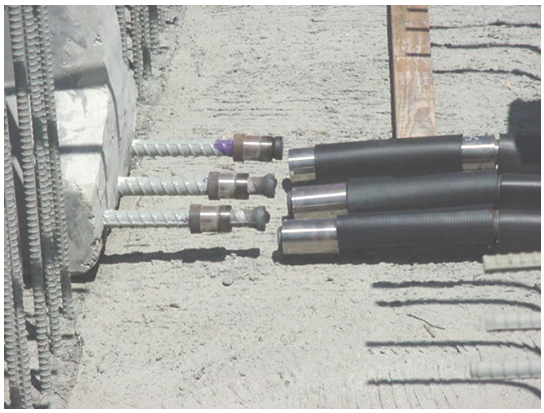

Fig. 15. Mechanical couplers for main girder reinforcement.

Fig. 16. View of completed bent cap beam ready for top reinforcement.

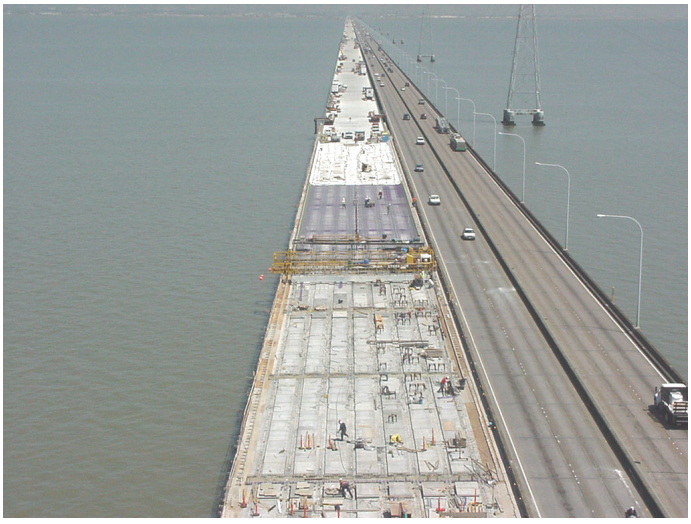

Fig. 17. San Mateo bridge near completion.

Fig. 18. San Mateo- Hayward bridge opening ceremony.

SEISMIC LOAD DEFINITION FOR STRUCTURES IN CANYON SITES

Mohammad Taghi Ahmadi
Professor, Civil Engineering Department, Faculty of Engineering,
Tarbiat-Modares University, Tehran, Iran, *mahmadi@modares.ac.ir*
Reza Tarinejad
Assistant Professor, Civil Engineering Department, Tabriz University, Tabriz, Iran

ABSTRACT

Hydraulic structures such as those appurtenant to dams are often located at either bottom or higher walls of canyons sites. Many of these canyons have sharp irregularities and steep walls with rather stiff rock formations. Today the significance of topographic seismic amplification is well-known although less characterized in design codes. Still the pattern of the non-uniform distribution of ground motion in canyon sites could not be assigned for a specific site due to lack of enough observations. In Iran seismic loads have been quite influential on the design of hydraulic structures although to the best of authors' knowledge there is no single design case in this country in which the topographic amplification phenomenon has been considered. In the present study the pattern recognition and magnitude quantification of this phenomenon has been made possible by the virtue of a novel algorithm based on the application of 3-D BEM in elasto-dynamics. Canyons of arbitrary geometries (non-prismatic, non-symmetric), with different but linear material properties, for a range of frequencies are considered. The algorithm is based on the synthesis of different frequency components of SH and SV waves to derive time histories (or spectra) of ground acceleration at arbitrary points in the site. To predict these, only a single accelerogram (or spectrum) attributed to a single point of the site is needed. Usually the "Free-Field" motion based on seismic hazard analysis and attributed to the valley bottom or to the far heights of the canyon, is sufficient. The validity of the methodology is verified by the observational ground motion data of earthquake of October 24, 2007 recorded at different elevations stations of Shafaroud dam site in northern Iran. By carrying out a limited sensitivity analysis (for wave types, frequencies, incidence directions, material properties and canyons geometries) it was understood that for most cases the exclusion of topographic amplification could lead to serious non-conservative errors in seismic load estimation for important hydraulic structures. Therefore as most of these structures such as water intake structure of underground power house, large spillways, etc. are located at points quite high above the canyon bottom it is recommended to use the present algorithm for correct seismic load definition. The algorithm could be also well employed for defining non-uniform ground motions for large extended structures such as large arch dams, long span bridges, etc. where enough observational data is lacking. However for this purpose further work is needed to account for the time lag between the ground motions at the foundation interface points.

INTRODUCTION

Topographic conditions play an important role on the modification of seismic ground motion. Therefore, their effects may become crucial in selection or simulation of ground motion for use in structural seismic response analysis.

As some historical cases Pacoima arch dam experienced at least 2 major earthquakes. In 1971 the San-Fernando earthquake induced PGAs of 0.49g and 1.25g at the bottom and on the top (15m higher than the dam crest) on the left abutment. This type of amplification happed during the Northridge earthquake too with PGAs of 0.43g and 1.58 g respectively [1, 2]. Furthermore in 2001 an amplification ratio of 5 was observed for acceleration during a small M4.3 earthquake.

This type of phenomena would cause great concern about structures located at higher elevations as well as the abutment rock mass wedges whose stability are very critical for dams. However almost all these structures are designed by assuming uniform ground motion regardless of their location in a canyon site. Among the seismic codes as far as we are aware of, only the EC-8 European code admits for the phenomenon by employing a 1.2 to 1.4 ratio prescription for hills. Therefore it is very demanding to learn how the ground motion pattern, spectra, and PGA differ for any specific valley. It is also crucial to understand what parameters are the major influential ones on the ground motion features in canyon sites. There are geometric parameters such as the valley cross section shape and span to depth ratio, the channel section variation trends etc. for which a 3D consideration is needed. There are several observations on the topographic amplification events some of which are denoted in Table 1.

Table 1. Some observation and research works on the topographic effect in major seismic events.

Earthquake	Event year	researchers	Publication date
Irpinia (Italy)	1980	Sirovitch [23]	1982
Chile	1985	Celebi and Hanks[21]	1986
Egion (Greece)	1995	Athanasopoulous et al.[16]	1999
Athens (Greece)	1999	Assimaki et al.[17]	2004
Chi-Chi (Taiwan)	1999	Sepulveda et al.[3]	2005
January 13 (California)	2001	Alves et al.[1]	2007

In some cases it has been made possible to estimate the topographical effects empirically (the 3 march 1985 Chile Earthquake [21], the 15 June 1995 Egion Earthquake in Greece [16], the 1999 Athens Earthquake in Greece [17], the 1994 Northridge Earthquake in California [22], and the 23 November 1980 Earthquake in Italy [23]). Also different analytical and numerical techniques have been adopted to quantify mathematically the topographic effects on the seismic wave scattering problems (e.g., Trifunac [4], Sanchez-Sesma [5,6,7], Paolocci [8], Zhang [9], Dravinski [10,11,12,13], Zhao [14], Luco [15], Athanasopoulos [16], Assimaki [17], Kamalian[18,19] and Geli [20]). The methods used as tools for such a task, consist of boundary element method (BEM), boundary integrals, finite element method (FEM), infinite element etc.

An up-to-date review paper of the published literatures on boundary integral equations and boundary element methods in elasto-dynamics is presented by Bouchon and Sanchez-Sesma recently [24].

As to adopt powerful analysis tools, issues such as the reduction of dimensionality, the fulfillment of radiation conditions at infinity, and the high accuracy of results, make the BEM attractive in engineering seismology and especially in evaluation of topographic effects. However while a great deal of work has been done on the two-dimensional elastic response of an isotropic medium, very little has been published on three-dimensional analyses.

In this research first the multi-domain boundary element method proposed in [25] is used to study the amplification of elastic waves by a three dimensional canyon of arbitrary shape. Incident plane harmonic compression, vertical shear and horizontal shear waves as denoted by P, SV, and SH-types respectively, are considered. The accuracy of the analytical method is tested through comparison with results of others studies and effects of different parameters are investigated. Some general rules for three-dimensional modeling of wave scattering with boundary element method are achieved. Also effects of different wave parameters (frequency and direction), material properties (shear wave velocity, damping and Poisson ratios) and canyon geometry are investigated. It is shown that deeper canyons induce larger amplification effects compared to shallower canyons for a given frequency. It is also shown that for a canyon widening toward its ends, maximum displacement for different components is usually greater compared to a prismatic canyon. However for a canyon narrowing toward ends, maximum displacement for different components is usually smaller than that of a prismatic canyon. It is also observed that for a non-prismatic canyon, the variation of displacement along the canyon can be different from that of a prismatic canyon depending on incident wave type, wave incident direction and frequency. This fact is also denoted in [17].

Finally techniques are proposed for defining the ground motion everywhere in a given canyon in terms of time history or spectrum once the motion of a single point on the canyon wall is known. Here a combination of SV and SH waves are considered for the total motion although in most cases the SH component is seemingly sufficient.

WAVE PROPAGATION AND METHODOLOGY

An arbitrarily shaped canyon of finite length is considered as illustrated in Fig. 1. Seismic body waves arrive from an arbitrary direction with angles of θ_h and θ_v with respect to the horizontal x- and the vertical z-axes, respectively. The half-space is characterized by the P and S wave velocities c_p and c_s, respectively. To compute the total displacement at the canyon site due to incident body waves, ground motion in free field conditions (u_{ff}) for the half-space without the canyon is determined first. Then the tractions corresponding to the displacements in the previous step are found at the canyon surface. Subsequently opposite of these tractions are applied as a traction boundary condition and the scattered displacements u_s are found. Finally the total displacements are obtained by superposition of the two displacements obtained in first and the latter steps, i.e.,

$u_{total} = u_{ff} + u_s$.

The scattered displacement vector u_s is now determined using the multi-domain boundary element technique as discussed in the following sections.

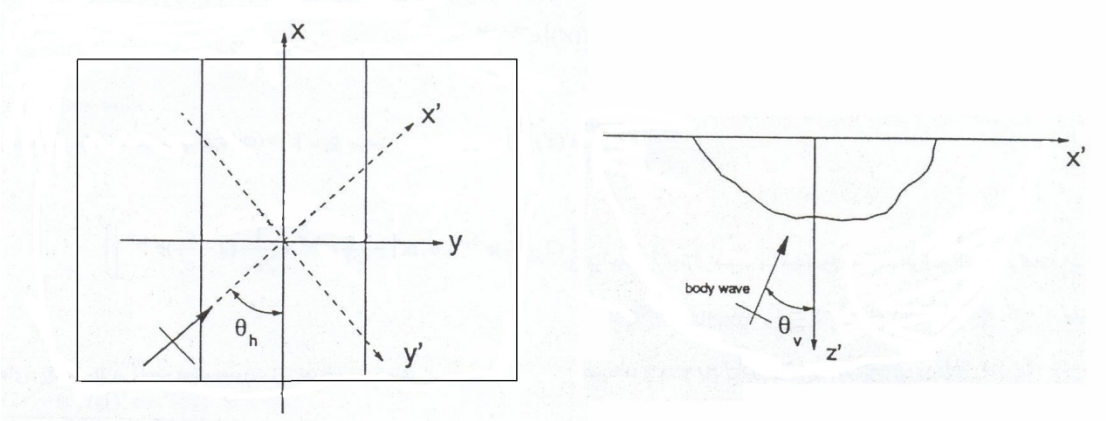

Fig. 1. An arbitrarily shaped canyon of finite length with incident waves arriving from arbitrary directions.

BACKGROUND THEORY AND BOUNDARY ELEMENT METHOD

The governing wave equation for an elastic, isotropic and homogeneous body is:

$$c_1^2 \nabla(\nabla . u) - c_2^2 \nabla \times \nabla \times u - \frac{\partial^2 u}{\partial t^2} = -b \tag{1}$$

in which u denotes the displacement, vector b denotes the body force vector, and c_1 and c_2 are the propagation velocities of compression (P) and shear (S) waves, respectively. The velocities are related to the properties of the medium through:

$$c_1 = (\lambda + 2\mu/\rho)^{0.5},\ c_2 = (\mu/\rho)^{0.5} \tag{2}$$

where λ and μ are the Lame constants and ρ is the mass density [26].
The corresponding governing boundary equation for an elastic, isotropic, homogenous body can be obtained using the well-known dynamic reciprocal theorem as:

$$c^i u^i + \int_\Gamma p^* u d\Gamma = \int_\Gamma u^* p d\Gamma \tag{3}$$

where p^* and u^* are the fundamental solution for traction and displacement respectively, at a point x when a unit Dirac delta load is applied at point i of the continuum body boundaries Γ. The independent coefficient c^i is a unit matrix for internal nodes and half a unit matrix for boundary nodes. In the BEM the variables u and p are discretized into the values at the so-called *collocation nodes*. The displacement and traction fields are interpolated over each element using a set of shape functions. The same shape functions are also used to approximate the geometry, *i.e.* the elements are iso-parametric. Discretization of Equation (3) yields:

$$c^i u^i + \sum_{j=1}^{ne} \left\{ \int_{\Gamma_j} p^* \Phi d\Gamma \right\} u^j = \sum_{j=1}^{ne} \left\{ \int_{\Gamma_j} u^* \Phi d\Gamma \right\} p^j \tag{4-a}$$

The expressions inside the braces can be replaced with the more familiar abbreviations:

$$c^i u^i + \sum_{m=1}^{n} \hat{H}^{im} u^m = \sum_{j=1}^{ne} G^{ij} p^j \tag{4-b}$$

$$G^{ij} = \int_{\Gamma_j} u^* \Phi d\Gamma \tag{4-c}$$

$$\hat{H}^{im} = \sum_{t} \int_{\Gamma_j} p^* \Phi_k d\Gamma \tag{4-d}$$

$$\begin{cases} H^{im} = \hat{H}^{im} & when \quad i \neq m \\ H^{im} = \hat{H}^{im} + c^i & when \quad i = m \end{cases} \tag{4-e}$$

Here n is the number of nodes, u^m is the displacement vector of node m, and p^j is the sum of all tractions of element j. Also t counts for all the elements to which node m belongs. Nodes in elements t are counted by k. Array Φ_k is the shape function diagonal matrix. In this research *quadratic* 9-node elements are used. The authors' studies lead to the fact that for obtaining accurate results, the element size should be smaller than one-fourth of the shear wavelength. After assembling all equations the following set of equations is obtained:

$$HU = G \tag{5}$$

in which H is a $3n \times 3n$ matrix, U is a $3n \times 1$ displacement vector, G is a $3n \times 3nne$ matrix, and P is a $3nne \times 1$ traction vector, and nne is the product of the number of elements and number of nodes. The problem has $3n$ unknowns that should be obtained by solving Equation (5).

FUNDAMENTAL SOLUTIONS

The fundamental solution in the frequency domain for the displacement is the solution to Eq. (1) for a harmonic point force with unit amplitude applied at the point $\boldsymbol{y}$ in the l direction, i.e.,

$$\rho b = \delta(r) e \tag{7}$$

where r is the distance between the *observation point x* and the *source point y* , e is the unit directional vector and δ is the delta Dirac function. In order to find the fundamental displacement solution, the principle of Helmholtz decomposition is used. The fundamental solution expressions are adopted from [26] and for the free-field surface displacements in the frequency domain are:

$$u^*_{lk} = \frac{1}{\alpha \pi \rho c_2^2} \left[\psi \delta_{lk} - \chi r_{,l} r_{,k} \right] \tag{8-a}$$

$$\psi = \frac{\exp(-k_2 r)}{r} + \left(\frac{1}{k_2^2 r^2} + \frac{1}{k_2 r}\right) \frac{\exp(-k_2 r)}{r} - \frac{c_2^2}{c_1^2} \left(\frac{1}{k_1^2 r^2} + \frac{1}{k_1 r}\right) \frac{\exp(-k_1 r)}{r} \tag{8-b}$$

$$\chi = \left(\frac{3}{k_2^2 r^2} + \frac{3}{k_2 r} + 1\right) \frac{\exp(-k_2 r)}{r} - \frac{c_2^2}{c_1^2} \left(\frac{3}{k_2^2 r^2} + \frac{3}{k_2 r} + 1\right) \frac{\exp(-k_1 r)}{r} \tag{8-c}$$

in which $\alpha = 4$, and δ_{lk} is delta Dirac function (with l and k being the coordinate directions of the point load and the generated traction, respectively) . Wave numbers $k_1 = \frac{i\omega}{c_1}$ and $k_2 = \frac{i\omega}{c_2}$

correspond to compression and shear waves, respectively. Here ω is the forcing function circular frequency and "*i* " is the unit imaginary number. The fundamental solution for the free-field surface tractions in the frequency domain is:

$$p^*_{lk} = \frac{1}{\alpha\pi}[(\frac{d\psi}{dr} - \frac{1}{r}\chi)(\delta_{lk}\frac{\partial r}{\partial n} + r_{,k}n_l) - \frac{2}{r}\chi(n_k r_{,l} - 2r_{,l}r_{,k}\frac{\partial r}{\partial n}) - 2\frac{d\chi}{dr}r_{,l}r_{,k}\frac{\partial r}{\partial n} + (\frac{c_1^2}{c_2^2} - 2)(\frac{d\psi}{dr} - \frac{d\chi}{dr} - \frac{\alpha}{2r}\chi)r_{,l}n_k] \quad (9\text{-a})$$

$$\frac{d\psi}{dr} = (-\frac{2}{r} - k_2 - \frac{3}{k_2 r^2} - \frac{3}{k_2^2 r^3})\frac{\exp(-k_2 r)}{r} + \frac{c_2^2}{c_1^2}(\frac{1}{r} + \frac{3}{k_1 r^2} + \frac{3}{k_1^2 r^3})\frac{\exp(-k_1 r)}{r} \quad (9\text{-b})$$

$$\frac{d\chi}{dr} = (-\frac{4}{r} - k_2 - \frac{9}{k_2 r^2} - \frac{9}{k_2^2 r^3})\frac{\exp(-k_2 r)}{r} + \frac{c_2^2}{c_1^2}(\frac{4}{r} + k_1 + \frac{9}{k_1 r^2} + \frac{9}{k_1^2 r^3})\frac{\exp(-k_1 r)}{r} \quad (9\text{-c})$$

The full space solution is utilized for the BE solution. Wave types of P, SH, and SV are the incident events coming from far field in different directions with different frequencies. The Rayleigh wave is not introduced as a loading event but its generation at the boundaries are essentially accounted for.

Internal damping is accounted for by using a complex shear modulus as $\mu = \mu + 2i\mu\zeta$ where ξ stands for viscous damping.

TREATMENT OF SINGULARITIES

The solution for the free-field displacement and subsequently the matrix *G* contain singularities because of the *1/r* term, a weak singularity encountered when the collocation node coincides with the integration node. To perform the numerical integration using standard Gauss-Legendre quadrature over an element where the collocation node belongs, a method proposed by Lachat [26] is used. In this method the element is divided into a number of triangles, each having one corner at the collocation node and the integration is performed over each of the triangles using a standard Gauss-Legendre quadrature rule over an equivalent collapsed quadratic element where the Jacobian tends to zero as $r \to 0$. This cancels out the *1/r* singularity. Furthermore the singularities of the free-field traction solution, and thus of the matrix *H*, are of the $1/r^2$ kind when the observation point coincides with the integration point. In this work a numerical method used to evaluate singular integrals for rigid body motion is adopted. This method normally applies only to closed domains. Ahmad and Banerjee generalized the method for the 2-D case by using the *enclosing elements technique* to cover open domain boundaries where parts of the boundary are not discretized [25]. Here their method is extended to the 3-D case.

BE MODEL VERIFICATION

The results obtained by this method for a 2-D SH wave of unit amplitude impinging normal to the semicircular canyon axis is compared first with the exact solution by Trifunac [4]. The results presented in Fig. 2 show the displacement amplitudes as a function of transverse coordinate y normalized by the canyon radius R for horizontal angle of $\theta_h = 45^\circ$,vertical angles of $\theta_v = 1^\circ$ or 45° and unit dimensionless frequency defined as $\Omega = \omega R/\pi c_2$. A similar comparison is presented

in Fig. 3 for $\theta_v = \theta_h = 0$, which corresponds to a vertically incident SH wave with particle motion perpendicular to the axis of the half-circle uniform canyon. For this test case the numerical result obtained by Zhang and Chopra [9] which is based on 2D approximation is used for the comparison.

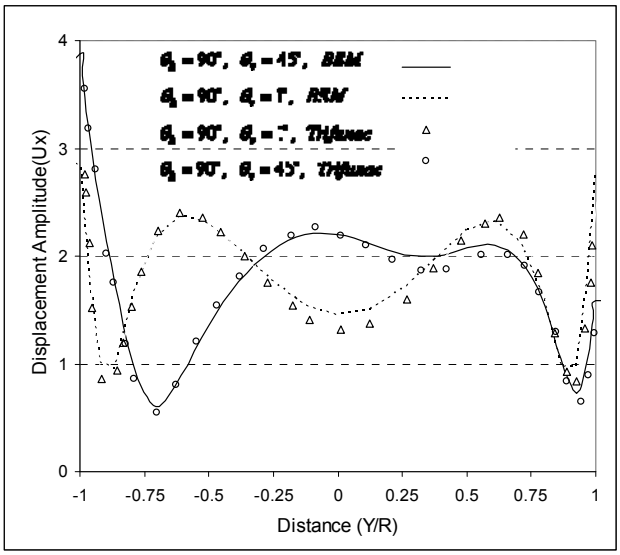

Fig. 2. Displacement amplitudes obtained by the BE method and Trifunac for incident SH-Wave with $\Omega = 1$.

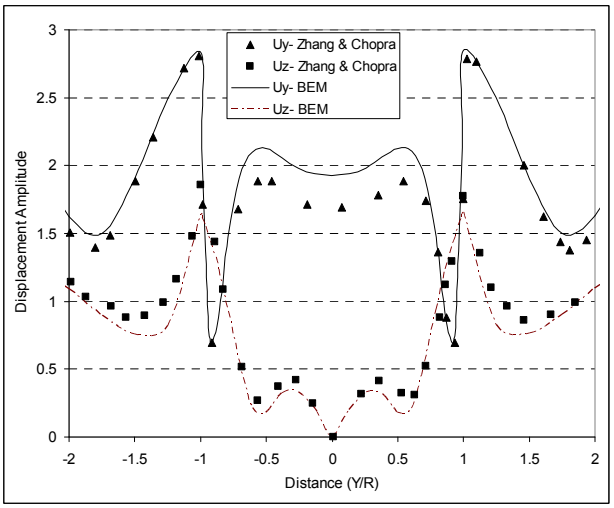

Fig. 3. Displacement amplitudes obtained by 3-D BE vs. Zhang and Chopra for incident SH-Wave with $\theta_h = 0$, $\theta_v = 0$ and $\Omega = 1$.

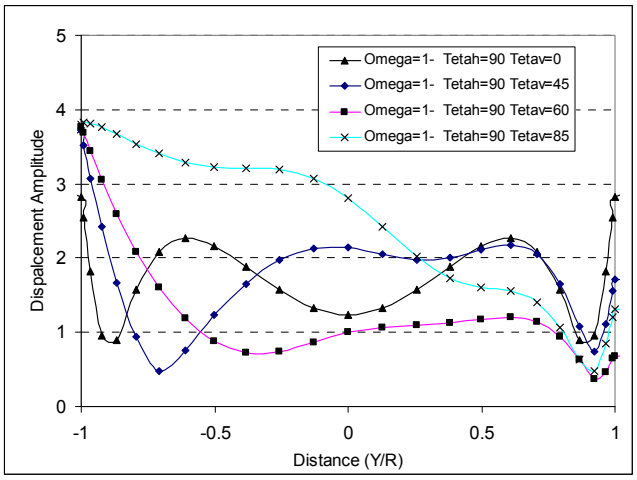

Fig. 4. The results obtained for different wave incident angles for incident SH-Wave.

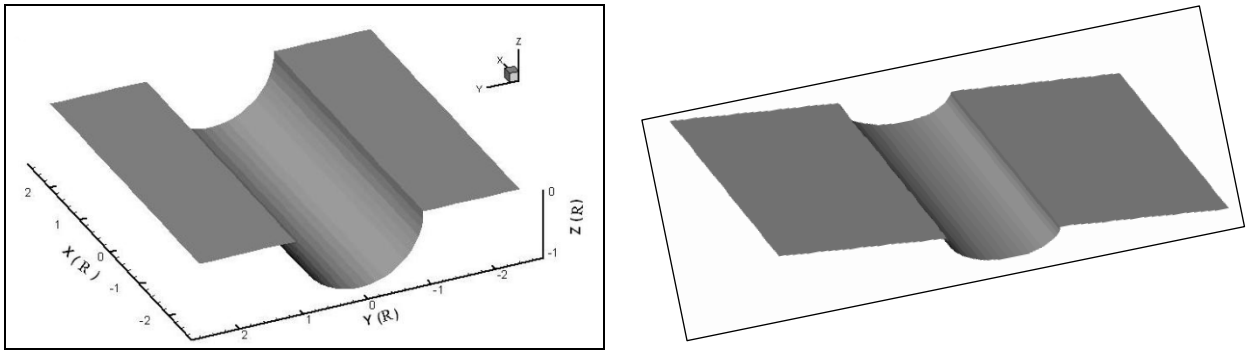

Fig. 5. A schematic view of the semi-circular (deep) vs. the semi-elliptical (shallow) canyon.

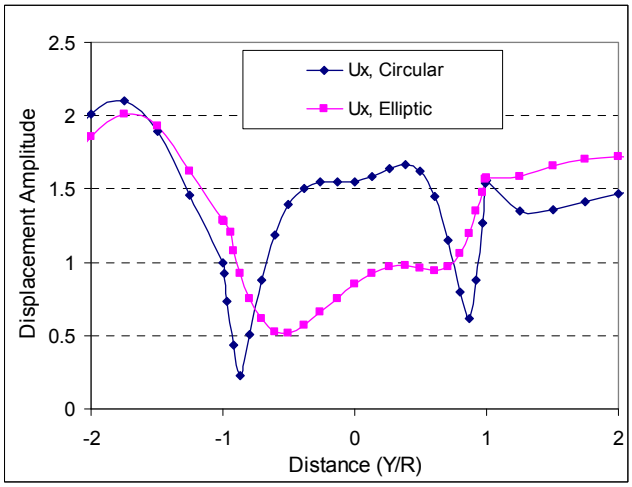

Fig. 6. Comparison of results obtained for two different shape canyon for incident SH-Wave with $\theta_h = 45$, $\theta_v = 45$ and $\Omega = 1$.

The results obtained for analysis with different wave incident angles are shown in Fig. 4. Further it is understood that the variation of displacements along the canyon with large dimensionless frequency is more complicated than that of a small one. The effects of damping in a reasonable interval (0. To 10 percent of critical) as well as the Poisson's ratio showed rather minor effects on the amplification pattern of the semi-circular valley. As shown in Figs. 5 and 6 results obtained for two different dimensionless frequencies show that the deep (circular) canyon has more amplification effect on displacement amplitude along the canyon in comparison to shallow (elliptical) canyon.

EFFECTS OF NON-PRISMATIC CANYON CROSS SECTION

Mosessian and Dravinsky in 1990 initiated the first 3-D BEM application for our purpose to show that 2-D models are valid only in limited incident angles and frequencies and for limited type of wave [13]. For SH wave the 2-D model is more difficult to confer. The interaction of P, SH and SV types of waves are also not possible to account for when 2-D models are used. Eshraghi and Dravinsky have shown that a 3-D model may differ sharply with that of a 2-D model in defining the motion field of canyons [12]. Besides it may be the case that a canyon is not uniform along its axis and thus the validity of 2-D models are severely challenged. Here three simple shapes are analyzed in order to investigate the effects of non-prismatic canyon cross sections. In the first model a canyon with a semi-circular cross section widens toward its ends, in the second model the canyon is prismatic, and in the third model the canyon narrows toward its ends. The radius of the cross section is assumed to be a linear function of the canyon length for the first and the third model as shown in Fig. 7.

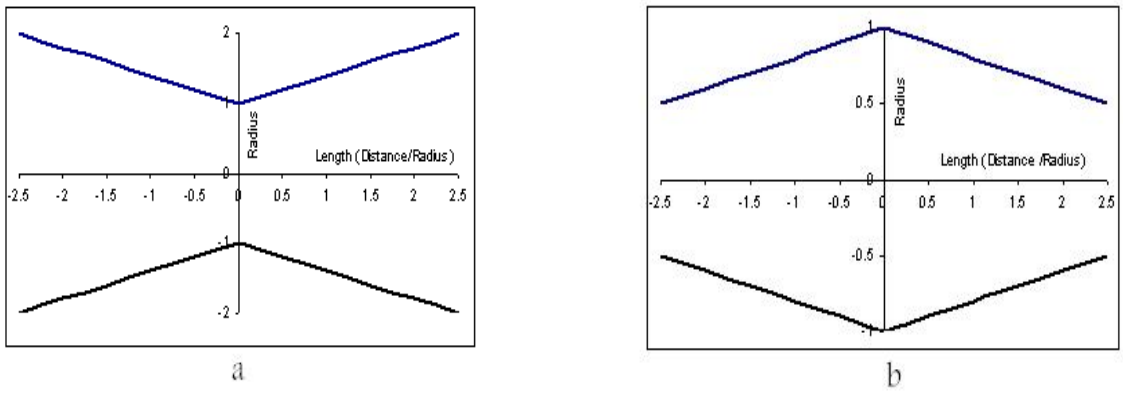

Fig. 7. Radius variation for non-prismatic semi-circular canyons, widening (a) and narrowing (b) toward their ends.

The results for a sample incident wave and dimensionless frequency is shown in Fig. 8. All these results present the displacement amplitude in the central cross-section (*x=0* plane) of the non-prismatic canyon with unit radius. Comparison of displacement components amplitudes with corresponding results obtained for prismatic canyon is shown in the same figure. This figure indicates that the responses of non-prismatic canyons are significantly different from that of the prismatic canyon. In general, the maximum displacement amplitude for the canyon widening toward the ends is in most cases larger than that for the prismatic canyon in the both cases of P-

and SV- waves. On the other hand, for the canyon narrowing toward the ends the maximum displacement amplitude is in most cases smaller than that of the prismatic canyon.

Therefore, for different kinds of seismic waves, the non-prismatic effect depends on how the variation of cross-section along the canyon is, and this means that assuming a prismatic shape for the canyon when it is truly non-prismatic may yield non-conservative results.

Concrete dams especially Arch dams are usually constructed in the narrowed cross section of the canyon. The non-prismatic effect of the canyon in seismic analysis of this kind of structures can have considerable effects on the obtained response of structures. It is thus concluded that for non-prismatic canyons, a 3-D solution is essential in order to obtain an accurate perspective of topography effects phenomena.

However when using the above methods as a tool, the errors are very sensitive to the valley length as 5 times the valley radius (R) is needed in each direction for semi-circular valleys. The free field length (in transverse direction) is taken as 1.5 R at each side. The program TDASC is developed with the aforementioned capabilities and used throughout the analyses for engineering application leading to seismic load definition.

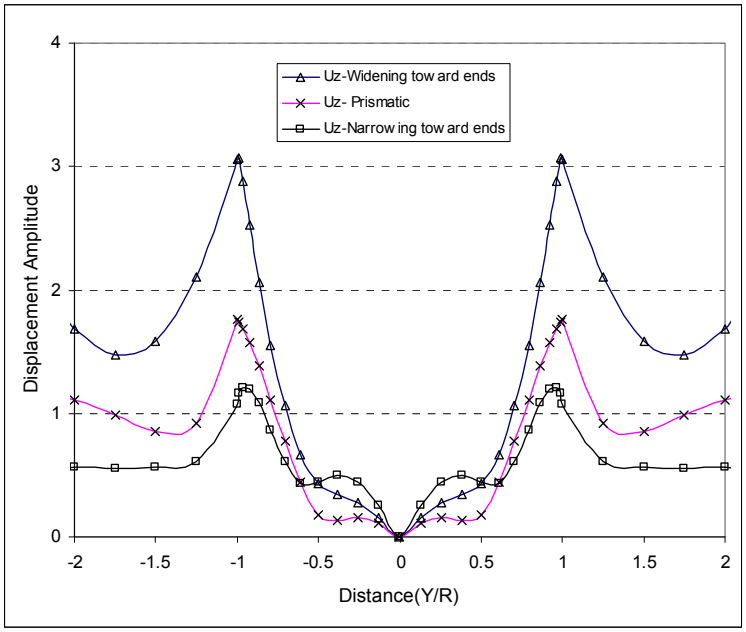

Fig. 8. Comparison of vertical displacement component amplitudes obtained for three different canyon cases: Prismatic, Widening toward ends and Narrowing toward ends due to incident SV-wave with $\theta_h = 90$, $\theta_v = 0$ and $\Omega = 1$.

ENGINEERING APPLICATION

It is well known that when the seismic wave lengths are in the order of surface canyon dimensions the ground motions of surface points are much influenced by these irregularities. For layered rock the variation of motion is more affected. Furthermore in measurement studies it is difficult to separate the effects of topography from that of the layers. This has made it difficult

for workers to succeed in achieving theoretical agreement with observational findings when 2-D models are used. However using a 2-D model Huang and Chiu in 1995 [27] showed that it is still possible to generate time history of a ground motion only if for the given canyon the source mechanism and the free field motion at the valley bottom is known and could appropriately be considered in 2-D models. Such conditions are rarely possible and a general 3-D method is well desired for actual applications.

VARIABLE RESPONSE SPECTRA FOR CANYONS

By means of the software devised in this research we could quantify the pattern and variation of the ground motion along the walls of different canyon shapes for different non-dimensional frequencies. Using these one can derive the response spectra at different locations along the valley walls. The prescribed free field site response spectrum (for flat ground) is attributed to the far left side of the canyon top. Here the Iranian seismic code 2800 normalized design response spectrum for ground type 1 was chosen for this purpose. According to usual earthquake postulations here it is generally assummed that the governing motion is due to the SH component of seismic waves incident vertically to the canyon. The shear wave velocity is assumed as 1500 m/sec throughout the analysis.

First trianglular canyons with different slopes are considered and the corresponding spectra for points A, to G are calculated as in Fig. 9. Here for the case of 45 degree slope it is clear that except for the lowest 3 points (E, F and G) an amplification is dominant in lower periods with a maximum factor of 1.5 for point C (Fig. 10). For the lower points de-amplification is almost generally happening with a maximum factor of 0.5 in point G.

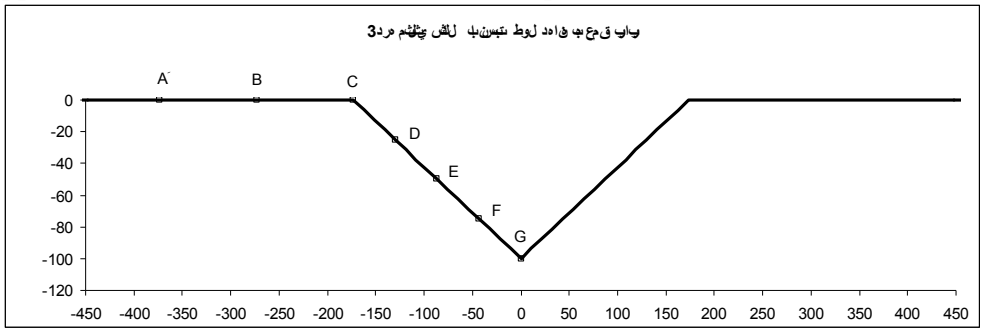

Fig. 9. Typical triangular section valley and its different considered points locations. (The axes scales do not apply to cases discussed here.)

Interesting to note that at the bottom of a trapezoidal valley (with span to height ratio of 3 and side slopes of 45 degrees) an amplification factor of some 1.5 is found at periods less than 0.5 seconds (Fig.11). This was also the case, although less pronounced, when trapezoids of other shape ratios were examined.

The same application of the free field spectrum to rectangular canyon shows similar trends. Here the case of such a canyon with aspect ratio of 4 (Fig. 12) shows very sensitive variation of the shape of "standard" spectra for valley bottom points staggering between amplification and de-amplification there for frequencies higher than about 2. Hz as in Fig.13.

It would also be very crucial if the flat ground spectrum is to be attributed to the bottom points. Many hydro power plants are usually located at the bottom of the valley specially in the US school of dams design.

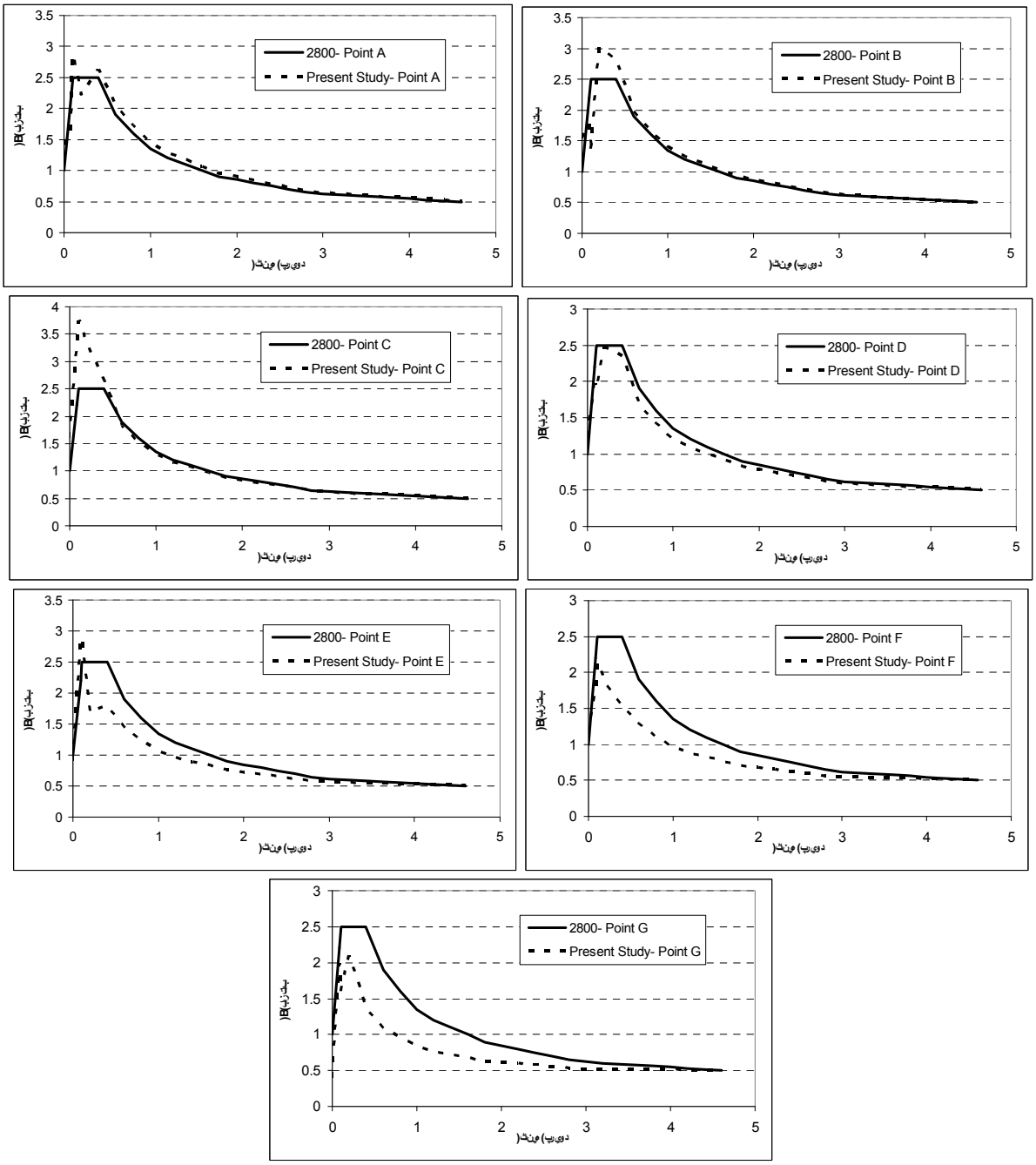

Fig. 10. Modified response spectra (acceleration versus period in seconds) for different points along the triangular canyon walls with slope of 45 degrees as compared with the flat ground spectrum.

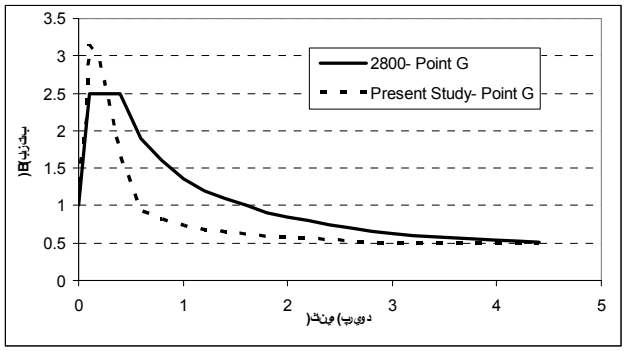

Fig. 11. Modified response spectrum (acceleration versus period in seconds) for the valley bottom central point G for trapezoidal canyon with side slope of 45 degrees and span to height ratio of 3, as compared with the flat ground spectrum (code 2800).

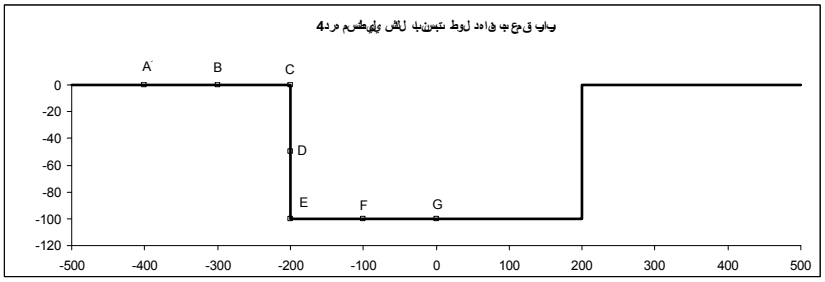

Fig. 12. Rectangular canyon with span to height ratio of 4.
(The dimensions are in meters although in different scales.)

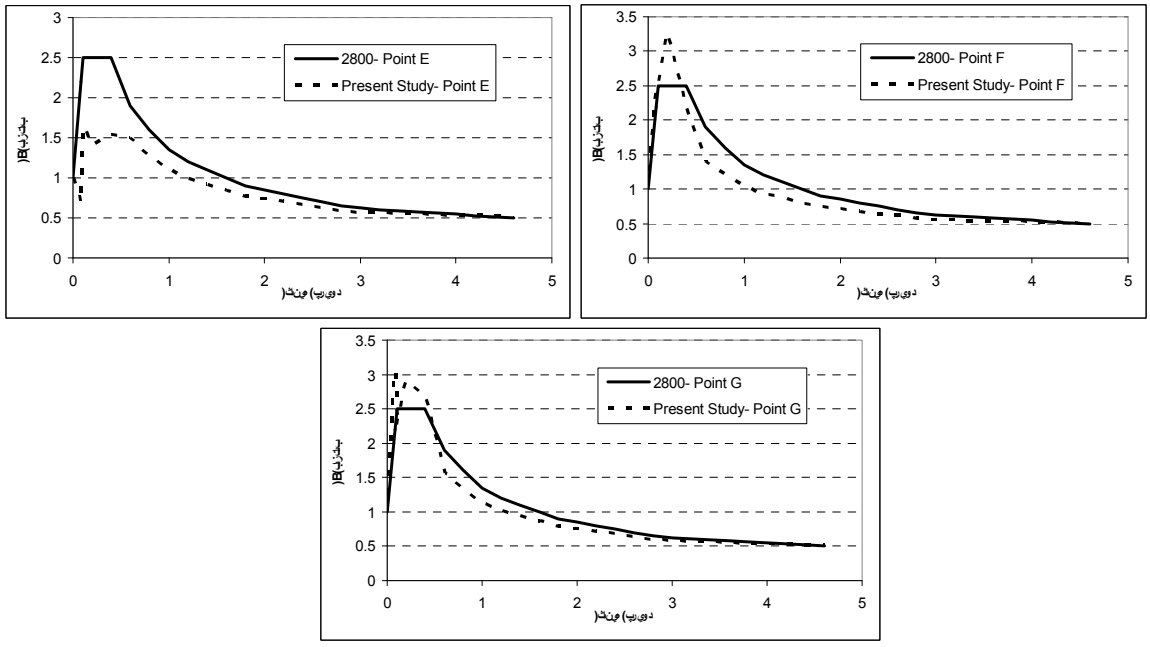

Fig. 13. Modified response spectrum (acceleration versus period in seconds) for the valley bottom points E(at wall foot), F, and G (at the valley bottom center) in rectangular canyon with span to height ratio of 4, as compared with the flat ground spectrum (code 2800).

DISCUSSION

1. It was obviously understood thus that the current practice might be far in error when dealing with uniform assumption of ground motion in valleys top, mid-height and even at the valley bottom. This error is not usually on the conservative side.
2. It is usually the case that in frequencies above 2. Hz, a range where usually the vibration modes of hydraulic structures and even concrete dams fall, for the wall foot point there is a de-amplification, whereas for the upper wall points there is amplification. But for the central points of valley bottom the case might be a pronounced amplification except for triangular canyons.
3. It is rather an easy task that for a given 3-D canyon shape and mechanical properties the prescribed flat ground spectrum be modified so as to define the exact situation of ground motion at any desired point of the valley where the structure is to be constructed.
4. Further research is to be followed to verify assumption of SH component dominancy, i.e., examining the SV components influence either individually or in combination with SH waves on the spectra.
5. The layered media fact may change the results substantially in some cases. Thus for any specific site not possible to assume as homogenous, this effect has to be considered. The problem is rather tedious when modeling the semi-infinite media with BE as it is very site dependent.

THE BASIC ASSUMPTIONS AND METHODOLOGY OF ACCELERATION TIME SERIES GENERATION

Once the location and mechanism of rupture of the hazardous fault is known the direction and type of the seismic waves should be carefully chosen as an extension of the 2-D works by Kojic [2] and also Huang and Chiu[27]. In the latter the recorded acceleration time history at different elevations of a Taiwanese dam canyon were compared with that of numerical estimation using a 2-D boundary integral method for the 1992 seismic event and based on a reference station record of the valley. As the fault was a near-field one with a strike of rather parallel to the canyon axis, only SH wave propagation in a specific direction was assumed with success. Alves [1] used three records set of the 2001 earthquake at the Pacoima dam canyon to generate the lost time history data of Northridge earthquake in the accelerographs array by employing transfer functions and accounting for the time delays.

There are only very few chances of obtaining such distributed multiple data for the purpose we seek. Thus it is very demanding to enable generating ground motion data for any arbitrary point of the canyon using only single given record of a specific valley.

Methodology

The assumptions used for time series generation are further taken as:

1. The direction of all components of P, SH, and SV waves at all frequencies are the same.
2. There is no phase lag between the different components of incident waves (SV, and SH).
3. At least one component of a ground acceleration record at a specific point in the canyon is known (base record).

4. The P wave components are not influential on the major shock interval of the ground motion time history.
5. Surface waves participation is negligible as they usually correspond to lower frequencies.
6. The canyon is composed of homogeneous elastic rock with no influential discontinuity.

The P-wave interval of the known record of the canyon (base record a(τ)) with duration τ, is utilized in a way to generate records a' (τ) matching the same frequency content. In this process the horizontal incident angle of the arriving waves is obtained. Thereafter assuming the same horizontal incident angle, the vertical incident angle is also found for the main shock (S-wave) interval of the base record a$(t-\tau)$ when matched with the generated record a'$(t-\tau)$. These are then employed to find incidents SH and SV components with the same frequency contents. In this try and error process the share factors of both components are also found. Finally based on thus obtained source parameters the boundary element model inputs are well obtained and should be used for generation of calculated time series at arbitrary points of the canyon as desired. Thereafter the comparison of the recorded and calculated time series shall be done. This process is introduced in Fig. 14.

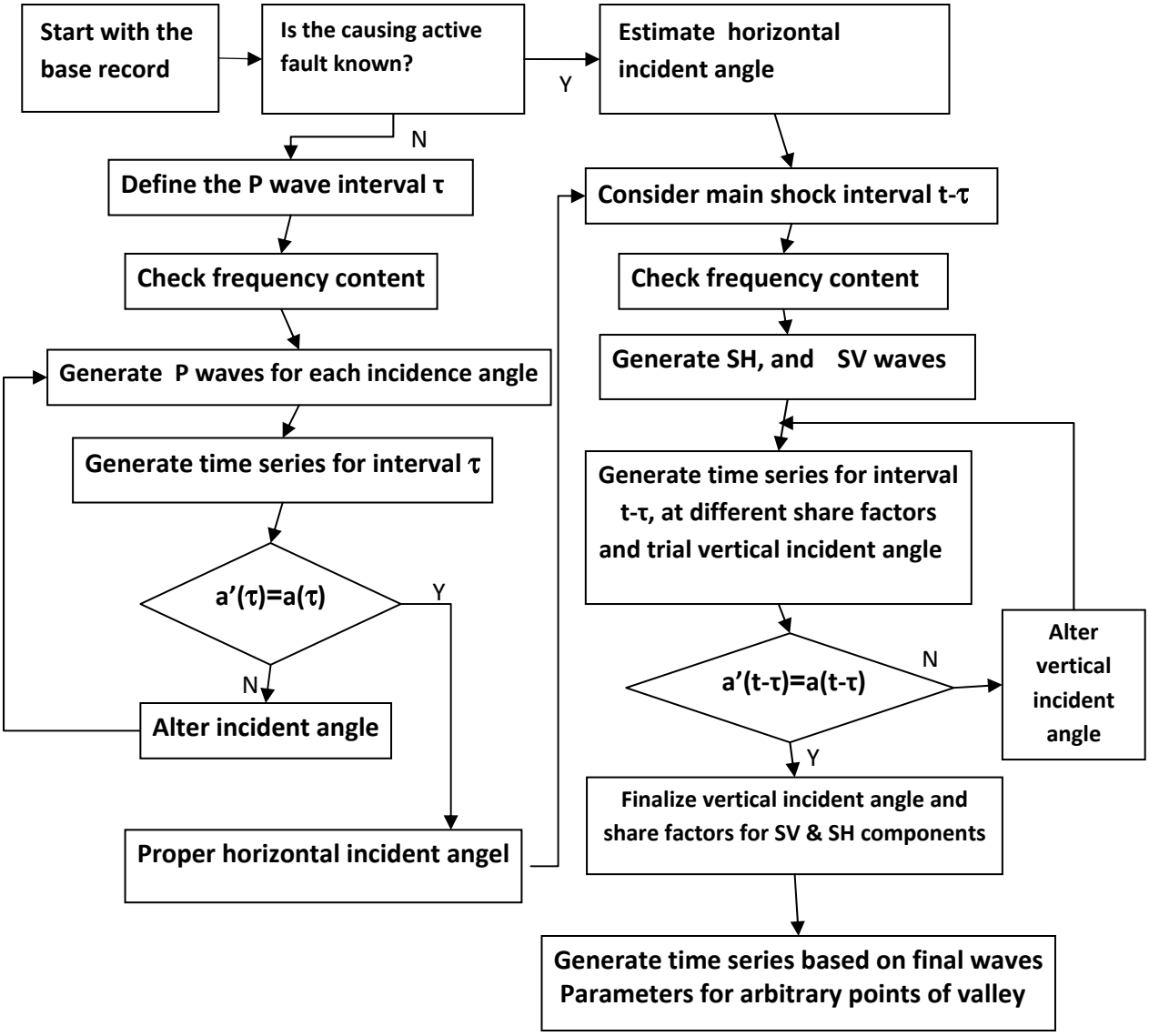

Fig. 14. Methodology of ground motion time series generation for arbitrary points of the canyon site using a given single base record.

Verification of the Algorithm

This issue is dealt with in the present work by considering the case of multi-station measurements done during the near-field earthquake of October 2007 at the Shafaroud dam site in Northern Iran.

Initially in our research Shafaroud dam site which consists of rather prismatic and homogeneous rock was going to be used for ambient vibration tests using 5 velocity-meter sensors (Fig. 15).

The sensors were located on firm rock with less weathering for micro tremor recordings.

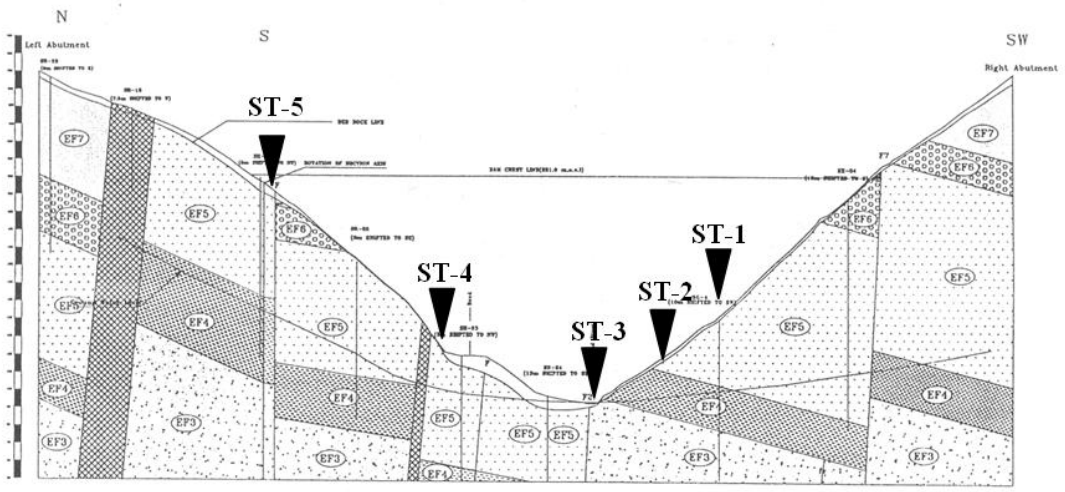

Fig. 15. Shafaroud dam canyon geology and recording stations.

However there came an interesting event of a real earthquake on the 24th of October 2007 (on the very first day of installation of the first 3 stations) with Magnitude 3.2 with focal depth of 14km at about 20 kilometers off the Caspian shore near the dam site according to the IIEES (Fig. 16).

Fig. 16. Location of October 2007 earthquake in respect to the Shafaroud dam site.

The peak values amplification between the top (station 1) and botom (station 3) are about 1.8 (for longitudinal displacement), 1.9 and 4.1(for transverse velocity, and acceleration respectively).

For modeling the phenomenon the aforementioned algorithm is employed. The geotechnical data of this dam site is rather uniform with average values as the shear modulus of 1.85 GPa and Poisson's ratio of 0.27 and the mass density of 2600 kg/m3. A quadratic mesh of 616 boundary elements and 2565 nodes is used as shown in Fig. 17.

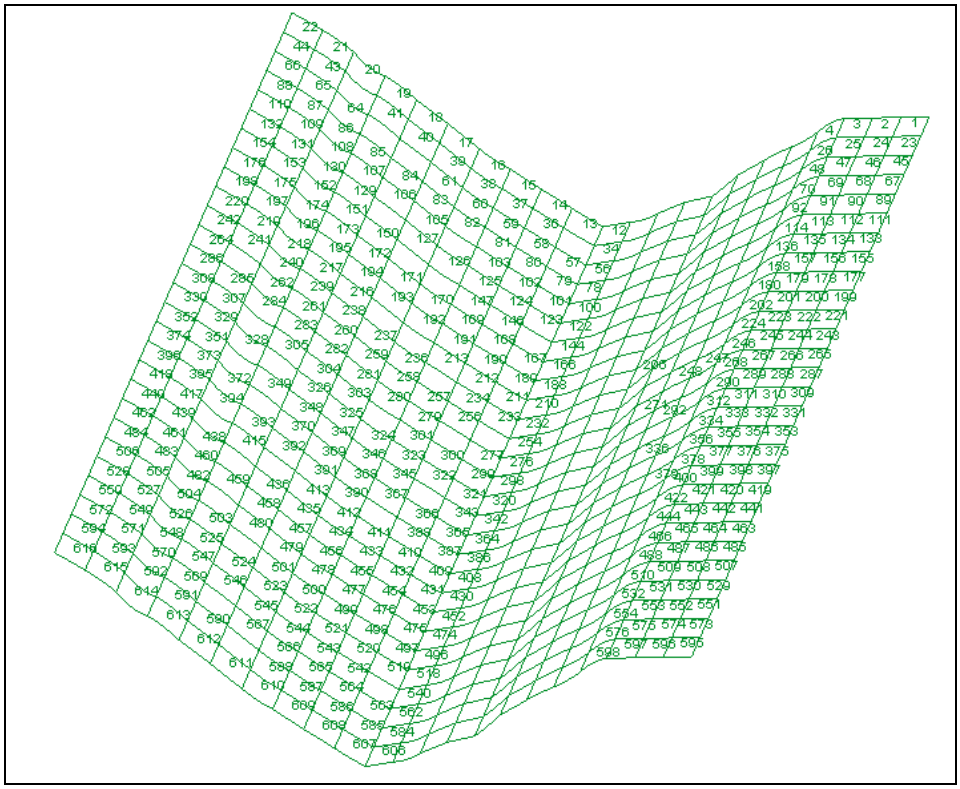

Fig.17. Boundary elements mesh of Shafaroud dam site.

As regarded to the fault location an horizontal incidence angel of 90 degrees ($\theta_h = 90^\circ$) in respect to the valley axis is prescribed. According to the algorithm of Fig. 14 the horizontal incident angel is obtained as $\theta_v = 0^\circ$.

Furthermore the share factors of 60% for SH and 40% for SV components are found when satisfying the original frequency content of the base record between 0. to 16 Hz. This range is in our domain of interest in earthquake engineering and also is compatible with the mesh dynamic response validity range. The recorded and computed records for station 1 are matched as shown in next Figures 18 and 19.

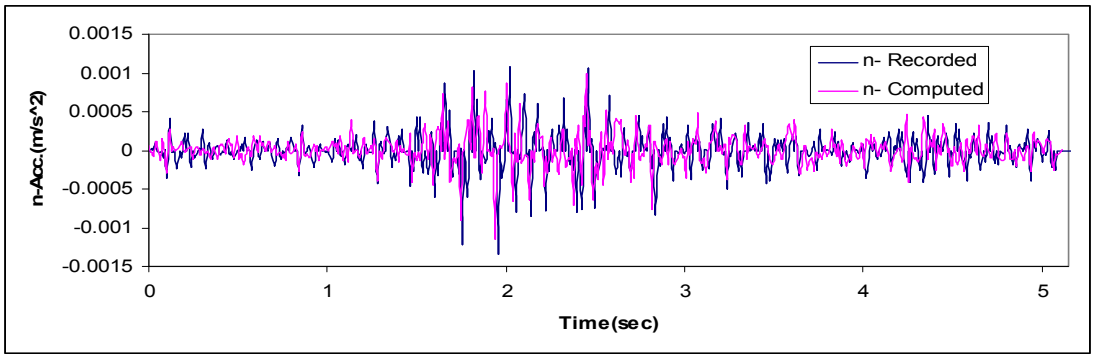

Fig.18. Typically generated ground acceleration record (using the proposed algorithm) versus actual measured one in Shafaroud Dam Site station 1 during the October 2007 earthquake.

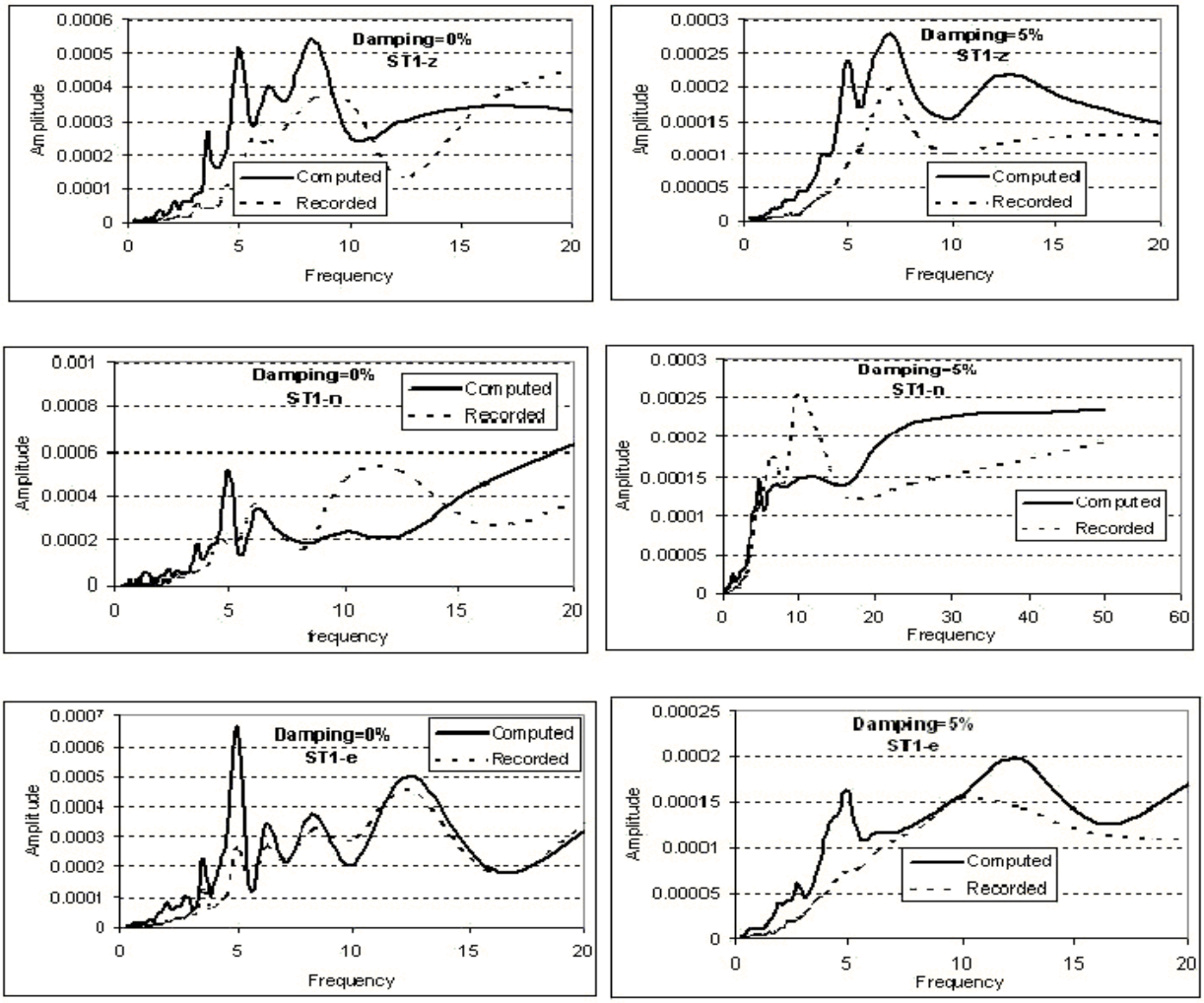

Fig. 19. Frequency content (acceleration response spectra) comparison for recorded components of station 1, vs. the calculated ones for damping factors of zero and five percents. Units are m/sec2 for accelerations and Hertz for frequencies.

The agreement is rather high in the frequency range of interest. Discrepancies should be due to material layer variability, geometric simplifications, and independent ground motion components searches. Thus verification of the algorithm seems so interesting and satisfactory.

CONCLUSION

A general 3-D elasto-dynamics BE code is devised in the frequency domain. An algorithm to find the desired ground motion features such as the PGA, site response spectra, and the time history of acceleration at any arbitrary point of 3-D canyon sites is proposed using a single actual or hypothetical spectrum (or accelerogram) attributed to the site. The agreement seems so promising. Although it is an approximation process but it is still of great use for seismic vulnerability assessment of old hydraulic structures as well as to prescribe realistic seismic input for structures to be built at arbitrary points of a specific canyon site. The process needs a try and error search but could be more precise once the features of the causing fault is known.

REFERENCES

[1] Alves, W.S., "Nonlinear analysis of Pacoima Dam with spatially Non-uniform Ground Motion", PhD Dissertation, California Institute of Technology, 2005

[2] Kojic, S.B., "Earthquake response of arch dams to non-uniform canyon motion" ,PhD Dissertation, Southern California University,1988

[3] Sepulveda, S.A., Murphy, W. & Petley, D.N., "Topographic controls on coseismic rock slides during the 1999 Chi-Chi earthquake, Taiwan, Journal of Engineering geology and Hydrogeology, 38(2), 189-196, 2005.

[4] Trifunac, M.D. Scattering of plane SH-waves by a semi-cylindrical canyon. *Earthquake Engineering and structural Dynamics* 1973; **1**: 267-281.

[5] Pedersen, H.A., Sanchez-Sesma, F.J., and Campillo, M. Three-Dimensional scattering by two-dimensional topographies. *Bulletin of the Seismological Society of America* 1994; **84**(4)**:**1169-1183.

[6] Sanchez-Sesma, F.J., and Luzon, F. Seismic response of three-dimensional alluvial valleys for incident P, S, and Rayleigh waves. *Bulletin of the Seismological Society of America* 1995; **85**(1): 269-284.

[7] Sanchez-Sesma, F.J., and Campillo, M. Topographic effects for incident P, SV, and Rayleigh waves. *Tectonophysics* 1993; **218**:113-125.

[8] Paolucci, R. Amplification of earthquake ground motion by steep topographic irregularities. Earthquake Engineering and Structural Dynamics *2002; **31**: 985-998*.

[9] Zhang, L. and Chopra, A. K. Three-Dimensional Analysis of spatially varying ground motions around a uniform canyon in a homogeneous half-space. Earthquake Engineering and Structural Dynamics *1991; **20**: 911-926.*

[10] Niu, Y. and Dravinski, M. Direct 3D BEM for scattering of elastic waves in a homogeneous anisotropic half-space. *Wave Motion* 2003; **38**(2): 165-175.

[11] Dravinski, M. Scattering of elastic waves by a general anisotropic basin. Part2: a 3D model. Earthquake Engineering and Structural Dynamics *2003; **32**(5): 653-670.*

[12] Eshraghi, H. and Dravinski, M. Scattering of plane harmonic SH, SV, P and Rayleigh waves by non-axisymmetric three dimensional canyons: a wave function expansion approach. Earthquake Engineering and Structural Dynamics *1989; **18**(7): 983-998.*

[13] Mossessian, T.K. and Dravinski, M. Amplification of elastic waves by a three dimensional valley. Part1: steady-state response. Earthquake Engineering and Structural Dynamics *1990; **19**:667-680.*

[14] Zhao, C., Valliappan, S. and Wang, Y.C. A numerical model for wave scattering problems in infinite media due to P- and SV-wave incidences. *International Journal for Numerical Methods in Engineering* 1992; **33**(8): 1661-1682.

[15] Luco, J.E., Wong, H.L. and De Barros, F.C.P. Three dimensional response of a cylindrical canyon in a layered half-space. Earthquake Engineering and Structural Dynamics *1990; **19**: 799-817.*

[16] Athanasopoulos, G.A., Pelekis, P.C and Leonidou, E.A. Effects of surface topography on seismic ground response in the Egion (Greece) 15 June 1995 earthquake. *Soil Dynamics and Earthquake Engineering* 1999; **18**: 135-149.

[17] Assimaki, D., Kausel, E. and Gazetas, G. Topography effects in the 1999 Athens earthquake: engineering issues in seismology. *Proc. 11th ICSDEE and 3rd ICEGE*, UC Berkeley 2004; 2: 31-38.

[18] Kamalian, M., Jafari, M.K., Sohrabi, A. , Razmkhah, A. and Gatmiri, B. Time-domain two-dimensional response analysis of non-homogeneous topographic structures by a hybrid BE/FE method. *Soil Dynamics and Earthquake Engineering* 2006; 26: 753-765.

[19] Kamalian, M., Jafari, M.K., Sohrabi, A. On time-domain two-dimensional site response analysis of topographic structures by BEM. *J. Seismological Earthquake Engineering* 2003; 5(2): 35-45.

[20] Geli, L., Bard, P.Y. and Jullien, B. The effect of topography on earthquake ground motion: a review and New results. *Bulletin of Seismological Society of America* 1988; **78**(1): 42-63.

[21] Celebi M. Topographical and geological amplifications determined from strong-motion and aftershocks records of the 3 march 1985 Chile earthquake. *Bulletin of the Seismological Society of America* 1987; **77**:1147-1167.

[22] Vahdani, S. and Wikstorm, S. Response of Tarzana strong ground motion site during the 1994 Northridge earthquake. *Soil Dynamics and Earthquake Engineering* 2002; **22**: 837-848.

[23] Sirovich, L. Southern Italy November 23, 1980 earthquake. *Proceedings of the Seventh European Conference of Earthquake Engineering,* Athens, Greece 1982; **7**: 419-429.

[24] Bouchon, M. , Sanchez-Sesma, F.J. Boundary integral equations and boundary elements methods in elastodynamics. Advances in Geophysics 2007; **48**: 157-189.

[25] Ahmad, S. and Banerjee, P.K. Multi-domain BEM for two dimensional problems of elastodynamics. *Int. Journal for Numerical Methods in Engineering* 1988; **26**: 891-911.

[26] Dominguez, J. *Boundary Elements in Dynamics;* Elsevier, 1993.
[27] Huang, H.C. and Chiu, H.C., "The effect of canyon topography on strong ground motion at Feitsui Damsite: Quantitive Results", Earth Eng and Struc Dyn,Vol24,1995
[28] Tarinejad, R., Ahmadi, M.T., and Harichandran, R.S., "Effect of non-prismatic 3D canyon on the scattering of seismic P- and SV- waves", 4th Int. Confer. Earthq. Geotec. Eng. 4ICEGE, Thessaloniki, Greece, 2007.
[29] Ahmadi M.T., Tarinejad R., "Seismic Load Definition for Hydraulic Structures in Canyon Sites," Applied Research Report, Water Resource Management Company, MOE, Iran, December 2008.

PUBLIC EDUCATION AND AWARENESS PROGRAM IN IRAN AND ITS ACHIEVEMENTS

Farokh Parsizadeh

Faculty member of Risk Management Research Center,
International Institute of Earthquake Engineering and Seismology, IIEES
parsi@iiees.ac.ir

ABSTRACT

Considering the constant threat of earthquakes and loss of human lives and resources in Iran, an effective risk reduction program requires maximum public participation; this can be achieved through effective and comprehensive public earthquake education with the objective of raising awareness and preparedness. With this view and answering to these important needs, the International Institute of Earthquake Engineering and Seismology (IIEES) is one of the main promoters and developers of earthquake risk reduction programs in Iran and implementer of the "Increasing public awareness and promoting a collective prevention and safety culture" component of the "Earthquake Risk Reduction Strategy of Iran". This paper will provide an overview of the program on the disaster management education for managers, general publics, and especially children's earthquake safety education in schools. This priority could be better highlighted by looking at the wide coverage of schools as well as the young age structure of Iran. This paper provides a brief summary of the comprehensive earthquake education program for increasing the public awareness and preparedness for earthquakes through an integrated educational program using all type of media, especially for schools and children.
Keywords: Earthquake, Disaster, Risk, Public education, Earthquake education, School safety, Children safety, Earthquake drill.

1. INTRODUCTION

Iran is located in one of the high seismic hazard regions of the world; it has experienced frequent devastating earthquakes and high human, social and property losses in the past decades. The establishment of IIEES in 1989 and the Manjil earthquake of 1990 became starting points in the earthquake risk reduction activities in Iran, especially in the area of building capacity, research, knowledge development, vulnerability reduction and public (especially children) awareness and preparedness. Based on the achievement and experience gained from the 13 years of earthquake risk reduction activities, and lessons learned from the Bam earthquake of 2003, the long term "Earthquake Risk Reduction Strategy of Iran" was developed and ratified with special emphasis on implementation. In other words, the Bam earthquake became a new turning point in the history of earthquake risk reduction in Iran with more incentive and support. By considering the comprehensive or "total" look at the earthquake from its cause to its effects, the new Iran long-term Strategy on Earthquake Risk Reduction (ISERR) is comprised of several components such as: policy change, increasing knowledge, improving the management quality in all related areas of risk, using advanced technology, code enforcement, public awareness, and increasing public preparedness for correct responses during and after earthquakes. It should be noted that the First Article of the new Strategy emphasizes the enhancement and promotion of the safety culture through increasing the awareness and preparedness of the policy maker and authorities, and the general public.

Considering the very young age structure of Iran as shown in Table (1), especially in the urban areas where the earthquake risk is high, "Safety Culture" can be effectively achieved if it gets started with children in schools. This young age structure and the high vulnerability of children make children and schools the key targets in the earthquake risk reduction activities. Earthquake preparedness education for children not only furthers their safety during earthquakes, but it can also play an effective role in the dissemination of knowledge and preparedness among families in the society. It helps the sustainable process of public educational programs to raise awareness, to create sensitivity and belief regarding the "facts of earthquakes" in order to take appropriate actions. Thus, the well thoughtout and comprehensively planned earthquake safety education program (with the full consideration of the principle: simple, clear and to the point) does not create fear or panic, results in less social and economic disruption, is consistent and not only creates a safety culture, but also creates strong public will and incentive for an effective implementation of risk reduction actions in the country.

Moreover, considering the fact that among the human losses, the loss and injury of children, the binding factor of a family, can create long-term psycho-social disorder in the society; thus saving their lives should have the highest priority in any risk reduction program and school building safety can play an important role. With this observation, one of the first and important outcomes of the new strategy was the program for the strengthening and reconstruction of vulnerable schools based on the law that was proposed and passed by the Iran Parliament with the allocation of $4 billion.

Table 1. Age Distribution (structure) of Iranian population in urban and rural areas. 36 % of the total population under 19. 40% of the urban area and 37% of the rural area population are under 19 years old.

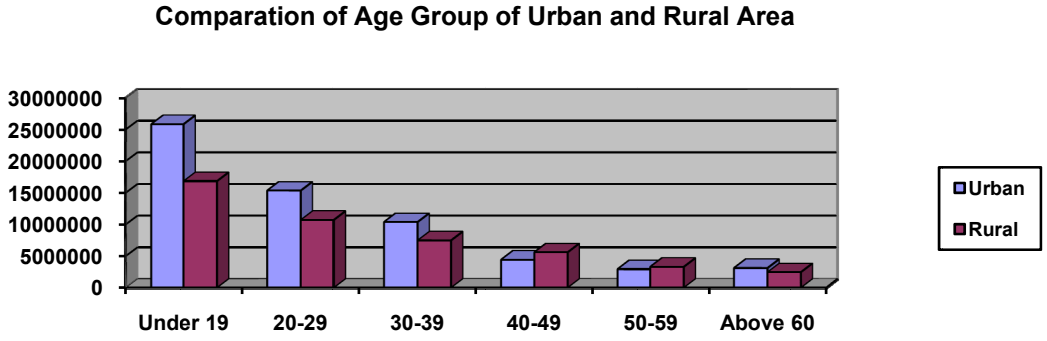

This paper provides an overview to the earthquake educational program and its achievement for the managers and policy makers in Section 2, for general public in Section 3 and for schools and children in Section 4.

2. DISASTER MANAGEMENT EDUCATION FOR THE MANAGERS

With the objective of raising awareness, knowledge and concern of policy makers, authorities, and managers on important factors (seismic hazard, vulnerability, management, etc.) contributing to the earthquake risk as well as the effective methods for its reduction and control, a special training program has been developed and implemented in almost all provinces through face to face discussion and training. The program contains information on the active faults, seismicity

and seismic hazard of each province as well as the related physical, human and economic risk in map form. This program has proven very effective in changing the perspectives on earthquakes and their risks held by city officials and managers.

Today the policy making body is much more concerned about earthquake risk and well aware that the only way to reduce risk is through preparedness and prevention. Development of a long term strategy for earthquake risk reduction; allocation of a 4 billion dollar budget for school safety; the ongoing retrofitting program for public funded buildings and infrastructures and lifelines; supporting risk mitigation activities; and talking about the need for earthquake risk reduction are some examples of the results of this awareness program. In other words, today we have passed the awareness step and are working our way towards helping the authorities know how to achieve an effective implementation outcome.

3. GENERAL PUBLIC EDUCATION

To achieve an acceptable level of earthquake preparedness, ,the public should first know the facts of earthquakes and their consequences in order to become sensitive and interested in learning about prevention measures. Thus public education should focus on: risk communication, showing the benefits of prevention and risk reduction, creating incentives, what is needed to be prepared, what to do during and after an earthquake, first aid, and finally how to help families and neighbors. In the entire program, it has been emphasized that the key factor in being prepared is prevention and living in a safe building. The results of the program, which was started in 1991, can be easily seen in the Iranian society. Today people are much more aware, a success in the first step of preparedness; but there is still a long way to go in order to become a prepared society. The following sections present some of the program activities that have been developed for this purpose.

3.1 Audio-Visual

Television and radio programs are focused on communicating the risk and providing continuous reminders to the public about the experience with past earthquakes. A 15-minute weekly TV program, 5 to 10-minute weekly programs on National Radio and special programs touch on various safety issues; these are useful for opening a dialogue with the public and answering their questions. The programs have resulted in decreasing fear and rumors and have created a channel of communication with people since they are continuous. Also broadcasting short films and TV programs such as: "*Earthquake and Rumor*" addressing the effects of unreliable rumors on social disruption; "*Paper House*" showing the effects of code violation and economic losses; "*Build lightweight structures*" and "*strengthening guidelines for buildings against earthquake"* teaching the key points that should be considered for safe design and construction , are examples of communication and teaching the public with a sense of humor and without causing fear, especially in rural areas. Also a series of clips on "*Earthquake and Safety, Rumors, and Earthquake Drills"* have been made and broadcast on national TV, touching on various issues related to building safety and on what to do during and after an earthquake.

Also on the occasion of National Earthquake Drill in Schools (see section 4.3) radio and TV channels have special programs for children and the general public to encourage all communities to be prepared for the drill. For example, in one week 6,276 minutes of programming were broadcast throughout the country during the 7th National School Drill (see Table 2 below).

Table 2. Number and duration of news and educational programs that were broadcast from national and local radio and T.V. during the week of the (7th National School Drill).

Type of Media	Educational Program		News		Total	
	Time/Min	Numbers	Time/Min	Numbers	Time/Min	Numbers
National T.V channels	781	23	96	42	877	65
National Radio channels	410	76	129	71	539	147
Local Radio and T.V channels	5,085	1,070	596	219	5,681	1,289
Total	6,276	1,169	821	332	7,097	1,501

3.2 Publication: Booklets, Pamphlets, Posters

Printed materials such as booklets, pamphlets, posters and articles in the newspapers have been used to show the facts on earthquakes and how to be prepared for them. For home and family these include "*Let's Reduce Earthquake Hazards*" and "*Earthquake Preparedness"* booklets; many pamphlets and posters such as *"Make Your House Safer against Earthquake*", each designed for different communities have been developed and disseminated through organizations. They all use simple language and attractive graphics and pictures to teach precautionary measures, how to become prepared, how to improve the safety of home interior, as well as what to do during and after an earthquake. *"Earthquake: Looking Deep Inside the Earth"* booklet provides simple scientific information on earthquake phenomenon for the educated general public. It covers information on earth structure, faults, seismotectonic, seismicity, seismic hazard and risk map of Iran as well as facts on earthquake predictions. For safety in offices and at work, "*Educational Guidelines for Earthquake Reduction in Office Buildings*" brochure, along with posters and audio tapes with short messages, have been prepared and distributed. Similar publications have been designed for hospitals, hotels, markets, metro, etc.

Considering the popularity of the Iranian newspaper, writing articles and organizing press interviews on special occasions have been effective teaching tools for generating public awareness and creating public will for safety. Street billboards and public exhibition stands are also being used to deliver a series of messages on awareness, and on safety and prevention measures.

4. SCHOOL EARTHQUAKE EDUCATION: AWARENESS AND PREPAREDNESS

Creating an earthquake safety culture should start with children and schools due to the young age structure of Iran and the loss of school children during earthquakes, especially around 10,000 of them during the Bam earthquake of 26 December 2003; this earthquake demonstrated that the youth are among the most vulnerable groups of the society. In Iran's population, 29.71% are between 5 to 19 years old (5-9 years:7.81%, 10-14 years:9.52% and 15-19 years:12.38%), including more than 14.4 million students in more than 2,067,326 classrooms as shown in Table

(3). It should be noted that in the past 10 years due to birth control policy the number of students have decreased by 2 million students, from 16,591,225 to 14,434,526 in 2007. Adding the 655,690 teachers and more than 1 million school staff members to the number of students will involve coverage of around 1/3 of Iran's 69 million population.

This young age structure and their high vulnerability make children and schools the key targets for the earthquake risk reduction activities in Iran. Earthquake preparedness education of children not only helps their safety during earthquakes, but it can play an effective role in the dissemination of knowledge and preparedness among the society and families. Finally, considering the fact that among the human losses, the loss and injury of children, since they are a binding factor of a family, can create long-term psycho-social disorder in the society; saving their lives should have the highest priority in any risk reduction program and school building safety can play an important role.

Thus the perspective of the national strategy is the undeniable need for the safety of children and creating and planting the seeds of the earthquake safety culture in the society; a comprehensive earthquake education and preparedness and earthquake building safety program has been initiated and developed by IIEES with the idea that the schools are the most important and fundamental community centers of a country, providing the basis for all aspects of sustainable development including technical, industrial, economic and social development. The IIEES program and activities are composed of:

- ✓ **Earthquake Awareness and Preparedness for all school levels**. Using direct and indirect methods to increase students' knowledge about earthquakes, the theoretical and practical program has been developed within the curriculum framework of the three different educational levels in Iran: one year Pre-School, 5 years of primary schools**,** 3 years of secondary schools, and 4 years of high schools. In primary school students learn about earthquakes and the proper decisions and activities which should be taken during an earthquake to ensure their safety. In secondary school and high school, the students learn about the emergency response activities which ensure their safety and well being before, during and after an earthquake. In fact they are taught about emergency first aid procedures, which would help them and their classmates survive until the rescue and relief teams arrives. The educational program is comprised of several formal and informal components:
  - Educating children and youngsters about earthquake preparedness at all school levels by including materials in textbooks, posters and films, and conducting drills, creating exhibitions, and conducting drawing and writing competitions, etc.
  - Conducting annual national drill in schools on November 8th.
  - Organizing annual art, painting and training exhibition.

Table 3. Distribution of Iranian students (rural and urban area, boys and girls), number of schools and classes in all 3 level of primary, secondary and high school (2007-2008).

	Primary		Secondary		High Schools	
	Total	**Rural**	**Total**	**Rural**	**Total**	**Rural**
Students	5,725,629	2,035,415	3,743,121	1,126,980	4,435,699	1,235,699
Schools	62,699	43,982	31,172	16,479	33,295	8,989
Classrooms	268,463	123,166	159,016	59,260	206,263	55,691

	Primary		Secondary		High Schools	
	Public & Private	Private	Public & Private	Private	Public & Private	Private
Girls	2,615,883	157,671	1,666,965	73,399	1879,215	128,050
Girls and Boys	5,332,002	393,627	3,479,736	228,534	3,692,059	316,295
Schools	59,439	3,260	28,239	2,518	23,300	5,559

	Primary		Secondary		High Schools	
	Girls	Girls & Boys	Girls	Girls & Boys	Girls	Girls & Boys
Urban and Rural	2,773,554	5,725,629	1,763,162	3,743,121	2,184,108	4,435,699
Rural	977,041	2,035,411	494,714	1,126,980	516,822	1,235,852

The role of school officials is to fully implement the program and integrate safety into the school's activities; the role of children and parents is to take the earthquake risk seriously, get educated, be aware, be prepared, and use the know-how before, during and after an earthquake.

a. Pre-school education

The education of pre-School students and kindergarten teachers has occurred since 1995 and has involved the development of special types of educational materials in the form of *Earthquake Song, Drawings, Earthquake Exercises, Computer Games, Story Books and Multimedia Educational Program (*see Figure 1 below).

Fig. 1. Teaching guidebook for pre-school teacher, children activities in park and exhibitions and story books.

b. Formal or theoretical education

Formal training materials have been integrated into school textbooks of the three different school levels with the objective of creating, expanding and consolidating the "Culture of Safety" in the society as well as reducing the human casualties and losses due to earthquakes and enhancing student knowledge about earthquakes. These programs have been designed and carried out by taking into consideration two factors relevant to the subject of the course as well as the age and physical capacity and socio-economic condition of the students.

The textbooks material for various school levels can be classified into the four categories as follows:

1. *Scientific subjects on earth and earthquakes:*
   Science books for 4th, 5th, 8th and 12th grades and geography books for 8th and 10th grades cover scientific materials on the earth structure, continental movements, earthquake phenomenon, faults, seismicity, and seismic hazard. Since the geography books are regionally prepared, they provide earthquake information related to the relevant province.
2. *Earthquake preparedness, response and recovery:*
   "Earthquake Preparedness" book for 8th and 9th grades and "Technology and Careers" book for the 8th grade covers materials on the most appropriate activities to be performed before, during and after a damaging earthquake, as well as a guideline for school preparedness and first aid.
3. *Technical and engineering aspects of safe building:*
   How to build a safe and earthquake resistant building is being taught in the construction major of the technical high schools. The curriculum and text book of this major has

been modified in order to make construction technicians aware and knowledgeable about building standards and the criteria of a seismically safe building.

4. *Social and cultural aspects of earthquakes:*
   "Social science" books for 3rd and 7th grades and "Persian literature" book for the 8th grade look at earthquakes from the social and literature points of views with the aim of creating self confidence and proper social behavior at the time of an earthquake.

To train the teachers of these courses, two "Teachers Guidebooks" have been published for the use of teachers and a special training program is being operated annually in each regional education offices. Each year millions of these books reach all school children at a very low price.

This nationwide program has been achieved with the close cooperation of the Ministry of Education, which set an example for other agencies that their cooperation will add awareness and safety. It has been more than a decade that the students are learning about earthquake safety and preparedness. The results and the program's effectiveness have been seen from the first year of program implementation when only a chapter on earthquake preparedness was inserted in the 8th grade geography book. The 8th grade students of the Sefidabeh village in a most remote part of Iran near Afghanistan saved their lives during the 1993 earthquake by taking proper shelter. And more recently during the 2003 Bam earthquake many school children stated that they saved their lives based on their learning in schools. During the March 2006 earthquake in Lorestan, many children and family members protected themselves by taking proper safety measures; this resulted in a low human casualty rate.

c. Extra-curricular or informal education

To complement the formal education, several activities such as extra-curricular activities have been designed, developed and implemented for the students within and outside the schools in the form of publications, drawing exhibitions, essay writing competitions, children safety campaigns, school earthquake safety councils, etc. It should be noted that the program has benefited from the maximum participation of educational, social, cultural, media organizations and NGO's for the successful implementation of the activities. The following section outlines some of the accomplishments that have been achieved.

i. Publications

Besides the textbook materials which are available to all school children, other educational publications on earthquake phenomenon and preparedness using simple science have been published for various ages and classes in the form of workbooks, booklets, brochures, and education-aid materials. Some of them are: *"E for Earthquake"* designed for the k-3 level with paintings and puzzles; "*Earthquakes: Understanding the Earthquake Phenomenon"* designed for the secondary school level, introduces simple experimental work and games for understanding earthquake science; *"What to do during earthquake in School"* describes simple guidelines for what to do and not to do during earthquakes*; "Earthquake Hazards Reduction at Educational Institutions*"; etc.

ii. Posters

Posters in schools and homes with the objective of delivering short and continuous messages are an effective medium to relay the quick safety message. Posters such as: *"What to do During an Earthquake"* for K-6; *"Earthquake Safety Provisions in Schools"*;

"Safety and Earthquake" for the 6 to 12 grade with the wide coverage have been distributed.

iii. School's Earthquake Safety Councils

To benefit from the maximum participation and cooperation of students and their parents for the improvement of school safety, the "School Earthquake Safety Council" is being formed with the following school teams based on the guideline given the 8th grade in the "Earthquake Preparedness" book: Nonstructural element safety team; Search and rescue team; First Aid team; and Fire Safety team. This council, with the help of "Teachers and Parents Councils" and using the expertise of parent volunteers, aims to improve school preparedness levels. This project, shown in Figure (2), was started in a few schools on an optional basis in 2000 and is expanding throughout the country as a voluntary school activity.

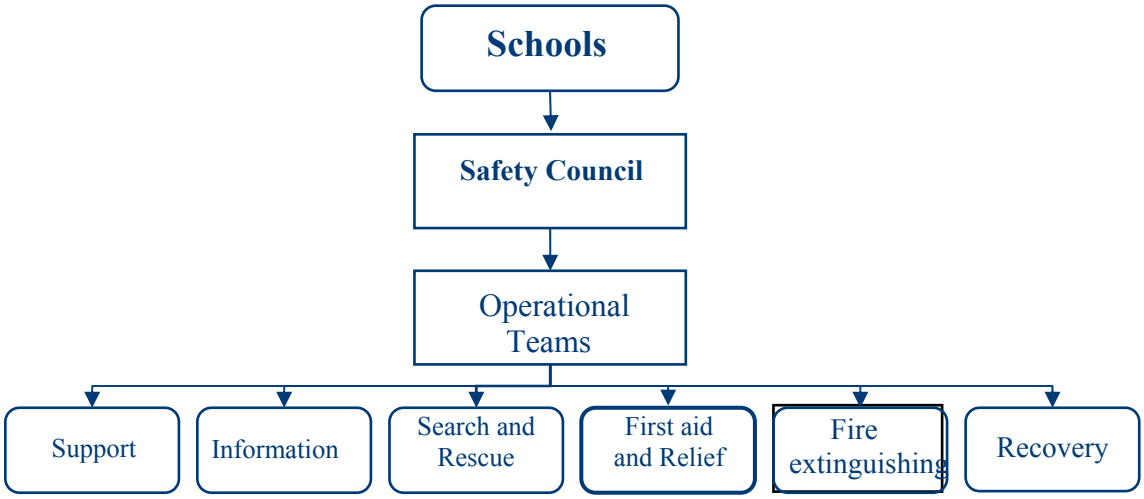

Fig. 2. Structure of School Safety Council and its guidebook.

iv. School Extra-Curricular Activities

The existence of a wide range of earthquake related educational material within the school curriculum provides a platform for the teachers to ask the students to perform activities related to earthquake safety. "Earthquake Safety and Preparedness" is a common topic for painting, writing composition, art work and other student projects. These activities can be considered an indicator of the effectiveness of the school education program and that earthquakes are in the minds and thoughts of children, which is a main step toward achieving the "Safety Culture".

4.1 Continuous Education Courses

To complement the student education, educational courses for all teachers and the employees of the Ministry of Education have been developed and are being implemented. The main purpose of these courses is to enhance the knowledge of teachers and their ability to transfer this knowledge to others. Special books and video tapes have been produced especially for the teachers. IIEES has organized various training programs for head teachers in the school systems.

4.2 National Earthquake Safety Drill

Another tool has been used to transfer the theoretical and textbooks learning into practice and prepare the students for the appropriate and quick responses during and after earthquake. The annual "Earthquake Safety Drill" program in school has been developed by IIEES with the main objectives of: improving and increasing children's skills, response and preparedness as well as to prepare them to become safety messengers in their homes and families. The idea was first tested in 1995 in 5 primary schools (one in each region) and it was concluded that due to the lack of awareness of young children and text book education, the planned program was not suitable for the primary school level. In 1997, after revision of the program, it was tested in 3 high schools in Tehran. After receiving a good response, it was followed by the second drill in all 1059 high schools in Tehran. After the comprehensive evaluation of the first three drills and revision of the program, the fourth drill was carried out in 15,499 high schools in Iran simultaneously on the 29th of November 1998. The level and type of activities of the drill were continuously updated and its coverage expanded. Since November 2003, the drills are being held annually on the "29th of November" of each year in all 154,804 Iranian schools with participation of more than 14.3 million students, making it a national event. Table (4) illustrates the expansion process of the safety drill in schools. It should be noted that if the 29th of November falls on a holiday, the drill will be done the day before or after. Learning from each year's experience, the quality of drills and the effective participation of the schools and students have improved

Considering that the drills are carried out simultaneously throughout the country, for coordination, cooperation and participation purposes, the "School Safety Drill" council, consisting of the representative of the Ministry of Education, Ministry of Science, Research and Technology, Ministry of Interior, Iran's Broadcasting organization, Iran's Red Crescent organization and IIEES, has been formed for their successful implementation . The process of preparing and holding drills is as follows:

- Preparing the earthquake drill guidelines for all schools.
- Producing the educational posters and sending them to the schools.
- Broadcasting different scientific and educational programs about earthquake safety on radio and TV channels one week before the drill.
- Delivering the "Earthquake and Safety" message to students in each school.
- Broadcasting a special program about the drill during the week of 29 November on national and regional radio.
- Broadcasting the "Earthquake & Safety" alarm on the morning of the 29th of November on national and regional radio for 30 seconds to start the national drill in all schools.
- Performing the correct sheltering "Drop, Cover and Hold" by the students in 30 seconds and evacuation after the drill.

Table 4. Development process of the School Earthquake Safety Drill.

	Year	School Level	No of schools	No of students	No of boys	No of girls	Coverage
First trial Drill	1996	Primary school	5	1000	600	400	Tehran
Second trial Drill	1997	High school	3	-	-		Tehran
Tehran Training drill	1998	High school	1,059	527,237	266,890	260,480	Tehran
First National Drill	1999	High school	15,499	4,580,688	2,324,907	2,255,781	National
2nd National Drill	2000	Secondary and High	45,000	11,000,000	5,776,000	5,224,000	National
3rd National Drill	2001	Secondary and High	48,000	11,800,000	6,176,000	5,624,000	National
4th National Drill	2002	Secondary and High	50,000	12,000,000	6,500,000	5,500,000	National
5th National Drill	2003	All levels	110,000	16,591,225	8,613,124	7,978,101	National
Special Post Bam Earth.	Feb. 2004	All levels	110,000	16,000,000	8,300,000	7,700,000	National
6th National Drill	2004	All levels	120,000	16,027,956	8,297,318	7,730,638	National
7th National Drill	2005	All levels	140,815	15,264,349	7,872,610	7,391,739	National
8th National Drill	2006	All levels	150,804	14,330,901	7,391,126	6,939,725	National
9th National Drill	2007	All levels	146,213	11,434,526	7,443,162	6,991,364	National

Note: The number of schools and students has been rounded up.

4.3 Educational Competitions, Exhibitions and Workshops

4.3.1 Drawing Competition and Exhibitions

To promote and encourage awareness among children and youth, the organization of drawing competitions and exhibitions with the following objectives has proven to be an effective approach:

- Investigating the ideas and concepts of the students about the earthquake phenomenon;
- Considering the effectiveness of previous educational efforts; and
- Creating incentive for understanding earthquakes and their effects.

Since 1992, bi-annual drawing contests entitled: "*Earthquake and Safety*" are held with the help of schools and the media for children ages 5 to 18. The one week exhibition of the selected drawing, along with side activities (games, play, science, etc.) designed for different age groups, has provided an exciting and attractive occasion for raising children awareness and preparedness levels since 1994. The assessment study on children knowledge and awareness level before and after the program shows the effectiveness of these kinds of activities.

With the objective of showing children that earthquake safety is an international issue and that the threat exists beyond Iran, the drawing competition and exhibitions are held in the Asian level with the cooperation of local organizations as well as by UNESCO, UNICEF, UN/ISDR, etc.

4.3.2 Writing Competition

To enhance safety culture among adolescents, bi-annual writing competitions with different themes, such as "*Earthquake Reduction*", "*Earthquake and Safety*", *"Earthquake Preparedness",* have been held around the following questions and issues since 1998:

- Describe an earthquake in the form of a fictitious story.
- If you were the mayor of a city, how would you make your city safe from earthquakes?
- What is if there is no access to mass media in the case of an earthquake? Write a story about the effects it may cause on people.
- The cooperation of young adults in earthquake hazard mitigation.
- What is the role of hospitals, fire stations and Red Crescent Society of the Islamic Republic of Iran in disaster management after an earthquake?
- Suppose you are the principal of a school, how would you attract the attention of the students for cooperating in earthquake programs?
- What is the role of earthquake safety drills?
- What do you expect as a citizen from the responsible authorities for hazard mitigation plans?
- What would you do in the case of a major earthquake?
- What is your idea about earthquake prediction?

Many useful ideas were drawn from these writing competitions and some of them were used for improving the public awareness program, opening dialogue with people and understanding their view. The proceeding of selected articles is being published and best papers receive awards in a ceremony which encourages better understanding and learning by children.

4.3.3 Earthquake and Safety Workshops

Every year, on the occasion of the National week of natural disaster reduction (week of October 11) and since 2007 on the Iran National Day of Earthquake (23rd of December on the occasion of the Bam earthquake), Earthquake and Safety workshops are held with the following goals:

- Increasing students and teachers awareness about earthquakes.
- Teaching the proper reactions and sheltering during earthquakes.
- Knowing the scientific principles about the earth and earthquakes.

The education process in workshops is direct and face to face, using the medium and materials such as computer software, video clips, audio cassettes, poems, drawings, games and etc.; the workshops have been welcomed by students, family members and teachers since they provide an attractive atmosphere for learning.

4.3.4 Special Program for Deaf Students

To reach-out to special students, a pilot program has been developed with the aim of identifying the common educational needs of deaf students before, during and after earthquakes. The program covers around 180 students and their teachers and parents. The preliminary result has shown the strong incentive among the deaf students for learning about earthquake and

preparedness, even more than the regular students (see Figure 2 below). These students are participating in the annual drill as well. It is envisioned that the coverage of this program will extend to all schools and all disabled and special students.

Fig. 2. Earthquake education workshop for deaf students.

5. CONCLUSION

The first article of "Earthquake Risk Reduction Strategy of Iran" is devoted to public awareness and preparedness and safety culture. The past studies and experiences in Iran and many parts of the world indicate that this objective can only be achieved through the implementation of a comprehensive, integrated and sustainable program. This paper provided a brief but comprehensive description of this program in Iran, with a special emphasis on the school safety program. The overall assessment, without any doubt, shows that the Iranian people, especially the children, are much more knowledgeable, aware and concern about earthquake safety today. This claim can be seen in all aspects, from the policy and legislation that has been passed for earthquake safety, to the allocation of funds and budgets, government support, and the strengthening of public buildings and infrastructures against earthquakes; this can also be seen in the effective measures that have been taken during recent earthquakes, especially during the March 2006 earthquake in Lorestan which saw a substantial reduction in human losses. The effect of school educational programs and other public earthquake education programs has resulted in a strong will in the government and public for reducing the high level of risk in schools. The allocation of $4 billion for the strengthening and reconstruction of vulnerable schools is a good example. However, there is still a long way to go to achieve a fully prepared and seismically safe community and for this stronger cooperation and participation of all of the society is necessary for enhancing public safety. Finally, the author strongly believes that the Iranian experience is a successful one, and can be shared and learned from.

REFERENCES

Fallahi.V. and Parsizadeh.F. Perspectives of Young Adult's on "Earthquake and Safety", IIEES Publication, (Persian -1997).

Rezaeepanah.N. and Parsizadeh.F. Analyzing Education Effects on Children and Young Adults "Earthquake and Safety", IIEES Publication, (Persian-1997).

Heshmati.V. and Parsizadeh.F. An Assessment of Awareness level among Iranian Children and Young Adults on Earthquake as a Natural Phenomenon and its Consequences, IIEES Publication, (Persian-2007).

Ashtiany.Ghafory.M and Parsizadeh.F. Educational Aspects of Disaster Management: Post-Earthquake Experiences. Iran Public Education and Awareness Program and its Achievements, World Conference on Disaster Reduction. Japan 2005.

Parsizadeh.F. An Insight in Iran's View on Earthquakes. The World Urban-Earthquake Conference in Fukui, 1998.

Parsizadeh.F. and Seif.A.E and Heshmati.V. National Earthquake and Safety Drill in Schools, IIEES publication, (Persian-2007).

Parsizadeh.F. and Seif.A.E Earthquake Safety Drill Guideline for School Principal, IIEES Publication (Persian-2007).
Parsizadeh.F. and Izadkhah.Y.O. Impact of the 2003 Bam, Iran, Earthquake on the Personnel and Functioning of Local Government Organizations, Special Issue on Bam Earthquake, Earthquake Spectra, Dec. 2005.
Parsizadeh.F. and Rezaeepanah.N. Assessing Children's Drawings: Earthquake and Safety, published by IIEES, (Persian-1997).
Parsizadeh.F and Heshmati.V., Planning Guides for preparation Before, During and After an Earthquake, Proceedings of the Second International Conference on Seismology and Earthquake Engineering SEE2, 1995.

ADVANCEMENTS IN URBAN SEISMIC RISK MODELING AND QUICK LOSS ESTIMATION FOR IRAN

Babak Mansouri[1] and Mohsen Ghafory-Ashtiany[2]

[1] Assistant Professor and Head of Emergency Management Department - Risk Management Research Center, International Institute of Earthquake Engineering and Seismology (IIEES), Tehran, Iran,
[2] Professor - International Institute of Earthquake Engineering and Seismology (IIEES), Tehran, Iran,

Keywords: urban risk modeling, vulnerability, quick loss estimation, GIS, remote sensing.

INTRODUCTION

Earthquake risk mitigation encompasses two main concepts: 1) seismic urban risk assessment before the occurrence of scenario earthquake(s) and 2) quick loss estimation based on damage detection after the event (even after days and weeks). The risk assessment part includes the creation of city inventories and the compilation of associated geodatabases, the evaluation and the implementation of different vulnerability functions for the built environment and finally, the derivation of proper risk algorithms applicable to buildings, road networks and more importantly to human casualties. The quick loss estimation is based on damage detection and takes advantage of various remote sensing techniques and applications in detecting the changes/damages on the ground surface. This paper explains the new advancements in using recent technologies and methodologies in the above contexts. Tehran is highly vulnerable to large earthquakes due to its surrounding active faults; hence, this metropolis is chosen as the case study for pre-event seismic risk assessment. However, the case of the Bam earthquake is selected for the post-event remote sensing damage detection for both optical and radar satellites.

URBAN RISK MODELING

Hazard Data

Active faults in the Tehran region have been investigated and mapped by Berberian et al. (2001), Abbassi et al. (1999) and Hessami (2003). A major source of earthquake hazard for Tehran is recognized as the "Mosha Fault" (important fault in central Alborz with the length of 220 km) that is farther from the city but poses the highest level of hazard on Tehran. Figure 2 shows the map of active faults and the associated seimicity in central Alborz surrounding Tehran. The "North Tehran Fault" with a length of 75km, and the "South and North Ray Fault" (a possible earthquake source for the southern part of the city) are other important seismic sources for Tehran. In order to consider all known possibilities (larger scale disaster management and insurance vision), the probabilistic seismic hazard microzonation map for a return period of 475 years developed by the IIEES (Jafari et al. 2005) shown in Figure 3 is used. Figure 4 depicts the microzonation map developed by JICA (2000) based on the scenario Ray fault model with a characteristic earthquake of 6.7 Mw in magnitude. It should be noted that the Ray fault (south and north faults combined) is not considered as the major source of earthquake risk for all of Tehran by most of the experts, but it has the high hazard potential for the southern part of Tehran (including district 17) and is expected to suffers severely from a large number of vulnerable

buildings; Thus the study of this scenario earthquake is useful from the emergency management response point of view.

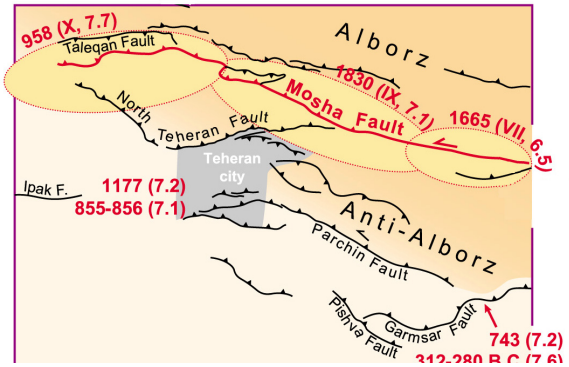

Fig. 1. Active fault map of central Alborz and associated seismicity (after Berberian et al. 2001).

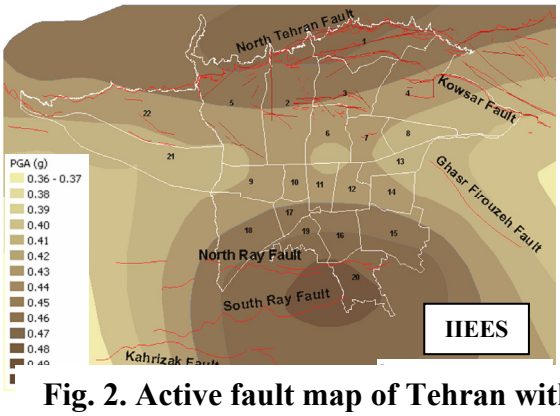

Fig. 2. Active fault map of Tehran with seismic hazard zonation at bedrock - PSHA 475 year return period (courtesy of IIEES).

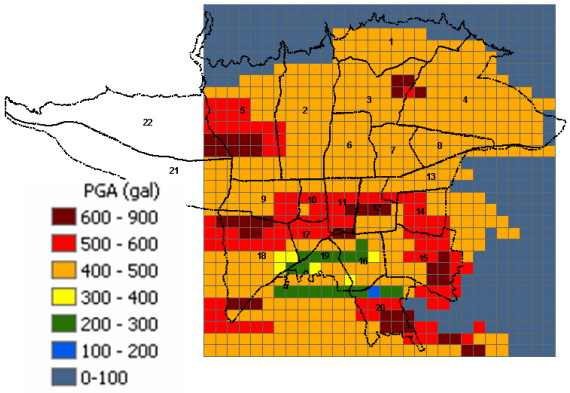

Fig. 3. IIEES probabilistic seismic hazard microzonation map (Jafari, et.al).

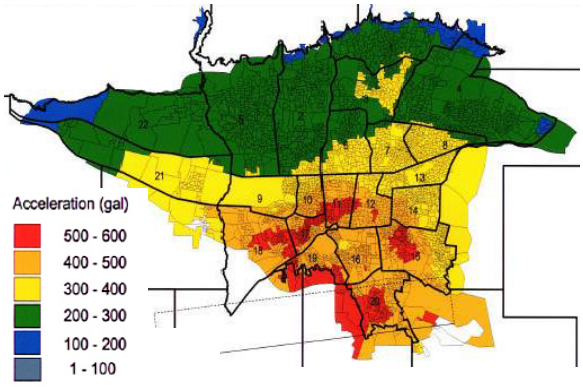

Fig. 4. Microzonation Map – Ray fault scenario reference (courtesy of JICA 2000).

Building Stock

A combination of urban databases describing city blocks and/or individual parcels have been acquired and compiled in the geodatabase. Very high resolution optical satellite data, aerial stereo-photos and also survey data was gathered and processed for Tehran. The height information was extracted from stereo-photography technique where it was complemented with survey data. The process involved the creation of the building stock database with 3D modeling pronouncing parcel details such as building height in digital format (Figure 5). The survey data provided some general building inventory information like: “landuse”, “number of stories”, “building age” and “building quality” (Figure 6).

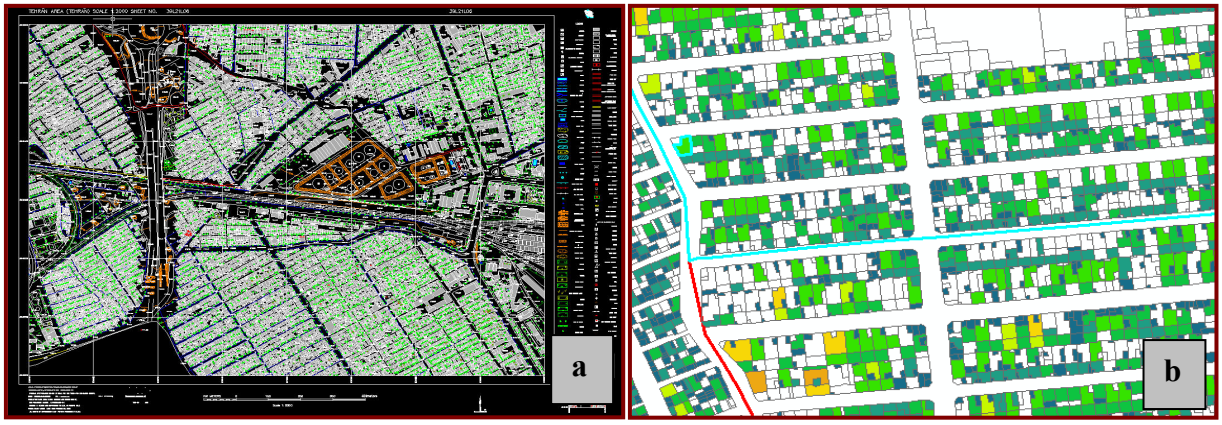

Fig. 5. (a) High resolution spatial and attribute from cartographic aerial photos (digitally 1:2000 scale stereo photos)
(b) Parcel survey data describing the building attributes.

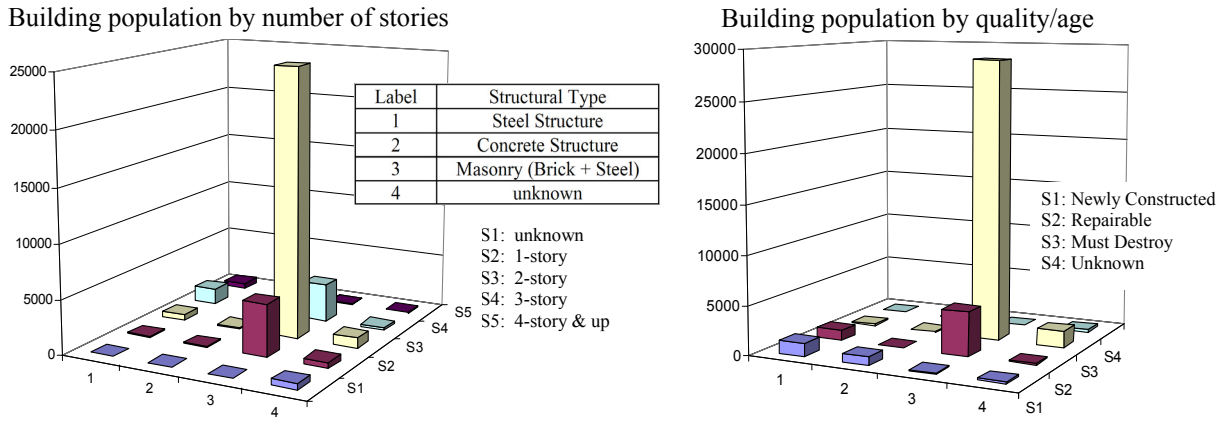

Fig. 6. Building stock general information for district 17 of Tehran.

Building Vulnerability

So-far most of the developed vulnerability functions of the structures are site specific by nature, because they are mainly dependent on local design and l construction practice, as well as local soil and hazard considerations. .Different damage functions have been generated using data and observation from worldwide and/or domestic past earthquakes and also by using suitable analytical methods.

A series of such curves were introduced for Tehran (Mansouri et al. 2008) and described as follows. Some worldwide vulnerability functions that can best represent the existing building stock in Tehran were selected. Some of these curves are derived from the Manjil-Iran earthquake or other countries such as Turkey with some modifications (JICA 2000) and Costa Rica as published by Sauter et al. (1978) as cases that resemble the study area. Some other damage functions were selected according to the ATC-13 and ATC-13-1 reports where the results are downscaled for the nonstandard constructions. Using an analytical modeling according to

HAZUS (Kircher et al 1997) and selecting/judging the parameters representing the local conditions of the region, 14 fragility curves were obtained.

The most common building typology in Tehran, especially in district 17 and other older urban settings encompasses the traditional un-reinforced masonry with bearing brick walls and steel and slightly-vaulted brick roofs (Figure 6). Darehzereshki et al. (2009) investigated 200 samples that represented the most common type of masonry structures in district 17 where finally 37 buildings were thoroughly investigated and modeled. The associated capacity curves were generated using a nonlinear static methodology. Using the EMS-98 damage grade definition and intersecting the capacity curves with the demand curve, performance points were found. Using a normal cumulative distribution function the following fragility curves were computed (Figure 7).

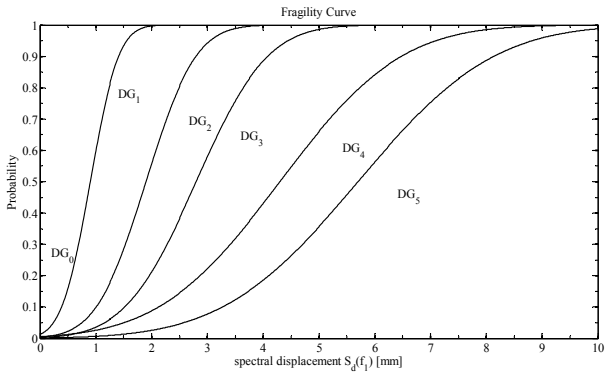

Fig. 7.- Fragility Curves for low-rise un-reinforced masonry buildings.

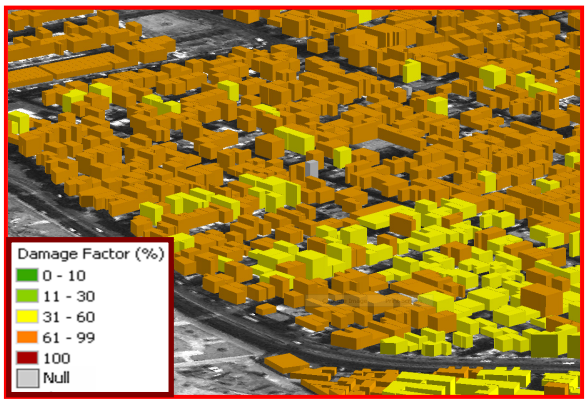

Fig. 8. 3D view of the seismic risk map adopted for a part of Tehran.

By relating these curves with the scenario microzonation data and applying the outcome to the inventory database (with parcel resolution), a spectrum of structural damage levels (with their proper probabilities) is evaluated within the extent of the city. Three-dimensional risk maps, in the cities, provide an excellent visual means to quickly evaluate the extent and the severity of potential building damages. These results can help in reducing the monetary loss and more importantly in devising measures to reduce the predicted human loss after the event. Figure 8 is an example of 3D seismic risk maps for a part of Tehran.

Human Casualty

Human loss is not a direct function of the earthquake intensity. It is mainly regarded as the consequence of building damage. Because of the importance of focusing on conventional masonry buildings, covering the largest part of the population, a model is presented in this research. The human vulnerability assessment for masonry buildings in Iran is based on an adaptation to the Hazus procedure using an event tree model judged for Iran. It is assumed that the casualty statistics of the Bam earthquake (December 2003) can relate to the case of the study area (Tehran) that is especially true for the older part of the city. Therefore, the empirical coefficients are obtained from the human loss statistics after the Bam event. The estimation pronounces the probability or the percentage of the building population for different severity

levels of injuries. It is also possible to calculate the loss during the day or at night considering different residential or commercial populations and locations.

The population statistics database reflects the information in each census zone (Iran Census Center). An interpolation procedure assigns the per-parcel population data from the census zone information considering the building footprints and the number of stories. In order to compute the human loss coefficients that describe the portion of the population affected by the earthquake, three levels of human casualty are defined according to the BAM post-disaster survey data. These three casualty levels are: "Uninjured", "Injured", and "Dead". This data also describes roughly three levels of structural loss as "Undamaged", "Damaged" and "Destroyed".

Fig. 9. BAM post disaster survey zones in GIS - overlaid on optical image (three levels of building damages in addition to three levels of human casualties).

For example the following simplified relationship can estimate the casualties for the unreinforced masonry building damages for the night case:

$$\begin{bmatrix} \#\text{ of Uninjured} \\ \#\text{ of Injured} \\ \#\text{ of Dead} \end{bmatrix} = \left(\frac{\#\text{ of Population}}{\#\text{ of Buildings}} \right) \begin{bmatrix} -0.073 & 1.040 & 0.650 \\ 0.071 & 0.047 & 0.062 \\ 1.001 & -0.087 & 0.289 \end{bmatrix} \begin{bmatrix} \#\text{ of Intact Buildings} \\ \#\text{ of Damaged Buildings} \\ \#\text{ of Destroyed Buildings} \end{bmatrix}$$

and $\#\text{of Uninjured} + \#\text{ of Injured} + \#\text{ of Dead} = \#\text{ of Population}$

Road Network Vulnerability

After a disastrous seismic event narrow roads are generally blocked. This is even more critical for older urban environments where building collapses occur in large numbers. In modeling the road network vulnerability, given a scenario microzonation map and sets of structural vulnerability functions, it is assumed that completely collapsed buildings that are adjacent to the roads are the main cause of the blockage.

The road network has been extracted from the 1:2000 scale digital maps using a semi-automated procedure in GIS. The modeling involves locating the completely collapsed buildings (or more sophistically to find the probability of a building being completely collapsed), finding the topology relationship to locate the parcels that are adjacent to each road, performing the proximity analysis in order to determine the parcel distance relative to the road and finally to calculate the blockage index (Figure 10). The blockage indices are obtained for completely collapsed buildings according to the building height "H" and road width "W" as a debris model. These criteria were first introduced in Iran by using Manjil field data (Iran earthquake of 1990) (Bahreini 1993).

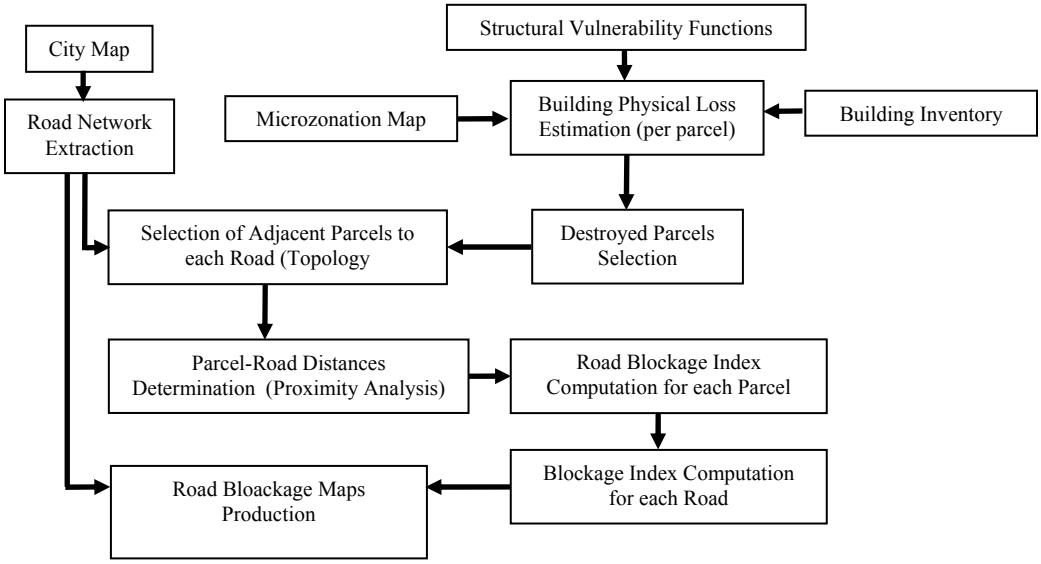

Fig. 10. Steps involved for road blockage calculation using GIS.

Determining the spatial distribution of the buildings and the road network, a Road Blockage Index (RBI) is assigned per each parcel. The probability of a building being completely damaged is combined with its RBI value. For each segment of the road, all contributing parcels are considered and their combined indices are aggregated. A road that is longer will have a higher probability of blockage unless the probability of at least one totally collapsed building that blocks the path (in the shorter road) is unity. On the other hand, when among all totally blocked pathways, the least amount of work and time in clearing the obstacles is of interest, then all contributing parcels must be considered. Figure 11 shows the road blockage chart for the area of study as an aggregation of the RBI value of all the contributing buildings.

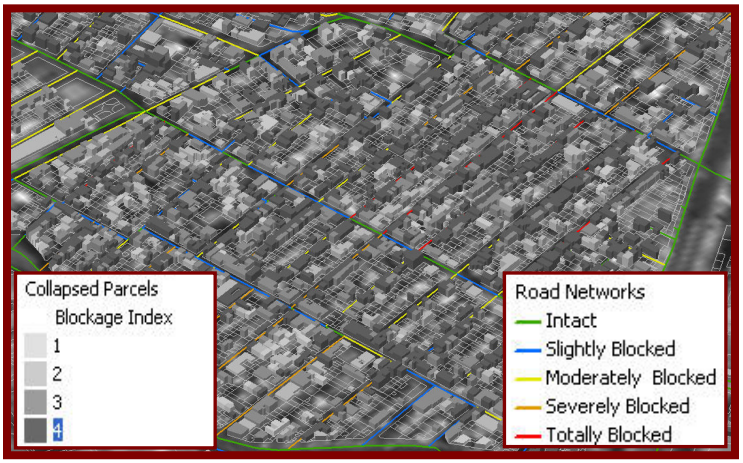

Fig. 11. Probabilistic road network blockage – part of Tehran.

QUICK LOSS ESTIMATION

Optical Remote Sensing

A parcel-based approach takes advantage of combining the information from the ancillary parcel data with Very High Resolution optical images. Effective spectral and spatial change detection features are chosen as the basic elements in a fuzzy classification. The procedure is applied and the entire city is classified for three damage grades, namely Slight, Moderate, and Severe. The reliability of the classification is computed and is high. Also the results were verified against a reported visual damage interpretation and good agreement is achieved for the collapse damage grade (Figure 12).

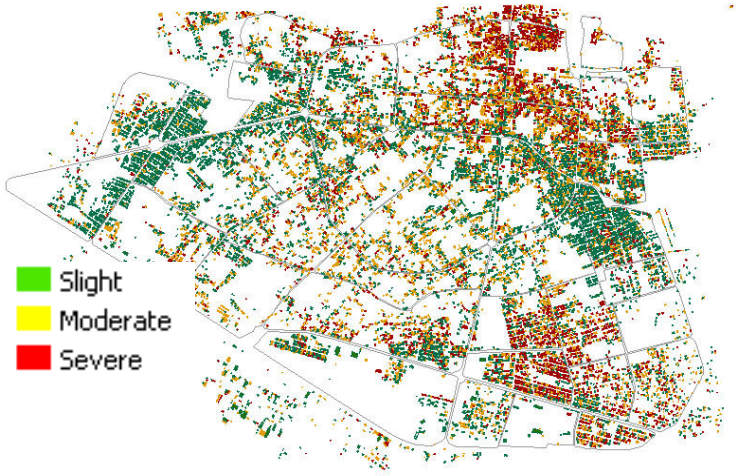

Fig. 12. Bam damage map using optical remote sensing data – an automated process.

Radar Remote Sensing

A Radar change index is studied (Mansouri et al. 2008) exploiting two "before" and a "before-after" image pairs. In this method, the radar change index is computed for each city parcel. The algorithm estimates the SAR signature using the RCS values with a calibration procedure. Figure

13 is the results of a statistical classification of the calibrated values of the change index that conforms well to the actual damages.

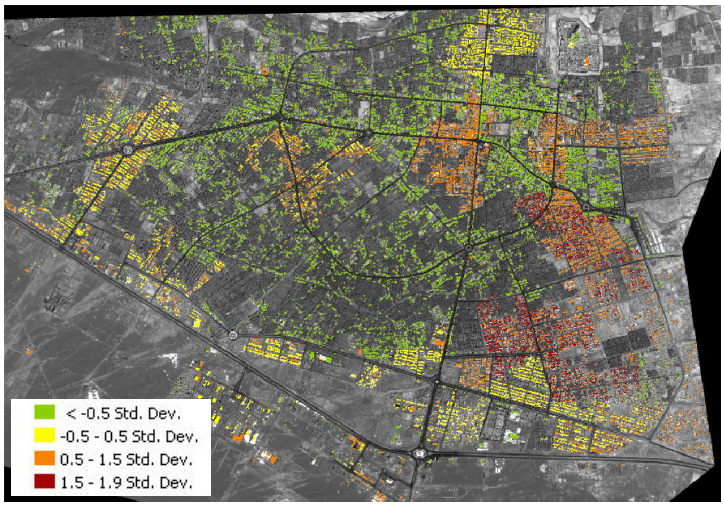

Fig. 13. Results of physical change/damage mapping in Bam using SAR data.

CONCLUSION

Seismic risk assessment of urban areas helps the authorities in devising strategies for lowering the unwanted consequences of earthquakes. Digital urban inventory, population statistics, different vulnerability functions for buildings, road networks and human casualty and also different risk algorithms were devised, compiled and implemented into GIS with a high level of information details. Urban risk maps are generated and the results can be effectively visualized in 3D.

After the occurrence of a devastating earthquake, the quick loss estimation will help the decision makers to have a realistic picture of the event and to find rational solutions. For this purpose a parcel-based approach for rapid building damage detection is presented that take advantage of combining the information from the ancillary city data in addition to the remote sensing (before and after) VHR optical images. Good correlation exists between the related damage map and the actual damage data for the “severe” class of building damages as investigated for the Bam earthquake (2003). Envisat satellite SAR data was also evaluated in the case of the Bam earthquake. The SAR cross power difference (before and after data sets) showed promise in detecting changes in urban areas when the index is calibrated for the sensor-parcel geometry.

ACKNOWLEDGEMENT

This paper represents the partial results of the IIEES project activated under the research contract number 327-8302. The support of NSF, The National Academies, and UCI is appreciated.

REFERENCES

Abbasi, M.R., Shabanian, E., 1999, "Fault Map of North Tehran", Published by International Institute of Earthquake Engineering and Seismology, Tehran, Iran.

Applied Technology Council, 1985, "Earthquake Damage Evaluation Data for California", ATC-13 Report, Redwood City, CA 94065

Bahreini, S. H., et al., (1993), The role of form, pattern and dwelling dimensions in seismic mitigation, volume one, Research Report, publication of Iranian Center for Disaster Response

Berberian, M., Yeats, R. S., 2001, "Contribution of archaeological data to studies of earthquaske history in the Iranian Plateau", Journal of Structural Geology 23 (2001) 563-584

Darrehzereshki M., 2009, "Development of Vulnerability Functions for Unreinforced Masonry Buildings for Tehran – District 17", Master's Thesis at IIEES.

HAZUS-FEMA, 2003,Technical Manual, "Multi-hazard Loss Estimation Methodology, Earthquake Model", HAZUS-MH MR1, Washington D.C.

Hessami K., Jamali F., and Tabassi H., 2003, "Active Fault Maps of Iran", Seismotectonic Dept., Seismology Research Center, IIEES, Iran

Jafari M. K., Amini Hosseini K., Hosseini M., Kamalian M., Askari F., Razmkhah A., Davoodi M., Mahdavifar M. R., Sohrabi Bidar A., and Keshavarz Bakhshayesh M., 2005, "Seismic Hazard Study", Final Report for Tehran Comprehensive Plan, International Institute of Earthquake Engineering and Seismology, IIEES, Iran

Japan International Cooperation Agency, JICA, 2000, "The Study on Seismic Microzoning of the Greater Tehran Area in the Islamic Republic of Iran", Final Report, Main Report, SSF JR 00-186

Kircher C. A., Nassar A. A., Kustu O., and Holmes, W. T., 1997, "Development of Building Damage Functions for Earthquake Loss Estimation", Earthquake Spectra, EERI, Vol. 13, November 1997, pp. 663-681

Mansouri B., and Ghafory-Ashtiany, 2008, "Seismic Risk Modeling and Quick Loss Estimation in Urban Areas using GIS and Remote Sensing Technologies", First International Conference on Remote Sensing Techniques in Disaster Management and Emergency Response in the Mediterranean Region, 22-24 Sept., Zadar, Croatia.

Mansouri B., Ghafory-Ashtiany M., Amini-Hosseini K., Nourjou R., and Mousavi M., (2009), 'Building Seismic Loss Model for Tehran using GIS', accepted for publication in Earthquake Spectra, EERI

Mansouri B., Ghafory-Ashtiany M., Amini-Hosseini K., Ghayamghamian M.R., Nourjou R., and Mousavi M., 2008, Urban Seismic Loss Estimation using Optical and Radar Satellite Imagery and GIS, International Institute of Earthquake Engineering and Seismology, contract #327-8302: Tehran, Iran, 2008.

Sauter F., and Shah, H. C., 1978, "Estudio de Seguro Contro Terremoto", Institute Nacional de Seguros, San Jose, Costa Rica.

Tavakoli B., and Tavakoli S. 1993, "Estimating the Vulnerability and Loss Functions of Residential Buildings", Natural Hazards, Vol. 7, No. 2

THE SEISMIC VULNERABILITY ASSESSMENT AND RETROFIT OF HIGHWAY AND RAILWAY BRIDGES IN IRAN

Shahrokh Maalek
School of Civil Engineering, University of Tehran
maalek@ut.ac.ir

EXTENDED ABSTRACT

In this paper, the results of a comprehensive program of work concerning the seismic vulnerability assessment of highway and railway bridges in Iran have been reported briefly. As a result of a preliminary investigation carried out on Tehran bridges by the author, a detailed qualitative and quantitative assessment program has been organized and supervised by the author and his team of experts, involving seventeen specialist firms (consulting engineers) and five universities, for the City Town Hall. The work included 110 junctions (more than 150 bridges). At the same time, the experiences gained in connection with a separate program of work on a rather large number of railway bridges have also been reported. In the latter studies, the author has acted as the director of the specialty committee appointed for the guidance and checking as well as the final approval of works which have been under investigation by ten firms (consulting engineers) and four universities.

A data base has been provided for the existing bridges as well as bridges under construction. The existing maps concerning the seismic zonation of Tehran as well as the map of the city have been digitized to provide a basis for a suitable GIS. The locations of bridges have been indicated and a computerized link has been provided between the bridge positions and their technical inventory gathered in the data base.

Tehran bridges have been categorized from different points of view (e.g. importance, structural and foundation systems, materials of construction, geometrical particulars, potential geotechnical hazards, date of design and construction, available information, history of repair, intended remaining service life, etc.). Important bridges which are expected to maintain their serviceability after a severe earthquake have been identified and a program has been developed that indicates the priorities of the actual retrofitting measures in relation to the available resources.

A system for rapid inspection and qualitative assessment of seismic vulnerability of various types of bridges has been presented. Also a method for a more detailed qualitative assessment has also been introduced for use in cases where a rapid evaluation may not lead to conclusive results.

A statistical data processing and mining system has been adopted in order to identify factors affecting the vulnerability of bridges and repetitive deficiencies.

Quantitative assessment of different classes of bridges have been carried out with the aid of dynamic analyses of realistic three dimensional finite element models with particular attention on the modeling of bearings and gaps and the geometric irregularities. Depending upon the category

of the bridge, an appropriate method of analysis has been employed for each of the bridges under consideration. The analysis methods included the response spectrum, the linear and the non-linear time history approaches. The analyses have included the vertical components of earthquake excitations, since many bridge sites in the city of Tehran are to be anticipated as quite hazardous due to effects caused by near field ground motions. For some of important bridges or those located on hazardous sites, attempts have been made to study the effects of multiple support excitations as well.

The results of both the qualitative and quantitative approaches have been compared and the results have been used to calibrate the rating methods introduced here. Damage indices by different proposed methods have been estimated and a brief discussion has been presented on some retrofit measures suitable for such bridges.

Common problems affecting the performance, retrofit measures and the implementation of a strategic planning for the maintenance, rehabilitation and retrofit of bridges have been discussed with the objective of the upgrading of the bridges under investigation to a higher level of safety and serviceability.

The program of non-destructive and destructive tests of the existing bridges has been prepared depending upon the availability of information and technical documents. In addition to normal geotechnical and geophysical tests, use has been made from geo-radar equipments, electromagnetic facilities, ultrasonic pile detectors, fatigue monitoring gauges and some other devices. The Down hole shear wave velocity measurements and the dynamic testing through forced vibration have also been been carried out, were needed. On the other hand, some testing procedures have been developed for the study of the cyclic behavior of elastomeric bearing pads as well as a procedure in which a combination of the operational model analysis has been used together with a series of the finite element analysis to indicate the shear modulus of existing elastomeric bearings.

The work also introduces a bridge inventory and a proposed bridge management system appropriate for highway and railway bridges in Iran. At the same time, some retrofit measures, which have been found to be particularly effective in the seismic retrofit of the bridges under investigation has been addressed. These measures include the use of various vibration isolation systems, locking devices, shock transmission units as well as some common passive damping devices to reduce the structural demand and more common methods of bridge retrofitting methods such as the inclusion of restrainers, shear keys, confinement of reinforced concrete piers and the provision of intermediate and end diaphragms and other measures to reduce the risk of local and overall buckling failure or fracture of steel bridges. For sites with the potentialities of liquefaction and/or lateral spreading, an area of particular attention has been concerned with various soil improvement methods.

The author has also been the chairman of the specialty committee for the preparation of a rather comprehensive guide (manual) for the seismic vulnerability assessment and retrofit of bridges for national highway and railway bridges. The basic concepts and the philosophy governing this manual have been described briefly.

Appendix

In the last session of the public seminar, on June 10, 2008, in Tehran, the participants suggested the following research topics for future seismic cooperation:

1. Assessment of seismic risk in historical structures and sites, including issues such as
   a. historical sites in ancient cities;
   b. upgrade design codes for historical buildings;
   c. decay of materials due to moisture, temperature, and other conditions;
   d. structural and architectural considerations;
   e. consideration of traditional structural materials, components, and systems and their variations in different parts of the country;
   f. social, economic, and political issues involved in seismic rehabilitation of historical structures and sites;
   g. lack of accessibility in older parts of historical sites; and
   h. cooperation with international organizations such as UNESCO.
2. Seismic rehabilitation of adobe and unreinforced masonry (URM) buildings in Iran.
3. Affordable seismic-resistant housing.
4. A collaborative program for seismic rehabilitation of 27,000 existing schools in Iran, mostly of unreinforced masonry (URM).
5. Development of seismic design guidelines for *existing* structures, including development of a few detailed case studies.
6. Simplified seismic design and rapid and economical construction of *new* homes and schools.
7. Public education and risk management, including preparation for major seismic events and training of local masons and construction companies for seismic construction.
8. Socio-economic aspects of earthquakes, including seismic loss estimation, costs of seismic mitigation measures, and seismic insurance in the U.S. and Iran.
9. Long-term cooperation on post-earthquake investigation and recovery.

10. Evaluation of the U.S. seismic design guidelines and standards, such as various FEMA seismic documents and ASCE-41, for their applicability to Iran.

11. Cooperation on seismic design and construction of steel buildings, including steel moment frames and braced buildings.

12. Cooperation on seismic design of tall buildings, including comparisons of seismic performance and design of tall buildings in California and Tehran.

13. Cooperation on seismic performance and rehabilitation of older "non-ductile" reinforced concrete buildings.

14. Cooperation on a coordinated and multidisciplinary research program on earthquake engineering and earth sciences such as
    a. seismic hazard,
    b. geology,
    c. seismology,
    d. geotechnical earthquake engineering, and
    e. structural earthquake engineering.

15. Seismic performance of lifelines, including transportation and electrical systems.

16. Creation of a dedicated website for U.S.-Iran seismic cooperation.

17. Research on multihazards, such as earthquakes, floods, and fires following earthquakes.

18. Research on seismic performance of old and new construction materials.

19. Research on seismic performance of soil and foundations.

20. Seismic performance of masonry bridges.

PEER REPORTS

PEER reports are available individually or by yearly subscription. PEER reports can be ordered at http://peer.berkeley.edu/publications/peer_reports.html or by contacting the Pacific Earthquake Engineering Research Center, 1301 South 46th Street, Richmond, CA 94804-4698. Tel.: (510) 665-3448; Fax: (510) 665-3456; Email: peer_editor@berkeley.edu

PEER 2009/02 *Improving Earthquake Mitigation through Innovations and Applications in Seismic Science, Engineering, Communication, and Response. Proceedings of a U.S.-Iran Seismic Workshop.* October 2009.

PEER 2009/01 *Evaluation of Ground Motion Selection and Modification Methods: Predicting Median Interstory Drift Response of Buildings.* Curt B. Haselton, Ed. June 2009.

PEER 2008/10 *Technical Manual for Strata.* Albert R. Kottke and Ellen M. Rathje. February 2009.

PEER 2008/09 *NGA Model for Average Horizontal Component of Peak Ground Motion and Response Spectra.* Brian S.-J. Chiou and Robert R. Youngs. November 2008.

PEER 2008/08 *Toward Earthquake-Resistant Design of Concentrically Braced Steel Structures.* Patxi Uriz and Stephen A. Mahin. November 2008.

PEER 2008/07 *Using OpenSees for Performance-Based Evaluation of Bridges on Liquefiable Soils.* Stephen L. Kramer, Pedro Arduino, and HyungSuk Shin. November 2008.

PEER 2008/06 *Shaking Table Tests and Numerical Investigation of Self-Centering Reinforced Concrete Bridge Columns.* Hyung IL Jeong, Junichi Sakai, and Stephen A. Mahin. September 2008.

PEER 2008/05 *Performance-Based Earthquake Engineering Design Evaluation Procedure for Bridge Foundations Undergoing Liquefaction-Induced Lateral Ground Displacement.* Christian A. Ledezma and Jonathan D. Bray. August 2008.

PEER 2008/04 *Benchmarking of Nonlinear Geotechnical Ground Response Analysis Procedures.* Jonathan P. Stewart, Annie On-Lei Kwok, Yousseff M. A. Hashash, Neven Matasovic, Robert Pyke, Zhiliang Wang, and Zhaohui Yang. August 2008.

PEER 2008/03 *Guidelines for Nonlinear Analysis of Bridge Structures in California.* Ady Aviram, Kevin R. Mackie, and Božidar Stojadinović. August 2008.

PEER 2008/02 *Treatment of Uncertainties in Seismic-Risk Analysis of Transportation Systems.* Evangelos Stergiou and Anne S. Kiremidjian. July 2008.

PEER 2008/01 *Seismic Performance Objectives for Tall Buildings.* William T. Holmes, Charles Kircher, William Petak, and Nabih Youssef. August 2008.

PEER 2007/12 *An Assessment to Benchmark the Seismic Performance of a Code-Conforming Reinforced Concrete Moment-Frame Building.* Curt Haselton, Christine A. Goulet, Judith Mitrani-Reiser, James L. Beck, Gregory G. Deierlein, Keith A. Porter, Jonathan P. Stewart, and Ertugrul Taciroglu. August 2008.

PEER 2007/11 *Bar Buckling in Reinforced Concrete Bridge Columns.* Wayne A. Brown, Dawn E. Lehman, and John F. Stanton. February 2008.

PEER 2007/10 *Computational Modeling of Progressive Collapse in Reinforced Concrete Frame Structures.* Mohamed M. Talaat and Khalid M. Mosalam. May 2008.

PEER 2007/09 *Integrated Probabilistic Performance-Based Evaluation of Benchmark Reinforced Concrete Bridges.* Kevin R. Mackie, John-Michael Wong, and Božidar Stojadinović. January 2008.

PEER 2007/08 *Assessing Seismic Collapse Safety of Modern Reinforced Concrete Moment-Frame Buildings.* Curt B. Haselton and Gregory G. Deierlein. February 2008.

PEER 2007/07 *Performance Modeling Strategies for Modern Reinforced Concrete Bridge Columns.* Michael P. Berry and Marc O. Eberhard. April 2008.

PEER 2007/06 *Development of Improved Procedures for Seismic Design of Buried and Partially Buried Structures.* Linda Al Atik and Nicholas Sitar. June 2007.

PEER 2007/05 *Uncertainty and Correlation in Seismic Risk Assessment of Transportation Systems.* Renee G. Lee and Anne S. Kiremidjian. July 2007.

PEER 2007/04 *Numerical Models for Analysis and Performance-Based Design of Shallow Foundations Subjected to Seismic Loading.* Sivapalan Gajan, Tara C. Hutchinson, Bruce L. Kutter, Prishati Raychowdhury, José A. Ugalde, and Jonathan P. Stewart. May 2008.

PEER 2007/03 *Beam-Column Element Model Calibrated for Predicting Flexural Response Leading to Global Collapse of RC Frame Buildings.* Curt B. Haselton, Abbie B. Liel, Sarah Taylor Lange, and Gregory G. Deierlein. May 2008.

PEER 2007/02 *Campbell-Bozorgnia NGA Ground Motion Relations for the Geometric Mean Horizontal Component of Peak and Spectral Ground Motion Parameters.* Kenneth W. Campbell and Yousef Bozorgnia. May 2007.

PEER 2007/01 *Boore-Atkinson NGA Ground Motion Relations for the Geometric Mean Horizontal Component of Peak and Spectral Ground Motion Parameters.* David M. Boore and Gail M. Atkinson. May. May 2007.

PEER 2006/12 *Societal Implications of Performance-Based Earthquake Engineering*. Peter J. May. May 2007.

PEER 2006/11 *Probabilistic Seismic Demand Analysis Using Advanced Ground Motion Intensity Measures, Attenuation Relationships, and Near-Fault Effects.* Polsak Tothong and C. Allin Cornell. March 2007.

PEER 2006/10 *Application of the PEER PBEE Methodology to the I-880 Viaduct.* Sashi Kunnath. February 2007.

PEER 2006/09 *Quantifying Economic Losses from Travel Forgone Following a Large Metropolitan Earthquake.* James Moore, Sungbin Cho, Yue Yue Fan, and Stuart Werner. November 2006.

PEER 2006/08 *Vector-Valued Ground Motion Intensity Measures for Probabilistic Seismic Demand Analysis*. Jack W. Baker and C. Allin Cornell. October 2006.

PEER 2006/07 *Analytical Modeling of Reinforced Concrete Walls for Predicting Flexural and Coupled–Shear-Flexural Responses*. Kutay Orakcal, Leonardo M. Massone, and John W. Wallace. October 2006.

PEER 2006/06 *Nonlinear Analysis of a Soil-Drilled Pier System under Static and Dynamic Axial Loading.* Gang Wang and Nicholas Sitar. November 2006.

PEER 2006/05 *Advanced Seismic Assessment Guidelines.* Paolo Bazzurro, C. Allin Cornell, Charles Menun, Maziar Motahari, and Nicolas Luco. September 2006.

PEER 2006/04 *Probabilistic Seismic Evaluation of Reinforced Concrete Structural Components and Systems.* Tae Hyung Lee and Khalid M. Mosalam. August 2006.

PEER 2006/03 *Performance of Lifelines Subjected to Lateral Spreading.* Scott A. Ashford and Teerawut Juirnarongrit. July 2006.

PEER 2006/02 *Pacific Earthquake Engineering Research Center Highway Demonstration Project.* Anne Kiremidjian, James Moore, Yue Yue Fan, Nesrin Basoz, Ozgur Yazali, and Meredith Williams. April 2006.

PEER 2006/01 *Bracing Berkeley. A Guide to Seismic Safety on the UC Berkeley Campus.* Mary C. Comerio, Stephen Tobriner, and Ariane Fehrenkamp. January 2006.

PEER 2005/16 *Seismic Response and Reliability of Electrical Substation Equipment and Systems.* Junho Song, Armen Der Kiureghian, and Jerome L. Sackman. April 2006.

PEER 2005/15 *CPT-Based Probabilistic Assessment of Seismic Soil Liquefaction Initiation.* R. E. S. Moss, R. B. Seed, R. E. Kayen, J. P. Stewart, and A. Der Kiureghian. April 2006.

PEER 2005/14 *Workshop on Modeling of Nonlinear Cyclic Load-Deformation Behavior of Shallow Foundations.* Bruce L. Kutter, Geoffrey Martin, Tara Hutchinson, Chad Harden, Sivapalan Gajan, and Justin Phalen. March 2006.

PEER 2005/13 *Stochastic Characterization and Decision Bases under Time-Dependent Aftershock Risk in Performance-Based Earthquake Engineering*. Gee Liek Yeo and C. Allin Cornell. July 2005.

PEER 2005/12 *PEER Testbed Study on a Laboratory Building: Exercising Seismic Performance Assessment*. Mary C. Comerio, editor. November 2005.

PEER 2005/11 *Van Nuys Hotel Building Testbed Report: Exercising Seismic Performance Assessment.* Helmut Krawinkler, editor. October 2005.

PEER 2005/10 *First NEES/E-Defense Workshop on Collapse Simulation of Reinforced Concrete Building Structures.* September 2005.

PEER 2005/09 *Test Applications of Advanced Seismic Assessment Guidelines.* Joe Maffei, Karl Telleen, Danya Mohr, William Holmes, and Yuki Nakayama. August 2006.

PEER 2005/08 *Damage Accumulation in Lightly Confined Reinforced Concrete Bridge Columns.* R. Tyler Ranf, Jared M. Nelson, Zach Price, Marc O. Eberhard, and John F. Stanton. April 2006.

PEER 2005/07 *Experimental and Analytical Studies on the Seismic Response of Freestanding and Anchored Laboratory Equipment.* Dimitrios Konstantinidis and Nicos Makris. January 2005.

PEER 2005/06 *Global Collapse of Frame Structures under Seismic Excitations*. Luis F. Ibarra and Helmut Krawinkler. September 2005.

PEER 2005//05 *Performance Characterization of Bench- and Shelf-Mounted Equipment.* Samit Ray Chaudhuri and Tara C. Hutchinson. May 2006.

PEER 2005/04 *Numerical Modeling of the Nonlinear Cyclic Response of Shallow Foundations.* Chad Harden, Tara Hutchinson, Geoffrey R. Martin, and Bruce L. Kutter. August 2005.

PEER 2005/03 *A Taxonomy of Building Components for Performance-Based Earthquake Engineering.* Keith A. Porter. September 2005.

PEER 2005/02 *Fragility Basis for California Highway Overpass Bridge Seismic Decision Making*. Kevin R. Mackie and Božidar Stojadinović. June 2005.

PEER 2005/01 *Empirical Characterization of Site Conditions on Strong Ground Motion.* Jonathan P. Stewart, Yoojoong Choi, and Robert W. Graves. June 2005.

PEER 2004/09 *Electrical Substation Equipment Interaction: Experimental Rigid Conductor Studies.* Christopher Stearns and André Filiatrault. February 2005.

PEER 2004/08 *Seismic Qualification and Fragility Testing of Line Break 550-kV Disconnect Switches.* Shakhzod M. Takhirov, Gregory L. Fenves, and Eric Fujisaki. January 2005.

PEER 2004/07 *Ground Motions for Earthquake Simulator Qualification of Electrical Substation Equipment.* Shakhzod M. Takhirov, Gregory L. Fenves, Eric Fujisaki, and Don Clyde. January 2005.

PEER 2004/06 *Performance-Based Regulation and Regulatory Regimes.* Peter J. May and Chris Koski. September 2004.

PEER 2004/05 *Performance-Based Seismic Design Concepts and Implementation: Proceedings of an International Workshop.* Peter Fajfar and Helmut Krawinkler, editors. September 2004.

PEER 2004/04 *Seismic Performance of an Instrumented Tilt-up Wall Building.* James C. Anderson and Vitelmo V. Bertero. July 2004.

PEER 2004/03 *Evaluation and Application of Concrete Tilt-up Assessment Methodologies.* Timothy Graf and James O. Malley. October 2004.

PEER 2004/02 *Analytical Investigations of New Methods for Reducing Residual Displacements of Reinforced Concrete Bridge Columns.* Junichi Sakai and Stephen A. Mahin. August 2004.

PEER 2004/01 *Seismic Performance of Masonry Buildings and Design Implications.* Kerri Anne Taeko Tokoro, James C. Anderson, and Vitelmo V. Bertero. February 2004.

PEER 2003/18 *Performance Models for Flexural Damage in Reinforced Concrete Columns.* Michael Berry and Marc Eberhard. August 2003.

PEER 2003/17 *Predicting Earthquake Damage in Older Reinforced Concrete Beam-Column Joints.* Catherine Pagni and Laura Lowes. October 2004.

PEER 2003/16 *Seismic Demands for Performance-Based Design of Bridges.* Kevin Mackie and Božidar Stojadinović. August 2003.

PEER 2003/15 *Seismic Demands for Nondeteriorating Frame Structures and Their Dependence on Ground Motions.* Ricardo Antonio Medina and Helmut Krawinkler. May 2004.

PEER 2003/14 *Finite Element Reliability and Sensitivity Methods for Performance-Based Earthquake Engineering.* Terje Haukaas and Armen Der Kiureghian. April 2004.

PEER 2003/13 *Effects of Connection Hysteretic Degradation on the Seismic Behavior of Steel Moment-Resisting Frames.* Janise E. Rodgers and Stephen A. Mahin. March 2004.

PEER 2003/12 *Implementation Manual for the Seismic Protection of Laboratory Contents: Format and Case Studies.* William T. Holmes and Mary C. Comerio. October 2003.

PEER 2003/11 *Fifth U.S.-Japan Workshop on Performance-Based Earthquake Engineering Methodology for Reinforced Concrete Building Structures.* February 2004.

PEER 2003/10 *A Beam-Column Joint Model for Simulating the Earthquake Response of Reinforced Concrete Frames.* Laura N. Lowes, Nilanjan Mitra, and Arash Altoontash. February 2004.

PEER 2003/09 *Sequencing Repairs after an Earthquake: An Economic Approach.* Marco Casari and Simon J. Wilkie. April 2004.

PEER 2003/08 *A Technical Framework for Probability-Based Demand and Capacity Factor Design (DCFD) Seismic Formats*. Fatemeh Jalayer and C. Allin Cornell. November 2003.

PEER 2003/07 *Uncertainty Specification and Propagation for Loss Estimation Using FOSM Methods.* Jack W. Baker and C. Allin Cornell. September 2003.

PEER 2003/06 *Performance of Circular Reinforced Concrete Bridge Columns under Bidirectional Earthquake Loading*. Mahmoud M. Hachem, Stephen A. Mahin, and Jack P. Moehle. February 2003.

PEER 2003/05 *Response Assessment for Building-Specific Loss Estimation.* Eduardo Miranda and Shahram Taghavi. September 2003.

PEER 2003/04 *Experimental Assessment of Columns with Short Lap Splices Subjected to Cyclic Loads.* Murat Melek, John W. Wallace, and Joel Conte. April 2003.

PEER 2003/03 *Probabilistic Response Assessment for Building-Specific Loss Estimation.* Eduardo Miranda and Hesameddin Aslani. September 2003.

PEER 2003/02 *Software Framework for Collaborative Development of Nonlinear Dynamic Analysis Program.* Jun Peng and Kincho H. Law. September 2003.

PEER 2003/01 *Shake Table Tests and Analytical Studies on the Gravity Load Collapse of Reinforced Concrete Frames.* Kenneth John Elwood and Jack P. Moehle. November 2003.

PEER 2002/24 *Performance of Beam to Column Bridge Joints Subjected to a Large Velocity Pulse.* Natalie Gibson, André Filiatrault, and Scott A. Ashford. April 2002.

PEER 2002/23 *Effects of Large Velocity Pulses on Reinforced Concrete Bridge Columns.* Greg L. Orozco and Scott A. Ashford. April 2002.

PEER 2002/22 *Characterization of Large Velocity Pulses for Laboratory Testing.* Kenneth E. Cox and Scott A. Ashford. April 2002.

PEER 2002/21 *Fourth U.S.-Japan Workshop on Performance-Based Earthquake Engineering Methodology for Reinforced Concrete Building Structures.* December 2002.

PEER 2002/20 *Barriers to Adoption and Implementation of PBEE Innovations.* Peter J. May. August 2002.

PEER 2002/19 *Economic-Engineered Integrated Models for Earthquakes: Socioeconomic Impacts.* Peter Gordon, James E. Moore II, and Harry W. Richardson. July 2002.

PEER 2002/18 *Assessment of Reinforced Concrete Building Exterior Joints with Substandard Details.* Chris P. Pantelides, Jon Hansen, Justin Nadauld, and Lawrence D. Reaveley. May 2002.

PEER 2002/17 *Structural Characterization and Seismic Response Analysis of a Highway Overcrossing Equipped with Elastomeric Bearings and Fluid Dampers: A Case Study.* Nicos Makris and Jian Zhang. November 2002.

PEER 2002/16 *Estimation of Uncertainty in Geotechnical Properties for Performance-Based Earthquake Engineering.* Allen L. Jones, Steven L. Kramer, and Pedro Arduino. December 2002.

PEER 2002/15 *Seismic Behavior of Bridge Columns Subjected to Various Loading Patterns.* Asadollah Esmaeily-Gh. and Yan Xiao. December 2002.

PEER 2002/14 *Inelastic Seismic Response of Extended Pile Shaft Supported Bridge Structures.* T.C. Hutchinson, R.W. Boulanger, Y.H. Chai, and I.M. Idriss. December 2002.

PEER 2002/13 *Probabilistic Models and Fragility Estimates for Bridge Components and Systems.* Paolo Gardoni, Armen Der Kiureghian, and Khalid M. Mosalam. June 2002.

PEER 2002/12 *Effects of Fault Dip and Slip Rake on Near-Source Ground Motions: Why Chi-Chi Was a Relatively Mild M7.6 Earthquake.* Brad T. Aagaard, John F. Hall, and Thomas H. Heaton. December 2002.

PEER 2002/11 *Analytical and Experimental Study of Fiber-Reinforced Strip Isolators.* James M. Kelly and Shakhzod M. Takhirov. September 2002.

PEER 2002/10 *Centrifuge Modeling of Settlement and Lateral Spreading with Comparisons to Numerical Analyses***.** Sivapalan Gajan and Bruce L. Kutter. January 2003.

PEER 2002/09 *Documentation and Analysis of Field Case Histories of Seismic Compression during the 1994 Northridge, California, Earthquake.* Jonathan P. Stewart, Patrick M. Smith, Daniel H. Whang, and Jonathan D. Bray. October 2002.

PEER 2002/08 *Component Testing, Stability Analysis and Characterization of Buckling-Restrained Unbonded Braces™.* Cameron Black, Nicos Makris, and Ian Aiken. September 2002.

PEER 2002/07 *Seismic Performance of Pile-Wharf Connections.* Charles W. Roeder, Robert Graff, Jennifer Soderstrom, and Jun Han Yoo. December 2001.

PEER 2002/06 *The Use of Benefit-Cost Analysis for Evaluation of Performance-Based Earthquake Engineering Decisions.* Richard O. Zerbe and Anthony Falit-Baiamonte. September 2001.

PEER 2002/05 *Guidelines, Specifications, and Seismic Performance Characterization of Nonstructural Building Components and Equipment.* André Filiatrault, Constantin Christopoulos, and Christopher Stearns. September 2001.

PEER 2002/04 *Consortium of Organizations for Strong-Motion Observation Systems and the Pacific Earthquake Engineering Research Center Lifelines Program: Invited Workshop on Archiving and Web Dissemination of Geotechnical Data, 4–5 October 2001*. September 2002.

PEER 2002/03 *Investigation of Sensitivity of Building Loss Estimates to Major Uncertain Variables for the Van Nuys Testbed.* Keith A. Porter, James L. Beck, and Rustem V. Shaikhutdinov. August 2002.

PEER 2002/02 *The Third U.S.-Japan Workshop on Performance-Based Earthquake Engineering Methodology for Reinforced Concrete Building Structures*. July 2002.

PEER 2002/01 *Nonstructural Loss Estimation: The UC Berkeley Case Study.* Mary C. Comerio and John C. Stallmeyer. December 2001.

PEER 2001/16 *Statistics of SDF-System Estimate of Roof Displacement for Pushover Analysis of Buildings.* Anil K. Chopra, Rakesh K. Goel, and Chatpan Chintanapakdee. December 2001.

PEER 2001/15 *Damage to Bridges during the 2001 Nisqually Earthquake.* R. Tyler Ranf, Marc O. Eberhard, and Michael P. Berry. November 2001.

PEER 2001/14 *Rocking Response of Equipment Anchored to a Base Foundation.* Nicos Makris and Cameron J. Black. September 2001.

PEER 2001/13 *Modeling Soil Liquefaction Hazards for Performance-Based Earthquake Engineering.* Steven L. Kramer and Ahmed-W. Elgamal. February 2001.

PEER 2001/12 *Development of Geotechnical Capabilities in OpenSees.* Boris Jeremi . September 2001.

PEER 2001/11 *Analytical and Experimental Study of Fiber-Reinforced Elastomeric Isolators*. James M. Kelly and Shakhzod M. Takhirov. September 2001.

PEER 2001/10 *Amplification Factors for Spectral Acceleration in Active Regions.* Jonathan P. Stewart, Andrew H. Liu, Yoojoong Choi, and Mehmet B. Baturay. December 2001.

PEER 2001/09 *Ground Motion Evaluation Procedures for Performance-Based Design.* Jonathan P. Stewart, Shyh-Jeng Chiou, Jonathan D. Bray, Robert W. Graves, Paul G. Somerville, and Norman A. Abrahamson. September 2001.

PEER 2001/08 *Experimental and Computational Evaluation of Reinforced Concrete Bridge Beam-Column Connections for Seismic Performance*. Clay J. Naito, Jack P. Moehle, and Khalid M. Mosalam. November 2001.

PEER 2001/07 *The Rocking Spectrum and the Shortcomings of Design Guidelines*. Nicos Makris and Dimitrios Konstantinidis. August 2001.

PEER 2001/06 *Development of an Electrical Substation Equipment Performance Database for Evaluation of Equipment Fragilities*. Thalia Agnanos. April 1999.

PEER 2001/05 *Stiffness Analysis of Fiber-Reinforced Elastomeric Isolators.* Hsiang-Chuan Tsai and James M. Kelly. May 2001.

PEER 2001/04 *Organizational and Societal Considerations for Performance-Based Earthquake Engineering.* Peter J. May. April 2001.

PEER 2001/03 *A Modal Pushover Analysis Procedure to Estimate Seismic Demands for Buildings: Theory and Preliminary Evaluation.* Anil K. Chopra and Rakesh K. Goel. January 2001.

PEER 2001/02 *Seismic Response Analysis of Highway Overcrossings Including Soil-Structure Interaction.* Jian Zhang and Nicos Makris. March 2001.

PEER 2001/01 *Experimental Study of Large Seismic Steel Beam-to-Column Connections.* Egor P. Popov and Shakhzod M. Takhirov. November 2000.

PEER 2000/10 *The Second U.S.-Japan Workshop on Performance-Based Earthquake Engineering Methodology for Reinforced Concrete Building Structures.* March 2000.

PEER 2000/09 *Structural Engineering Reconnaissance of the August 17, 1999 Earthquake: Kocaeli (Izmit), Turkey.* Halil Sezen, Kenneth J. Elwood, Andrew S. Whittaker, Khalid Mosalam, John J. Wallace, and John F. Stanton. December 2000.

PEER 2000/08 *Behavior of Reinforced Concrete Bridge Columns Having Varying Aspect Ratios and Varying Lengths of Confinement.* Anthony J. Calderone, Dawn E. Lehman, and Jack P. Moehle. January 2001.

PEER 2000/07 *Cover-Plate and Flange-Plate Reinforced Steel Moment-Resisting Connections*. Taejin Kim, Andrew S. Whittaker, Amir S. Gilani, Vitelmo V. Bertero, and Shakhzod M. Takhirov. September 2000.

PEER 2000/06 *Seismic Evaluation and Analysis of 230-kV Disconnect Switches*. Amir S. J. Gilani, Andrew S. Whittaker, Gregory L. Fenves, Chun-Hao Chen, Henry Ho, and Eric Fujisaki. July 2000.

PEER 2000/05 *Performance-Based Evaluation of Exterior Reinforced Concrete Building Joints for Seismic Excitation.* Chandra Clyde, Chris P. Pantelides, and Lawrence D. Reaveley. July 2000.

PEER 2000/04 *An Evaluation of Seismic Energy Demand: An Attenuation Approach.* Chung-Che Chou and Chia-Ming Uang. July 1999.

PEER 2000/03 *Framing Earthquake Retrofitting Decisions: The Case of Hillside Homes in Los Angeles.* Detlof von Winterfeldt, Nels Roselund, and Alicia Kitsuse. March 2000.

PEER 2000/02 *U.S.-Japan Workshop on the Effects of Near-Field Earthquake Shaking.* Andrew Whittaker, ed. July 2000.

PEER 2000/01 *Further Studies on Seismic Interaction in Interconnected Electrical Substation Equipment.* Armen Der Kiureghian, Kee-Jeung Hong, and Jerome L. Sackman. November 1999.

PEER 1999/14 *Seismic Evaluation and Retrofit of 230-kV Porcelain Transformer Bushings*. Amir S. Gilani, Andrew S. Whittaker, Gregory L. Fenves, and Eric Fujisaki. December 1999.

PEER 1999/13 *Building Vulnerability Studies: Modeling and Evaluation of Tilt-up and Steel Reinforced Concrete Buildings.* John W. Wallace, Jonathan P. Stewart, and Andrew S. Whittaker, editors. December 1999.

PEER 1999/12 *Rehabilitation of Nonductile RC Frame Building Using Encasement Plates and Energy-Dissipating Devices.* Mehrdad Sasani, Vitelmo V. Bertero, James C. Anderson. December 1999.

PEER 1999/11 *Performance Evaluation Database for Concrete Bridge Components and Systems under Simulated Seismic Loads.* Yael D. Hose and Frieder Seible. November 1999.

PEER 1999/10 *U.S.-Japan Workshop on Performance-Based Earthquake Engineering Methodology for Reinforced Concrete Building Structures.* December 1999.

PEER 1999/09 *Performance Improvement of Long Period Building Structures Subjected to Severe Pulse-Type Ground Motions*. James C. Anderson, Vitelmo V. Bertero, and Raul Bertero. October 1999.

PEER 1999/08 *Envelopes for Seismic Response Vectors.* Charles Menun and Armen Der Kiureghian. July 1999.

PEER 1999/07 *Documentation of Strengths and Weaknesses of Current Computer Analysis Methods for Seismic Performance of Reinforced Concrete Members.* William F. Cofer. November 1999.

PEER 1999/06 *Rocking Response and Overturning of Anchored Equipment under Seismic Excitations.* Nicos Makris and Jian Zhang. November 1999.

PEER 1999/05 *Seismic Evaluation of 550 kV Porcelain Transformer Bushings.* Amir S. Gilani, Andrew S. Whittaker, Gregory L. Fenves, and Eric Fujisaki. October 1999.

PEER 1999/04 *Adoption and Enforcement of Earthquake Risk-Reduction Measures.* Peter J. May, Raymond J. Burby, T. Jens Feeley, and Robert Wood.

PEER 1999/03 *Task 3 Characterization of Site Response General Site Categories*. Adrian Rodriguez-Marek, Jonathan D. Bray, and Norman Abrahamson. February 1999.

PEER 1999/02 *Capacity-Demand-Diagram Methods for Estimating Seismic Deformation of Inelastic Structures: SDF Systems*. Anil K. Chopra and Rakesh Goel. April 1999.

PEER 1999/01 *Interaction in Interconnected Electrical Substation Equipment Subjected to Earthquake Ground Motions.* Armen Der Kiureghian, Jerome L. Sackman, and Kee-Jeung Hong. February 1999.

PEER 1998/08 *Behavior and Failure Analysis of a Multiple-Frame Highway Bridge in the 1994 Northridge Earthquake.* Gregory L. Fenves and Michael Ellery. December 1998.

PEER 1998/07 *Empirical Evaluation of Inertial Soil-Structure Interaction Effects.* Jonathan P. Stewart, Raymond B. Seed, and Gregory L. Fenves. November 1998.

PEER 1998/06 *Effect of Damping Mechanisms on the Response of Seismic Isolated Structures.* Nicos Makris and Shih-Po Chang. November 1998.

PEER 1998/05 *Rocking Response and Overturning of Equipment under Horizontal Pulse-Type Motions.* Nicos Makris and Yiannis Roussos. October 1998.

PEER 1998/04 *Pacific Earthquake Engineering Research Invitational Workshop Proceedings, May 14–15, 1998: Defining the Links between Planning, Policy Analysis, Economics and Earthquake Engineering.* Mary Comerio and Peter Gordon. September 1998.

PEER 1998/03 *Repair/Upgrade Procedures for Welded Beam to Column Connections.* James C. Anderson and Xiaojing Duan. May 1998.

PEER 1998/02 *Seismic Evaluation of 196 kV Porcelain Transformer Bushings.* Amir S. Gilani, Juan W. Chavez, Gregory L. Fenves, and Andrew S. Whittaker. May 1998.

PEER 1998/01 *Seismic Performance of Well-Confined Concrete Bridge Columns.* Dawn E. Lehman and Jack P. Moehle. December 2000.

ONLINE REPORTS

The following PEER reports are available by Internet only at http://peer.berkeley.edu/publications/peer_reports.html

PEER 2009/103 *Performance Evaluation of Innovative Steel Braced Frames.* T. Y. Yang, Jack P. Moehle, and Božidar Stojadinović. August 2009.

PEER 2009/101 *Report of the First Joint Planning Meeting for the Second Phase of NEES/E-Defense Collaborative Research on Earthquake Engineering.* Stephen A. Mahin et al. July 2009.

PEER 2008/104 *Experimental and Analytical Study of the Seismic Performance of Retaining Structures.* Linda Al Atik and Nicholas Sitar. January 2009.

PEER 2008/103 *Experimental and Computational Evaluation of Current and Innovative In-Span Hinge Details in Reinforced Concrete Box-Girder Bridges. Part 1: Experimental Findings and Pre-Test Analysis.* Matias A. Hube and Khalid M. Mosalam. January 2009.

PEER 2008/102 *Modeling of Unreinforced Masonry Infill Walls Considering In-Plane and Out-of-Plane Interaction.* Stephen Kadysiewski and Khalid M. Mosalam. January 2009.

PEER 2008/101 *Seismic Performance Objectives for Tall Buildings.* William T. Holmes, Charles Kircher, William Petak, and Nabih Youssef. August 2008.

PEER 2007/101 *Generalized Hybrid Simulation Framework for Structural Systems Subjected to Seismic Loading.* Tarek Elkhoraibi and Khalid M. Mosalam. July 2007.

PEER 2007/100 *Seismic Evaluation of Reinforced Concrete Buildings Including Effects of Masonry Infill Walls.* Alidad Hashemi and Khalid M. Mosalam. July 2007.